



Journal which deals with research, Innovation and Originality



Table of Content

Topics	Page no
Chief Editor Board	3-4
Message From Associate Editor	5
Research Papers Collection	6-547

IJERGS

CHIEF EDITOR BOARD

- 1. Dr Chandrasekhar Putcha, Outstanding Professor, University Of California, USA**
- 2. Dr Shashi Kumar Gupta, , Professor, New Zealand**
- 3. Dr Kenneth Derucher, Professor and Former Dean, California State University, Chico, USA**
- 4. Dr Azim Houshyar, Professor, Western Michigan University, Kalamazoo, Michigan, USA**
- 5. Dr Sunil Saigal, Distinguished Professor, New Jersey Institute of Technology, Newark, USA**
- 6. Dr Hota GangaRao, Distinguished Professor and Director, Center for Integration of Composites into Infrastructure, West Virginia University, Morgantown, WV, USA**
- 7. Dr Bilal M. Ayyub, professor and Director, Center for Technology and Systems Management, University of Maryland College Park, Maryland, USA**
- 8. Dr Sarâh BENZIANE, University Of Oran, Associate Professor, Algeria**
- 9. Dr Mohamed Syed Fofanah, Head, Department of Industrial Technology & Director of Studies, Njala University, Sierra Leone**
- 10. Dr Radhakrishna Gopala Pillai, Honorary professor, Institute of Medical Sciences, Kirghistan**
- 11. Dr Ajaya Bhattarai, Tribhuwan University, Professor, Nepal**

ASSOCIATE EDITOR IN CHIEF

- 1. Er. Pragyan Bhattarai , Research Engineer and program co-ordinator, Nepal**

ADVISORY EDITORS

- 1. Mr Leela Mani Poudyal, Chief Secretary, Nepal government, Nepal**
- 2. Mr Sukdev Bhattarai Khatry, Secretary, Central Government, Nepal**
- 3. Mr Janak shah, Secretary, Central Government, Nepal**
- 4. Mr Mohodatta Timilsina, Executive Secretary, Central Government, Nepal**
- 5. Dr. Manjusha Kulkarni, Asso. Professor, Pune University, India**
- 6. Er. Ranipet Hafeez Basha (Phd Scholar), Vice President, Basha Research Corporation, Kumamoto, Japan**

Technical Members

- 1. Miss Rekha Ghimire, Research Microbiologist, Nepal section representative, Nepal**
- 2. Er. A.V. A Bharat Kumar, Research Engineer, India section representative and program co-ordinator, India**
- 3. Er. Amir Juma, Research Engineer ,Uganda section representative, program co-ordinator, Uganda**
- 4. Er. Maharshi Bhaswant, Research scholar(University of southern Queensland), Research Biologist, Australia**

IJERGS

Message from Associate Editor In Chief



Let me first of all take this opportunity to wish all our readers a very happy, peaceful and prosperous year ahead.

This is the Fourth Issue of the Third Volume of International Journal of Engineering Research and General Science. A total of 225 research articles are published and I sincerely hope that each one of these provides some significant stimulation to a reasonable segment of our community of readers.

In this issue, we have focused mainly on the ongoing trends and its improvisation and gave focus to Student works. We also welcome more research oriented ideas in our upcoming Issues.

Author's response for this issue was really inspiring for us. We received many papers from many countries in this issue than previous one but our technical team and editor members accepted very less number of research papers for the publication. We have provided editors feedback for every rejected as well as accepted paper so that authors can work out in the weakness more and we shall accept the paper in near future. We apologize for the inconvenient caused for rejected Authors but I hope our editor's feedback helps you discover more horizons for your research work.

I would like to take this opportunity to thank each and every writer for their contribution and would like to thank entire International Journal of Engineering Research and General Science (IJERGS) technical team and editor member for their hard work for the development of research in the world through IJERGS.

Last, but not the least my special thanks and gratitude needs to go to all our fellow friends and supporters. Your help is greatly appreciated. I hope our reader will find our papers educational and entertaining as well. Our team have done good job however, this issue may possibly have some drawbacks, and therefore, constructive suggestions for further improvement shall be warmly welcomed.

Er. Pragyan Bhattarai,

Associate Editor-in-Chief, P&R,

International Journal of Engineering Research and General Science

E-mail -Pragyan@ijergs.org

Landslide Hazard Zonation Using Remote Sensing and GIS Technology: A Case Study of Landslide Prone Area near Mahabaleshwar, Maharashtra, India

Rakesh L. Metha¹, Supriya R. Koli², Vivek R. Koli³

Walchand College of Engineering, Sangli, metha.rakesh@gmail.com

Abstract— Landslide is routine geological process on earth's crust, but recorded under disasters due to loss of lives and property. Prevention and mitigation of disaster can be planned if detected prior to the occurrence. The proposed paper is detection and mapping tool of probable mass movements and its destruction potential. The area surrounded by pre occurred landslide at Bhilar in Maharashtra is chosen for the present study. The effort has been made to study the Geo-informatics approach containing Remote sensing data and GIS as software integrated tool towards Landslide Hazard zonation. The various Spectral signatures and the image interpretation keys with respect to slope instability and various image data to identify Pre-occurred events and vulnerable sites are studied and used. The multivariate statistical analysis in the form of Information value method has been implemented along with the spatial analysis to obtain Landslide Susceptibility and Hazard Zonation. The methodology considers factors in the form of various thematic layers like lithology, slope, morphology, slope aspect, soil, relief, drainage, land use and pre-occurred landslides in the area generated using remote sensing data and GIS tools. From landslide hazard zonation map the hazardous locations are extracted from the study area and checked by the post analysis during field visit. The vulnerability zonation mapping and analysis of settlement and infrastructural facilities in high risk zone has been carried out. The present study demonstrates high degree of hazardousness at Bhilar and Godvali.

Keywords— Landslide hazard zonation, remote sensing, GIS, Landslide Susceptibility, Thematic layers, Information value method, Landslide Vulnerability.

INTRODUCTION

The landslides are hazards usually triggered by the neo-tectonic movements, earthquakes, heavy precipitation and those induced due to land-use changes such as felling of trees, agriculture, mining and road cutting in hilly terrain. Landslide is a general term used to describe the down-slope of soil, rock and organic material under the influence of gravity. The remote sensing and GIS based approach to map and study methodology involves generation of geomorphic map, NDVI map, soil map, slope map, DEM, drainage and lineament map, land use / land cover change map. LANDSAT TM and ASTER images have been used to generate a few of these thematic maps. Existing literature have also been referred to generate the thematic maps. To identify the vulnerable areas, the above-mentioned parameters were analyzed in a GIS by assigning appropriate ranks and weights. The result is a landslide hazard zonation map showing regions with varying degrees of vulnerability to landslides. It is opined that such a map (which is derived from the analysis of the causative factors) will enable to propose and implement suitable mitigating measures, thus preventing loss of life and property in the hilly area.

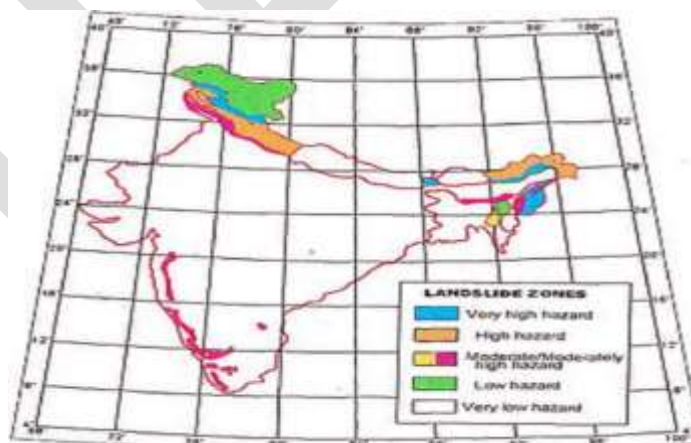


Figure 1 Landslide Hazard Zonation for India

Landslide hazard is one of the most significant hazards that affect different parts of India every year during the rainy season. It has been observed that Himalaya ranges, North east India, Nilgiris, Western Ghats and Eastern Ghats, are affected by this hazard every year and suffer heavy losses in terms of life, infrastructure and property.

Landslides affect at least 15 per cent of the land area of India—an area which exceeds 0.49 million km² (ndma.gov.in). The landslide situation in the country is further compounded by increased vulnerabilities related to rapidly growing population, unplanned urbanization and fast-paced industrialization, rapid development in high risk areas, environmental degradation and climate change. It is observed that impact of landslide is felt more severely by people who are socioeconomically weak because their habitats are located in vulnerable areas and not designed to withstand the impact of natural disasters.

This study aims at proposing the strategy for Landslide hazard zonation mapping to formulate an efficient methodology to delineate the Landslide hazard areas. Integration of remote sensing and GIS allows most accurate and most updated data base on land information. It has been found to be very useful tool in combination with spatial data and very useful deriving the ideas for efficient management and mitigation during the landslide disaster(Raju, n.d.). Also in developing various layers like slope map, drainage map, flow direction map, flow accumulation map, land use map, soil map, settlement map and various point maps with different attributes(Raju, n.d.). Information in thematic mapping which in turn can be utilized in predicting and presenting the generated landslide hazard data. The remote sensing data provides synoptic view of a fairly large area in the narrow and discrete bands of the electromagnetic spectrum at regular intervals (Aggarwal, 2004). The multi spectral data enable generating timely, reliable and cost Effective information after applying various image interpretation keys to discover the parameters of landslide hazard.

2. Study Area

In Western Ghats (declared as World Heritage by UNESCO) many human habitats, tourist places & highways are vulnerable to landslide .Hence we have chosen “hilly areas near Panchgani” as our study area which connects two major tourist regions of Maharashtra. This Area is blocked many times in rainy season because of landslide & hence due attention must be given to Hazard Zonation Mapping & mitigate recommendations. Landslide hazard zonation helps in identifying strategic points and geographically critical areas prone to landslides along this highway. In this study, a methodology has been developed to identify landslide prone areas using Remote Sensing and tools of GIS environment like ILWIS software.

3. Methodology

3.1 Landslide hazard Zonation

Most popularly, “Natural hazard” is defined as possibility of hazardous occurrences within a given area and in a given period of time. (Hearn and Griffiths, land surface evaluation for engineering practice, 2001) It incorporates three components: magnitude, geographical location and time. Landslide hazard zonation (LHZ) refers to "the division of the land surface into homogenous domains and their ranking according to degrees of potential hazard due to mass movement".(Krishnan, 2015)Landslide hazard is presented with spatial distribution of hazard classes(landslide hazard zonation).”(D et al., 2007) Demarcation or mapping of these zones demands understanding of influencing processes in the study area and factors causing landslides.

3.2 Data Source

The analysis is based on maps from Survey of India and Geological Survey of India and satellite imageries. A landslide occurrence database was generated from GPS measurements were taken during field survey. Various thematic maps pertaining to slope, aspect, drainage, flow accumulation, lithology, and land cover are generated with the help of ILWIS software for Bhilar and Godvali area. The slope and slope aspect layers were derived from ASTER DEM in ILWIS, while flow accumulation is analyzed from drainage in ILWIS. The NDVI analysis was undertaken to enhance the spectral variation in LANDSAT ETM+ (2005) satellite imageries in order to derive meaningful land use/land cover classification(Journal and Geomatics, 2011).

Table 1 Illustration of Data type/source used for analysis.

SR. NO.	DATA TYPE	DATA DESCRIPTION	USE/PURPOSE
1	Topographical Map	Scale- 1: 50,000	Thematic Vector Data generation, Correlation with Remote Sensing Data
2	Satellite Data ASTER LANDSAT ETM+ 2005	Spatial Resolution 30 m	Digital elevation model: Slope, Aspect, Drainage network and Density
	Google Earth Images 2005	Spatial Resolution 30m	Land use/Land cover
	Google Earth Images 2010	Spatial Resolution 1m	Land use/Land cover, Pre-occurred landslides, Settlement
3	Geological Map	Scale- 1:2,50,000	Geology: Lithology and geo-coding and geo-

			referencing
4	GPS Data	Co-ordinates and altitudes	Landslide Location
5	Field Data	Lithology, Slopes, Vegetation, Settlement	Vulnerability Assessment and Accuracy verification

3.3 Input Parameters and Data Preparing:

The thematic layers were used for the landslide hazard analysis are listed below:

- Slope
- Drainage
- Lithology
- Land use
- Slope Aspect
- Roads
- Pre-occurred Landslides
- Settlement

The outcome of image processing is a set of thematic maps that are utilized as data inputs in different layers. The data is integrated using GIS technique to analyze the layers.

3.4 Information Value Method

Method adopted for the study area is a statistical method, namely the Information Value Method (Yin and Yan, 1988). The information value is calculated using the following formula (Van Westen, 1993)(Balasubramani and Kumaraswamy, 2013):

$$\text{Prior Probability} = \text{nslide} / \text{nmap}$$

$$\text{Information Value} = \log [(\text{nsc} / \text{nc}) / \text{Prior Probability}]$$

Where: nmap = Total number of pixels in the map
nslide = Total number of landslide pixels
nc = Number of pixels in each class
nsc = Number of pixels containing slide

Negative values indicate negative correlation with landslides
Values around 0 indicate uncertainty or no evidence
Positive values indicates strong correlation with landslide.

For calculation of information value, each class of the thematic map is crossed with the landslide map (map x) with the active landslides. Cross tables were created which contain the pixel information value for the various classes of the individual layers. After crossing the landslide with all the individual layers, all the final maps were integrated together to derive a landslide hazard map. The equation for the final map is:

$$\text{Landslide Hazard Map} = \text{Slide Slope} + \text{Slide Flow Accu} + \text{Slide Litho} + \text{Slide L Cover} + \text{Slide Asp} + \text{Slide Rd} + \text{Slide Settle}$$

Where:

Slide Slope = Landslide and Slope Cross Weighted Map
Slide Flow Accu = Landslide and Flow Accumulation Cross Weighted Map
Slide Litho = Landslide and Lithology Cross Weighted Map
Slide L Cover = Landslide and Land Cover Cross Weighted Map
Slide Asp = Landslide and Aspect Cross Weighted Map
Slide Rd = Landslide and Road Density Cross Weighted Map
Slide Settle = Landslide and Settlement Cross Weighted Map

Following 7 parameters have been used. Before starting calculation the weights are assigned as per their importance. The weights are assigned by studying anaglyph, expert's opinion and actual site visits.

Table 2 Parameters with weights for statistical analysis

Parameter Maps	Weights
Slope	7
Drainage/ Flow Accumulation	6
Lithology	5
Land cover	4
Aspect	3
Roads	2
Settlement	1

4. ANALYSIS FOR LANDSLIDE HAZARD ZONATION:-

4.1 Digital Elevation Model (DEM): The DEM tile was imported in ILWIS environment and proper georeferenced was assigned to it along with WGS 84 coordinate system. Then the sub map was extracted to cover the study area. It has been observed that the minimum R.L. is about 840M in Kudali main stream and the top R.L. is about 1380M near west of Panchgani and east of Bhilar. To enhance the accuracy the digitized contour map was prepared from slicing the DEM by 20 M. the sliced DEM was vectored into polygon and then into segment map. This segment map was assigned the respective contour value in value domain. Again the same contour map was interpolated with 0.01 M precision to develop the new final DEM.

4.2 Digitized contour map: Digitized contour map of 20 M interval was prepared after slicing the DEM. It shows that, the contours are ranging between 800m to 1380m R.L. in the study area. It is observed that in certain elevation range the contours are much closed and nearly basic volcanic rock is present in the form of lava sheets. This area is being eroded since 53 million years. And has given rise to present contour pattern. Ridges, platu, valleys and the main stream, spurs of the hills are easily recognized from the contour patterns. The main function of the contour map was to prepare the enhanced DEM with 0.01 M precision.

4.3 Elevation sliced map: This is the layer prepared after slicing the DEM. It shows slicing of the study area into thirteen different zones of elevation range with 20 M precision. The layer was used to extract the contour data.

4.4 Slope map in degree: This is important layer in landslide hazard zonation mapping as slope is first causative factor of landslide. From slope stability point of view, the slope map was classified in three groups as Blue color indicates the slope from 0° to 13° as gentle slopes; Yellow color indicates the slope from 13° to 50° as slide prone slopes and red color indicates the slope from 50° to 90° as steep stable slopes.

4.5 Slope aspect map: The slope aspect map was prepared from DEM. This map shows the ground slope direction with respect to North. It has been observed that in this particular area the slope aspect has a little control over landslide. After studying pre occurred landslides, the slope aspect map was also considered in Information Value Method. Slope aspect map has been sliced into 8 directions. (N1 and N2 both indicates Northward slopes).

4.6 Flow direction map: This map indicates the flow direction of the study area. Each pixel is assigned with direction out of eight in which the precipitated water may flow. It is used to prepare the flow accumulation map by calculating the number of pixels, from the upstream direction flowing towards each pixel. This layer is the pre-requisite raster for the flow accumulation map. It has not been used in Information Value Analysis.

4.7 Flow accumulation map: It indicates the number of pixels flowing towards any particular pixel. With the prior information of resolution and rainfall data, it is easy to calculate the volume of water that may accumulate at selected pixel, for known rainfall. Since water plays very important role in landslides the flow accumulation has been used as high weighted layer in the Information Value Technique. Pre occurred landslides have been associated with the maximum flow accumulation. Maximum flow accumulation in soft overburden on slide prone slopes enhances the susceptibility. In the final layer of Information Value Method the maximum landslide susceptible areas have been found in the flow accumulation zones.

4.8 Village Map: The village map has been added over each layer combination for getting the relative position of spatial features with respect to village settlement.

4.9 Road Map: Contoured topographic map and the satellite data are collectively used to prepare the road map. Road map is simply a vector segment layer digitized on map and satellite imagery. Road vector after converting to raster was used to analysis vulnerability in Information Value method. In present study area only three major stretches of the roads have found to be landslide prone. They are associated with vulnerable settlement. In the hilly areas excavation for the roads has found to be one of the important causes of landslide. Therefore the raster road map was used in Information Value Method with the weightage.

4.10 ETM+ DATA: Out of 8 bands of Landsat 7 ETM+ band 4, 3 and 2 i.e. 1NIR and 2 Visible bands were used for the remote sensing study of the area. The FCC was prepared from extracted portion of the study area. NDVI layers and various band combinations were prepared and same were utilized for supervised classification of the area. It has been observed that the area consists of the E-W ridges alongside the river Kudali. Various slopes, Lava flows, Mini water sheds, Lateritic Platu's, Forest and Vegetation Cover, Barren Land, Settlements were identified by using the image interpretation keys. The identified classes were co-related with topographic map and field observations. Then the imagery was classified for getting the output layer of land cover map. Some pre occurred landslides were identified from both ETM+ and high resolution Google Earth (IKONOS) imagery and the same information was used in calculating prior probability. By using the ASTER DEM as DTM the stereopair of the same imagery have been prepared. They were viewed as an anaglyph models, so as to realize the probabilistic accuracy of the outcome of the information value method used for hazard zonation.

4.11 Google Earth Data: The google earth data has been processed from high resolution IKONOS PAN to develop the PAN sharpened MSS merged data product giving the true color composites. Therefore the same was utilized to extract the information of settlement details, roads, lithology, vegetation and the pre occurred landslide events. After the image interpretation the various related thematic layers were on screen digitized and converted into the required raster data set to be used in information value method.

4.12 Land Cover Map: From supervised classification of multiband layer combination of ETM+ data the land cover map was prepared. This raster was directly used for information value method. Since it is having relatively low spatial resolution and also the lower thematic resolution it was given a less weightage in information value method.

4.13 Lithology Map: In the study area basaltic rocks are very common. Because of highly oxidizing and humid conditions prevailed in the past, the basalts were weathered to form thick layers of lithomarge clays later on converted to the capping of laterite. Therefore basalts capped by laterite is a common lithology of the area. During the field visit the basaltic outcrops were marked on map along with their RLs. It has been observed that above certain RL the lithomarge clay layers are outcropping and above that entire area is covered by laterites. Therefore elevation data was sliced to get the general lithology map of the area.

5.0 Calculations for Information Value by Statistical Relationship of various Classes with Active Landslides:

5.1 Landslide Hazard Zonation

By overlaying all these crossed layers new output in the form of Landslide hazard zonation has been obtained.

Table 3 Landslide Hazard Zonation

LANDSLIDE HAZARD ZONES	AREA (Sq.km)	% OF TOTAL AREA
Very Low	2.377215	7.03
Low	6.1312996	18.13
Moderate	13.9574223	41.28
High	9.7868371	28.94
Very High	1.5618777	4.62

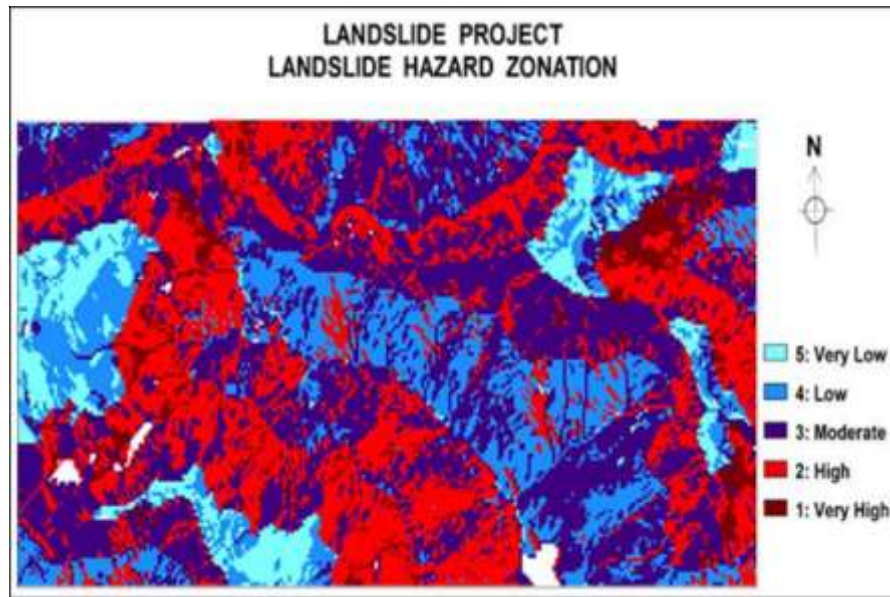


Figure 2 Landslide Hazard Zonation

5.2 Landslide Susceptibility Zonation

Form all zones only susceptible zone is delineated to focus on most hazard zone. By slicing operation the entire study area is divided in only two zones as susceptible zone and safe zone.

Table 4 Landslide Susceptibility Zonation

LANDSLIDE HAZARD ZONES	AREA (Sq.km)	% OF TOTAL AREA
Relatively Stable	29.752840.0	87.86%
Landslide Susceptible	4.110155.5	12.14%
Total	33.862995.5	100

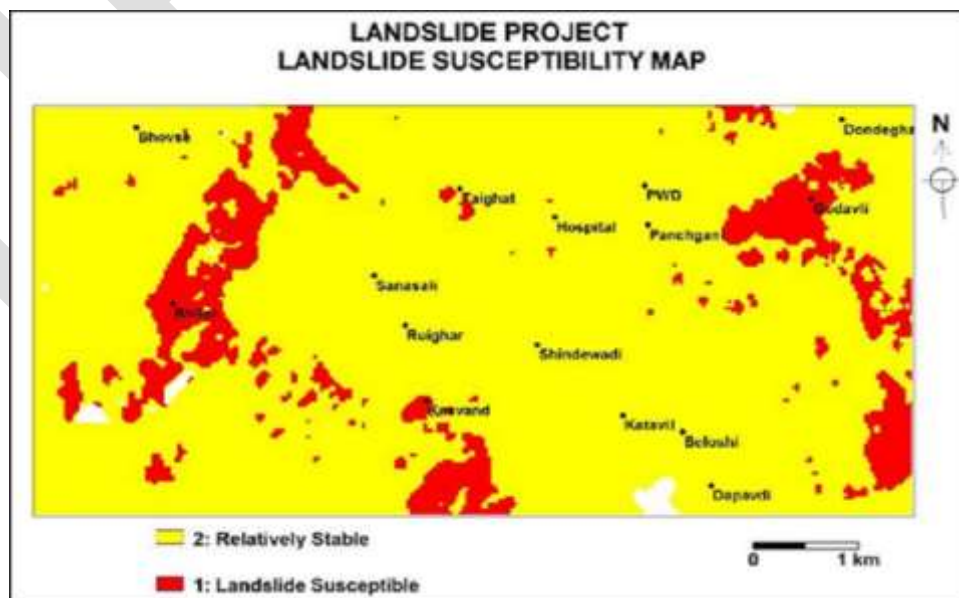


Figure 3 Landslide Susceptibility Map

5.9 Vulnerability Zonation Details:

By slicing operation the entire study area is divided in only two zones as susceptible zone and safe zone. For dividing the map in various zones slicing is done.

Table 5 Vulnerability Assessment Details:

LANDSLIDE HAZARD ZONES	AREA (Sq.km)	% OF TOTAL AREA
No Infrastructure	31.0200062	90.82
Safe Road	1.1602520	3.40
Non Vulnerable Settlement	1.2783225	3.74
Vulnerable Settlement	0.4797196	1.40
Vulnerable Road	0.2166176	0.63
Total:	34.1549179	100

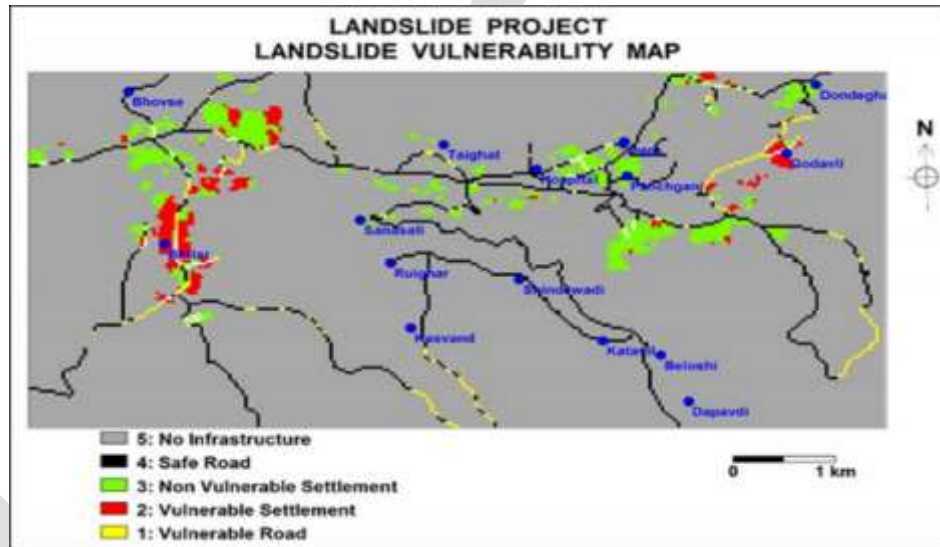


Figure 4 Landslide Vulnerability Map

From the information value method the Landslide Hazard Zonation, Landslide Susceptibility Zonation and Landslide Vulnerability Zonation has been obtained. From the statistical analysis the area of hazardous and vulnerable area has been calculated.

IMMEDIATE TROUBLE POINT LOCATIONS:

Following locations from the study area, demand immediate attention due to having high degree of landslide hazard. Efficient planning should be done to avoid the possibility of landslides and to reduce loss of economy.

Table 6 Immediate Trouble Point Location

SR. NO	LATTITUDE	LONGITUDE
1	17°55'25.9"	73°46'04.5"
2	17°55'12.8"	73°45'57.3"
3	17°55'01.8"	73°45'53.7"
4	17°54'57.1"	73°45'48.2"
5	17°54'50.8"	73°45'43.3"
6	17°54'40.8"	73°45'57.6"
7	17°54'33.6"	73°45'59.1"
8	17°54'30.7"	73°46'04.6"
9	17°54'26.4"	73°46'37.3"
10	17°54'25.9"	73°46'41.3"
11	17°53'50.1"	73°47'08.1"
12	17°55'59.4"	73°48'37.1"
13	17°55'19.7"	73°48'52.9"
14	17°55'57.5"	73°48'41.6"
15	17°54'53.9"	73°49'26.6"

7. Results and discussion:

Integration of Remote Sensing along with Geographical Information System (GIS) allows most reliable, accurate and updated database for land and water resource. Lack of land in hilly terrain has forced people to construct buildings on steep slopes with small or no retaining measure.

For the very first time in Maharashtra the information value method has been adopted and implemented by overlaying all the thematic layers to obtain Landslide hazard zonation map. This map is divided in five risk zones as Very Low, Low, Moderate, High, and Very High. In further part of the research from obtained hazard zonation map the only susceptible zone have been delineated to focus on most hazardous zone. This susceptibility map divides the entire study area in only two zones as susceptible zone and safe zone. This facilitates us to focus only on the most hazardous zone. This most hazardous zone map overlaid on landslide susceptibility map with settlement and road to obtain vulnerability zonation map.

The obtained vulnerability zonation map incorporated unnoticed area of Godvali which has shown equal risk for Godvali settlement as in Bhilar, therefore ground trothing visit immediately arranged to verify the accuracy of obtained output. It has been revealed that the settlement of Godvali is along deep and steep valley with flow accumulation passing from both sides. The entire settlement is on sloping ground which is having ground slope about 10°. According to Young's slope classification it is steep for settlement. Some sliding movements has been noticed along with considerable creep towards the valley. This has proved the results obtained are satisfactory having utmost accuracy. According to vulnerability assessed results over 34 percent area is liable to high-severe landslide risk and within this about 5 per cent has very high to severe risk while about 29 per cent of the total area has high risk of landslide occurrence. Such areas include Bhilar and Godvali on eastern slopes of the hill. About 59 per cent area of the study area has low to moderate risk of landslides. The analysis shows that unmapped hilly terrain of Mahabaleshwar Tehsil may also lie under hazardous zone of landslide of varying magnitude.

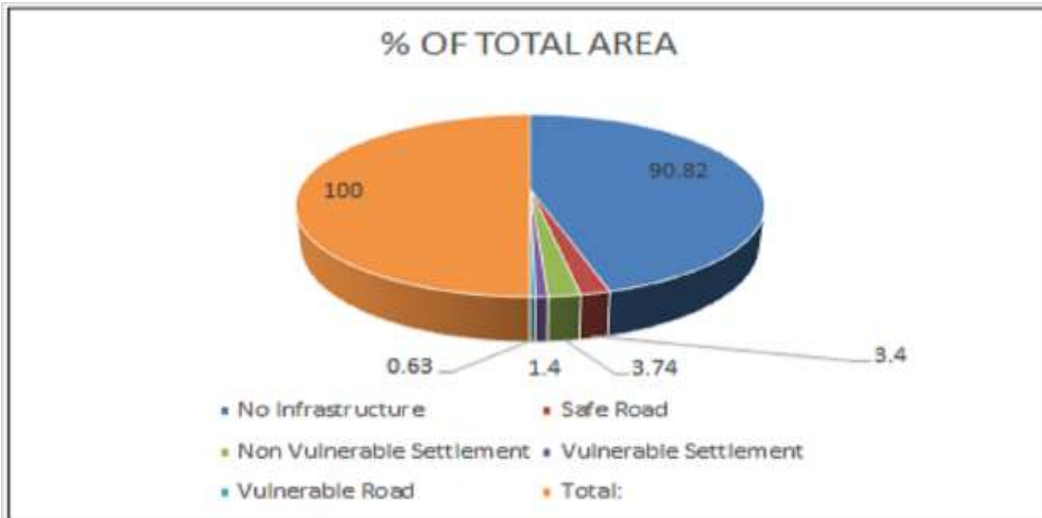


Figure 5 Graph showing Landslide Vulnerability Zonation classification

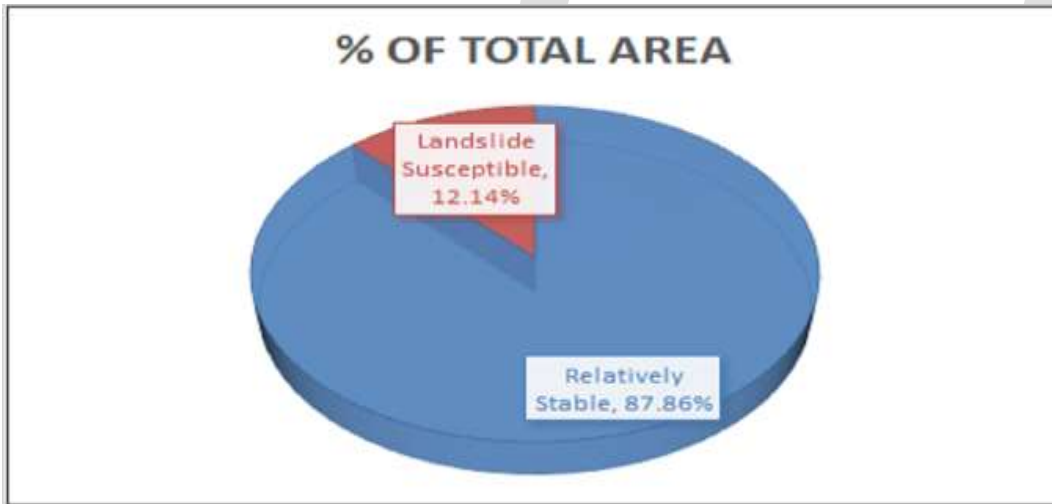


Figure 6 Graph showing Landslide Susceptibility Zonation Classification

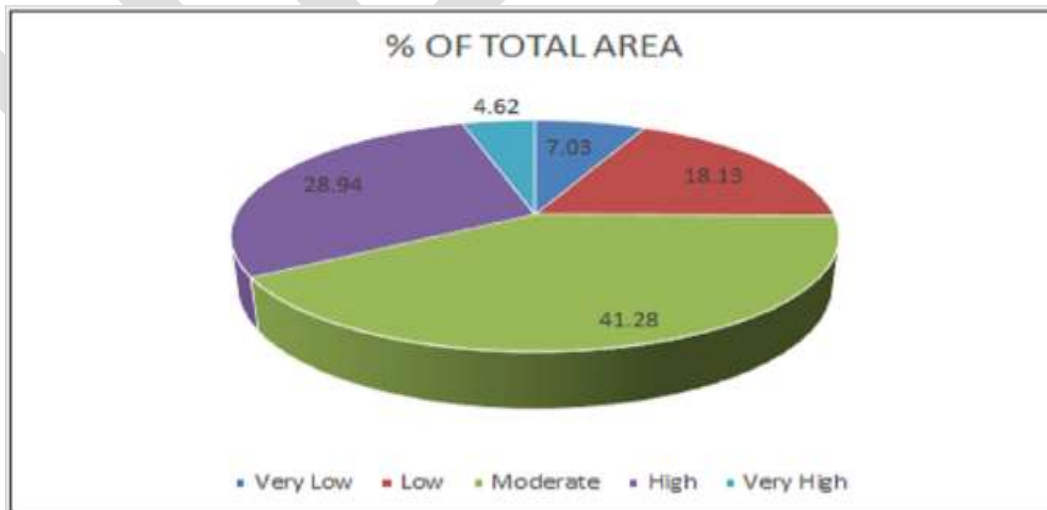


Figure 7 Graph showing Landslide Hazard Zonation Classification

REFERENCES:

1. A, A., C, K., B, P., 2011. Application of remote sensing data and GIS for landslide risk assessment as an environmental threat to Izmir city (West Turkey). Environmental Monitoring assessment. DOI: 10.1007/s10661-011-2352-8
2. Aggarwal, S., 2004. Principles of remote sensing. Satellite Remote Sensing and GIS Applications in Agricultural Meteorology 23–38.
3. Ahmed, B., 2014. Landslide susceptibility mapping using multi-criteria evaluation techniques in Chittagong Metropolitan Area, Bangladesh. Landslides. DOI: 10.1007/s10346-014-0521-x
4. Anbalagan, R., Chakraborty, D., Kohli, A., 2008. Landslide hazard zonation (LHZ) mapping on meso-scale for systematic town planning in mountainous terrain. J. Sci. Ind. Res. (India). 67, 486–497.
5. Balasubramani, K., Kumaraswamy, K., 2013. Application of Geospatial Technology and Information Value Technique in zonation mapping: A case study of Giri Valley, Himachal Pradesh. Disaster Advances 6, 38–47.
6. BL, D., RK, G., 1994. Remote sensing and Vegetation. Proceedings Natl. Academy Sci. 299–333.
7. Chandel, V.B.S., Brar, K.K., Chauhan, Y., 2011. RS & GIS Based Landslide Hazard Zonation of Mountainous Terrains A Study from Middle Himalayan Kullu District, Himachal Pradesh, India. International Journal of Geomatics and Geosciences 2, 121–133.
8. Chung, C.-J.F., Fabbri, A.G., 2008. Validation of spatial prediction models for landslide hazard mapping. Special. Issue Landslides GIS 30, 451–472.
9. D, P., AP, G., GB, S., 2007. GIS based landslide hazard mapping in Jhimruk River basin, West Nepal. J. Nepal Geol. Soc. 36, 25.
10. Ilija, I., Tsangaratos, P., Koumantakis, I., Rozos, D., 2010. Application of a Bayesian Approach in GIS model for evaluating Landslide Susceptibility. Case study Kimi area, Euboea, Greece. Bulletin of the Geological Society of Greece XLIII, No.3, 1590–1600.
11. Kanungo, D.P., Arora, M.K., Sarkar, S., Gupta, R.P., Landslide Susceptibility zonation (LSZ) mapping - a review. Journal of South Asia Disaster Studies 2, 81–106.
12. Krishnan, N., Subramani T., 2015. Land Slides Hazardous Zones by Using Remote sensing and GIS. International Journal of Application in Engineering & Management. 4, 211–222.
13. Lallianthanga, R.K., Lalbiakmawia, F., Lalramchuana, F., 2013. Landslide Hazard Zonation of Mamit town, Mizoram, India using remote sensing and GIS technique. International Journal of geology, Earth and Environmental Sciences 3, 184–194.
14. Lee, S., Pradhan, B., 2006. Probabilistic landslide hazards and risk mapping on Penang Island, Malaysia. Journal of Earth System Science 115, 661–672. DOI: 10.1007/s12040-006-0004-0
15. Mancini, F., Ceppi, C., Ritrovato, G., 2010. GIS and statistical analysis for landslide susceptibility mapping in the Daunia area, Italy. Natural Hazards and Earth System Science 10, 1851–1864. DOI: 10.5194/nhess-10-1851-2010
16. Nithya, S.E., Prasanna, P.R., 2010. An Integrated Approach with GIS and Remote Sensing Technique for Landslide Hazard Zonation. International Journal of Geomatics and Geosciences 1, 66–75.
17. Oledzki, Jan Romuald, 2004. Geoinformatics – an integrated spatial research tool. Miscellanea Geographica 11, 323–332.
18. Pardeshi, S.D., Autade, S.E., Pardeshi, S.S., 2015. Landslide hazard assessment : recent trends and techniques. Springer plus 1–11. DOI: 10.1186/2193
19. Pourghasemi, H.R., Pradhan, B., Gokceoglu, C., Moezzi, K.D., 2012. Terrigenous Mass Movements. Springer VIII, 23–50. DOI: 10.1007/978-3-642-25495-6
20. R.K., Lallianthanga, F., Lalbiakmawia, 2013. Micro-Level Landslide Hazard Zonation of Saitual Town, Mizoram, India Using
21. Remote Sensing and GIS Techniques. International Journal of engineering sciences & Research Technology 2.
22. Raju, P.L.N., Fundamentals of Geographical Information system. Satellite Remote Sensing and GIS Applications in Agricultural Meteorology 103–120.
23. Regmi, A.D., Devkota, K.C., Yoshida, K., Pradhan, B., Pourghasemi, H.R., Kumamoto, T., Akgun, A., 2014. Application of frequency ratio, statistical index, and weights-of-evidence models and their comparison in landslide susceptibility mapping in Central Nepal Himalaya. Arabian Journal of Geosciences 7, 725–742. DOI: 10.1007/s12517-012-0807-z
24. Sarkar, S., Kanungo, D.P., Patra, A K., Kumar, P., 2006. GIS Based Landslide Susceptibility Mapping — A Case Study in Indian Himalaya. Disaster Mitigation of Debris Flows, Slope Failures and Landslides 617–624.
25. Srileka, S., 2014. Landslide Hazard Zonation of Sirumalai Hills using Remote Sensing and GIS. International Journal of Scientific and Research Publications 4, 1–10.
26. Wu, T., Abdel-Latif, 2000. Prediction and mapping of landslide hazard. Canadian Geotechnical Journal 37, 781–795.
27. Yager, K., 2006. A CIESIN Thematic Guide to Social Science Applications of Remote Sensing. Social Science 1–68.
28. Yin, K. L. and Yan, T. Z., (1988) Statistical Prediction Model for Slope Instability of Metamorphosed rocks. In: Bonnard, C. (ed.)
29. Proceeding Fifth International Symposium on Landslides, Lausanne, Balkema, Rotterdam, the Netherlands, 2, 1269-1272.

Book References:

1. Buckley, D., Rights, A.L.L., Permission, R., 1998. David J. Buckley Principal GIS Consultant Innovative GIS Solutions, Inc. February 1997.
2. Kingma, N.C., 2011. Multi-hazard risk assessment Distance education course Risk City Exercise book 2011 Risk city dataset.
3. Noam Levin, 1999. Fundamentals of remote sensing. GIS unit, the Society for the Protection of Nature in Israel
4. Parkash, S., 2012. Compressive Landslides Risk Management, National institute of Disaster Management, New Delhi, India

Thesis and Reports:

1. Gaurav, K., 2009. Stochastic Modelling of Land Cover (dynamic) Elements to Assess Landslide Vulnerability Stochastic Modelling of Land Cover (dynamic) Elements to Assess Landslide Vulnerability.
2. Khats, P., 2005. Urban Multi-Hazard Risk Analysis Using GIS and Remote Sensing : A Case Study of a Part of Kohima Town, India.
3. Westen, C. van, Krol, B., 2015. Combining landslide research with capacity building : the experience of the United Nations University – ITC School for Disaster Geo-information Management

Web References:

1. <http://ndma.gov.in/en/learn-about-disasters/natural-disaster/landslides/zone-map.html> (last accessed 5 July 2015)
2. www.bhuvan.nrsc.gov.in (last accessed 2 July 2015)
3. www.earthexplorer.usgs.gov (last accessed 5th July 2015)
4. www.srtm.csi.cgiar.org (last accessed 5th July 2015)
5. www.libutexas.edu (last accessed 1 July 2015)
6. www.geoportal.icimod.org (last accessed 25 June 2015)
7. www.itc.nl.html (last accessed 29 June 2015)

Software Project Risk Management by using Six Sigma Approach

Khadija Zafar

Department of Computer Science, University of Agriculture, Faisalabad, Pakistan

Email: khadija.zafar83@gmail.com

ABSTRACT- Risk controlling in software projects is considered to be a most important contributor to project success. Six Sigma is being used in the industries and business sectors as a project management method to authenticate goal of near to excellence in process accomplishment and execution. It is one of applications in several organization and business processes to attain major performance enhancement in different industrial and business sectors including the IT sector. Six Sigma require across-the- board framework for effective risk management because root cause analysis (RCA) is still the primary and most important practice used for managing risks in this methodology. In this research, we have endeavoured to put forward an investigation in order to improve quality and productivity of Six Sigma projects, predominantly in the IT development projects. The study also included detailed overview of the current methods being practiced for risk identification, mitigation and management in Six Sigma.

Keywords — Risk Management, DMAIC, DMADV, Six Sigma, Risk Management

I. INTRODUCTION

In modern software projects, security and risk management are not just something one might do if there are time and resources. Software Project Development and its Execution is on the whole a difficult task as we are going to produce new product, proper research is required before development process, beside that we are facing high risk factors too. Though, we have methodologies to identify a number of risks in earlier stages but probability of failure is still very high. The major issue is that same techniques and methodologies cannot be applied on every type of project as the risk type for every project differs [6].

Our objective in this research is to provide a methodology for risk management that can serve in several aspects. Technically, it would help project managers to adopt methodology which will be best fit for their projects. On the other hand, it would help for further studies that aim to improve the software development process by identifying risk in earlier stages of development [6].

Security has become an important part of the end product. Six Sigma is a quality standard used in industries and corporate sectors. So it has always been a burning issue to research, methods and tools to identify and eliminate risk from IT projects. We are motivated with the specialized tools and techniques offered by Six Sigma, Six sigma is a series of best practices that can enhance manufacturing procedures and reduce defects, so it is also called a problem solving methodology. As we know risk identification and management is a major issue in every industry including IT in real time environment. Therefore, it's a collective effort for this research. We have focused on both approaches of six sigma: - measure-analyse-improve- control (DMAIC) and define-measure-analyse-design-verify (DMADV) also called Design for Six Sigma (DFSS). Six Sigma is based on DMAIC idea and focuses on to discover the core cause of the problem using statistical methods. Risk analysis includes risk identification and to minimize their effects to make a successful project.

In this paper we have analysed different techniques and methodologies currently using in software development life cycle. We have shown their capability to identify and manage risks during SDLC. Suggestions made for choosing better methodology for different types of projects for development of risk management process [8].

Risk identification and its mitigation collectively called as risk management which is a core part of any project. In six sigma this part of a critical phase called Risk Cause Analysis (RCA). For this purpose first of all core reason is identified that can cause defects in final product, then a table is designed in which defects/risks are prioritized and found their severity to apply tools accordingly. In this paper we have given an overview of existing techniques used for risk management. In the end we have concluded whole literature review in the form of a table and conclusion.

II. LITERATURE REVIEW

Sinovec and Hribar [1] in their research they applied different software quality prediction techniques to indicate existing faults in software project and financial management. They have analyzed three case studies including Nokia, Ericson and Tesla for the purpose of research. They pointed out that if we want to improve software fault handling process we should have best understanding of software faults, their distribution and association with prediction model. With this knowledge we can apply improvement techniques more efficiently to avoid loss of resources. They suggest that Product Life Cycle Management (PLCM) supports to transform customer needs into desired product with best use of resources and avoiding risks.

Vojo and Bubevsk [2] discovered that the conservative approach to Risk Assessment and Management in Software Testing is based on investigative models and statistical analysis and projected a model. They showed that investigative models are fixed, so they do not give any explanation for the inbuilt changeability and uncertainty of the testing process, which is a clear deficit. In this paper they presented application of Six Sigma and Simulation in Software Testing. In Six Sigma we have two techniques DMAIC and DMADV, they adopted one of them that is (define-measure-analyze-improve-control) DMAIC in testing process to evaluate and mitigate the risk to make delivery of the product on time, achieving the required quality goals.

Tariq [3] find out that Six Sigma with its countless implementations in many organizational and business procedures can help in project management methodology. It also supports in accomplishing goals near to perfection in process performance. Six Sigma is supported by the momentum of Plan-Do-Check-Act; it can help manufacturing industries, businesses and institutions to attain major performance perfection. Six Sigma involve DMAIC and DMADV methods for attaining a standard of high quality. In this paper they analyze critically the applications, techniques and tools of Six Sigma range that are used for improvement of quality and efficiency of the different business procedures. Their research also present an analysis of processes used for risk recognition and lessening in Six Sigma.

Ekananta [4] explored that software development project is an unsafe task due to the ambiguity of the consumer requirements, the complications of the method, and the fuzzy nature of the manufactured goods. Keeping in view all these circumstances, risk management is not easy and costly to put into practice. A perfect software development project is depends upon the preliminary planning about scope of the project, schedule, cost and available resources for that particular project. This research combines together COCOMO and Fuzzy logic. They validate their approach with business data and shown that fuzzy-ExCOM offered improved risk evaluation outcomes with a better understanding to risk recognition contrast to the original Expert COCOMO technique.

Haneen [5] make comparison of existing software development procedures. To choose the technique that will best suits for a particular software development depends upon many factors. Most significant feature is to identify how uncertain that project would be. Another important issue is to evaluate each tactic and chose best one that will also support risk management. This paper reveals that they look into the situation of risk and risk management in the most well known software development procedure models including waterfall, v-model, incremental development, spiral, and agile development method. Their research will help researchers and project managers to choose best methodology that will help them in development and for risk management too.

Tariq [6] again investigate that Six Sigma is being used as project management methodology in different manufacturing industries and business sectors to authenticate their goals near to exactness in process completion and implementation. In this paper, they projected a framework for risk recognition and management to get better quality and output of six sigma projects especially the IT development projects. This research paper also covers a condensed overview of the existing techniques being in practiced for risk detection in Six Sigma projects. The proposed framework will help us to identify risks in real time environment by using six sigma tools and techniques to produce better quality products in IT sector.

Abbas [7] describe that ERP systems are compound software systems that business organizations use to administer their resources. From first step of development of ERP system life cycle to its end it supposed to face plenty of risks that have to be identified and suitable actions should be taken to overcome or avoid these risks, so it could not effects the whole project life cycle. They proposed a system Enterprise Sustainability Risk Management (ESRM) for ERP projects for their successful completion. Their results shown that like other risk Staff risks is a major risk that should be identified as it has affect the end results. ESRM can also be used for project other than ERP as it is a general model to manage risks.

Azlin [8] conclude that Risk management (RM) has always been the burning issue for the software project management

studies. The major purpose of RM is to identify risk and its associations and then to make strategy for its elimination according to its nature. In this paper they make comparison of different models for risk management. They conclude that risk should be identified during requirement gathering from experts and customers. This paper also gives information about the results of the survey regarding the most wanted features for risk management tool (RMT). After concluding results, the authors suggested, planned and developed the tool to automate the Boehm's Risk Management process.

Frank [9] aims in their empirical study was to clarify managerial and customer related challenges in software developing companies that affect the software testing process and how afterwards these challenges affect software quality building. This research pointed out testing challenges which negatively affect the quality of the product. Finally it was concluded that software quality also based on organizational structure and movement of information from customer to development team. The team leader play an important role in this process, if he will provide correct information about the required product, the result will be near to perfection otherwise, it will led to errors, ambiguities and failure of the project.

Irena [10] presented their paper a model system integration technical risk assessment model (SITRAM), which is based on Bayesian belief networks (BBN) joined with parametric models (PM). They proposed a theoretical modeling approach to deal with the problem of System integration technical risks (SITR) measurement in the beginning of a system life cycle. The suggested approach includes a set of BBN models which represents associations between risk causing elements, and complement PMs which is used to supply input data to the BBN models. Initially, BBN model is used to identify risks, PMs provides risk relationships and then combine them to form a hybrid model by selecting Boehm's approach.

Shihab [11] said that a lot of research is being conducted to find out the ways to assure software quality. One line work that has been getting an escalating total of interest is Software Defect Prediction (SDP), where calculations and forecast are prepared to conclude where future defects would appear. He provides an approach that will predict major defects and also provide a simplified model of SDP that is easily understandable. While development risky changes may not make defects but they can delay the release of product. In his proposed approach we can predict risky changes and implementation of SDP for predicting risks before they become a part of coding.

Janjua [12] proposed responsibilities for „risk managers „as they assumed to be responsible for the whole process of risk management. But in of software engineering field this term “risk manager” is not clearly defined and having uncertainty over the term's meaning. After studying many research papers about risk management but we still don't have clear picture about the person who will handle all these tasks of risk management. It is difficult for an organization to find a professional Risk Manager for software development project so it is suggested to make team leader as risk manager as they already have risk analysis, management and software engineering knowledge.

3) TABLE 1: ANALYSIS OF RISK MANAGEMENT TECHNIQUES

Author	Method/Technique	Key characteristics	Key points
Sinovic I and L.Hribar [1]	PLCM	Identified existing faults in software projects using three case studies.	PLCM supports to convert customer need into end product and avoiding risks.
Vojo and Bubevsk [2]	DMAIC technique of six sigma	Six sigma metrics used to determine probability of defects in testing.	Six sigma is combined with CMMI for performance driven improvement.
Usman [3]	Six sigma, DMAIC and	Critical analysis of different	An approach into the current perceptive,

	Lean	techniques for quality and productivity of an organization.	practices and applications of Six Sigma.
Ekananta [4]	Fuzzy technique and COCOMO	A model proposed by combining Fuzzy technique and COCOMO.	Proposed model provides identification, analysis and prioritization of risks.
Haneen [5]	Highlights risky areas of leading software development models.	Comparison of leading SDLC model with respect to risk management.	Investigated state of risk in each software development methodology.
Tariq [6]	Risk identification using six sigma	Identification of a number of unpredicted risks and their	Proposed framework can be used for IT project and other projects as well.
Abbas [7]	Risk identification, reduction and control in	statistical analysis Identification of staff risks that effects project failures.	Proposed ERMS as generic model for risk management
..	ERP projects		
Azlin [8]	Boehm's RM process	Steps of RM process based on Boehm's model	Developed the tool to automate the Boehm's RM process.
Shihab [9]	Proactive risk management	Identifies how SDP research helps software engineers.	SDP used for prediction of defects before coding.
Frank [10]	Grounded theory research method	Identification of Customer and organizational challenges	Organizational structure also effects software quality.
Irena [11]	SITRAM, BBN	Identification of risks and relations between risk factors	Proposed model combines BNN and Boehm's model
Janjua[12]	Comparison of different theories about risk managers	Classifications of risk managers according to their role in RM.	Identification of responsibilities of risk managers.

IV. CONCLUSIONS

This study highlighted a significant overview of different techniques that can significantly get better the quality and output of different organizations particularly related to IT. A proper research lacks that can combine together the risk management in operating environment with the organizational tactics. Besides, this study also insight into the credible processes that can be efficiently implement for risk detection within the Six Sigma framework [3]. This study also highlighted the significance of six sigma approach in achieving better quality, capability, efficiency and stability of procedures. Six Sigma had already been implemented by a numerous organizations worldwide but the research in this domain is still in its premature phase. The base of six sigma is variation reduction [6].

This study also analyzed the various approaches used for risk management in different circumstances. In this research we

started from risk identification, then goes with different models and approaches used for this purpose including the role of risk managers in managing risk properly and the structure of the organization which also effects the project management. We can say that Six Sigma provides a better approach for quality and risk management with cooperation of an experienced risk manager.

REFERENCES:

1. Sinovic I and L. Hribar. How to Improve Software Development Process using Methimatical model for pridiction and elements of six sigma methodology. *MIPRO*, May 24-28, Opatija, Croatia.2010
2. Bubevski Vojo 2010. An Application of Six Sigma and Simulation in Software Testing Risk Assessment:
3. Third International Confe rence on Software Testing. *Verification and Validation*. DOI . 10, 1109/ICST. London, United Kingdom, 2010
4. Usman Muhammad Tariq and Muhammad Naeem .Khan. An Insight into Risk Identification, Quality and Productivity Enhancement using Six Sigma: *Journal of Education and Vocational Research* Vol. 2. 24-33. Islamabad, Pakistan,2011.
5. Ekanta,Manalif, Luiz Fernando Capretz and Ali Bou Nassif. 2012. Fuzzy-ExCOM Software Project Risk Assessment: 11th International Conference on Machine Learning and Applications. *IEEE*. Ontario, Canada.
6. Haneen Hijazi., Thair Khmour and Abdusalam Alarabyat. 2012. A Review of Risk Management in Different Software Development Methodologies: *International Journal of Computer Applications* (0975 – 8887) Volume 45– No.7. Salt, Jordan
 - a. Tariq Muhammad Usman and Muhammad .Naeem Khan .2012. Six Sigma based Risk Identification and Mitigation Framework for Projects Execution: *Information Management and Business Review*. Vol. 4, No. 2, pp. 79-85, Islamabad, Pakistan.
7. Fakhar Muhammad Zaman, Dr Muhammad Abbas and Madiha Waris. 2013. Risk Management System for ERP Software Project: *Science and Information Conference*. October 7-9. London, UK
 - a. Shihab Emad. 2014. Practical Software Quality Prediction: *IEEE International Conference on Software Maintenance and Evolution*. Canada.
8. Frank Philip Seth, Ossi Taipale and Kari Smolander. 2014. Organizational and Customer related Challenges of Software Testing: An Empirical Study in 11 Software Companies.*IEEE*. Lappeenranta, Finland.
9. Irena Loutchkina, Lakmi C. Jain, Thong Nguyen and Sergey Nesterov. 2014. Systems“ Integration Technical Risks“ Assessment Model (SITRAM): *IEEE Transactions on Systems, Man, And Cybernetics Systems*. Vol. 44, No. 3.
 - a. Azlin Nordin Lili, .Muhammad Abdullah , Farihin Diyana Muhamad Fadzil and Nor Aqila S.yamira Roselan. 2014. Requirements Elicitation and Analysis: Towards the Automation of Software Project Risk Management: 8th MalaysianSoftware Engineering Conference (MySEC, IEEE). Gombak, Malaysia.
10. Janjua Uzair.Iqbal, Alan Oxley and Jafreezal Bin Jaafar. 2014. Classification of Software Project Risk Managers: *Established on Roles and Responsibilities*. IEEE. Perak, Malaysia

Time Critical Emergency Message Dissemination in VANETs

Anees A S, Bibin Varghese Kurien

PG Scholar, Department of ECE, CAARMEL Engineering College, Pathanamthitta, Kerala
Assistant Professor, Department of ECE, CAARMEL Engineering College, Pathanamthitta, Kerala

Email:aneeskacd@gmail.com

Abstract: Here we propose a multi-hop broadcasting protocol for time critical emergency message dissemination in Vehicular ad hoc networks (VANETs). Here we use a partitioning protocol which consists of three mechanisms. First, Selection of emergency message using different mechanisms (e.g cross layer broadcast protocol). Second is multiple sectoring, partitioning the total region into different sectors (number of sectors depending on the density of vehicle in particular region). Third, transfer this emergency message into nearby sectors and Road Side Unit (RSU).It enables a faster and more reliable emergency message dissemination by shortening the channel access time and reducing the contention period jitter. VANET is not restricted up to Vehicle-to-Vehicle communication, it also takes advantages of road side units. Using directional antennas as road side units it influence the system performance. Antenna positioning related to road geometry is also important.

Keywords: VANETs, Inter vehicle communications, Emergency Message, Road side units (RSU), On Board Unit (OBU), Multiple Sectoring, Dedicated Short Range Communication (DSRC), Cross Layer Broadcast Protocol (CLBP).

INTRODUCTION

The number of vehicles rapidly increased in several countries, the rate of growth of new roads is much lower than that of vehicles. For these reasons number of accidents will increase and also traffic congestion. It becomes more severe if an accident occurs. One possible solution for reduce these problems is to use wireless communication among vehicles. Due to recent advances in wireless communication now a days, inter vehicle communication becomes a realistic solution. The vehicular ad hoc network (VANET) is a kind of wireless ad hoc network which deploys the concept of continuous varying vehicular motion. Here, the moving vehicles act as nodes. Vehicular networks are composed of mobile nodes, vehicles equipped with On Board Units (OBU), and stationary nodes called Road Side Units (RSU) attached to infrastructure that will be deployed along the roads. Both OBU and RSU devices have wireless/wired communications capabilities [1]. OBUs communicate with each other and with the RSUs in ad hoc manner. Vehicular Ad-hoc Networks are expected to implement a variety of wireless technologies such as Dedicated Short Range Communications (DSRC) which is a type of Wi-Fi. Other Wireless Technologies are Cellular, Satellite and Wi-MAX. Vehicular Ad-hoc Networks can be viewed as component of the Intelligent Transportation Systems (ITS) [2].

The main objective of VANET is to help a group of vehicles to set up and maintain a communication network among them without using any central base station or any controller. The most prominent feature of VANETs is the high mobility of the nodes. A vehicle can communicate with another vehicle directly which is called Vehicle to Vehicle (V2V) communication, or a vehicle can communicate to an infrastructure such as a Road Side Unit (RSU), known as Vehicle-to-Infrastructure (V2I). If the network has very less vehicle then it becomes more challenging to send a packet from source to destination. There is a need for faster and more practical solution for emergency message dissemination. Here we propose a multi-hop broadcast protocol for time critical emergency message dissemination in VANETs. This mechanism involved is spread the message in its communication range of vehicles and identify emergency situation gave priority to the particular one. Next is sectoring the communication range for the convenience of message transmission. Last step is, send this message through RSU in a wide range. In this technique it is important to cover at least one sector in a particular region. In reality direct communication is susceptible to interference and blocked by physical obstacles such as large buildings and mountains. Vehicles takes on the role of sender, receiver, and router to broadcast information to the vehicular network. Every vehicle that is participating in the VANET turns into wireless router. When any vehicle goes out of the particular signal range the connection drop out and in place of that new connection is established. The vehicles in this model is equipped with On Board Communication devices(OBU) and a data base unit, which use sensors for communication and sensors for GPS. A broadcast service is used to inform the drivers about an emergency situation. The data rate is not an important issue here because each vehicle wants to receive only warning alert messages.

As a cooperative approach, vehicular communication systems can be more effective in avoiding accidents and traffic congestions than if each vehicle tries to solve these problems individually. Generally vehicular networks are considered to contain two types of nodes;

vehicles and roadside stations. Both are Dedicated Short Range Communications (DSRC) devices. DSRC works in 5.9 GHz band with bandwidth of 75 MHz and approximate range of 1000m. The primary goal of VANET is to provide road safety measures where information about vehicle's current speed, location coordinates are passed with or without the deployment of infrastructure.

RELATED WORK

Trinary Partitioned Black-Burst Based Broadcast Protocol: Existing work consists of trinary partitioned black-burst-based broadcast protocol (3P3B), it consists of two primary mechanisms. First, a mini distributed inter-frame space (DIFS) in a medium access control (MAC) sublayer is introduced to give the time-critical EMs a higher access priority to the communication channel compared with other messages. Second, a trinary partitioning is designed to iteratively partition the communication range into small sectors. The trinary partitioning mechanism allows the farthest possible vehicle in the farthest sector from the sender node to perform forwarding to increase the dissemination speed by reducing the number of forwarding hops.

Binary-Partition-Assisted Broadcast Protocol: Binary partition assisted broadcast protocol (BPAB) aims to reduce and stabilize the broadcast delay. BPAB achieves a good message progress speed by selecting the farthest forwarder [3]. This protocol deploys a combination of a binary partitioning and a novel contention mechanism. The binary partitioning scheme constantly divides the communication area into multiple partitions. The binary partition of this scheme stems from a similar concept compared with that of OB-VAN, but it introduces fewer time slots than OB-VAN during the selection of the next-hop forwarder. Only vehicles in the farthest partition contend with each other during the forwarding phase in this scheme. Thus, the collision rate is reduced, and the contention duration is stabilized. It is also shown that BPAB demonstrates a good performance in terms of the average dissemination speed compared with the other protocols, such as UMB and SB.

SYSTEM MODEL

The vehicle in the model is equipped with on board communication devices (On Board Units) and a data base unit, which contain control information. Here we use sensors for communication and sensors for GPS. Vehicles in the road can directly communicate themselves or through road side units. The figure shows detailed view of system model. The vehicle-to-roadside communication configuration represents a single hop broadcast where the roadside unit sends broadcast information to all vehicles in its surrounding area. The vehicle communicates with RSU for sending, forwarding and receiving information from one node to another. RSU is further connected to infrastructural network and therefore allows the vehicles to access the internet for non-safety applications. Vehicle-to-roadside communication provides a high bandwidth link and enables high data rate transmission between vehicles and roadside units. GPS to identify location and speed of a vehicle, or vehicle based sensor data wherein the location and speed data is derived from the vehicle's computer and is combined with other data such as latitude, longitude, or angle to produce a richer, more detailed situational awareness of the position of other vehicles.

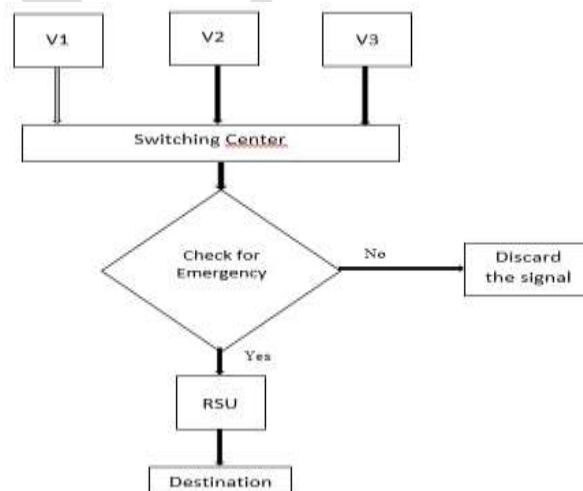


Fig.1 Basic Operations

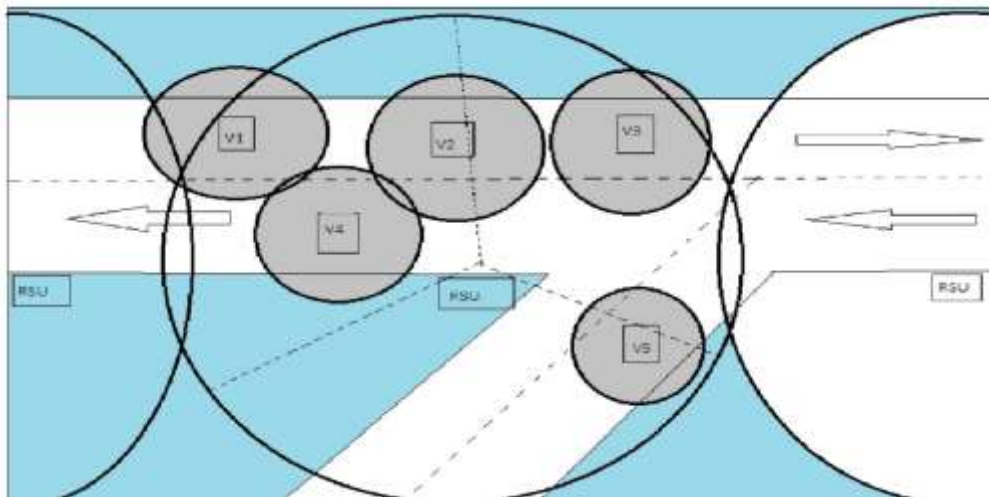


Fig 2. System model: Network Specifications

CROSS LAYER BROADCAST PROTOCOL

Cross Layer Broadcast Protocol (CLBP) is used for emergency message dissemination in VANETs. It is aiming to improve transmission reliability, minimizing the message redundancy, and to reduce the transmission delay. Here we use request-to-send/ clear-to-send (RTS/CTS) scheme to select an appropriate relaying node. Specifically, after receiving a broadcast RTS (BRTS) frame, each relay candidate starts its back-off timer to reply a broadcast CTS (BCTS) frame based on the calculated relaying metric. After a successful BRTS/BCTS handshake, one node is successfully selected as the next hop relay to forward the broadcast message in the desired propagation direction.

The figure 2. shows that the vehicles are randomly moving in a highway with 4 lanes, and half of the lanes are used for vehicles driving to one direction and other half are used for vehicles driving to the another direction. Each blocks are separated by safety distance in order to avoid vehicle collision. E1 is the source node that initiates an emergency message, and V4 is the current broadcast node. Node V1,V2 and V3 will not reply a BCTS frame to V4. Whereas V5 is eligible for relaying the message and starts a back-off timer upon receiving a BRTS frame. This guarantees that the emergency message will be efficiently forwarded along the the desired propagation direction. Emergency messages are served with highest priority.

Multiple Sectoring

One of the important step here is to select next hop forwarder. This can be done by multi-sectoring mechanism as shown in Figure 3. Each vehicle in a particular RSU has its own communication range which always includes large number of vehicle. We can divide the communication area of a RSU into multiple sectors according to presence of vehicles. In this figure we partitioning the communication area of RSU into three equal sectors (number of sectors can be increased according to particular situation). The regions are R1, R2, R3. Out of these three regions vehicles present only in first two regions R1 and R2. In region R1 which includes vehicles V1,V2 and V5, the region R2 include V3,V4 and V6. There is no vehicle present in the third region. Vehicles in the region R1 (V1,V2 and V5) can communicate themselves and to RSU. Similar situation in case of region R2. Hence connection is established between every vehicles. Most advantage of this system is we can use sectored antenna in particular regions.

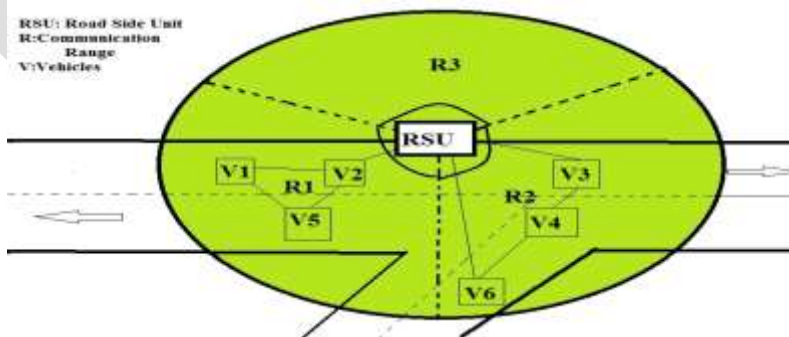


Fig 3. Sectoring in Communication region

We investigate the use of IEEE 802.11e to provide priority based service differentiation. The messages' importance leads to different message priorities which pose their own particular requirements on the communication system in terms of delay and reliability. For example, when an accident occurs, accident related messages will be transmitted. These messages must be sent immediately with high reliability and low delay. Therefore, these messages should have a higher priority compared with congestion related messages created during a traffic congestion period. This unavoidable contention can lead to significant message errors, causing low communication reliability. Higher priority messages will be transmitted more times than lower priority messages, resulting in higher reliability for higher priority messages.

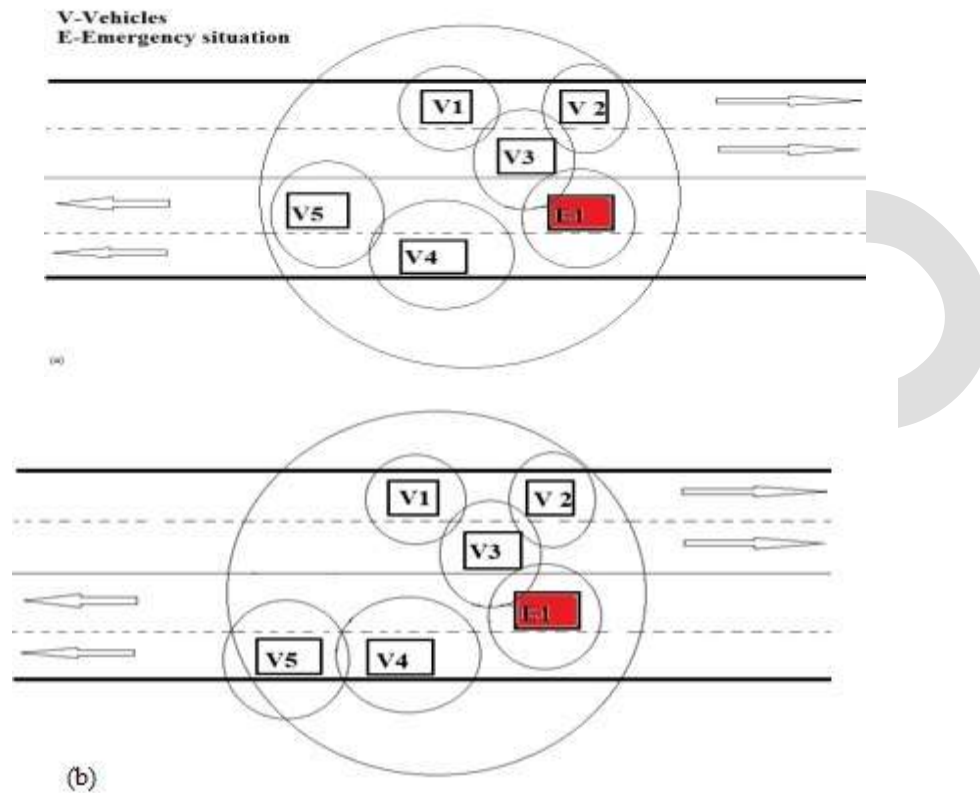


Fig 4. (a) E1 approaching other vehicles (b) Other vehicles changing their location

Figure 4(a) shows a four lane road, each pair in opposite directions. Also has vehicles and road side unit (RSU) with their communication range. Vehicles V1, V2 and V3 are move in one direction and remaining V4, V5 and E1 are in opposite direction. The red colour in the figure indicate emergency situation. The emergency signal is transmitted to each neighbouring vehicle and road side unit. Hence all the vehicles in the communication range of particular RSU get the emergency signal. The On Board Unit (OBU) in each vehicle can have the capability to the location and speed of emergency vehicle. Hence the drivers can change the location of others according to emergency vehicles path. Figure (b) shows position of vehicle V5 is changing according to location of E1. The present RSU transmit this emergency situation to near RSU and continuing till the emergency message reaches its destination.

Communication Standards for VANET

Dedicated Short Range Communication (DSRC)

It is developed by USA and is used in short to medium range communications service that is used for V2I and V2V communication. The United states Federal Communications Commission (FCC) had allocated 750 MHz of spectrum i.e from 8.5 GHz to 9.25 GHz to be used by Dedicated Short Range Communication (DSRC). DSRC spectrum has 7 channels with each channel 100 Mhz wide. Out of 7 channels, six channels are used for service purpose and remaining one for control purpose[5].

Wireless Access in Vehicular Environment (WAVE) (IEEE 1609.11p)

In 2003, American Society for Testing and Materials (ASTM) sets ASTM-DSRC which was totally based on 802.11 MAC layer and IEEE 802.11a physical layer. The main problem with IEEE 802.11a with Data Rate of 54 Mbps is it suffers from multiple overheads. Vehicular scenarios demands high speed data transfer and fast communication because of its high topological change and high mobility. For this the DSRC is renamed to IEEE 802.11p Wireless Access in vehicular Environments (WAVE) by the ASTM 2313 working group. This works on MAC layer and physical layers. WAVE consists of Road Side Unit (RSU) and On-Board Unit (OBU). WAVE uses OFDM technique to split the signals. The following figure 1.3 shows the WAVE, IEEE 802.11p, IEEE 1609 and OSI model.

DATA DISSEMINATION

Here network simulator 2 is used, nodes are deployed in the environment. Here each vehicle have an individual id and location, when an vehicle enters into RSU range its id and location is registered in RSU. RSU acts as a server to transfer the requested information to the requested vehicle. When a vehicle (Source node) "V1" request a packet to RSU to verify its id and location then transfer the packet to requested vehicle ie (Destination Node). In this model, when a vehicle "V1" request a data to Road Side Unit the RSU will verify its Id and location if the ID and location is registered in RSU it transfer the packet to the requested vehicle. The vehicle must be in the optimal location and it is fixed by the service provider when we design the node creation model is mainly used to reduce packet drops as well as to reduce delay while packet transfers.

Simulation Results

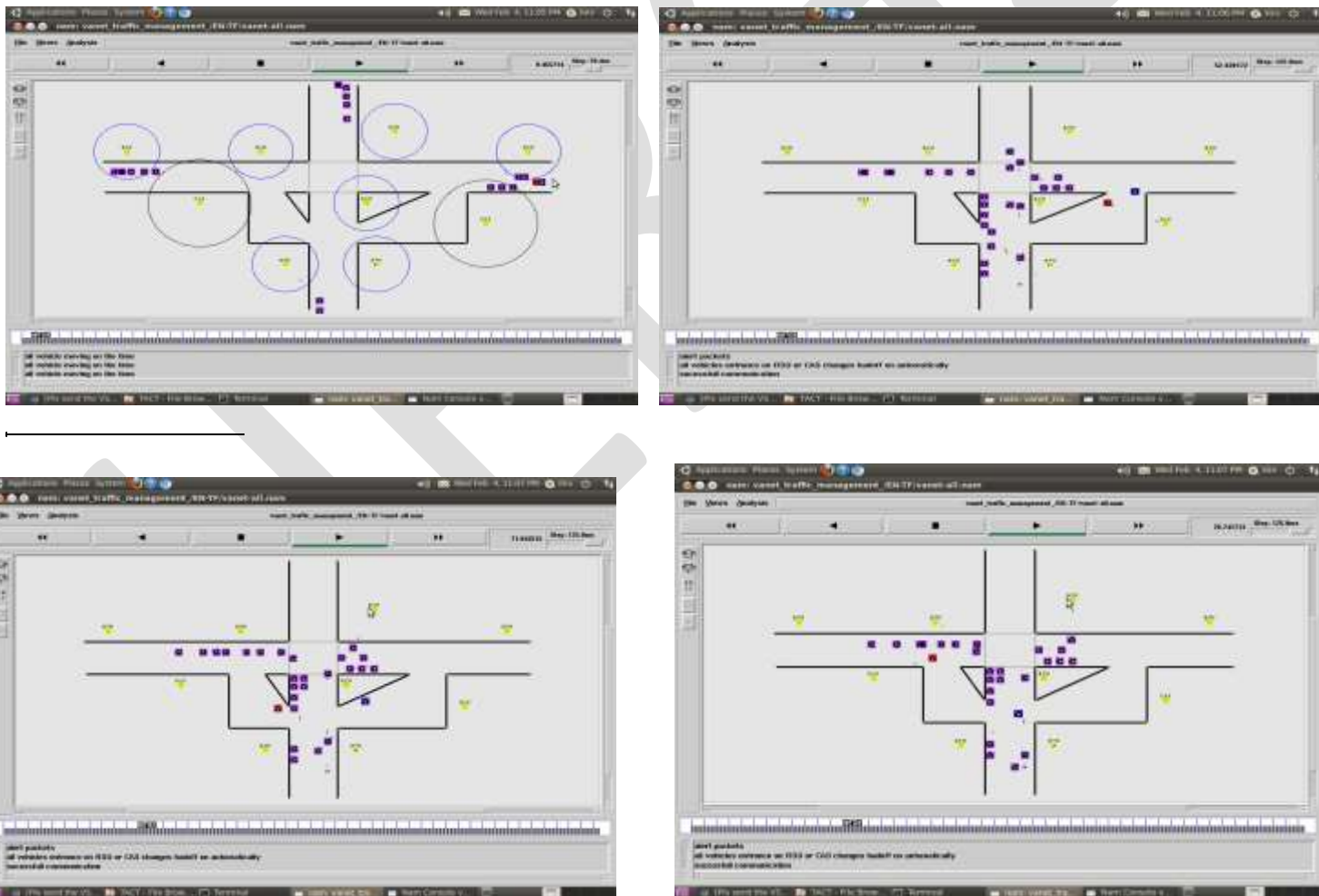


Fig.5 Different stages in message dissemination: messages are spread by road side units and also from one vehicle to another, easy path is calculated which have less in traffic, emergency vehicle follows the easy path and reaches the destination easily.

Performance of each parameter from simulation



Fig.6 Packet transmission comparison



Fig.7 Packet transmission delay graph

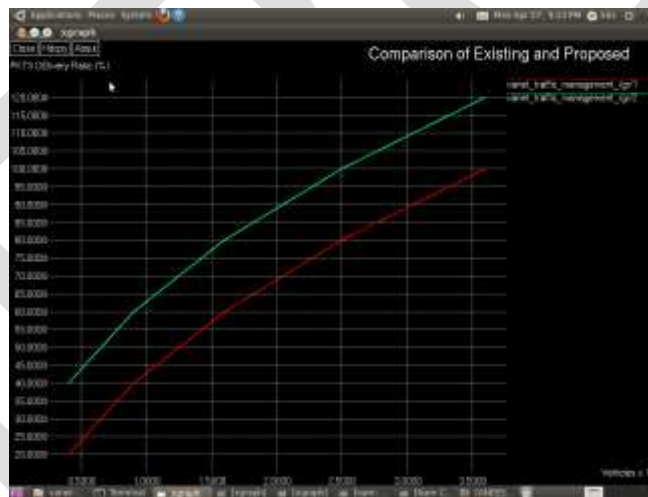


Fig.8 comparison of packet delivery ratio (PDR)

Conclusion

In this paper we have proposed a system for efficient time critical emergency message dissemination in VANETs. Here we use a cross layer broadcast protocol and multiple sectoring technology. In this system that is able to share Infrastructure to vehicle and Vehicle to Vehicle Communication with Messages very accurately. So towards this goal the system i.e. Design and Implementation of inter infrastructure and vehicle to vehicle communication for traffic information sharing messages from a moving vehicle and vehicle to vehicle communication. It is demonstrated through simulation results that the proposed system outperforms the benchmark protocols in terms of the average delay, average message dissemination speed, and average packet delivery ratio (PDR). Hence our proposed system conclude that for every vehicle it becomes very easier to deal with the traffic issues and many more accidental scenarios that come across due to the lack of real time road side issues.

REFERENCES:

- [1] Trinary Partitioned Black-Burst-Based Broadcast Protocol for Time-Critical Emergency Message Dissemination in VANETs , Chakkaphong suthaputchakun , IEEE Transaction on vehicular technology, Vol.63, No. 6, July 2014.
- [2] Pankaj Joshi, Jaswinder Kaur, Inderjeet Singh Gill, Heterogeneous Configuration: A Better Approach to Analyze VANET, International Journal of Computer Applications (0975 – 8887) Volume 118 – No.19, May 2015
- [3] On Roadside Unit Antenna Measurements for Vehicle-to-Infrastructure Communications, Veronika Shivaldova*, Alexander Paier, Dieter Smely, Christoph F. Mecklenbräuer.
- [4] http://www.rpublication.com/ijca/ijca_index.htm, Privacy-Preserving and Priority Based Congestion Control for VANET, Deivanai.P, Mrs.K.Sudha, Issue 5, Volume 1 (Jan.- Feb. 2015, ISSN: 2250-1797.
- [5] A Survey On Vehicular Ad-Hoc Network, Bhuvaneshwari.S1, Divya.G2, Kirithika.K.B3 and Nithya.S4, **ISSN (Print) : 2320 – 3765** **ISSN (Online): 2278 – 8875**

Switched Inductor Quadratic Buck Converter

Rosemary Mathai¹, Sheela Joseph², Sini Paul³
M.Tech Student¹, Professor², Associate Professor³
rosemarymathai.mec@gmail.com

Abstract— A dc-dc converter featuring a steep step down of the input voltage is presented. The proposed converter uses two quadratic buck converters integrated with switched inductor structure. The structure formed by two inductors and two diodes is known as switched inductor structure. When the switch is on, the inductors are charged in series and when the switch is off, the inductors are discharged in parallel in switched inductor structure. The dc voltage conversion ratio of this converter has a quadratic dependency on duty cycle, providing a large step down. The stress voltage over the switches is reduced as compared to the quadratic buck converter. A complete theoretical analysis of the converter is done in continuous conduction mode. Also simulation results are presented which verify the theoretical analysis.

Keywords— quadratic, switched inductor, switch voltage stress, voltage conversion ratio

INTRODUCTION

The conventional buck converter whose voltage conversion ratio is the duty cycle, cannot provide a steep step-down of the line voltage, as required by modern applications. Certain applications such as microprocessors and on-board voltage regulators in PCs and laptops require very wide voltage step-down factor. The buck converter when integrated with switched inductor structure [2], high voltage conversion can be achieved. But the switch voltage stress is greater than input voltage. The buck quadratic PWM soft-single-switched (SSS) converter can provide a voltage conversion which have a quadratic dependency on duty cycle, but again switch stress is greater than input voltage [3]. The quadratic buck self-resonant (SR) PWM converter can achieve quadratic voltage gain and also switch stress is low [4]. But the number of switches is three and number of components is high.

The quadratic buck converter can achieve quadratic voltage gain and also one switch is used [5]-[7]. Here also switch voltage stress is high. Then double quadratic buck converter can achieve quadratic voltage gain and switch voltage stress is less than input voltage [1].

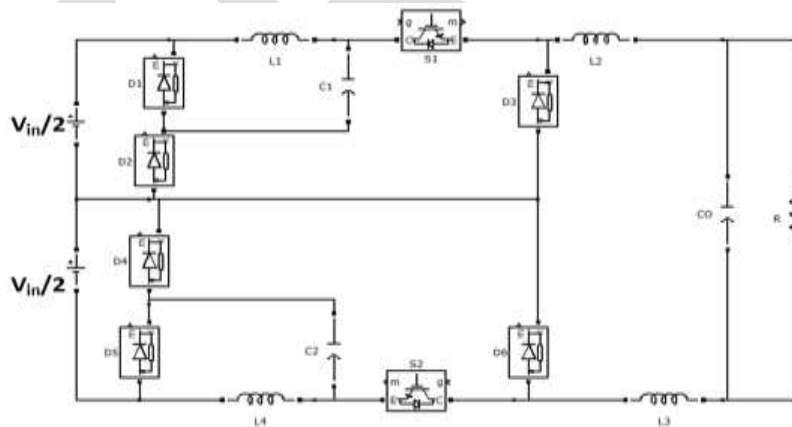


Fig 1: Double quadratic buck converter

Double quadratic buck converter is shown in fig.1 [1]. The double quadratic buck converter is characterized by average output voltage to be lower than input voltage, and the voltage of intermediate capacitor also to be lower than the input voltage. Furthermore, it has high gain ratio compared to the conventional buck converter. In this structure, both the power supply and the intermediate capacitor will behave as voltage source. The load should behave as a current source and the current on the intermediate capacitor is given by the difference between the current across the inductor L_1 and the current in the switch S_1 . Because of its symmetrical topology, the lower components have the same behavior of the respective upper component.

When switched inductor structure is combined with buck, buck-boost, Cuk, Sepic, Zeta converters to get a step down function. In this paper two quadratic buck converter are integrated with switched inductor structure to obtain a steep step down of the input voltage.

SWITCHED INDUCTOR QUADRATIC BUCK CONVERTER

The proposed converter is shown in fig.2. For symmetry, the value of inductors L_1 and L_4 are equal and also L_2 and L_3 . Also, the capacitors $C_1=C_2$ and voltage across each capacitor is taken as $V_C/2$. When compared to double quadratic buck converter, the proposed converter uses only one source.

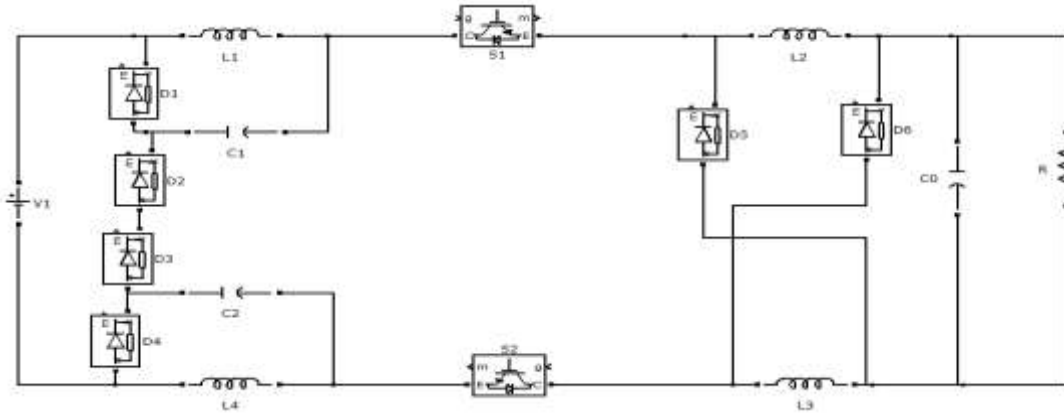


Fig 2: switched inductor quadratic buck converter

PRINCIPLE OF OPERATION

Fig.2 shows the basic circuit diagram of the switched inductor quadratic buck converter in CCM. The inductors L_1 , L_2 and diodes D_4 , D_5 form the switched inductor structure. There are two stages of operation for this circuit.

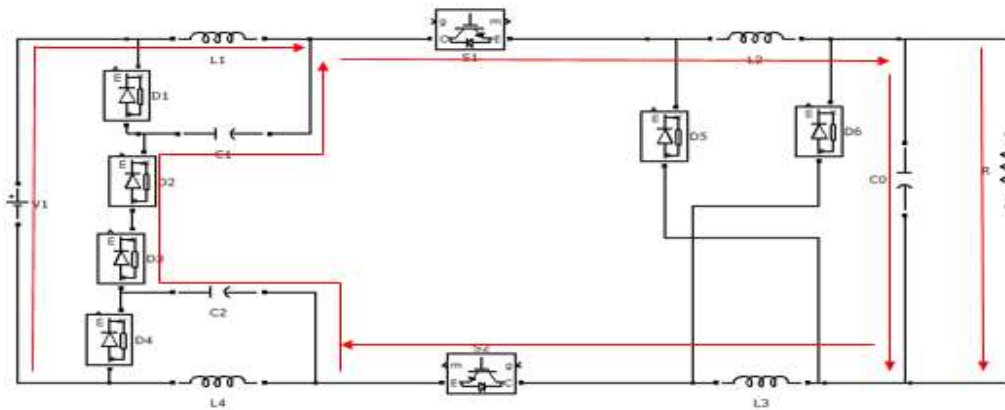


Fig 3: mode 1 operation

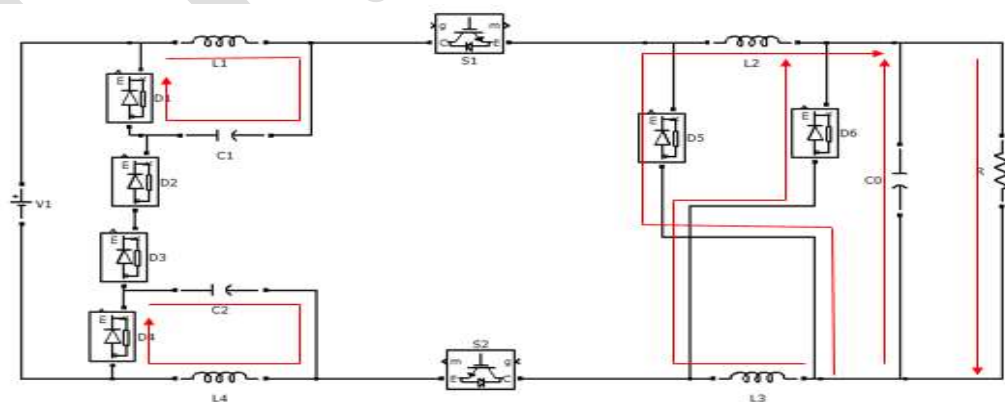


Fig 4: Mode 2 operation

The equivalent circuit corresponding to stage 1 is shown in fig.3. During this interval, both the switches are ON. The input voltage V_1 appears in series across the inductors. The voltage across L_1 is given by

$$v_{L1}(t) = \frac{V_1 - V_C}{2} = L_1 \frac{di_{L1}(t)}{dt}$$

The current through L_1 is given by,

$$i_{L1}(t) = \frac{1}{L_1} \int_0^t v_{L1}(t) dt = \frac{V_1 - V_C}{2L_1} (t) + i_{L1}(0),$$

Where $i_{L1}(0)$ is the initial current in the inductor L_1 at time $t=0$. The peak current through L_1 is

$$i_{L1}(DT) = \frac{V_1 - V_C}{2L_1} DT + i_{L1}(0),$$

And the peak to peak current of L_1 is

$$\Delta i_{L1} = i_{L1}(DT) - i_{L1}(0) = \frac{V_1 - V_C}{2L_1} DT$$

The voltage across inductor L_2 is given by

$$v_{L2}(t) = \frac{V_C - V_0}{2} = L_2 \frac{di_{L2}(t)}{dt}$$

Similarly,

The peak to peak current of L_2 is

$$\Delta i_{L2} = i_{L2}(DT) - i_{L2}(0) = \frac{V_C - V_0}{2L_2} DT$$

The equivalent circuit corresponding to stage2 is shown in fig.4. During this interval, both the switches are OFF. The inductor L_1 and L_4 begins to discharge through capacitors C_1 and C_2 respectively. The voltage across L_1 is given by

$$v_{L1}(t) = \frac{-V_C}{2}$$

The current through L_1 is given by,

$$i_{L1}(t) = \frac{-V_C}{2L_1} (t - DT) + i_{L1}(DT),$$

Where $i_{L1}(DT)$ is the initial current in the inductor L_1 at time $t=DT$. At time $t = T$, the value of inductor current is

$$i_{L1}(T) = \frac{-V_C}{2L_1} (T - DT) + i_{L1}(DT),$$

Thus, the peak to peak current of L_1 is

$$\Delta i_{L1} = i_{L1}(T) - i_{L1}(DT) = \frac{-V_C}{2L_1} T(1 - D)$$

The voltage across inductor L_2 is given by

$$v_{L2}(t) = -V_0$$

Similarly,

And the peak to peak current of L_2 is

$$\Delta i_{L2} = i_{L2}(T) - i_{L2}(DT) = \frac{-V_0}{2L_2} T(1 - D)$$

CIRCUIT ANALYSIS

By the principle of volt-sec balance, the average steady state DC voltage across the inductor is zero. Let us first derive the voltage-time relation for L_1 .

$$\frac{(V_1 - V_C)}{2} DT + \left(\frac{-V_C}{2}\right)(1 - D)T = 0$$

Yielding,

$$V_C = DV_1$$

Similarly, applying volt-sec balance for L_2 ,

$$\frac{(V_C - V_0)}{2} DT + (-V_0)(1 - D)T = 0$$

Yielding,

$$V_0 = \frac{DV_C}{2 - D}$$

Thus, voltage gain

$$\frac{V_0}{V_1} = \frac{D^2}{2 - D}$$

The peak value of inductor current is given by,

$$i_{L2}(DT) = \frac{(V_C - V_0)}{2L_2} DT + i_{L2}(0)$$

At boundary between continuous and discontinuous modes, the inductor current is zero, i.e., $i_{L2}(0)=0$. Therefore, above eq. reduces to

$$\Delta i_{L2} = i_{L2}(DT) = \frac{(V_C - V_0)}{2L_2} DT$$

Similarly,

$$\Delta i_{L1} = i_{L1}(DT) = \frac{V_1 - V_C}{2L_1} DT$$

Since, the L-C filter networks are similar to the conventional buck stage, the equations for minimum values of filter capacitors can be obtained by similar methods.

$$C_{0min} = \frac{(1 - D)V_0 T_s^2}{8L_2 \Delta V_{C0}}$$

$$C_{1min} = \frac{(1 - D)V_C T_s^2}{8L_1 \Delta V_C}$$

SIMULATION RESULTS

The switched inductor quadratic buck converter with the following specifications is considered: $V_1 = 400\text{ V}$, $f_s = 50\text{ kHz}$ and duty ratio, $D = 0.5$ and is constructed using MATLAB/Simulink simulator. The ripple voltage at the output is designed to be 1% of the average output voltage. The ripple current in the inductor is designed to be 10% of the total current, in continuous conduction mode. Using the design equations obtained in above section, the values of inductors and capacitors are found to be: $L_1 = 8\text{ mH}$, $L_2 = 0.866\text{ mH}$, $C_0 = 1\text{ }\mu\text{F}$ and $C_1 = 22\text{ }\mu\text{F}$. Fig. 5 shows the Simulink diagram of the proposed converter.

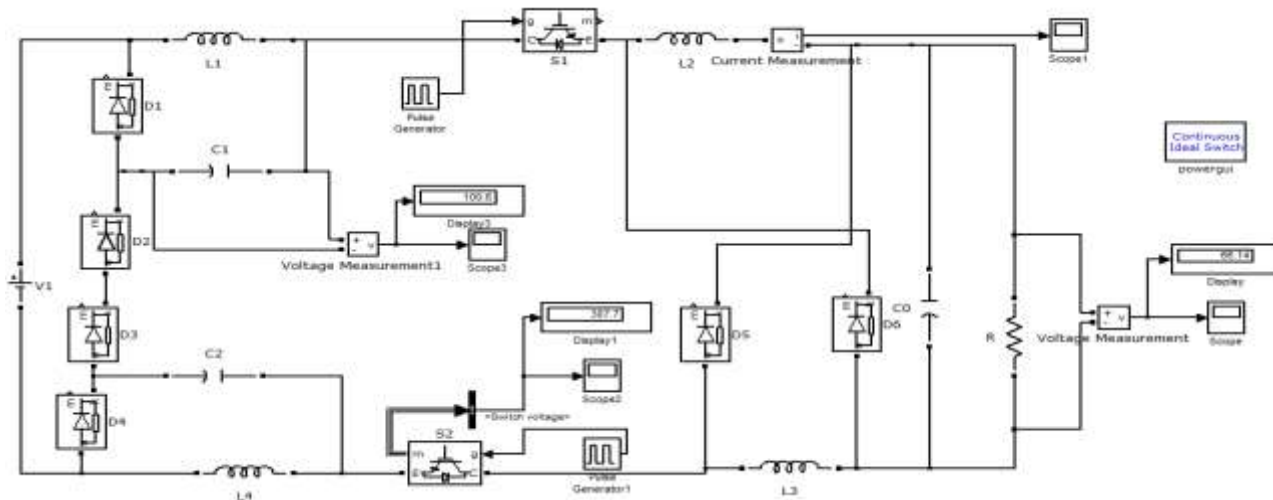


Fig 5: Simulink model of switched inductor quadratic buck converter

Gate pulse is given with a duty ratio of 50%. The gate pulse given to both the switches are same and is shown in fig.6. The voltage stress across the switch is measured to be 300V and is shown in fig. 7. The output voltage is shown in fig. 8 and is measured to be 66V.

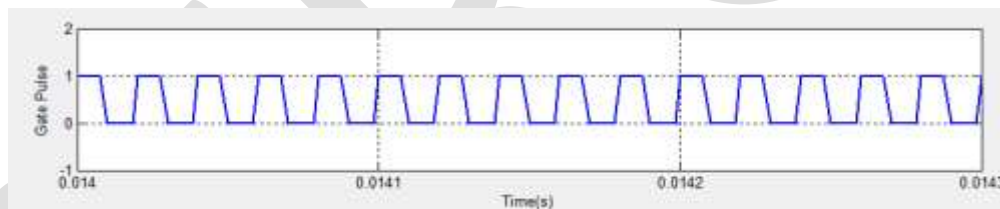


Fig 6: Gate pulse to switch

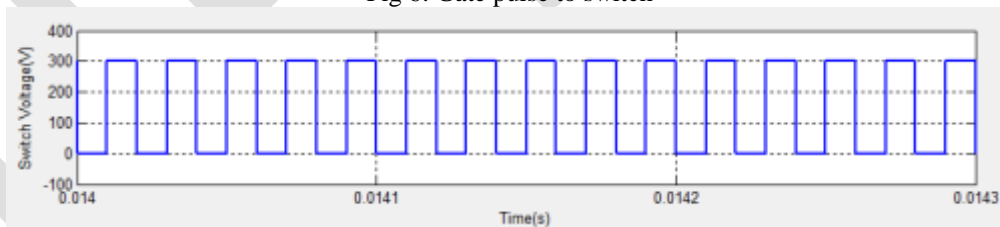


Fig 7: Voltage across the switch

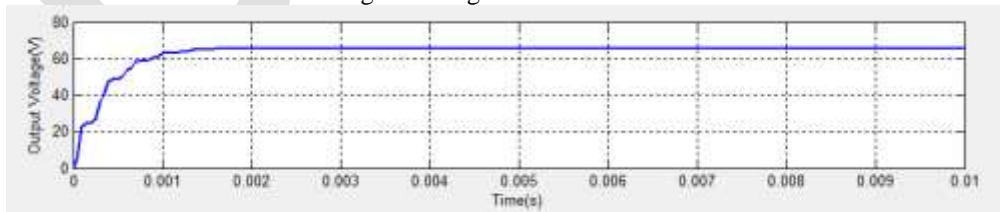


Fig 8: Output Voltage

Then the performance analysis of four converters is done. The performance comparison is done with following parameters: Input voltage=400V, switching frequency=50 kHz, Duty Cycle=50%. The performance is summarized in the following table.

Table 1: Comparison of topologies

Converter Type	Output Voltage(V)	Switch Voltage(V)
Conventional Buck Converter	200	400
Quadratic Buck Converter	100	600
Double Quadratic Buck Converter	100	300
Switched Inductor Quadratic Buck Converter	66	300

From the table it can be seen that when switched inductor quadratic buck converter is used high voltage conversion can be achieved with less switch voltage stress.

CONCLUSIONS

The study of switched inductor quadratic buck converter is presented in this paper. The stages of operation and circuit analysis of the proposed converter is done in continuous conduction mode. Simulation results are presented for continuous conduction mode and show low value in the output voltage over the input voltage, providing the high conversion rate of the converter. With the help of proposed converter, high switching frequencies can be obtained. From the above table, it can be seen that switched inductor quadratic buck converter can provide steep step down of the voltage and reduced switch voltage stress can be obtained.

REFERENCES:

- [1] Francieli L. de Sa, Caio V. B. Eiterer, Domingo Ruiz-Caballero, Samir A. Mussa, "Double Quadratic Buck Converter," IEEE Proc. In Circuits and Systems, pp. 36-43, 2013.
- [2] Boris Axelrod, Yefim Berkovich, Adrian Ioinovici, "Single-Stage Single-Switch Switched-Capacitor Buck/Buck-Boost-Type Converter," IEEE Trans. On Aerospace and Electronic Systems, vol. 45, no. 2, pp. 419-430, April 2009.
- [3] Lucio dos Reis Barbosa, Joao Batista Vieira, Luiz Carlos de Freitas, Marcio da Silva Vilela and Valdeir Jose Farias, "A Buck Quadratic PWM Soft-Switching Converter Using a Single Active Switch," IEEE Trans. on Power Electronics, vol. 14, no. 3, pp. 445-453, May 1999.
- [4] Vincius Miranda Pacheco, Acrisio Jose do Nascimento, Valdeir Jose Farias, Joao Batista Vieira, and Luiz Carlos de Freitas, "A Quadratic Buck Converter with Lossless Commutation," IEEE Trans On Industrial Electronics, vol. 47, no. 2, pp. 264-272, April 2000.
- [5] Carbajal Gutierrez, "Modeling of a Single-Switch Quadratic Buck Converter," IEEE Trans. on Aerospace And Electronic Systems, vol. 41, no. 4, pp. 1451-1457, Oct. 2005.
- [6] Agasthya Ayachit and Marian K. Kazimierzuk, "Steady-State Analysis of PWM Quadratic Buck Converter in CCM," IEEE Proc. on Aerospace and Electronic Systems, pp. 49-52, 2013.
- [7] Agasthya Ayachit and Marian K. Kazimierzuk, "Power Losses and Efficiency Analysis of the Quadratic Buck Converter in CCM," IEEE Proc. In Circuits and Systems, pp.463-466, 2014
- [8] Boris Axelrod, Yefim Berkovich, Adrian Ioinovici, "Switched-Capacitor/Switched-Inductor Structures for Getting Transformerless Hybrid DC-DC PWM Converters," IEEE Trans. On Circuits and Systems, vol. 55, no. 2, pp. 687-696, Mar. 2008.
- [9] Yuanmao Ye, K. W. E. Cheng, "A Family of Single-Stage Switched-Capacitor-Inductor PWM Converters," IEEE Trans. On Power Electronics," vol. 28, no. 11, pp. 5196-5205, Nov. 2013.
- [10] K. I. Hwu , T. J. Peng, "A Novel Buck-Boost Converter Combining KY and Buck Converters," IEEE Trans. On Power Electronics," vol. 27, no. 5, pp. 2236-2241, May. 2012.
- [11] Il-Oun Lee, Shin-Young Cho, and Gun-Woo Moon, "Interleaved Buck Converter Having Low Switching Losses and Improved Step-Down Conversion Ratio," IEEE Trans. On Power Electronics," vol. 27, no. 8, pp. 3664-3675, May. 2012.
- [12] Yu Chen, Zhihao Zhong, and Yong Kang, "Design and Implementation of a Transformerless Single-Stage Single-Switch Double-Buck Converter With Low DC-link Voltage, High Step-Down, and Constant Input Power Factor Features," IEEE Trans. On Power Electronics," vol. 29, no. 12, pp. 6660-6671, Dec. 2012

MARKET SURVEY, FORCE CALCULATION AND TESTING OF GARLIC ON INNOVATIVE FORCE CALCULATING MACHINE

Dhananjay G. Dange

Dr. S. K. Choudhary

A. P. Ninawe

Mechanical Engineering Department

Professor

Assistant Professor

K.D.K.C.E.

Mechanical Engineering Department

Mechanical Engineering Department

Nagpur, India

K.D.K.C.E. Nagpur, India

K.D.K.C.E Nagpur, India.

dangedhananjay08@gmail.com

skc14763@gmail.com

free1rhyme@rediffmail.com

Abstract – This paper presents the market survey related to garlic, its types and weight of garlic clove, garlic bulb and also the number of garlic clove included in the garlic bulb according to its type and weight. Also this paper presents the technique of calculating the various forces related to garlic like peeling force, breaking force, crushing force etc. In this paper, also it mentions about the young's modulus of garlic and this technique is also useful for other types of products like ground nut, onion, almond, coconut etc. These are based on a systematic study of the garlic peeling process and testing of a prototype model of force instrument.

Keywords – Garlic peeling force, force instrument, young's modulus of garlic, garlic breaking force, garlic crushing force, types of garlic, and weight of garlic.

INTRODUCTION

Garlic is the most important foreign exchange earning spicy vegetable crop, commercially grown in India. India is one of the leading Garlic producing countries. Garlic has digestive, carminative and anti-rheumatic properties. It is used in Ayurveda formulation since ancient times for curing muscular pain, giddiness, lungs, heating intestinal ulcer, etc. Garlic is consumed as green as well as dried in the spice form and as ingredient to flavor the various vegetarian, non-vegetarian dishes and pickles. Good tasty pickles, chutneys, curry powders are prepared from Garlic cloves.

Very little work has been done on the garlic peeling and it is restricted to traditional peeling methods only. Traditional peeling methods viz.; hand peeling, flame peeling, oven peeling and chemical peeling are being used in processing industries, big restaurants, hotels and kitchens. These are laborious, time consuming, cost intensive and restrict speed of processing activity. Because of its typical shape, the mechanical peeling of garlic is still untouched by process engineers. Keeping this in view, a study was undertaken with the main objective of development of a garlic peeler.

The paper gives the information about the types of garlic and its weight which is available in Indian market. Also the paper gives the information about the method of calculation of force required to peel the garlic and also its force calculating machine and about young's modulus of garlic clove.

MARKET SURVEY

• TYPES OF GARLIC

According to market survey and observation, we can categorized the garlic broadly in three type

1. Single clove garlic
2. Multi clove garlic
3. Himalayan garlic

1. Single Clove Garlic

In single clove garlic, there is only a clove in garlic bulb. Its weight ranges between 5gm-10gm and its cost in market is near about 500 Rs. /Kg.

It is generally used for medical purpose in "AYURVED".

2. Multi Clove Garlic

It is a type of garlic which is plenty available in market. It is used mainly in food product. Its weight ranges between 12gm-35gm.

3. Himalayan Garlic

Himalayan garlic is a subtype of multi clove garlic. According its name, its production is taken in Himalayan area. If we compare Himalayan garlic with the other types of garlic, the Himalayan garlic is greater in size, shape and weight.

Its weight is near about 100gm. It contains 12-15 cloves in single garlic bulb which has weight up to 10gm.

• WEIGHT OF GARLIC

1. Single Clove Garlic

Weight, $W = 5\text{gm to }10\text{gm}$; (Single Clove)

2. Multi Clove Garlic

- i. Bulb Weight, $W = 30\text{gm to }35\text{gm}$; (Maximum)
No. of Clove = 26 to 30
Weight of single Clove = 1gm to 1.25gm
- ii. Bulb Weight, $W = 25\text{gm to }30\text{gm}$
No. of Clove = 22 to 26
Weight of single Clove = 1gm to 1.25gm
- iii. Bulb Weight, $W = 20\text{gm to }25\text{gm}$
No. of Clove = 18 to 22
Weight of single Clove = 1gm to 1.25gm
- iv. Bulb Weight, $W = 16\text{gm to }20\text{gm}$
No. of Clove = 14 to 18
Weight of single Clove = 1gm to 1.25gm
- v. Bulb Weight, $W = 12\text{gm to }15\text{gm}$; (Minimum)
No. of Clove = 10 to 14
Weight of single Clove = 1gm to 1.25gm

3. Himalayan Garlic

Weight up to, $W = 100\text{gm}$

No. of Clove = 12 to 15

Weight of Single Clove = Up to 10gm

FORCE CALCULATION

For finding or calculating the breaking force of garlic bulb, peeling force of garlic clove and crushing force of garlic clove, I developed the force instrument by using the spring, plates and nut and bolts which is work on the principle of," the applied force on the spring is the product of a stiffness of that spring and its deflection in the direction of force applied."

For calculating the force, some experimentation is carried out by using the force instrument. The force instrument is consisting of the spring, two moving plate, and one fix plate and tightening nut. By using the formula $F = K \times X$ it is possible to

calculate the gradual force required to break or peel the garlic bulb or clove respectively. First garlic bulb or clove is fixed in between two movable plates. After fixing it, it is started to tighten the nut up to breaking the garlic bulb or breaking the cover of garlic clove. Then measuring the displacement and multiplying it with stiffness of spring it will get the gradual force required to break or peel the garlic bulb or clove respectively. Where, F is a gradual force required to break the garlic bulb or to peel the garlic clove, K is the spring constant and X is the displacement of the spring after tightens the nut.

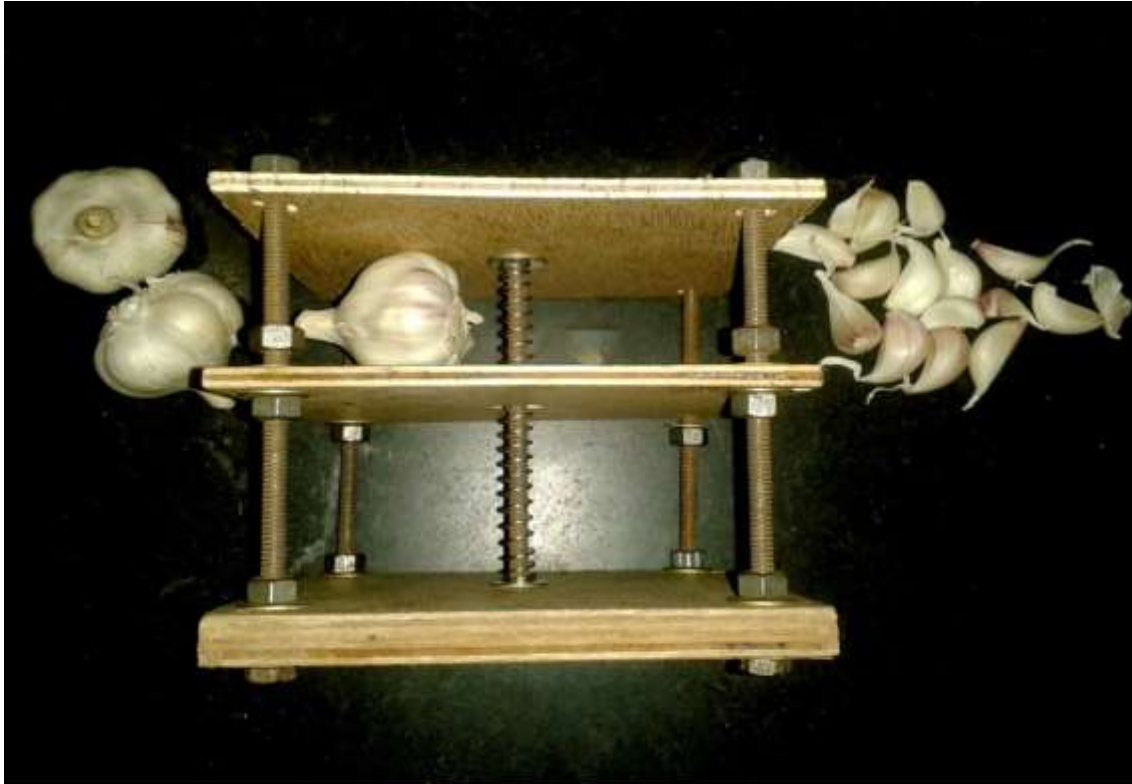


Fig. – Force Instrument

STIFFNESS OF SPRING

The “Stiffness” is the ratio of Load (W in Newton) per Deflection (X in mm). The stiffness is also known as “Spring Ratio” or “Spring Constant” and it is denoted by $[K]$.

Therefore, **Stiffness, $K = \text{Load } (W) / \text{Deflection } (X)$**

For calculating the spring stiffness, we collect the following data.

Observation

Original length of spring, $L = 95\text{mm}$.

<i>Weight, W</i>			<i>Total Length, T_L, mm</i>	<i>Deflection, mm</i>	
gm	Kg	N		T _L – L	X
50	0.05	0.49	96	96 – 95	1
100	0.1	0.98	96.5	96.5 – 95	1.5
150	0.15	1.47	97	97 – 95	2
200	0.2	1.96	98	98 – 95	3
250	0.25	2.45	98.5	98.5 – 95	3.5
300	0.3	2.94	100	100 – 95	5
350	0.35	3.43	101	101 – 95	6
400	0.4	3.92	101.5	101.5 – 95	6.5
500	0.5	4.90	103	103 – 95	8
600	0.6	5.88	105	105 – 95	10
700	0.7	6.86	107	107 – 95	12

Table – Observation of Deflection of Spring

Now, using the equation,

$$\text{Stiffness, } K = \text{Load (W)}/\text{Deflection (X)}$$

Sample calculation of stiffness

From observation table taking a any value of force like 2.45 N and its respective value of deflection is 3.5 mm.

$$\text{Weight } W = 2.45 \text{ N}$$

$$\text{Deflection } X = 3.5 \text{ mm}$$

$$\text{Therefore } K_5 = W/X = 2.45/3.5 = 0.70 \text{ N/mm}$$

Results

<i>Sr. No. (K_n)</i>	<i>W/X</i>	<i>Stiffness, N/mm</i>
K ₁	0.49/1	0.49
K ₂	0.98/1.5	0.65
K ₃	1.47/2	0.74

K ₄	1.96/3	0.65
K ₅	2.45/3.5	0.70
K ₆	2.94/5	0.59
K ₇	3.43/6	0.57
K ₈	3.92/6.5	0.60
K ₉	4.90/8	0.61
K ₁₀	5.88/10	0.59
K ₁₁	6.86/12	0.57

Table – Stiffness of Spring

Now calculating the average stiffness of spring by using the equation

$$K = (K_1 + K_2 + K_3 + \dots + K_n) / n$$

Therefore Stiffness of Spring K,

$$K = (0.49 + 0.65 + 0.74 + 0.65 + 0.70 + 0.59 + 0.57 + 0.60 + 0.61 + 0.59 + 0.57) / 11$$

$$K = 0.61 \text{ N/mm}$$

So, now we have the value of stiffness of spring. So we can calculate the breaking force of garlic bulb, peeling as well as crushing force of garlic clove.

By using the force measuring instrument, now are calculate the force required to crush wet garlic clove, using following equation,

$$\text{Crushing Force, } F = K \times X \text{ Newton}$$

Where, K – Stiffness of spring, N/mm

X – Deflection of spring, mm

Observation during Experiment

Total length of spring, $L_T = 95\text{mm}$

Deflected length of spring, $L_O = 81\text{mm}$

$$\therefore \text{Deflection of spring, } X = L_T - L_O$$

$$X = 95 - 81$$

$$\therefore X = 14\text{mm}$$

∴ Crushing Force, $F = 0.61 \times 14$

$$F = 8.54 \text{ N (Gradually Applied)}$$

So, by using this force instrument and basic principle of it's working, we already calculate the range of breaking force of garlic bulb, force of peeling and crushing of garlic clove and these ranges are as follows,

- Force required to break the garlic bulb varies between
 $F_{\text{Break}} = 4.88 \text{ N to } 6.1 \text{ N}$
- Force required to peel the garlic clove varies between
 $F_{\text{Peeling}} = 1.83 \text{ N to } 3.05 \text{ N}$
- Force required to crush the garlic clove varies between
 $F_{\text{Crush}} = 7.32 \text{ N to } 8.54 \text{ N}$

Also by using this force instrument we can calculate the force of breaking, peeling, crushing of other objects like ground nut, onion, almond, coconut and many more.

YOUNGS MODULUS OF GARLIC CLOVE

This force instrument is very useful for calculating the young's modulus of garlic. By using this force instrument we already calculate the young's modulus of garlic. And for that we perform the following experiments.

For calculating the modulus of elasticity we require the value of stress and strain developed in garlic. For that we first calculate the force and then by using the force and area we calculate the stress developed in a garlic pixel.

Also we have known the value of original length of garlic pixel and change in length of garlic pixel.



Fig. – Garlic Pixel

For calculating the young's modulus of garlic clove, following observation is done.

Stiffness, $K = 0.61 \text{ N/m}^2$,

Force, $F = K \times X$,

Dimension of garlic pixel = $7 \times 7 \times 13 \text{ mm}$,

Cross section area of garlic pixel, $A = 4.9 \times 10^{-5} \text{ m}^2$,

Stress developed in a garlic pixel, $\sigma = F/A$,

Deflection of a garlic pixel, $X = 95 - \delta_x$

Stress developed in a garlic pixel

Sr. No.	δ_x	$X, \text{ mm}$	$F, \text{ N}$	$\sigma, \text{ N/m}^2$
1	94.5	0.5	0.305	6224.5
2	94	1	0.61	12449.0
3	93.5	1.5	0.915	18673.5
4	93	2	1.22	24898
5	92.5	2.5	1.525	31122.4
6	92	3	1.83	37346.9
7	91.5	3.5	2.135	43571.4
8	91	4	2.44	49795.9
9	90.5	4.5	2.745	56020.4
10	90	5	3.05	62244.9
11	89.5	5.5	3.355	68469.4
12	89	6	3.66	74693.9

Table – Stress in Garlic Pixel

Original length of Garlic pixel = 13 mm,

l = Change in length

ΔL = Original length – Change in Length

$$= L - l$$

Strain, $\epsilon = \Delta L/L$

Strain developed in a garlic pixel

Sr. No.	L, mm	l, mm	ΔL , mm	ϵ
1	13	12.5	0.5	0.03846
2	13	12	1	0.07692
3	13	11.5	1.5	0.11538
4	12	11	1	0.08333
5	11.5	10.5	1	0.08696
6	11	10	1	0.09091
7	10.5	9.5	1	0.09524
8	10	9	1	0.1
9	9.5	8.5	1	0.10526
10	9	8	1	0.11111
11	8.5	7.5	1	0.11765
12	8	7	1	0.12500

Table – Strain in Garlic Pixel

Up to Sr. No. 1 to 3 from stress and strain table, the respective values are in the elastic region and from Sr. No. 4 to 12; the values are in plastic region. Therefore, for finding the young’s modulus taking the value up to Sr. No. 3.

Sample calculation of young’s modulus

$$\text{Young’s modulus, } E = \text{stress/strain} = \sigma/\epsilon, \text{ N/m}^2$$

Taking $\sigma_1 = 6224.5 \text{ N/m}^2$ from stress table and $\epsilon_1 = 0.03846$ from strain table.

$$\text{Therefore, } E_1 = \sigma_1/\epsilon_1 = 6224.5/0.03846 = 1.62 \times 10^5$$

Within elastic limit, the values of elasticity are as follows

$$E_1 = 1.62 \times 10^5 \text{ N/m}^2$$

$$E_2 = 1.62 \times 10^5 \text{ N/m}^2$$

$$E_3 = 1.62 \times 10^5 \text{ N/m}^2$$

So from the above values we can conclude that the value of young's modulus of is $E = 1.62 \times 10^5 \text{ N/mm}^2$.

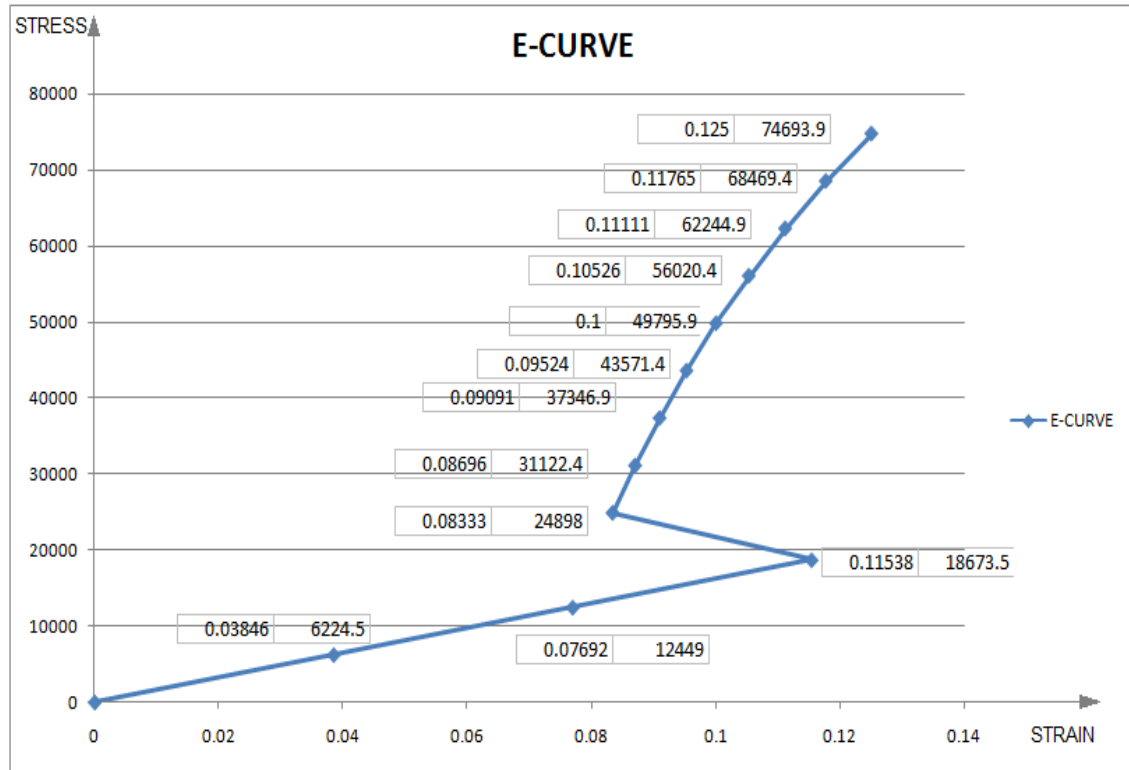


Fig. – Stress Strain Curve of Garlic Pixel

CONCLUSION

- Thus the testing of garlic using innovative force calculating machine are as follows
 - Force required to break the garlic bulb varies between $F_{\text{Break}} = 4.88 \text{ N to } 6.1 \text{ N}$
 - Force required to peel the garlic clove varies between $F_{\text{Peeling}} = 1.83 \text{ N to } 3.05 \text{ N}$
 - Force required to crush the garlic clove varies between $F_{\text{Crush}} = 7.32 \text{ N to } 8.54 \text{ N}$
- Young's modulus of garlic calculated by using force calculating machine is equal to $1.62 \times 10^5 \text{ N/m}^2$.

REFERENCES:

[1] Prof. B. D. Shiwalkar, "Design Data Book", Denett Publication, 2015 Edition.

[2] Prof. B. D. Shiwalkar, "Design of Machine Elements", Denett Publication, Third Edition.

[3] Farazdak Haideri, "A Text Book of Mechanical System Design", Third Edition, Chapter 2, Page No. 149 – 241.

[4] E. J. Hearn, "Mechanics of Materials I", Third Edition, University of Warwick, United Kingdom, Chapter 1, Page No. 1-8.

[5] Thammaiah Gowda, Jagadeesha T, D. V. Girish, "Mechanical Vibrations", Tata Mcgraw Hill Education Private Limited, Page No. 44, Topic – Spring Element.

[6] S. Ramamrutham, R. Narayanan, "Strength of Materials", Dhanpat Rai Publication Company, Page No. 116-118

IJERGS

Comparison of geopolimer & Ferrocement mortar with varying volume percentage and Specific surface of mesh

Swapna S. Yedshikar¹, Prof. Dr. A. S. Kasnale².

¹Student of M.E. Structure, M.S.Bidve Engineering College, Latur-413512, Maharashtra - India

E-mail: swapna.yedshikar4@gmail.com. Contact No.: +91 - 9422654175.

² Associate Professor Department of Civil Engg, M.S.Bidve Engineering College, Latur-413512, Maharashtra - India

E-mail: askasnale@yahoo.com

Abstract— The major factors in the global warming is Production of cement which releases CO₂ in atmosphere. Efforts are needed to make concrete more environmental friendly by reducing or replacing the cement by other cementitious material or industrial waste like fly ash. Geopolymer is a new development in the world of mortar in which cement is totally replaced by fly ash and activated by alkaline solutions to act as a binder in the concrete mix. Experimental investigation has been carried out to study the effect of different volume fraction % of steel mesh on compressive strength and split tensile strength of Ferrocement and geopolimer mortar. Activated liquid to fly ash ratio of 0.6 by mass was maintained in the experimental work on the basis of past research. Sodium silicate solution with Na₂O = 16.37%, SiO₂ = 34.35% and H₂O = 49.28% and sodium hydroxide solution having 13M concentration were maintained throughout the experiment. Geopolymer mortar cylinders of 150*300 mm size were cast. The temperature of heating was maintained at 90⁰C for 8 hours duration after demoulding. Test results show that compressive strength and split tensile strength of geopolimer mortar increases with increase in volume fraction percentage and specific surface of steel mesh as compare to ferrocement mortar.

Keywords - Fly ash, steel mesh, Sodium silicate, sodium hydroxide, Volume fraction, Specific surface, Compression test, Tensile test.

1. INTRODUCTION

World production of hydraulic cements is close to one thousand million tons per year. Every year the production of Portland cement is increasing with the increasing demand of construction industries[1,2]. The worldwide, near about 3% annual increase in production of Portland cement [6,9]. Therefore the rate of release of carbon dioxide into the atmosphere during the production of Portland cement is also increasing[3]. Among the greenhouse gases, CO₂ contributes about 65% of global warming [7, 8]. The green house gas emission from the production of Portland cement is about 1.35 billion tons annually, which is about 7% of the total greenhouse gas emissions [9]. Portland cement production is under critical review due to high amount of carbon dioxide gas released to the atmosphere. The climatic change due to global warming is one of the major issues concerning with the environmental pollution. So there must be an alternative to OPC. fly. In the past few decades, it has emerged as one of the possible alternative to OPC binders due to their reported high early strength and resistance against acid and sulphate attack apart from its environmental friendliness. Davidovits [4] was developed amorphous to semi-crystalline three dimensional silico-aluminate materials in 1979 called as geopolimer. Geopolymer mortar is a new material in which cement is totally replace by low calcium fly ash and activated by alkaline solutions. Low-calcium fly ash based geopolimer concrete possess high compressive strength [6,9], undergoes very little drying shrinkage and moderately low creep [10], and shows excellent resistance to sulphate and acid attack [7, 8]. They are not suffering from alkali-aggregate reaction and possess excellent fire resistant [6]. Geopolymer is produced by a polymeric reaction of alkaline liquid with source material of geological origin or byproduct material such as fly ash. In terms of reducing global warming, geopolimer technology could reduce approximately 80% of CO₂ emission to the atmosphere caused by cement and aggregate industry. This favorable behavior can be attributed to the type of matrix formation in geopolimer mortar. It has been reported that the stress strain relationship of fly ash based geopolimer mortar is almost similar to that of ordinary Portland cement mortar. The most common alkaline liquid used in geopolimerisation is a combination of sodium hydroxide or potassium hydroxide and sodium silicate or potassium silicate. Davidovits found that geopolimer cements has very low mass loss of 5%-8% when samples were immersed in 5% sulphuric acid and hydrochloric acid solutions.

1.2.1 Salient feature of geopolymer

Geopolymers can meet a “zero waste” objective because they can be produced from materials that are themselves waste products, such as fly ash, blast furnace slag, rice husk ash, metakaoline etc. The properties of alkali-activated fly ash are influenced, by a set of factors related to the proportioning of ingredients of the mixture and the curing conditions. Also, the earlier studies have manifested the high potential of these materials that could be used in the near future in the construction industry, especially in the pre-cast industry. The development of fly ash-based geopolymer mortar is one of the needs to the ‘greener’ mortar for sustainable development. Fly ash based geopolymer mortar has excellent compressive strength and is suitable for structural applications. The elastic properties of hardened mortar and the behavior and strength of structural members are similar to those of Portland cement mortar. The scope of the present study is to check suitability of geopolymer mortar as a substitute to cement mortar on the basis of compressive strength and split tension test on cylinder. It is expected that the final outcome of the research will have beneficial effect on generalizing the use of geopolymer mortar in the field of civil engineering construction in general and pre-cast construction in particular.

□ MATERIALS USED

i) Fly ash: Low calcium processed fly ash procured from Dirk India Private Limited, Nashik under the trade name Pozzocrete-83 is used in the present investigation.

ii) Sand: - Locally available sand conforming to zone II with specific gravity 2.74, water absorption 3.41% and fineness modulus 3.039.

iii) Alkaline activator : . In this case the mixture of Sodium Hydroxide (NaOH) and Sodium Silicate (Na₂SiO₃) is used as alkaline Solution. Sodium hydroxide in pellets form.

iv) Water : The fresh drinking water should be used in the mortar

v) steel mesh: The steel mesh of 1.5 mm diameter, 15 mm spacing (with galvanized coating) with tensile strength of 512 N/mm² and yield strength of 406 N/mm² has been used as reinforcement

Table No. 2.1 : Details of Steel Mesh

%of steel	Specific surface area (mm ²)	Weight of required steel (gm)	Size of steel mesh (mm X mm)
0.5	1.33	208	280 X 383
1	2.67	416	280 X 766
1.5	4.00	624	280 X 1149
2	5.33	832	280 X 1532

2.2 Preparation of sodium hydroxide solution

The sodium hydroxide (NaOH) solids were dissolved in water to make the solution. The mass of NaOH solids in a solution varied depending on the concentration of the solution expressed in terms of molar, M. For instance, NaOH solution with a concentration of 13M consisted of 13x40 = 520 grams of NaOH solids (in flake or pellet form) per liter of the solution, where 40 is the molecular weight of NaOH. The mass of NaOH solids was measured as 361.11 grams per kg of NaOH solution of 13M concentration. The sodium silicate solution and the sodium hydroxide solution were mixed together at least one day prior to use to prepare the alkaline liquid. On the day of casting of the specimens, the alkaline liquid was mixed together with the extra water (if any) to prepare the liquid component of the mixture.

III. Experimental program

In the present investigation, solution-to-fly ash ratio is considered as 0.60 which gives comparatively cohesive and workable mixes. Following parameters are fixed to study the effect of activators(NaOH and Na₂SiO₃).

1. Mix proportion 1:3
2. Molarity..... 13
3. Solution to fly ash ratio..... 0.6
4. Type of curing Oven
5. curing Temperature 90°C

- 6. Curing time (duration) 8hours
- 7. Test Period 3days

3.1 Mixing, Casting, Compaction and Curing

Mixture of fly ash and graded sand is taken in a bowl of capacity 6 kg. Homogeneous mix was made in the bowl-using trowel. Then the dry mix was spread on the non-absorbent steel plate in thick layer. Then prepared solution was added and thoroughly mixed for 3 to 4 minutes so as to give uniform colour. It was found that the fresh fly ash-based geopolymer mortar was viscous, cohesive and dark in colour. The amount of water in the mixture played an important role on the behavior of fresh mortar.

After making the homogeneous mix, workability of fresh geopolymer mortar was measured by flow table apparatus. Then 48 cylinders of size 150 mm X 300 mm were cast in three layers with placing 0.5%, 1%, 1.5% & 2% steel mesh (V_f) and 12 cylinders were cast with geopolymer mortar and ferrocement mortar without mesh. As per the percentage of volume fraction, mesh was placed in cylindrical form in cylinder mould as shown in fig. Each layer of mortar was well compacted by tamping rod of diameter 20 mm and vibrator machine. After compaction of mortar, the top surface was leveled by using trowel and also struck the sides of mould by using hammer so as to expel air if any present inside the mortar. After 24 hours of casting, all cylinders were demoulded and then placed in an oven for thermal curing (heating) at (90°C) temperature and for 8 hrs duration. For GPM, After specified period of heating at required temperature, oven was switched off. To avoid the sudden variation in temperature, the mortar cylinders were allowed to cool down up to room temperature in an oven. After 24 hours, specimens were removed from oven and weight of each specimen was taken for determination of mass density and then tested for compressive strength and split tensile strength. 60 cylinders were cast and tested 30 for compressive strength & 30 for split tensile strength after specified curing period.

IV. Tests and Results :

4.1 Compressive strength : Compressive strength of mortar cylinders was tested after curing and tested after three days of casting. Testing procedure of GPM is similar to that of cement mortar.

4.2 Split tensile test: The split tensile strength at an age 3 & 28 days has been evaluated for mortar GPC and OPC mix are reported in Table . Average split tensile strength of 3 cylinders (150mmx300mm) for all concrete mixes are given in table.

4.3 Specific Surface of Reinforcement : The specific surface of reinforcement is the total surface area of reinforcement divided by the volume of composite that is, the surface area of bonded reinforcement per unit volume of composite.



Fig 4.1 & 4.2 Specimen at Testing & mesh in cylinder mould.

Table 4.1: : Experimental Results

Sr.No.	Steel %	Ferrocement Mortar		Geopolymer Mortar	
		Average Compressive Strength (N/mm ²)	Average Split Tensile strength (N/mm ²)	Average Compressive Strength (N/mm ²)	Average Split Tensile strength (N/mm ²)
1	0	21.71	1.55	24.58	2.55
2	0.5	23.43	1.84	28.94	2.96
3	1.0	26.47	2.8	33.41	4.74
4	1.5	27.58	3.09	36.32	5.39
5	2.0	27.82	3.27	39.1	5.58

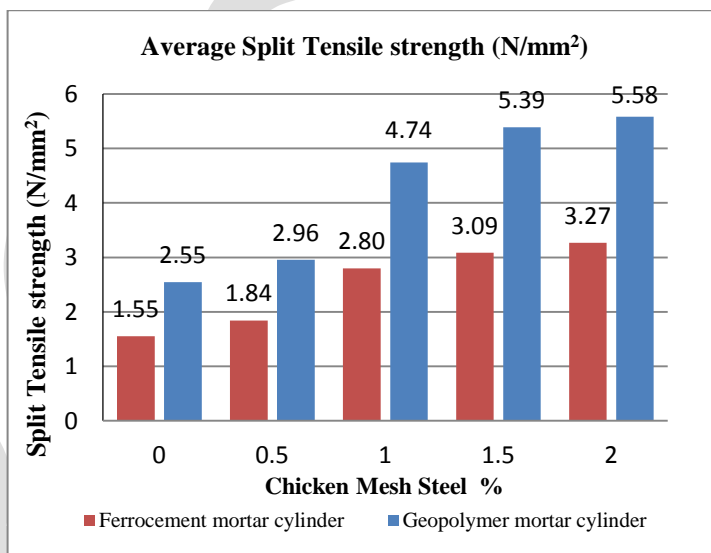
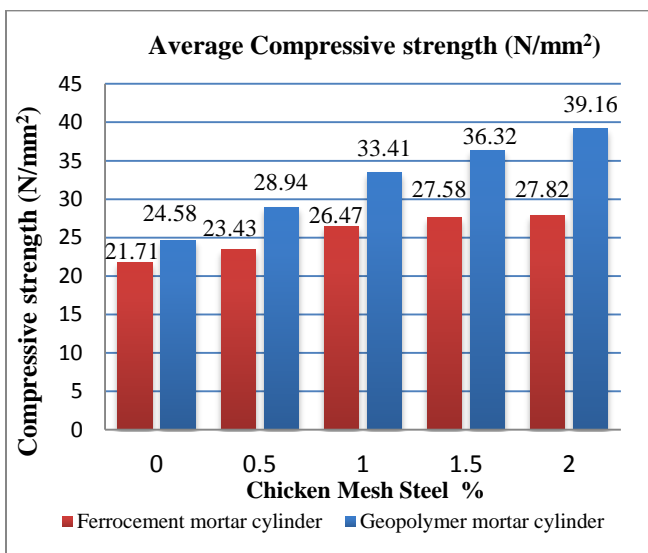


Fig. 4.3 & 4.4 strength comparison of FCM & GPM

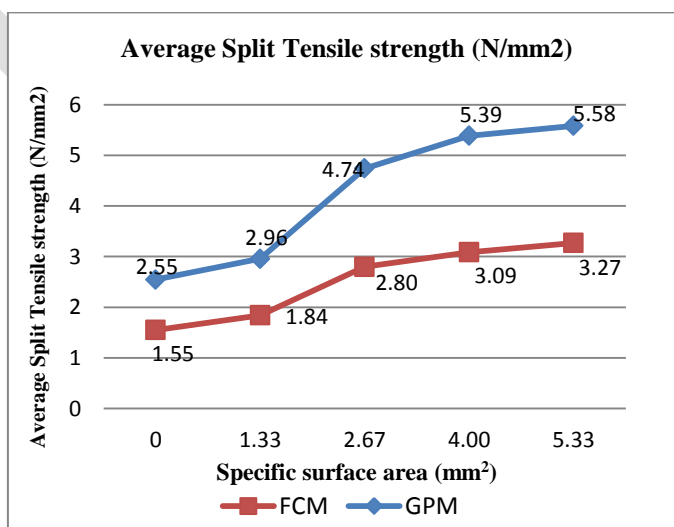
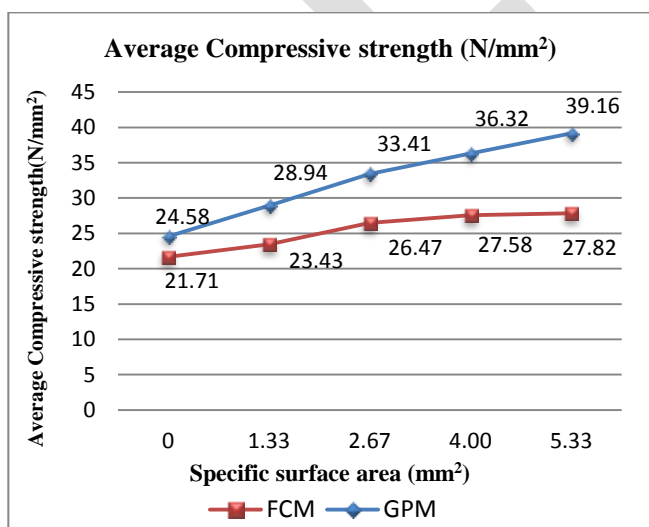


Fig. 4.5 & 4.6 : Average Compressive & Split tensile strength w.r.t. Specific surface For GPM

VI. CONCLUSION

On the basis of results obtained during the experimental investigations, following conclusions were drawn:

- Compressive and split tensile strength increases by increasing volume fraction % (0.5,1,1.5,2) of steel mesh.

- In 0.5% steel mesh, It gives 13.21% and 60.86% more compressive strength and split strength in GPM than FCM respectively.
- It is concluded that if we doubles the volume fraction (1%) of same size mesh with the specific surface of specimen increased by 100% and therefore increased in compressive Strength is observed to be 26% . Further using 1.5% V_f i.e. increases specific surface by 200% increase compressive Strength around by 32%. Further if specific surface is increased by 300% i. e. using 2% V_f , the corresponding compressive Strength of GPM increased by 41% than FCM.
- It is concluded that if we doubles the volume fraction (1%) of same size mesh with the specific surface of specimen increased by 100% and therefore increased in split tensile strength is observed to be 69% . Further using 1.5% V_f i.e. increases specific surface by 200% increase tensile strength around by 74%. Further if specific surface is increased by 300% i. e. using 2% V_f , the corresponding tensile strength of GPM increased by 70% than FCM.
- Different percentage of volume fraction also affecting specific surface. From experiment it is noted that the specific surface is increases in multiples of % of wire mesh.

GPC utilizes the industrial waste for producing the binding material in concrete, hence it can be considered as eco-friendly material and gives more strength than FCM. The environmental issues associated with the production of OPC are too many, responsible for some of the CO₂ emissions, So there must be an alternative to OPC. The reduced CO₂ emissions of GPC make them a good alternative to OPC.

REFERENCES:

- [1] Malhotra V. M. and Ramezani pour A. A., "Fly ash in Concrete", Canada Centre for Mineral and Energy Technology (CANMET) September 1994, pp.1-253.
- [2] Bapat J.D., "Performance of Concrete with Blended Cement", Two days seminar on Advances in concrete technology at Bharati Vidyeeth, Pune, 16-17 January 2003, pp. 24-29.
- [3] Christy C Freeda and Tensing D. "Greener building ", Asian journal of Civil Engineering(Building and Housing),2011, Vol. 12, No.1, pp. 87-105. Carola Edvardsen and Karsten Tollose, "Environmentally Green Concrete Structures", FIB-Symposium on Concrete and Environment in Berlin, October 2001, pp.178-192.
- [4] Suri S.B., "Fly Ash based Innovative building products for construction -Part-II", CE and CR , January 2012, pp134-142.
- [5] Patankar S.V., Ghugal Y.M., Jamkar S.S., "Mix Proportioning of fly ash based Geopolymer concrete" ACI Materials Journal 17 July 2015.
- [6] Davidovits Joseph, "Geopolymeric Reaction on the Economic future of cements and concretes: World Wide Mitigation of carbon dioxide Emission" Proceedings of the Second International Conference Geopolymère 99, , France, 30 June to 02 July 1999, pp111-121.
- [7] Joseph Davidovits, Luigi Buzzi, Philippe Rocher, Domingo Jimeno, Carlo Marini and Sandro Tocco, "Geopolymeric Cement Based on Low Cost Geologic Materials. Results from the European Research Project Geocistem", Proceedings of the second international conference geopolymer-99, France, 30 June to 2 July 1999 pp 83-96.
- [8] Joseph Davidovits "Environmentally Driven Geopolymer Cement Application", Proceedings of the third international conference geopolymer 2002, Melbourne, Australia, 28-29 Oct 2002, pp223-235
- [9] Zosin A. P., Priimak T.I. and Avsaragov Kh.B, "Geopolymer materials Based on Magnesia-Iron Slags for Normalization and Storage of radioactive wastes " Atomic Energy, 1998, Vol 85, No. 1, pp 510-514.
- [10] Rangan B.V., Djwantoro Hardjito, Steenie E Wallah and Dody M.J. Sumajouw, "Studies on fly-ash based Geopolymer concrete", Proceedings of the Geopolymer; Green chemistry and Sustainable Development Solutions, World Congress Geopolymer 2005, pp133-137
- [11] Davidovits Joseph, "geopolymers: Inorganic Polymeric New materials", Journal of Thermal Analysis, 1991, Vol.37, No.2, pp
- [12] Davidovits Joseph, " Chemistry Of Geopolymeric Systems, Terminology", Proceedings of the Second International Conference Geopolymer 99, France, 30 June to 02 July 1999, pp. 9-39
- [13] Patankar S.V. and Jamkar S.S., "Effect Of Various Parameters In Activation of Fly Ash Based Geopolymer Mortar", Proceedings of International Conference on Advances in Concrete and Construction, ICACC-2008 7-9 Feb, 2008, Hyderabad, India pp 270-279.

Implementation of Role Based Access Control on Encrypted Data in Hybrid Cloud

Gajanan Ganorkar, Prof. A.B. Deshmukh, Prof M.D.Tambhakhe

Information Technology Email:g.ganorkar7691@gmail.com Contact: 8600200142

Abstract— As we know that cloud technology provides the way for storing the data. Nowadays cloud system is used for storing the large amount of user data. But there is issue of security of data in cloud storage that how we control and prevent unauthorized access to users data which is stored in cloud. To overcome this situation there is one well known access control model which is Role Based Access Control (RBAC), this model provides flexible controls and management by having two mapping, User to Role and Role to Privileges on data. This is the well known model which can be used for protecting the data in the cloud storage. Although this Role Based Access model can be used for storing the data securely in cloud system which is uploaded by the owner of data, but this model assume that there is existence of trusted administrator who is going to manage all the user and role of organization which is not actually happen in real condition. In this paper we are have implemented the Role Based Encryption (RBE) scheme which can be implemented with the RBAC model for storing data securely in the cloud system. In this system user of any role who has been added by the admin of organization will have to remind only his decryption key which will be given by the admin to user when user will be added to the particular role. Based on this we have build up the hybrid cloud storage architecture which is consist of both public and private cloud, in which data will be able to store data in public cloud and organization secure data will be store on the private cloud. Access to the private cloud will be provided to only administrator of organization. Also the size of the cipher text remains constant regardless of the no. of user's in the particular role. User having higher role will be able to access the data of low level role's data. Depending on the different condition different report will be generated

Keywords— Encryption, Decryption, Public Cloud, Private Cloud, RBAC Policy, RBE Scheme, Security

I. INTRODUCTION

With increase in the large amount of data that need to be stored, cloud storage has attracted much attention in recent times because of its ability to deliver resource for storage to user on demand in cost effective manner. There are different infrastructures associated with the cloud [4]. One of this is a public cloud which is available to any user and user who want to use it can use in pay-as-you-go manner. Whereas private cloud is an internal cloud which is built and operated by the single organization, potentially there could be several benefits of storing data to public cloud [5]. Only organization has full access over the private cloud and private cloud cannot be accessed by the external parties. And hence we can say that private cloud is more secure than that of the public cloud.

In this research paper we have addressed the issue of storing the data on public cloud securely. Public cloud is formed by two or more data centered which are distributed geographically at different location. User does not know that where the actual data is stored and there is a strong perception that user have lost control over the data after it is uploaded to the cloud. In order to provide the control to the user for their data which is stored in the public cloud some suitable access control and mechanism is required. And this policies must restrict data access to only those user intended by the owner of data.

In this research paper we have implemented the secure RBAC (Role Based Access Control) based cloud system where access control policies will be enforced by the new Role Based Encryption (RBE) scheme. This RBE scheme enforces RBAC policies on encrypted data stored in the cloud. In this RBE scheme [13] owner of the data will encrypt the data and this encrypted data will be access by only that user which have appropriate role specified by the RBAC policy. If the user who want to access the data which is in encrypted form, if he satisfies the particular role then and only then he will be able to decrypt the data and he will be provided decryption key after satisfying the particular role. After getting the decryption key he will be able to decrypt the data and will be able to see the original content of the file that owner has uploaded to the public cloud. As shown in Fig1. We can see that public cloud is accessible to any user because data canters of public cloud can be located anywhere hence user will never know where his data is stored. In contrast to this private cloud is accessible to only administrator of the organization, Thus from this discussion we can conclude that hybrid cloud is best where shared information can be stored into public cloud and secure information can stored on the private cloud.

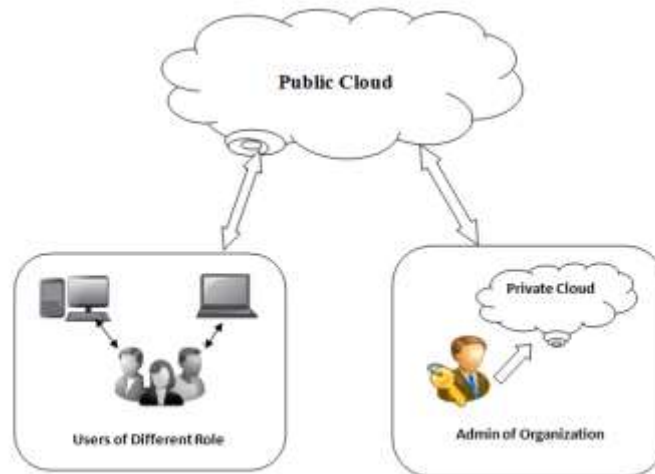


Fig1. Hybrid Cloud

In traditional access control systems, enforcement is carried out by trusted parties which are usually the service providers. In a public cloud, as data can be stored in distributed data centers, there may not be a single central authority which controls all the data centers. Furthermore the administrators of the cloud provider themselves would be able to access the data if it is stored in plain format. To protect the privacy of the data, data owners employ cryptographic techniques to encrypt the data in such a way that only users who are allowed to access the data as specified by the access policies will be able to do so. We refer to this approach as a policy based encrypted data access. The authorized users who satisfy the access policies will be able to decrypt the data using their private key, and no one else will be able to reveal the data content. Therefore, the problem of managing access to data stored in the cloud is transformed into the problem of management of keys which in turn is determined by the access policies. In this paper, we present the design of a secure RBAC based cloud storage system where the access control policies are enforced by a new role-based encryption (RBE) that we proposed in the paper.

This RBE scheme enforces RBAC policies on encrypted data stored in the cloud with an efficient user revocation using broadcast encryption mechanism described in [5]. In proposed RBE scheme, the owner of the data encrypts the data in such a way that only the users with appropriate roles as specified by a RBAC policy can decrypt and view the data. The role grants permissions to users who qualify the role and can also revoke the permissions from existing users of the role. The cloud provider (who stores the data) will not be able to see the content of the data if the provider is not given the appropriate role. Proposed RBE [12] scheme is able to deal with role hierarchies, whereby roles inherit permissions from other roles. A user is able to join a role after the owner has encrypted the data for that role. The user will be able to access that data from then on, and the owner does not need to re-encrypt the data. A user can be revoked at any time in which case, the revoked user will not have access to any future encrypted data for this role. With our new RBE scheme [12], revocation of a user from a role does not affect other users and roles in the system. In addition, we outsource part of the decryption computation in the scheme to the cloud, in which only public parameters are involved.

By using this approach, our RBE scheme achieves an efficient decryption on the client side. We have also used the same strategy of outsourcing to improve the efficiency of the management of user to role memberships, involving only public parameters. Based on the proposed RBE scheme, we have developed a secure cloud data storage architecture using a hybrid cloud infrastructure. This hybrid cloud architecture is a composite of private cloud and public cloud, where the private cloud is used to store only the organization's sensitive structure information such as the role hierarchy and user membership information. The high level architecture of the hybrid cloud storage system is illustrated in Fig1.

In this architecture, the users who wish to share or access the data only interact with the public cloud; there is no access for public users to access the private cloud, which greatly reduces the attack surface for the private cloud. We have developed a secure cloud storage system using the new RBE scheme and hybrid cloud architecture. The most frequently used system operations such as encryption of data by a data owner, decryption of data by a cloud user have been benchmarked. The result shows that the encryption and decryption time for a given data size is constant regardless of the number of roles and users that have the access to the cloud.

II. LITERATURES REVIEW & RELATED WORK

There exist many hierarchy access control scheme [2], [6] ,[10] Which have been constructed based on hierarchical key management (HKM) schemes and approaches using HKM schemes to enforce RBAC policies for data storage are discussed in [1], [9] ,[6]. But this scheme has disadvantages that when the user's access permission is revoked, all the keys known to this user as well as all the public values related to these keys need to be changed. In the traditional control access system, enforcement is carried out by trusted parties which are usually service provider. As we know in public cloud data can be distributed at different data centre. Furthermore when owner of data upload any data to cloud the service provider itself was able to access that particular document. This raised to security issue of the document. To protect the data, data owner uses the cryptographic encryption scheme to encrypt the data in such a way that user who has decryption key was able to decrypt the data and see the original content of the data. But this scheme leads to the problem of management of keys. To overcome the drawback of above system; there is Role Based Access Control (RBAC) model which can be used to protect data which is stored in the cloud.

Although cryptographic RBAC scheme have been developed recently to secure data outsourcing, but these scheme assumes the existence of trusted administrator managing all the users and roles, which is not realistic in large-scale system. In this project work we proposed Role Based Encryption (RBE) scheme [4] which can be used efficiently with RBAC scheme to provide security to data which is stored in the cloud storage. However the revocation of user in this scheme require the update of the all the role related parameter. Another scheme was proposed [11] in this scheme the size of the cipher text increases linear with the number of all the ancestor roles. In addition if user belongs to different roles, multiple key need to be posses by this user. Moreover, the management of the user membership for each individual role requires the use of the system secret keys.

Motivation

There exist as RBAC policy i.e. User to role and role to data mapping .In RABC policy different role are created and different user are added to the role .User are added to the role according to their position and qualification in the organization. But in previous system organization has to fully trust on the service provider that they will provide security to the data of organization which may lead to the insecurity of data in cloud.Organnization doesn't know that where there data is actually stored .They simply fill that they lost control over the data which is uploaded by them.They has to fully trust on the cloud service provider.

Objectives

As we know that if we simply upload the document to the cloud the owner of the data doesn't know where actually his data is saved .The cloud provider itself is able to see the original content of the file which may lead to data access in illegal way. To overcome this situation we have implemented RBAC policy in hybrid cloud. In which all the secure information will be stored on the private cloud and public related information will be available on the public cloud. By storing their sensitive data to private cloud user knows that where the data is actually stored .He doesn't have to worry about where his data is stored .We have implemented RBAC policy and has given permission to user to access data according to his position and qualification.

Need

1. For storing the secure data in cloud.
2. For successfully implementation of RBAC policy.
3. To overcome the problem of management of keys.

III. SYSTEM ANALYSIS

A. Existing System

Existing system refers to the system that is being followed till now. Presently all the functionalities that can be carried out in the RBAC policy are done only by the cloud service provider. That any organization want to implement RBAC policy they has to fully trust on the cloud provider that they will provide security to the organization data. But this may lead to insecurity of data service provider may itself see the original content of data. In this existing system security was handled only by the cloud service provider and organization has to fully trust on them which may lead to sometimes insecurity of the data. Some of the main disadvantage is time consuming are as follows:

Limitatations of Existing System.

- Lack of security of data
- Organization has to fully trust on the service provider.
- Service provider itself was able to see the content of file.
- Document was uploaded to the sever in plaintext format

To avoid all these limitations and make the system working more accurately it needs to be computerized using proper database functionality.

B. Proposed System

For designing this system some modern technology is used to expose the functionality of, which is based on the Service Oriented Architecture. The technology which is used cloud Technology Integration and Interoperability of RBAC policy with Hybrid cloud, systems will contribute to more effective and efficient. Hybrid cloud is a cloud computing environment which uses a mix of on-premises, private cloud and public cloud services with orchestration between the two platforms. By allowing workloads to move between private and public clouds as computing needs and costs change, hybrid cloud gives businesses greater flexibility and more data deployment option [3].

A public cloud is one based on the standard cloud computing model, in which a service provider makes resources, such as applications and storage, available to the general public over the Internet. Public cloud services may be free or offered on a pay-per-usage model. Data centers of public cloud are located at different centres even the user who uses the public cloud service don't know where his data is actually stored in opposite side private cloud is organization cloud user of private cloud know that where the actual data is store they don't have to bother about the security of the data.

In this research paper we have addressed the issue of storing the data on public cloud securely. Public cloud is formed by two or more data centres which are distributed geographically at different location. User does not know that where the actual data is stored and there is a strong perception that user have lost control over the data after it is uploaded to the cloud. In order to provide the control to the user for their data which is stored in the public cloud some suitable access control and mechanism is required. And this policies must restrict data access to only those user intended by the owner of data.

In this research paper we have proposed the secure RBAC based cloud system where access control policies will be enforced by the new Role Based Encryption (RBE) scheme. This RBE scheme enforces RBAC policies on encrypted data stored in the cloud. In this RBE scheme owner of the data will encrypt the data and this encrypted data will be access by only that user which have appropriate role specified by the RBAC policy. If the user who want to access the data which is in encrypted form, if he satisfies the particular role then and only then he will be able to decrypt the data and he will be provided the decryption key after satisfying the particular role. After getting the decryption key he will be able to decrypt the data and will be able to see the original content of the data that owner has uploaded to the public cloud.

As we know that in previous system there was some disadvantage of the traditional system i.e. to overcome this situation we have proposed the RBE scheme which can be efficiently used with RBAC scheme. To implement this project we are going to implement the hybrid cloud. This RBE scheme will contain the following four parameter.

- System administrator who has authority to generate the key for the user.
- RM is a role manager who manages the user membership of the role.
- Owners are the parties who wish to store the data securely over the cloud.
- Users are the parties who want to access the data and decrypt data stored on the cloud by the owner of the data.

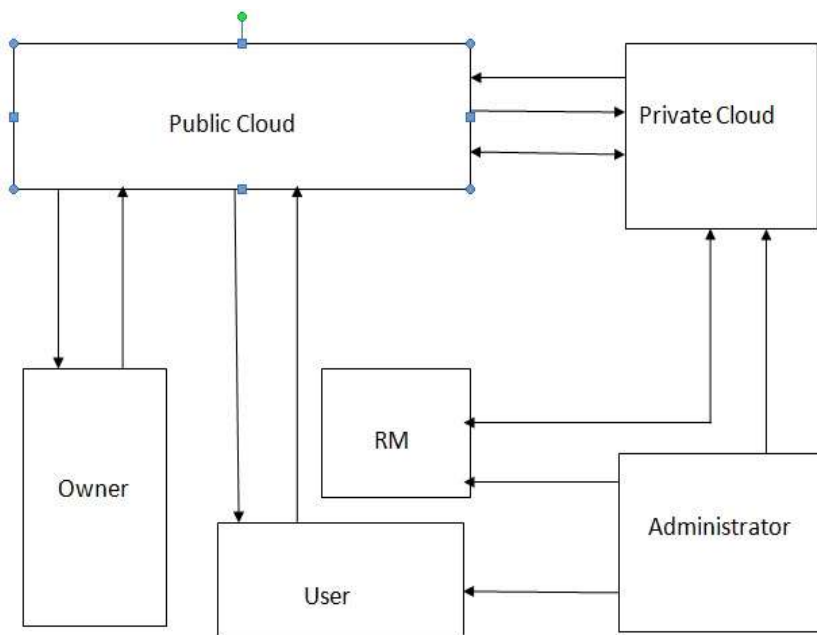


Fig2. System Architecture

As shown in above Fig2. Our system architecture is as follows the role of each component is as follows.

Owner:

Owners are the user of organization or they may be external parties who want to encrypt the data to the cloud and want is should be access by the other user. When owner of data will upload data to the cloud he will specify to whom this data should be accessed i.e. he will select the role based on the organization role hierarchy and will select the role to whom this data should be accessed.

Public Cloud:

We know that the public cloud is untrusted, because data centres of public cloud is located at different location we even don't know where our data is actually stored. Data stored in the public cloud could be accessed by unauthorized parties, such as employees of the cloud provider and users from other organizations who are also using services from the same cloud. An untrusted public cloud may deny a user's request for accessing stored data in the cloud or provide users within correct data. Such behaviours will result in the users not being able to access the data stored in cloud, but will not cause violation of RBAC policies.

Private Cloud:

As we know that private cloud is secure than public cloud because private cloud is a organizations cloud ,organization know that where the data is stored they don't have to worry about where there data is actually stored they already know it this was not possible in case of public cloud. In our project we are going to store all the security related data to the private cloud.

User:

User is the party who wish to access the data from the cloud which is uploaded by owner of data. Each user is authenticated by the administrator of the role-based system; upon successful authentication, the user is given a secret key which is associated with the identity of the user. User has not directly access to the private cloud they have only access to the public cloud.

Role Manager:

Role manager will add different role and will generate id related to the role .After this role manager will send this data to the private cloud. This role related data will be access by administrator of organization .Only role manager and administrator of organization will have direct access to the private cloud.

Administrator:

System administrator will add different user to different role which are generated by the Role Manager. He will be able to remove the particular user from the particular role. He will generate user decryption key and will send it to user via email or text message. Only Role Manager and Administrator have direct access to the private cloud.

IV. IMPLEMENTATION OF SYSTEM

In this research paper we address the issue of storing the data in the cloud. We have successfully implemented RBAC policy in hybrid cloud. Hybrid cloud consists of private cloud and public cloud. In this system we have created five roles for the organization ie.Role Hierarchy consist of following. SA is a system administrator that has the authority to generate he keys for users and roles, and to define the role hierarchy. RM is a role manager who manages the user membership of a role. Owners are the parties who want to store their data securely in the cloud. Users are the parties who want to access and decrypt the stored data in the cloud. Cloud is the place where data is stored and it provides interfaces so all the other entities can interact with it.

Private Cloud Module:

In this paper we have created 2 applications in our project one is for admin side and another is for user side. We have deployed these two applications successfully on this server, for deploying these two applications we have created two servers and deploy this two application successfully on this server. First we will go through the private cloud which is for the administrator and role manager of the organization. The application which is developed for private cloud which will be accessed by only by the administrator and role manager of organization.

Public Cloud Module:

As from the proposed system application which is developed for the public cloud will be access by the user, here user may be the part of organization or he may be external party. Now if any users who want to upload the file to particular role.

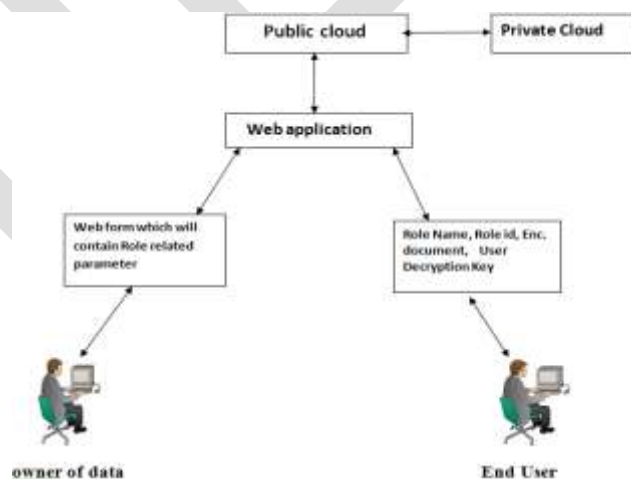


Fig3. Access to Application

As shown in Fig2. Flow of the system flow will be as follows.

Role manager will generate the different role and id related to that role and will upload this data to the private cloud. Then administrator of the organization will add different role and user to different role and will generate user decryption key. This generated user decryption key will be send to the user via mail or text message. Only admin will have access to the private cloud. Public cloud will be accessed by the user and owner of data. As shown in fig the owner who wish to upload the data for particular role. He will get the role related parameter on the public cloud and getting this information he will encrypt the document and will add encryption key to it. Now this encrypted document will be uploaded to the public cloud. Now when any user who want use any document he will have to satisfy the particular role if he satisfy the particular role then and only then he will get the document decryption key. From this we can conclude the size of the cipher text remain same although the number of user increases.

A. Owner of data

As shown in fig3. We can see that owner may be the external user or within the organization. When he wants to upload the document in encrypted form in cloud he will add the following parameter.

- Encrypted Document
- Role Name
- Role ID
- Decryption key of Document

After this document will be in encrypted form and all the secure information will be stored on private cloud.

B. User

Now when the owner of data upload the file to the cloud The User who wish to use that file or want to decrypt the file ,he must have the decryption key of that particular file then and only then he will be able to decrypt the file. When he wants to decrypt the file he will have to enter the following parameter

- Role Name.
- Role Id.
- User Decryption key (dk).

All the information enters by the use will be verified at private cloud. If all the information which is passed or entered by user is true or verified then he will be given the decryption key of the file. If that user decryption key is not present then user will not be given the file decryption key.

System Evaluation:

We come to following conclusion when the different operation is performed on the system.

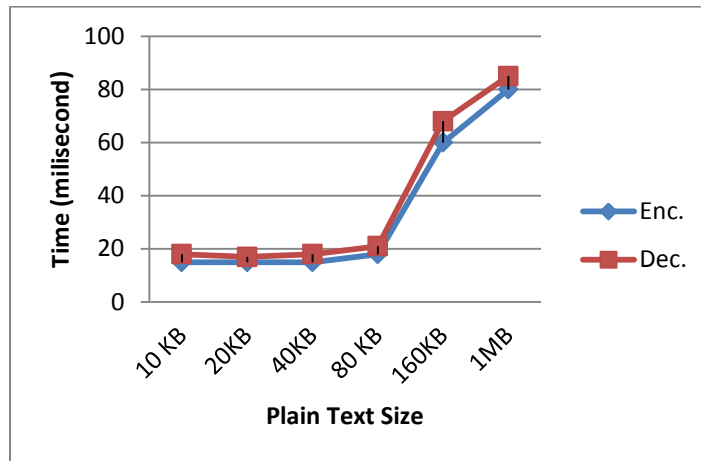


Fig4. Response for Different size

From the above graph it can be observed that system is taking same time for encryption and decryption time when the size of document is same. But time is increasing for both encryption and decryption operation when the size of the document get increase.

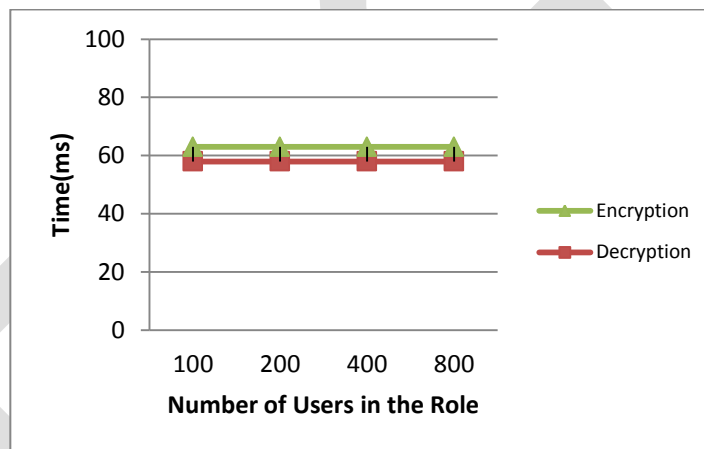


Fig5. Response for Different number of user

From the above graph it can be observed that response for encryption and decryption time is same regardless of the no user existing in the system.

5. APPLICATION

This policy can be implemented in any organization where role hierarchy plays an important role. The organization which wish to upload the document to the cloud with security. This policy provide the full security to the documents. This project can be used in colleges or company need to provide the access to the file to appropriate role and to user. As we know that there exists the different role and user in these organization and can be implemented easily.

6. CONCLUSION

As from the previous studies we can understand that the current system have lots of drawbacks. And from the Literature studies we come to understand that, there is insecurity to the document or data which is uploaded to the cloud. So, to overcome some of these drawback we have develop this project i.e. Implementation of Role Based Access Control on Encrypted Data in Hybrid Cloud which is the great improvement over previous system. The RBAC policy in Hybrid Cloud system was thoroughly checked and tested with dummy data and thus is found to be very reliable and user friendly. And it is also checked that weather is following the mapping Data to user and user to role. In this we have checked all the condition and it observed that it satisfy all the condition which was assume to be follows.

ADVANTAGES

- It is fast, efficient and reliable
- Avoids data redundancy and inconsistency
- Size of the cipher text remain constant regardless of no of user and roles.
- Provides more security and integrity to data

7. ACKNOWLEDGEMENT

I would like to express my deep and sincere thanks to Prof. A. B. Deshmukh and Co. guide Prof. M.D.Tambhakhe for their unstinted support and valuable guidance directing the course of action in the necessary and new direction and imparting me the knowledge to work satisfactory and to be able write and present this report. I would like to express my sincere thanks to our principal Dr. S. A. Ladhake for giving their valuable support. I am also thankful to Head of Department (IT) Prof. Dr. V. S. Gulhane for providing their support and necessary facilities, without whom this work would have been a goal at infinity.

REFERENCES:

- [1] C.Blundo, S. Cimato, S.D.C.di Vimercati,A.D. Santis S. Foresti, S. Foresti, S. Parabosch, et al.,”Efficient key management for enforcing access control in outsourced scenarios,” in SEC(IFIP), vol. 297. New York, NY, USA:Springer – Verlag, May 2009, pp. 364-375
- [2] H. R. Hassen, A. Bouabdallh, H. Bettahar, and Y. Chllal, “Key management for content ” Access control in hierarchies,” Comput. Netw. vol. 51, no 11, pp. 3197 – 3219, 2007.
- [3] <http://searchcloudcomputing.techtarget.com/defination/hybrid-cloud>.
- [4] L. Zhou, V. Varadharajan, and M. Hitchens, “Enforcing role-based access control for secure data storage in the cloud,” Comput. J., vol. 54, no. 13, pp. 1675–1687, Oct. 2011.
- [5] M. Armbrust, A. Fox, R. Griffith, A.D. Joseph, R. H. Katz, A.Konwinski, et Al., “A view of Cloud Computing ,” Common. ACM, vol. 53, no. 4, pp. 50-58 2010.
- [6] M .J. Atallh, K. B. Frikken, and M.Blanton, “Dynamic and efficient keymanagment”For access control in hierarchy,” Computt.Netw. Common. Sec., Nov. 2005, pp. 190-202.
- [7] P. Samarati and S. D. C. di Vimercati, “Data protection in outsourcing scenarios: Issues and directions,” in Proc. ASIACCS, Apr. 2010. pp. 1-14
- [8] R. Canetti, S. Halevi, and J. Katz, “Chosen-ciphertext security from identity-based Encryption,”in EUROCRYPT (Lecture Notes in Computer Science), vol.3027.New York, NY, USA: Springer-Verlag, 2004, pp.207-222.
- [9] S. D. C. Di Vimercati, S. Foresti, S. Jajodia, S. Paraboschi, and P. Samarati,”Over Encryption: Mangment of access control evolution on outsourced data,” in proc. VLDB, Sep. 2007, pp. 123-134.
- [10] S. G. Akl and P.D. Taylor, “Cryptographic solution to problem of access control in HierarchyTrans,” ACM Trans. Comput. Syst., vol. 1. No. 3, pp. 239-248, 1983.
- [11] S. Yu, C. Wang, K. Ren, and W. Lou, “Achieving secure, scalable, and fine-grained data Access control in cloud computing,” in Proc. IEEE INFOCOM, Mar 2010,pp.534-542.
- [12] Y. Zhu, H.Hu, G. –J. Ahn, H. Wang and S.-B Wang, “Provably secure role–based encryption with revocation mechanism,” Comput. JSci Techno vol 26, no. 4, pp. 697 -710, 2011.
- [13] Lan Zhou, Vijay Varadharajan, and Michael Hitchen “Achieving Secure Role-Based Access Control on Encrypted Data in Cloud Storage” IEEE TRANSACTIONS ON INFORMATION FORENSICS AND SECURITY, VOL. 8, NO. 12, DECEMBER 2013

A Real-Time Monitoring and Contamination Detection in Water Distribution Systems using 32-Bit Microcontroller

G.Vasudevan
M Tech [Embedded Systems]
Dept. of ECE,
Princeton College of Engineering and
Technology

B. Sudhir Kumar, M.Tech & MS
Assoc. professor and HOD
Dept. of ECE,
Princeton College of Engineering and
Technology

Abstract :-The aim of the Proposed Project is a Microcontroller based Low-Cost Sensor Network for Real-Time Monitoring and Contamination Detection in Potable and non- Potable Water Distribution Systems and also updates the information to the consumers and concerned authorities by using GSM module. In the existing system, it is just monitor the water level and electrical conductivity manually (off-line) and report to concerned authorities only in metropolitan areas. The objective of the project is to present a conceptual model of embedded based real time monitoring the water quality and also contamination detection for both potable and non-potable water distribution systems. In this proposed system we are using different sensors for water level and contamination detection. The main goal is the design and development of low cost system that can be used at the premises of consumers. This system can also be used in customer oriented manner to continuously monitor qualitative water parameters and fuse multi parametric sensor data for assessing the water quality. A 32-bit Microcontroller and associated sensor network can detect water contamination continuously according to water conductivity and temperature. Depends on these parameters microcontroller computes the other related contaminants and transmits same data to consumers and some authorities by using GSM module. Our approach is based on the development of low cost sensor nodes for real time and in-pipe monitoring and assessment of water quality on the fly. The main sensor node consists of electrochemical and optical sensors which can be used to monitor the water quality. From the sensor node we are sending monitored values to control room (ARM board) through RS232 serial cable.

Keywords: Water quality monitoring, flat surface sensors, Oxidation reduction potential sensor (ORP) and multisensory system, and sensor networks, arsenic & bacterial contamination detection.

I. INTRODUCTION

Immaculate drinking water is a critical for the wellbeing and prosperity of all people and creatures. In addition, it is additionally essential for farming utilization for good product yielding and natural way of life linkage (root zone) wellbeing issues. An ease and comprehensive methodology is a microcontroller based sensor system for continuous observing and pollution recognition for both drinking and non-drinking water dissemination frameworks and in addition for customer locales.

It is critical for accurate on-line (real-time) water quality observing frameworks than the current lab based techniques, which are too ease back to create operational reaction and don't give a level of general wellbeing security continuously.

Conventional strategies for water quality checking and control include the manual accumulation of water tests at different areas and at diverse times, trailed by research centre scientific procedures keeping in mind the end goal to portray the water quality.

Such methodologies are no more thought to be productive. It has a few disadvantages:

- a) The absence of continuous water quality data to empower discriminating choices for general wellbeing security (long time holes in the middle of testing and identification of defilement).
- b) Poor spatiotemporal scope (little number areas are tested).
- c) It is work serious and has generally high expenses (work, operation and hardware).

In this way, there is a reasonable requirement for nonstop on-line water quality checking with proficient spatio-fleeting determination.

The proposed framework comprises of a top of the line 32-bit microcontroller, sensor hub comprises of a few in-channel electrochemical and optical sensors and accentuation is given on minimal effort, lightweight execution and dependable long time operation. Such execution is suitable for huge scale arrangements empowering a sensor system approach for giving spatiotemporally rich information to water purchasers, water organizations and powers. Exploratory results show that this economical framework is equipped for identifying these high effect contaminants at genuinely low fixations. The outcomes show that this framework fulfils the on-line, in-channel, low organization operation expense and great location precision criteria of a perfect early cautioning framework. Broad writing and statistical surveying is performed to distinguish minimal effort sensors that can dependably screen a few parameters, which can be utilized to gather the water quality. Taking into account those parameters a sensor cluster is produced alongside a few Microsystems for simple sign moulding, handling, logging, and remote presentation of information.

At long last, calculations for intertwining on-line multi sensor estimations at neighbourhood level are created to evaluate the water tainting danger. Investigations are performed to assess and approve these calculations on deliberate tainting occasions of different amassing of *Escherichia coli* microscopic organisms and substantial metals (arsenic).

Drinking water utilities (water investigation and dispersion) are confronting new difficulties in their ongoing operation as a result of restricted water assets, escalated spending plan necessities, developing populace, maturing framework, progressively stringent regulations and expanded consideration towards protecting water supplies from inadvertent or conscious sully.

Fast recognition (and reaction) to occasions of tainting is basic because of the possibly extreme results to human wellbeing. Ruptures in physical and pressure driven respectability of a water conveyance framework can prompt the deluge of contaminants crosswise over channel dividers, through breaks, and by means of cross associations. The mixture of dangerous (small scale organic, concoction, and so forth) specialists which can deliver unfavourable impacts on people because of various courses (ingestion, inward breath and dermal) of presentation. US Environmental Protection Agency (USEPA) has completed a broad trial assessment of water quality sensors to survey their execution on a few sully.

The main conclusion was that many of the chemical and biological contaminants used have an effect on many water parameters monitored including Turbidity (TU), Oxidation Reduction Potential (ORP), Electrical Conductivity (EC) and pH. Thus, it is feasible to monitor and infer the water quality by detecting changes in such parameters.

Water quality monitoring systems should provide good balance between cost and ease of implementation-maintenance, however to ensure their survival must demonstrate operational benefits (such as better water quality, decreased operating costs or reduced customer complaints).

The objective of the project is to present a conceptual model of embedded based real time monitoring the water quality and also contamination detection for both potable and non-potable water distribution systems. In this proposed system we are using different sensors for water level and contamination detection. This approach can achieve more reliable quality monitoring due to the large spatiality distribution development and possibility of correlating quality measurements from various sensors.

II. PROPOSED METHOD:

The main goal is the design and development of low cost system that can be used at the premises of consumers. This system can also be used in customer oriented manner to continuously monitor qualitative water parameters and fuse multi parametric sensor data for assessing the water quality. A 32-bit Microcontroller and associated sensor network can detect water contamination continuously according to water conductivity and temperature. Depends on these parameters microcontroller computes the other related contaminants and transmits same data to consumers and some authorities by using GSM module. A user/consumer can view the presented data regarding quality of water and it will be used accordingly. The below shows a functional block diagram proposed the low cost system for both potable and non-potable water comprising of multi sensor network and 32-bit microcontroller development board, GPRS/GSM module etc.

A preliminary version of this article has appeared. In this article, we present an improved hardware platform, develop a new advanced contamination event detection algorithm and provide an experimental evaluation and validation of system and event detection algorithms in the presence of Real microbiological and chemical contamination events. In addition, several water monitoring micro systems (sensor nodes) have been developed for large scale water monitoring based on wireless sensor networks (WSNs) technology. A sensor hub is created for checking saltiness in ground water and the water temperature in surface waters. We have built up a WSN and a vitality gathering framework (in view of a sun powered board) to screen nitrate, ammonium and chloride levels in streams and lakes. Vitality reaping systems alongside hibernation techniques assume a critical part in expanding the lifetime of sensor hubs. A study on vitality collecting for WSNs is given. a self-governing vessel furnished with water sensors is proposed to gather tests from lakes utilizing the A* look calculation. More productive route calculations for a gathering of vessels with impediment shirking are introduced. Aside from the progressing examination towards the configuration and advancement of sensors and small scale frameworks another parallel Research heading is that of the improvement of programming and calculations for the identification of water quality irregularities and tainting occasions. At present openly accessible instrument is CANARY programming created at Sandia National Laboratories in a joint effort with the USEPA. CANARY shows conceivable defilement occasions by utilizing a scope of Mathematical and measurable procedures to distinguish the onset of atypical water quality occurrences from online crude sensor Data. Other occasion recognition and information acceptance approaches are given and references therein.

Software Requirements:

- Kiel compiler.
- Embedded C.
- Flash Magic.

Hardware Requirements:

- Microcontroller unit.
- Temperature sensor.
- Conductivity sensor.
- Oxidation Reduction Potential sensor(ORP)
- Power supply.
- LCD.

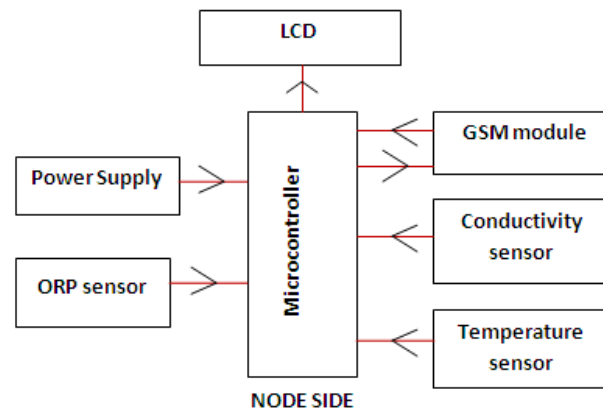


Fig 1. Block Diagram

III. SENSORS WORKING PRINCIPLE

A. Oxidation Reduction Potential (ORP)

Oxidation refers to any chemical action in which electrons are transferred between atoms. Oxidation and reduction always occur together. ORP is a reliable and cost effective method to measure the effectiveness of water disinfection sanitizers (chlorine, sodium hypochlorite, bromine and ozone) in real time.

As the measured value of ORP increases, the solution has more potential to oxidize and thus to destroy any unwanted organisms. WHO adopted an ORP standard for drinking water disinfection of 650 mV. Research has shown that at 650-700 mV of ORP, bacteria such as E.coli and Salmonella are killed on contact.

ORP level can also be viewed as the level of bacterial activity of the water because a direct link occurs between ORP level and Coliform count in water. The table 4.2 represents ORP levels and relative Coliform counts. Level of coli form count (E.coli) in drinking water indicates the water has been contaminated with faecal material that may contain disease causing microorganisms, such as certain bacteria, viruses, or parasites.



Fig 2: ORP Sensors

B. pH sensor implementation:

The pH value is a good indicator of whether water is hard or soft. The pH of pure water is 7. In general, water with a pH lower than 7 is considered acidic, and with a pH greater than 7 is considered basic. The normal range for pH in surface water systems is 6.5 to 8.5, and the pH range for ground water systems is between 6 and 8.5.

The modern pH electrode is a combination electrode composed of two main parts: a glass electrode and a reference electrode as shown in below Figure. pH is determined essentially by measuring the voltage difference between these two electrodes. At the tip of the electrode is the thin membrane that is a specific type of glass that is capable of ion exchange. It is this element that senses the hydrogen ion concentration of the test solution. The reference electrode potential is constant and is produced by the reference electrode internal element in contact with the reference-fill solution that is kept at a pH of seven.

The output of the pH electrode produces DC voltage (mV), 1pH indicates $\pm 59.4\text{mV}$ for full scale range. An ideal electrode at 25°C will produce 0 mV when placed in a solution with a pH of seven.



Fig 3 pH sensor

C. Temperature Sensor

LM35 is a precision IC temperature sensor with its output proportional to the temperature (in $^{\circ}\text{C}$). The sensor circuitry is sealed and therefore it is not subjected to oxidation and other processes. With LM35, temperature can be measured more accurately than with a thermistor. It also possesses low self heating and does not cause more than 0.1°C temperature rise in still air. The operating temperature range is from -55°C to 150°C . The output voltage varies by 10mV in response to every $^{\circ}\text{C}$ rise/fall in ambient temperature, i.e., its scale factor is $0.01\text{V}/^{\circ}\text{C}$. The sensor generates an output voltage proportional to the suspended particles and has a linear response.

Advantages & Applications:

Quality of water delivered to consumers Using low cost, low power and tiny in-pipe sensors. The main contribution of this project is the design and development of a low cost system that can be used at the premises of consumers to continuously monitor qualitative water parameters and fuse multi-parametric sensor response in order to assess the water consumption risk.

III. RESULTS

A modular but holistic approach is adopted for the design and development of the system. Modularity enables the simultaneous instrumentation and sampling of all parameters and the decomposition of several operations like calibration, upgrades and repair or replacement of faulty parts. The overall system architecture under discussion is presented in Fig. 1 and is comprised of the following three subsystems: a central measurement node (LPC2148 MCU based board) that collects water quality measurements from sensors, implements the algorithm to assess water quality and transmits data to other nodes, a control node (ARM/Linux web server based platform) that stores measurement data received from the central measurement node in a local database and provides gateway to the internet, visualize data (charts), and sends email/sms alerts and finally a tiny notification node(s) (PIC MCU based board) that receives information from the central measurement node through an interconnected Zig Bee RF transceiver and provides local near-tap notifications to the user (water consumer) via several interfaced peripherals (LED, LCD, Buzzer). It should be noted that the central measurement node serves as the sensor node. The idea is to install these sensor nodes in many consumer sites in a spatially-distributed manner to form a WSN that will monitor the drinking water quality in the water distribution system from the source to the tap.

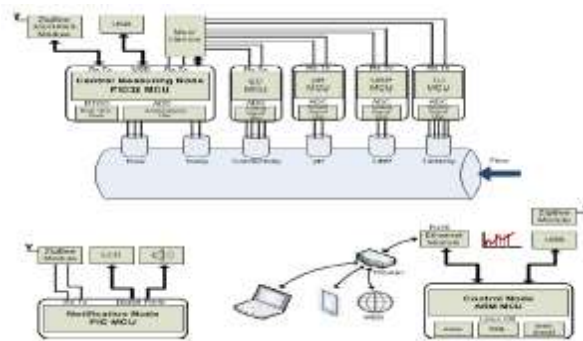


Fig 4 System architecture

The objective of the event detection algorithms is to activate a trigger event (alarm) when normalized sensor outputs exhibit sudden and significant changes, given that these changes are bounded within the quality ranges suggested by drinking water quality standards (see Table II, quality range). The detection of water quality changes that are outside the expected quality ranges (min/max violations) is easier and can be done by a weighted multi-parameter cost function in the form of $RO = \sum_i w_{oi} J_i$, where J_i are binary variables that indicate whether parameter i has been violated and w_{oi} are non negative weights which imply the significance of the violation of each parameter i . If $RO = 0$ no violation is assumed, however as $RO > 0$ increases the water contamination risk is also increases. As previously indicated, the objective in this paper is to detect anomalies when water quality changes are inside the expected quality ranges by fusing the multi-sensor data. Therefore a risk indicator RI function is defined that takes a value $RI = 1$ if a contamination event is detected or $RI = 0$ otherwise. The first event detection algorithm is denoted as Vector Distance Algorithm (VDA) and the risk indicator RVDA I function used in this algorithm is estimated based on the Euclidian distance between the normalized sensor signal vector \mathbf{N} and the normalized control signal vector \mathbf{N}_0 of pure (clean) water. In fact, developing and deploying sensors for all contaminants would not be feasible (too many contaminants which translates to very high cost). On the other hand, many contaminants cause changes in some parameters of the water that can be easily monitored. Therefore, by monitoring these changes we can infer possible contamination events, even though this approach may suffer from some false alarms, it can be compensated/eliminated by the large scale deployment and the possibility of correlating the decisions from various sensor nodes which is the topic of our future work.

Microbiologically (E.coli) contaminated drinking water:

The first experiment considers the case of microbiologically (E.coli) contaminated drinking water. Most E. coli strains are in general harmless to humans, but some types can cause serious food and water poisoning. However, the presence of E.coli is used to indicate that other pathogenic organisms may be present (often of faecal origin). According to WHO guidelines & EU Drinking Water Directive E.coli parametric value is 0 CFU/100mL. Fig. 10(a) presents the measurements received using the developed sensor node when the following concentrations of E.coli were injected: 5×10^{-2} , 5×10^{-1} , 5×10^0 , 5×10^1 , 5×10^3 , 5×10^4 , 1×10^7 CFU/mL. It is evident that TU and EC sensors responded well when microbiological contaminants injected in chlorinated potable water. ORP sensors have responded with delay and pH sensor has a spiky type of response. Fig. 10(b) presents the output signals of the Vector Distance Algorithm (VDA) and Polygon Area Algorithm (PAA). The results of Fig. 10(b) indicate that both algorithms miss the detection of 5×10^{-2} CFU/mL because sensors responses were very close to background levels (no anomalies occurred). It should be noted that the performance of PAA algorithm is better and given that it utilizes less information, PAA algorithm is better than the VDA algorithm.

2) Chemically (Arsenic) contaminated drinking water:

The second experiment considers the case of chemically (Arsenic) contaminated drinking water. Water contamination by toxic heavy metals and especially arsenic contamination is a common problem encountered in many countries due to undue deposition of mining, agricultural, industrial and urban wastes in water resources. Arsenic is known to affect negatively the mental and central nervous

system function, to damage the blood composition, lungs, kidneys, liver, and other vital organs, as well as it contributes to certain neurological

(b) E.Coli bacteria contamination detection.

Fig.10. Experiments with E.coli bacteria degenerative processes and causes skin cancer. According to WHO guidelines & EU Drinking Water Directive Arsenic parametric value is 10_{g/L} (it was 50_{g/L} in the previous directives). Fig. 11(a) presents the measurements received using the developed sensor node when the following concentrations of Arsenic were injected: 5, 10, 25, 50, 125, 500, 1000 _{g/L}. Arsenic solutions created from a standard solution of 1000mg/L As. Unfortunately, almost all sensors did not respond at low arsenic contamination. However, at concentrations above 25 _{g/L} ORP and pH sensors have responded and at higher concentrations (above 500_{g/L}) all sensors responded well. Fig. 11(b) presents the output signals of the Vector Distance Algorithm (VDA) and Polygon Area Algorithm (PAA). The results of Fig. 11(b) indicate that both algorithms miss the detection of 5 and 10 _{g/L} because sensors responses were very sluggish and close to background levels and that the VDA algorithm exhibits two false alarms. Therefore, the performance of PAA algorithm is again better (sharp response, no false alarms) than the VDA algorithm.



Fig 5 LPC 2148,32 bit-Microcontroller board



Fig 6 GSM module.



Fig 7. Final Result

IV. CONCLUSION

In this article, the design and development of a low cost sensor node for real time monitoring of drinking water quality at consumer sites is presented. The proposed sensor node consists of several in-pipe water quality sensors with flat measuring probes. Unlike commercially available analyzers, the developed system is low cost, low power, lightweight and capable to process, log, and remotely present data. Moreover, contamination event detection algorithms have been developed and validated to enable these sensor nodes to make decisions and trigger alarms when anomalies are detected. Such implementation is suitable for large deployments enabling a sensor network approach for providing spatiotemporally rich data to water consumers, water companies and authorities. In the future, we plan to investigate the performance of the event detection algorithms on other types of contaminants (e.g. nitrates) and install the system in several locations of the water distribution network to characterize system/sensors response and wireless communication performance in real field deployments. Finally, we plan to investigate network-wide fusion/correlation algorithms to assess water quality over the entire water distribution system.

REFERENCES:

- [1] T.P. Lambrou, C.C. Anastasiou , C.G. Panayiotou, A Nephelometric Turbidity System for Monitoring Residential Drinking Water Quality, in Sensor Networks Applications, Experimentation and Logistics, 2009
- [2] T.P. Lambrou, C.G. Panayiotou and C.C. Anastasiou, A Low-Cost System for Real Time Monitoring and Assessment of Potable Water Quality at Consumer Sites, in IEEE Sensors 2012, 28-31 Oct 2012.
- [3] S. Zhuiykov, Solid-state sensors monitoring parameters of water quality for the next generation of wireless sensor networks, Sensors and Actuators B: Chemical, Volume 161, Issue 1, pp 1-20, 2012

- [4] A. Aisopou, I. Stoianov, N. Graham, In-pipe water quality monitoring in water supply systems under steady and unsteady state flow conditions: A quantitative assessment, *Water Research*, 46(1), pp. 235-246, 2012
- [5] S. Panguluri, G. Meiners, J. Hall, J.G. Szabo, *Distribution System Water Quality Monitoring: Sensor Technology Evaluation Methodology and Results*, U.S. Environmental Protection Agency, EPA/600/R-09/076, 2009
- [6] J. Hall, A.D. Zaffiro, R.B. Marx, P.C. Kefauver, E.R. Krishnan, R.C. Haught, and J.G. Herrmann, On-line Water Quality Parameters as Indicators of Distribution System Contamination, *Journal AWWA*, 2007
- [7] M.V. Storey, B. Gaag, B.P. Burns, Advances in on-line drinking water quality monitoring and early warning systems, *Water Research*, Volume 45, Issue 2, January 2011, Pages 741-747, ISSN 0043-1354
- [8] Hach HST, *GuardianBlue Early Warning System Brochure*, 2008
- [9] JMAR, *BioSentry Contamination Warning System Technical Overview*, 2006
- [10] i::scan, *Multi-parameter spectrophotometer probe*, 2012
- [11] Whitewater Technologies, *BlueBox Intelligent Water Analytics System Brochure*, 2012
- [12] D. Hart, S. McKenna, K. Klise, V. Cruz and M. Wilson, CANARY: A Water Quality Event Detection Algorithm Development Tool. in *World Environmental and Water Resources Congress*, 2007.
- [13] World Health Organization *Guidelines for drinking-water quality*, fourth edition, 2011
- [14] European Communities *Drinking Water Regulations (No.2)*, 2007
- [15] U.S. Environmental Protection Agency 2012 Edition of the *Drinking Water Standards and Health Advisories*, EPA 822-S-12-001
- [16] J.C. Chou, C.C. Chen, and C.C. Lee, Development of Microcontroller Applied to Chlorine Ion Measurement System, *IEEE Sensors Journal*, vol. 12, no 6, pp. 2215-2221, 2012
- [17] M. Yunus and S. Mukhopadhyay, Novel planar electromagnetic sensors for detection of nitrates and contamination in natural water sources, *IEEE Sensors Journal*, vol. 11, no 6, pp. 1440-1447, 2011
- [18] C.N. Haas, M.A. Meyer, and M.S. Paller, Microbial alterations in water distribution systems and their relationship to physical-chemical characteristics, in *Journal of American Water Works Association*, 1983
- [19] K.N. Power and L.A. Nagy, Relationship between bacterial regrowth and some physical and chemical parameters within Sydney's drinking water distribution system, in *Water Research*, 1999

DEVELOPMENT OF HIGH PERFORMANCE MACHINING TECHNIQUES THROUGH DATA MINING AND INTERPRETATION: MODELLING FOR TEMPERATURE DISTRIBUTION OF NIMONIC 90

Kartik Mittal, Nitin Agrawal

Department of Mechanical Engineering, IIT Delhi

Email Id: kartikmittal.iitd@gmail.com, nitinagrawaljmp@gmail.com

Contact Number: 8010080095

Abstract- Nickel based super alloys are fast gaining relevance and importance in the aerospace and steam power industries, as they have high strength to weight ratio, and exhibit superior mechanical properties. In addition, they possess high resistance at high temperatures; maintaining their resistance to corrosion, thermal shock, creep and erosion at elevated temperatures. Nickel based alloys contain a high percentage of Nickel and Chromium elements, and a continuous face centered cubic austenitic phase with poor thermal diffusivity, which is formed after various surface treatments. The austenitic phase contributes to the high yield strength and results in poor machinability of Nickel based alloys.

The basic problem in machining of Nickel based alloys is their high chemical activity at high cutting forces and temperatures. Most of the tool coatings (TiN, TiC, TiSn, etc.) have higher chemical affinity with Nickel based alloys. So, chemical diffusion between the tool and the machined work-piece takes place, thus affecting the tool life and machined surface quality. To be able to accurately predict the temperature distribution across the Nickel based work piece, we developed a 3D simulation for temperature modelling of Nimonic 90 during turning and then contrasted the values predicted by the model with the actual experimental values. Tweaking the various variables, we can find out the optimum parameters to be used while machining so as to have the desired temperature distribution across the work piece.

Keywords- Nimonic 90, Temperature Modelling, Experimental Verification, Turning, Machining Parameters, Tool Wear, Deform 2D

Introduction

Nimonic 90 is a recently developed Nickel based heat resistant super alloy, with considerable content of Cobalt and Chromium. Machining of such heat resistant super alloys has been an ongoing research field due to increasing application of these alloys as well as the apparent problems with their processing, owing to their low thermal conductivity and high temperature strength.

Any variations in the machining process of the Nickel super alloys might deteriorate the quality and performance of the products made from them, which is of considerable significance in the aerospace industry. To predict the machining characteristics in advance and help reduce the cost of manufacturing resulting from improper machining, suitable modelling techniques are called for. Modelling is one of the most widely used tools in the study of machining processes due to its several advantages in design, validation and control of the machining process. The numerical simulation instead of relying on experimentation is very useful to predict the thermal and mechanical properties of both the work-piece and tool without spending undue time in experimentation. The accuracy of the simulation depends mainly on the input values which imparts huge importance to understanding how the input parameters effect the predictive machining model.

Vaz et al, (2007) attributed the complexity in modelling of metal cutting to the diversity of physical phenomena available, including thermo-mechanical coupling, contact-friction, and material failure. The large and localized plastic deformation and complex contact conditions are the principal difficulties one faces while modelling machining processes.

Finite Element Modeling is presently the most widely used modelling technique in the machining area owing to advances in the field of software computing. Ezilarasan et al., (2014) attributed the various physical phenomena taking place from micro to macro scale during machining for the interaction between the workpiece and tool becoming very complex and highly stochastic. In addition, several variables like the properties and condition of the work material, tool material, tool geometry, cutting parameters, dynamic performances of the machine tool and clamping conditions are also interlinked. Analysis and control thus naturally become a challenging task in any machining process, but modelling provides a solution to this. Since cutting force and temperature play a prominent role in dictating the performance of the machined surface of the work materials, this paper uses Finite Element Analysis to predict these machining characteristics.

While Lagrangian finite element formulation deforms the mesh grid along with the material, a Eulerian formulation of a continuous medium fixed the grid in space. This paper uses Deform 2D software, based on the implicit Lagrangian computation routine with continuous adaptive remeshing, for the FEM analysis. The Finite Element tool in the software is capable of converting large scale problems in magnitude and complexity into solvable 2D problems. The domain is divided into nodes and elements which store the values calculated at various time intervals during the simulation process. The large non-steady state calculations are reduced to smaller steady state equations and solved one step at a time over the course of the simulation.

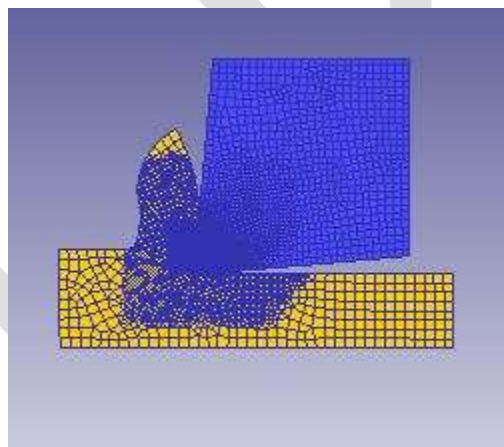


Fig.1: Simulation in Progress in DEFORM 2D

Modelling in Deform 2D occurs in three consecutive steps, Pre-processing, Simulation and Post-processing. The preprocessor uses a graphical user interface to assemble the data required to run the simulation. The orthogonal cutting process is modelled as a plane strain problem which assumes the geometry to have a unit depth with both front and back faces constrained. The simulation assumes that the objects will behave identically in any given cross-section across the width and height of the object. Data on conditions of the process environment, type of physical process and discrete time steps is fed to the pre-processor. It also generates a mesh within the workpiece and tool, after specifying their border geometry and taking data about the mesh density. To perform a simulation, a database containing the process data and simulation controls is prepared. The control, material, object and inter-object options of the

preprocessor allow for interactive input of the simulation parameters. The specified database is executed as simulation steps are generated. The results of the simulation are displayed through the post-processor in graphical and alphanumeric form.

Objectives and Deliverables

- *Temperature modelling of Nimonic 90 during turning:* A temperature model would be developed using Deform 2D for accurate prediction of work piece and tool characteristics through simulation.
- *Conducting a comprehensive Force Analysis:* Use the model so developed to measure the forces acting on tool in order to ensure the overall accuracy.
- *Verification of the theoretical model using experiments:* To compare the cutting force curve as well as the temperature profile generated using the theoretical model with the values obtained during experiments.

Literature Review

Nimonic alloys are one class of nickel based super alloys developed to give superior creep resistance and are commonly used in wrought form. Nimonic type alloys gain their superior high temperature properties basically from the precipitation of Ni-Al-Ti compounds within a Ni-Cr matrix. Raman and Padmanabhan, (1995) carried out a comparative study of AISI 304 LN stainless steel and Nimonic 90 under strain cycling and depicted the superior characteristics of Nimonic 90 over AISI 304. They showed the higher energy absorption capacity of Nimonic 90 as well as the fact that it exhibited longer fatigue lives at all strain amplitudes. Nimonic 90 also displayed a much shorter transition life, thus proving its superior credentials.

Maranhao and Davim, (2010) studied the influence of friction coefficient at the tool-chip interface on cutting and feed forces, cutting temperature, plastic strain and strain rate and maximum shear stress during machining of stainless steel. Their experimental validation revealed that friction modelling at the tool chip interface had a significant effect on the values of the modelled cutting parameters. It was thus shown that the friction coefficient has a huge bearing on cutting and feed forces, plastic strain and stress, as well as the cutting temperature and so, must be carefully chosen for precise results.

Numerous research papers have been published to evaluate the machining characteristics of nickel based alloys. Machining characteristics in the case of nickel based alloys take center stage as the life of components manufactured from these alloys depends intimately on these characteristics, which is of significant importance in industries like aerospace and steam power.

Aspinwall et al, (2007) studied the machining of nickel based alloys with profiled super abrasive grinding wheels experimentally while Kortabarria et al, (2011) developed different residual stress profiles using different dry facing conditions for Inconel 718. Wei, (2002) studied the feasibility of using milling or grinding as alternatives for the current EDM process to machine shaped hole in Inconel 718 while Soo. et al, (2011) estimated the machinability and surface characteristics of RR1000 Nickel based alloy in drilling and milling process.

One of the biggest applications of the Nimonic alloys is in the gas turbine aero engine industry, where designs strive to achieve greater power, reduced weight and improved fuel economy. Studies show that under the thermal and mechanical loading conditions experienced by turbine blades, the major deformation mechanisms are creep dominated. Creep life for any material depends intimately on its operating temperatures, and can be said to be halved for every 10-15 degree Celsius increase in temperature. This highlights the importance of study of the thermal characteristics during machining of Nimonic alloys. G. F. Harrison and T. Homewood, (1994) somewhat successfully demonstrated the use of the Graham and Walles Creep equation to predict the creep characteristics of Nimonic super alloys.

Developing a temperature model for turning of Nimonic 90 makes a study of its hot working characteristics essential. Srinivasan and Prasad, (1995) found the Nimonic alloys to exhibit a high temperature domain representing the process of dynamic recrystallization in their hot working processing maps, which can be attributed to the presence of carbon in the form of interstitials in the alloys. Also, Nimonic 90 was found to exhibit cracking at temperatures of less than 875 degrees Celsius, which is the γ' dissolution temperature.

The composition of Nimonic 90 comprises mainly of Nickel, Cobalt and Chromium.

Carbon.....	0.13 max.
Silicon.....	1.0 max.
Copper.....	0.2 max.
Iron.....	1.5 max.
Manganese.....	1.0 max.
Chromium.....	18.0-21.0
Titanium.....	2.0-3.0
Aluminum.....	1.0-2.0
Cobalt.....	15.0-21.0
Boron.....	0.02 max.
Sulfur.....	0.015 max.
Lead.....	0.0020 max.
Zirconium.....	0.15 max.
Nickel.....	Balance

Property	Metric	Imperial
Density	8.18 g/cm ³	0.296 lb/in ³
Melting point	1370 °C	2500 °F
Co-Efficient of Expansion	12.7 µm/m.°C (20-100 °C)	7.1x10 ⁻⁶ in/in.°F (70-212 °F)
Modulus of rigidity	82.5 kN/mm ²	11966 ksi
Modulus of elasticity	*213 kN/mm ² **227 / 240 kN/mm ²	30894 ksi 32924 / 34810 ksi

* Solution Annealed + Aged **Spring Temper and Aged

Article.aspx?ArticleID=4199

Methodology

Before embarking on the modelling and subsequent simulation of our model, we decided to become familiar with the material under study, i.e., Nimonic 90 by reading in depth about it. We became acquainted with the various uses of the material, as well as the numerous problems faced while machining it in order to derive relevance of its temperature modelling. We then conducted extensive research detailing the effect of various turning parameters on the temperature profile of the work-piece and read about the research work being done on developing temperature profiles during machining of other Nickel based work-pieces. This extensive literature review enabled us to become familiar with the material as well as the process and the subsequent effects of varying parameters.

The next objective was to develop a theoretical model that could accurately depict the temperature profile of the work-piece with varying process parameters. Firstly, the super alloy's composition as well its physical properties as a function of temperature were procured and then used to define Nimonic 90 as a new material in the software. The tool insert to be used for experiments was then finalized to be CNMG 120408-THM, a high performance Tungsten Carbide (WC) insert. Its geometrical properties were then found

and used to design the insert in the SolidWorks CAD package. The simple workpiece designer provided in Deform 2D was used to develop a prototype of the work piece as temperature profile is largely independent of the size of the workpiece.

The default temperature of both the workpiece and tool was taken to be 35 degrees Celsius. Since no lubricants were used during experimental validation, the heat transfer coefficient was taken at its default value of (45 N/sec/mm/C) while the friction coefficient was modified to 0.6 as this displayed the best correlation with the experimental results. The mesh density was taken to be 2000 for the tool insert, with relative positioning while the workpiece had 25 elements through uncut chip thickness. The simulation steps were taken to be 1500, with data being saved after every 10 steps. For calculating the tool wear, the following model was used.

$$w = \int apVe^{-b/T} dt$$

P = interface pressure;
v = sliding velocity;
T = interface temperature (in degrees absolute);
dt = time increment;
a,b = experimentally calibrated coefficients

After careful setup of all the input parameters, the model was then simulated to generate the temperature profile, load diagram, the stress map, strain and velocity profiles among other information.

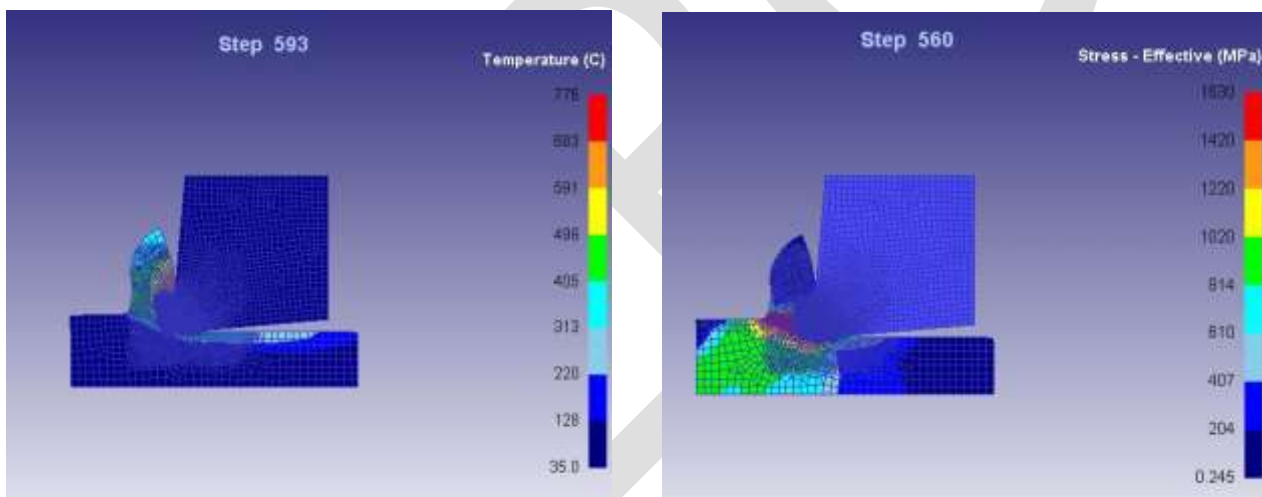


Fig. 2: a) Temperature Profile, b) Effective Stress Map developed using theoretical model at Vc = 40m/min and Feed Rate = 0.12 mm/rev

The modelling was done across a 5*5 matrix, with cutting velocity varying from 20 m/min to 100 m/min and the feed rate changing from 0.06 mm/rev to 0.14 mm/rev. For the purpose of experimental validation, observations were taken only across a 2*2 matrix with cutting velocity at 40 m/min and 60 m/min and the feed rate at 0.06 mm/rev and 0.08 mm/rev. Any more experimental data would have been redundant since if the model correlated well with the experimental results for these input parameters, it would be a reliable model and would be able to predict accurately the characteristics for other input parameters too.

Due to a lack of hardware, the temperature profile validation was unfortunately not possible. Resultantly, only the cutting forces analysis using a Kistler piezo- electric tool post dynamometer was conducted with a Nimonic 90 work piece and CNMG 120408-

THM insert. The resultant cutting force curves were recorded and compared with the theoretical model's predictions for similar input parameters.

Results

As predicted by the model thus developed, the work piece temperature variation with time has been plotted for a constant cutting speed of 20 m/min and feed rates varying from 0.06 mm/rev to 0.14 mm/rev. As Fig 3. Clearly depicts, the work piece temperature rises with increasing feed rate for a constant cutting velocity, which correlates well with the experimental results and is consistent with the theoretical background.

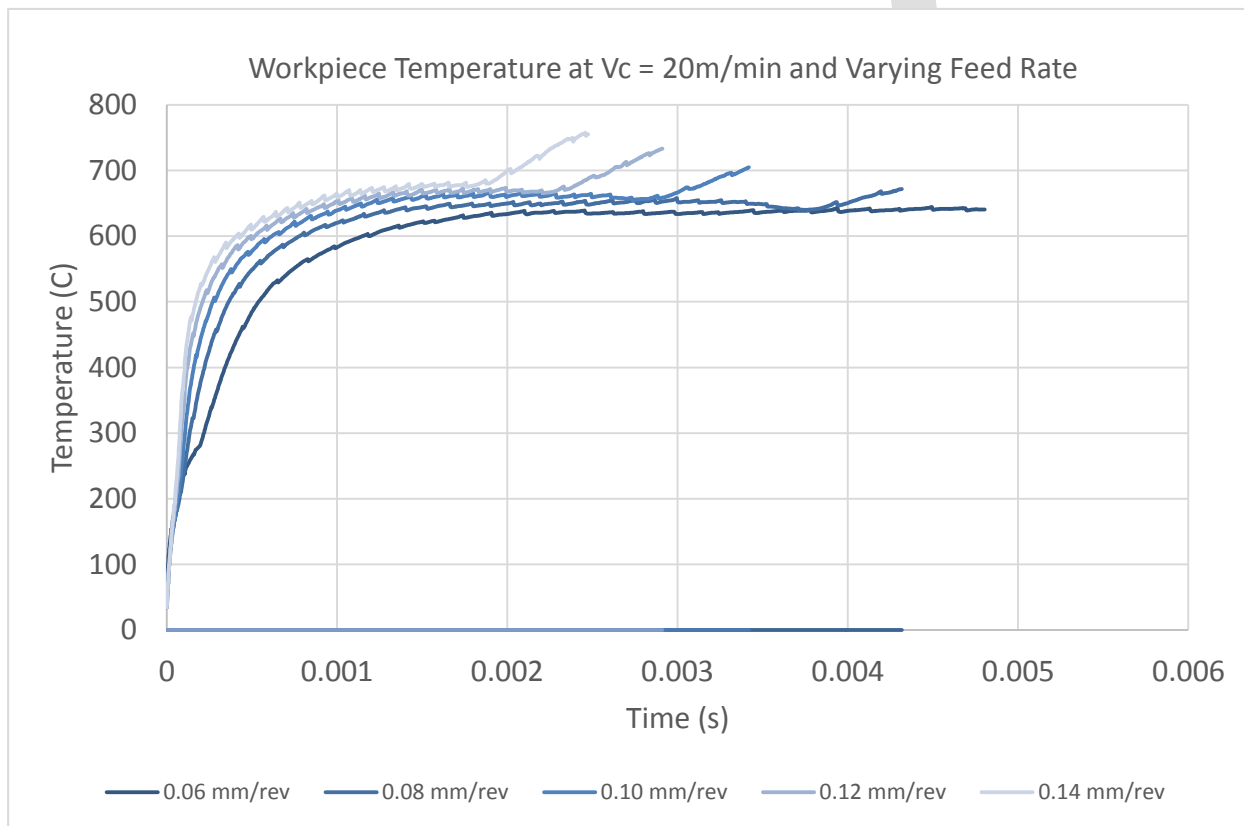


Fig. 3: Workpiece temperature at constant cutting velocity and varying feed rate

A plot of the work piece temperature at a constant feed rate of 0.08 mm/rev and increasing cutting velocity has been plotted in Fig. 4. As expected, the work piece temperature rises with rising cutting velocity due to the generation of increasing frictional force. A notable observation is that the work piece temperature distribution is more diffused and spaced for the varying cutting speed case as against the varying feed rate case where the curves almost coincide.

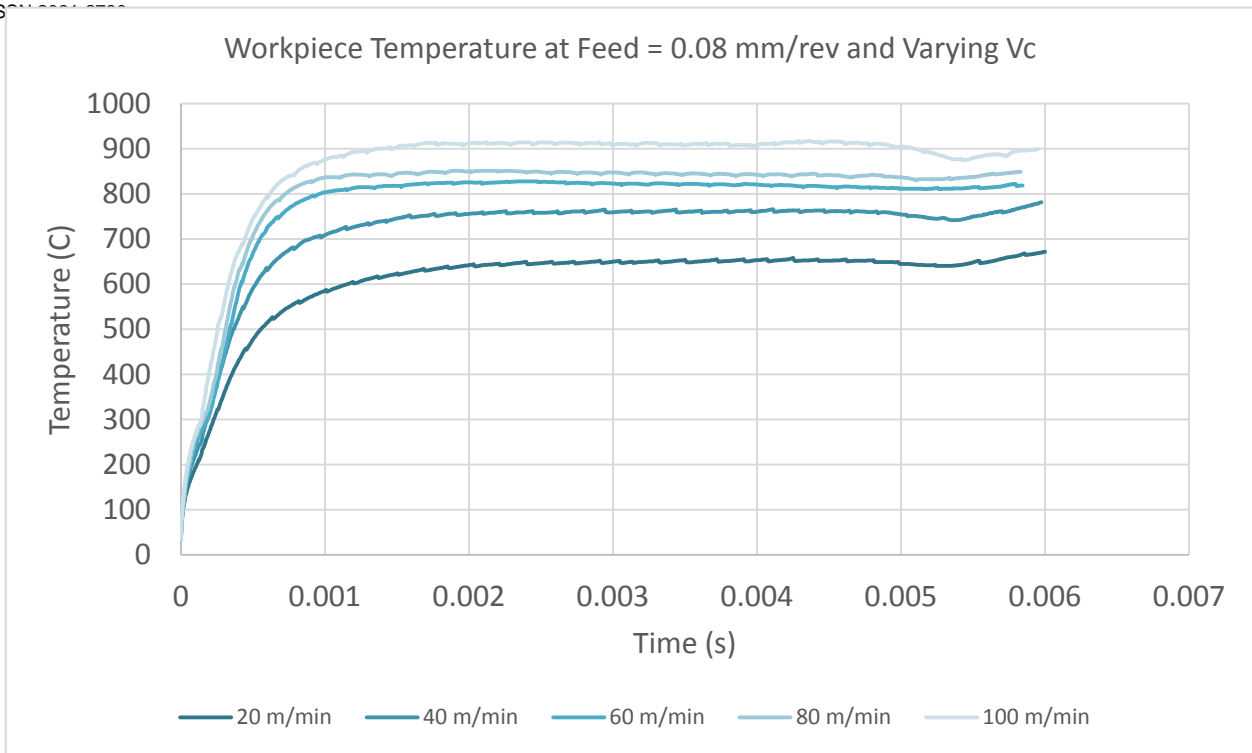


Fig. 4: Workpiece temperature for varying cutting velocity and at a constant feed rate

Similarly, the tool temperature for constant cutting speed and varying feed rate as well as at constant feed rate and varying cutting velocity has been plotted in Fig. 5 and 6 respectively. They show a similar trend as for the workpiece, that is, the temperature rises with increasing cutting velocity as well as feed rate. This is to be expected as has been shown in numerous experiments historically and has been proven through several theories.

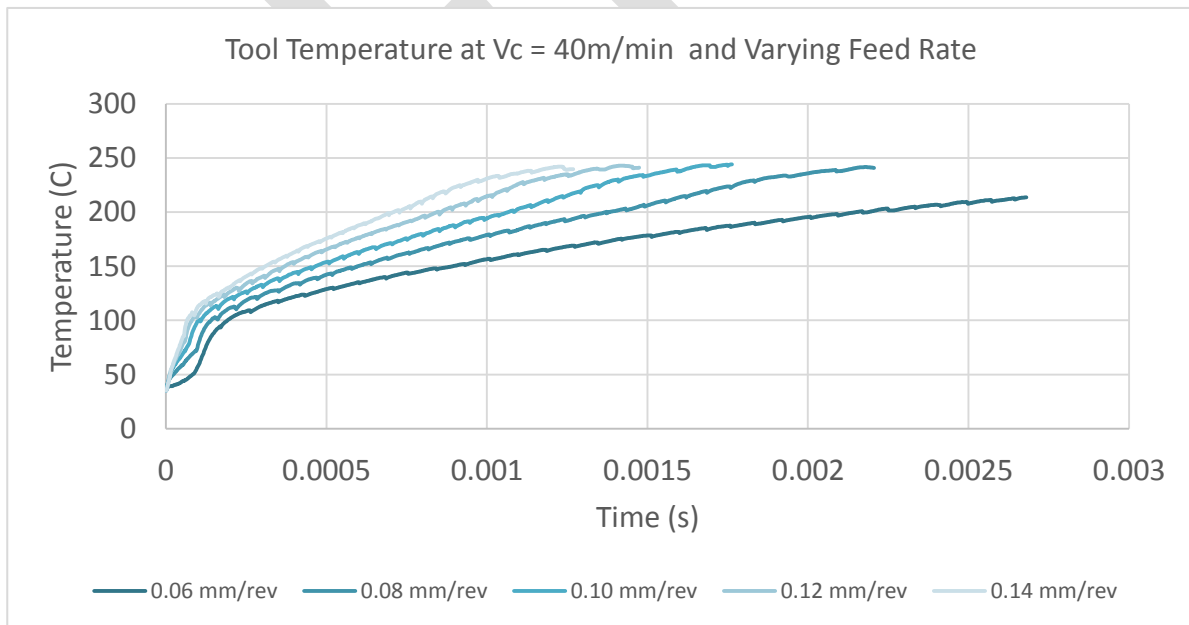


Fig. 5: Tool temperature at constant cutting velocity and varying feed rate

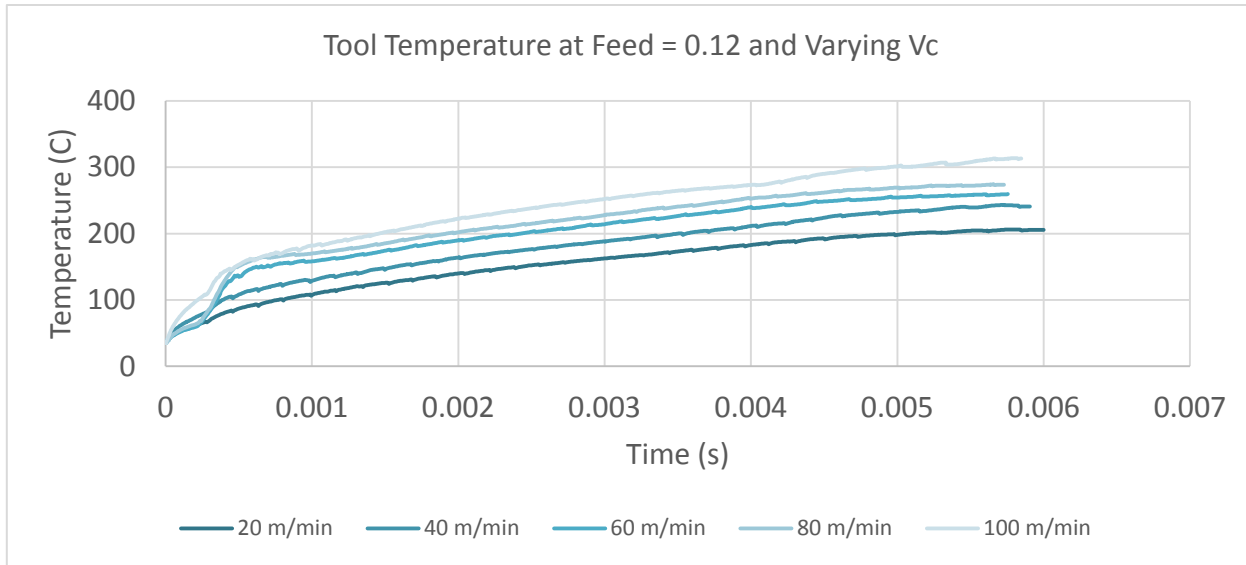


Fig. 6: Tool temperature at constant feed rate and varying cutting velocity

	0.06 mm/rev	0.08 mm/rev	0.10 mm/rev	0.12 mm/rev	0.14 mm/rev
20 m/min	640.4	671.8	704.8	733	757.7
40 m/min	758	781	807.5	839.4	860
60 m/min	821	825.6	839.1	849	853.3
80 m/min	847.1	849.4	864	875.2	880.4
100 m/min	911.4	916	919	946.4	953

Fig. 7: Maximum Work-piece Temperature with varying Cutting velocity and Feed rate

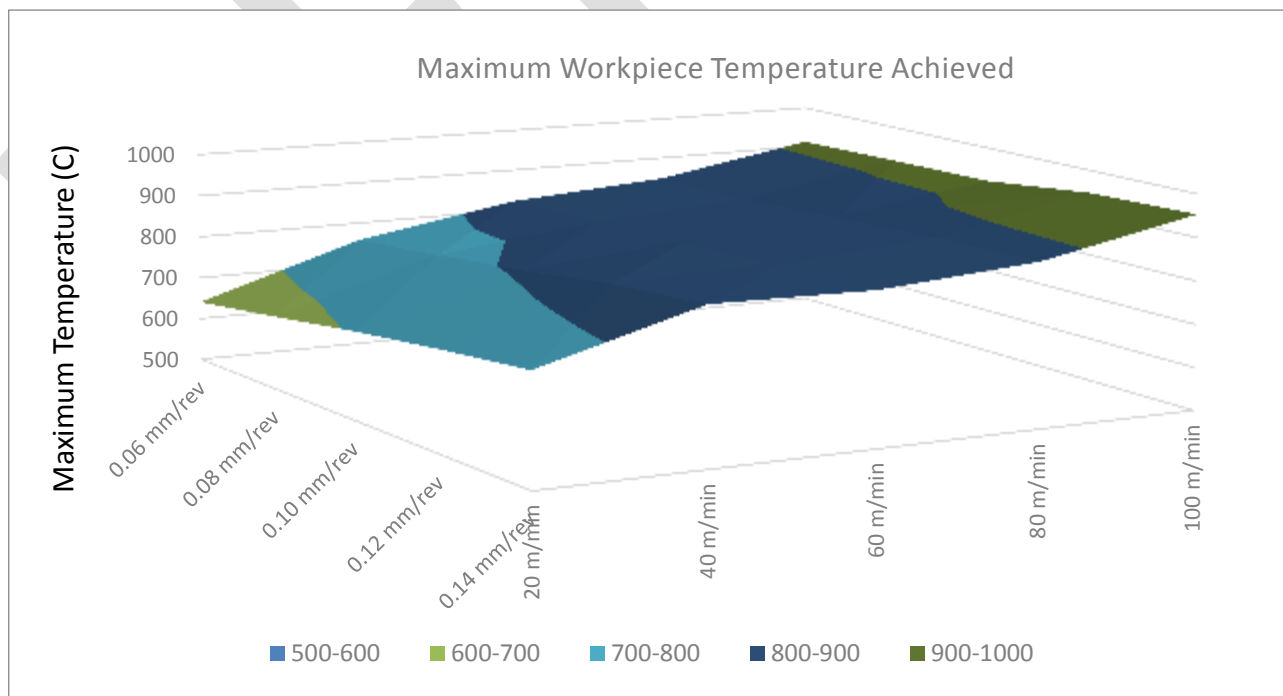


Fig. 8: 3D Plot showing the variation of Maximum Work-piece temperature with Cutting Velocity and Feed Rate

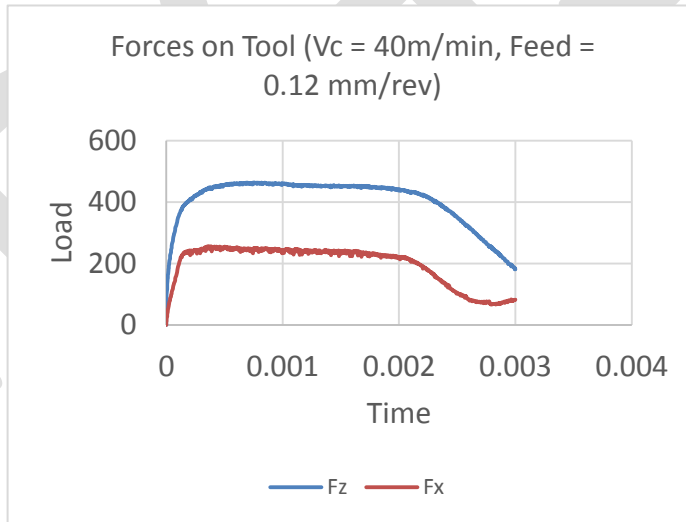
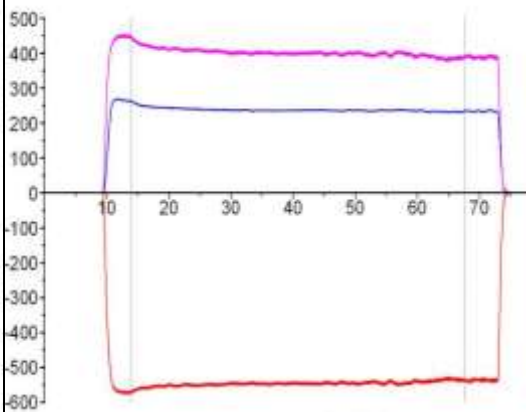
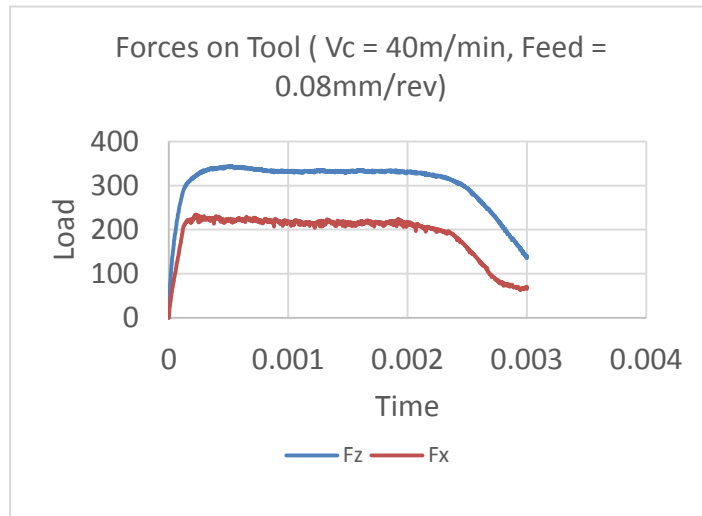
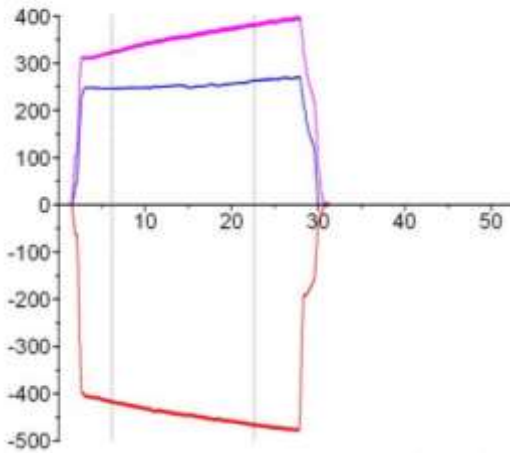


Fig. 10

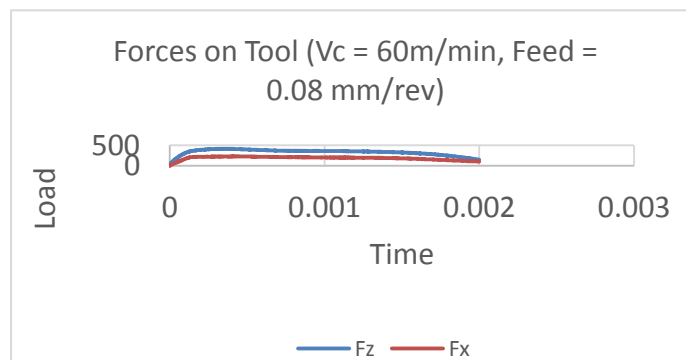
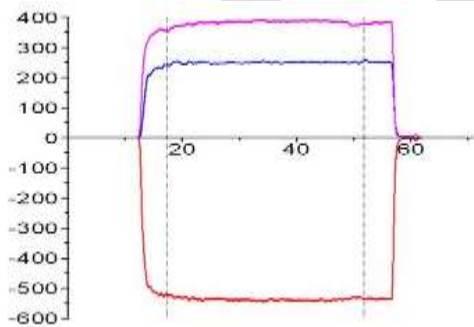


Fig. 11

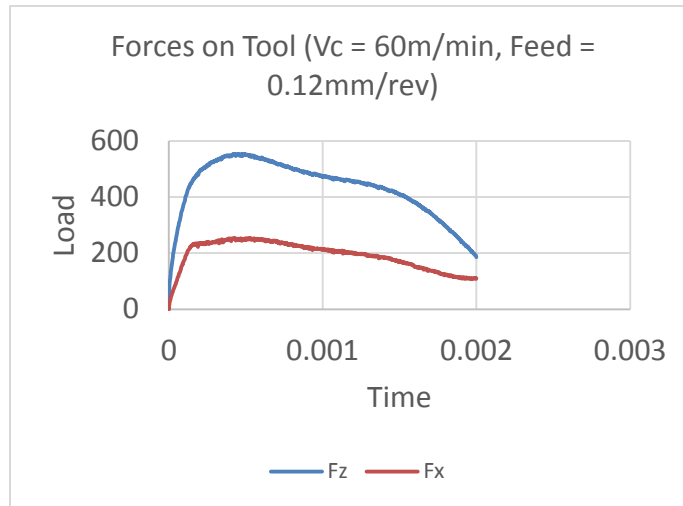
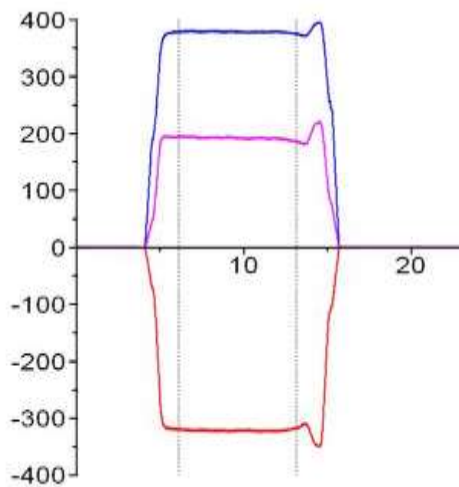


Fig. 12

Figures 9, 10, 11 and 12 show the experimental observations as well as the theoretical predictions for the forces acting on the tool for a 2*2 matrix of varying cutting velocity as well feed rate. The figures clearly depict that the theoretical predictions for the cutting forces are quite close and within the margin of error, thus correlating well with the experimental findings. The cutting forces show a marked increase with rising feed rate for a constant velocity while they are almost constant when the feed rate is held constant and cutting velocity is increased. This is consistent with the theoretical background of the effect of cutting velocity and feed rate on the cutting forces. The model thus turns out to be quite reliable while simulating and predicating the cutting forces.

Conclusion

While the experimental validation for temperature profiling could not be conducted due to lack of appropriate hardware, it can be concluded that since the model correlates well with the experimental results for cutting speed and proves to be quite reliable, it is expected to be accurate while predicting temperature profiles too. The model thus developed is quite consistent with experimental findings and may well be used in the future for accurate prediction of temperature and cutting forces during turning of Nimonic 90.

REFERENCES:

- [1] Vinod Kumar, Kamal Jangra and Vikas Kumar, "Effect of WEDM parameters on machinability of Nimonic 90", National Conference on Trends and Advances in Mechanical Engineering, YMCA University of Science & Technology, Faridabad, Haryana, Oct 19-20, 2012
- [2] G. F. Harrison and T. Homewood, "The application of the Grahan and Walles Creep Equation to Aeroengine superalloys"
- [3] S. Ganesh Sundara Raman and K. A. Padmanabhan, "A comparison of the room temperature behavior of AISI 304 LN stainless steel and Nimonic 90 under strain cycling", *Int. J. Fatigue*, Vol. 17, No. 4, pp. 271-277, 1995
- [4] D.C. Lou, J.K. Solberg, O.M. Akselsen, N. Dahl, "Microstructure and property investigation of paste boronized pure nickel and Nimonic 90 superalloy", *Materials Chemistry and Physics* 115 (2009) 239–244
- [5] N. Srinivasan and Y. V. R. K. Prasad, "Hot working characteristics of Nimonic 75, 80A and 90 superalloys: A comparison using processing maps", *Journal of Materials Processing Technology* 51 (1995) 171-192
- [6] C. Ezilarasan, V.S. Senthil kumar, A. Velayudham, "Theoretical predictions and experimental validations on machining the Nimonic C-263 super alloy", *Simulation Modelling Practice and Theory* 40 (2014) 192–207

- [7] C.A. Van Luttervelt, T.H.C. Childs, I.S. Jawahir, F. Klocke, P.K. Venuvinod, Y. Altintas, E. Armarego, D. Dornfeld, I. Grabec, D. Lindstrom, B. Leopold, D. Lucca, T. Obikawa, H. Shirakashi H. Sato, "Present Situation and Future Trends in Modelling of Machining Operations", Progress Report of the CIRP Working Group 'Modelling of Machining Operations', Annals of the CIRP 47 (1998) 587–626.
- [8] J. Paulo Davim, P. Reis, C. Maranhao, "Finite element simulation and experimental analysis of orthogonal cutting of an aluminium alloy using polycrystalline diamond tools", Int. J. Mater. Product Technol. 37 (2010).
- [9] M. Vaz Jr., D.R.J. Owen, V. Kalhori, M. Lundblad, L.-E. Lindgren, "Modelling and simulation of machining processes", Arch Comput. Methods Eng. 14 (2007) 173–204.
- [10] C. Maranhao, J. Paulo Davim, "Finite element modelling of machining of AISI 316 steel: numerical simulation and experimental validation", Simulat. Modell. Pract. Theory 18 (2010) 139–156.
- [11] E. Ceretti, C. Lazzaroni, L. Menegardo, T. Altan, "Turning simulations using a three-dimensional FEM code", J. Mater. Process. Technol. 98 (2000) 99–103.
- [12] W. Grzesik, M. Bartoszuk, P. Niesłony, "Finite element modelling of temperature distribution in the cutting zone in turning processes with differently coated tools", Proceedings of the 13th International Scientific Conference on Achievements in Mechanical and Materials Engineering, Poland, 2005, pp. 18–19.
- [13] E. Ceretti, "FEM simulations of segmented chip formation in orthogonal cutting: further improvements", Proceedings of the CIRP International Workshop on Modeling of machining Operations, Atlanta, GA, 1998, pp. 257–263.
- [14] S.L. Soo, D.K. Aspinwall, R.C. Dewesa, "3D FE modelling of the cutting of Inconel 718", J. Mater. Process. Technol. 150 (2004) 116–123.
- [15] Aspinwall D.K., Soo S.L., Curtis D.T., Mantle A.L. (2007), "Profiled Superabrasive Grinding Wheels for the Machining of a Nickel Based Superalloy". Annals of the CIRP Vol. 56, pp 335-338.
- [16] Kortabarria A., Madariaga A., Fernandez E., Esnaola J.A., Arrazola P.J, (2011) "A comparative study of residual stress profiles on Inconel 718 induced by dry face turning". Procedia Engineering 19, pp 228 – 234.
- [17] Wei X. (2002), "Experimental study on the machining of a shaped hole Ni – based super – heat –resistant alloy". Journal of materials Processing Technology 129, pp 143-147.
- [18] Soo S.L., Hood R. , Aspinwall D.K. , Voice W.E., Sage C. (2011), "Machinability and surface integrity of RR1000 nickel based superalloy". Manufacturing Technology 60, pp 89–92

Spectrum Sensing In TVFF Channels for Cognitive Radios with Combined Sensing Technique

Anoop S, Nirosha R

PG Scholar, Department of ECE, CAARMEL Engineering College, Pathanamthitta, Kerala
Assistant Professor, Department of ECE, CAARMEL Engineering College, Pathanamthitta, Kerala

Email:anoopspillai004@gmail.com

Abstract: Cognitive radios are indispensable to shift paradigm from conventional exclusive spectrum assignment to dynamic spectrum access. They can boost up spectrum utilization significantly, by dynamically accessing unused primary spectrum while bringing no harm to primary users. The envisioned radio calls for fast and accurate spectrum sensing. Researchers are focusing on cooperative spectrum sensing to improve reliability but still there is room for improvement in local spectrum sensing. In cooperative spectrum sensing, it will be hard to cooperate with local network nodes in a short time as cognitive radio has to operate in heterogeneous wireless networks. Most of the renowned local spectrum sensing technique in the literature up to now is matched detection, although it is reliable but computationally complex. Other well-known local sensing techniques are energy detection and matched filter detection. This paper proposes an adaptive local spectrum sensing scheme, in which cognitive radio can adopt one-order matched filter or energy detector for spectrum sensing on the basis of estimated SNR, which is calculated in advance for available channels. Simulation results indicate that we can achieve reliable results equal to one-order matched filter detection with less mean detection time.

Keywords: Cognitive radio networks, Spectrum sensing, Energy detection, Matched filter detection.

INTRODUCTION

With the increase of customers in wireless network services, the demand for radio spectrum is also increasing significantly. The trend of new wireless devices and applications is expected to continue in coming years which will increase the demand for spectrum. The conventional fixed spectrum assignment policy is a big hurdle in the innovation of new technologies. In 2008, the Federal Communication Commission (FCC) allowed the unlicensed fixed and personal/portable devices in rural and urban area [1].

Cognitive Radio (CR) is a key technology that can help mitigate scarcity of spectrum. The most essential task of CR is to detect licensed user/Primary User (PU); if PU is absent, then spectrum is available for cognitive radio user/Secondary User (SU) and is called spectrum hole/white space. The process of detection of PU is achieved by sensing radio environment and is called spectrum sensing [2-4]. The prime concerns of spectrum sensing are about two things first, the primary system should not be disturbed by Communication and secondly, spectrum holes should be detected efficiently for required throughput and quality of service (QoS) [5].

RELATED WORK

Here in this thesis we are considering the main two spectrum sensing techniques for cognitive radios which are energy detection and matched filter detection. Energy detection is a simple technique that has short sensing time, but its performance is poor under low Signal to Noise Ratio (SNR) conditions [12]. The firmness on whether the signal is present or absent on the channel can be expedited if we pass the signal through a filter that will accentuate the useful signal and suppress the noise signal [11]. A Matched Filter will peak out the signal component at some instant of time and suppress the noise amplitude at the same time. If Signal is present on the channel, a large peak at this instant will occur and if the signal is absent, no such peak will appear. This prearrangement will make it possible to decide whether the signal is present or not in the channel. A matched filter detection technique is the optimal linear filter used to maximize the signal to noise ratio (SNR) in the presence of additive white Gaussian noise [9]. Cooperation among CUs are established to estimate the PU's presence or absence, fusion Centre (FC) is used to take the overall resolution about the PU's.

ENERGY DETECTION METHOD

Figure 1 depicts the block diagram of the energy detector. The elementary approach behind the energy detector is the estimation of the power of the received signal $r(t)$ [8]. To evaluate the power of the received signal, the output of the band pass filter of bandwidth W is

squared and integrated over an interval T. Finally, the integrated value is compared with a threshold λ_1 to decide whether the PU is present or not .

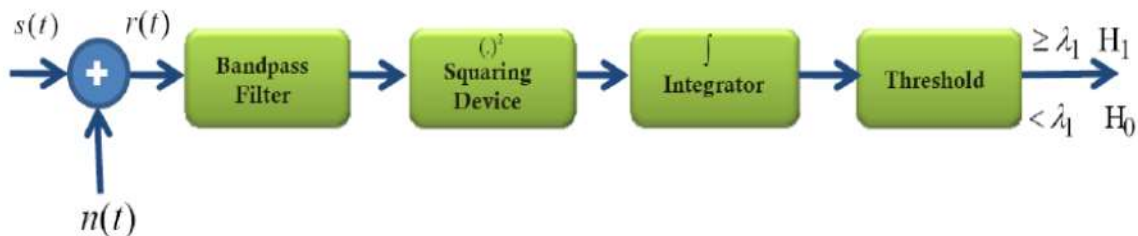


Fig 1: Block diagram of energy detection

The block diagram for the energy detection technique is shown in the Figure 1. In this method, signal is passed through band pass filter of the bandwidth W and is integrated over time interval. The output from the integrator block is then compared to a predefined threshold. This comparison is used to discover the existence of absence of the primary user [7]. The threshold value can set to be fixed or variable based on the channel conditions. The ED is said to be the Blind signal detector because it ignores the structure of the signal. It estimates the presence of the signal by comparing the energy received with a known threshold ν derived from the statistics of the noise. Analytically, signal detection can be reduced to a simple identification problem, formalized as a hypothesis test,

$$y(k) = n(k) \dots \dots \dots H_0$$

$$y(k) = h * s(k) + n(k) \dots \dots \dots H_1$$

Where $y(k)$ is the sample to be analysed at each instant k and $n(k)$ is the noise of variance σ^2 . Let $y(k)$ be a sequence of received samples $k \in \{1, 2, \dots, N\}$ at the signal detector, then a decision rule can be stated as,

$$H_0 \dots \text{if } \epsilon < \nu$$

$$H_1 \dots \text{if } \epsilon > \nu$$

Where $\epsilon = |E y(k)|^2$ The estimated energy of the received signal and ν is chosen to be the noise variance σ^2 [10].

MATCHED FILTER METHOD

A matched filter (MF) is a linear filter designed to maximize the output signal to noise ratio for a given input signal [3]. When secondary user has a priori knowledge of primary user signal, matched filter detection is applied. Matched filter operation is equivalent to correlation in which the unknown signal is convolved with the filter whose impulse response is the mirror and time shifted version of a reference signal [6]. The operation of matched filter detection is expressed as:

$$Y[n] = \sum_{k=-\infty}^{\infty} h[n - k] x[k] \quad (3)$$

Where 'x' is the unknown signal (vector) and is convolved with the 'h', the impulse response of matched filter that is matched to the reference signal for maximizing the SNR [2]. Detection by using matched filter is useful only in cases where the information from the primary users is known to the cognitive users [10].



Fig 2: Block diagram of Matched Filter Detection

Figure 3.6 depicts matched filter based spectrum sensing method for primary user detection [5]. Considering that a complete signal information of the primary user signal is required in this case the matched filter method is not really recommended by the system designers to suit our purpose here unless when the complete signal information is known to the secondary user.

THE COMBINED SENSING TECHNIQUE

Here we are combining the two well-known sensing techniques explained above for the better sensing results [1]. The block diagram representation of such an idea is shown below in Fig 3.

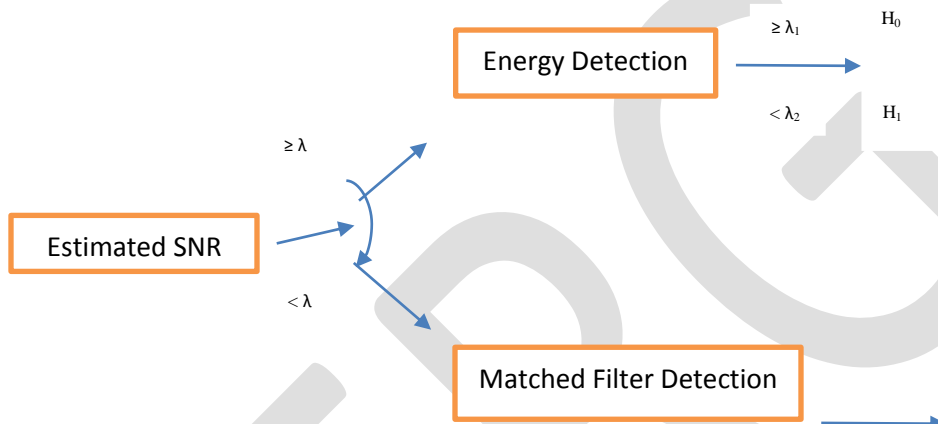


Fig 3: Block diagram of combined sensing technique.

In this method first we find the SNR from the environment and according to a threshold value the signal is fed to either Energy detection method or Matched filter method. If the value is less than or equal to the threshold we fed it to ED and if not then fed it to MF detector. By doing so the effective sensing efficiency is improved and we obtain a better probability of detection than if either of one is individually used[4].

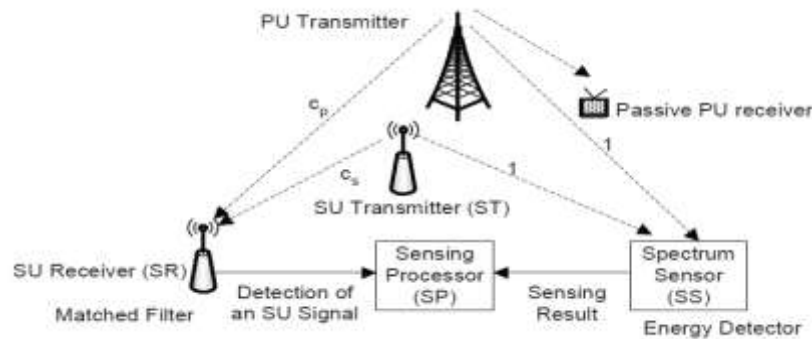


Fig 4: Working of combined sensing method.

Simulation Results

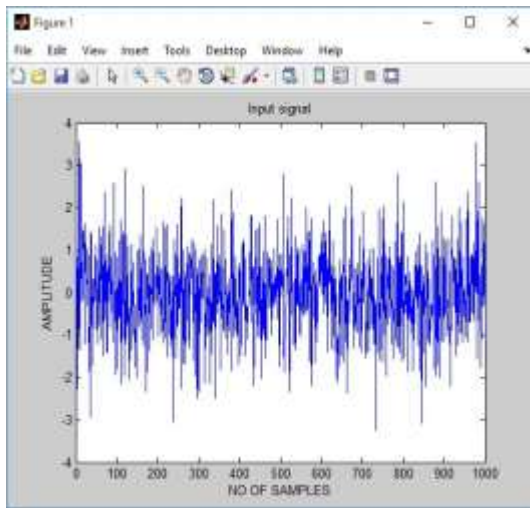


Fig 5: Input Signal

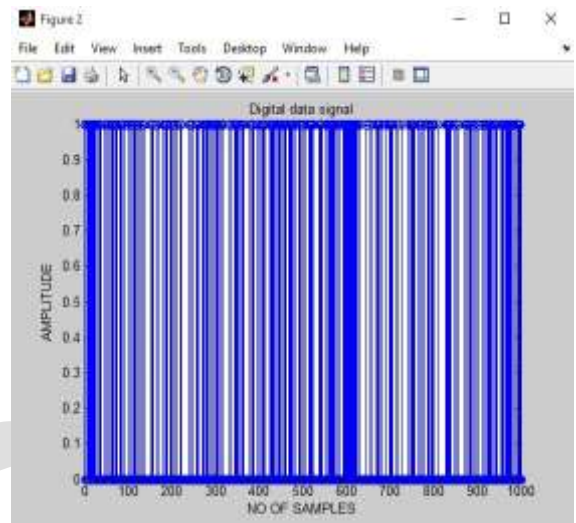


Fig 6: Digital Data Signal

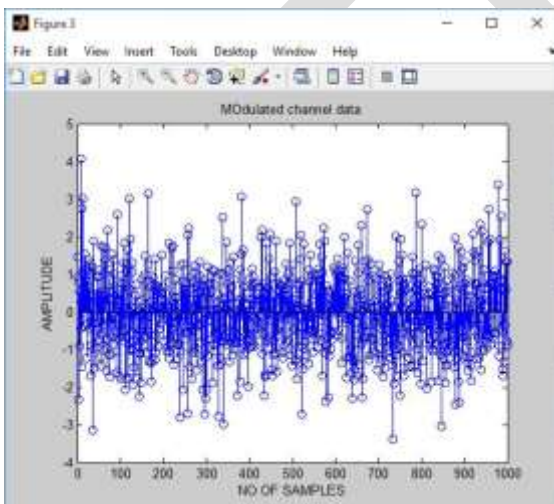


Fig 7: Modulated Channel Data

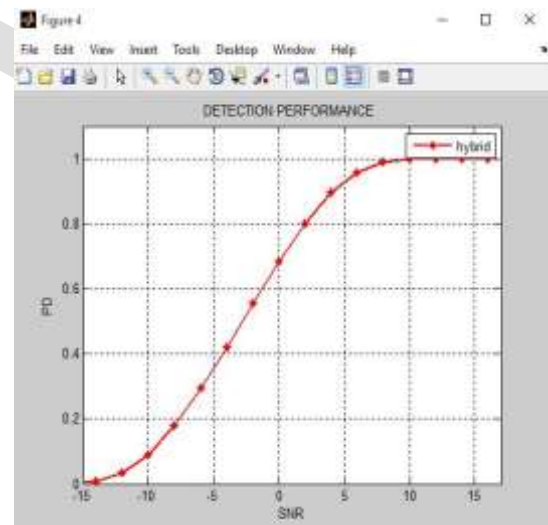


Fig 8: Detection Performance

Conclusion

In order to sense the spectrum holes consistently and resourcefully, in this paper we propose matched filter and ED method based cooperative spectrum sensing in CR networks. Here we adapt the advantages of both Energy detection methods and Matched Filter Detection method. Initially we are taking the signal data and fed it to both these detectors and by acting as a combined unit the resultant detection process stands out among the individual performances.

REFERENCES:

- [1] S. Haykin, "Cognitive Radio: Brain-Empowered Wireless Communications", IEEE Journal on Selected Areas in Communications, vol. 23,2005, pp. 201-220.
- [2] K. Yau, P. Komisarczuk and P.D. Teal, "Cognitive Radio-based Wireless Sensor Networks: Conceptual Design and Open Issues", IEEE34th Conference on Local Computer Network,2009, pp. 955-962.
- [3] Federal Communications Commission (FCC), Spectrum Policy Task Force, ET Docket no.2,2002, pp. 1-135.
- [4] R.W. Broderson, A. Wolisz, D. Cabric, S.M.Mishra and D. Willkomm, "CORVUS: A CognitiveRadio Approach for Usage of Virtual Unlicensed Spectrum", White Paper, University of California, Berkeley, Technical Report, 2004.
- [5] A. Ghasemi and E.S. Sousa, "Collaborative Spectrum Sensing for Opportunistic Access in Fading Environments", Ist IEEE Symposium onNew Frontiers in Dynamic Spectrum Access Network, 2005, pp. 131-136.
- [6] F. F. Digham, M.S. Alouini and M.K. Simon,"On the Energy Detection of Unknown Signals Over Fading Channels", IEEE International Conference on Communications, vol. 5, 2003,pp. 3575-3579.
- [7] Lei Zhang and Shaquan Xia, "A New Cooperative Spectrum Sensing Algorithm for Cognitive Radio Networks", Proceedings of ISECS International Colloquium on Computing, Communication, Control, and Management, vol. 1, 2009,pp. 107-110.
- [8] Sina Maleki, Sundeep Prabhakar Chepuri andGeert Leus, "Energy and Throughput Efficient Strategies for Cooperative Spectrum Sensing in Cognitive Radios", IEEE 12th InternationalWorkshop on Signal Processing Advances inWireless Communications, 2011, pp. 71-75.
- [9] Z. Quant, S. Cui and A.H. Sayed, "Optimal Linear Cooperation for Spectrum Sensing in Cognitive Radio Networks", IEEE Journal of Selected Topics in Signal Processing, vol. 2,2008, pp. 28-45.
- [10] T. Kieu-Xuan and I. Koo, "A Cooperative Spectrum Sensing Using Fuzzy Logic for Cognitive Radio Networks", KSII Transactions on Internet and Information Systems, vol. 4, 2010, pp. 289-304.
- [11] T. Kieu-Xuan and I. Koo, "Cooperative Spectrum Sensing using Kalman Filter based Adaptive Fuzzy System for Cognitive Radio Networks",KSII Transactions on Internet and Information Systems, vol. 6, 2012, pp. 287-304.
- [12] Waleed Ejaz, Najam Ul Hasan and Hyung SeokKim, "SNR Based Adaptive Spectrum Sensing for Cognitive Radio Networks", International Journal of Innovative Computing, Information and Control, vol. 8, 2012, pp. 6095-6105.

Detection of Ovary Cyst using Kirsch Template

Anju R.S

P.G Scholar, Dept of CSE, BMCE, Kollam, Kerala, India

anjurs89@gmail.com

Radhakrishnan B

Professor, Dept. of CSE, BMCE, Kollam, Kerala, India

radhak77@rediffmail.com

Abstract: Ultrasound imaging of ovary is used to determine infertility problems. Now a days it is quite common. For effective treatment, information like shape, position, size and presence of cyst are important. Today detection of cyst is done by medical experts in non automatic way. This method often results inaccurate and incorrect determination. In this paper, a new automatic detection of follicles in ultrasound images of ovary is proposed. Four stages are involved like preprocessing, segmentation, feature extraction and classification. In preprocessing stage gaussian low pass filter is used for removing speckle noise in ultrasound image of ovary. Proposed algorithm use kirsch template for segmentation. Features extracted from the segmented image is used to classify normal ovary or cystic ovary.

Keywords: Ovary, Ultrasound image, Follicle, gaussian low pass filter, Speckle Noise Kirsch template, Feature Extraction.

1. INTRODUCTION

The ovary is an ovum-producing reproductive organ, often found in pairs as part of the vertebrate female reproductive system[1]. The ovaries are the site of production and periodical release of egg cells, the female gametes. In the ovaries, the developing egg cell (or oocyte) grows within the environment provided by follicles. Follicles are composed of different types and number of cells according to the stage of their maturation, and their size is indicative of the stage of oocyte development[2].

An ovarian cyst is any fluid-filled sac within the ovary. Most ovarian cysts are related to ovulation being either follicular cysts or corpus luteum cysts. Other types include cysts due to endometriosis, dermoid cysts, and cystadenomas[3]. Many small cysts occur in both ovaries in polycystic ovarian syndrome. Pelvic inflammatory disease may also result in cysts. Rarely cysts may be a form of ovarian cancer. Diagnosis is undertaken by pelvic examination with an ultrasound or other testing used to gather further details[4].

Ultrasound is sound waves with frequencies which are higher than those audible to humans. Ultrasound images also known as sonograms are made by sending pulses of ultrasound into tissue using a probe. The sound echoes off the tissue; with different tissues reflecting varying degrees of sound. These echoes are recorded and displayed as an image to the operator[5]. By analyzing ultrasound image of ovary help the doctor to determine whether it is cystic or not. Sometimes cyst may lead to infertility problems. For proper treatment of infertility, information like shape size, position are important. Non automatic detection of cyst in ultrasound image can be very demanding and inaccurate. To overcome those problems an automatic method is desirable. In this paper, a new automatic detection of cyst is proposed.

The literature on computer assisted approaches for follicle detection is rare. Potocnik and Zazula segmented ultrasound image of ovary using optimal thresholding[6]. This method use edges for finding ovary boundaries and thresholding. But it does not give optimal results. Again they were use active contour method for segmentation. But it is difficult to determine the parameters for snakes automatically[7]. Cigale and Zazula use cellular neural network for follicle segmentation. It was not promising work. Main disadvantage in this method is difficult to find the parameters for determining follicles[8]. Hiremath and Tegnoor segmented ultrasound image of follicle using edge based segmentation. Gaussian low pass filter is used in the preprocessing stage for noise removal[9]. Ultrasound images have high amount of speckle noise. The speckle is most often considered a dominant source of multiplicative noise and should be filtered out without affecting important features of the image[10].

In this paper, a new and improved algorithm for follicle detection is proposed. Four stages involved like preprocessing, segmentation, feature extraction and classification. Here speckle noise in the ultrasound image is reduced by using gaussian low pass filter and kirsch template method is used for segmentation. Features are extracted from the segmented image is used for classification. Main objective of this paper is to classify normal ovary and cystic ovary.

The paper is organized as follows. In section 2 describes new and improved proposed method for follicle determination. In section 3 shows the experimental results and section 4 concludes the paper.

2. METHODOLOGY

Ovarian follicles are spherical fluid- filled structures [8]. They grow from 8 to 10 mm on an average. Only the dominant follicle can reach as much as 17 to 25 mm in diameter . The small follicles of 2 to 3 mm can also be perceived in the ultrasound images of ovaries. In the middle of the ovary, other structures can also be found, such as blood vessels, lymphatic glands.

The block diagram used for follicle detection in this proposed method is shown in fig.1[11].Ultrasound image is an input to the algorithm. Our aim is to locate cystic portion from the image. Within the study of female fertility it is essential to know what your ovarian reserve is. Currently is still counting ovarian follicles, the truest estimate of ovarian reserve in a given patient. Ultrasound also allows us to follow the evolution and growth of follicles both in spontaneous cycle as in a stimulated cycle fertility treatment[12]. Sample ultrasound image is shown in fig.2. By this proposed algorithm we can know about the status of ovary whether it will affect infertility.

In this method mainly four steps are involved. Ultrasound image is preprocessed by Contourlet transform. Speckle noise can be reduced by this denoising method compared to gaussian low pass filter. Kirsch template is used for segmenting cystic portion from remaining region. Then features are extracted from the segmented image like major axis and minor axis. These features are used for classification.

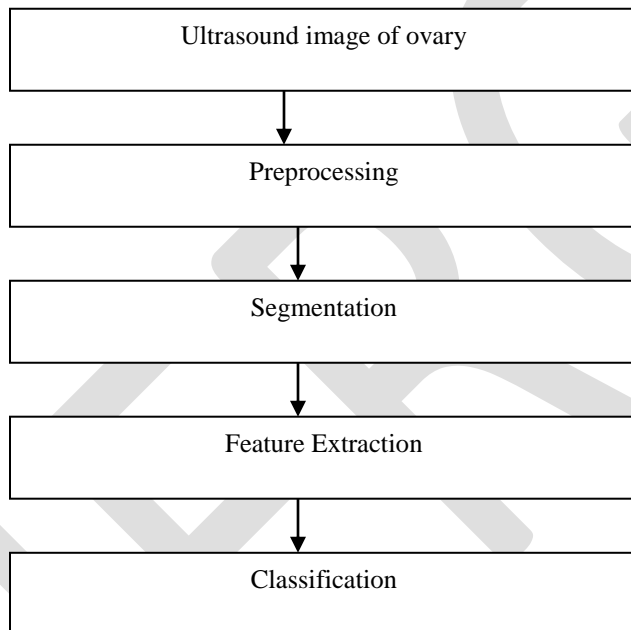


Fig.1 Block diagram of proposed algorithm



Fig.2 Sample ultrasound image of ovary

A. Preprocessing

An efficient representation of visual information is one of the important tasks in image processing applications such as denoising. Ultrasound image is an input to this stage. Due to speckle noise in ultrasound image gives incorrect results. So this step is important. Gaussian low pass filter is used for noise reduction. This will yield better result compared to other noise removal methods.

B. Segmentation

The image after noise removal will be the input for segmentation process. Kirsch template is used for segmentation. In this phase we compared with other methods, but kirsch template method yield better result. Correctly segment the cystic portion from remaining portion. Resulting image are broken due to noise. The broken edges are filled by using morphological dilation with appropriate structuring element like disc. Any unwanted edges are removed by using erosion operation.

C. Feature Extraction

Feature extraction means extracting particular characteristics that can be used to classify images. Ovarian follicles are elliptical like structures. So we can consider as an ellipse and features can be extracted. Major axis, minor axis length of ellipse is extracted from the segmented image. By using these two measurement we can calculate the ratio of major axis and minor axis. Ratio is an important feature descriptor in this algorithm.

D. Classification

Training Phase

In this phase calculated ratio is an important information. Here we compute the ratio for regions known to be follicle in the segmented image. From our experimental study ratio for follicle region is 1.42 .

Testing Phase

We can compute ratio of newly segmented image. By comparing ratio with our experimental value and classify whether it is cystic ovary or not.

3.EXPERIMENTAL RESULTS

Ultrasound image is an input to our proposed system. Images are collected from ultrasound gallery. The experimentation is done using 20 images, out of which 10 are used for testing phase and 10 for training phase. Typical results are shown in fig 3.

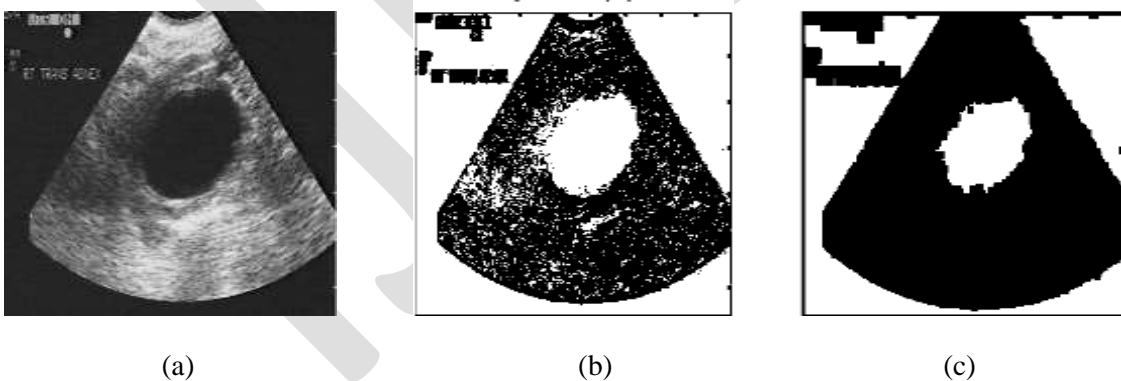




Fig.3 Results:a)Original image b)Segmented image c)dilated image d)eroded image e)detected cyst

4.CONCLUSION

In this paper a new automated method for follicle detection is proposed. It helps significantly to improve the quality of diagnosis and treatment of patients. Ultrasound images are used as input. Gaussian low pass filter is used for noise removal in ultrasound image. Kirsch template is used for segmenting cyst portion. By extracting features from the segmented image is used for classification. The experimental results are in good agreement with the manual follicle detection by medical experts, and thus demonstrate efficiency of the method.

REFERENCES:

- [1] Daftary, Shirish; Chakravarti, Sudip (2011). Manual of Obstetrics, 3rd Edition. Elsevier. pp. 1-16. ISBN 9788131225561.
- [2] Salama S, Arbo E, Lamazou F, Levailant JM, Frydman R, Fanchin R (April 2010). "Reproducibility and reliability of automated volumetric measurement of single preovulatory follicles using SonoAVC". Fertil. Steril. 93 (6): 2069-73.
- [3] Qublan HS, Abdel-hadi J (2000). "Simple ovarian cysts: Frequency and outcome in girls aged 2-9 years". Clinical and experimental obstetrics & gynecology 27 (1):51-3. [PMID 10758801](#)
- [4] Caspi, B.; Zbar, AP.; Mavor, E.; Hagay, Z.; Appelman, Z. (Mar 2003). "The contribution of transvaginal ultrasound in the diagnosis of acute appendicitis: an observational study.". Ultrasound Obstet Gynecol 21.
- [5] Kollmann M, Martins WP, Raine-Fenning N (2014). "Terms and thresholds for the ultrasound evaluation of the ovaries in women with hyperandrogenic anovulation". Hum. Reprod. Update 20 (3): 463-4.
- [6] B.Potocnik, D.Zazula, The XUltra project-Automated Analysis of Ovarian ultrasound images, Proceedings of the 15th IEEE symposium on computer based medical systems (CBMS'02)
- [7] Cigale B and Zazula D, Segmentation of ovarian ultrasound images using cellular neural networks, Proc. 7th Inter .work. systems, signals and image processing (Maribor, Slovenia 2000) 33-36.
- [8] P.S.Hiremath and Jyothi R Tegnoor, Recognition of Follicles in Ultrasound Images of Ovaries using Geometric Features, Proc. 2nd IEEE International Conference on Biomedical and Pharmaceutical Engineering (ICBPE-09), 2-4 Dec. 2009, Singapore, ISBN 978-1-4244-4764-0/09
- [9] P.S.Hiremath and Jyothi R Tegnoor, Recognition of Follicles in Ultrasound Images of Ovaries using Geometric Features, Proc. 2nd IEEE International Conference on Biomedical and Pharmaceutical Engineering (ICBPE-09), 2-4 Dec. 2009, Singapore, ISBN 978-1-4244-4764-0/09
- [10] P.S.Hiremath and Prema Akkasaliger, Despeckling medical ultrasound images using the contourlet transform, 4th AMS Indian International Conference on Artificial Intelligence (IICAI-09), 16-18 Dec. 2009, Tumkur, India
- [11] P.S.Hiremath and Jyothi R Tegnoor, (2010), —Automatic Detection of Follicles in Ultrasound Images of Ovaries using Edge based Method, International Journal of Computer Applications (IJCA), Special issue on RTIPPR(2):No.3, Article 8, pp 120-125, ISSN 0975-8887.

[12] [12]M. J. Lawrence, R.A.Pierson, M.G.Eramian, E. Neufeld, "Computer assisted detection of polycystic ovary morphology in ultrasound images," In Proc. IEEE Fourth Canadian conference on computer and robot vision (CRV'07), pp. 105-112, 2007.

IJERGS

AUTOMATED DETECTION OF SHADOW REGIONS IN HIGH RESOLUTION SATELLITE IMAGES

¹Mahak Khurana, ²Vaishali Wadhwa

¹Mtech. Student, N.C. College of Engineering

¹Khuranamahak@gmail.com, 09050669567

Abstract— High-Resolution (HR) satellite image is a commanding basis of data for detecting and extracting information about urban constructions. Shadow in HR satellite imageries is capable of providing a high level of detail, which makes them a reliable and highly vital basis of information. Nevertheless, to extract shadows, the automated detection of shadows from images must be perfect. In this paper, we present a global thresholding practice for automated detection of shadow regions from remotely sensed data. This thresholding scheme detects both shadow and vegetation regions of a High Resolution Satellite Image at the same time.

Keywords— High Resolution Satellite Image, Shadow detection, Vegetation mask, Shadow mask, Thresholding, Otsu method, Histogram.

INTRODUCTION

High Resolution (HR) satellite images are one of the most significant data input source to be utilized for the purpose of object detection. However, due to urban constructions which are built above ground, such as buildings, bridges etc., shadows are the most common component accompaniments for these constructions that can be seen in the HR images. A shadow indicates the shape of the object which is casting it.

Satellite images are the type of images that are taken by artificial satellites and contain portion of Earth. In that kind of imagery, image data is captured at specific frequencies across the electromagnetic spectrum. In most cases, the spectral range of satellite images is broader than that of the visible light. In the high resolution (HR) satellite images, the following spectral bands exist with corresponding wavelength intervals:

- Blue: 450 - 515...520 nm
- Green: 515...520 - 590...600 nm
- Red: 600...630 - 680...690 nm
- Near-infrared (NIR): 750 - 900 nm

The existence of NIR band provides valuable information for detecting natural regions and shadows in the satellite image. The satellite image can be visualized by using red, green, blue channels as its standard order (called true-color), as well as mapping NIR, red, green channels to red, green, blue. This is called false-color. This visualization is much useful for identifying vegetative regions. Figure 1.1 shows an example satellite image in true-color and false-color respectively.

For detecting a specific target such as building, road, vehicle, etc; it is essential to obtain a spatial resolution as high as possible. This can be done by a process called pan sharpening.



(a)

(b)

Figure 1.1: A satellite image shown in two different visualizations. (a) True color visualization. (b) False color visualization.

Along with the multispectral image data, a single grayscale image, whose spectral resolution is higher than the multispectral image, is also acquired by the optical sensor. This grayscale image is called panchromatic image. The pan sharpening process fuses the high resolution panchromatic image and low resolution multispectral image together to obtain a single high resolution multispectral image. Figure 1.2 shows an example image pan sharpened using a commercial GIS tool called Geoimage:



(a)

(b)

(c)

Figure 1.3: Pan sharpening process applied on a satellite image. (a) High-resolution panchromatic image. (b) Low-resolution multispectral image. (c) Resulting high-resolution pan sharpened image.

Shadow detection from HR satellite images is not an easy task and all image processing techniques for detecting shadows still rely on the estimation of shadow areas. The reliable and accurate detection of building objects from the HR satellite images is a leading task and is also very active ground of research. The shadow line of the object will be shorter in the case of a rise in a horizontal receiving surface and longer where there is a drop in this surface for the other objects in the urban areas. Also, the subsistence of trees, their shadows and shadows from the non-built-up areas (such as vehicles), can disfigure the real boundaries of shadows (the geometric form such as buildings) and give a random shape to the built-up objects, when they coalesce with an object's shadows. Moreover, the shadow region of an object in image will be larger in the summer season than its equivalent in the winter due to the sun's position in the sky vault and its angle and elevation. Spectrally, non-shadow regions, such as water, generally exhibit the same pixel intensity values or darkness with shadow regions of the objects in images that grounds for an error in detecting shadows.

DETECTION OF VEGETATION AREAS

The pixels corresponding to the vegetation regions have very high reflectance values in the NIR band; while having low reflectance values in the red band. This is because of the emission / absorption characteristics of healthy vegetation. Live green plants need a specific range of solar radiation; between 400 nm 700 nm, to carry on the photosynthesis process. This spectral range is called photo synthetically active radiation and abbreviated as PAR. The wavelength of NIR radiation is longer than 700 nm. Therefore, the radiation with wavelength inside the NIR spectral region is scattered / emitted by the leaf cells; otherwise these rays would overheat and damage the leaves. Hence, healthy vegetation has high reflectance values in NIR spectral region. On the other hand, chlorophyll pigments in leaves absorb the light rays with wavelength equivalent to red, causing red reflectance to have low value. Among these, the most widely used index is Normalized Difference Vegetation Index (NDVI). The formula for calculating NDVI is simply:

$$R = (NIR - RIB) / (NIR + RIB)$$

NIR and *RIB* represent the normalized near-infrared and red image bands, respectively.

For every pixel, the NIR is calculated and an NDVI map is generated for whole image. The decision whether a pixel belongs to a vegetated area or not is made by simply applying Otsu's automatic thresholding method. Figure 2.1 shows an example image of detected vegetation regions in a residential area

It can be seen from its arithmetic characterization that the NDVI of an area containing intense vegetation shade will tend towards the positive values (say 0.3 to 0.8) while clouds and snow fields will be illustrated by the negative values of this index. Further objects on Earth visible from space include:

- free standing water (e.g., oceans, seas, and rivers) which have relatively low reflectance in both shadowlike(spectral) bands and hence, upshot a very low positive or even slightly negative NDVI values, and
- Soils which usually reveal a near-infrared spectral reflectance somewhat greater than the red are inclined to produce somewhat small positive NDVI values (say 0.1 to 0.2).

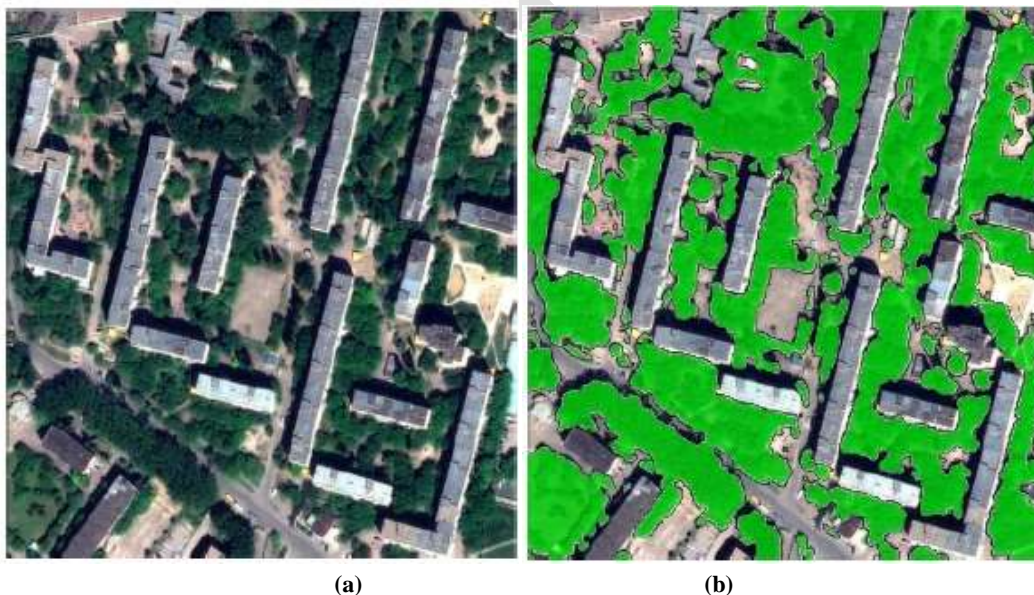


Figure 2.1: Vegetation detection example. (a) Sample image with large vegetation area. (b)Vegetation regions detected using NDVI thresholding.

For every test site, we employ automatic thresholding method to locate the optimum threshold of the histogram of the NDVI ratio values computed from the above equation, and relate that threshold on the NDVI ratio map to compute a binary vegetation mask. To spot the shadow areas, Otsu method is applied to the histogram of the ratio map

DETECTION OF SHADOWS

The approach generates a false color image in which NIR, red and green bands are employed. The algorithm is simple; first, the false color image is normalized and converted to Hue-Saturation-Intensity (ρ_{HSI}) color space. Then, a ratio map (ρ_{RM}), in which the normalized saturation (ρ_S) and the normalized intensity (ρ_I) values are compared with a ratio, is generated:

$$\rho_{RM} = \frac{\rho_S - \rho_I}{\rho_S + \rho_I}$$

To detect the shadow areas, as utilized in the case of vegetation extraction, Otsu's method is applied to the histogram of the ratio map, ρ_{RM} . Due to the fact that the thresholding scheme detects both shadow and vegetation regions at the same time, the regions that belong to the vegetation are subtracted to obtain a binary shadow mask. This approach provided successful shadow detection results for various satellite images and the major advantage is that it is independent from manual thresholds. Figure 3.1 and 3.2 shows example of detected shadow regions.



(a) (b)
Figure 3.1: Shadow detection example. (a), Sample image , (b) Shadow detection result

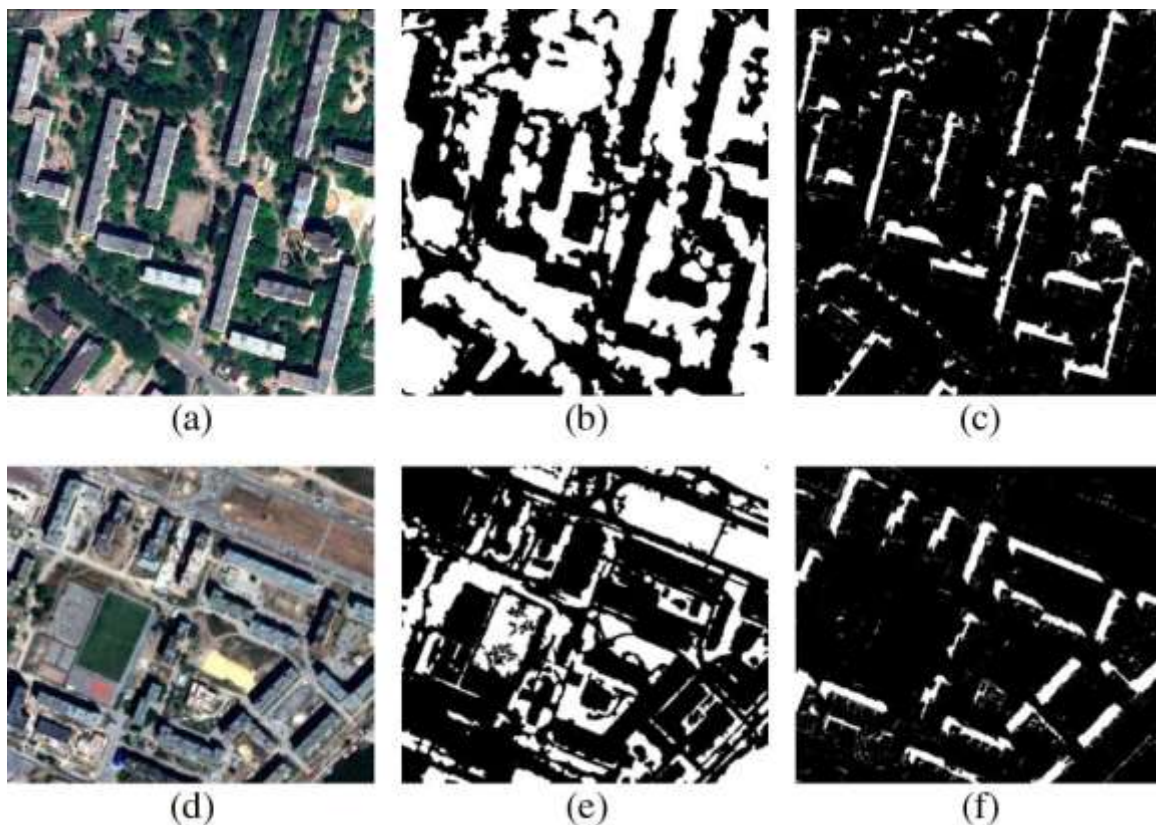


Figure 3.2 : (a), (d) High Resolution satellite image, the generated (b), (e) Vegetation masks and (c), (f) shadow masks

IMAGE THRESHOLDING: OTSU'S THRESHOLDING METHOD

Image thresholding techniques are indispensable in the course of object detection. This is in spite of the verity that the thresholding techniques are a straightforward blueprint for partitioning an image into inaccessible features, they are nonetheless effectual. Alternatively, the thresholding techniques which are applied on HR satellite images for shadow detection are requisite to be more efficient, taking into account the dissimilar characteristics of the worn and old images. As well, the fully automated algorithms of shadow detection regularly call for advance constraining assumptions about extracting shadow regions from HR satellite images in order to run them suitably and acquire reliable exactness of the shadow masks.

In this paper, we bring in, thresholding that is determined to segment the image into two brightness regions which correspond to background and object. Several methods have been proposed to automatically select the threshold. Otsu formulates the threshold selection problem as a discriminant analysis where the gray level histogram of image is divided into two groups and the threshold is determined when the variance between the two groups is the maximum. Even in the case of unimodal histogram images, that is, the histogram of a gray level image does not have two obvious peaks; Otsu's method can still provide satisfactory result.

Thresholding usually involves *analyzing the histogram*

- Different features give rise to distinct features in a histogram
- In general the histogram peaks corresponding to two features will overlap. The degree of overlap depends on peak separation and peak width.

Otsu is an automatic thresholding method, that automatically selects the best threshold 't' in a given Image histogram. It assumes 2 groups are present in the image:

- Those that are $\leq t$.
- Those that are $> t$.

For every possible t:

- Calculate within group variances:
 1. probability of being in group 1; probability of being in group 2
 2. determine mean of group 1; determine mean of group 2
 3. calculate variance for group 1; calculate variance for group 2
 4. calculate weighted sum of group variances
- Remember which t gave rise to minimum.

Otsu's thresholding method is based on selecting the lowest point *between two classes* (peaks).

- Frequency and Mean value:

Frequency:

$$\omega = \sum_{i=0}^T P(i) \quad P(i) = n_i / N$$

N: total pixel number

Mean:

$$\mu = \sum_{i=0}^T iP(i) / \omega$$

n_i: number of pixels in level i

- Analysis of variance (variance=standard deviation²)

Total variance:

$$\sigma_t^2 = \sum_{i=0}^T (i - \mu)^2 P(i)$$

Between-classes variance (δ_b^2):

The variation of the mean values for each class from the overall intensity mean of all pixels:

$$\delta_b^2 = \omega_0 (\mu_0 - \mu_t)^2 + \omega_1 (\mu_1 - \mu_t)^2,$$

Substituting $\mu_t = \omega_0 \mu_0 + \omega_1 \mu_1$, we get:

$$\delta_b^2 = \omega_0 \omega_1 (\mu_1 - \mu_0)^2$$

$\omega_0, \omega_1, \mu_0, \mu_1$ stands for the frequencies and mean values of two classes, respectively.

- The criterion function involves *between-classes* variance to the total variance is defined as:

$$\eta = \delta_b^2 / \delta_t^2$$

- All possible thresholds are evaluated in this way, and the one that maximizes η is chosen as the optimal threshold

Matlab function for Otsu's method:

function level = graythresh (I)

GRAYTHRESH compute global threshold using Otsu's method. Level is a normalized intensity value that lies in the range [0, 1].

Now, If **reference value** > **T (i, j)**, then **1** at pixel position (referring to the edges of shadows of an object within an image)

Else **0** at pixel position (background image)

Example:

```
>>n=imread ('nodules1.tif');  
>> tn=graythresh (n)  
tn = 0.5804  
>> imshow (im2bw (n, tn))
```

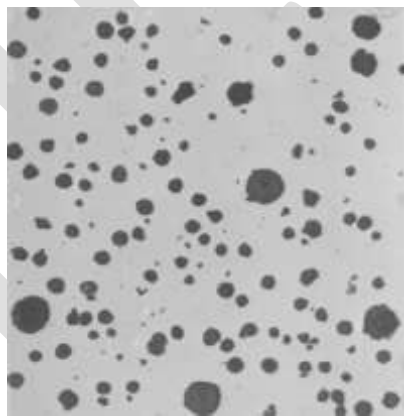


Figure 4.1: Nodules1.tif

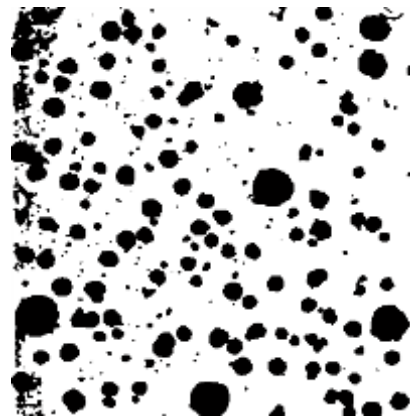


Figure 4.2: Nodules1 after thresholding

ACKNOWLEDGMENT

I want to say thanks to NCCE for the cooperation in completing my work. Specially, I thanks to my guide Ms. Vaishali Wadhwa for her help in performing my Research Paper work and complete it on the time. Without her help I cannot able to complete my work. Last but not least I want to say thanks to my parents who helped me very much and understand my work load.

CONCLUSION

The automated detection of shadows from VHR satellite images is a significant method in applications for building detection, illumination direction analysis from the sun, and the spatial distribution of the object casting the shadow. In this paper, a thresholding technique has been proposed that can handle image with fuzzy boundaries amid the image's object and background. This thresholding scheme detects both the shadow and the vegetation regions of a High Resolution Satellite Image at the same time more reliably and accurately.

REFERENCES:

- [1] N. M. Salih M. Kadhim, M. Mourshed, M. T. Bray, "Shadow Detection From Very High Resolution Satellite Image Using Grab cut Segmentation And Ratio-Band Algorithms", The International Archives of the Photogrammetry, Remote Sensing and Spatial Information Sciences, Volume XL-3/W2, 2015.
- [2] D.M. Tsai and Y. H. Chen, "A fast histogram-clustering approach for multilevel thresholding," Pattern Recognition Letters, Vol. 13, No. 4, 1992, pp. 245-252
- [3] N. Otsu, "A threshold selection method from gray-level histogram," IEEE Transactions on System Man Cybernetics, Vol. SMC-9, No. 1, 1979, pp. 62-66.
- [4] W. H. Tsai, "Moment-preserving thresholding: a new approach," Computer Vision, Graphics, and Image Processing, Vol. 29, 1985, pp. 377-393.
- [5] J. C.Yen, F. J.Chang, and S. Chang, "A new criterion for automatic multilevel thresholding," IEEE Transactions on Image Processing, Vol. 4, No. 3, 1995, pp. 370-378.
- [6] S. Wang and R. Haralick, "Automatic multithreshold selection," Computer Vision, Graphics, and Image Processing, Vol. 25, 1984, pp. 46-67.
- [7] P. K. Sahoo, S. Soltani, A. K. C. Wong, and Y. Chen, "A survey of thresholding techniques," Computer Vision Graphics Image Processing, Vol. 41, 1988, pp. 233-260.
- [8] T. Pun, "A new method for gray-level picture thresholding using the entropy of the histogram," Signal Processing, Vol. 2, 1980, pp. 223-237.
- [9] J. N. Kapur, P. K. Sahoo, and A. K. C. Wong, "A new method for gray-level picture thresholding using the entropy of the histogram," Computer Vision Graphics Image Processing, Vol. 29, 1985, pp. 273-285.
- [10] Shabnam Jabari, "Building Detection in Very High Resolution Satellite Image", ASPRS 2014 Annual Conference Louisville, Kentucky, March 23-28, 2014
- [11] J. R. Jensen, *Introductory Digital Image Processing: A Remote Sensing Perspective*. Upper Saddle River, NJ: Prentice-Hall, 2005.
- [12] N. Otsu, "A threshold selection method from gray-level histograms," Automatic, vol.11, pp. 285-296, 1975.
- [13] S. Aksoy, I. Z. Yalniz, and K. Ta, sdemir, "Automatic detection and segmentation of orchards using very high resolution imagery," IEEE Trans. Geosci. Remote Sens., vol. 50, no. 8, pp. 3117-3131, Aug. 2012.
- [14] S. U. Lee and S. Y. Chung, "A comparative performance study of several global thresholding techniques for segmentation," Computer Vision Graphics Image Processing, Vol. 52, 1990, pp. 171-190.

ZCS BRIDGELESS BOOST PFC RECTIFIER

Anna Joy¹, Neena Mani², Acy M Kottalil³

¹ PG student, annajoykandathil@gmail.com, 8111948255

Abstract— A new bridgeless single-phase ac–dc converter with a natural power factor correction (PFC) is proposed. Compared with existing single-phase bridgeless topologies, the proposed topology has the merits of less component counts. The absence of an input diode bridge and less conduction losses; hence, improved thermal management compared to existing PFC rectifiers is obtained. The proposed topology is designed to work in resonant mode to achieve an automatic PFC close to unity in a simple and effective manner. The resonant mode operation gives additional advantages such as zero-current turn-on in the active power switches.

Keywords— Bridgeless AC-DC Converters, Power-factor correction, Resonant power conversion, Zero Current Switching, Total harmonic distortion, Pseudo boost converters, Voltage gain

INTRODUCTION

Power factor correction (PFC) techniques are becoming necessary for many types of electronic equipment especially in the telecommunication and computer industries to meet harmonic regulations. Also, higher power density and lower system cost are always very desirable features, especially for low power supplies. Most of the PFC rectifiers utilize a boost or buck-boost topology converter at their front end due to its high power factor (PF) capability. However, a conventional PFC scheme has lower efficiency due to significant losses in the diode bridge. During each switching cycle interval, the current flows through three power semiconductor devices. The forward voltage-drop across the bridge diodes degrades the converter efficiency, especially at low-line input voltage [1]. Pseudo boost converters are thus named because the voltage transfer ratio of pseudo boost converter is similar to that of conventional boost converter, with no relation to the resonant parameters and switching frequency. A bridgeless PFC circuit allows the current to flow through a minimum number of switching devices compared to the conventional PFC circuit. Accordingly, the converters conduction losses can be significantly reduced, and higher efficiency and lower cost can be obtained. However, most of the previous proposed bridgeless PFC converters have at least one of the following drawbacks:

1) high components count, 2) Components are not fully utilized over whole ac-line cycle, 3) complex control, 4) dc output voltage is always higher than the peak input voltage, 5) lack of galvanic isolation, and 6) due to the floating ground, some topologies require additional diodes and/or capacitors to minimize EMI. In order to overcome most of these problems, an interesting topology has been introduced with reduced component count. However, the proposed topology in still suffers from having at least two semiconductors in the current conduction path during each switching cycle. In [4], a zero current switch topology is presented. This topology has reduced-component count; however, the load is floating with respect to the input. A novel low count topology has been introduced in [5]. The proposed topology has low-component count with an input stage similar to a boost converter. Here a new bridgeless PFC circuit based on the modified boost converter is introduced and presented. Compared with existing single phase bridgeless topologies. The proposed topology has low component count, a single control signal, and non-isolating output. Since the topology operates in discontinuous conduction mode, the proposed converter is intended for low power applications. The converter components are fully utilized during the positive and negative ac-line cycle [9].

Pseudo naming comes because this converters have voltage transformation ratio same as that of conventional boost converter, but it is independent of resonant parameters and duty ratio. Voltage conversion ratio can be further increased by quasi resonant technique [10].

BRIDGELESS RESONANT PSEUDO-BOOST PFC RECTIFIER

Introduction

The Bridgeless Resonant Pseudo boost PFC Converter circuitry consists of two MOSFET switches, two power diodes, resonant inductor and capacitor. At input side, LC filter is provided. The Bridgeless Resonant Pseudo boost PFC Rectifiers are designed to operate in discontinuous-conduction mode (DCM) during the switch turn-on interval and in resonant mode during the switch turn off intervals. As a result, the switch current stress is similar to the conventional DCM PFC converter, while the switch voltage stress is higher [1]. Moreover, the two power switches Q1 and Q2 can be driven by the same control signal, which significantly simplifies the control circuitry. Basic circuit of Bridgeless Resonant Pseudo boost PFC Rectifier is shown in Fig 3.1. Referring to Figure 2.1, the switching conduction sequences are as follows:

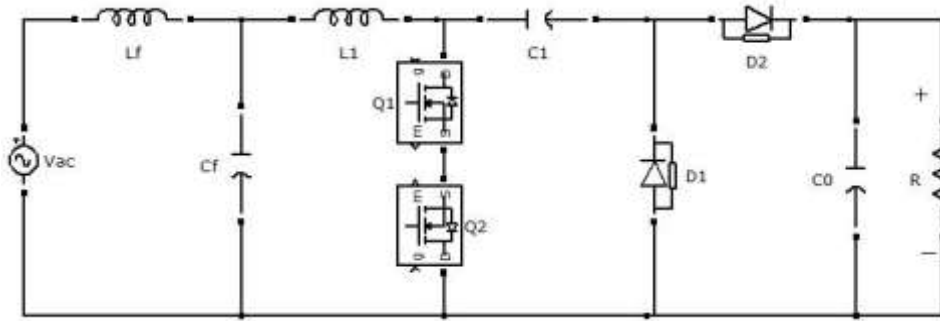


Figure 2.1: The Bridgeless Resonant Pseudo boost PFC Rectifier

During positive ac-line cycle, Q_1, D_{Q2}, D_2, D_1, X (all switches are off); and 2) during negative ac-line cycle, Q_2, D_{Q1}, D_1, D_2, X . On the other hand, the switching conduction sequences for the converter are as follows: 1) during positive ac-line cycle, Q_1, D_{Q2}, D_1, D_2, X and 2) during negative ac-line cycle, Q_2, D_{Q1}, D_2, D_1, X . Thus, during each switching period T_s , the current path goes through only two or one semiconductor devices instead of three. As a result, the total conduction losses of the semiconductor devices will be considerably lower compared to the conventional bridgeless PFC converters. In addition, the following assumptions are made: input voltage is pure sinusoidal, ideal lossless components, the switching frequency (f_s) is much higher than the ac line frequency (f_L), and the output capacitor C_0 is large enough such that the output voltage can be considered constant over the whole line period. Based on these assumptions, the circuit operations in one switching period T_s in a positive ac-line cycle can be divided into four distinct topological stages.

From simulation results, for an input voltage 110 V, f_s (switching frequency) = 50 kHz, simulation is performed in MATLAB Ra2010. The parameters used includes $L_f = 1\text{mH}$ and $C_f = 1\ \mu\text{F}$, $L_1 = 100\ \mu\text{H}$, $C_1 = 65\text{nF}$ and $R_L = 500$. Output voltage is obtained as 242V and output current as 0.4A. Output voltage step up. Switching frequency used is 50 kHz. Power factor is obtained near unity, 0.92 and Total Harmonic Distortion is only 2%. Output power is nearer to 100 W, so it is used only for low power application.

Working Principle

Resonant Pseudo boost PFC Rectifiers are designed to operate in discontinuous- conduction mode (DCM) during the switch turn-on interval and in resonant mode during the switch turn off intervals. As a result, the switch current stress is similar to the conventional DCM PFC converter, while the switch voltage stress is higher. Moreover, the two power switches Q_1 and Q_2 can be driven by the same control signal, which significantly simplifies the control circuitry. However, an isolated gate drive is required for the power switch Q_1 .

Table I: Tabulation of simulated results

Input Voltage	110 V
Input Current	1.5 A
Input Power Factor	0.92
THD	2%
Output Voltage	242 V
Output Current	0.4 A

ZCS BRIDGELESS BOOST PFC RECTIFIER

For further improving voltage conversion ratio of conventional boost converters a new converter can be designed. An alternative approach to soft switching in modified boost converters is to use quasi-resonant (QR) techniques that can be cheaply implemented by using only a few passive components. This converter can operate with soft-switching and PFC in low line applications. It is

economical because it requires only two active switches and two diodes for the main power circuit and a few passive components for soft switching. ZCS bridgeless boost PFC rectifiers are shown in fig 3.1.

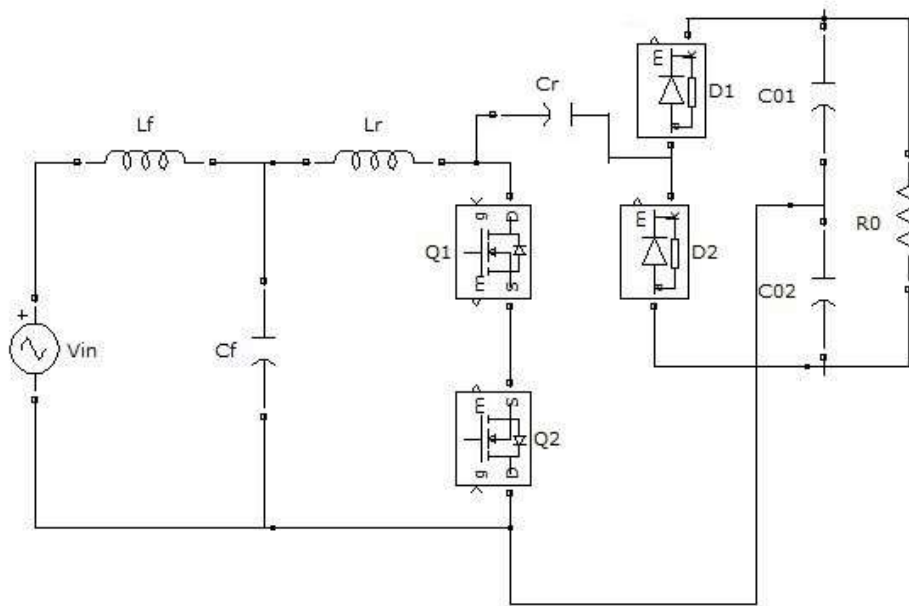


Figure 3.1: ZCS Bridgeless boost PFC Rectifier

Operational modes:

Stage 1: This stage starts when the switch Q_1 is turned-on. The body Diode of Q_2 is forward biased by the inductor current I_{L1} . Diodes are reverse biased by the voltage across C . In this stage, the current through inductor L_1 increases linearly with the input voltage, while the voltage across capacitor C_1 remains constant at voltage V_X .

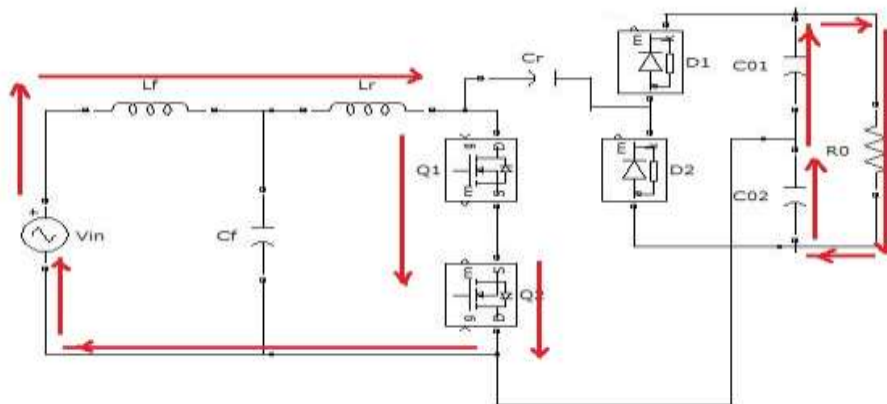


Figure 2.1: Mode 1 of ZCS Bridgeless boost PFC Rectifier

Stage 2: This stage starts when switch Q_1 is turned OFF and diode D_1 is turned ON simultaneously providing a path for the inductor currents I_{L1} . As a result, diode D_2 remains reverse biased during this interval. The series tank consisting of L_1 and C_1 are excited by the input voltage V_{AC} . The stage ends when the resonant current I_{L1} reaches zero. During this stage, capacitor C is charged until it reaches a peak value as shown in Figure 2.2

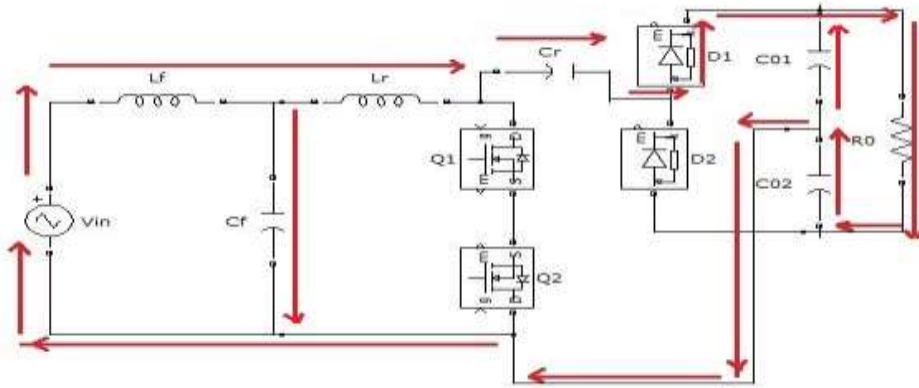


Figure 2.2: Mode 2 of ZCS Bridgeless boost PFC Rectifier

Stage 3: During this stage diode D_1 is forward biased to provide a path during the negative cycle of the resonating inductor current I_{L1} . This stage ends when the inductor current reaches zero. Thus, during this stage diode D_2 is switched ON under zero current conditions. Assuming the constant input voltage over a switching period, the capacitor is discharged until it reaches a voltage V_X .

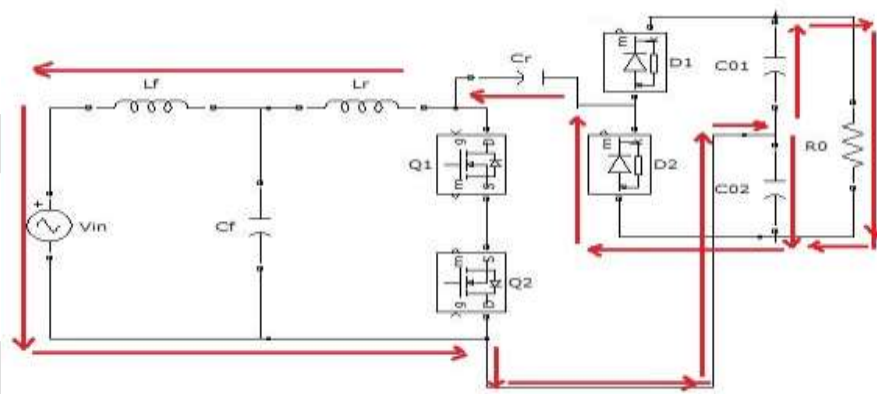


Figure 2.3: Mode 3 of ZCS Bridgeless boost PFC Rectifier

Stage 4: During this stage all switches are in their off-state. The inductor current is zero, while the capacitor voltage remains constant (V_X). It shall be noted that for this converter to operate as specified, the length of this stage must be greater than or equal to zero.

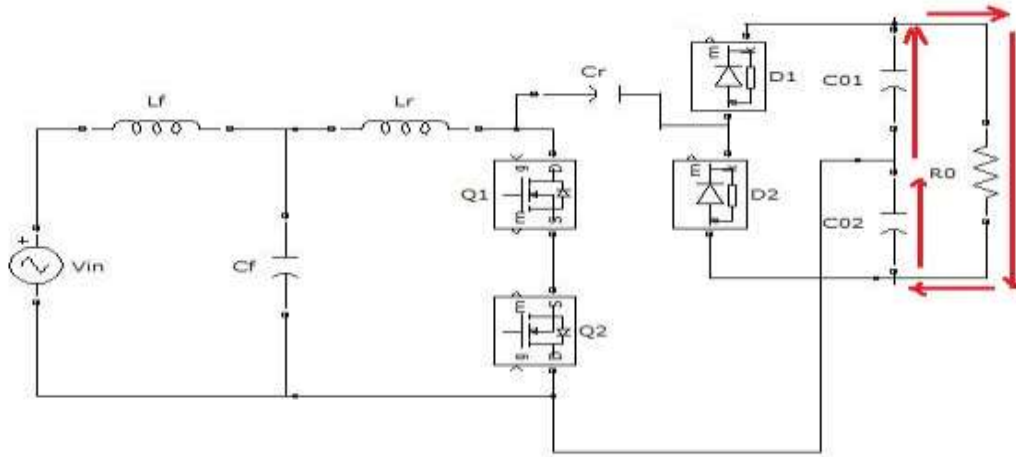


Figure 2.4: Mode 4 of ZCS Bridgeless boost PFC Rectifier

DESIGN OF COMPONENTS

Design procedure of this converter is explained with the following specifications.

Input Voltage, $V_{in} = 110$ V

Output Voltage, $V_o = 275$ V

Duty Ratio, $D = 40$ %

Power Factor, $pf = 0.98$

Switching Frequency $f_s = 50$ kHz

In order to perform the analysis and derive equations independent of any particular parameter, all equations derived in this paper are normalized using the following base quantities:

Base voltage = Output voltage, V_0

Base Impedance = $Z_0 = \sqrt{\left(\frac{L_1}{C_1}\right)}$

Base Current = $\frac{V_0}{Z_0}$

Base Frequency = $\frac{\omega_r}{2\pi}$

To ensure DCM operation, normalised switching frequency, $F = \frac{f_s}{f_r}$

The values of circuit components are calculated as follows:

1. Voltage Conversion Ratio, $M = \frac{V_o}{V_m} = 2.4$

2. Critical Inductance, $L_1 \leq \frac{R_L T_s}{4} \times \left(\frac{F}{\pi}\right)^2 = 163 \mu H$

3. Resonant Capacitance, $C_1 = \frac{1}{L_1 2\pi (f_r)^2} = 65 nF$

SIMULATION MODEL AND RESULTS

For an input voltage 110 V, f_s (switching frequency) = 50 kHz, simulation is performed in MATLAB Ra2010. The parameters used includes $L_f = 1\text{ mH}$ and $C_f = 1\ \mu\text{F}$, $L_l = 100\ \mu\text{H}$, $C_l = 65\text{ nF}$ and $R_l = 500$. Fig 4.1 shows the Simulink model of a ZCS Bridgeless boost PFC Rectifier.

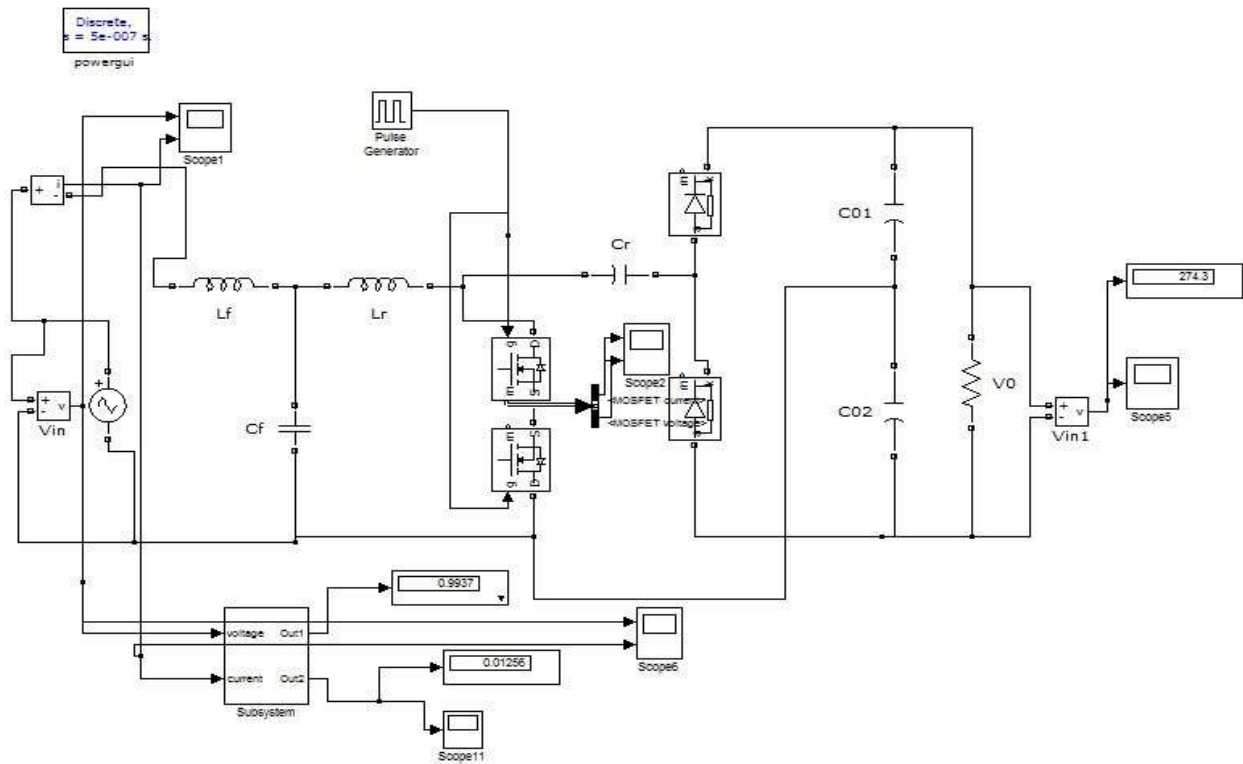
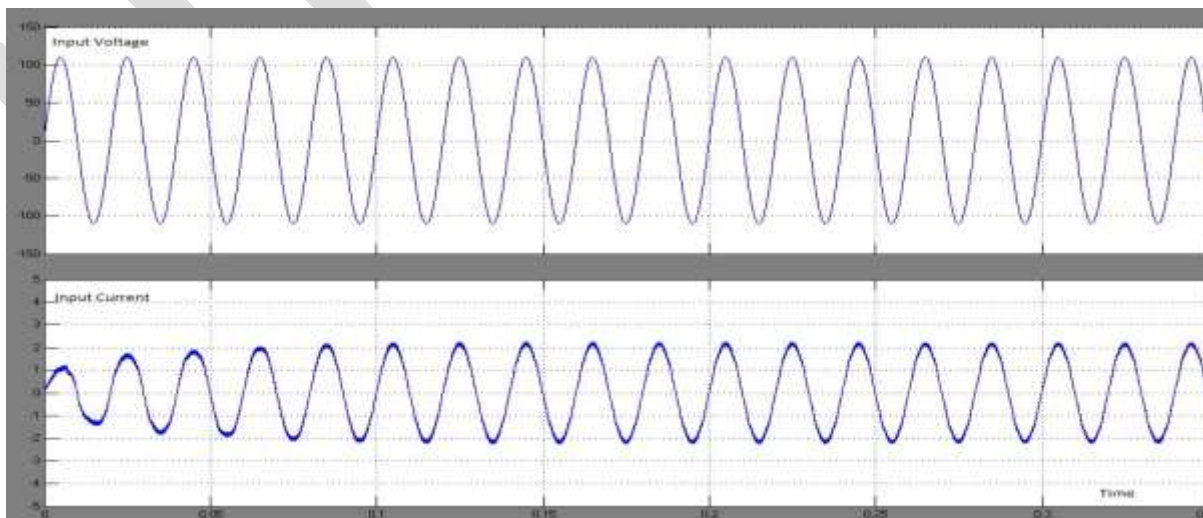


Figure 4.1: Simulink Model of ZCS bridgeless boost PFC Rectifier

For input voltage 110 V and input current 1.5A, output voltage is obtained as 274 V. Switching frequency used is 50 kHz. Power factor is obtained near unity, 0.99 and Total Harmonic Distortion is only 1%. Output power is nearer to 100 W, so it is used only for low power application.



Power factor correction is observed from the input voltage and current waveforms, these are in phase. PF is measured as 0.92. Switching frequency is taken as 50 kHz and duty ratio 50%. Discontinuous conduction mode is operated.

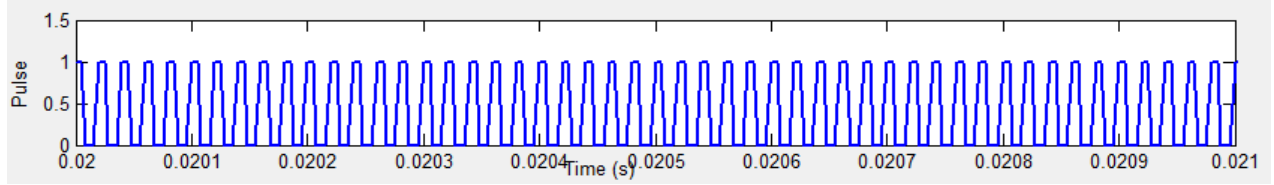
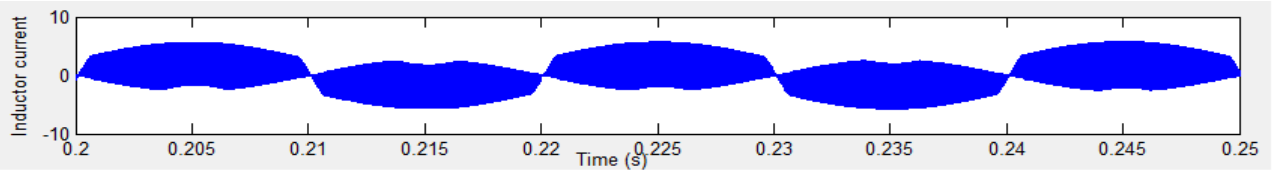
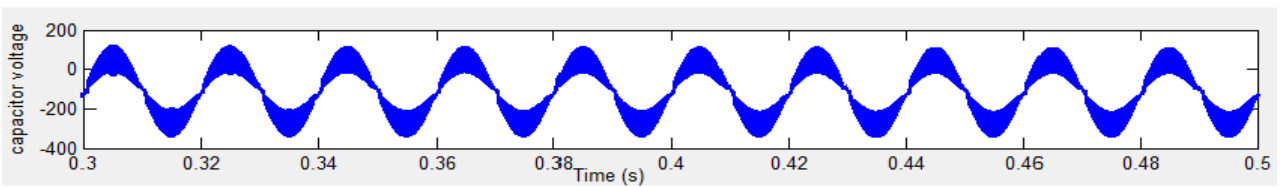


Fig 4.3: Switching Pulses



(a)



(b)

Fig 4.4: (a) Inductor Current (b) Capacitor Voltage

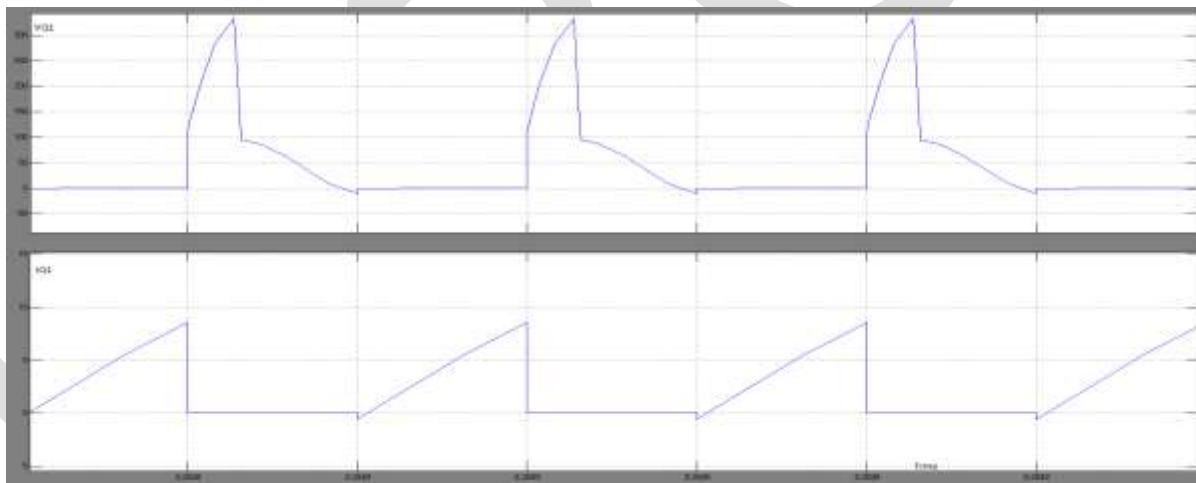


Fig 4.5: Voltage and Current across the switch

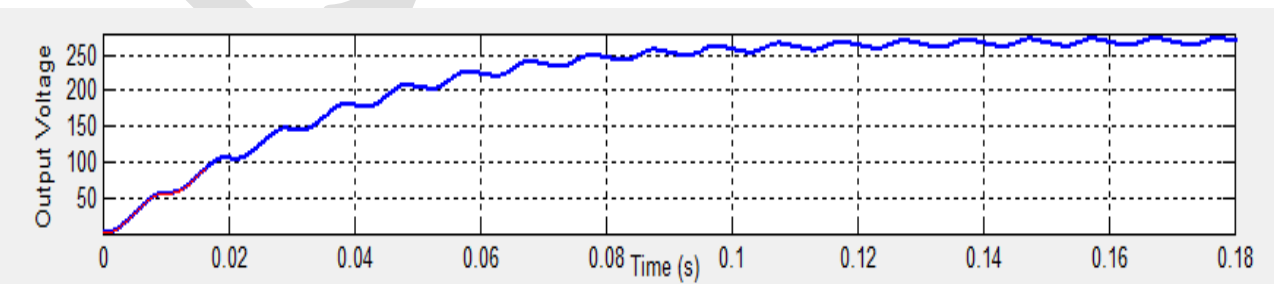


Fig 4.6: (a) Output Voltage of ZCS bridgeless boost PFC rectifier

For input voltage 110 V, output voltage boost upto 274 V. Voltage conversion ratio is increased to 2.4 where less than 2 for conventional type. Zero Current switching can be observed from the fig 4.5. ZCS Bridgeless boost PFC rectifier gives high step up conversion and high input power factor 0.99. Total harmonic distortion is only 1 to 2%.

Table II: Tabulation of simulated results

Input Voltage	110 V
Input Power factor	0.99
THD	0.012
Output Voltage	274 V
Voltage Gain	2.4

CONCLUSIONS

A new AC to DC converter with low component count and its topology derivation have been presented. The components of this topology are fully utilized over the whole line cycle. The two power switches in the proposed topology can be driven by the same control signal, which significantly simplifies the control circuitry. Voltage transfer ratios of ZCS bridgeless boost PFC rectifier is greater than conventional boost converters. Analysis, component stresses, design constraints, and simulation results of the converter have been presented. For an input voltage 110 V, switching frequency is 50 kHz. Output voltage is obtained as 274 V with high input power factor 0.99 and less THD(1-2%). Output Power is nearer to 100 W, so it is used only for low power applications. simulation is performed in MATLAB Ra2010

REFERENCES:

- [1] Abbas A. Fardoun, Esam H. Ismail, Mustafa A. Al-Sa_ar and Ahmad J. Sabzali, "A Bridgeless Resonant Pseudoboost PFC Rectifier" IEEE Trans. Power Electron., vol. 29, no.11, pp. 384397, Nov 2014.
- [2] Manfred Reddig, Dr. Wenqi Zhou, "True Bridgeless PFC - Stages with Advanced Current Measuring Circuit," IEEE Trans.Power Electron., Dec. 2011.
- [3] Fellipe S. Garcia, Jos A. Pomilio, and Giorgio Spiazzi, "Modeling and Control Design of the Interleaved Double Dual Boost Converter", Trans.Power Electron., vol. 24, no. 12, pp. 28862896, Dec. 2011.
- [4] K. Mino, H. Matsumoto, S. Fujita, Y. Nemoto, D. Kawasaki, R. Yamada, and N. Tawada "Novel Bridgeless PFC Converters with Low Inrush Current Stress and High Efficiency," International Power Electronics Conference., Feb.2010.
- [5] M. Mahdavi, H. Farzanehfard, New Bridgeless PFC Converter with Reduced Components, , International Conference on Electronic Devices, Systems and Applications,2011.
- [6] J. Marcos Alonso,Juan Via, David Gacio Vaquero, Gilberto Martinez, and Ren Osorio, "Analysis and Design of the Integrated Double Buck Boost Converter as a High-Power-Factor Driver for Power-LED Lamps" ,IEEE Trans.Industrial Electron.,vol.59, no.4, april 2012.
- [7] Dylan Dah-Chuan Lu and Wenfei Wang Bridgeless Power Factor Correction Circuits with Voltage-Doubler Con_figuration,, IEEE PEDS. Ind. Electron., Dec 2011.
- [8] W.-Y. Choi, J.-M. Kwon, B.H. Kwon, "Bridgeless dual-boost rectifier with reduced diode reverse-recovery problems for power-factor correction", IET power electronics, Vol. 1, No. 2, pp. 194202, october 2007.
- [9] [9] Bin Su and Zhengyu Lu, "An Interleaved Totem-Pole Boost Bridgeless Rectifier With Reduced Reverse-Recovery Problems For Power Factor Correction",IEEE Transactions On Power Electronics, Vol. 25, No.6, June 2010.
- [10] Gerry Moschopoulos, Praveen K Jain, "A Novel single-phase soft switched rectifier with unity power factor and minimal Component count", IEEE Transactions On Industrial Electronics,Vol. 51, No.3, June, 2004
- [11] Mohammad Mahdavi, Hosein Farzanehfard, "Bridgeless SEPIC PFC Rectifier With Reduced Components and Conduction Losses", IEEE Transactions On Power Electronics,Vol. 58, No.9, September 2011.
- [12] T. Nussbaumer, K. Raggl, and J. W. Kolar, "Design guidelines for interleaved single-phase boost PFC circuits," IEEE Trans. Power Electron.,vol. 56, no. 7, pp. 2559–2573, Jul. 2009.

Video Background Extraction:A Survey

Vinky Dhingra, Vaishali Washwa

Kurukshetra University, vinky.dhingra87@gmail.com 9050334375

Abstract— This paper reviews the studies involved in background subtraction techniques. Object detection is basically the most important step in video analysis. There are various studies which are aimed at detecting the objects in video sequences. But due to fast illumination change in a visual surveillance system, many of them are not tolerant to dynamic background. There are various background subtraction algorithms for detection of moving objects, but many of them fail with slow-moving objects or in poor image qualities of videos and does not distinguish shadows from moving objects. Among all the background extraction techniques, Multibackground model and Robust thresholding are the most efficient which can deal with the problem such as occurrence of shadow in its foreground.

Keywords— Background subtraction, Object detection, Thresholding, Multibackground model, visual surveillance system, moving objects, Illumination change.

INTRODUCTION

Identification of dynamic behavior of objects from a video sequence is a critical and fundamental task in video surveillance. It plays a significant role in human tracking and detection traffic analysis and monitoring and recognition of gestures in human-machine interface. Background subtraction is a basic term for the processes which aim to segment dynamic foreground objects from a static background. There is a crucial distinction between the background detection stages and background modeling, which constitute the complete subtraction process. The two stages of background subtraction are *overlapping* and *co-relating*. The modeling stage maintains and creates a model of the scene in the background. The detection process segments the current image into dynamic (foreground) and static (background) regions based on its background model. The resulting detection masks are then put back into the modeling process so as to avoid coincidence of foreground objects and background model. Developing an appropriate algorithm for background subtraction is a challenging task. It should be robust with respect to changes in illumination. Second, it must ignore the detection of dynamic background objects such as rain, snow, moving flowers and shadows casted by dynamic objects. Its internal background model must give a quick reaction to changes occurring in the background like starting and stopping of an object. The huge flow of traffic poses challenge to a background subtraction algorithm. The vehicles move at an accurate speed when the signal is green, but stop when signal turns red. The vehicle then remains static until the signal turns green. An appropriate background subtraction algorithm should deal with the dynamic objects that first merge into background and then become foreground after certain time. In addition, to meet the real-time requirements of various applications, a background subtraction algorithm should not be expensive and possess lesser memory requirements, while still be able to identify dynamic objects in the video accurately. In order to deal with these challenges, various background models and measures bound up to different optimization strategies have been developed in the past years. These techniques are more robust to instability in the background than other background subtraction techniques. In this paper, we have compared few most implemented background subtraction techniques on video sequences representing different challenges. The aim of this study is to find how better sophisticated techniques are compared to simple background subtraction techniques. To compare the processing power and the amount of memory required by each technique at run time.

PREVIOUS WORK

[1] In 2010, Parisa Darvish Zadeh Varcheie Michael Sills-Lavoie and Guillaume-Alexandre Bilodeau proposed an important background subtraction technique. The background is identified by rectangular areas shown by the color histogram and a text measure.

It is modeled at various scales to examine motion more accurately. This background model and Gaussian Mixture model are combined. The presence of rectangular regions filters out small motions such as data acquisition noise and swaying vegetation. The Gaussian Mixture background subtraction method then executes the work by defining foreground detection in rectangular areas where motion is detected. In Comparison to the Gaussian Mixture method, RECTGAUSS-*Tex* gives lesser false positive detection for same kind of true and positive results. The algorithm was implemented with various videos against multiple illumination resolutions and changes. The obtained results show that RECTGAUSS-*Tex* outperforms Gaussian Mixture method as it has same TPR, but lesser FPR. For the used data sets, it outperforms Code-book, TBMOD and KDE using their default parameters. Although the algorithm used eight such parameters, six among them are stable, only two required tuning. This motion detection algorithm can be implemented at various scales to adjust the object shape precision which is needed for an application that means Detection can be performed at coarse scale with large rectangles and without applying Gaussian Mixture method.

[2] In 2012, Vinayak G Ukinkar, Makrand Samvatsar published their work. They proposed an approach for detection of object in moving background. This approach is suitable for object detection in outdoor and indoor environment and is robust for fast illumination changes in the video sequences. It avoids detecting dynamic background objects such as rain, moving leaves, snow, and shadows of moving objects. And its background model reacts faster to change in background such as start and stopping of objects.

[3] In 2012, Y. Benezeth¹ P.-M. Jodoin, B. Emile, H. Laurent, C. Rosenberger presented a comparative study of background subtraction algorithms. The study of several background subtraction methods is presented. The approaches range from general background subtraction with global thresholding to more critical statistical techniques and have been executed and tested on various videos. The aim of this study is to lay down a solid analytic basis to identify the advantages and drawbacks of the widely implemented object detection techniques. The techniques are compared on the basis of their robustness to various types of video, memory used by them, and the computation overhead they need. The effect of the Markovian prior and some of the post processing operators are examined. The videos used in the study come from benchmark databases and possess different challenges like camera jitter and poor signal-to-noise ratio.

[4] In 2013 Kalyan Kumar Hati, Pankaj Kumar Sa, and Banshidhar Majhi, stated an intensity range based object detection method for videos with static background and stationary cameras. The method uses two different algorithms. They model background from initial few frames and separate the object using local thresholding. The efficiency of these techniques is described by comparative study of competitive methods. Both quantitative measures as well as videos show better performance and the techniques have a strong ability for real time applications.

[5] Farah Yasmin Abdul Rahman, Aini Hussain, Wan Mimi Diyana Wan Zaki, Halimah Badioze Zaman, and Tahir cited improvement in Background Subtraction Techniques. They presented a hybrid technique that uses SDGD filters having four basic BGS methods, namely RA, RGA, FD and AM. This method improves segmentation performance, as shown by *F*-score values. This technique was implemented on different videos from various databases, and each video was captured indoors and outdoors and showed various scenes. An ANN classifier is used to distinguish non human and human images. This work emphasizes on BGS techniques, such as Gaussian average, approximate median and running average. In this study, they have removed the limitation by identifying all edge pixels.

[6] In 2013, Harsha Varian Helena Choithwani Tina Gyanchandani Dashrath Mane Kajal Sahatiya Shruti Gangan proposed a paper, they introduced many Background subtraction and modeling techniques with a problem which has inclusion of Shadow as Object in the foreground. The process of removing shadow by using invariance against illumination changes and improvements in obtaining the foreground data in comparison to previous background subtraction techniques have been discussed. Processing overhead is higher in this method. Alternative frames are considered to reduce time. The technique of classification of pixels possesses the same problem of excess computation.

[7] A review has been carried out by Hemavathy R, Dr. Shobha G to know the advantages and drawbacks of the techniques used in tracking and detection of the objects in both static and dynamic environments. A study is carried out to identify the problems faced in static and dynamic environment. Many algorithms are there to track the dynamic object in stationary and dynamic environments. Static technique does not pose any difficulty as compared to the dynamic techniques. In stationary environment condition is that the background will be static in the video and the foreground is dynamic in the whole video. The foreground can be of single object or multiple objects and these objects can be tracked and detected from the first frame. Videos having natural scenes comprised of several moving objects. Objects of interest often move along complicated backgrounds that are themselves moving in dynamic

conditions. Many issues have been taken into consideration prior to the object is decided as moving entities in dynamic background. An observation is tube carried out on the video frames to check whether an object is moving or not.

[8] In 2014, A technique to detect dynamic objects in video by using a textual representation been cited in a paper by PRANAM JANNEYAND GLENN GEERS. Experimental results have verified that the methodology is effective to noise, low frame rate, illumination changes, and other camera-associated noise. The proposed algorithms approach improves the performance of other algorithms that are frequently used. Traffic videos taken in night time are still a challenging task which is still to be implemented using this proposed methodology. They have also stated a framework to estimate traffic density by using a foreground object detection-based method. They have successfully developed a process, such as showcasing its use for video analysis applications such as traffic density estimation

CONCLUSION

Much work has been carried out towards obtaining the best background model which works in real time. Most efficient of these algorithms would be to use a static frame without any foreground object as a base background model and use a simple threshold based frame subtraction to obtain the foreground. This is not suited for real life situations where normally there is a lot of movement through cluttered areas, objects overlapping in the visual field, shadows, lighting changes, and effects of moving elements in the scene (e.g. swaying trees), slow moving objects, and objects being introduced or removed from the scene. When dealing with a video for background subtraction then frames have to be stored in buffer and that requires a large buffer size and increase memory requirements. When a video or picture is shooting from the camera then various noises, illumination variation, shadow etc poses threat to background subtraction.

REFERENCES:

- [1]. Deepak Kumar Rout, Sharmistha Puan, " Video Object Detection in Dynamic Scene using Inter-Frame Correlation based Histogram Approach" International Journal of Computer Applications (0975 – 8887) Volume 82 – No 17, November 2013, pp19-24
- [2]. Yannick Benezeth, Pierre-Marc Jodoin, Bruno Emile, H'el'ene Laurent, Christophe Rosenberger. Comparative study of background subtraction algorithms. Journal of Electronic Imaging, Society of Photo-optical Instrumentation Engineers (SPIE), 2010.
- [3]. Hemavathy R, Dr. Shobha G, " Object Detection and Tracking under Static and Dynamic environment: A Review" International Journal of Advanced Research in Computer and Communication Engineering Vol. 2, Issue 10, October 2013 pp4095-4100
- [4]. Vinayak G Ukinkar, Makrand Samvatsar, "Object detection in dynamic background using image segmentation: A review" IJERA, ISSN: 2248-9622 Vol. 2, Issue 3, May-Jun 2012, pp.232-236
- [5]. Kalyan Kumar Hati, Pankaj Kumar Sa, and Banshidhar Majhi, " Intensity Range Based Background Subtraction for Effective Object Detection" IEEE Signal Processing Letters, Vol. 20, No. 8, August 2013, Pp759-762
- [6]. Bo Liu, Yan Lin, Guan Guan, " A Method of Multi-scale Edge Detection for Underwater Image" Journal of Information & Computational Science 10: 2 (2013) 345–354
- [7]. CHI Jian-nan, ZHANG Chuang, ZHANG Han, LIU Yang, YAN Yan-tao, " Approach of Moving Objects Detection in Active Video Surveillance" Joint 48th IEEE Conference on Decision and Control and 28th Chinese Control Conference Shanghai, P.R. China, December 16-18, 2009
- [8]. Parisa Darvish Zadeh Varcheie, Michael Sills-Lavoie and Guillaume-Alexandre Bilodeau, " A Multiscale Region-Based Motion Detection and Background Subtraction Algorithm" Sensors 2010, ISSN 1424-8220, 1041-1061
- [9]. Caius SULIMAN, Cristina CRUCERU, Florin MOLDOVEANU, " Kalman Filter Based Tracking in an Video Surveillance System" 10th International Conference on DEVELOPMENT AND APPLICATION SYSTEMS, Suceava, Romania, May 27-29, 2010
- [10]. Pranam Janney And Glenn Geers, " A Robust Framework For Moving-Object Detection And Vehicular Traffic Density Estimation" Arxiv:1402.0289v1 [Cs.CV] 3 Feb 2014

- [11].Harsha Varwani Heena Choithwani, " Understanding various Techniques for Background Subtraction and Implementation of Shadow Detection" IJCTA Vol 4 (5),822-827
- [12] Farah Yasmin Abdul Rahman, AiniHussain, WanMimiDiyanaWanZaki, HalimahBadiozeZaman, and NooritawatiMdTahir, "Enhancement of Background Subtraction Techniques Using a Second Derivative in Gradient Direction Filter" Hindawi Publishing Corporation Journal of Electrical and Computer Engineering Volume 2013
- [13] Hemavathy R, Dr.Shobha G, "Object Detection and Tracking under Static and Dynamic environment: A Review" International Journal of Advanced Research in Computer and Communication Engineering Vol. 2, Issue 10, October 2013pp4095-4100
- [14] Deepak Kumar Rout, SharmisthaPuhan, "Video Object Detection in Dynamic Scene using Inter-Frame Correlation based Histogram Approach" International Journal of Computer Applications (0975 – 8887) Volume 82 – No 17, November 2013,pp19-24
- [15] Olga Zoidi, AnastasiosTefas, Member, IEEE, and Ioannis Pitas, Fellow, IEEE "Visual Object Tracking Based on Local Steering Kernels and Color Histograms" IEEE transaction on circuits and system for video technology VOL:25 NO:3 YEAR 2013.
- [16] PranamJanney And Glenn Geers, "A Robust Framework For Moving-Object Detection And Vehicular Traffic Density Estimation" Arxiv:1402.0289v1 [Cs.CV] 3 Feb 2014
- [17] Bo Liu, Yan Lin, Guan Guan, "A Method of Multi-scale Edge Detection for Underwater Image" Journal of Information & Computational Science 10: 2 (2013) 345–354

SINGLE PIXEL DEPENDENT PREDICTION WITH DOWNSAMPLING AND INTERPOLATION

Anuja Ann Mani, Cinly Thomas

PG Scholar, Dept of CSE, BMCE, Kollam, Kerala, India

anujabava@gmail.com,

Abstract— In the past decades, video coding technologies have greatly promoted the development of digital multimedia contents related industry. To satisfy the rapid increasing demand for high-definition (HD) and ultra-HD (UHD) video contents, a higher requirement for more efficient video coding has been brought forward. In this paper we propose a new approach for efficient video compression. We mainly focus on intraframe coding that performs compression techniques on any one of the frames in video sequence. A single pixel based lossless prediction (SPLP) along with downsampling and interpolation is used to achieve a better compression ratio compared to existing system. SPLP is an enhancement of H.264/MPEG-4 standard, which employs pulse code modulation for better prediction. Along with SPLP, a checker board pattern downsampling and adaptive weighted interpolation techniques are used to improve the performance.

Keywords— SPLP, Checkerboard downsampling, adaptive weighted downsampling, Differential pulse code modulation, H.264, Bilinear Interpolation, MDDI.

1. INTRODUCTION

Video compression reduces or removes redundant data so that a video file can be effectively transmitted and stored. The process of video compression involves the application of an efficient algorithm to the source video to create a compressed file that is ready for transmission and storage. Various video coding standards are available. Most popular compression standards are JPEG, motion JPEG, H.261, H.263, MPEG, H.264 etc.

Our existing system, mode dependent downsampling and interpolation (MDDI) ^[1] method divides the pixels in a given image into two sub-images namely even row wise pixel image and odd row wise pixel image using a uniform downsampling ^{[2],[3]} method. For the odd downsampled pixel image, bilinear interpolation ^[4] is applied to predict other even sampled pixels. Then we applies H.264 intra prediction ^{[5],[6],[7]} into the odd pixels to develop an adaptive downsampling structure. Then residual of both the odd wise sampled and even wise sampled pixels are calculated and encoding is applied on both residual. On the odd row wise sampled image H.264 intra prediction is applied, where coding performance is based on the rate-distortion (RD) measurement.

There are some limitations in our existing system and they are:

- The Prediction Mode Selection complexity is more.
- Bit rate ratio can be improved further in most of the cases.
- The Hardware complexity is more in most of the algorithms which can be lessened.
- The time complexity can be reduced further.
- Edge details can't be preserved.
- Can improve residual quality further

To overcome all this drawbacks we go for a new method named single pixel dependent lossless prediction (SPLP) along with checkerboard downsampling and adaptive weighted interpolation.

2. PROPOSED METHOD

We propose three changes for our existing system to improve the intra frame coding. First we replace uniform downsampling with checkerboard pattern downsampling [8] in order to preserve the edge details. Then an adaptive weighted interpolation [9] can be taken instead of bilinear interpolation so that we can improve the residual quality and thereby can improve the compression rate. Then we are giving a proposal of replacing H.264 with SPLP [10] which will further improve the compression rate. The block diagram for the proposed method is given in Fig.1

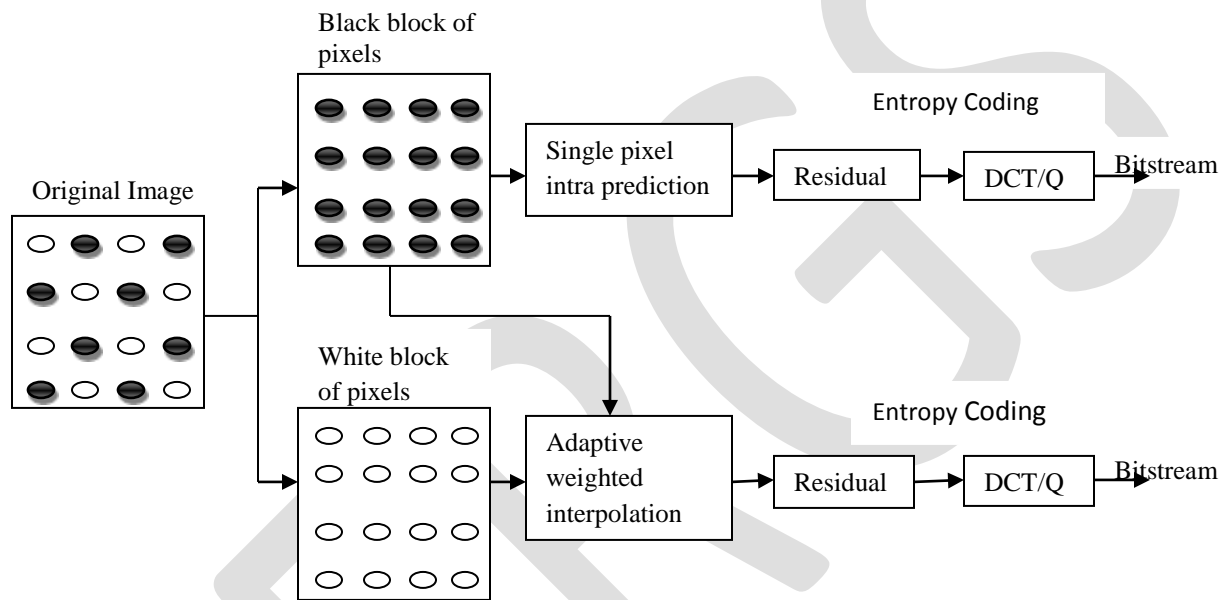


Fig.1: Block diagram for proposed method

Let I be the original (full resolution) color image and ID is a down sampled image based on chess board fashion. For example 8 x 8 images are first level downsized using chess board pattern gives 8x4 image and the second level downsizing using chess board given 4x4 image. We would get 2 blocks namely black block of pixel and white block of pixel.

Adaptive weighted interpolation would be applied to black block of pixels. In the adaptive weighted interpolation, the gradients are found by finding the differences of the pixel values in both horizontal and vertical position. The vertical gradient can be found by finding the difference between pixel values A and D as shown in Fig.2. The horizontal gradient can be found by finding the difference between pixel values B and C such that

Vertical gradient $V = (A-D)$

Horizontal gradient $H = (B-C)$

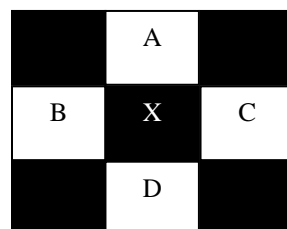


Fig.2: Adaptive weighted interpolation pattern

The threshold can be fixed such that its value should be greater than the sum of vertical and horizontal gradient. Then the value of X can be calculated such that

$$X = \frac{(A + B + C + D)}{4}$$

We add the weighted coefficients to the pixel values in some cases. If the horizontal gradient is greater than the threshold value, we add the weighted coefficients such that the values of horizontal pixels should be greater than the values of vertical pixels. It is denoted as

$$X = \frac{(W1B+W1C+W2A+W2D)}{4} \quad \text{for } W1 > W2$$

If the vertical gradient is greater than the threshold value, we add the weighted coefficients such that the values of vertical pixels should be greater than the values of horizontal pixels. It is denoted as

$$X = \frac{(W1A+W1D+W2B+W2C)}{4} \quad \text{for } W2 > W1$$

After applying adaptive weighted interpolation method we can calculate the residual by subtracting the result from white block of pixels. Then need to do discrete cosine transformation and quantization on the residual to achieve better compression.

SPLP is a new source pixel based prediction technique for lossless intra coding technique which is applied again to the black block of pixels. It employs DPCM (Differential Pulse Code Modulation)^{[11],[12]} and it is developed as an enhancement of intra frame coding of H.264/MPEG-4 AVC standard. Identification of a source block adaptively among the sixteen micro blocks of a macro block in 4:4:4 format is based on visual perceptual considerations for both luma and chromo components. From the selected source block, SPLC selects a source pixel adaptively within the block. Using the selected source pixel SPLP predicts other pixels in the selected source block and then predicts all pixels in the remaining fifteen micro blocks in a macro block using this source block.

The prediction is carried out using DPCM. The philosophy of predictive techniques is to remove inter pixel redundancy between successive pixels. In order to reduce the time complexity in mode selection, the residual of predicted pixel is calculated by using only the two directional modes 1 and 2 of DPCM rather than all of its nine modes. Finally, the residuals are encoded with the arithmetic entropy coder.

Advantages of proposed system:

- Reducing the time complexity during the Prediction Mode Selection phase of the lossless Intraframe coding algorithms was identified as one of the pressing needs in lossless Intraframe video compressions techniques.
- Proposed prediction technique which keeps one pixel as source to predict the entire pixels in the source micro block of a given macro block. The source micro block will be subsequently used for predicting the other micro blocks in the macro block, which can make efficient block wise compression.
- Proposed system could improve the compression ratio substantially. These algorithms work on a new pixel based prediction technique to predict the pixel, increasing the data redundancy leading to much improved compression ratio and use Differential Pulse Code Modulation for prediction.
- The pixel based algorithms SPLP can achieve a substantial reduction in the hardware complexity in preprocessing by reducing the number of modes to just two to predict the pixels in the macro block in comparison with the other algorithms which use between 4 modes and 9 modes.
- Edge details could be preserved by applying adaptive checkerboard pattern downsampling.
- Adaptive weighted interpolation helps in improving the residual quality and thereby improving the compression rate.

3. CONCLUSION

In this paper, an improved prediction method along with two efficient techniques is proposed for better compression of videos. The techniques we preferred here are single pixel based intra prediction (SPLP), an adaptive weighted interpolation and a checker board downsampling method. The use of SPLP technique reduces the time complexity and coding complexity. The proposed techniques preserve the edge details and improve the residual quality. So we could achieve a significant performance improvement with the decrease in complexity.

REFERENCES

- [1] Quingbo Wu, Hongliang Li, —Mode dependent downsampling and interpolation scheme for high efficiency video codingl, Signal Processing: Image Communication 28 (2013)581–596.
- [2] W.Lin, L.Dong, —Adaptive downsampling to improve image compression at low bit ratesl, IEEE Transactions on Image Processing 15 (9) (2006) 2513–2521.
- [3] X. Wu, X. Zhang, X. Wang, —Low bit-rate image compression via adaptive downsampling and constrained least squares upconver- sionl, IEEE Transactions on Image Processing 18 (3) (2009) 552–561.
- [4] K.T. Gribbon and D.G. Bailey, —A Novel Approach to Real-time Bilinear Interpolationl, IEEE International Workshop on Electronic Design, Test and Applications, 2004.
- [5] T. Wiegand et al., —Overview of the H.264/AVC video coding standardl, IEEE Trans. on CSVT, vol. 13, no. 7, pp. 560–576, July 2003.
 - a. ITU-T Recommendation H.264 and ISO/IEC 14496-10 (MPEG-4) AVC, —Advanced Video Coding for Generic Audiovisual Servicesl (Mar. 2005).
- [6] Veerendra Nath. D, M.V. Srikanth, —Video Compression by Using H.264/MPEG-4 AVC by Exploiting Spatial Correlationl, International Journal of Advanced Research in Computer Science and Software Engineering, Volume 4, Issue 8, August 2014.
- [7] S. J. Lebonah, D. Minola Davids, —A Novel Coding using Downsampling Technique in Video Intraframe, International Conference on Emerging Technology Trends on Advanced Engineering Research, 2012.
- [8] Sang Jun Park, Changki Min, Jechang Jeong, Gwanggil Jeon, —Adaptive Weighting Scheme for Edge-based Line Interpolationl, IEEE Fourth Pacific-Rim Symposium on Image and Video Technology , Nov. 2010, 320 – 324.
- [9] Krishnan. N, Selvakumar R. K., Vijayalakshmi. P, Arulmozhi. K., —Adaptive Single Pixel Based Lossless Intra Coding for H.264 / MPEG-4 AVCl, IEEE international Conference on Computational Intelligence and Multimedia Applications, (volume 3), Dec. 2007, 63-67.
- [10] O'Neal, J.B, Jr., —Differential pulse code modulation with entropy codingl, IEEE transaction on Information Theory(volume 22, Issue:2), Mar 1976, 169-174.
- [11] Farvardin. N, Modestino. J. W, —Rate distortion performance of DPCM schemes for autoregressive sourcesl, IEEE transaction on Information theory (volume 31, Issue:3), May 1895, 402-418

Study of Interesting Security Issues in Mobile Computing

Girish S¹, Sangamesh C J² Priya R Kamath³
Asst.Prof CSE¹, MCA², CSE³ Department, Sahyadri College of Engineering & Management
AdyarMangalore- 575009 India
[^1giriat@gmail.com](mailto:giriat@gmail.com)
[^2sangamesh.mca@sahyadri.edu.in](mailto:sangamesh.mca@sahyadri.edu.in)
[^3priya.cs@sahyadri.edu.in](mailto:priya.cs@sahyadri.edu.in)
Mobile No: 8197954105

Abstract- This paper is an answer to the question: "What is unique and conceptually different about mobile computing?" The paper begins by describing a set of constraints intrinsic to mobile computing, and examining the impact of these constraints on the design of distributed systems. Next, it summarizes the key results of the Coda and Odyssey systems. Finally, it describes the research opportunities in five important topics relevant to mobile computing: caching metrics, semantic callbacks and valuers, resource revocation, analysis of adaptation, and global estimation from local observations.

1. Introduction

What is really different about mobile computing? The computers are smaller and bits travel by wireless rather than Ethernet. How can this possibly make any difference? Isn't a mobile system merely a special case of a distributed system? Are there any new and deep issues to be investigated, or is mobile computing just the latest fad?

This paper is my attempt to answer these questions. The paper is in three parts: a characterization of the essence of mobile computing; a brief summary of results obtained by my research group in the context of the Coda and Odyssey systems; and a guided tour of fertile research topics awaiting investigation. Think of this paper as a report from the front by an implementer of mobile information systems to more theoretically-inclined computer scientists

1.1. Constraints of Mobility

Mobile computing is characterized by four constraints:

- *Mobile elements are resource-poor relative to static elements.*

For a given cost and level of technology, considerations of weight, power, size and ergonomics will exact a penalty in computational resources such as processor speed, memory size, and disk capacity. While mobile elements will improve in absolute ability, they will always be resource-poor relative to static elements.

This research was supported by the Air Force Materiel Command (AFMC) and ARPA under contract number F196828-93-C-0193. Additional support was provided by the IBM Corp. and Intel Corp. The views and conclusions contained here are those of the authors and should not be interpreted as necessarily representing the official policies or endorsements, either express or implied, of AFMC, ARPA, IBM, Intel, CMU, or the U.S. Government. was provided by the IBM Corp. and Intel Corp. The views and conclusions contained here are those of the authors and should not be interpreted as necessarily representing the official policies or endorsements, either express or implied, of AFMC, ARPA, IBM, Intel, CMU, or the U.S. Government.

- 4) *Mobility is inherently hazardous.*

A Wall Street stockbroker is more likely to be mugged on the streets of Manhattan and have his laptop stolen than to have his workstation in a locked office be physically subverted. In addition to security concerns, portable computers are more vulnerable to loss or damage.

- 5) *Mobile connectivity is highly variable in performance and reliability.*

Some buildings may offer reliable, high-bandwidth wireless connectivity while others may only offer low-bandwidth connectivity. Outdoors, a mobile client may have to rely on a low-bandwidth wireless network with gaps in coverage.

- 6) *Mobile elements rely on a finite energy source.*

While battery technology will undoubtedly improve over time, the need to be sensitive to power consumption will not diminish. Concern for power consumption must span many levels of hardware and software to be fully effective.

These constraints are not artifacts of current technology, but are intrinsic to mobility. Together, they complicate the design of mobile information systems and require us to rethink traditional approaches to information access.

1.2. The Need for Adaptation

Mobility exacerbates the tension between autonomy and interdependence that is characteristic of all distributed systems. The relative resource poverty of mobile elements as well as their lower trust and robustness argues for reliance on static servers. But the need to cope with unreliable and low-performance networks, as well as the need to be sensitive to power consumption argues for self-reliance.

Any viable approach to mobile computing must strike a balance between these competing concerns. This balance cannot be a static one; as the circumstances of a mobile client change, it must react and dynamically reassign the responsibilities of client and server. In other words, mobile clients must be *adaptive*.

1.3. Taxonomy of Adaptation Strategies

The range of strategies for adaptation is delimited by two extremes, as shown in Figure 1. At one extreme, adaptation is entirely the responsibility of individual applications. While this *laissez-faire* approach avoids the need for system support, it lacks a central arbitrator to resolve incompatible resource demands of different applications and to enforce limits on resource usage. It also makes applications more difficult to write, and fails to amortize the development cost of support for adaptation.

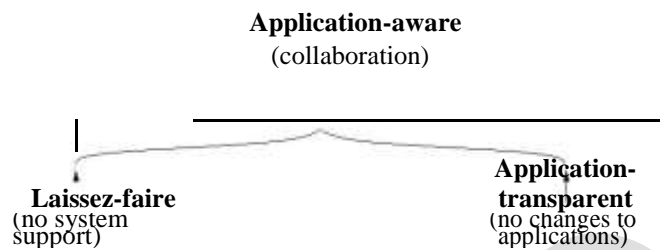


Figure 1: Range of Adaptation Strategies

The other extreme of *application-transparent adaptation* places entire responsibility for adaptation on the system. This approach is attractive because it is backward compatible with existing applications: they continue to work when mobile without any modifications. The system provides the focal point for resource arbitration and control. The drawback of this approach is that there may be situations where the adaptation performed by the system is inadequate or even counterproductive.

Between these two extremes lies a spectrum of possibilities that we collectively refer to as *application-aware adaptation*. By supporting a collaborative partnership between applications and the system, this approach permits applications to determine how best to adapt, but preserves the ability of the system to monitor resources and enforce allocation decisions.

1.4. The Extended Client-Server Model

Another way to characterize the impact of mobile computing constraints is to examine their effect on the classic client-server model. In this model, a small number of trusted server sites constitute the true home of data. Efficient and safe access to this data is possible from a much larger number of untrusted client sites. Techniques such as caching and read-ahead can be used to provide good performance, while end-to-end authentication and encrypted transmission can be used to preserve security.

This model has proved to be especially valuable for scalability [16]. In effect, the client-server model decomposes a large distributed system into a small nucleus that changes relatively slowly, and a much larger and less static periphery of clients. From the perspectives of security and system administration, the scale of the system appears to be that of the nucleus. But from the perspectives of performance and availability, a user at the periphery receives almost standalone service.

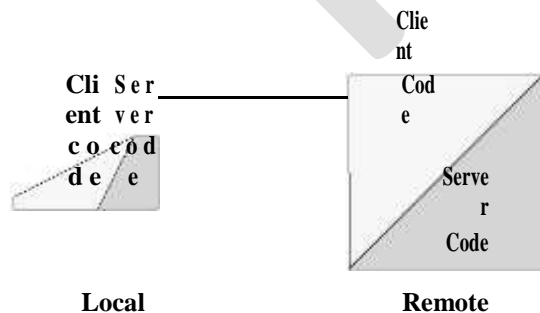


Figure 2: Temporary Blurring of Roles

Coping with the constraints of mobility requires us to rethink this model. The distinction between clients and servers may have to be temporarily blurred, resulting in the *extended client-server model* shown in Figure 2. The resource limitations of clients may require certain operations normally performed on clients to sometimes be performed on resource-rich servers. Conversely, the need to cope with uncertain connectivity requires clients to sometimes emulate the functions of a server. These are, of course, short-term deviations from the classic client-server model for purposes of performance and availability. From the longer-term perspective of system administration and security, the roles of servers and clients remain unchanged.

2. Summary of Coda and Odyssey Results

We have been exploring application-transparent adaptation since about 1990. Our research vehicle has been the *Coda File System*, a descendant of AFS [2]. Coda has been in active use for five years, and has proved to be a valuable testbed [13]. Coda clients are in regular use over a wide range of networks such as 10 Mb/s Ethernet, 2 Mb/s radio, and 9600 baud modems.

Since the research contributions of Coda have already been extensively documented in the literature, we only provide a high-level summary of the key results here:

Disconnected operation

Coda has demonstrated that disconnected operation is feasible, effective, and usable in a distributed Unix file system [3, 4, 17]. The key mechanisms for supporting disconnected operation include hoarding (user-assisted cache management), update logging with extensive optimizations while disconnected, and reintegration upon reconnection.

Optimistic replication

Coda was one of the earliest systems to demonstrate that an optimistic replica control strategy can be used for serious and practical mobile computing [6]. It incorporates several novel mechanisms to render this approach viable. These include log-based directory resolution [5], application-specific file resolution [7], and mechanisms for conflict detection, containment and manual repair.

Support for weak connectivity

Coda has shown that weak connectivity can be exploited to alleviate the limitations of disconnected operation [12]. The mechanisms needed to accomplish this include adaptive transport protocols, a rapid cache validation mechanism, a trickle reintegration mechanism for propagating updates, and model-based cache miss handling for usability.

Isolation-only transactions

In the context of Coda, a new abstraction called isolation-only transaction has been developed to cope with the detection and handling of read-write conflicts during disconnected operation [9]. This abstraction selectively incorporates concepts from database transactions, while making minimal demands of resource-poor mobile clients and preserving upward compatibility with Unix applications.

Server replication

Coda has shown how server replication can be used to complement disconnected operation [15]. Although this is not particularly relevant to mobility, it is an important result in distributed systems because it clarifies the relationship between first-class (i.e., server) replicas and second-class replicas (i.e., client caches). It also represents one of the first demonstrations of optimistic replication applied to a distributed system with the client-server model.

More recently, we have begun exploration of application-aware adaptation in *Odyssey*, a platform for mobile computing. An preliminary prototype of Odyssey has been built [14, 18], and a more complete prototype is under development. The early evidence is promising, but it is far too early for definitive results.

3. Fertile Topics for Exploration

We now turn to the discussion of promising research topics in mobile computing. By its very nature, this section of the paper is highly

speculative and will raise far more questions than it answers. Further, this is a selective list: it is certainly not intended to be complete. Rather, my goal is to give the reader a tantalizing glimpse of the rich problem space defined by mobile computing.

In choosing the five topics discussed below, I have followed two guidelines. First, these problems are more likely to be solved by rigor and analysis than by implementation and experience. Second, each of these problems is real, not contrived. Good solutions and insights to these problems will strongly impact the mobile computing systems of the future.

Each topic is presented in two parts: a brief discussion that lays out the problem space of the topic, followed by a sample of open questions pertaining to it. Again, my aim in posing these questions is not to be exhaustive but to offer food for thought.

3.1. Caching Metrics

Caching plays a key role in mobile computing because of its ability to alleviate the performance and availability limitations of weakly-connected and disconnected operation. But evaluating alternative caching strategies for mobile computing is problematic.

Today, the only metric of cache quality is the *miss ratio*. The underlying assumption of this metric is that all cache misses are equivalent (that is, all cache misses exact roughly the same penalty from the user). This assumption is valid when the cache and primary copies are strongly connected, because the performance penalty resulting from a cache miss is small and, to a first approximation, independent of file length. But the assumption is unlikely to be valid during disconnected or weakly-connected operation.

The miss ratio also fails to take into account the timing of misses. For example, a user may react differently to a cache miss occurring within the first few minutes of disconnection than to one occurring near the end of the disconnection. As another example, the periodic spin-down of disks to save power in mobile computers makes it cheaper to service a certain number of page faults if they are clustered together than if they are widely spaced.

To be useful, new caching metrics must satisfy two important criteria. First, they should be consistent with qualitative perceptions of performance and availability experienced by users in mobile computing. Second, they should be cheap and easy to monitor. The challenge is to develop such metrics and demonstrate their applicability to mobile computing. Initial work toward this end is being done by Ebling [1].

3.1.1. Some Open Questions

- What is an appropriate set of caching metrics for mobile computing?
- Under what circumstances does one use each metric?
- How does one efficiently monitor these metrics?
- What are the implications of these alternative metrics for caching algorithms?

3.2. Semantic Callbacks and Validators

Preserving cache coherence under conditions of weak connectivity can be expensive. Large communication latency increases the cost of validation of cached objects. Intermittent failures increase the frequency of validation, since it must be performed each time communication is restored. A lazy approach that only validates on demand could reduce validation frequency; but this approach would worsen consistency because it increases the likelihood of stale objects being accessed while disconnected. The cost of cache coherence is exacerbated in systems like Coda that use anticipatory caching for availability, because the number of objects cached (resident set size) is much larger than the number of objects in current use (working set size).

The Coda solution is to maintain cache coherence at multiple levels of granularity and to use callbacks [11]. Clients and servers maintain version information on individual objects as well as entire subtrees of them. Rapid cache validation is possible by comparing version stamps on the subtrees. Once established, validity can be maintained through callbacks. This approach to cache coherence trades precision of invalidation for speed of validation. It preserves correctness while dramatically reducing the cost of cache coherence under conditions of weak connectivity. Usage measurements from Coda confirm that these potential gains are indeed achievable in practice [12].

The idea of maintaining coherence at multiple granularities can be generalized to a variety of data types and applications in the following way:

- 1 a client caches data satisfying some predicate P from a server.
- 2 the server remembers a predicate Q that is much cheaper to compute, and possesses the property Q implies P . In other words, as long as Q is true, the cached data it corresponds to is guaranteed to be valid. But if Q is false, nothing can be inferred about

that data.

- 3 On each update, the server re-evaluates Q . If Q becomes false, the server notifies the client that its cached data might be stale.
- 4 Prior to its next access, the client must contact the server and obtain fresh data satisfying P .

We refer to Q as a *semantic callback* for P , because the interpretation of P and Q depends on the specifics of the data and application. For example, P would be an SQL select statement if one is caching data from a relational database. Or it could be a piece of code that performs a pattern match for a particular individual's face from a database of images. Q must conform to P : a simpler select statement in the first case, and a piece of code that performs a much less accurate pattern match in the second case. In Coda, P corresponds to the version number of an object being equal to a specific value (x), while Q corresponds to the version number of the encapsulating volume being unchanged since the last time the version number of the object was confirmed to be x .

Semantic validation can be extended to domains beyond mobile computing. It will be especially valuable in geographically widespread distributed systems, where the timing difference between local and remote actions is too large to ignore even when communication occurs at the speed of light. The predicate Q in such cases serves as an inexpensive *validator* for cached data satisfying some complex criteria.

Consider the example of a transcontinental distributed system in the United States. Even at the speed of light, communication from one coast to the other takes about 16 milliseconds. A round trip RPC will take over 30 milliseconds. During this time, a client with a 100 MIP processor can execute over 3 million instructions! Since processor speed can be expected to increase over time, the lost computational opportunity represented by this scenario will only worsen.

Over time, the synchronous model implicit in the use of RPC will become increasingly untenable. Eventually, very wide-area distributed systems will have to be structured around an asynchronous model. At what scale and timeframe this shift will occur depends on two factors: the substantially simpler design, implementation, and debugging inherent in the synchronous model, and the considerably higher performance (and hence usability) of the asynchronous model.

One promising asynchronous model is obtained by combining the idea of cheap but conservative validation with the style of programming characterized by optimistic concurrency control [8]. The resulting approach bears some resemblance to the use of hints in distributed systems [19], and is best illustrated by an example.

Consider remote control of a robot explorer on the surface of Mars. Since light takes many minutes to travel from earth to Mars, and emergencies of various kinds may arise on Mars, the robot must be capable of reacting on its own. At the same time, the exploration is to be directed live by a human controller on earth — a classic command and control problem.

This example characterizes a distributed system in which communication latency is large enough that a synchronous design paradigm will not work. The knowledge of the robot's status will always be obsolete on earth. But, since emergencies are rare, this knowledge will usually differ from current reality in one of two benign ways. Either the differences are in attributes irrelevant to the task at hand, or the differences can be predicted with adequate accuracy by methods such as dead reckoning. Suppose the robot's state is P , as characterized in a transmission to earth. Based on some properties, Q , of this state, a command is issued to the robot. For this command to be meaningful when it reaches the robot, Q must still be true. This can be verified by transmitting Q along with the command, and having the robot validate Q upon receipt. For this approach to be feasible, both transmitting and evaluating Q must be cheap.

There are, of course, numerous detailed questions to be answered regarding this approach. But it does offer an intriguing way of combining correctness with performance in very wide-area distributed systems.

3.2.1. Some Open Questions

4. Under what circumstances are semantic callbacks most useful? When are they not useful?
5. What forms can P and Q take for data types and applications in common use? How does one estimate their relative costs in those cases?
6. Can P and Q really be arbitrary code? Are there restrictions necessary for efficiency and practicality?
7. How does one derive Q from P quickly? Are there restrictions on P that make this simpler?

How does one trade off the relative cost and benefit of P and Q ? Is the tradeoff space discrete or continuous? Can this tradeoff be made adaptive?

3.3. Algorithms for Resource Revocation

Application-aware adaptation complicates the problem of resource management. In principle, the system owns all resources. At any

time, it may revoke resources that it has temporarily delegated to an application. Alas, reality is never that simple. A variety of factors complicate the problem.

First, some applications are more important than others. Any acceptable revocation strategy must be sensitive to these differences. Second, the cost of revoking the same resource may be different to different applications. For example, reducing the bandwidth available to one application may result in its substantially increasing the amount of processing it does to compensate. A similar reduction in bandwidth for another application may result in a much smaller increase in processing. A good revocation strategy must take into account these differential impacts. Third, there may be dependencies between processes that should be taken into account during revocation. For example, two processes may have a producer-consumer relationship. Revoking resources from one process may cause the other to stall. More complex dependencies involving multiple processes are also possible. Unless revocation takes these dependencies into account, hazards such as deadlocks may occur.

Revocation of resources from applications is not common in current systems. Classical operating systems research has focused on resource allocation issues rather than resource revocation. As a result there is currently little codified knowledge about safe and efficient techniques for revocation. This deficiency will have to be remedied as application-aware adaptation becomes more widely used.

3.3.1. Some open questions

- How does one formulate the resource revocation problem?
- How does one characterize the differential impact of revocation on different applications?
- What strategies does one use if multiple resources must be simultaneously revoked?
- How does one distinguish between resources whose revocation is easy to recover from and those it is expensive or impossible to recover from?
- How does one handle deadlocks during revocation?
-

3.4. Analysis of Adaptation

How does one compare the adaptive capabilities of two mobile clients? The primary figure of merit is *agility*, or the ability of a client to promptly respond to perturbations. Since it is possible for a client to be more agile with respect to some variables (such as bandwidth) than others (such as battery power), agility should be viewed as a composite metric.

A system that is highly agile may suffer from *instability*. Such a system consumes almost all its resources reacting to minor perturbations, hence performing little useful computation. The ideal mobile client is obviously one that is highly agile but very stable with respect to all variables of interest.

Control theory is a domain that might have useful insights to offer in refining these ideas and quantifying them. Historically, control theory has focused on hardware systems. But there is no conceptual reason why it cannot be extended to software systems. Only careful investigation can tell, of course, whether the relevance is direct and useful or merely superficial.

3.4.1. Some open questions

- What are the right metrics of agility?
- Are there systematic techniques to improve the agility of a system?
- How does one decide when a mobile system is "agile enough"?
- What are the right metrics of system stability?
- Can one develop design guidelines to ensure stability?
- Can one analytically derive the agility and stability properties of an adaptive system without building it first?

3.5. Global Estimation from Local Observations

Adaptation requires a mobile client to sense changes in its environment, make inferences about the cause of these changes, and then react appropriately. These imply the ability to make global estimates based on local observations.

To detect changes, the client must rely on local observations. For example, it can measure quantities such as local signal strength, packet rate, average round-trip times, and dispersion in round-trip times. But interpreting these observations is nontrivial. A change in a given quantity can be due to a multiplicity of non-local phenomena. For example, packet rate will drop due to an overload on a distant server. But it will also drop when there is congestion on an intermediate network segment. If an incorrect cause is inferred from an observation, the adaptation performed by the client may be ineffective or counterproductive.

At present there is no systematic theory to guide global estimation from local observations. The problem is especially challenging in

the absence of out-of-band communication, because the client cannot use an alternative channel to help narrow the diagnosis on the main communication channel.

3.5.1. Some Open Questions

- Are there systematic ways to do global estimation from local estimates?
- Can one bound the error in global estimates?
- What is the relationship of global estimation to agility of adaptation? Can one quantify this relationship?
- Can one provide system support to improve global estimation? For example, do closely-synchronized, low-drift clocks on clients and servers help?
- Can one quantify the benefits of out-of-band channels? For example, how much does the presence of a low-latency, low-bandwidth channel help with estimates on a parallel high-latency, high-bandwidth channel?

Acknowledgements

This paper is the result of many years of interaction and brainstorming with members of the Coda and Odyssey projects. These members include Jay Kistler, Puneet Kumar, David Steere, Lily Mummert, Maria Ebling, Hank Mashburn, Brian Noble, Masashi Kudo, Josh Raiff, Qi Lu, Morgan Price, Hiroshi Inamura, Tetsuro Muranaga, Bob Baron, Dushyanth Narayanan, and Eric Tilton.

I wish to thank Vassos Hadzilacos and Yoram Moses, the program chairmen of the Fourteenth and Fifteenth ACM Symposia on Principles of Distributed Computing respectively, for giving me the opportunity to present these thoughts as an invited speaker at PODC '95 and as an invited paper in the proceedings of PODC '96. I also wish to thank Matt Zekauskas and Brian Noble for their help in reviewing and improving the presentation of the paper.

4. Conclusion

The tension between autonomy and interdependence is intrinsic to all distributed systems. Mobility exacerbates this tension, making it necessary for mobile clients to tolerate a far broader range of external conditions than has been necessary hitherto.

Adaptation is the key to mobility. By using local resources to reduce communication and to cope with uncertainty, adaptation insulates users from the vagaries of mobile environments. Our research is exploring two different approaches to adaptation: application-transparent and application-aware. Our experience with Coda confirms that application-transparent adaptation is indeed viable and effective for a broad range of important applications. In circumstances where it is inadequate, our initial experience with Odyssey suggests that application-aware adaptation is the appropriate strategy.

In closing, it is worth speculating on the long-term impact of mobility on distributed systems. In his book *Mind Children*, my colleague Hans Moravec draws an analogy between the seminal role of mobility in the evolution of biological species, and its influence on the capabilities of computing systems [10]. Although Hans' comments are directed at robotic systems, I believe that his observation applies equally well to a much broader class of distributed computing systems involving mobile elements. Mobility will influence the evolution of distributed systems in ways that we can only dimly perceive at the present time. In this sense, mobile computing is truly a seminal influence on the design of distributed systems.

REFERENCES:

- [1] Ebling, M.R. Evaluation and Improving the Effectiveness of Caching Availability, PhD thesis, Department of Computer Science, Carnegie Mellon University, 1997 (in preparation).
- [2] Howard, J.H., Kazar, M.L., Menees, S.G., Nichols, D.A., Satyanarayanan, M., Sidebotham, R.N., West, M.J. Scale and Performance in a Distributed File System. *ACM Transactions on Computer Systems* 6(1), February, 1988.
- [3] Kistler, J.J., Satyanarayanan, M. Disconnected Operation in the Coda File System. *ACM Transactions on Computer Systems* 10(1), February, 1992.
- [4] Kistler, J.J. *Disconnected Operation in a Distributed File System*. PhD thesis, Department of Computer Science, Carnegie Mellon University, May, 1993.
- [5] Kumar, P., Satyanarayanan, M. Log-Based Directory Resolution in the Coda File System. In *Proceedings of the Second International Conference on Parallel and Distributed Information Systems*. San Diego, CA, January, 1993.
- [6] Kumar, P. *Mitigating the Effects of Optimistic Replication in a Distributed File System*. PhD thesis, School of Computer Science, Carnegie Mellon University, December, 1994.
- [7] Kumar, P., Satyanarayanan, M. Flexible and Safe Resolution of File Conflicts. In *Proceedings of the 1995 USENIX Technical Conference*, New Orleans, LA, January, 1995.
- [8] Kung, H.T., Robinson, J. On Optimistic Methods for Concurrency Control. *ACM Transaction on Database Systems* 6(2), June, 1981.
- [9] Lu, Q., Satyanarayanan, M. Improving Data Consistency in Mobile Computing Using Isolation-Only Transactions. In

- Proceedings of the Fifth Workshop on Hot Topics in Operating Systems*. Orcas Island, WA, May, 1995.
- [10] Moravec, H. *Mind Children*. Harvard University Press, Cambridge, MA, 1988.
- [11] Mummert, L.B., Satyanarayanan, M. Large Granularity Cache Coherence for Intermittent Connectivity. In *Proceedings of the 1994 Summer USENIX Conference*. Boston, MA, June, 1994.
- [12] Mummert, L.B., Ebling, M.R., Satyanarayanan, M. Exploiting Weak Connectivity for Mobile File Access. In *Proceedings of the Fifteenth ACM Symposium on Operating Systems Principles*. Copper Mountain Resort, CO, December, 1995.
- [13] Noble, B., Satyanarayanan, M. An Empirical Study of a Highly-Available File System. In *Proceedings of the 1994 ACM Sigmatics Nashville, TN, May, 1994. Conference*.
- [14] Noble, B., Price, M., Satyanarayanan, M. A Programming Interface for Application- Aware Adaptation in Mobile Computing. *Computing Systems* 8, Fall, 1995.
- [15] Satyanarayanan, M., Kistler, J.J., Kumar, P., Okasaki, M.E., Siegel, E.H., Steere, D.C. Coda: A Highly Available File System for a Distributed Workstation Environment. *IEEE Transactions on Computers* 39(4), April, 1990.
- [16] Satyanarayanan, M. The Influence of Scale on Distributed File System Design. *IEEE Transactions on Software Engineering* 18(1), January, 1992.
- [17] Satyanarayanan, M., Kistler, J.J., Mummert, L.B., Ebling, M.R., Kumar, P., Lu, Q. Experience with Disconnected Operation in a Mobile Computing Environment. In *Proceedings of the 1993 USENIX Symposium on Mobile and Location-Independent Computing*. Cambridge, MA, August, 1993.
- [18] Steere, D.C., Satyanarayanan, M. Using Dynamic Sets to Overcome High I/O Latencies During Search. In *Proceedings of the Fifth Workshop on Hot Topics in Operating Systems*. Orcas Island, WA, May, 1995.
- [19] Terry, D.B. Caching Hints in Distributed Systems, *IEEE Transactions in Software Engineering* SE-13(1), January, 1987

Stress and Displacement Analysis of Rectangular Stainless Steel Plate with Elliptical Cut-out of Different Orientation

S. Sambhu Prasad¹, G. Panduranga²

¹Professor & Principal, Department of Mechanical Engineering, Pragati Engineering College, Andhra Pradesh, India

principal@pragati.ac.in

²Assistant Professor, Department of Mechanical Engineering, Pragati Engineering College, Andhra Pradesh, India

panduranga.g@pragati.ac.in

Abstract— The study of stress and displacement analysis of rectangular stainless steel plate of size 300mm X 100mm X 10mm with elliptical cutout of size 40 mm major axis and 20mm minor axis at the centre of the plate with different orientation is carried out by using finite element formulation. The 3D plate is designed in CATIA V5 tool and analysis is carried out in ANSYS package. The plate with cutouts is often used in modern engineering like aerospace, mechanical and civil engineering applications. It is mainly focused on the study of stress concentration induced at the abrupt change of the cross section of the plate due to cutout. The changes of the stresses and displacements have been calculated for the different orientation of the cutout and are tabulated and discussed in this paper.

Keywords— Stress concentration, CATIA V5 and ANSYS.

INTRODUCTION

The plate with cutouts/openings is made into structure in order to full fill the requirement of service requirements in many engineering applications. Mainly in aerospace and marine applications high strength and low weight are the important parameters. So the basic structural members like plates with openings or cutouts are provided. But this cutouts leads to discontinuity in the cross section of the structural member and penetrates the strength. The flow of stress is disturbed with the discontinuity of the area and the concentration of the stress will be more at this critical area. This stress concentration increases the stress levels and it is high concern in the design of the total structure.

Stress Concentration:

Stress concentration is localized high stress due to the abrupt change or irregularities present in the cross section of the structural member. The localized stresses are found out by a factor nothing but the stress concentration factor. It is denoted by K_t . The stress concentration factor K_t is defined as the ratio of maximum stress at the cutout edge and nominal edge.

$$K_t = \frac{\text{Maximum stress}}{\text{Nominal stress}} = \frac{\sigma_{max}}{\sigma_{nom}}$$

DESCRIPTION OF THE PROBLEM

A rectangular plate of dimensions 300mmX100mmX10mm with an elliptical hole of size 40mm in major diameter and 10mm in minor diameter oriented at 0, 45, 90 and 135 degrees is located at the centre of the plate. This plate is subjected with a tensile load along the length of the plate at one end and constrained at the other end. The stresses developed at the vicinity of the elliptical hole. The solid body is designed by using CATIA V5 and the analysis is carried out by ANSYS software. The actual analysis is done is shown in the figure 1. The plate with cutout is subjected with the same load but stress developed and displacements for the each plate varies as the orientation of the elliptical cutout. As per the orientation of the elliptical cutout, the stress flows in the plate are different so that we can find out the critical orientation in which the stress levels will be more. The plate material considered in this problem is stainless steel. The dimensions and mechanical properties for the stainless steel are tabulated below.

Plate Material	Stainless Steel
Plate Dimensions	Length = 300 mm; Width =100 mm; Thickness=10 mm
Elliptical Cutout Dimensions	Major diameter = 40 mm; Minor Diameter = 20 mm
Young's Modulus	1.93e+11 Pa
Poisson's Ratio	0.31
Density	7750 kg/m ³
Tensile Yield Strength	2.07e+8 Pa
Tensile Ultimate Strength	5.86e+8 Pa

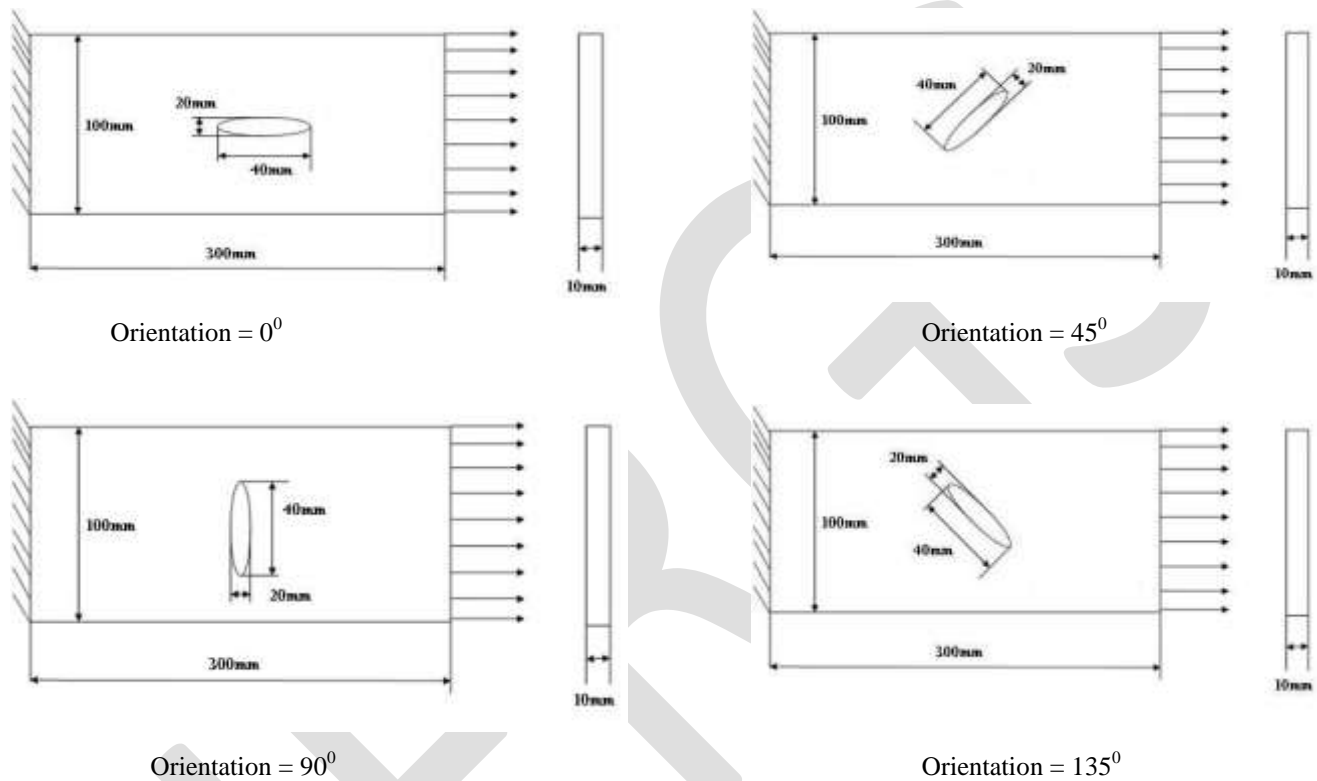


Figure1. The rectangular plate with elliptical cutouts with different orientations

MODELLING:

Introduction to CATIA V5

As per the dimensions taken, the plate is designed in 3D model using CATIA V5 software. CATIA [5- 7] (Computer Aided Three Dimensional Interactive Application) in 1980's in later implementation this company improved its feasibility and released the latest versions one by one i.e., V5R5, V5R7, V5R8.....V5R19, V5R21. CATIA is much faster and more accurate. Once a design is completed. 2D and 3D views are readily obtainable. The ability to changes in late design process is possible. It provides a very accurate representation of model specifying all other dimensions hidden geometry etc. It provides clear 3D models, which are easy to visualize and understand. CATIA provides easy assembly of the individual parts or models created it also decreases the time required for the assembly to a large extent. The designed plate is saved in IGS format so that the designed model can be easily opened in the ANSYS software.

The Sketcher workbench is a set of tools that helps to create and constrain 2D geometries. Features (pads, pockets, shafts, etc...) may then be created solids or modifications to solids using these 2D profiles. The part modeled in this paper is shown in the figure 2. The rectangular plate with elliptical cutout at the centre is created using simple profiles, lines and arcs. The geometries are constrained to conform to certain dimensions like lengths and diameters.

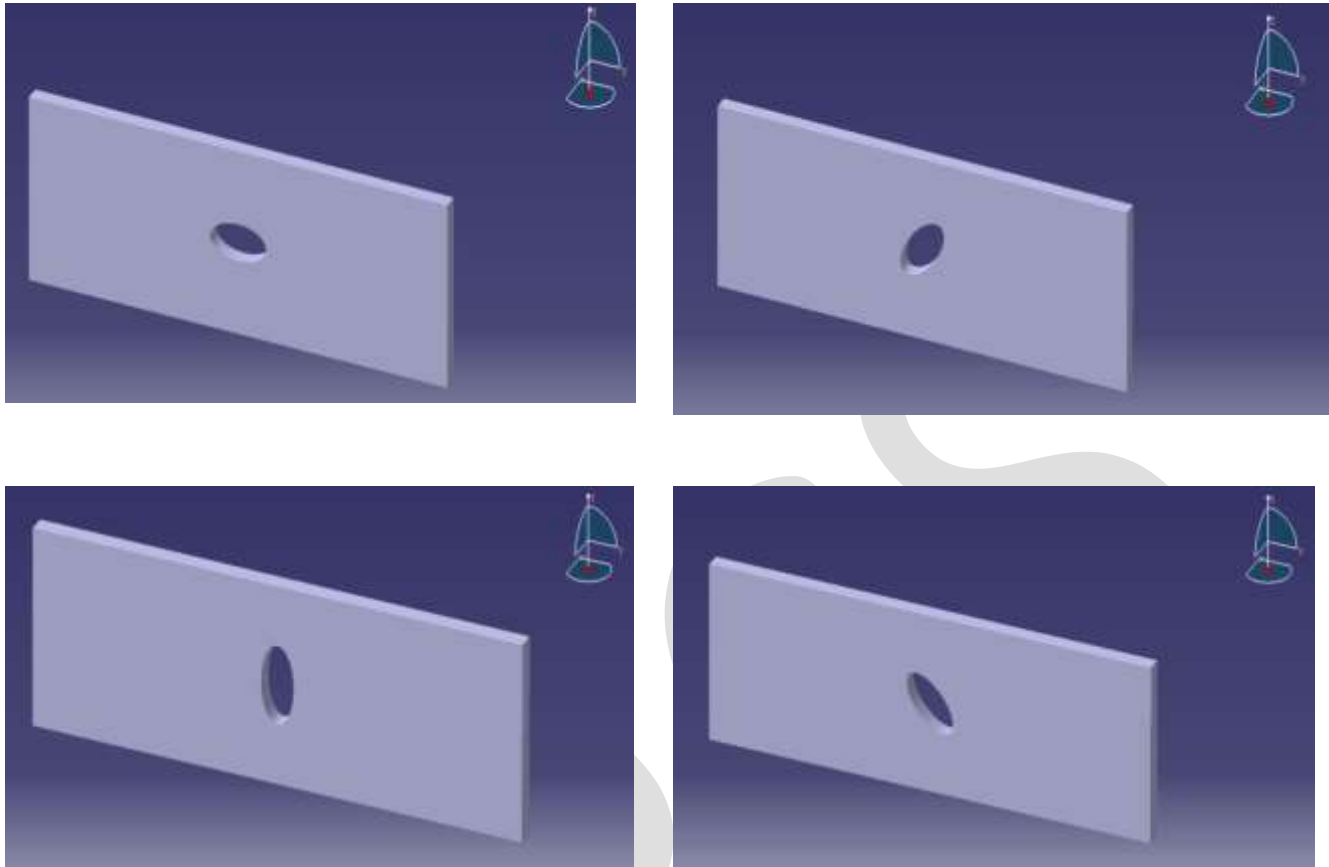


Figure2. Rectangular plate with elliptical cutout solid model design in CATIA V5

ANALYSIS:

Introduction to ANSYS

ANSYS is computer simulation software, mostly used for doing the analysis in the field of structural Mechanics, Multi physics, Fluid Dynamics, Explicit Dynamics, Electromagnetic, Hydrodynamics.

The following are the analysis steps involved in the ANSYS. They may be

Preprocessing

- Define element type, real constants, and material properties
- Define geometry Processors

Solution

- Define type of analysis
- Set boundary conditions
- Apply loads
- Initiate finite element solution

Post processing

- Review results using graphical displays and tabular listings
- Verify against analytical solutions

The modeled plate is opened in the ANSYS tool and static analysis is carried out by applying a force 3KN at the one of the plate. The other end is fully constrained by keeping all degrees of freedom is zero. The material properties like Young's modulus (E) for the plate is 1.93×10^{11} Pa, Poisson's ratio = 0.31 and Density 7750 kg/m^3 are given. The meshing operation is done and applied loads and displacements according to the requirements.

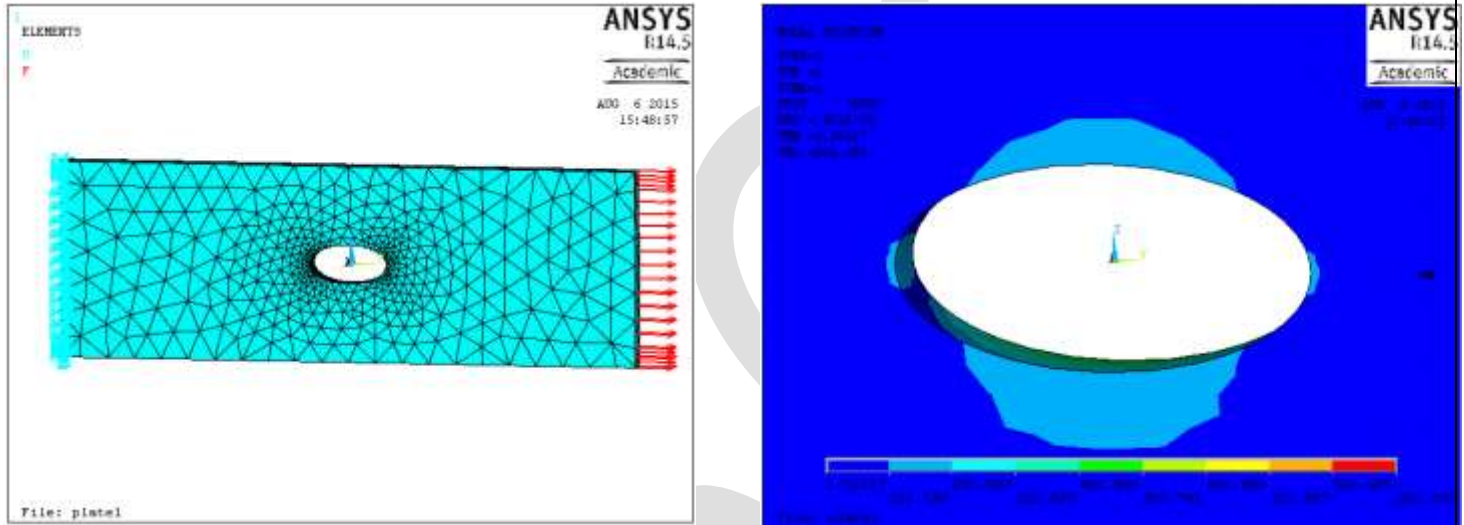


Figure 3: Plate with elliptical cutout with an orientation of 0 degrees and its stress distributions

The analysis of the rectangular plate with elliptical cutout with 0 degree orientation is done. The maximum displacement 0.431×10^{-5} m and maximum stress of 958.51 Pa is obtained.

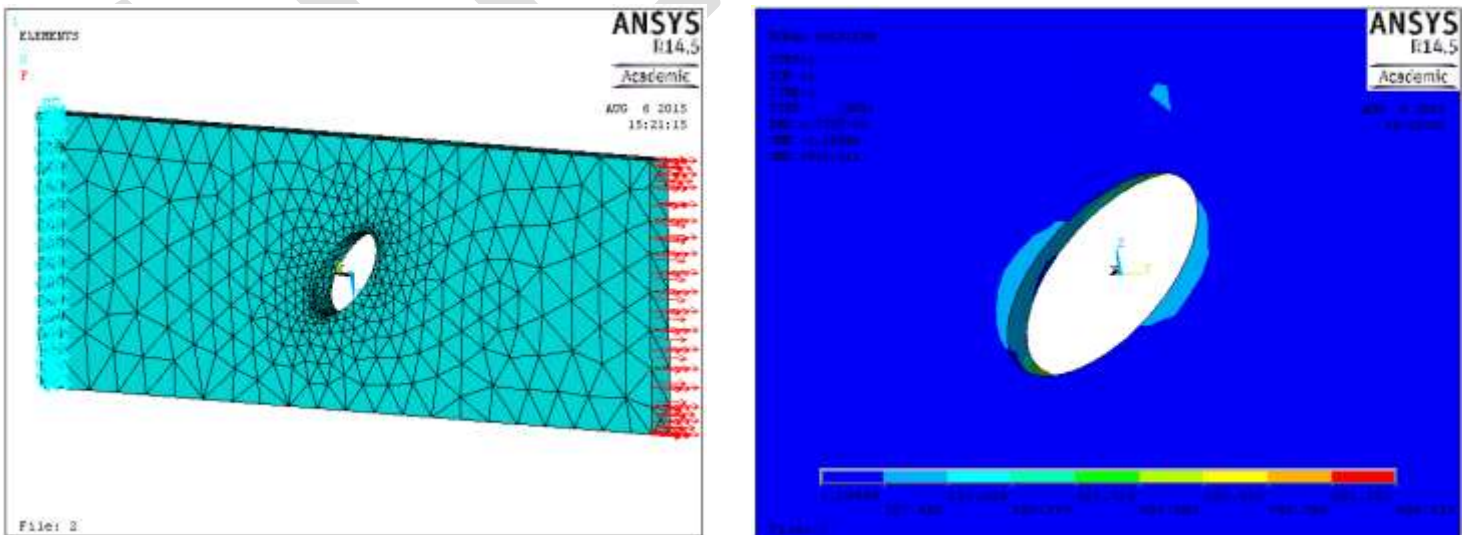


Figure 4: Plate with elliptical cutout with an orientation of 45 degrees and its stress distributions

The analysis of the rectangular plate with elliptical cutout with 45 degree orientation is done. The maximum displacement $0.776E-5$ m and maximum stress of 902.3 Pa is obtained.

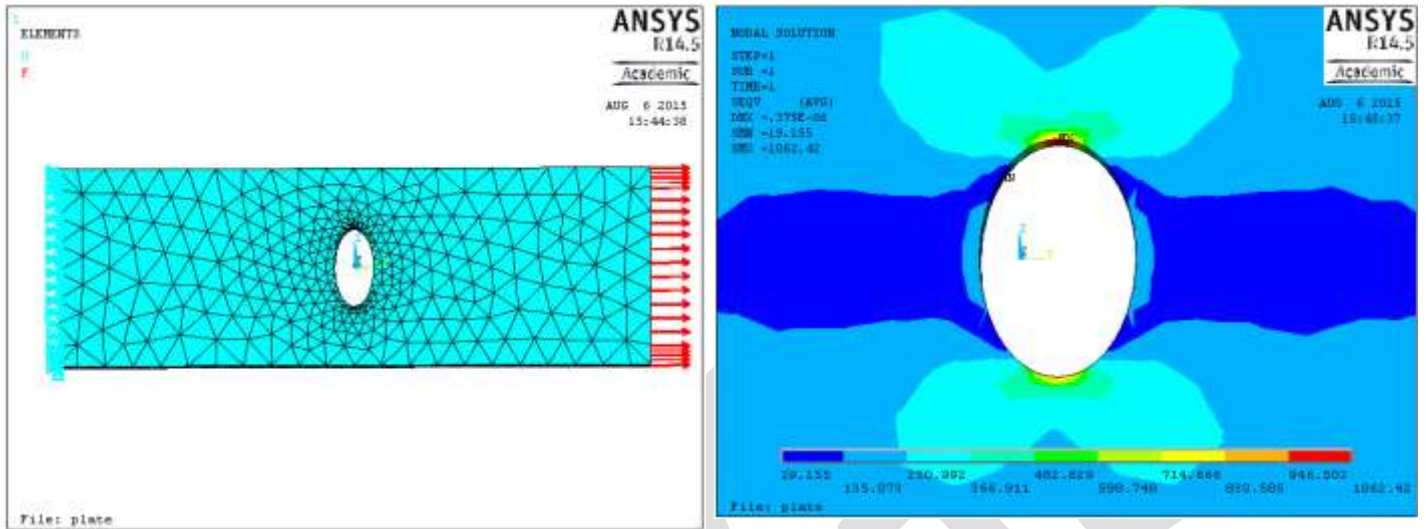


Figure 5: Plate with elliptical cutout with an orientation of 90 degrees and its stress distributions

The analysis of the rectangular plate with elliptical cutout with 90 degree orientation is done. The maximum displacement $0.375E-6$ m and maximum stress of 1062.42 Pa is obtained.

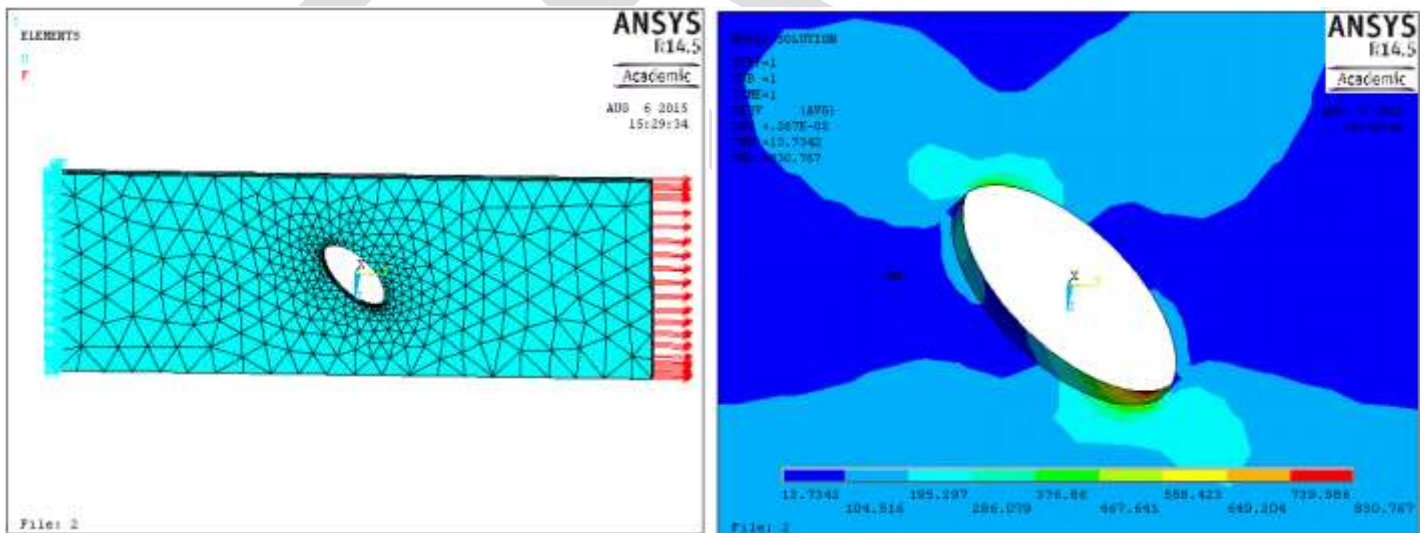


Figure 6: Plate with elliptical cutout with an orientation of 135 degrees and its stress distributions

The analysis of the rectangular plate with elliptical cutout with 135 degree orientation is done. The maximum displacement $0.267E-5$ m and maximum stress of 830.7 Pa is obtained.

RESULTS

After analysis is done the values of the maximum stress values and maximum displacements are observed and tabulated below.

Table 1: Von-Mises stress and displacements in the rectangular plate with elliptical cutout

S.NO	Cutout Orientation	Stress Values (Pa)	Displacements (m)
1	0 ⁰	958.51	0.431E-5
2	45 ⁰	902.3	0.776E-5
3	90 ⁰	1062.42	0.375E-6
4	135 ⁰	830.7	0.267E-5

ACKNOWLEDGMENT

I really thank to the management of Pragati engineering college for providing good systems and licensed software for doing this analysis.

CONCLUSION

After successful completion of the analysis the following conclusions can be made.

- ANSYS provides a very suitable way of determining stress induced in any body.
- The maximum stress concentration observed at the corners of the elliptical hole.
- As expected, the maximum stresses concentrated in the case of elliptical hole at 90⁰ orientations.
- The maximum displacements observed in the plate with elliptical cutout at 45⁰ orientations.
- ANSYS gives a more intuitive feel to the designer by displaying stress contours throughout the plate.

REFERENCES:

- [1] G. C. Mekalke, M. V. Kavade, S. S. Deshpande, "Analysis of plate with a circular hole by FEM" IOSR Journal of Mechanical and Civil Engineering (IOSR-JMCE) ISSN: 2278-1684, PP: 25-30
- [2] Dheeraj Gunwant, J. P. Singh, "Stress and Displacement Analysis of a Rectangular Plate with Central Elliptical Hole" International Journal of Engineering and Innovative Technology (IJEIT) Volume 3, Issue 3, September 2013
- [3] T. K. Paul, and K. M. Rao, "Stress analysis in circular holes in FRP laminates under transverse load," Computers & Structures, vol. 33(4), pp. 929-935, 1989.
- [4] R. A. Chaudhuri, "Stress concentration around a part through hole weakening laminated plate," Computers & Structures, vol. 27(5), pp. 601-609, 1987.
- [5] B. C. Patle, D. V. Bhope, "Evaluation of Stress Concentration Factors In Plate with Oblique Hole", Journal of Mechanical and Civil Engineering, Vol. 2 (2), pp. 28-32, 2012.
- [6] D. S. Sharma, Nirav P. Patel, Khushbu C. Panchal, "Stress distribution around triangular hole in orthotropic plate", Nuicone 10, 2010.
- [7] Jike Liu, Chengwu Cai, "Analytical solution to stress concentration problem in plates containing rectangular hole under biaxial tensions", Journal of Acta Mechanica Solida Sinica, Vol. 21, No. 5, 2008.
- [8] Jianlin Wang, Steven L. Crouch, Sofia G. Mogilevskaya, "A complex boundary integral method for multiple circular holes in an infinite plane", Journal of Engineering Analysis with Boundary Elements, Vol. 27, pp. 789-802, 2003.
- [9] Mohsen Mohammadi, John R. Dryden, Liying Jiang Stress concentration around a hole in a radially inhomogeneous plate International Journal of Solids and Structures 48 (2011) 483–491.
- [10] E. S. Folias and J.-J. Wang On the three-dimensional stress field around a circular hole in a plate of arbitrary thickness Computational Mechanics 1990;6(3):379–391.
- [11] A text book of Machine design by R.S Khurmi and J.K Gupta , 2005 Eurasia publishing house (pvt.) ltd

COMPARATIVE STUDY OF SELF-LIFT DC-DC CONVERTERS WITH HIGH VOLTAGE GAIN

Ajith Ashokan, Dr. Babu Paul, Jeena Joy

PG Student, Assistant Professor, Assistant Professor, Mar Athanasius College of Engineering, Kothamangalam, Kerala
ajithashokan135@gmail.com, 8129246511

Abstract— This paper discussed about two DC-DC converters with same design and different voltage gain. The voltage conversion ratio is different. Compared with the classical Cuk and buck–boost converters, the converter increases the voltage boost ability significantly using the switched capacitor and self-lift techniques. Here we discussed enhanced self-lift Cuk converter and self-lift Luo converter. It is featured with single power switch operation, common ground, transformerless structure, and clear energy delivery process. This compare study is done by MATLAB 2013a.

Keywords— Boost ability, DC–DC converter, Voltage gain, Cuk converter, Luo converter.

INTRODUCTION

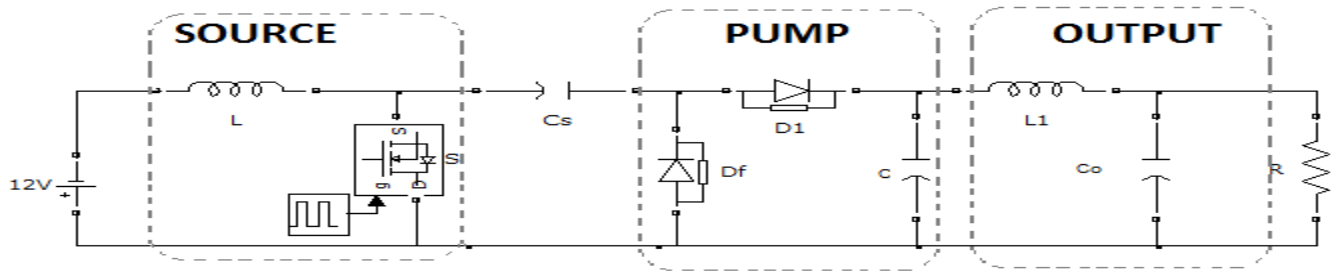
Many applications of switch-mode DC-DC converters require higher conversion rates. An alternative solution to this problem is to use n-stages connected in cascade, Such that the total conversion rate can be increased by an order of n. However, the resulting problems, energy losses, multiple power switches, and large switching surges in transformers significantly increase the control complexity and the cost of these converters [1]. The use of the voltage multiplier technique applied to the classical non-isolated DC–DC converters in order to obtain high step-up static gain, reduction of the maximum switch voltage, zero current switching turn-on. The diodes reverse recovery current problem is minimized and the voltage multiplier also operates as a regenerative clamping circuit, reducing the problems with layout and the EMI generation. These characteristics allows the operation with high static again and high efficiency, making possible to design a compact circuit for applications where the isolation is not required. The operation principle, the design procedure and practical results obtained from the implemented prototypes are presented for the single-phase and multiphase DC–DC converters [2]. The derived circuits can increase the voltage-conversion ratios under the single power switch condition, but the number of passive components is also obviously increased. Classical nonisolated DC–DC topologies, such as switched-capacitor (SC), switched-inductor (SL), hybrid SC/SL, and voltage-lift (VL) techniques, have been greatly explored. The main advantage of SC techniques is the absence of inductors, thus making it very small in size and high in power density[3][4]. Switched-capacitor technology is widely used in low power DC–DC converter. This method can reduce the high pulse current which usually causes serious problem in traditional converters. The well-known one is the charge pump circuits. They are widely used in low power DC–DC converter, especially in power management of the integrated circuits. Usually, they use high-frequency switching actions and only use capacitors to transfer the energy [5]-[8].

In this paper, the concept of the voltage self-lift techniques has been integrated into an SC cell, and consequently, a new step-up circuit is proposed on the basis of the classical converter.

SELF-LIFT CUK CONVERTER

Introduction

The concept of the voltage self-lift techniques has been integrated into an SC cell, and consequently, a new step up circuit is on the basis of the classical Cuk converter. As shown in Fig 1. Compared with the conventional Cuk prototype, two additional components (diode D_1 and capacitor C_1) are added into the circuit. However, the relative positions of the other components are kept invariant in the new circuit. Different from the Cuk prototype, a π -type low-pass filter C_1 - L_1 - C_o is constructed, and it results in the different voltage conversion mechanism. The voltage gain will be increase from $D/(1-D)$ to $(1)/(1-D)$. The voltage conversion is negative to positive polarity [9].

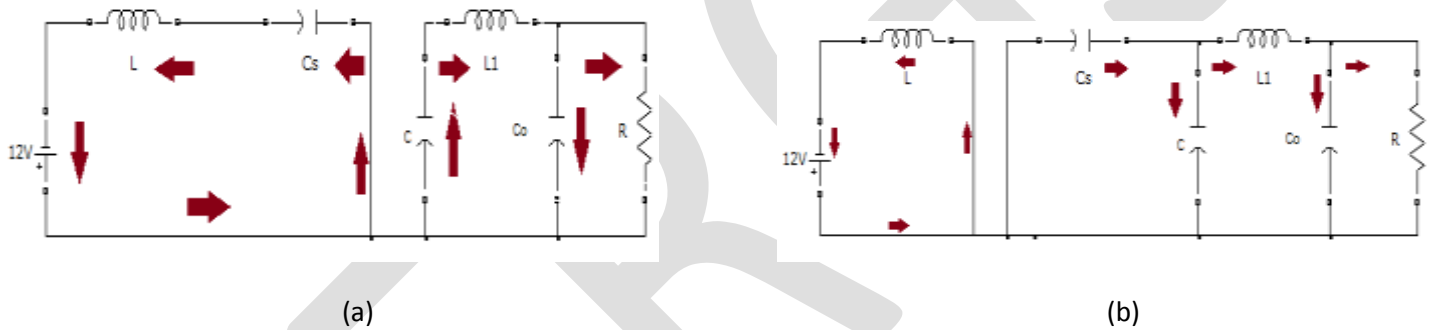


Self-lift cuk converter.

For the convenience of analysis, the whole circuit is divided into three different sections, as described in Fig. 1. L_1 belongs to the source section, and it performs the function of storing and transferring the energy from the source voltage V_{in} to C_s under the switching operation of S . C_1 , D_1 , and D_f form a pump section, in which C_1 is charged by C_s during each cycle and absorbs the energy stored in C_s like a pump. An output section formed by L_1 and C_o is combined with the pump section to perform the output filter function for the voltage of C_1 .

Working Principle

The converter structure operates in Continuous Conduction Mode (CCM). This circuit contains two mode of operation: a) ON Period, b) OFF Period.



Equivalent circuits. (a) Switching ON. (b) Switching OFF.

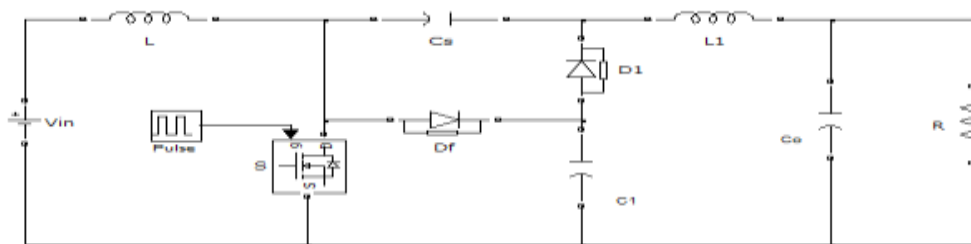
Mode 1 (During Switch ON): The equivalent circuit during switching ON is shown in Fig 2(a) When switch S turns ON, D_1 is ON, and D_f is OFF. C_1 performs characteristics to lift the output capacitor voltage V_{co} by the capacitor voltage V_{cs} .

Mode 2 (During Switching OFF): The equivalent circuit during switching OFF is shown in Fig 2(b). When S turns OFF, D_1 is OFF, and D_f is ON. C_1 performs characteristics to lift the output capacitor voltage V_{co} by the capacitor voltage V_{cs} .

SELF-LIFT LUO CONVERTER

Introduction

Voltage-lift technique is a popular method used in electronic circuit design. Applying this technique can effectively overcome the effect of the parasitic elements, and largely increase the voltage transfer gain.

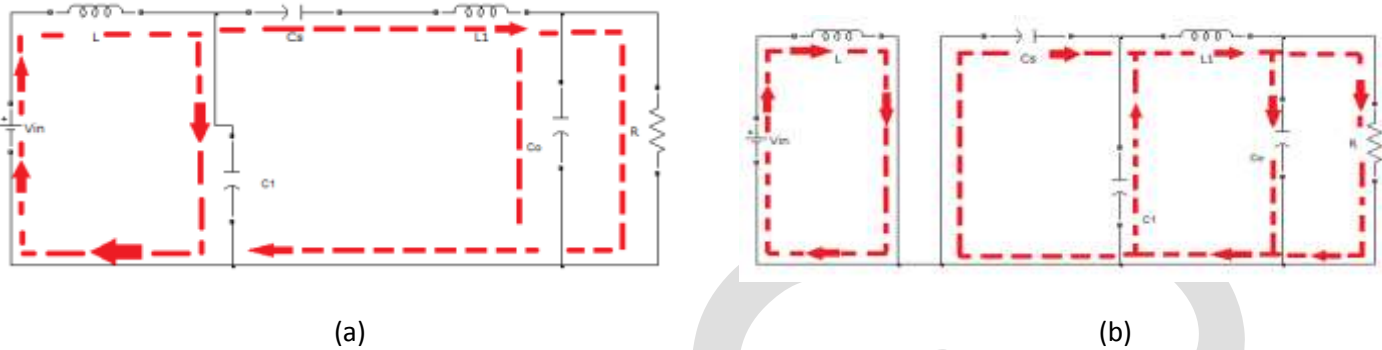


Self-lift cuk converter

Compared with above converter, number of the elements is equal and same design. The arrangements of the circuits are different. In this arrangement the voltage gain will be increase from $D/(1-D)$ to $(2-D)/(1-D)$. The voltage conversion is positive to positive polarity [10]-[12].

Working Principle

The converter structure operates in Continuous Conduction Mode (CCM). This circuit contains two mode of operation: a) OFF Period, b) ON Period



Equivalent circuits. (a) Switching OFF. (b) Switching ON.

Mode 1 (During Switching OFF): The equivalent circuit during switching OFF is shown in Fig 4(a) When S turns OFF, D_1 is OFF, and D_f is ON. The capacitors C_1 and C_s are charging by source. C_1 and C_s perform characteristics to lift the output capacitor voltage V_{co} .

Mode 2 (During Switching ON): The equivalent circuit during switching ON is shown in Fig 4(b) When switch S turns ON, D_1 is ON, and D_f is OFF. The capacitors C_1 and C_s are discharging through load. C_1 and C_s perform characteristics to lift the output capacitor voltage V_{co} .

DESIGN OF COMPONENTS

Design of Inductor L

Take input voltage $V_{in} = 12 V$ and output voltage $V_o = 32 V$, so the duty ratio $D = 0.63$ refers in equation Switching frequency $f = 50 kHz$ and $\Delta i_L = 0.3 A$. The peak to peak current variation of i_L $\Delta i_L = \frac{DV_{in}}{Lf}$

$$\therefore L = \frac{DV_{in}}{\Delta i_L f} \quad (1)$$

Design of Capacitor C_s

The peak to peak current variation of V_{cs} , $\Delta V_{cs} = \frac{V_o}{R.f.C_s}$, Ripple voltage $\Delta V_{cs} = 0.06 mV$ and load resistance $R = 100 \Omega$.

$$\therefore C_s = \frac{V_o}{R.f.\Delta V_{cs}} \quad (2)$$

Design of Capacitor C_1

The peak to peak current variation of V_{c1} , $\Delta V_{c1} = \frac{V_o(1-D)}{R.f.C_1}$, Ripple voltage $\Delta V_{c1} = 0.1 mV$ and load resistance $R = 100 \Omega$.

$$\therefore C_1 = \frac{V_o(1-D)}{R.f.\Delta V_{c1}} \quad (3)$$

Design of Inductor L_1

The peak-to-peak current variation of i_{L_1} can be calculated by the area A of a triangle with width $T/2$ and the height $V_{c1}/2$,

$$L_1 = \frac{V_o(1-D)}{8RC_1f^2\Delta i_{L_1}} \quad (4)$$

Design of Capacitor C_o

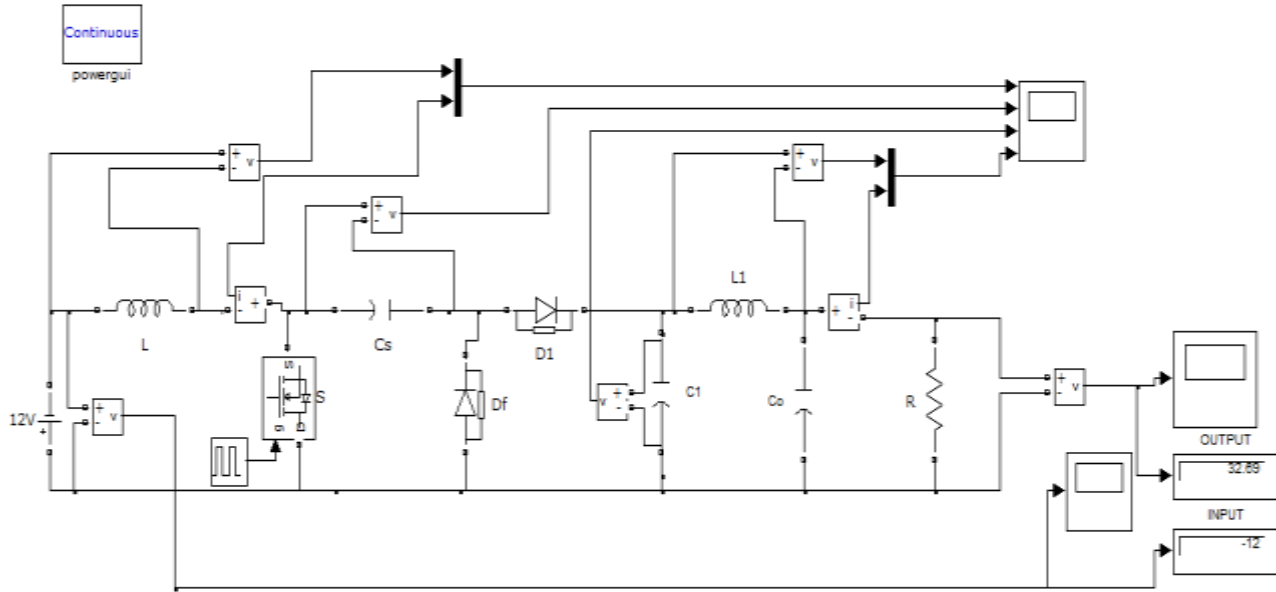
The peak-to-peak voltage variation of V_o is calculated by the area B of a triangle with width $T/2$ and the height $\Delta iL_1/2$

$$\therefore C_o = \frac{V_o(1-D)}{64Rf^3.L_1C_1\Delta V_{co}} \quad (5)$$

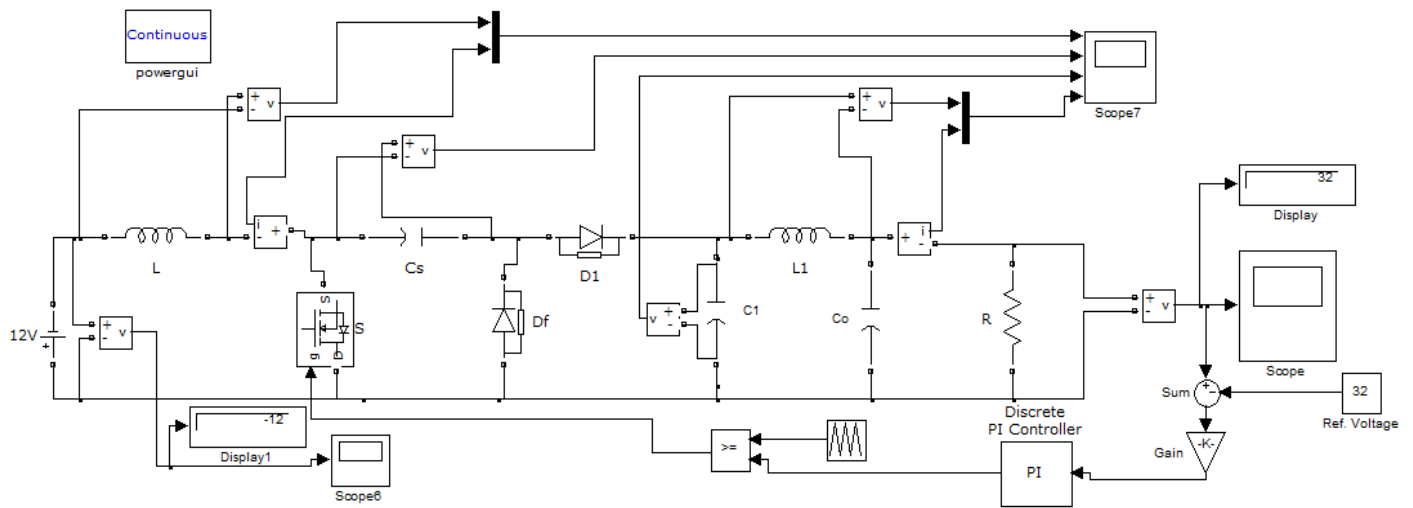
SIMULATION MODEL AND RESULTS

Self-Lift Cuk Converter Model

The simulation of the Cuk converter is done with the help of MATLAB SIMULINK. Here, discussed about two type of model, one is open model and other one is closed loop. In closed loop, PI controller is used for feedback signal.



(a)



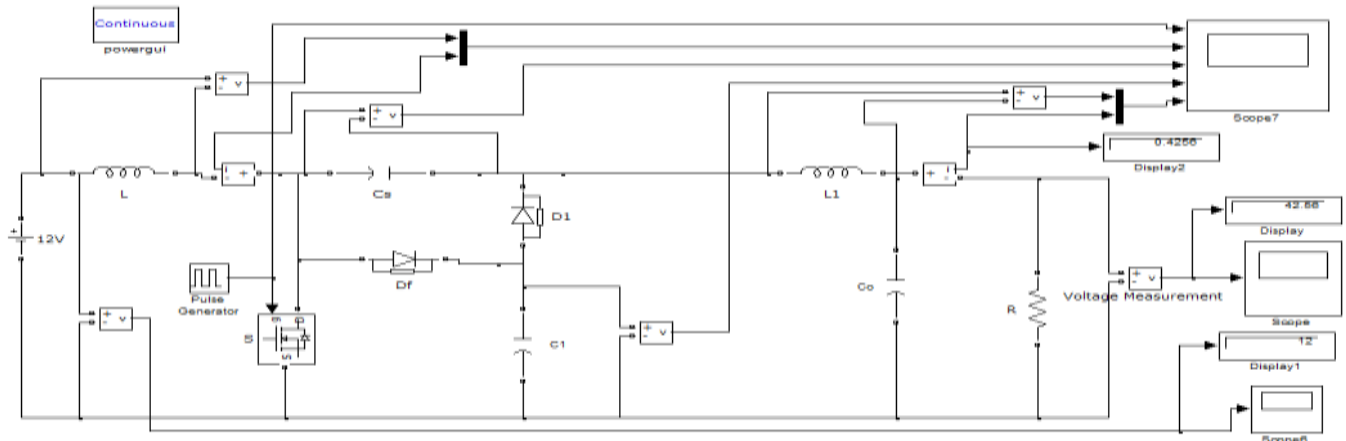
(b)

Self-lift Cuk converter model. (a) Open. (b) Closed.

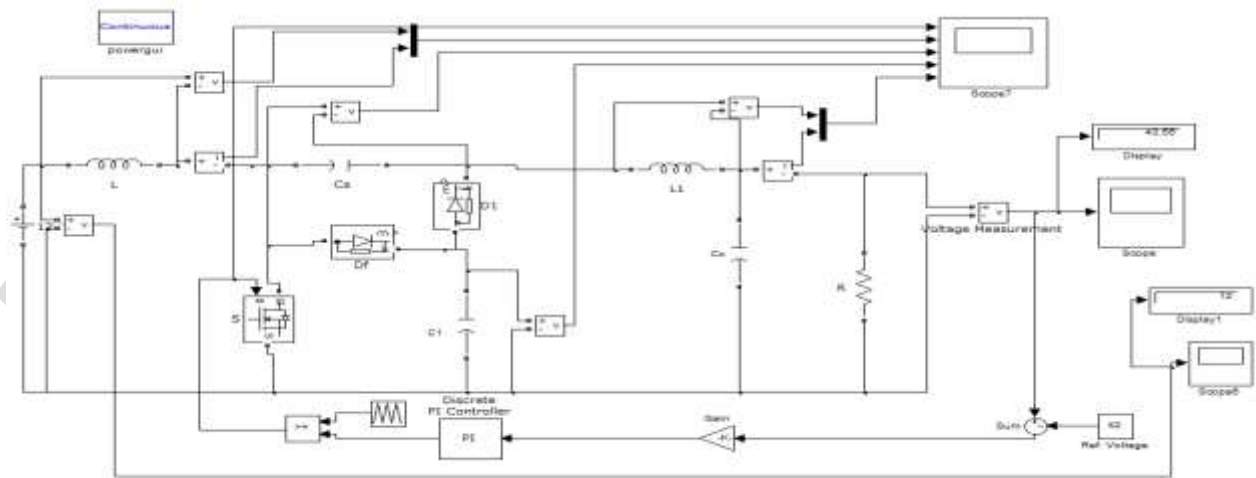
The main circuit parameters are chosen as follows: For an input voltage is 12V with load = 100Ω, $L = 500\mu H$, $C_s = 110\mu F$, $C_1 = 22\mu F$, $L_1 = 500\mu H$, $C_o = 47\mu F$ and $f = 50\text{ kHz}$. All the components are assumed ideal, and the voltage conversion aim is set as +32 V, as shown in Fig. 5(a). In order to increase the performance of the system closed path is provided. PI controller is used for controller purpose. The closed loop configuration of converter using PI controller, with $K_p=0.01$ and $K_i=0.75$ Pulse is created with the help of relational operator. Direct output of relational operator is given to gate signal.

Self-Lift Luo Converter Model

The simulation of the Luo converter is done with the help of MATLAB SIMULINK. Here, discussed about two type of model, one is open model and other one is closed loop. In closed loop, PI controller is used for feedback signal.



(a)



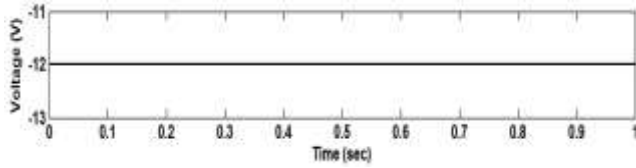
(b)

Self-lift Luo converter model. (a) Open. (b) Closed.

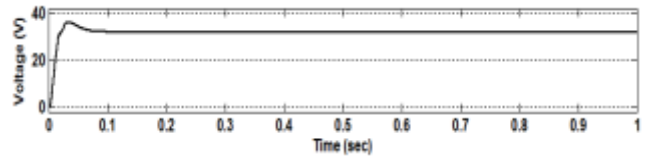
The models of self-lift Luo converter in open and closed model are shown in Fig. 6(a) and (b), respectively.

Self-Lift Cuk Converter Results

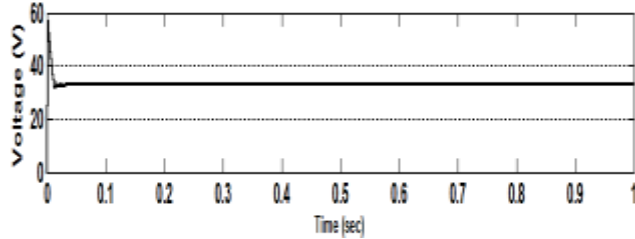
The input voltage of the converter is 12 V. Input voltage wave form is shown in Fig 7(a). Output voltage of the Cuk converter in open model is 32.69 V is shown in Fig 7(b). The output voltage of the Cuk converter in closed model is 32V and reference voltage is 32 V is shown in Fig 7(c). Input current of the converter is 1.92 A is shown in Fig 7(d). Output current of the converter is 3.269 A, current waveform is shown in Fig 7(e). Duty ratio is 63% as shown in Fig. 7(f).



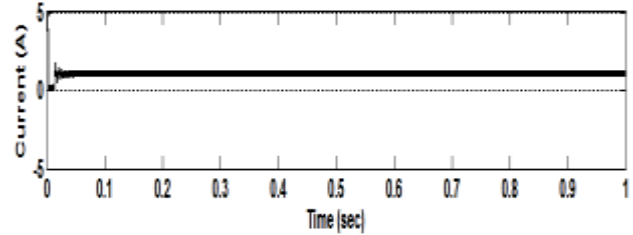
(a)



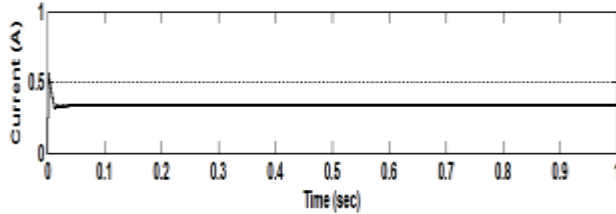
(b)



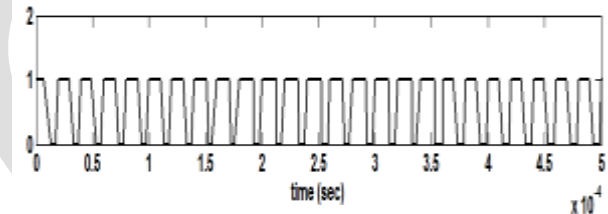
(c)



(d)



(e)

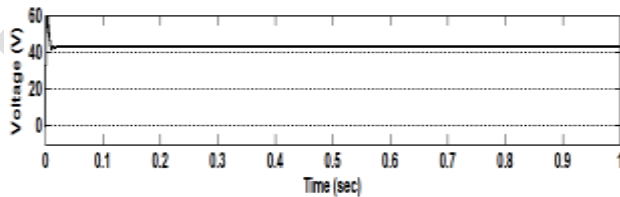


(f)

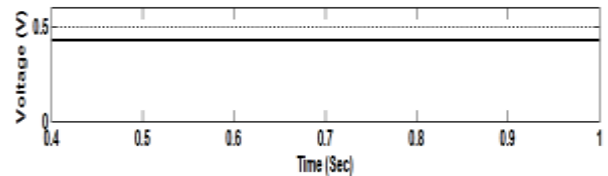
Simulated results in self-lift Cuk converter (a) Input Voltage (b) Output Voltage in open (c) Output Voltage in Closed (d) Input Current (e) Output Current, (f) Switching pulse

Self-Lift Luo Converter Results

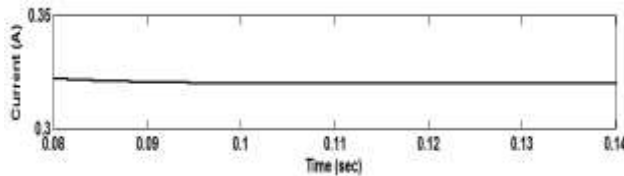
The input voltage of the converter is 12 V. Output voltage of the Cuk converter in open model is 42 V is shown in Fig 8(a). Output current of the converter is 0.42 A, current waveform is shown in Fig 8(b). Input current of the converter is 3.4 A is shown in Fig 8(c). Duty ratio is 63% as shown in Fig. 8(f).



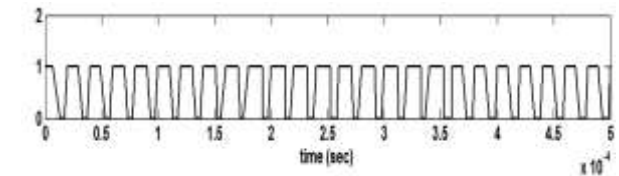
(a)



(b)



(c)



(d)

Simulated results in self-lift Luo converter (a) Output Voltage (b) Output Current (c) Input Current, (d) Switching pulse

CONCLUSION

By an in-depth topology analysis, it is known that the circuit (i.e., enhanced self-lift Cuk converter) can increase the voltage boost ability of the classical Cuk converter to a higher level. A negative to positive conversion path is provided to make it suitable for negative DC-voltage source with respect to the common ground. It also has the characteristics of high efficiency smooth currents at both sides, and small ripples in simple structures. It might be developed and used in the areas of various DC distributed power systems. Here input voltage is -12 V, and output is 32v

In Luo converter voltage boosting capability is increase, with equal number of elements and same design. A positive to positive conversion path is provided. Here input voltage 12V and output is 42 V. These works is done by MATLAB SIMULINK 2013a

REFERENCES:

- [1] J.A.Morales-Saldana, E. E. C. Gutierrez, and J. Leyva-Ranos, "Modelling of switch-mode dc-dc cascade converters," *IEEE Trans. Aerosp. Electron. Syst.*, vol. 38, no. 1, pp. 295–299, Jan. 2002.
- [2] F. Zhang, L. Du, F. Z. Peng, and Z. Qian, "A new design method for high-power high-efficiency switched-capacitor dc-dc converters," *IEEE Trans. Power Electron.*, vol. 23, no. 2, pp. 832–840, Mar. 2008.
- [3] B. Axelrod, "Switched Capacitor/Switched-Inductor Structures For Getting Transformerless Hybrid DC-DC PWM Converters."
- [4] M. Prudente, L. L. Pfitscher, G. Emmendoerfer, E. F. Romanelli, and R. Gules, "Voltage multiplier cells applied to non-isolated dc-dc converters," *IEEE Trans. Power Electron.*, vol. 23, no. 2, pp. 871–887, Mar. 2008.
- [5] M. Zhu and F. L. Luo, "Voltage-lift-type Cuk converters: Topology and analysis," *IET Power Electron.*, vol. 2, no. 2, pp. 178–191, Mar. 2009.
- [6] J. Sun and V. Mehrotra, "Orthogonal winding structures and design for planar integrated magnetics," *IEEE Trans. Ind. Electron.*, vol. 55, no. 3, pp. 1463–1469, Mar. 2008.
- [7] M. Zhu and F. L. Luo, "Series SEPIC implementing voltage lift technique for dc-dc power conversion," *IET Power Electron.*, vol. 1, no. 1, pp. 109–121, Mar. 2008.
- [8] M. D. Seeman and S. R. Sanders, "Analysis and optimization of switched capacitor dc-dc converters," *IEEE Trans. Power Electron.*, vol. 23, no. 2, pp. 841–851, Mar. 2008.
- [9] Miao Zhu and Fang Lin Luo, "Enhanced Self-Lift Cuk Converter for negative to positive voltage conversion" *IEEE Trans. Power Electron.*, vol. 25, no. 9, pp. 841–851, Sept. 2010.
- [10] Fang Lin Luo, Ph.D. and Hong Ye, Ph.D. "DC/DC Conversion Technique and Twelve Series Luo-converters", chapter 14, 2007
- [11] Rashid M. H. "Power Electronics: Circuits, Devices and Applications" Second edition, **Prentice-Hall**, USA, 1993.

A Triclass Image Segmentation using Adaptive K-means Clustering and Otsu's Method

Parvathy U S, Stephe Sara Philipose
P.G Scholar, Dept of CSE, BMCE, Kollam, Kerala, India
Parvathyus125@gmail.com

Abstract— Image segmentation is used to cluster an image based on features or regions of an image. So each cluster represents each segment. There are different segmentation algorithms, in which thresholding segmentation has an important role. Thresholding is used to obtain binary of an image, in which one state represent the foreground and the complementary represent the background. Among the various thresholding methods otsu method is the best with respect to the time and accuracy. Here we present the modification of otsu method by combining it with adaptive k-means clustering algorithm. Based on the otsu's threshold and two mean values, the algorithm separate it into three regions such as background, foreground and the TBD (to-be-determined) region. The further processing carried out in this TBD region, which is between the two mean values. In this region we apply the adaptive k-means algorithm. The process stops until no cluster left with the image. The new method can achieve good performance in some challenging cases, such as identifying weak objects and revealing fine structures of complex objects while the added computational cost and time is minimal.

Keywords — Binarization, Segmentation, Threshold, Otsu's Method, Triclass Segmentation, Adaptive k-means Clustering.

INTRODUCTION

Image segmentation is useful in any context where an image (such as a photograph) is to be in any way analyzed automatically by computer [5]. image processing and computer vision applications usually require binary images (i.e. black and white) as an introductory step in order to do further processing. The simplest way to use image binarization is to choose a threshold value, and classify all pixels with values above this threshold as white, and all other pixels as black. By choosing a particular intensity value as threshold, the thresholding segmentation can be broadly classified into global and local thresholding. In the global thresholding, partition the image histogram using a single global threshold value. In the local thresholding, divide an image into sub images and threshold these individually. The global thresholding method is simple and time efficient. So our method is coming under the category of global thresholding.

The otsu method is one of the best global binarization technique, and this method is widely used in pattern recognition, document binarization and computer vision [2]. It is trying to find one threshold value for the whole image. The aim of the method is to find the threshold value where the sum of foreground and background spreads is at its minimum. However, since Otsu's threshold is biased towards the class with a large variance, it tends to miss weak objects or fine details in images. For example in biomedical images, nuclei and axons may be imaged with very different intensities due to uneven staining or imperfect lightening conditions. At that situations, algorithm like otsu's method raising difficulty to segment them successfully. It works well with clearly scanned images, but it performs unsatisfactorily for those poor quality images that have low contrast and non-uniform illumination [4]. A quad-tree approach was developed to segment images by combining a centroid clustering and boundary estimation methods but the approach only works under the assumption that the histogram consists of Gaussian distributions only[4]. In [8] the main image segmentation algorithm has been reviewed and gives some valuable characteristics of image segmentation algorithm. The authors have classified Otsu algorithm as thresholding region based segmentation algorithm. Also the complexity rate of Otsu thresholding algorithm is very high and processing rate is very slow. By concluding here, in order to improve the performance of the Otsu algorithm, combine it with other algorithms [9]. In this paper [10], the Otsu method works on global thresholding while the K means method work on the local thresholding. Both methods produce good segmentation result but K means give better results comparatively to Otsu. Otsu method takes comparatively more time and increases the complexity of the algorithm. In this technique, clustering is based on the identification of k elements in the data set that can be used to create an initial representation of clusters. even though the method seems to be straight forward, it suffers from the fact that it may not be easy to clearly identify the initial k elements [3]. In triclass method [4], it is comparatively better performance than all other methods, but fine parts of weak object is missing and initial threshold selection is also difficult.

In this method performs better than the iterative method. It is based on otsu method, but it perform better than the standard application. Initially, Segment the image using otsu's thresholding. Then we get a threshold value from this method. Then calculate two mean values with this threshold. So divide the image into three classes, using this mean. Then separate the image by less than first mean as background, greater than the second mean as the foreground and in-between these two mean values is represented as the TBD (to-be-determined) region. Then apply the adaptive k-means clustering method in the to-be-determined region. Combine the clusters with the foreground by checking the white pixel. This fusion continues until there is no cluster left.

The paper is organized as in the next section includes the related methods of the proposed methods. Then the next includes the proposed work and the flowchart of that. Ultimately this includes the conclusion.

RESEARCH METHODOLOGY

Here there are two methods are used, one is otsu's method and other one is adaptive k-means clustering.

- **Otsu's method**

Otsu's method searches the histogram of an image to find a threshold that binaries the image into two classes, the background with a mean of μ_0 and the foreground with a mean of μ_1 , without loss of generality, here we assume that the foreground is brighter than the background, i.e., $\mu_1 > \mu_0$. The calculation of threshold T is as follows

$$T = \operatorname{argmin}_T \sigma_{\omega}^2(T) \quad (1)$$

Where

$$\sigma_{\omega}^2(T) = q_0(T)\sigma_0^2(T) + q_1(T)\sigma_1^2(T) \quad (2)$$

Where the subscript 0 and 1 denote the two classes, background and foreground, respectively, and q_i and σ_i , $i = [0, 1]$ are the estimated class probabilities and class variances, respectively. These quantities are calculated as

$$q_0 = \sum_{i=1}^T P(i) \quad (3)$$

$$q_1 = \sum_{i=T+1}^k P(i) \quad (4)$$

And the individual class variance are given as

$$\sigma_0^2(T) = \sum_{i=1}^T [i - \mu_0(T)]^2 \frac{P(i)}{q_0(T)} \quad (5)$$

$$\sigma_1^2(T) = \sum_{i=T+1}^k [i - \mu_1(T)]^2 \frac{P(i)}{q_1(T)} \quad (6)$$

Where we assume that the pixel values of the images are from 0 to k. So from the above equations we can see that T is function of the pixel values of both the foreground and the background. If the signal intensity changes, it may affect T in such a way that the segmentation result may become less optimal [7].

- **Adaptive k-means clustering**

The adaptive K-means (AKM) clustering algorithm starts with the selection of K elements from the input data set. The K elements form the seeds of clusters and are randomly selected. This function is also used to compute distance between two elements. An important consideration for this function is that it should be able to account for the distance based on properties that have been normalized so that the distance is not dominated by one property or some property is not ignored in the computation of distance. In most cases, the Euclidean distance may be sufficient. For example, in the case of spectral data given by n-dimensions, the distance between two data elements

$$E_1 = \{E_{11}, E_{12}, \dots, E_{1n}\} \quad (7)$$

And

$$E_2 = \{E_{21}, E_{22}, \dots, E_{2n}\} \quad (8)$$

$$\text{Then } \sqrt{(E_{11} - E_{12})^2 + (E_{12} - E_{22})^2 + \dots + (E_{1n} - E_{2n})^2} \quad (9)$$

It should be pointed out that for performance reasons, the square root function may be dropped. In other cases, we may have to modify the distance function. Such cases can be exemplified by data where one dimension is scaled different compared to other dimensions, or where properties may be required to have different weights during comparison. With the distance function, the algorithm proceeds as follows: Compute the distance of each cluster from every other cluster. This distance is stored in a 2D array as a

triangular matrix. We also note down the minimum distance d_{min} between any two clusters C_{m1} and C_{m2} as well as the identification of these two closest clusters. For each unclustered element E_i , compute the distance of E_i from each cluster. For assignment of this element to a cluster, there can be three cases as follows:

1. If the distance of the element from a cluster is 0, assign the element to that cluster, and start working with the next element.
2. If the distance of the element from a cluster is less than the distance d_{min} , assign this element to its closest cluster. As a result of this assignment, the cluster representation, or centroid, may change. The centroid is recomputed as an average of properties of all elements in the cluster. In addition, we recomputed the distance of the affected cluster from every other cluster, as well as the minimum distance between any two clusters and the two clusters that are closest to each other.
3. If the distance of the element from a cluster is less than the distance d_{min} , assign this element to its closest cluster. As a result of this assignment, the cluster representation, or centroid, may change. The centroid is recomputed as an average of properties of all elements in the cluster. In addition, we recomputed the distance of the affected cluster from every other cluster, as well as the minimum distance between any two clusters and the two clusters that are closest to each other.

The above three steps are repeated until all the elements have been clustered. There is a possibility that the algorithm identifies a number of singletons or single-element clusters, if the distance of some elements is large from other elements. These elements are known as outliers and can be accounted for by looking for clusters with an extremely small number of elements and removing those elements from clustering consideration, or handled as exceptions [3].

PROPOSED METHOD

From different literatures it is found that the otsu threshold segmentation is found to be accurate, the idea of dividing an image's histogram iteratively into 3 classes. The idea of dividing an image's histogram iteratively into three classes is illustrated at the bottom of Fig. 1.

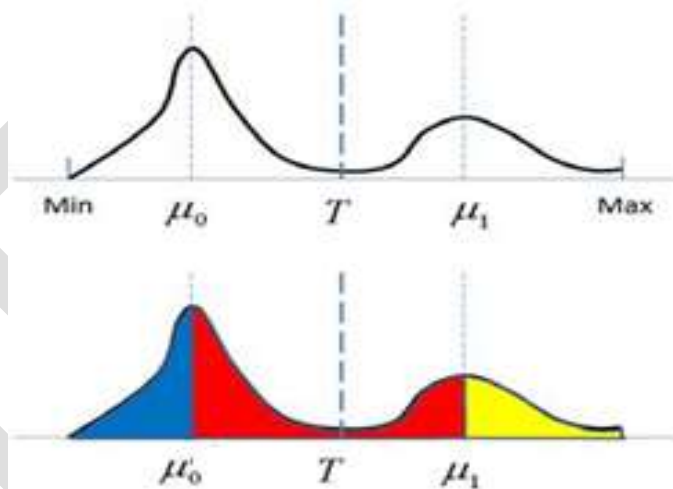


Fig.1. Histogram divided into three classes using mean

In top of Fig.1 shows that the Otsu's method binarizes an image to two classes based on threshold T . Bottom shows that our method classify the histogram into three classes, namely the foreground region with pixel values greater than μ_1 (shown in yellow), the background region with pixel values less than μ_0 in blue, and the third region, called TBD, in red.

For an image u , at the first iteration, Otsu's method is applied to find a threshold T , and denote the means of the two classes separated by T as μ_0 and μ_1 for the background and foreground, respectively. Then we classify regions whose pixel values are greater than μ_1 as foreground F and regions whose pixel values are less than μ_0 as background B . For the remaining pixels $u(x, y)$ such that $\mu_0 \leq u(x, y) \leq \mu_1$ we denote them as the TBD class Ω . So our process assumes that the pixels that are greater than the mean of the "tentatively" determined foreground are the true foreground. Similarly, pixels with values less than μ_0 are for certain the background. But the pixels in the TBD class, which are the ones that typically cause misclassifications in the standard Otsu's method, are not decided at once and will be further processed [4].

The second procedure is start with the TBD region. The adaptive k-means clustering is applied in this region. The AKM estimates the correct number of clusters and obtains the initial centers by the segmentation of the norm histogram in the linear normed space consisting of the data set, and then performs the local improvement heuristic algorithm for K-means clustering in order to avoid

the local optima. So we obtain clusters according to the images [6]. Take the first cluster and the foreground, which is greater than the μ_1 . Fuse this two by comparing the amount of white pixels, and take the output and fuse it with the second cluster, this continue until there is no cluster remaining. And then combine with the background. These steps are described in the flowchart shown in the Fig.2. This method can detect the fine details of weak objects clearly, because the TBD region has the confusion about background and foreground, in that region we applied the clustering technique, so we will get the clear picture of background and foreground. And also this method is parameter free and cost effective method.

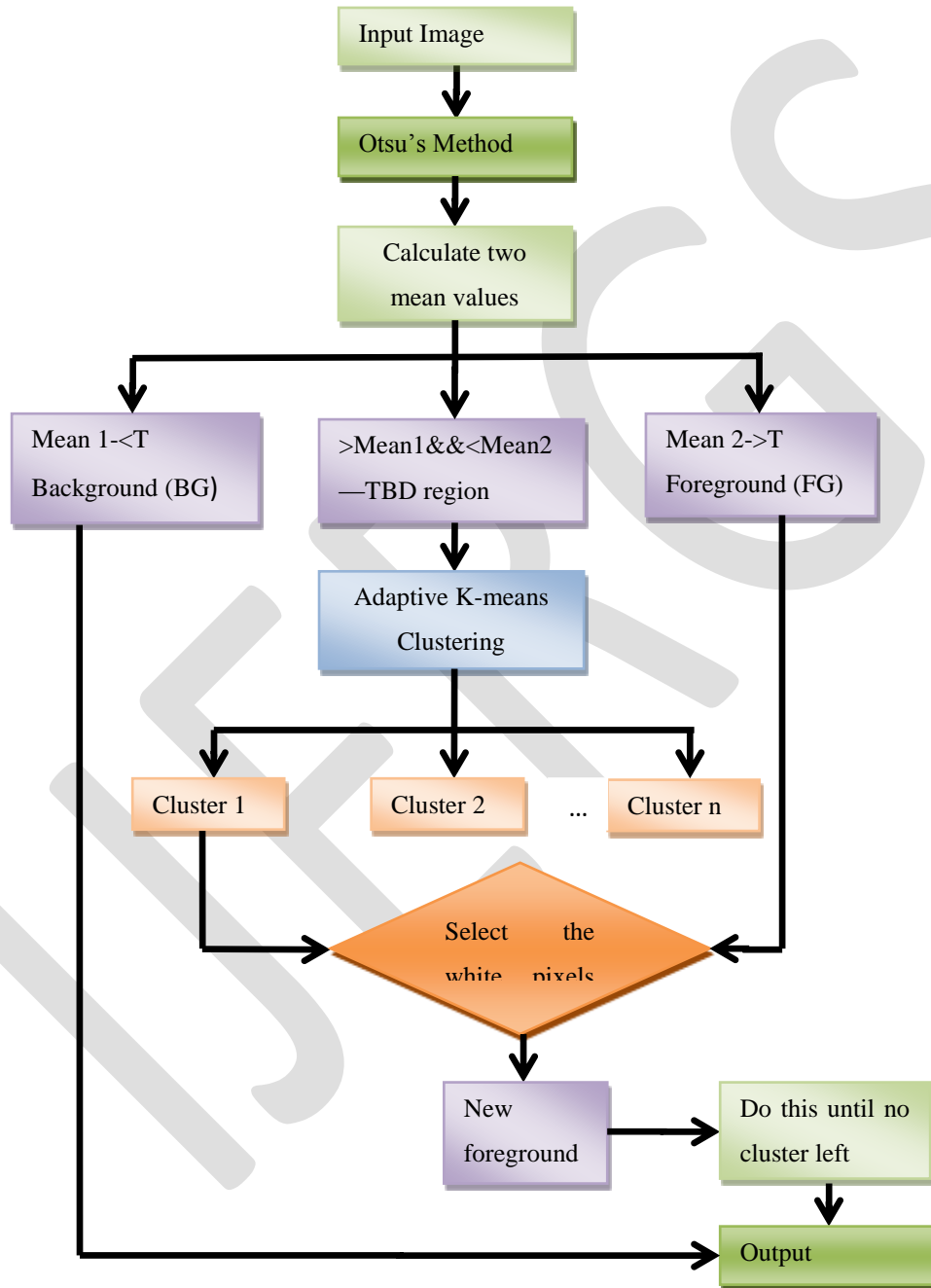


Fig.2. Flowchart of the proposed system

CONCLUSION

The otsu method is to divide the image into foreground and background, but it fails in some times to detect the weak objects clearly. Otsu can be used as a preprocessing technique in document binarization and pattern recognition.

So in this paper represent an enhancement of otsu's method. Instead of dividing in to classes, here represent 3 classes. One is foreground one is background and a newly determined region. Apply adaptive cluster in this region. Because this algorithm is a fully automatic way to cluster an input color or gray image using k-means principle, and here you do not need to specify number of clusters or any initial seed value to start iteration. This algorithm automatically finds number of cluster and cluster center iteratively. It is very fast implementation of clustering without knowing number of clusters. Then fuse the clusters with the foreground region by comparing the intensity. Finally combines with the background.

This method is parameter free and there is no complexity coding required. Also it perfectly determines the weak objects with minimal time and cost.

REFERENCES:

- [1] M. Huang, W. Yu, and D. Zhu, "An improved image segmentation algorithm based on the Otsu method," in Proc. 13th ACIS Int. Conf. Softw. Eng., Artif. Intell., Netw. Parallel Distrib. Comput., Aug. 2012, pp. 135–139
- [2] Ann Josy John, Merlin Mary James, "A New Tri Class Otsu Segmentation With K-means clustering in brain image segmentation," International Journal of Advanced Research in Computer Engineering & Technology (IJARCET), Volume 4 issue 3, march 2015
- [3] Sajiv K. Bhatia, "Adaptive k-means clustering"
- [4] Hongmin Cai, Zhong Yang, Xinhua Cao, Weiming Xia, and Xiaoyin Xu, "A New Iterative Triclass Thresholding Technique in Image Segmentation," IEEE Transactions on Image Processing, VOL. 23, NO. 3, March 2014.
- [5] Matthew Kerwin, "Comparison of Traditional Image Segmentation Techniques and Geostatistical Threshold"
- [6] [Chen, Hailin](#); [Wu, Xiuqing](#); [Hu, Junhua](#), "Adaptive K-means clustering algorithm"
- [7] Nobuyuki Otsu, "A Threshold Selection Method from Gray-Level Histograms", IEEE Transactions on Systems, Man, and Cybernetics, VOL. SMC-9, NO. 1, JANUARY 1979.
- [8] W. X. Kang, Q. Q. Yang, R. R. Liang, "The Comparative Research on Image Segmentation Algorithms", IEEE Conference on ETCS, pp. 703-707, 2009.
- [9] Miss Hetal J. Vala, Prof. Astha Baxi, "A Review on Otsu Image Segmentation Algorithm", ISSN: 2278 – 1323 International Journal of Advanced Research in Computer Engineering & Technology (IJARCET) Volume 2, Issue 2, February 2013 387.
- [10] L. Dongju and Y. Jian, "Otsu method and k-means," in Hybrid Intelligent Systems, 2009. HIS '09. Ninth International Conference on, vol. 1, 2009, pp. 344–349.
- [11] Y. Zhang and L. Wu, "Fast document image binarization based on an improved adaptive Otsu's method and destination word accumulation," J. Comput. Inf. Syst., vol. 7, no. 6, pp. 1886–1892, 2011.
- [12] M. Cheriet, J. N. Said, and C. Y. Suen, "A recursive threshold technique for image segmentation," IEEE Trans. Image Process., vol. 7, no. 6, pp. 918–921, Jun. 1998

Analysis of MANET Characteristics, Applications and its routing challenges

Mayur Bhalia

Electronics & Communication Engineering, mayur.bhalia@gmail.com

Abstract-In the last few years; we have seen that the field of mobile computing drastically changes due to the economical, widely available wireless devices. However, current devices, applications and protocols are mainly focused on cellular or WLAN, without including the MANET (Mobile Ad-Hoc Network).

Keywords- MANET, Security, Routing, Bandwidth, Power

INTRODUCTION

A MANET is an autonomous collection of mobile devices like laptops, smart phones, wireless sensor, etc) which will communicate with each other over using wireless links and helps in the distributed form to provide the necessary network functionality where the fixed network infrastructure is not available. This type of network, operating as a stand-alone network or more than one points of connection to cellular network or the Internet, provides the way for new and exciting applications. If we talk about application scenarios include, emergency operations like flood, earthquake, etc., in auditorium for a conference, personal network etc. In this paper, we can see the potential of a MANET for different kind of applications using Ad-Hoc Networks and also we will see challenges to face by protocol and network developers. These challenges include network and resource discovery, routing problem, Internet connectivity, Security, Network lifetime, power consumption at node level, temporary network without any established infrastructure or centralized administration, security challenges to provide secure communication, etc.

The growth of wireless communication including mobile communication field is at very much high level during the last few decade. Currently second generation (2G) and third generation cellular systems have been reached probably at saturation level, which enables worldwide mobile connectivity. Now a day, Mobile users are using their smart phones to check email and browse the Internet. Recently, an increasing number of WLAN hot spots is rising, which will allow travelers with portable computers to surf the Internet from any feasible locations like airports, railway stations, hotels, school or college campus as well as other public locations. Presently, third generation (3G) provides higher data rates, location-based or person requirement based services.

Even though, all these networks are usually wireless networks, they required a fixed network infrastructure with centralized administration for their operation, which will consumes a lot of time and money for setup and maintenance. Another thing, wireless interfacing ranges is short in different devices like as laptops, Personal Digital Assistants, Tablet PCs, smart phones, etc. But, these kinds of devices are small in size, economical and more users oriented. This will provides a new concept of wireless network in which mobile devices form a self creating network, self organizing network and self-administering network, called a mobile ad hoc network[1].

Mobile Ad Hoc Networks (MANETs) has become one of the most favorite areas of research now a day because of its challenges related to its protocols. MANET is the new emerging technology which enables users to communicate without any need of any fixed infrastructure, because of this; sometimes it is also called an infrastructure less network. Due to some advance features like cheaper, small and more powerful devices make MANET a fastest growing network. A MANET is self-organizing and adaptive. Device in mobile ad hoc network should be able to find out the presence of other devices in the same network and perform necessary set up to communicate and sharing of data and service with it. MANET allows the devices to maintain connections to the network as well as easily adding and removing devices to and from the network. Opposed to infrastructure wireless networks, where each user directly communicates with an access point or base station, a mobile ad hoc network, or MANET, does not rely on a fixed infrastructure for its operation as shown in the Fig. 1 for peer to peer communication.

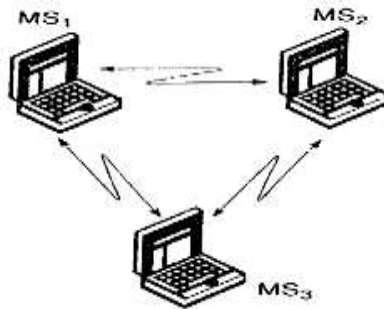


Fig. 1 Peer to peer Mobile Ad-Hoc Network (MS stands for Mobile Station)

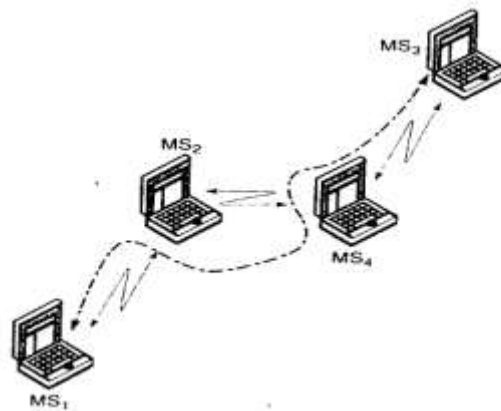


Fig. 2 Multi-hop Mobile Ad-Hoc networks (MS stands for mobile Station)

Fig. 2, shows the multi-hop ad hoc network, where more than one node or device is able to communicate with each other. In addition, in MANET all devices are free to join or leave the network and they may move randomly anywhere within the range of network, which results in continuous change in network topology, which may generate the problem of communication in between every device. In this energy constrained, dynamic network topology, multihop environment, nodes need to organize themselves dynamically in order to provide the necessary network functionality without any fixed infrastructure or central control or we can say administration[7].

CHARACTERISTICS

1) Autonomous network:

In this kind of a network, no centralized administration is available to manage the operation of the different mobile nodes or devices because individually every node is working as a router also.

2) Constrained of Energy for operation:

Few or every node in a MANET may depend on batteries for their energy because of its mobility. For these nodes, a most important condition is optimum power management.

3) No need of fixed Infrastructure:

In this kind of network, all nodes or devices are mobile and able to connect with each other at any moment as per its need.

4) Dynamic network topology:

Nodes are free to move randomly anywhere in the network. So, the dynamic network topology will come in to the picture in which, because of nodes, the topology of the network is randomly changes at unpredictable times.

5) Band-width optimization:

The capacity of a Wireless links in the sense of number of nodes is very much lower as compare to the wired networks. So, in this network, the problem of congestion will arise when an application demands more number of nodes to join the network, results in higher network capacity where the optimum use of bandwidth will come into the picture.

6) Physical Security:

Wireless links mean the risk of security will be higher, like in to a peer to peer communication or a shared wireless medium

is accessible for network users as well as attackers. Firewall for any attacks must be considered into the wireless network [8].

APPLICATIONS

As we have seen the salient characteristics of MANET, we will switch over to the few applications of MANET, where the above characteristics must be considered. Due to many advantages, MANETs are used in many fields like commercial as well as in military.

Application	Used final area of an application
Commercial field	Mobile offices, Vehicular services like way guidance, road and weather conditions, taxi cab network, inter-vehicle networks
Educational field	In college campus or in Universities campus during arrange any kind of meeting or to deliver a lecture to the students/faculties
For Gaming Zone	To play any kind of Multi-user games
Networks based on sensor	Used in different home applications based on sensors which will interfaced with consumer electronics products
Device network	It can establish a wireless communication link between more than one mobile device

ROUTING PROTOCOL to overcome the routing

challenges of MANET, different Protocols are used. With the help of different protocols, many challenges are solved but still many problems arise when in actual manner MANET will be implemented. Let's see few protocols which are used for MANET.

MANET routing protocols are mainly categorized into three:

1. Topology based routing
2. Location based routing
3. Energy awareness based routing

1. TOPOLOGY BASED ROUTING:

Here in topology based routing protocol; it uses the knowledge of instantaneous connectivity of the network with significance condition of the network links. Here, the routing protocols are again classified into three subtypes, which are mainly focused on the time at which the routes are going to be discovered and updated. Different routing protocols are shown in Fig. 3.

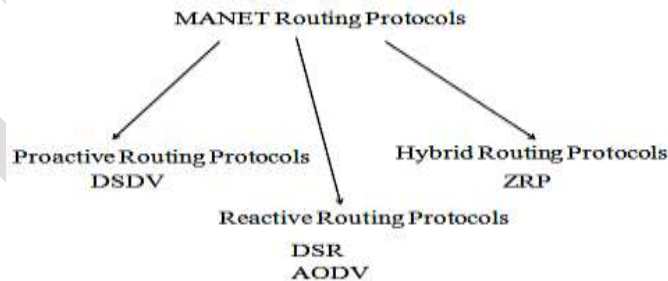


Fig.3 MANET routing protocol

The routing types are as mentioned below:

- 1.1. Proactive Routing Protocol (Table Base)
- 1.2. Reactive Routing Protocol (Demand Base)
- 1.3. Hybrid Routing Protocol

1.1 PROACTIVE ROUTING PROTOCOLS

Proactive routing protocols are maintained consistently and latest routing information between every communicating pair of nodes in the network by circulating, route updates at every fixed time intervals. These protocols are sometimes referred to as table base or table driven protocols because of the every routing information is notified in tables. The main characteristic of proactive protocol is that the each node in the network will maintain a route to every other node available on the same network at any times

continuously. Periodic updates in the table consist of routing information exchanges between each node at a particular time intervals, which is already set. Example of a Proactive Routing Protocol is DSDV.

A) *DSDV (Destination Sequence Distance Vector) :*

In DSDV routing protocol, every node, available, in the network, maintains a routing table, in which all the possible destinations within the network to reach at every destination are notified. Each route entry is marked with a specific sequence number. Nodes are periodically transmitting routing table updates to the network in order to maintain table consistency, throughout. Route updates contains the information in the form of address of few node, the number of path to reach the destination, the sequence number of a destination as well as a sequence number that indentifies the update continuously.

1.2 REACTIVE ROUTING PROTOCOLS

As per the requirement of a communication path from one node to another node a query reply dialog does the work. Thus, the latency goes high but here as per need only control messages is used. Example of different Reactive routing protocols are AODV, DSR, etc.,

A) *AODV(Ad-Hoc On Demand Distance Vector):*

AODV is based on DSDV protocol with some improvement in it. AODV protocol minimizes the number of route broadcasting by destination node for create a route on an on-demand basis for communication purpose. Here, route discovery is basis on-demand. So, the route request is forward to the neighbors as per demand, and so on for whole network until either the destination node or an intermediate node with a latest route to the destination is located.

1.3 HYBRID ROUTING PROTOCOLS

This kind of protocols is the combination of proactive and reactive routing protocols. Hence, recently, several hybrid routing protocols are proposed. Out of them one is ZRP.

A) *ZRP(Zone Routing Protocol):*

ZRP topology divided in between zones and searching to utilize different routing protocols for intra-zone and inter-zone, based on the weaknesses and strengths of these protocols. ZRP is routing protocol can be used within same zone and between different zones. The size of the zones is defined by a parameter which is describing the radius in hops. Intra-zone routing is handled by a proactive protocol since these protocols keep an up to date routing information of the zone topology, which results in minimum latency when communicating with nodes available in intra-zone. Whether, inter-zone routing will be under the control of reactive protocol.

2. LOCATION BASED ROUTING:

Location based routing uses the actual position in any area of nodes to make routing decision. Location information can be obtained through some mechanism or by using Global Positioning System (GPS).

A) *Location-Aided Routing (LAR) protocol*

It is an example of Location Based routing. The central point of LAR is working on request zone in which the flooding rate, of routing request packets in a small group of nodes, is less. To create this kind of request zone, the zone should be defined of the destination. The route discovery process in LAR is like the nodes within the request zone forward the message, others discard the message. On receipt of the route request packet, the destination sends back a route reply packet which contains its current location. Then the routing request packet is broadcast within the request zone.

3. ENERGY AWARENESS ROUTING:

Each node maintains multiple entries of routing in routing tables, one for each of the power levels available on the wireless medium. Routing table corresponding to the power level is built and maintained by transferring hello messages in between nodes at power level. So, the number of entries in routing table of nodes is corresponds to the number of nodes reachable by using power level. Thus, the number of entries in routing tables gives the total number of network nodes.

ROUTING CHALLENGES

Even though many routing protocols are available for MANET, still problems are arising related to the following field like[4]:

- a. Security
- b. Bandwidth optimization
- c. Energy limitation
- d. Parties within the network want their communication to be secure.

Out of all these problems, in present scenario all the researchers are focused on power efficient routing protocol.

CONCLUSION

The continuous evolution in the field of communication is driving a new alternative way for wireless communication, in which devices are in mobile condition which creates a self-creating, self-organizing and self-administering wireless network, known as a MANET. Its flexibility, infrastructure less, auto-configuration, low cost applications make it an essential part of wireless environments. Integration of MANET with other wireless networks and fixed infrastructures will be an essential part of the future 4G (fourth-generation) communication networks. Many routing protocol are used for MANET but technically still more number of challenges to be solved related to devices, security, routing protocols, power constraint and services.

REFERENCES:

- [1] "WIRELESS COMMUNICATIONS" by Andrea Goldsmith, Cambridge University Press, 2005.
- [2] IETF MANET Working Group: <http://www.ietf.org/html.charters/manet-charter.html>
- [3] MANET: Vulnerabilities, Challenges, Attacks, Application, IJCEM International Journal of Computational Engineering & Management, January 2011
- [4] An Overview of MANET: History, Challenges and Applications, Indian Journal of Computer Science and Engineering (IJCS),Feb, 2012
- [5] " Mobile ad hoc networking: imperatives and challenges." By Chalmtac, Jennifer
- [6] A Comprehensive Performance Analysis of Proactive, Reactive and Hybrid MANETs Routing Protocols, IJCSI International Journal of Computer Science Issues, November 2011
- [7] Ad Hoc Mobile Wireless Networks Protocols and Systems, by C.K. Toh, Publishers Pearson
- [8] Secure routing in mobile wireless ad hoc networks. Ad Hoc Networks, by Gupte, Singhal, 2003
- [9] Experimental Comparison Of Hybrid And Proactive Manet Routing Protocols By Peter Sholander, Andreas And Paul

Combined Contrast Stretching and Homomorphic Normalised Filtering for Color Image Enhancement

Megha Rajan, Radhakrishnan B, Raji P G

P.G Scholar, Dept of CSE, BMCE, Kollam, Kerala, India.

megharajan592@gmail.com,

Abstract— Image enhancement area in image processing provides a wide range of techniques which can be used for enhancing images quality as well as the natural look of the image. This paper proposes the enhancement techniques which enhances the image and protects the image from losing the natural look. To improve image under varying lighting conditions, contrast normalization along with homomorphic filtering based illumination normalization method is proposed in this paper. In this work the effect of illumination is effectively normalized by the homomorphic filtering and the contrast is normalized by contrast stretching. The resulted image is not only enhances illumination effect but also preserves edges and details that will facilitate the further processing task.

Keywords— Image enhancement, image processing, illumination, contrast normalization, homomorphic filtering, illumination normalization, contrast stretching,

INTRODUCTION

In image enhancement, when different techniques are used the chance of degradation of natural look and the contrast are higher. The enhancement will work well on grey scale images but in case of color images the enhancement sometimes results in over enhancement or contrast degradation. The contrast enhancement is a widely using image enhancement technique. The contrast in an image is the difference between the color and the brightness that makes an object in the scene distinguishable. The brightness is the feature of vision that defines how much light the source reflects makes the source appears to be reflecting the light. But the brightness and the lightness are two different aspects. Their are direct enhancement techniques [1],[2] and indirect enhancement techniques [3] [4]. Direct methods define a contrast measure and try to improve it. Indirect methods, on the other hand, improve the contrast through exploiting the under-utilized regions of the dynamic range without defining a specific contrast term [5].

The contrast can also be defined as the amount of color or the grey scale differentiation value that exists between various images. Many image enhancement algorithms, such as the Retinex based algorithms [6], the unsharp masking algorithms [7], the histogram equalization (HE) algorithms [8], etc., have been proposed. Part of the algorithms focus on detail enhancement, but usually result in unnatural looks, such as light source confusion and artifacts. Hence, some others attempt to reduce over-enhancement at the cost of the details [9].

Retinex theory assumes that the sensations of color have a strong correlation with reflectance, and the amount of visible light reaching observers depends on the product of reflectance and illumination [10]. Most Retinex-based algorithms extract the reflectance as the enhanced result by removing the illumination, and therefore they can enhance the details obviously [6], [11]. But it is impossible to exactly remove the illumination for the scenes of unsmooth depth. Some center/surround algorithms take the local convolution of the lightness instead of the illumination without considering the limit of the reflectance [6], [7]. In fact, the reflectance should be within 0 and 1, which means the surface cannot reflect more light than that it receives. Moreover, it is unreasonable to simply remove the illumination which is essential to represent the ambience [12]. The bright-pass filter which is used to preserve the natural look in the non-illumination images also restricts the reflectance to 0 and 1. This will give the output as grey scale image. But the complexity of implementing the bright-pass filter is more compared with the other enhancement algorithms [9].

The unsharped masking algorithms decompose the image into the low frequency and high frequency terms and then processing it independently. The classical unsharp masking algorithm can be described by the equation: $v = y + \gamma(x - y)$ where x is the input image, y is the result of a linear low-pass filter, and the gain $\gamma(\gamma > 0)$ is a real scaling factor. The signal $d = x - y$ is usually amplified ($\gamma > 1$) to increase the sharpness. However, the signal contains 1) details of the image, 2) noise, and 3) over-shoots and under-shoots in areas of sharp edges due to the smoothing of edges. While the enhancement of noise is clearly undesirable, the enhancement of the under-shoot and over-shoot creates the visually unpleasant halo effect. Ideally, the algorithm should only enhance the image details. This

requires that the filter is not sensitive to noise and does not smooth sharp edges [7].

HE technique is simple but widely-used for image enhancement. Since conventional HE algorithms may result in over enhancement, many algorithms with restrictions, such as brightness preservation [8], [13] and contrast limitation [14], have been proposed. Brightness preservation is useful in the applications that need to preserve the intensity. However, for non-uniform illumination images, brightness preservation is disadvantageous to detail enhancement in the areas of inappropriate intensity, such as the dark areas. Contrast limited algorithms restrain over-enhancement by redistributing the histogram in such a way that its height does not go beyond the clip limit. But, it is not easy to fix the clip limit for the images of seriously non-uniform illumination, in which the histograms of different areas are quite different [9].

In the image enhancement using contrast enhancement Quantitative evaluation is not trivial, as there do not exist any universally accepted measure of contrast or ideally enhanced images as references. Measures of dispersion (local and global) such as variance, standard deviation and entropy have been used to evaluate contrast enhancement. Quantitative evaluation of contrast enhancement should be based upon appropriate measurement of contrast at all image pixels. Any reasonable measure of contrast should be at least crudely tuned according to the retinal visual system and such a measure would then probably be more credible and universally acceptable [15].

In the naturalness preserved image enhancement algorithm the three major issues are discussed such as the naturalness preservation, the intensity decomposition and the illumination effect. Firstly the lightness order error measure for the naturalness preservation is proposed to assess enhanced images. Secondly, the image is decomposed through the brightpass filter, which insures the reflectance is restricted in the range of 0 and 1. Thirdly, a bi-log transformation is proposed to process the illumination so that the illumination will not flood details due to spatial variation while the lightness order is preserved. But when implementing the brightpass filter, the complexity of the process increases and it is time consuming [9].

Therefore, we propose a method which enhances the image by decomposing the image into reflectance and illumination and then transforming the image for final result.

METHODOLOGY

In this paper we propose the image enhancement technique which can be used in color images. This method uses mainly three methods. The first method is the contrast stretching, which stretches the intensity values which improves the contrast. Then the resulted image is processed with homomorphic filtering. The image can be expressed as the product of illumination and reflectance. In this paper the homomorphic filtering is used, where the image is decomposed to reflectance and illumination. Illumination and reflectance are not separable, but their approximate location in the frequency domain may be located. Then the resulted image is processed by normalizing the image. For the images with the varying lighting conditions the contrast adjustment is necessary for preserving the edges as well as the details contained in the image. Normalization is a process that changes the range of pixel intensity values. It simultaneously normalizes the brightness across an image and increases the contrast. In this the normalization is done in the basis of the illumination component of an image.

PROPOSED WORK

For the enhancement of the image and the preservation of the edges and the details of the image, the image is subjected to contrast stretching, then the output is transformed using the transformation functions and then the output is normalized to get the final enhanced output image.

In this method the image is first decomposed into the RGB components. Where, output of the decomposition will be three different grey scale images. Then the contrast normalization of the image is done to these three images. Then the contrast normalization is done by the contrast stretching technique.

Then the image is decomposed to the illumination and reflectance component. Where the illumination is the light absorbed by the object and the measure of light get illuminated. The reflectance is the amount of light that is reflected from the object. The illumination and reflectance of an image is described as the pixel intensity, where the amount of light reflected from the object in the scene, is the product of the illumination and the reflectance of the objects presented in the scene, which can be expressed as:

$$I(x, y) = il(x, y) * R(x, y) \quad (1)$$

In this paper the decomposition of the image is done by homomorphic filtering. The basic theory of the homomorphic filtering starts with taking the natural log of the model as described in the equation (2). Since illumination and reflectance combine multiplicatively, the components are made additive by taking the logarithm of the image intensity, so that these multiplicative components of the image can be separated linearly in the frequency domain.

$$\ln(I(x, y)) = \ln(il(x, y)) + \ln(R(x, y)) \quad (2)$$

then the result is transformed using the Fourier transformation function

$$F(\ln(I(x, y))) = F_I(x, y) = F(\ln(il(x, y))) + F(\ln(R(x, y))) \quad (3)$$

Where the equation (3) can be replaced as

$$F_I(x, y) = F_{il}(x, y) + F_r(x, y) \quad (4)$$

Then apply the filter function $H(x, y)$

$$E(x, y) = F_I(x, y)H(x, y) = F_{il}(x, y)H(x, y) + F_r(x, y)H(x, y) \quad (5)$$

Then the inverse fourier transformation is applied

$$F^{-1}E(x, y) = F^{-1}(F_{il}(x, y)H(x, y)) + F^{-1}(F_r(x, y)H(x, y)) \quad (6)$$

Then the enhanced result I^1 , can be obtained by taking the exponential function of the result

$$I^1 = e^{E(x, y)} \quad (7)$$

The transformation of the image is done on the basis of illumination transformation on reflectance component of an image. The illumination normalization is done as the next step to the resulted image obtained after applying equation (7) on the image. The dynamic range expansion in various applications is usually to bring the image into a specified range which is more familiar to the senses. The normalization also works in the same perspective that it transforms the n dimensional grey scale image into a new image. As the output of the image decomposition is the grey scale image, normalization can be applied to the three components that is the RGB components of the image. Then the three components of the image after normalization is subjected to synthesizing to form a single color image. The proposed system is explained briefly in the below figure.

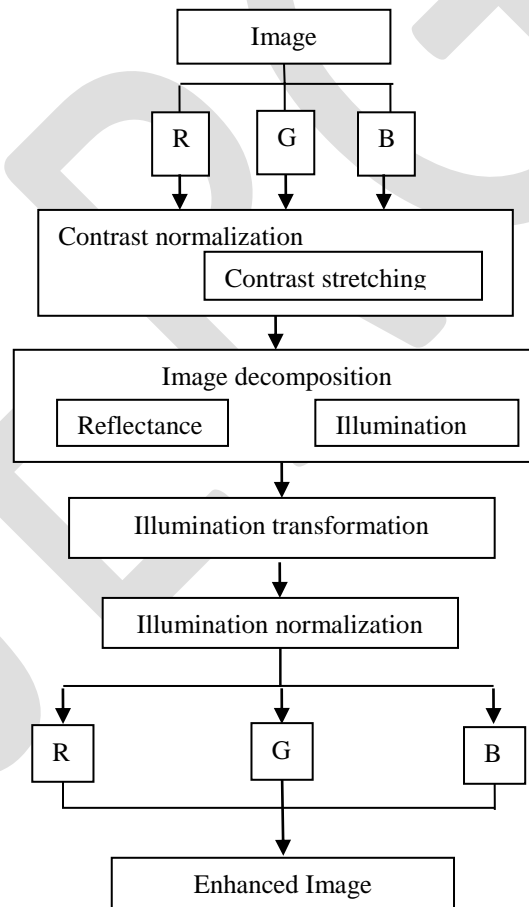


Fig 1 Overview of the proposed system

CONCLUSION

This paper proposes the methodology that will enhance the image without losing its natural look. For different images the lighting conditions may vary according to the scene. To enhance the images under the varying lighting conditions the contrast normalization along with the homomorphic filtering is effective and easy way to obtain the result. As the filtering is based on the illumination, the contrast is stretched and the resulted image will enhance the illumination effect as well as preserves the edges and the details of the image. So that the resulted images obtained by the proposed method are visually pleasing and preserves the natural look

of the image.

REFERENCES:

- [1] H.-D. Cheng and H. J. Xu, "A novel fuzzy logic approach to contrast enhancement," *pattern Recognit.*, vol. 33, no. 5, pp. 809–819, May 2000.
- [2] A. Beghdadi and A. L. Négrate, "Contrast enhancement technique based on local detection of edges," *Comput. Vis, Graph., Image Process.*, vol. 46, no. 2, pp. 162–174, May 1989.
- [3] R. Sherrier and G. Johnson, "Regionally adaptive histogram equalization of the chest," *IEEE Trans. Med. Imag.*, vol. MI-6, no. 1, pp. 1–7, Jan. 1987.
- [4] A. Polesel, G. Ramponi, and V. Mathews, "Image enhancement via adaptive unsharp masking," *IEEE Trans. Image Process.*, vol. 9, no. 3, pp. 505–510, Mar. 2000.
- [5] T. Arici, S. Dikbas, and Y. Altunbasak, "A histogram modification framework and its Application for image contrast enhancement," *IEEE Trans. Image Process.*, vol. 18, no. 9, pp. 1921–1935, Sep. 2009.
- [6] D. J. Jobson, Z. Rahman, and G. A. Woodell, "Properties and performance of a center/surround retinex," *IEEE Trans. Image Process.*, vol. 6, no. 3, pp. 451–462, Mar. 1996.
- [7] G. Deng, "A generalized unsharp masking algorithm," *IEEE Trans. Image Process.*, vol. 20, no. 5, pp. 1249–1261, May 2011.
- [8] C. Wang and Z. Ye, "Brightness preserving histogram equalization with maximum entropy: A variational perspective," *IEEE Trans. Consum. Electron.*, vol. 51, no. 4, pp. 1326–1334, Nov. 2005.
- [9] Shuhang Wang, Jin Zheng, Hai-Miao Hu, and Bo Li, "Naturalness preserved enhancement algorithm for non-uniform illumination images," *IEEE Trans. Image Process.*, vol. 22, no. 9, pp. 3538–3548, Sep. 2013.
- [10] M. Bertalmio, V. Caselles, and E. Provenzi, "Issues about retinex theory and contrast enhancement," *Int. J. Comput. Vis.*, vol. 83, no. 1, pp. 101–119, 2009.
- [11] D. J. Jobson, Z. Rahman, and G. A. Woodell, "A multi-scale retinex for bridging the gap between color images and the human observation of scenes," *IEEE Trans. Image Process.*, vol. 6, no. 7, pp. 965–976, Jul. 1997.
- [12] B. Li, S. Wang, and Y. Geng, "Image enhancement based on Retinex and lightness decomposition," in *Proc. IEEE Int. Conf. Image Process.*, Sep. 2011, pp. 3417–3420.
- [13] H. Ibrahim and N. Kong, "Brightness preserving dynamic histogram equalization for image contrast enhancement," *IEEE Trans. Consum. Electron.*, vol. 53, no. 4, pp. 1752–1758, Nov. 2007.
- [14] A. M. Reza, "Realization of the contrast limited adaptive histogram equalization (CLAHE) for real-time image enhancement," *J. VLSI Signal Process.*, vol. 38, no. 1, pp. 35–44, 2004.
- [15] D. Sen and S. K. Pal, "Automatic exact histogram specification for contrast enhancement and visual system based quantitative evaluation," *IEEE Trans. Image Process.*, vol. 20, no. 5, pp. 1211–1220, May 2011

A Heuristic Method For Energy Hoarding In Wireless Sensor Networks

Eulia Mariam Mathew, Tintu Mary John

PG Scholar, Department of ECE, CAARMEL Engineering College, Pathanamthitta, Kerala
Assistant Professor, Department of ECE, CAARMEL Engineering College, Pathanamthitta, Kerala

Email:eulia.mathew@gmail.com

Abstract: In the past few years, we have seen a fast expansion in the field of mobile computing due to the production of inexpensive, widely available wireless devices. In contrast, current devices applications and protocols in WSN are mainly focused on energy consumption and life time of network. To provide the required network functionality in WSN and to sustain network life time it process selective routing protocol. Most of the battery powers drain in data aggregation than processing and the network would affect in case of any particular node failure. To address this problem, the energy efficient Multi-sink path selection strategy is proposed, where each source node finds its sinks on its surroundings. If the destination is not reachable by its sink, each sink find its next sink and perform traffic through that sink. This paper presents the techniques in Multipath selection to enhance the lifetime of the sensors in WSN.

Keywords: Wireless sensor network, Multisink, Path selection strategy, Network life time

INTRODUCTION

A wireless sensor network is a collection of nodes organized into a cooperative network. Every node has its own processing capability, may contain multiple types of memory (program, data and flash memories), have a RF transceiver(usually with a single omni-directional antenna), have a power source (e.g., batteries and solar cells), that mainly accommodates numerous sensors and actuators .Such systems can revolutionize the way to live and work. Currently, wireless sensor networks are beginning to be deployed at an accelerated pace. This can be considered as the Internet becoming a physical network. This new skill is stimulating with unrestrained prospective for numerous application areas. Most current deployed sensor networks involve relatively small amount of sensors, wired to a central processing unit in which every signal processing is performed.

Wireless sensor networks are composed of a large number of sensor nodes deployed in a field. Each sensor nodes is equipped with battery with extremely limited processing capabilities. These wireless sensor networks are capable to maintain many new applications, including habitat monitoring [1] and agricultural monitoring [2]. In such wireless sensor networks (WSN), sensors send data packets to sink nodes through multi-hop wireless links. As the size of the network increases, the sensors near the sink nodes will dissipate energy faster than other sensors as they need to forward a larger number of messages, and prolonging the lifetime of whole network becomes a critical problem. Reducing energy utilization is the most important objective in the design of a sensor network. These constraints have led to intensive research efforts on designing energy-efficient protocols.

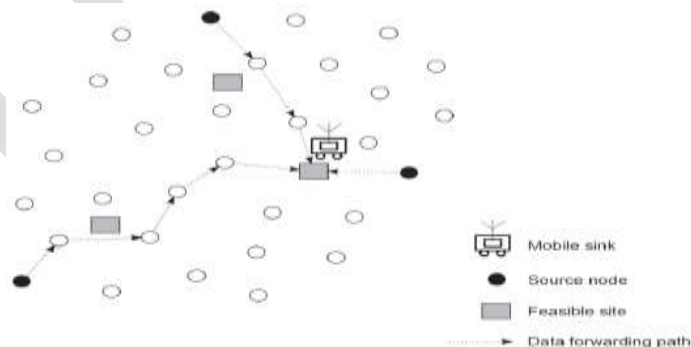


Fig 1: Mobile sink performing data collection in a WSN

RELATED WORK

Due to the battery resource constraint, it is a critical issue to save energy in wireless sensor networks, particularly in large sensor networks. Considering this issues many researches and surveys are made in wireless sensor network. In this section, we exhibit an overview of various works that examine the energy efficient routing protocols and also various methodologies for energy consumption for wireless sensor network along with its limits. Multi-constrained QoS multipath routing(MCMP) [3] is mainly designed to avoid probabilistic programming problem i.e. end –to –end and soft QoS problem. MCMP is developed according to linear programming approach and then to deterministic approximation to define end-to-end and soft QoS problems

Energy Constrained Multipath Routing(ECMP) [4] is the extended version of MCMP to provide energy-efficient communication. ECMP introduces an energy optimization problem. Energy optimization problem is constrained by reliability, delay and geo-spatial energy consumption to provide multi-constrained QoS routing in sensor networks. Thus, ECMP satisfy delay and reliability requirement. Delay-Constrained High-Throughput Protocol for Multipath Transmission (DCHT) [5] is the modified version of Directed Diffusion that uses multipath routing approach to support high-quality video streaming in low-power wireless sensor networks. The protocol introduces a novel path reinforcement method and uses a new routing cost function that takes into account the expected transmission count (ETX) [6] and delay metrics to discover high-quality paths with minimum end-to end delay. The utilized path reinforcement strategy and routing metric in DCHT greatly improves the performance of the original Directed Diffusion by constructing multiple low-latency high-quality paths.

Energy-Efficient Multipath Routing Protocol [7] distributes the network traffic over the multiple node-disjoint paths. Whenever an event occurs, a sensor node in the event area is selected as the source node. The selected source node initiates the route discovery process and transmits multiple Route-request messages to its neighbouring nodes. Route-request messages include different path IDs to construct multiple node-disjoint paths from the selected source node towards the sink node. All the intermediate nodes select one of their best next-hop neighbouring nodes that are not included in any other paths during the route discovery process. Sink node upon reception of the first Route-request message, sets its timer to fulfil the path establishment process in an acceptable period. All the paths discovered after the timer timeouts are considered as low-quality paths and the Route-request messages received from these paths are discarded by the sink node. Then, the sink node assigns different data rates to the established paths.

SYSTEM ARCHITECTURE

Several studies have demonstrated the benefits of using a mobile sink to reduce the energy consumption of nodes and to prevent the formation of energy holes in wireless sensor networks (WSNs). However, these benefits are dependent on the path taken by the mobile sink, mainly in delay-sensitive applications, as all sensed data must be composed within a given time constraint. An approach projected to address this challenge is to form a hybrid moving pattern in which a mobile-sink node only visits rendezvous points (RPs), as opposed to all nodes. Sensor nodes that are not RPs forward their sensed data via multi hopping to the nearest RP. The essential problem then becomes computing a tour that visits all these RPs within a given delay bound. Determining the optimal tour, however, is an NP-hard problem. To deal with this problem, a methodology called weighted rendezvous planning (WRP) is proposed, whereby every sensor node is assigned a weight corresponding to its hop distance from the tour and the number of data packets that it forwards to the closest RP.

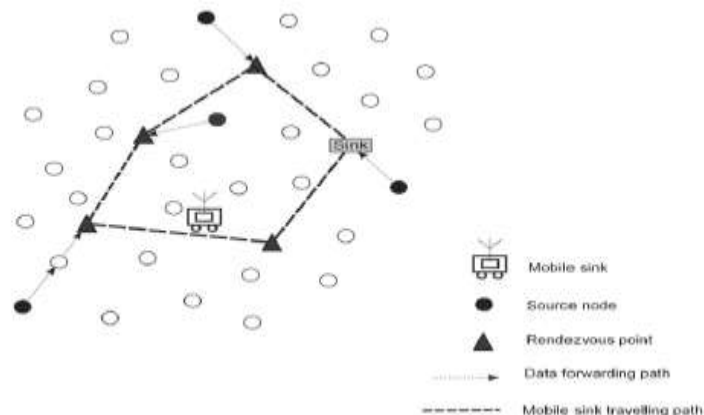


Fig 2: Hybrid movement pattern for a mobile sink node.

In WSNs with a mobile sink, one fundamental problem is to determine how the mobile sink goes about collecting sensed data. One approach is to visit each sensor node to receive sensed data directly. This is essentially the well-known traveling salesman problem (TSP), where the goal is to find the shortest tour that visits all sensor nodes. To this end, researchers have proposed the use of rendezvous points (RPs) to bound the tour length. This means a subset of sensor nodes are designated as RPs, and non-RP nodes simply forward their data to RPs. A tour is then computed for the set of RPs, as shown in Fig 2. As a result, the problem, which is called rendezvous design, becomes selecting the most suitable RPs that minimize energy consumption in multihop communications while meeting a given packet delivery bound. A secondary problem here is to select the set of RPs that result in uniform energy expenditure among sensor nodes to maximize network lifetime. A DEETP is an NP hard problem and propose a heuristic method, which is called weighted rendezvous planning (WRP), to determine the tour of a mobile-sink node. In WRP, the sensor nodes with more connections to other nodes and placed farther from the computed tour in terms of hop count are given a higher priority. In order to design the routing algorithm the following node models are considered. In large density applications, the sensor node should be transmits the sensed data to mobile sink within time constraint. The proposed system the cluster head transmits to Rendezvous point rather than all sensor nodes. Due to Processing overhead of Rendezvous point is not appropriate for large and delay sensitive applications. To overcome this problem, the proposed method is a heuristic method for energy hoarding in wireless sensor networks. The sensor nodes are organized into clusters. Within a cluster, nodes transmit data to cluster head (CH) through routing protocol. In the clustering process, Cluster Head is elected for each cluster. CH have a responsibilities for collecting data from each sensor node and transmits data to nearest Rendezvous point. High energy first (HEF) clustering algorithm is used for selecting cluster head with high ranking of residual energy of each sensor node. This algorithm is used for minimizes the energy depletion throughout sensor network field. The travelling Path of the Mobile Sink to visit all Rendezvous point which can be considered as a NP Hard problem. This problem taken as delay-aware energy efficient path (DEETP) and solved as Weighted Rendezvous Planning (WRP) algorithm. WRP algorithm calculating weight for each sensor node which can be computed by hop distance and number of packets forwarded.

ASSUMPTIONS

The assumptions that are made during this work are.

- 1) The communication time between the sink and sensor nodes is negligible, as compared with the sink node's traveling time. Similarly, the delay due to multihop communications including transmission, propagation, and queuing delays is negligible with respect to the traveling time of the mobile sink in a given round.
- 2) Each RP node has sufficient storage to buffer all sensed data.
- 3) The sojourn time of the mobile sink at each RP is sufficient to drain all stored data.
- 4) The mobile sink is aware of the location of each RP.
- 5) All nodes are connected, and there are no isolated sensor nodes.
- 6) Sensor nodes have a fixed data transmission range.
- 7) Each sensor node produces one data packet with the length of b bits in time interval D .

SIMULATION RESULTS

The simulation results and performance comparison of the mobile node and multipoint sink routing protocols is analyzed. Important parameters are compared with single mobile node and Multisink mobile nodes such as energy consumption and throughput. When mobile node fails to transmit data the communication established is difficult. But in the case of Multisink point no node fails to communicate and transmits the data without network overheads. Comparing to existing method the traffic size and network overheads of Multisink point is low.

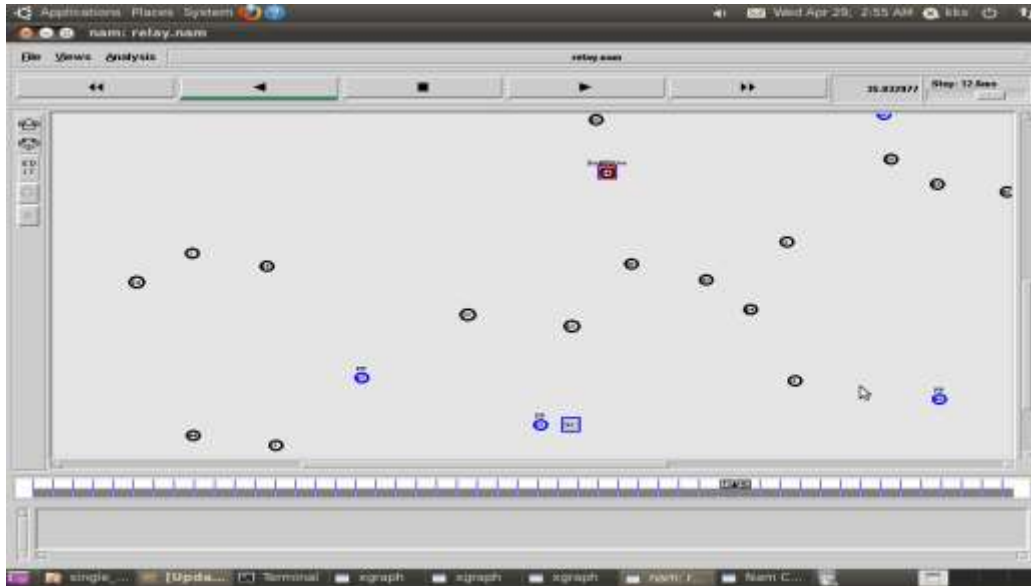


Fig 3: A WSN consisting of base station and a single mobile sink node using WRP algorithm

Figure 3 shows a single mobile sink collecting data from each Rendezvous Point and relaying back to the base station using WRP algorithm for computing the path to cover the RPs in shortest time possible.



Fig 4: Sensor nodes are arranged into clusters for maximum accessibility for the multisink mobile nodes

The sensor nodes are arranged into clusters in order to prolong network lifetime and for maximum conservation of energy. Multiple sink nodes are used. This is useful in case a mobile sink runs out of energy. WRP maps out a route for the mobile sinks to collect the data from RPs; here the RPs are represented by Gateway as shown in Figure 4.



Fig 5: Multisink mobile nodes collect data from each cluster via gateway

The blue coloured nodes show the cluster heads(CH) in each cluster in Figure 5. They are selected by the High Energy First Clustering algorithm. This selects the node having highest energy to be the CH. When the CH gets depleted of energy, a new cluster head is selected. The energy-depleted CH is represented by the black coloured nodes. CH accumulates the data from their respective cluster and transmits to the visiting mobile sink nodes who in turn relays the data to the base station. Mobile sinks are yellow coloured in the figure.

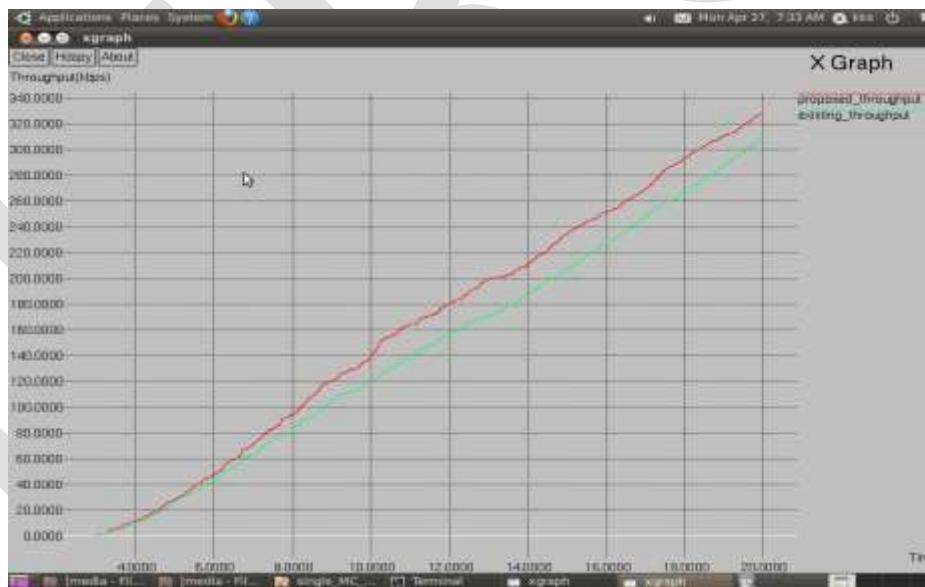


Fig 6: Throughput comparison

Figure 6 shows the throughput comparison when WRP is used. Throughput increases significantly when mobile sinks using WRP is used.

CONCLUSION

In this paper WRP, which is a novel algorithm for controlling the movement of a mobile sink in a WSN. WRP selects the set of RPs such that the energy expenditure of sensor nodes is minimized and uniform to prevent the formation of energy holes while ensuring sensed data are collected on time. The proposed method is a heuristic method for energy hoarding in wireless sensor networks. The sensor nodes are organized into clusters. Within a cluster, nodes transmit data to cluster head (CH) through routing protocol. Clustering algorithm is to choose the highest-ranking residue energy of sensor as a cluster head. This algorithm is used for minimizing energy depletion and maximizing the network lifetime. A mobile sink that preferentially visits areas of RP will prevent energy holes from forming in a WSN. These Multisink nodes and path selection strategy techniques are used for reliable communication and also to prolong the network lifetime.

REFERENCES:

- [1] Mainwaring, J. Polastre, R. Szewczyk, D. Culler, and J. Anderson, "Wireless sensor networks for habitat monitoring," Proc. 1st ACM Int'l Workshop on Wireless Sensor Networks and Applications, 2002.
- [2] J. Burrell, T. Brooke, and R. Beckwith, "Vineyard computing: sensor networks in agricultural production," IEEE Pervasive Computing, Vol. 3, Issue. 1, 2004.
- [3] Huang, X.; Fang, Y. Multiconstrained QoS Multipath Routing in Wireless Sensor Networks. J. Wirel. Netw. 2007, 14, 465–478.
- [4] Bagula, A.; Mazandu, K. Energy Constrained Multipath Routing in Wireless Sensor Networks. In Proceeding of the 5th International Conference on Ubiquitous Intelligence and Computing, Oslo, Norway, 23–25 June 2008;
- [5] Lu, Y.M.; Wong, V.W.S. An Energy-Efficient Multipath Routing Protocol for Wireless Sensor Networks. Int. J. Commun. Syst. 2007, 20, 747–766.
- [6] Li, S.; Neelisetti, R.K.; Liu, C.; Lim, A. Efficient Multi-Path protocol for Wireless Sensor Networks. Int. J. Wirel. Mobile Netw. 2010, 2, 110–130.
- [7] Couto, D.S.J.D.; Aguayo, D.; Bicket, J.; Morris, R. A High-Throughput Path Metric for Multi-Hop Wireless Routing. Wirel. Netw. 2005, 11, 419–434.
- [8] G. Xing, T. Wang, W. Jia, and M. Li, "Rendezvous design algorithms for wireless sensor networks with a mobile base station," in Proc. 9th ACM Int. Symp. Mobile ad hoc Network Computing., Hong Kong, China, pp. 231–240, May 2008.

Authenticated Anonymous Secure Routing Using Trust Model Technique

Aswathi Rajan, Kiran Krishnan

PG Scholar, Department of ECE, CAARMEL Engineering College, Pathanamthitta, Kerala
Assistant Professor, Department of ECE, CAARMEL Engineering College, Pathanamthitta, Kerala

Email:aswathirajan03@gmail.com

Abstract: Anonymous communications are vital for several applications of the mobile unplanned networks (MANETs) deployed in someone environments. A significant demand on the network is to produce unidentifiability and unlinkability for mobile nodes and their traffics. Though variety of anonymous secure routing protocols is projected, the necessity isn't absolutely glad. The present protocols are susceptible to the attacks of pretend routing packets or denial-of-service (DoS) broadcasting, even the node identities are protected by pseudonyms. A brand new routing protocol is projected, i.e., documented anonymous secure routing (AASR), to satisfy the necessity and defend the attacks. Additional specifically, the route request packets are documented by a gaggle signature, to defend the potential active attacks while not unveiling the node identities.

Keywords: Anonymous Routing, Authenticated Routing, Mobile Adhoc Network, Trust Management.

INTRODUCTION

MANETS rely on wireless transmission, a secured way of message transmission is important to protect the privacy of the data. An insecure ad-hoc network at the edge of communication infrastructure may potentially cause the entire network to become vulnerable to security breaches. There is no central administration to take care of detection and prevention of anomalies in Mobile ad hoc networks. Mobile devices identities or their intentions cannot be predetermined or verified. Therefore nodes have to cooperate for the integrity of the operation of the network. However, nodes may refuse to cooperate by not forwarding packets for others for selfish reasons and not want to exhaust their resources. Various other factors make the task of secure communication in ad hoc wireless networks difficult include the mobility of the nodes, a promiscuous mode of operation, limited processing power, and limited availability of resources such as battery power, bandwidth and memory. Therefore nodes have to cooperate for the integrity of the operation of the network. Nodes may refuse to cooperate by not forwarding packets for others for selfish reasons and not want to exhaust their resources. A community of ad-hoc network researchers has proposed, implemented, and measured a variety of routing algorithms for such mobile, wireless networks. While these ad-hoc routing algorithms are designed to generate less routing protocol traffic than the above-mentioned shortest-path routing protocols in the face of a changing topology, they nevertheless compute shortest-path routes using either topological information concerning the entire network, or topological information concerning the entire set of currently used paths between sources and destinations. Thus, their ability to find routes depends similarly on describing the current wide-area topology of the network to routers.

In this work, we focus on the MANETs in adversarial environments, where the public and group key can be initially deployed in the mobile nodes. We assume that there is no online or localization service available when the network is deployed. We propose an authenticated anonymous secure routing (AASR) to overcome the pre-mentioned problems. The primary challenge in building a Manet is mobilisation every device to ceaselessly maintain the knowledge needed to properly route traffic. Such networks could operate by themselves or is also connected to the larger web [3]. They will contain one or multiple and totally different transceivers between nodes. This leads to an extremely dynamic, autonomous topology.

RELATED WORK

The main focus is to discuss the anonymous communication protocols that have been proposed already for MANETs. Most of the works are based on onion routing protocol in which data is enclosed in a series of encrypted layers to form an onion by a series of proxies communicating over encrypted channels.

Kong and Hong [2] proposed Anonymous On-Demand Routing (ANODR) Protocol is the first one to provide anonymity and unlinkability for routing in MANET. ANODR uses one-time public or private key pairs to attain anonymity and unlinkability but fails to assure content unobservability. An efficient anonymous routing for MANET which provides advantages for ANODR protocol is

that routing performance changes notably when different cryptosystems are used to implement the same function. Seys and Preneel [4] proposed Anonymous Routing (ARM) Protocol uses one-time public or private key pairs and go behind only anonymity in route discovery and data forwarding. Yang [5] proposed Discount ANODR performs lower computation and communication complexities at the cost of a small reduction of privacy but provides only source anonymity and routing privacy. Qin [6] proposed On-Demand Lightweight Anonymous Routing (OLAR) scheme which involves the secret sharing scheme which is based on the properties of polynomial interpolation mechanism to reach anonymous message transfer without per-hop encryptions and decryptions. The only job for a forwarder is to perform additions and multiplications which is less expensive than traditional cryptographic operations. Pan and Li [7] proposed Efficient Strong Anonymous Routing (MASR) Protocol which uses onion routing scheme to achieve anonymity but leads to routing overhead and high computational cost. Efficient Anonymous Routing Protocol for Mobile Ad Hoc Networks adapts onion routing algorithm to achieve anonymity. In this the node that participates in the protocol, encrypts the whole message with a trust key and says Hello to its preceding nodes within the expiration time. This approach detects the malicious nodes and isolates the node from the network. V-routing based on proactive routing protocol which hides the location and identity of the communication parties but it provides less security for the data. Zhang [9] proposed Anonymous On-Demand Routing (MASK) enables anonymous on-demand routing protocols with high routing efficiency by comparing with ANODR which is very much sensitive to node mobility that may lower routing efficiency. Dong [10] proposed Anonymous routing protocol with multiple routes (ARMR) communications in mobile ad hoc networks and anonymous and secure reporting (ASR) of traffic forwarding activity in mobile ad hoc networks which makes use of one-time public or private key pairs which achieve anonymity and unlinkability. ARMR uses one-time public-keys and bloom filter to find out multiple routes for mobile ad hoc networks and ASR is designed to achieve stronger location privacy, which ensures nodes on route does not have any information on their distance to the source or destination node. Anonymous Location-Aided Routing in Suspicious MANETs uses group signature but this protocols are not suitable for practical approach to routing in mission-critical location-based environment because there is no analysis on protocols performance for privacy and security.

AASR NODE MODEL

In order to design the routing algorithm the following node models are considered.

Destination Table: we tend to assume that a supply node is aware of all its attainable destination nodes. The destination info, together with one in all destinations' name, public key, and therefore the pre-determined trapdoor string destination are going to be keeping within the destination table. Once a session to the destination is established, the shared radially symmetrical key's needed for information encryptions within the session. Such radially symmetrical keys generated by the supply node before causing the route requests, and keep within the destination table when receiving the route reply. As an example sample entry of the destination table is (DestNym, Dest String, Dest Public Key, Session Key).

Neighbourhood Table: We assume that each node domestically exchanges info with its neighbours. It will generate completely different pseudonyms to speak with different neighbours. The neighbours security associations are established likewise because the shared regular keys. The data is kept in a very neighbourhood table. For instance, a sample entry of the neighbourhood table is (Neighbour Nym, Session Key).

Routing Table: When a node generates or forwards a route request, a replacement entry are created in its routing table that stores the request's anonym and also the secret verification message during this route discovery. Such associate entry is marked within the standing of "pending". If associate RREP packet is received and verified, the corresponding entry within the routing table are updated with the anonymous next hop and also the standing of "active". Meanwhile, a replacement entry is created within the node's forwarding table. As an example, a sample entry of the routing table is (ReqNym, DestNym, VerMsg, Next hop Nym, Status). Note that, to modify the notation, we have a tendency to ignore the timestamp data of the entry within the table. 4) Forwarding Table: The forwarding table records the switch data of a long time route. We have a tendency to adopt the per hop name because the symbol for packet switch, just like the VCI (virtual channel identifier) in ATM networks. In every entry of the forwarding table, the route name is generated by the destination node, whereas the node pseudonyms of the previous and next hop square measure obtained when process the connected RREQ and RREP packets. For instance, a sample entry of the forwarding table is (RtNym, Prev hop Nym, Next hop Nym).

AASR PROTOCOL DESIGN

In this section, we present the design of AASR protocol. Considering the nodal mobility, we take the on-demand adhoc routing as the base of our protocol, including the phases of route discovery, data transmission, and route maintenance. In the route discovery phase, the source node broadcasts an RREQ packet to every node in the network. If the destination node receives the RREQ to itself, it will reply an RREP packet back along the incoming path of the RREQ. In order to protect the anonymity when exchanging the route information, we redesign the packet formats of the RREQ and RREP, and modify the related processes. We use a five-node network to illustrate the authenticated anonymous routing processes. The network is shown in Fig.1, in which the source node S discovers a route to the destination node D.

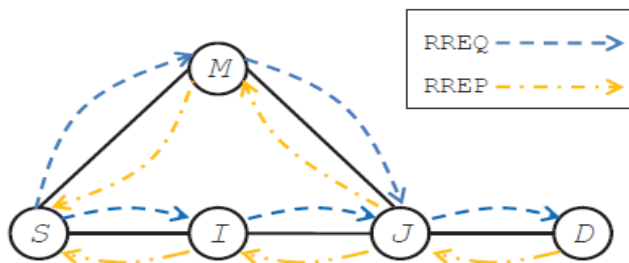


Fig 1: Network topology

Anonymous Route Request

1) Source Node: We assume that S initially knows the information about D, including its pseudonym, public key, and destination string. The destination string *dest* is a binary string, which means “You are the destination” and can be recognized by D. If there is no session key, S will generate a new session key K_{SD} for the association between S and D. Then, S will assemble and broadcast an RREQ packet in the format.

$$S \rightarrow *: [RREQ; N_{sq}; V_D; V_{SD}; Onion(S)] GS$$

where RREQ is the packet type identifier; N_{sq} is a sequence number randomly generated by S for this route request; V_D is an encrypted message for the request validation at the destination node; V_{SD} is an encrypted message for the route validation at the intermediate nodes; $Onion(S)$ is a key encrypted onion created by S. The whole RREQ packet is finally signed by S with its group private key GS.

2) Intermediate Node: The RREQ packet from S is flooded in T. Now we focus on an intermediate node I, as shown in Fig. 1. We assume that I has already established the neighbour relationship with S and J. I knows where the RREQ packet comes from. I checks the N_{sq} and the timestamp in order to determine whether the packet has been processed before or not. If the N_{sq} is not known in the routing table, it is a new RREQ request; if the N_{sq} exists in the table but with an old timestamp, it has been processed before and will be ignored; if the N_{sq} exists with a fresh timestamp, then the RREQ is a repeated request and will be recognized as an attack.

3) Destination Node: When the RREQ packet reaches D, D validates it similarly to the intermediate nodes I or J. Since D can decrypt the part of V_D , it understands that it is the destination of the RREQ. D can obtain the session key K_{SD} , the validation nonce N_V , and the validation key K_V . Then D is ready to assemble an RREP packet to reply the S's route request.

B. Anonymous Route Reply

1) Destination Node: When D receives the RREQ from its neighbour J, it will assemble an RREP packet and send it back to J. The format of the RREP packet is defined as follow:

$$D \rightarrow *: (RREP; N_{rt}; (K_V; Onion(J))K_{JD})$$

where RREP is the packet type identifier; Nrt is the route pseudonym generated by D; Kv and Onion(J) are obtained from the original RREQ and encrypted by the shared key K_{JD} . The intended receiver of the RREP is J.

2) Intermediate Node: We assume that J has already established a neighbour relationship with I, D, and M. If J receives the RREP from D, J will navigate the shared keys in its neighbourhood table, and try to use them to decrypt. In case of a successful decryption, J knows the RREP is valid and from N_D , and J also obtains the validation key Kv. Then J continues to decrypt the onion part. J knows the next hop for the RREP.

3) Source Node: When the RREP packet reaches S, S validates the packet in a similar process to the intermediate nodes. If the decrypted onion core NS equals to one of S's issued nonce, S is the original RREQ source. Then the route discovery process ends successfully. S is ready to transmit a data along the route indicated by Nrt.

C. Anonymous Data Transmission

Now S can transmit the data to D. The format of the datapacket is defined as follows:

$S \rightarrow D: (DATA; Nrt; (Pdata)KSD)$

where DATA is the packet type; Nrt is the route pseudonym that can be recognized by downstream nodes; the data payload is denoted by Pdata, which is encrypted by the session key KSD.

D. Routing Procedure

The routing algorithm can be implemented based on the existing on-demand ad hoc routing protocol like AODV or DSR. The main routing procedures can be summarized as follows:

- 1) During route discovery, a source node broadcasts an RREQ packet in the format.
- 2) If an intermediate node receives the RREQ packet, it verifies the RREQ by using its group public key, and adds one layer on top of the key-encrypted onion. This process is repeated until the RREQ packet reaches the destination or expired.
- 3) Once the RREQ is received and verified by the destination node, the destination node assembles an RREP packet in the format of (9), and broadcasts it back to the source node.
- 4) On the reverse path back to the source, each intermediate node validates the RREP packet and updates its routing and forwarding tables. Then it removes one layer on the top of the key-encrypted onion, and continues broadcasting the updated RREP in the format.
- 5) When the source node receives the RREP packet, it verifies the packet, and updates its routing and forwarding tables. The route discovery phase is completed.
- 6) The source node starts data transmissions in the established route in the format. Every intermediate node forwards the data packets by using the route pseudonym.

SIMULATION RESULTS

We implement the proposed AASR protocol in ns-2 by extending the AODV module to support the cryptographic operations.

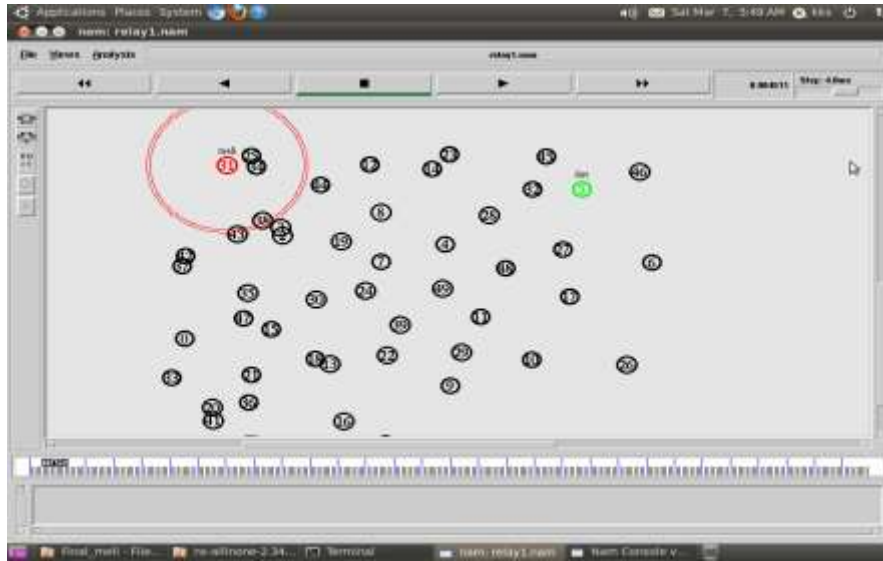


Fig 2: Entering of malicious node into the network.

Entering of malicious node to the network is shown in the figure 2. While entering the network all the normal nodes will send the fake request to the malicious node. Normally the fake node will reply but some cases it will not reply to this request. To avoid this all the nodes will send the fake request to the malicious node. If any of the node receives a reply from the malicious node, it will broadcast to all the nodes in the network.

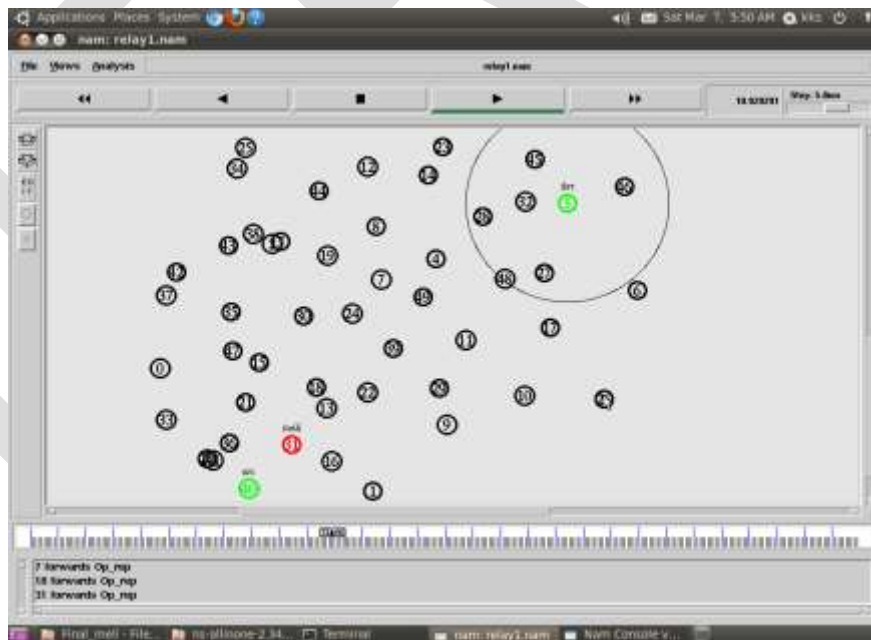


Fig 3: Malicious node entered in the network

In figure 3 the malicious node entered the network and all other nodes are checking and sending the fake request to the malicious node .

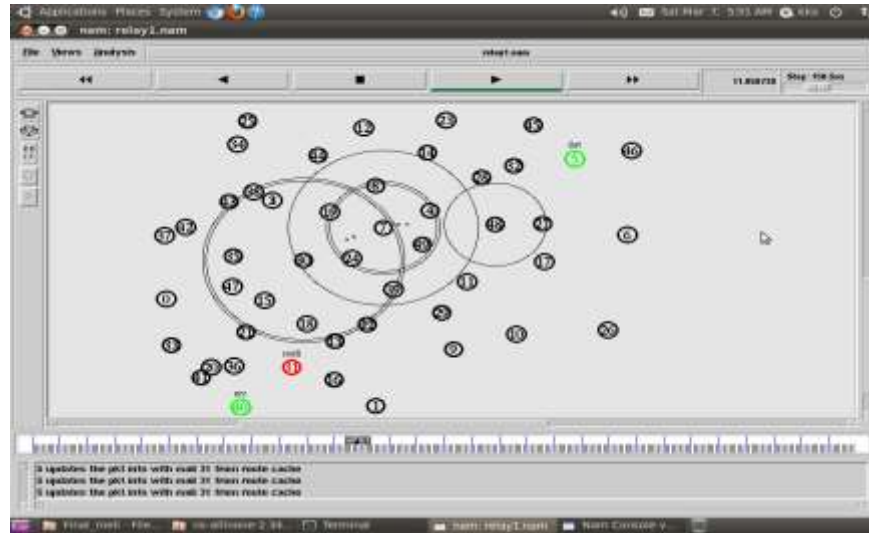


Fig 4: Malicious node identification

In figure 4 the malicious node is identified by all nodes because of the broadcast message. Now all the nodes will eliminate the malicious node from their route. And it will eliminate the path with the malicious node. Data is transmitted to the destination without any failure by avoiding the malicious node in the network.

CONCLUSION

In this paper, we tend to style associate genuine and anonymous routing protocol for MANETs in adversarial environments. The route request packets are genuine by cluster signatures, which might defend the potential active anonymous attacks while not unveiling the node identities. The key-encrypted onion routing with a route secret verification message is intended to not solely record the anonymous routes however conjointly forestall the intermediate nodes from inferring the important destination. This paper gives the information about AASR in network. Which provide different information that useful for achieving propose work with respect to scenario.

REFERENCES:

- [1] Wei Liu and Ming Yu. Aasr: Authenticated anonymous secure routing for manets in adversarial environments. IEEE TRANSACTIONS ON VEHICULAR TECHNOLOGY, VOL. X, NO. Y,, March 2014.
- [2] J.Kong and X. Hong, "ANODR: Anonymous On Demand Routing with Untraceable Routes for Mobile Ad hoc networks," in Proc. ACM MobiHoc'03, Jun. 2003, pp. 291–302.
- [3] J. Kong, X. Hong, and M. Gerla, "ANODR: An identity-free and on demand routing scheme against anonymity threats in mobile ad hoc networks," IEEE Trans. on Mobile Computing, vol. 6, no. 8, pp. 888–902, Aug. 2007.
- [4] S. Seys and B. Preneel, "ARM: Anonymous Routing protocol for mobile ad hoc networks," Int. Journal of Wireless and Mobile Computing, vol. 3, no. 3, pp. 145–155, Oct. 2009.
- [5] Y. Liu, J. Markus, and W. Susanne, "Discount Anonymous On Demand Routing for Mobile Ad hoc Networks," in Proc. 2nd International Conference on Security and Privacy in Communication Networks, Baltimore, 2006, pp. 1-10.

[6] Q. Yang, H. Dijiang, and K. Vinayak, "OLAR: On-demand Lightweight Anonymous Routing in MANETs," in Proc. 4th International Conference on Mobile Computing and Ubiquitous Networking, Tokyo, 2008, pp. 72-79.

[7] P. Jun, and L. Jianhua, "MASR: An Efficient Strong Anonymous Routing Protocol for Mobile Ad Hoc Network," in Proc. International Conference on Management and Service Science, Wuhan, 2009, pp. 1-6.

[8] R. Song, L. Korba, and G. Yee, "AnonDSR: efficient anonymous dynamic source routing for mobile ad hoc networks," in Proc. ACM Workshop Security of Ad Hoc and Sensor Networks (SASN'05), Nov. 2005

IJERGS

Flow pattern analysis of melted aluminum in shot sleeve of pressure dies casting and minimizing the defect

Rupesh Kumar Tiwari, Trilok Raj Chauhan

Assistant Professor, ITM University Gwalior India, Email: rupeshtiwari9999@gmail.com

Abstract— Cold chamber high pressure die casting, (HPDC), is a vital business process for the production of complex near net shape aluminum and magnesium alloy castings. The investigations were carried out mainly using the aluminum alloy. High Pressure Die Casting (HPDC) is a complex process that results in casting defects if organized inappropriately. Though, finding out the optimum construct is a quite uphill task as eliminating one of the casting defects (for example, porosity) can result in occurrence of other casting defects. The purpose of the project is to improve current modeling and understanding of defects formation in HPDC machines. An attempt has been made to analysis the flow behavior of metal (Aluminum) in HPDC injection chamber. The flow in the injection chamber of pressure die casting machines is analyzed using a model based on the shallow-water approximation which takes into account the effects of wave reflection against the end wall of the chamber. The results of the model for wave profiles, volume of air remaining in the injection chamber at the instant at which the molten metal reaches the gate to the die cavity, and optimum values of the parameters characterizing the law of plunger motion are observed to reduce the porosity defect. We found that, although the shallow water model does not provide a very accurate estimation of the mass of entrapped air in the injection chamber for certain ranges of working conditions, it does describe reasonably well the influence of the acceleration parameters and the initial filling fraction on the entrapped air mass, and can be of help in selecting operating conditions that reduce air entrapment while keeping the injection chamber filling time as low as possible.

Keywords— CFD, Fluent, Gambit, Simulation, HPDC machine etc.

INTRODUCTION

Many researchs have been done in various domains like technology development, material development, etc to improve the pressure die casting process. Now a days, HPDC process is finding its application in numerous fields, consequently majority of researchers are paying attention towards utilizing the HPDC process in the areas like casting complex shapes, casting light weight components etc.

Sulaiman, Shamsuddin et al. (1997) ^[1] explain the Simulation of the molten metal flow along runner and gating system of pressure die casting is carried out to determine the pressure applied by the plunger of the injection system through the casting process and how angle of the runner and gating system influence it. The result shows that smaller branch angle will require less pressure to fill the runner and gating system. The time required to fill the runner and gating system takes longer when smaller branch angle is used.

X.P. Niu et al. (1999) ^[2] studied that High pressure die casting usually contain gas porosity due to the entrapment of air or gas in the melt during the very high speed injection . The benefit of with evacuated die cavity through mould filling was assessed. It was establish that volume of gas porosity in the casting were considerably diminished by applying vacuum aid during die casting. As a consequence, the density and mechanical properties, mainly tensile strength and ductility were improved. The result of vacuum support on the porosity distribution and mechanical strength of the castings were deliberated. An optimum injection speed was also identified for producing high performance castings. After heat treatment, vacuum assisted die cast parts showed much less surface blistering when compared to conventional die cast parts

K. H. Lee et al. (2000) ^[3] studied that a feasibility study of the partial squeeze and vacuum die casting process was performed to make defect free casting product with excellent mechanical properties. The mixture of vacuum effect before injection and the squeezing effect after injection results in exceptional flaw free die casting . In the die casting procedure the injection stroke can originate a jet of liquid to strike the far end of the mold cavity and then spatter back. This creates extreme turbulence which generates a plenty of air, and results flawed castings.

J. Lopez et al. (2001) ^[4] studied on the optimum plunger acceleration law in the slow shot phase of pressure die casting machine. The purpose is to examine a plunger acceleration that is supposed to diminish air trap in the slow shot stage of the pressure die casting to decrease porosity in parts. The results of the model for wave profiles, volume of air remaining in the injection chamber at the instant at which the molten metal reaches the gate to the die cavity, and optimum values of the parameters characterizing the law of plunger motion, are evaluated with the mathematical results obtained.

Haijing Mao (2004) ^[5] studied that externally solidify product (ECP) in the cold chamber die casting process has been done. The fraction of melt which solidifies in the shot sleeve before the metal is injected into the die cavity is referred to as externally solidified product. The objectives of this research is to examine what amount of ESP will travel into die cavity and final location of ESP in the casting.

Kallien, Lothar H (2009) ^[6] studies that Gas injection is a special technique which allows the production of hollow structure. The advantage of gas injection are free design of thick and thin wall in one part. In this process the cavity is filled with molten metal and after the partial solidification by the gas is injected in to the cavity. After total freezing the gas pressure is released. The result shows that the injection is applicable for relative complex geometries. Further release will deal with the optimization of the process with respect to later application in production and optimization of the internal surface structure that depends on the pressure and the alloy.

M. Sahu et al. (2009) ^[7] studied a CFD model of fully developed of laminar flow in a pipe is derived. Fluent is CFD software package to simulate fluid flow problem. Geometry and grid generation is done is GAMBIT which is further analyse in FLUENT. A solution can be obtain by following nine steps

1. Create geometry in GAMBIT.
2. Mesh geometry in GAMBIT
3. Set boundary type in GAMBIT
4. Set up problem in FLUENT
5. Solve
6. Analyze result
7. Refine mesh

Yoshifumi kuriyama et al. (2011) ^[8] studied an optimum velocity control of Die casting plunger accounting for air entrapment has been done. Die casting has the disadvantage, however, of air entrapment reducing product strength because it forces molten metal at high speed into a mold using a plunger. A multistage velocity control pressure die casting machine is used. Projection velocity is in between 0.02 to 5.0 m/s and acceleration between 4.23 and 4.61 m/s². We set the Die temperature in between 110 to 150 degree celcius and molten metal temperature is 660 to 680 degree celcius. Evaluation of air entrapment amount - Using FLOW-3D to determine the air entrapment amount in the molten metal caused by plunger movement. Using casting CAE, we analyzed fluidity behavior, the amount of air trapped, and the amount of air shutting caused by a plunger moving to evaluate their effect on product quality.

Matti sirvio et al. (2012) ^[9] studied the simulation of the wave formation in the shot sleeve and all of its effects, such as air entrapment. By including the parameters and attributes of the die casting machine in simulation model, it is achievable to simulate the filling perfectly.

The present research explains the benefits of the Shot Sleeve simulations to achieve improved casting system design in HPDC castings. Investigation of filling is utilized to decide upon the size, location of the gate and runner design to make certain complete filling of the mould. Shot sleeve simulations in High Pressure Die Casting process ensures the minimum air entrapment during the pre-filling phase. The low velocity of the plunger enables the air to escape via parting line or vents.

Kuo, T.H et al. (1993) ^[10] studied the simulation in high pressure die casting by computer aided engineering (CAE). The filling and solidification behaviour related to product quality and defect forming mechanism. It reduce trial and error in workshop as the process is virtually realized and verified by computer. CAE simulation of the entire casting system reveals filling and solidification behavior in the casting process and identifies the necessary information related to product quality and defect formation.

Paul Robbins (2012) ^[11] studied the vacuumed assisted casting. The benefit of vacuum assisted die casting are many such as rejections due to porosity are virtually eliminated, excellent surface quality is practically ensured, product density and strength are increased, less casting pressure is required. The gap between the plunger and the wall of the shot sleeve is necessarily very small- only 0.004 in. If at any time during the slow part of the shot, the gap becomes much greater than this, air is likely to be sucked through gap.

Brevick, J. R et al. (1994) ^[12] studied the effect of entrapped gas in porosity of Aluminum Horizontal Cold Chamber Die Casting. Duran. M et al. (1991) ^[13] in their research tried to minimize air entrapment in the shot sleeve of a die casting to reduce porosity. Thome, M. C et al. (1993) ^[14] modelled fluid flow in horizontal cold chamber die casting shot sleeves. Sekhar, J. A et al. (1979) ^[15] studied the effect of pressure on metal die heat transfer coefficient during solidification.

METHODOLOGY

Shot sleeve related parameter

The parameters like

- Acceleration
- Stage velocities
- Diameter

The above parameters determining the formation of wave patterns which can be a crucial factor in deciding whether air becomes entrapped in molten metal. Shot command delay in the first process parameter is to be selected carefully. Another process parameter to be optimized is the first stage velocity. The vents should be big enough to let the air escape and also the runner should not have sharp corners.

CFD Software

- Commercial: Fluent, Comsol, CFX, Star-CD
- In-house codes: Edge (FOI), DLR-Tau (German Aerospace Center), Fun3D (NASA), Sierra/Premo (American Aerospace)
- Open Source: Open FOAM, FEniCS, OpenFlower

What is FLUENT?

FLUENT is a state-of-the-art computer program for modeling fluid flow and heat transfer in complex geometries. FLUENT gives total mesh exibility as well as the capability to explain your own problems applying unstructured meshes which can be create intricate geometries with comparative simplicity. FLUENT also allows you to refine or coarsen your grid based on the flow solution. FLUENT is written in the C computer language and makes full use of the exibility and power offered by the language. As a result, accurate dynamic memory distribution, efficient data structures, and supple solver run are all feasible. FLUENT also utilizes a client/server architecture, which permits it to run different concurrent processes on client desktop workstations. This architecture permits capable execution, interactive control, and complete flexibility between diverse types of operating systems. All functions required to compute a solution and display the results are accessible in FLUENT through an interactive, menu-driven interface.

Explaining how to use FLUENT cannot be done without discussing GAMBIT first. GAMBIT is an application that is distributed along with FLUENT. As of this writing, it is owned and distributed by ANSYS, Inc. GAMBIT is used as a tool to generate or import geometry so that it can be used as a basis for simulations run in FLUENT. It can either build a model or import existing geometries from various other CAD applications. With a geometry in place it generates a mesh for the surface and volume of the geometry allowing it to be used for computational fluid dynamics. FLUENT is able to read geometries generated in GAMBIT and model fluid flow within the. It can be modeled using CFD.

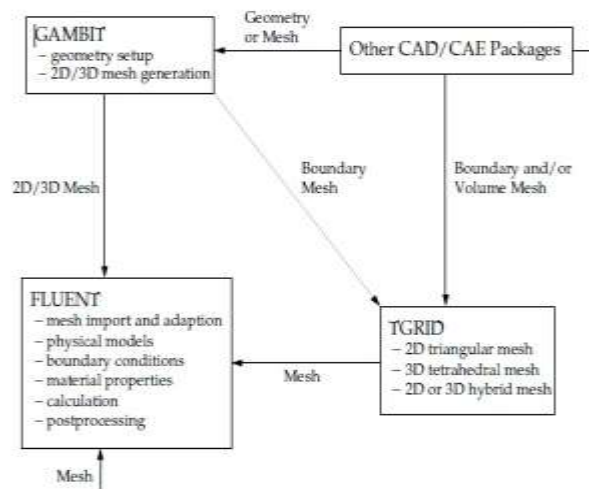


Fig 1. Basic fluent structure

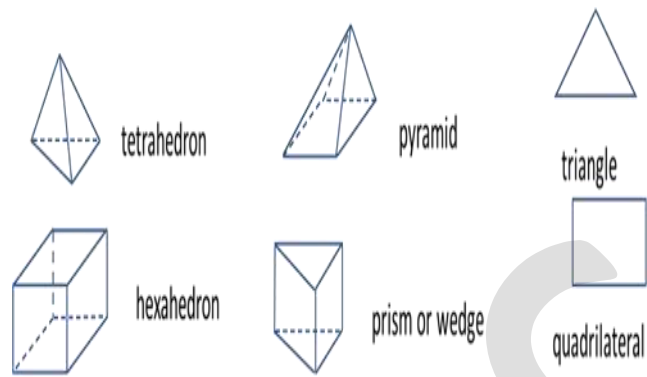


Fig 2 Types of grid

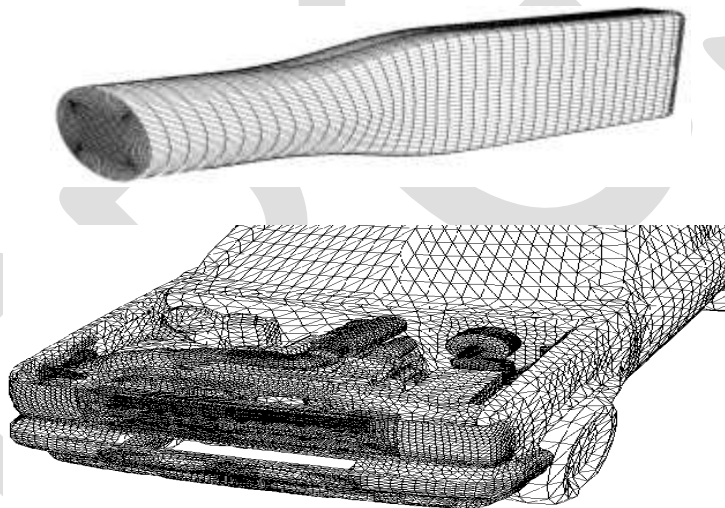


Fig 3. Grid shape in simple and complex geometry

Terminology-

- Cell – Control volume into which the domain is broken up.
- Node – Grid point
- Cell center – Center of cell
- Edge – Boundary of face
- Face – Boundary of cell
- Domain - Group of nodes, cells and faces

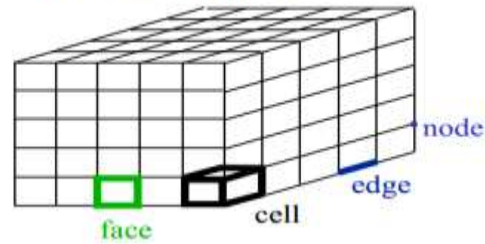
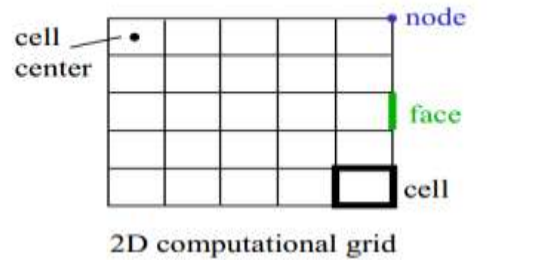


Fig 4. Domain type

CFD Procedure

I. Formulate the Flow Problem

The initial step is to generate the flow problem by answering to the questions as follows:

- What is the objective of the analysis?
- What geometry should be included?
- What are the freestream and/or operating conditions?
- What dimensionality of the spatial model is required? (1D, quasi-1D, 2D, axisymmetric, 3D)
- How the flow domain should look resemble to?
- What sequential modeling is suitable? (steady or unsteady)
- What is the nature of the viscous flow? (inviscid, laminar, turbulent)
- How should the gas be modeled?

II. Model the Geometry and Flow Domain

The body about which flow is to be analyzed requires modeling. This usually done using CAD. Rough estimates of the geometry and some simplifications may be involved to permit analysis with relative ease. Simultaneously, decisions are made as to the extent of the finite flow domain in which the flow is to be simulated. The geometry and flow domain are modeled in such a manner as to provide input for the grid generation. Thus, the modeling often takes into account the structure and topology of the grid generation.

III. Establish the Boundary and Initial Conditions

Since a finite flow domain is specified, physical conditions are required on the boundaries of the flow domain. The simulation usually begins from an initial solution and subsequent iterative results in final solution.

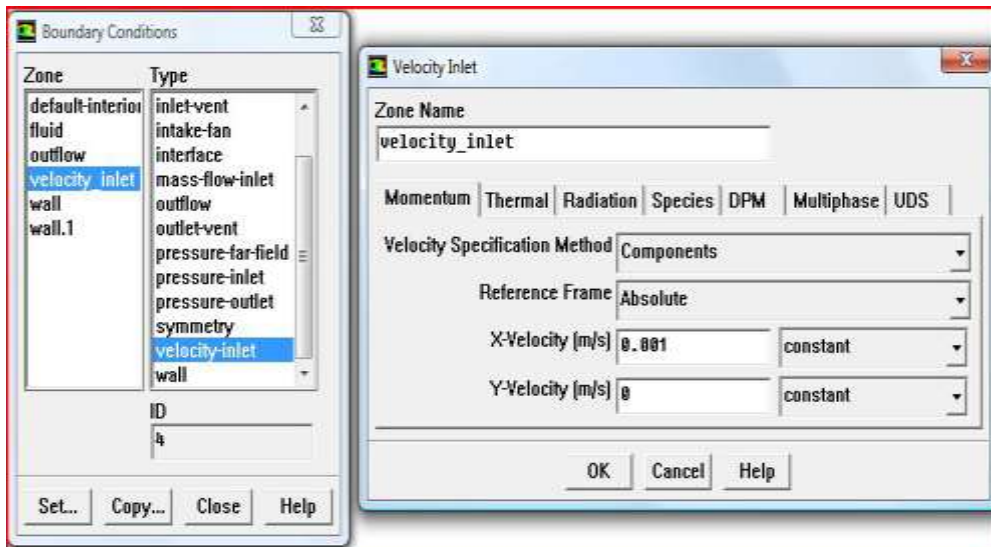


Fig 5. Boundary condition and velocity inlet window

IV. Generate the Grid

The grid creation defines the structure and topology. At present the entire cases under consideration are multi-block, structured grids; though, the grid blocks may be abutting, contiguous, non-contiguous, and overlapping. The grid should exhibit some minimal grid quality as defined by measures of orthogonality (especially at the boundaries), relative grid spacing (15% to 20% stretching is considered a maximum value), grid skewness, etc.

V. Establish the Simulation Strategy

The strategy for performing the simulation involves determining such things as the use of space-marching or time-marching, the choice of turbulence or chemistry model, and the choice of algorithms.

VI. Establish the Input Parameters and Files

A CFD codes generally requires that an input data file be created listing the values of the input parameters consisted with the desired strategy. Further the a grid file containing the grid and boundary condition information is generally required. The files for the grid and initial flow solution need to be generated.

VII. Perform the Simulation

The simulation is carryout with a variety of possible alternatives for interactive or batch processing and distributed processing.

VIII. Monitor the Simulation for Completion

The solution is examined to find out whether "converged" solution has been achieved or not.

IX. Post-Processing involves extracting the desired flow properties (thrust, lift, drag, etc...) from the computed flowfield.

X. Make Comparisons of the Results

The computed flow properties are judge against the experimental studies to ascertain the legitimacy of the calculated results.

XI. Sensitivity Analysis

The sensitivity of the results is investigated with respect to the following parameters:

- Dimensionality
- Flow conditions
- Initial conditions
- Marching strategy
- Algorithms
- Grid topology and density
- Turbulence model
- Chemistry model
- Flux model
- Artificial viscosity
- Boundary conditions
- Computer system

XII. Document

Documenting the findings of an analysis involves describing each of these steps in the process.

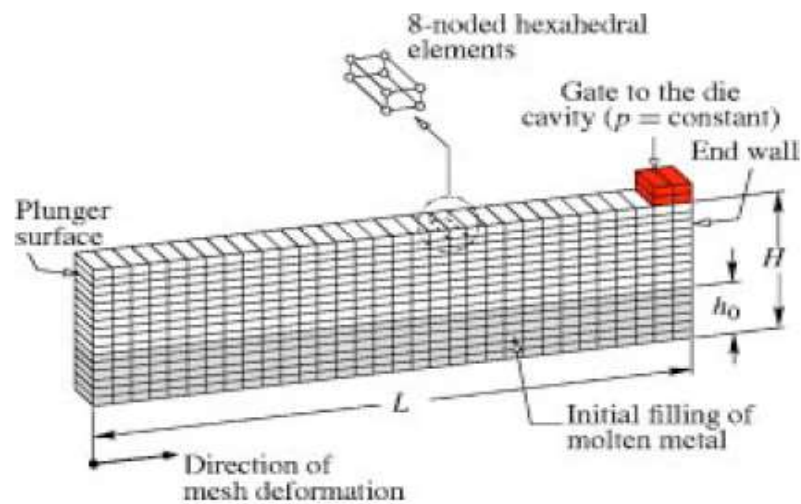


Fig 6. Grid formation in domain

EXPERIMENT

In order to achieve the goal of this experiment work, i.e. to establish the correlation between software analysis and real time condition, high pressure die casting machine is used. For the practical work Indore based industry “Triyami Tools” provide the HPDC machine. Two parts have been prepared, Engine cover and the automotive foot rests. The material used for this experiment is aluminium. It should be pointed out that the cast plates were also subjected to thermal treatments, i.e. Solution Treatment (T4: 2 hr at 470oC), Aging (Stress-Relief) (T5: 2 hr at 200oC), and Solution Treatment +Aging (T6).



Fig 7. HPDC Machine

- **For engine cover**
 60 tonnes machine is used.
 80000 KPa pressure is required.
 Shot sleeve diameter 40 mm
 Locking force 60 tonnes
- **For Foot rests**
 60 tonnes machine is used.
 100000 KPa pressure is required.
 Shot sleeve diameter 40 mm
 Locking force 60 tonnes



Fig 8. Engine cover and footrests

Specification

Die cast parts can vary greatly in size and therefore require these measures to cover a very large range. As a result, die casting machines are designed to each accommodate a small range of this larger spectrum of values. Sample specifications for several different hot chamber and cold chamber die casting machines are given below.

Machine	DC60	DC120	H-160D	H-250D	H-400D	H-660D
Locking force	60	120	160	250	400	660

Injection force (adjustable)	10	13	20	35	38.5	65
Hydraulic ejection force	4	6	10	15	22	43
Initial plunjer stroke(mm)	250	275	300	350	400	600
Plunjer dia (mm)	30-45	50-65	40-80	50-85	60-110	50-120
Max injection pressur (kg/cm ²)	800	1035	1600	1780	2600	3310

Table 1. Specification of HPDC machine

Both hot chamber and cold chamber die casting machines are typically characterized by the tonnage of the clamp force they provide. The required clamp force is determined by the projected area of the parts in the die and the pressure with which the molten metal is injected. Therefore, a larger part will require a larger clamping force. Also, certain materials that require high injection pressures may require higher tonnage machines. The size of the part must also comply with other machine specifications, such as maximum shot volume, clamp stroke, minimum mold thickness, and platen size.

HPDC machine and setup

Die casting is a manufacturing process that can produce geometrically complex metal parts through the use of reusable molds, called dies. The die casting process involves the use of a furnace, metal, die casting machine, and die. The metal, typically a non-ferrous alloy such as aluminum or zinc, is melted in the furnace and then injected into the dies in the die casting machine. There are two main types of die casting machines - hot chamber machines (used for alloys with low melting temperatures, such as zinc) and cold chamber machines (used for alloys with high melting temperatures, such as aluminum). The differences between these machines will be detailed in the sections on equipment and tooling. However, in both machines, after the molten metal is injected into the dies, it rapidly cools and solidifies into the final part, called the casting. The steps in this process are described in greater detail in the next section.

RESULTS

ANALYSIS OF FLOW

- Material used- Aluminium
- Inlet Velocity- 1 m/s
- Software used- Gambit and Fluent
- Gambit is used for mesh generation and Fluent for flow Analysis.

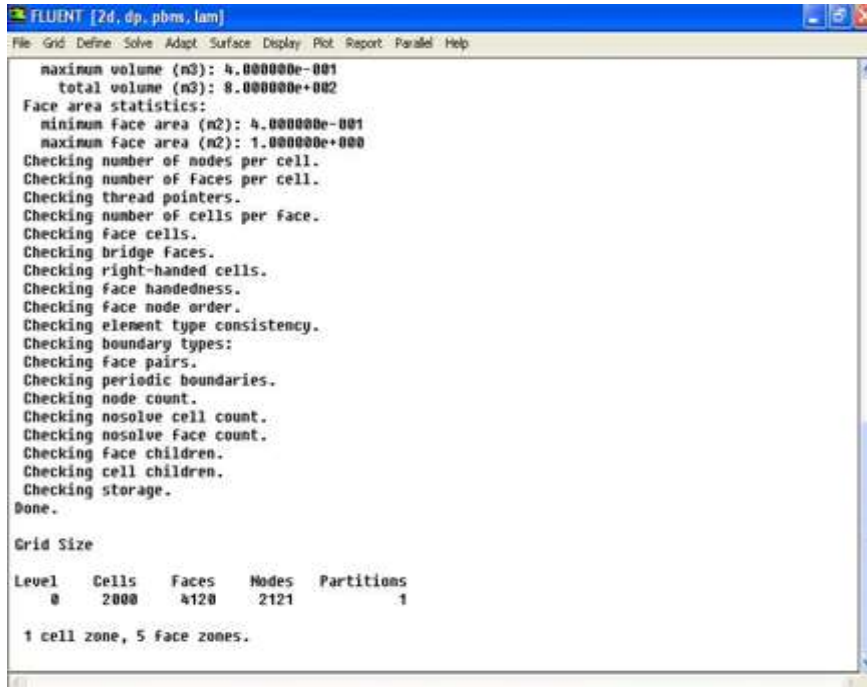


Fig 9. Grid size details

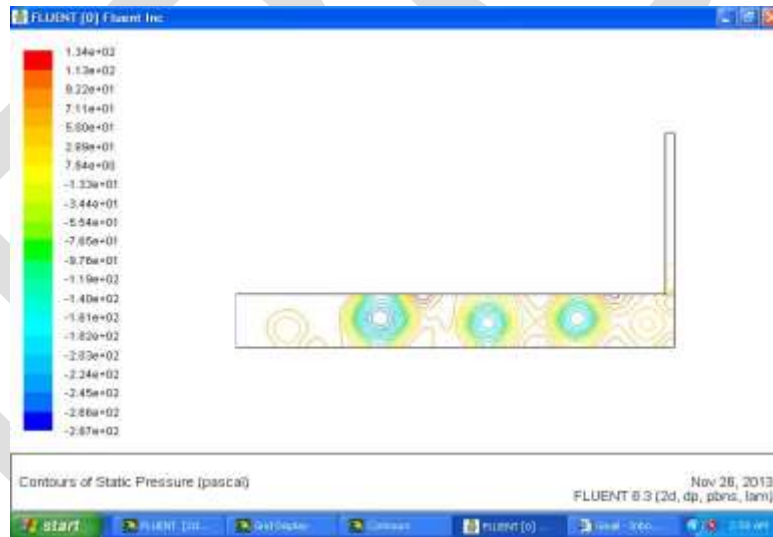


Fig 10. Pressure plot at velocity 1m/s

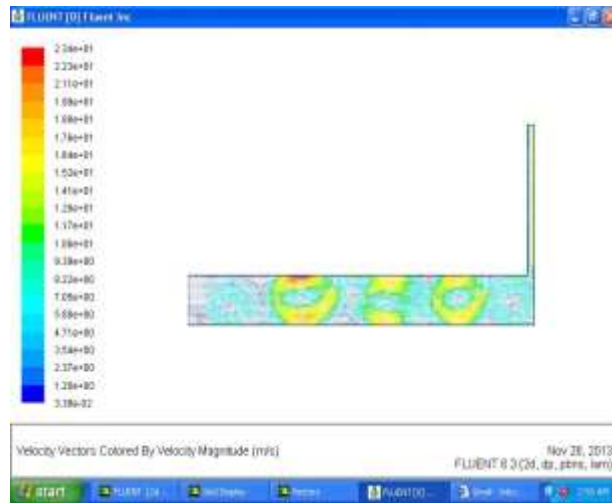


Fig 11. Velocity plot to 1m/s

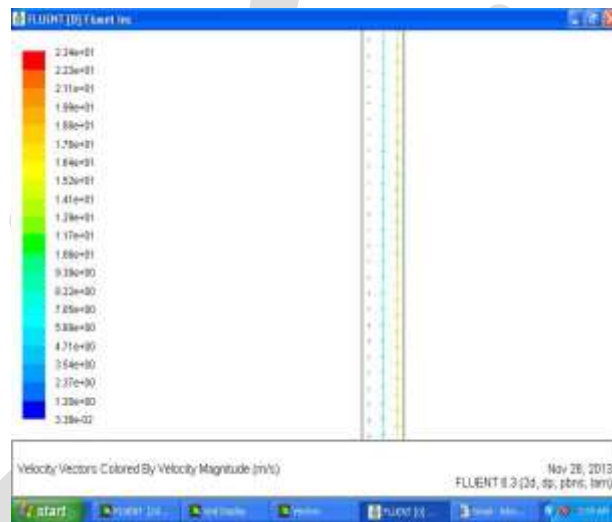


Fig 12. Zoom to runner

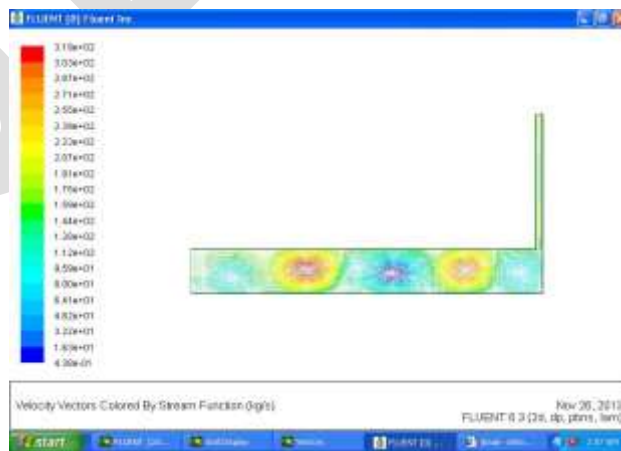


Fig 13. Stream function plot

- Increasing the velocity to 3 m/s for the same model

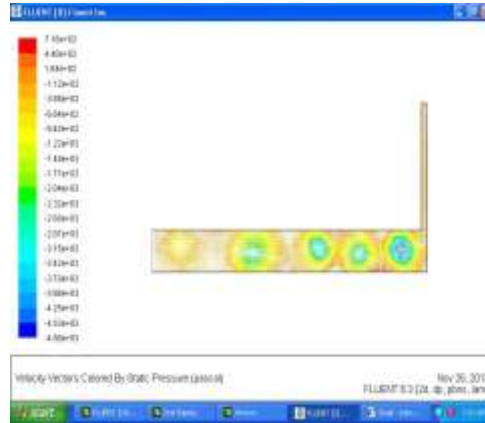


Fig 14. Pressure plot 3 m/s

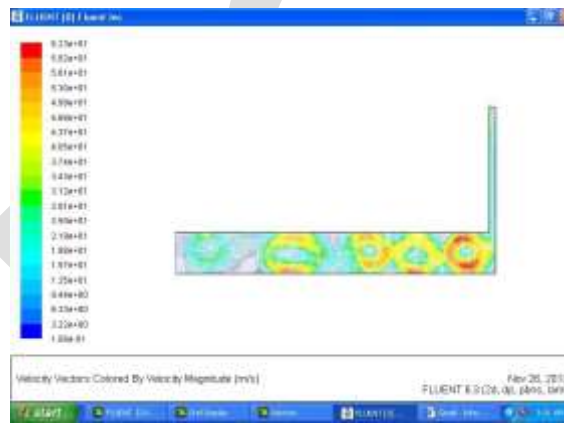


Fig 15. Velocity plot at 3 m/s



Fig 16. Velocity plot (zoom to runner)



Fig 17. Stream function plot

The stream function can be used to plot [streamlines](#), which represent the trajectories of particles. Since streamlines are [tangent](#) to the velocity vector of the flow, the value of the stream function must be constant along a streamline

- When the velocity is increased by 5m/s for the same model



Fig 18. Flow behavior at 5 m/s

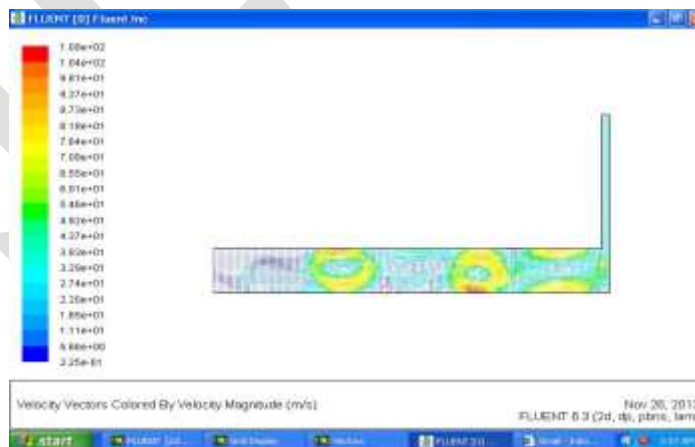


Fig 19. Velocity plot

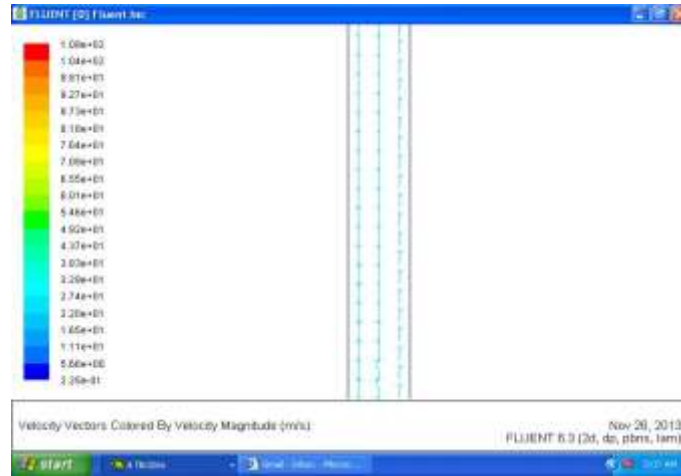


Fig 20. Zoom to runner

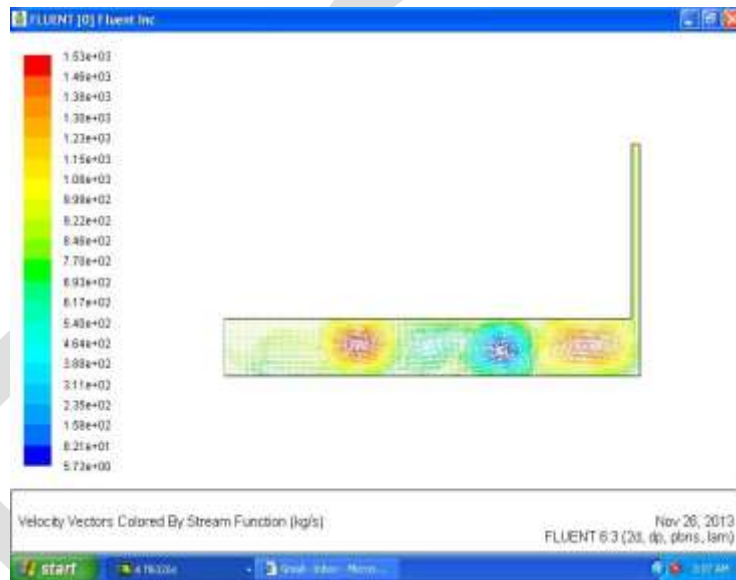


Fig 21. Stream function plot

- Preparation of Engine cover in 3-D visualize the grid structure

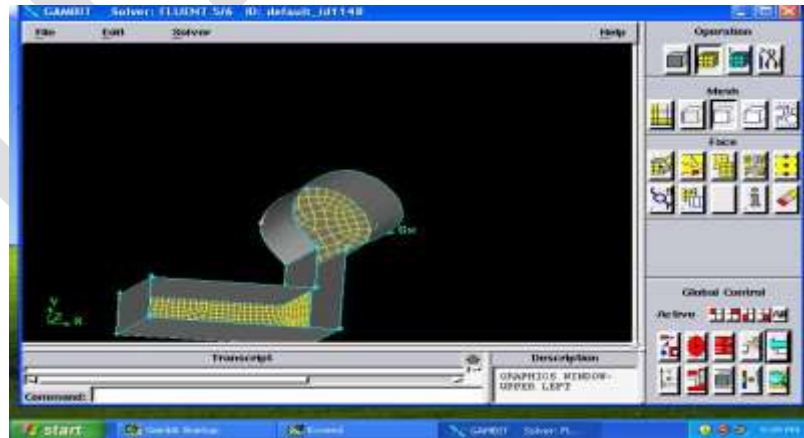


Fig 22. Model of engine cover

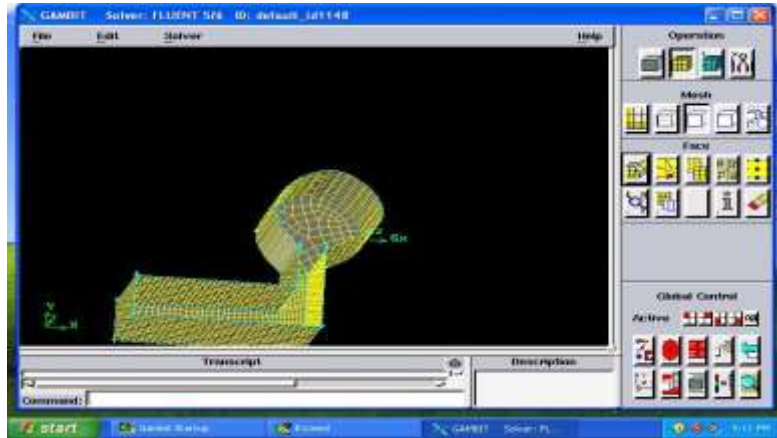


Fig 23. Fully meshed model

- Flow behaviour at 40000 KPa

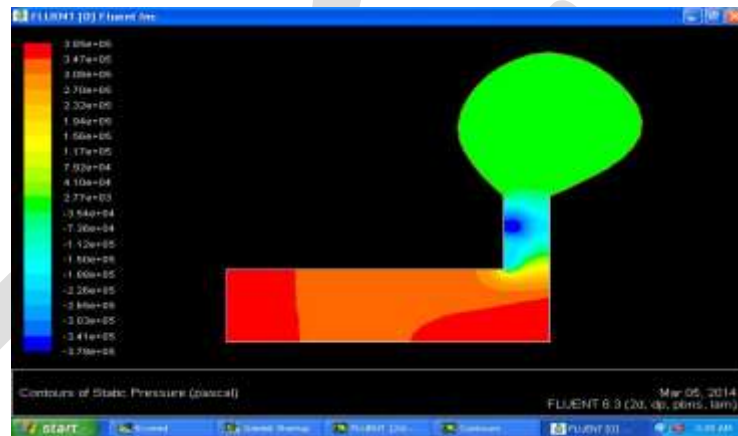


Fig 24. Pressure graph when the pressure is 40000 Kpa

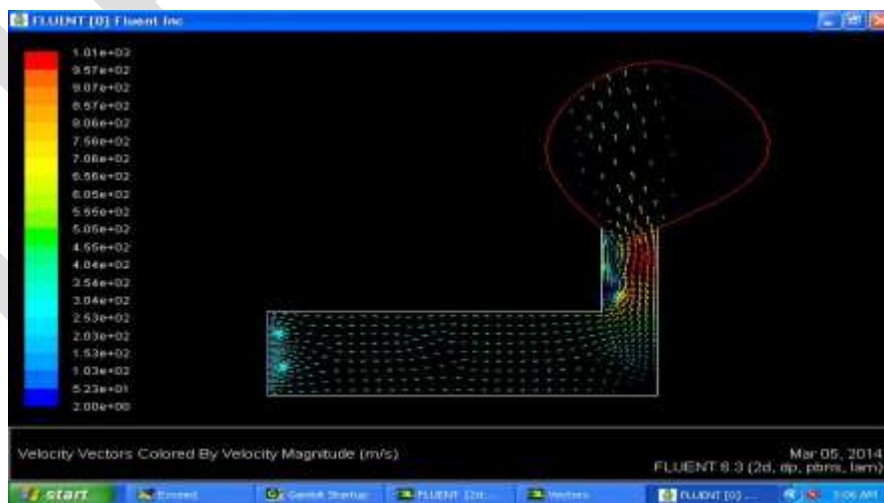


Fig 25. Velocity plot

- Flow behaviour at 60000 KPa

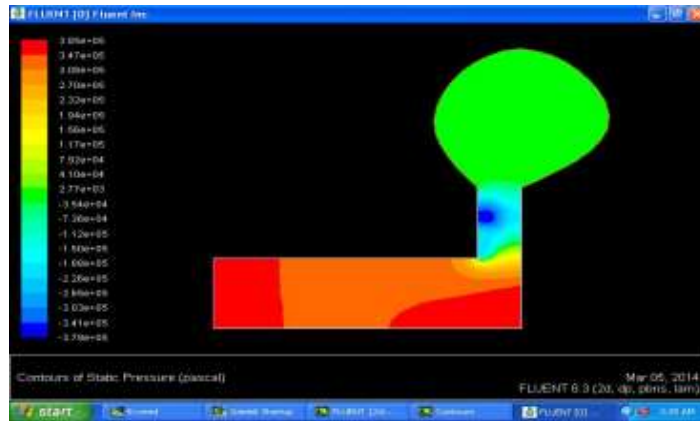


Fig 26. Pressure based plot at 60000 Kpa

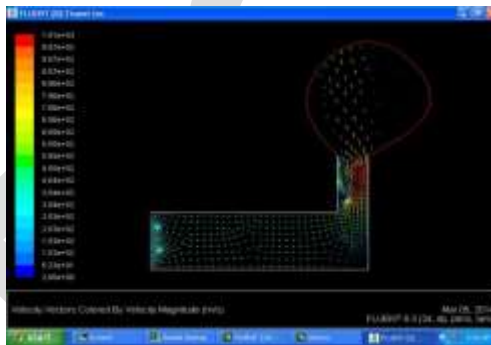


Fig 27. Velocity plot

Flow behaviour at 80000 KPa

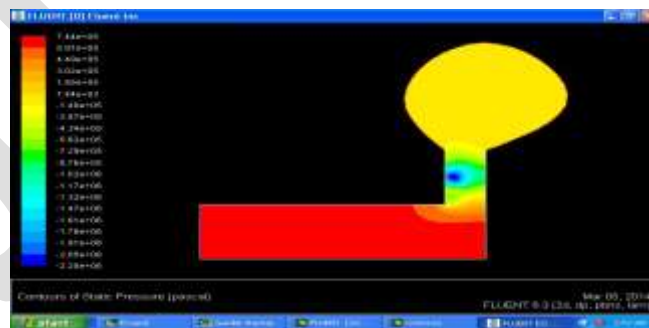


Fig 28. Pressure based plot

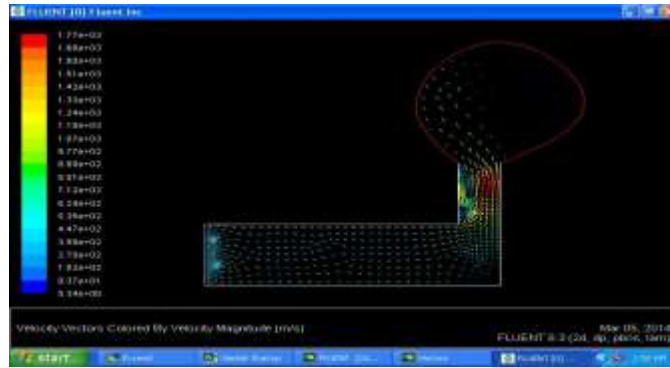


Fig 29. Velocity plot

- 3-D model of foot rests

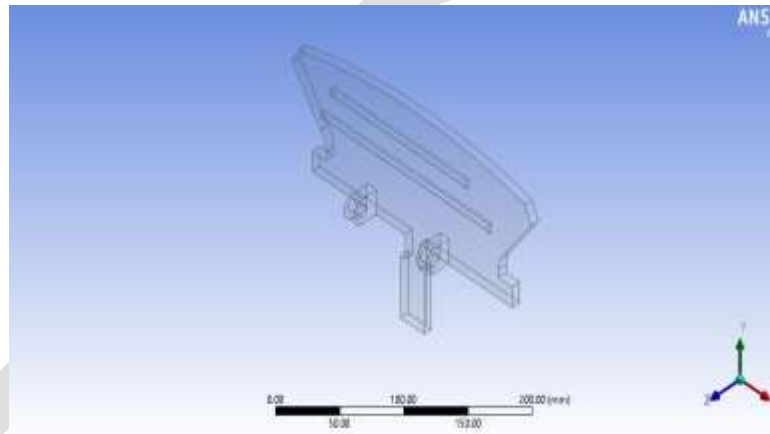


Fig 30. 3d model of footrest

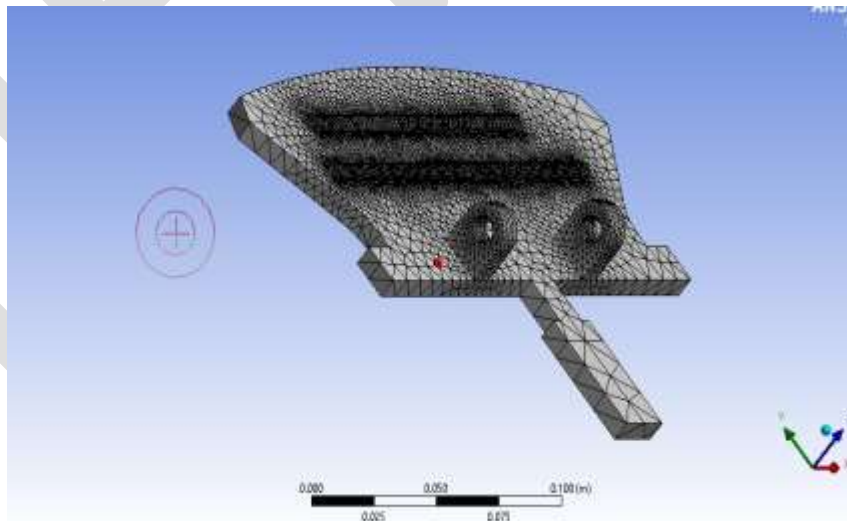


Fig 31. Meshing of structure

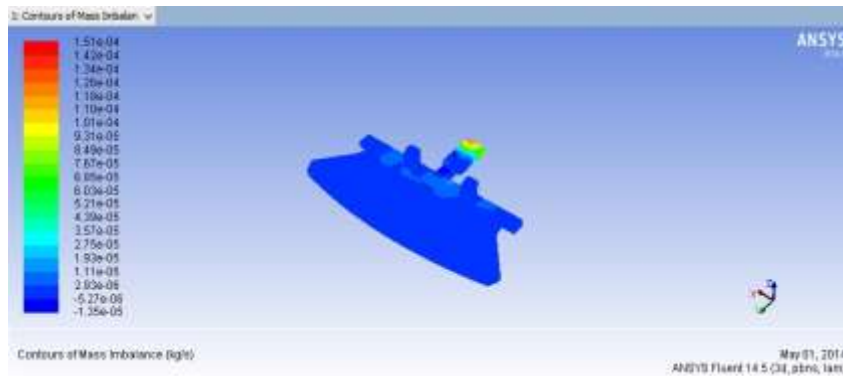


Fig 32. Contour of Residual

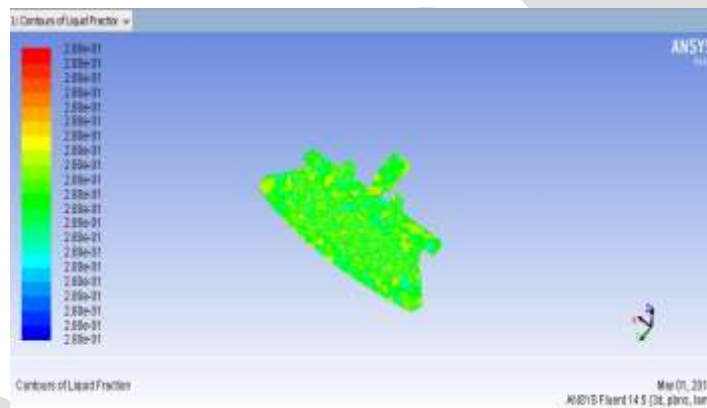


Fig 33. Solidification of casting

Result and Discussion

Graph plot between Pressure and Velocity.

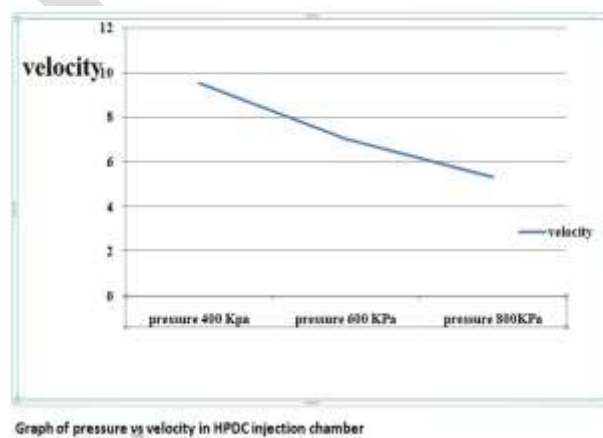


Fig 33. Plot between pressure and velocity

- Analysis from experiment and software as the pressure increases ,the velocity decrease
- For every change in pressure there is change in flow behaviour of liquid aluminium.
- This lead to the conclusion that for a specific size of injection chamber there is a fixed range of pressure.

- The smaller the branch angle, the less the applied pressure at the plunger is needed. This is because smaller branch angle offers less resistance to the metal flow which is also a reason for the back flow of molten metal in injection chamber.

When a pressure of 40000 kPa is applied by a plunger of 40 cm diameter to a specific area of cavity, the velocity of the liquid aluminium inside the injection chamber increases. As the pressure is further increased to 60000 kPa the velocity of the molten metal inside the injection chamber gradually decreases. The actual pressure at which the casting process takes place i.e 80000 kPa the velocity decreases, which also satisfy the Bernoulli's principle.

From the graph above it has been observed that, when the pressure 40000 kPa is applied, there is frequent change in the pressure inside the injection chamber which can be seen from the change of colour in the pressure graph, but when the actual pressure of 80000 kPa is applied, which is suitable for model prepared (engine cover), the large variation of pressure inside the injection chamber decreases. Thus for the specific area of casting there must be a fixed range of pressure.

CONCLUSION

An attempt has been made to analysis the flow behaviour of metal (Aluminium) in HPDC injection chamber. The future work involves the experiment on the basic of which the final parameter for minimizing the defect will be decided. Analysis of the flow behaviour is observed on the basis of graph plotted with the help of GAMBIT which is a application that is distributed along with FLUENT. FLUENT is able to read geometries generated in GAMBIT and model fluid flow within. The formation of vortex has been seen in the graph due to the pressure variation.

Several simulations were carried out using different combinations of plunger speed and movement to demonstrate importance of right plunger movement profiles. For every change in pressure there is change in flow behaviour of liquid aluminium. This lead to the conclusion that for a specific size of injection chamber there is a optimum value of pressure.

Future Scope

- Improvement of the casting quality by minimising the entrapped air during the shot sleeve process.
- Optimisation of the whole casting process by controlling filling with optimal plunger movement.

REFERENCES:

- [1] Sulaiman, Shamsuddin, and Tham Chee Keen. "Flow analysis along the runner and gating system of a casting process." *Journal of materials processing technology* 63.1 (1997): 690-695.
- [2] Niu, X. P., et al. "Vacuum assisted high pressure die casting of aluminium alloys." *Journal of Materials Processing Technology* 105.1 (2000): 119-127.
- [3] Kim, E. S., K. H. Lee, and Y. H. Moon. "A feasibility study of the partial squeeze and vacuum die casting process." *Journal of Materials Processing Technology* 105.1 (2000): 42-48.
- [4] Faura, F., J. Lopez, and J. Hernandez. "On the optimum plunger acceleration law in the slow shot phase of pressure die casting machines." *International Journal of Machine Tools and Manufacture* 41.2 (2001): 173-191. Thompson, Joe F. "Grid generation techniques in computational fluid dynamics." *AIAA journal* 22.11 (1984): 1505-1523.
- [5] Mao, Haijing. *A numerical study of externally solidified products in the cold chamber die casting process*. Diss. The Ohio State University, 2004.
- [6] Kallien, Lothar H. "Using Gas Injection in High Pressure Die Casting Technology." *113th Metalcasting Congress, Las Vegas, Nevada*. (2009).
- [7] Sahu, M., et al. "Developed laminar flow in pipe using computational fluid dynamics." *7th International R & D Conference on Development and Management of Water and Energy Resources, 4-6 February 2009, Bhubaneswar, India*. 2009.
- [8] Kuriyama, Y., K. Yano, and S. Nishido. "Optimization of Pouring Velocity for Aluminium Gravity Casting." *Fluid Dynamics, Computational Modeling and Applications* (2012).
- [9] Sirviö, M. and Martikainen, H. "**Simultaneous engineering between workshops and foundries**". *Int. Conf. on Best Practices in the Production, Processing and Thermal Treatment of Castings*. Singapore,
- [10] Kuo, T.-H., and Hwang, W.-S., 1998, "Flow Pattern Simulation in Shot Sleeve Injection of Diecasting," *AFS Transactions, Vol. 106, pp. 497-503*.
- [11] [www.castool.com/sites/default/files/publications/vacuum assisted die casting todays most significant technology print.pdf](http://www.castool.com/sites/default/files/publications/vacuum_assisted_die_casting_todays_most_significant_technology_print.pdf), Paul Robbin: 2012.
- [12] Brevick, J. R., Armentrout, D. J., and Chu, Y., 1994, "Minimization of Entrained Gas Porosity in Aluminum Horizontal Cold Chamber Die Casting," *Transactions of NAMRI/SME, Vol. 22, pp. 41-46*.

- [13] Duran, M., Karni, Y., Brevick, J., Chu, Y., and Altan, T., 1991, "Minimization of Air Entrapment in the Shot Sleeve of a Die Casting Machine to Reduce Porosity," Technical Report ERC/NSM-C-91-31, The Ohio State University.
- [14] Thome, M. C., and Brevick, J. R., 1993, "Modeling Fluid Flow in Horizontal Cold Chamber Die Casting Shot Sleeves," *AFS Transactions, Vol. 101, pp. 343-348.*
- [15] Sekhar, J. A., G. J. Abbaschian, and R. Mehrabian. "Effect of pressure on metal-die heat transfer coefficient during solidification." *Materials Science and Engineering* 40.1 (1979): 105-110, 10 - 12 Oct. 1995. Paper 17-1-6

IJERGS

Contrast Enhancement Based on BAT Algorithm

Pooja, Jyoti Rani

GZS PTU Campus, Bathinda, gargaarzo05@gmail.com, 9478002224

Abstract— In this research paper, an algorithm is developed to produce better contrast enhancement which is inspired from nature and calculates the upper and lower limit for each sliding window. These upper and lower limits are used to calculate the local mean and global mean. It is based on contrast objective function; this is parabolic logarithmic threshold function. The results show that, the method is able to produce better contrast sensitivity and pleasing visuals as compared to older methods(histogram equalization, adaptive histogram equalization, fusion of pyramid and Gaussian , ant colony optimization method etc). The corpus of image consists of both gray and color images. Other than these other evaluation values like loudness, pulse rate, frequency show that this method provides better contrast ratio.

Keywords- Bat algorithm, Contrast Enhancement, Fusion Method

INTRODUCTION

Contrast enhancement is a commonly used operation in Image Processing. Contrast, is a property of image which makes the visual appearance better by adding color grading in the image. Contrast is calculated in terms of color and brightness of the object and other objects within same view of field. Contrast enhancement is the operation which is used in Medical images. It plays an important role for processing scientific images such as X-rays or satellite images. There are many methods proposed to enhance the contrast of an image. The most simplest and effective method for contrast enhancement is Histogram Equalization. The basic idea behind Histogram Equalization was to rescale the gray levels of image. Histogram Equalization removed the annoying artifacts and unwanted noise. The limitation of histogram equalization was that it applied on entire image whereas this limitation was overcome by Adaptive histogram Equalization which operated on small regions/blocks.

The improved version of Adaptive histogram Equalization was Contrast Limited Adaptive Histogram Equalization which partitioned images into contextual regions and then histogram equalization was applied. This process evens out the distribution of gray pixel values and make out the hidden details visible to human. To improve contrast there was a Dualistic Sub Image Histogram Equalization in which the original image was decomposed into two equal sub images based on its gray level probability density function. On the basis of normalized law function they changed the sub histogram through weighting process and then equalized the weighted sub Histogram Enhancement of contrast using Weighted Threshold Histogram Equalization with Improved Switching Median Filter. The general idea adopted by WTHE was to modify the histogram and assigned weight and threshold to each pixel before equalization. Filtering played a vital role in signal processing and main goal of filtering was to enhance fine details of an image. The image was enhanced by WTHE then it passed through Improved Switching Filter, in improved switching median filtering it modified the corrupted signal without affecting uncorrupted signal and reduced the impulse noise created during enhancement. The performance of this method was evaluated by Absolute Mean Brightness Error (AMBE), Measure of Enhancement (EME), PSNR, and MSE. There were few bio inspired algorithms applied for contrast enhancement such as Ant Colony Optimization, Improving Ant Colony Optimization, Local and Global Contrast Algorithm, Firefly Algorithm.

PROPOSED WORK

Bat Algorithm

1. Objective function $f(x)$, $x = (x_1; \dots; x_d)^T$

2. Initialize the bat population x_i for $i = 1, \dots, n$

$v_i =$ pulse distance/ time

$f_i = f_{\min} + [f_{\max} - f_{\min}] * \beta$

where β is frequency adjustment constant.

3. Let A_{\min} to A_{\max} be the loudness range dependent upon frequency and emission rate as the emission rate slows when the loudness increases and vice versa.

4. Let λ be the wavelength at a fixed value

For each iteration,

x_0 be the starting search point.

Get Position x , Loudness A , frequency f , Wavelength λ

Generate Random solution.

If new solution is better than old solution

Terminate

Else

5. Update position, loudness, frequency, emission rate.

Generate Random number between 0 and 1.

If ($\text{rand} > p_e$)

Select best solution

Generate local solution among best solution

If ($\text{rand} < A_i$) and $f(x_1) < f(x_2)$)

Accept solution

Increases p_e (pulse emission rate) and reduce A (loudness)

End

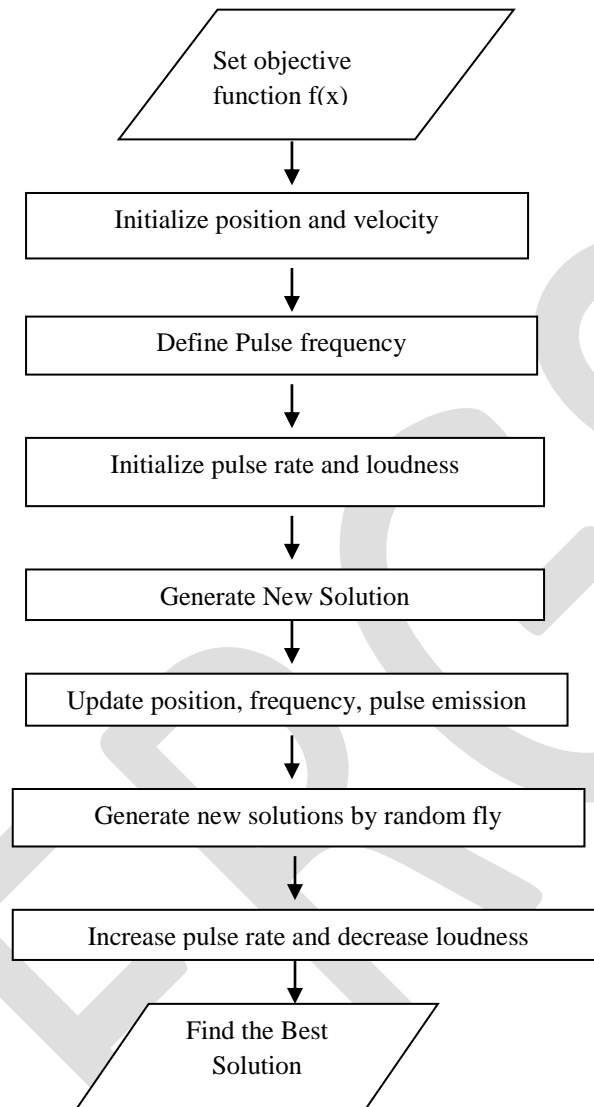
Table I
Showing BAT Parameters and its values

Sno	BAT Parameters	Values
1	Population Size (Bat Number)	20
2	Loudness	0.5
3	Minimum Frequency	0.1
4	Maximum Frequency	2
5	Pulse Rate	0.4
6	Number of Generation(Iterations)	1000
7	f(x), x = (x1; :::; xd) Objective Function	[0,1]
8	Upper Bound	4
9	Lower Bound	1
10	Design of Experiment for Optimal parameters method	5

Table II
Showing Research Parameters and its values

Sno	Research Parameters	Values
1	Number Of Images	15
2	Size of Images	8KB-1.12MB
3	Contrast Upper value	1
4	Contrast Lower value	0.1

FLOW CHART



RESULTS

In the previous work researchers enhanced the contrast of an image but with some limitations such as unwanted noise, artifacts, more computation time. In the current research work it is wise to enhance the contrast of an image by using nature inspired algorithms which gives the better results

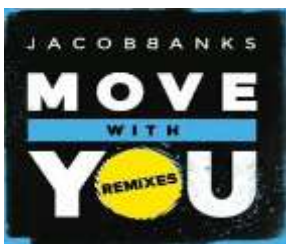


Fig1 : (a) Original Image (b) Apply fusion method of Pyramid and Gaussian (c) Proposed Method



(a)



(b)

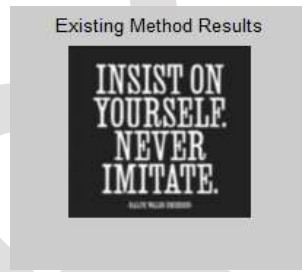


(c)

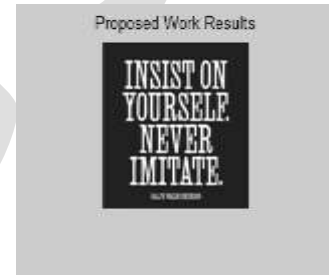
Fig2 : (a) Original Image (b) Apply fusion method of Pyramid and Gaussian (c) Proposed Method



(a)



(b)

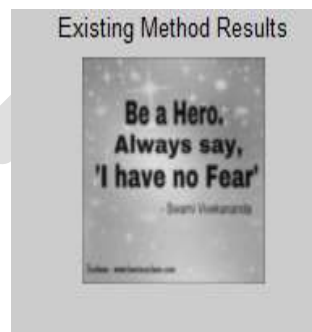


(c)

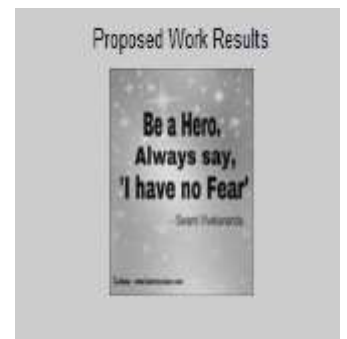
Fig3 : (a) Original Image (b) Apply fusion method of Pyramid and Gaussian (c) Proposed Method



(a)



(b)



(c)

Fig4 : (a) Original Image (b) Apply fusion method of Pyramid and Gaussian (c) Proposed Method

Table III

Comparison with Existing Method

Images	Fusion of Gaussian and Pyramid	Proposed Method
Fig 1	84.5738	87.7512
Fig 2	97.8488	99.2395
Fig 3	66.050	73.6042
Fig 4	39.7182	43.1568

This table shows that the proposed method which is bat based contrast enhancements gives better results as compared to existing method which was based on fused based.

CONCLUSION

In summary, we can say that contrast enhancement methods must be able to produce images that are not just pleasing to human eyes and perception, but also must be able to produce more information within the content of image. There are many methods implemented till date, and most of the methods were based upon stretching the edges of objects. In such a way, difference in gray levels or color levels increases and the image does not lose its quality, or may introduce unwanted artifacts when image is reproduced after contrast enhancement algorithm applications. In this research work, we were able to do a better treatment in context of contrast, as it is apparent from the evaluation parameters. The results produced by proposed method shows better results as compared to the existing fusion based method. The existing method gives values in terms of grey level variance 40.5807, 63.9614, 66.050 of some images whereas proposed method gives 44.5555, 65.0935, 73.6042 and this shows the better contrast enhancement.

FUTURE SCOPE

In future, we suggest the proposed method may be extended for medical images that follow some standards like Health Level 7 (HL7), as these images need multi-resolution, multi-contrast view to satisfy at particular diagnostic process.

REFERENCES:

- [1] Chao Zuo, Qian Chen, Xiubao Sui, and Jianle Ren, "Brightness Preserving Image Contrast Enhancement Using Spatially Weighted Histogram Equalization" volume11, No 1, January 2014
- [2] Kesharee Singh Yaduwanshi, Nitin Mishra " Contrast Enhancement of HDR images using linear transformation and kernel padding" volume5(2),2014
- [3] Shyam Lal , Mahesh Chandra ," Efficient Algorithm for Contrast Enhancement of Natural Images, vol 11, No1 , January 2014

- [4] Shih-Chia Huang, Fan-Chieh Cheng, and Yi-Sheng Chiu, "Efficient Contrast Enhancement Using Adaptive Gamma Correction with Weighing Distribution, volume 22, issue 3, march 2013
- [5] Qing Wang, Rabab Ward , "Fast Image/Video Contrast Enhancement based on WTHE"
- [6] Amiya Halder , "Dynamic Contrast Enhancement Algorithm", volume 74 no-12 july 2013
- [7] Ritu Chauhan, Sarita Singh Bhadoria , " An improved image contrast enhancement based on histogram equalization and brightness preserving weight clustering histogram equalization", 2011 International Conference on Communication Systems and Network Technologies (CSNT), vol., no., pp.597,600, 3-5 June 2011
- [8] Nirmal Singh, Maninder Kaur, K.V.P Singh , "Parameter Optimization Using PSO", volume 2, issue 3 , 2013
- [9] R.Sharmila, R.Uma , " A new approach to image contrast enhancement using weighted threshold equalization with improved switching median filter" volume 7, issue 2 , 2014
- [10] Pooja Mishra ,Mr.KhomLal Sinha, " Different Approaches of Image Enhancement" (2014)

An Efficient Content-Based Image Retrieval System Based On Dominant Color Using a Clustered Database

Joby Elsa Abraham, Kavitha V K

P.G Scholar, Dept of CSE, BMCE, Kollam, Kerala, India.

Email : Jobyeabraham@gmail.com

Abstract— Last years the importance and abundance of image retrieval systems had a big growth. During the searching process the color feature of the images is one of the most significant characteristics. Since the color-based comparison and retrieval has a variety of widely used techniques. In this paper we introduce a Dominant Color extraction scheme through which we extract color feature of the image. After extracting the dominant colors we use quantization to represent the extracted dominant colors within a limit. Based on quantized value we cluster the database and do the indexing to store images. Whenever a query image given to the system it will not search the whole database, just identify the cluster and search the image. Similarity measure used in our paper is a modified Euclidean distance measure. With the proposed feature experiments were carried out in image databases, and that was found the precision of retrieval has significantly improved and the time complexity of retrieval of images is reduced.

Keywords— CBIR, Dominant Colors, Dominant Color Descriptor, Similarity Measure, Quantization, Clustering, Indexing, query image, thresholding, RGB color space.

INTRODUCTION

Over the past few years Content-Based Image Retrieval has become an exciting and in-depth area of research. The relevance of visual information retrieval in many areas such as fashion and design, crime prevention, medicine, law, and science makes this research field one of the important and fastest growing in information technology. Image retrieval has come a long way where it started off with text-based retrieval. However, there are many problems associated with retrieving images based on text such as manual annotation of keywords, differences in perceptions and interpretations, and a few others. Due to this, researchers came up with CBIR where images are retrieved based on automatically derived low-level features (human vision related), middle-level features (objects related), or high-level features (semantic related). Among these features, the low-level features are the most popular due to its simplicity. One of the important low-level features is color as it plays an important role in CBIR due to its robustness to complex background and independent of image size and orientation.

In the current version of the MPEG-7 Final Committee Draft, several color descriptors have been approved including number of histogram descriptors and a dominant color descriptor (DCD). MPEG-7 specifies seven color descriptors [3,4]. It includes dominant colors, scalable color histogram, color structure, color layout, and GoF/GoP color. In [15], the authors have shown that the early perception in human visual system performs dominant color identification, and eliminates the fine details and colors in small areas. Therefore, for macroscopic level, human perceive images as a combination of dominant colors no matter how the exact color distribution. In MPEG-7, DCD provides an effective, compact, and intuitive salient color representation, and describe the color distribution in an image or a region of interesting but it lacks certain semantic information. This feature descriptor contains two main components: (1) representative colors and (2) the percentage of each color. These prominent colors and their percentages may only lead to retrieve many dissimilar images that share the same biggest DC. Usually, the dissimilarity occurs when the background color of an image has the largest percentage. Due to this so many enhancements are done to the MPEG-7 DCD. In [8], a semantic feature is added to the DCD to improve its accuracy in an object-based image retrieval application and it is considered as feature level-based solution to the background dominance problem. In this paper, we will develop an effective color extraction scheme for the image retrieval from the large database.

Besides, MP7DCD's quadratic similarity measure (QSM) that is used by Deng et al.[14]and Yamada et al.[13] has some drawbacks. In [10,12], one can see the first simple changes that were made to improve QSM. Authors in [11] also propose a palette histogram similarity measure to solve QSM problem. Moreover in [6], a new similarity measure was proposed to achieve a good performance compared with QSM and all the aforementioned modifications [10–12]. In [8] they used mutual color ratio (MCR),

which alleviates their dependencies on the biggest DC. In this present work, a modification will be applied to all the above dissimilarity measures to improve their performance. In order to increase the retrieval we propose a new clustered and indexed database in this work. In all the former works the database may be clustered or indexed but not clustered and indexed which does not assure good performance. In the present work the new database will be developed which assures a good time complexity

The paper is organized in the following way. Section 2 is concerned with explicating dominant color extraction scheme and the similarity measures. Section 3 is mainly concerned with the proposed color extraction scheme, the newly proposed modification that helps improve the similarity measure and introduces new clustered and indexed database. Section 4 illustrates the extensive experiment that contains visual results. Finally comes the conclusion in Section 5.

RELATED WORKS

Last decade has witnessed great interest in research on Content-based Image Retrieval. Many techniques have been done with respect to content-based image retrieval (CBIR). Most proposed CBIR [2, 5] techniques automatically extract low-level features (e.g. color, texture, shapes and layout of objects) to measure the similarities among images by comparing the feature differences. Color, texture and shape features have been used for describing image content. Color is one of the most widely used low-level visual features and is invariant to image size and orientation [1]. As conventional color features used in CBIR, there are color histogram, color correlogram, and dominant color descriptor (DCD).

Color histogram is the most commonly used color representation, but it does not include any spatial information. Color correlogram describes the probability of finding color pairs at a fixed pixel distance and provides spatial information. Therefore color correlogram yields better retrieval accuracy in comparison to color histogram. Color autocorrelogram is a subset of color correlogram, which captures the spatial correlation between identical colors only. Since it provides significant computational benefits over color correlogram, it is more suitable for image retrieval. DCD is MPEG-7 color descriptors [3,4]. DCD describes the salient color distributions in an image or a region of interest, and provides an effective, compact, and intuitive representation of colors presented in an image. However, DCD similarity matching does not fit human perception very well, and it will cause incorrect ranks for images with similar color distribution [7, 16]. In [6], Yang et al. presented a color quantization method for dominant color extraction, called the linear block algorithm (LBA), and it has been shown that LBA is efficient in color quantization and computation. For the purpose of effectively retrieving more similar images from the digital image databases (DBs), Lu et al. [9] uses the color distributions, the mean value and the standard deviation, to represent the global characteristics of the image, and the image bitmap is used to represent the local characteristics of the image for increasing the accuracy of the retrieval system. In [8] they used a weighted DCD for content based image retrieval for increasing the performance of MPEG-7 DCD. In our present work we will replace the DCD by a Dominant Color extraction scheme.

In other hand, similar to the dynamic quantization-based histogram, MP7DCD [13] also uses QSM with some modification to measure the dissimilarity between the query image and database images. However, QSM is not void of serious drawbacks. For instance, it does not match human color perception [6,11]. Therefore, some extensions to QSM have been proposed in Ma et al. [10], Mojsilovic et al. [12]. Po and Wong [11] propose a merging palette histogram for similarity measure (MPHSM). Yang et al. [6] propose a similarity measure that simulates human color perception. In [8] a modified DC-based similarity measure is proposed. In our work new similarity measure is proposed by the separation of RGB values.

Addition to this, in our present work we will introduce a new clustered and indexed database to increase the performance level and this will help to reduce the image retrieval time complexities. In the former works they used only clustering or indexing approach and not both approach together. As we use both approaches it increases the retrieval performance. Other great advantage we considered in our work is reduced time complexity for the retrieval.

PROPOSED SYSTEM

When we are considering Content-based Image Retrieval the foremost operation is feature extraction. The proposed method is based on Dominant Color feature of an image, so the first step is to identify the Dominant Color. Using the quantization technique we limits the dominant color from the image into a certain limit. The images are grouped into different clusters using the quantized values and indexed. Color indexing is used to index the images in the clusters and stores the image into the database. Whenever the query image arrives as the first step we will do the feature extraction and quantization. Most advantage in our work is reduced time complexity in retrieving images from the database because the clusters are identified for query image. So instead of searching the whole database, only need to search the corresponding cluster. A block diagram for the proposed system is shown in the Fig 1.

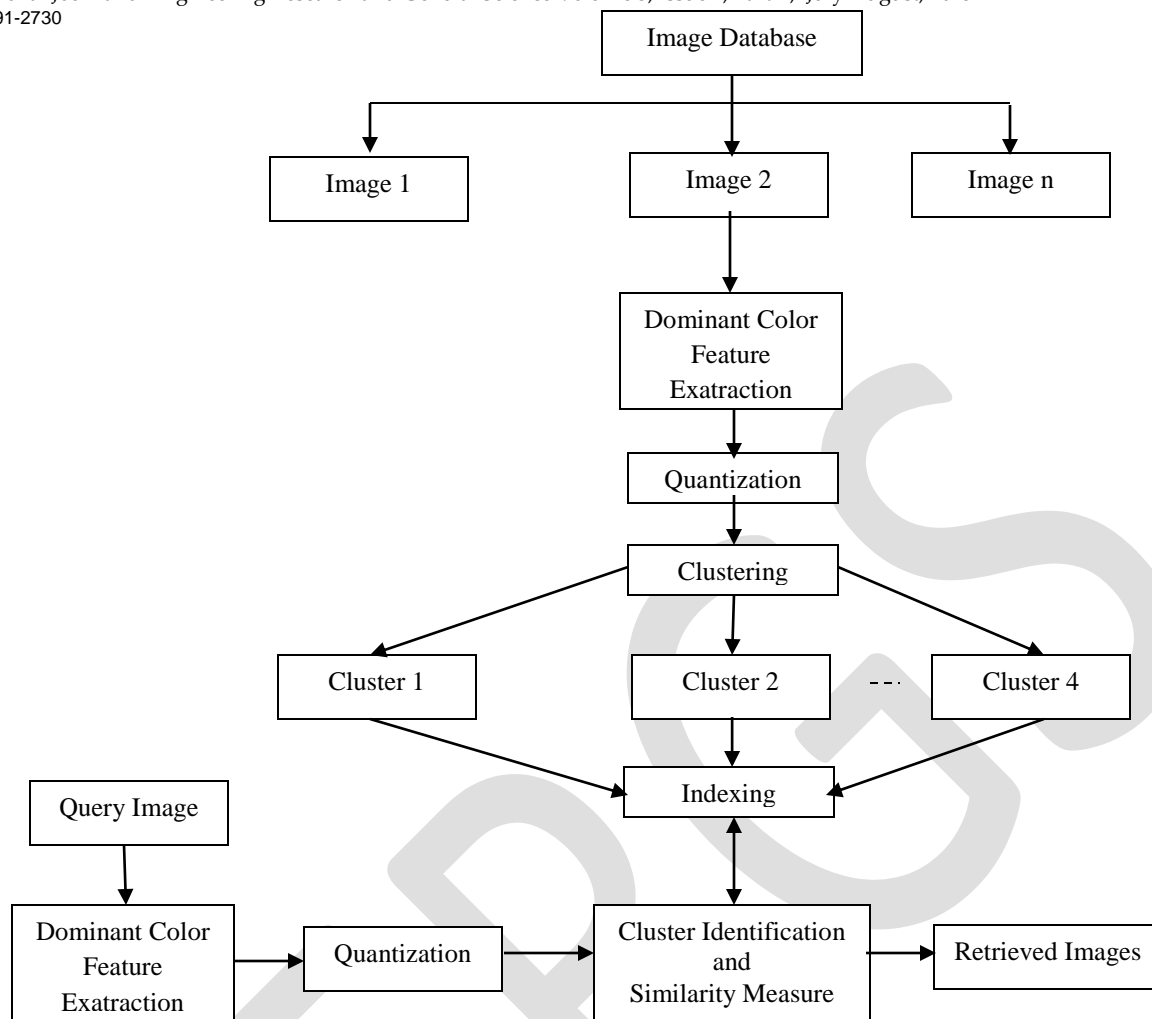


Fig 1 A Block Diagram for Proposed System

Dominant Color Extraction

When we are extracting the color feature of an image, first need is to fix a color space. We are using a RGB color space for the color feature extraction. The separation of RGB is done by using the thresholding technique and stores into R, G and B. Mean value of red, blue and green color are calculated an stored into $m_i(l)$. Among these values the dominant colors are identified by calculating the percentage of each red, green and blue component separately. The color has the highest percentage considered as the dominant color. Dominant Colors are extracted using the formulas given below:

$$DC_r(l) = \frac{m_r(l)}{m_r(l)+m_g(l)+m_b(l)} \times 100$$

$$DC_g(l) = \frac{m_g(l)}{m_r(l)+m_g(l)+m_b(l)} \times 100$$

$$DC_b(l) = \frac{m_b(l)}{m_r(l)+m_g(l)+m_b(l)} \times 100$$

In the above I is the image, $DC_r(l)$, $DC_g(l)$ and $DC_b(l)$ are dominant colors in R, G and B components and $m_r(l)$, $m_g(l)$ and $m_b(l)$ mean values of red, blue green colors respectively. We choose the color with the highest percent as the dominant color and quantized it into eight color values of a fixed limit.

Clustering and Indexing

Clustering done as just the grouping of the images based on the quantized color values. We are giving a different threshold value and cluster the images into different small cluster. Indexing is done to the each cluster as a labeling part. We use color indexing with the help of a color histogram. The images are stored in the different cluster and labeled through indexing. Whenever a query image arrives, extract the dominant color from the image and do the quantization. The cluster in which the image belongs to is identified by using the index values.

Similarity Measure

Searching large databases of images is a challenging task especially for retrieval by content. Most search engines calculate the similarity between the query image and all the images in the database and rank the images by sorting their similarity. Similarity measure is used to subtract the two images. We use the modified Euclidean distance here. Let I_1 and I_2 are two images, then the similarity measured as

$$SIM(I_1, I_2) = \sqrt{(DC_r(I_2) - DC_r(I_1))^2 + (DC_g(I_2) - DC_g(I_1))^2 + (DC_b(I_1) - DC_b(I_2))^2}$$

In the above measure DC_r , DC_g and DC_b are dominant color values in red, green and blue component.

EXPERIMENTAL RESULTS

To show the practical relevance of the proposed CBIR system, retrieval experiments are conducted. The technique is evaluated based on recall and precision. A recall rate can be defined as the number of relevant documents retrieved by a search divided by the total number of existing relevant documents (which should have been retrieved). A precision rate on the other hand is the number of relevant documents retrieved by a search divided by the total number of documents retrieved by that search.

For the experiments we selected database corel images of ground truth. It consists of 10 categories with each category comprising of 100 images. The categories include mountain, elephant, dinosaurs, African people, buses, horses, flowers, buildings, food, and beaches. The size of the images is 256×384 and other corel database with Image size 128×85 which contain butterflies, cars, etc



Fig 2 Images in the Database

The total number of relevant correctly retrieved images and the total number of retrieved images obtained from each of the query performed is recorded. For each query, the recall and precision values will be interpolated. The average precision at each recall level for each image category is then calculated. The time complexity also calculated and time taken for the retrieval is less than other systems.

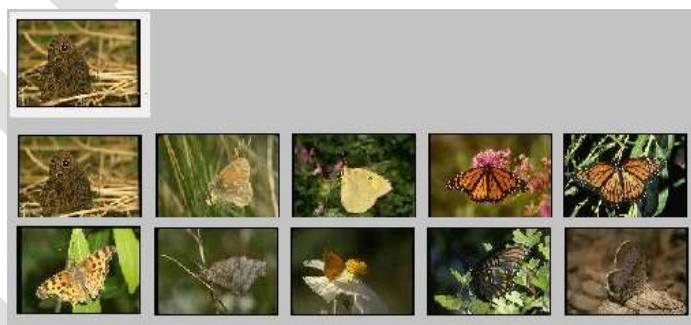


Fig 3 Retrieval Result

CONCLUSION

In this paper we introduced a Content-based Image Retrieval System based on dominant color using a clustered database. The system uses quantization technique to limits the dominant color from the image into a certain level. In our work the images were grouped into different clusters using the quantized values and indexed. Whenever the query image given to the system, it identifies the cluster to which the image belongs. So instead of searching the whole database it searches the corresponding cluster and retrieves the images. Experiments shows that the retrieval time complexity is reduced compare to other systems and the precision rate is also good.

REFERENCES:

- [1] Ritendra Datta, Dhiraj Joshi, Jia Li, James Z. Wang, "Image retrieval: ideas, influences, and trends of the new age", *ACM Computing Surveys* 40 (2) (2008) 1–60.
- [2] W. Niblack et al., "The QBIC Project: Querying Images by Content Using Color, Texture, and Shape," in *Proc. SPIE*, vol. 1908, San Jose, CA, pp. 173–187, Feb. 1993.
- [3] B. S. Manjunath, Jens-Rainer Ohm, Vinod V. Vasudevan, and Akio Yamada, "Color and Texture Descriptors", *IEEE TRANSACTIONS ON CIRCUITS AND SYSTEMS FOR VIDEO TECHNOLOGY*, VOL. 11, NO. 6, JUNE 2001.
- [4] Thomas Sikora "The MPEG-7 Visual Standard for Content Description—An Overview" *IEEE TRANSACTIONS ON CIRCUITS AND SYSTEMS FOR VIDEO TECHNOLOGY*, VOL. 11, NO. 6, JUNE 2001.
- [5] M. Sticker, and M. Orenko, "Similarity of Color Images," in *Proc. SPIE Storage and Retrieval for Image and Video Databases*, pp.381-392, Feb. 1995.
- [6] Nai-Chung Yang, Wei-Han Chang, Chung-Ming Kuo, Tsia-Hsing Li, "A fast MPEG-7 dominant color extraction with new similarity measure for image retrieval", *Journal of Visual Communication and Image Representation* 19 (2) (2008) 92–105.
- [7] Chia-Hung Wei, Yue Li, Wing-Yin Chau, Chang-Tsun Li, "Trademark image retrieval using synthetic features for describing global shape and interior structure", *Pattern Recognition* 42 (3) (2009) 386–394.
- [8] Ahmed Talib, Massudi Mahmuddin, Husniza Husni, Loay E. George, "A weighted dominant color descriptor for content-based image retrieval", *J. Vis. Commun. Image R.* 24 (2013) 345–360.
- [9] P. Howarth and S. Ruger, "Robust texture features for still-image retrieval", *IEE. Proceedings of Visual Image Signal Processing*, Vol.152, No. 6, December 2005.
- [10] W.Y. Ma, Y. Deng, B.S. Manjunath, "Tools for texture/color based search of images", *Proc. SPIE Hum. Vis. Electron. Imaging II* 3106 (1997) (1997) 496–507.
- [11] L.M. Po, K.M. Wong, "A new palette histogram similarity measure for MPEG-7 dominant color descriptor", *IEEE Int. Conf. Image Process. (ICIP'04)* 3 (2004) 1533–1536.
- [12] A. Mojsilovic, J. Kovacevic, J. Hu, R.J. Safranek, S.K. Ganapathy, "Matching and retrieval based on the vocabulary and grammar of color patterns", *IEEE Trans. Image Process.* 9 (1) (2000) 38–54.
- [13] A. Yamada, M. Pickering, S. Jeannin, L.C. Jens, "MPEG-7 Visual Part of Experimentation Model Version 9.0-Part 3 Dominant Color". *ISO/IEC JTC1/SC29/WG11/N3914*, Pisa, 2001.
- [14] Y. Deng, B.S. Manjunath, C. Kenney, M.S. Moore, H. Shin, "An efficient color representation for image retrieval", *IEEE Trans. Image Process* 10 (1) (2001)140–147.
- [15] K.-M. Wong, L.-M. Po, K.-W. Cheung, "Dominant color structure descriptor for image retrieval", *IEEE Int. Conf. Image Process.*, 2007. *ICIP 2007* 6 (2007) 365–368.
- [16] *ISO/IEC 15938-3/FDIS Information Technology*, "Multimedia Content Description Interface", Part 3 Visual Jul. 2001, *ISO/IEC/JTC1/SC29/WG11 Doc. N4358*

Analysis of Plain Circular Journal Bearing lubricated with Micropolar Fluid

Pallavi Jagdale,

[#]Mechanical Engineering Department, DYPIET, Pimpri

¹pallavi.jadhav293@gmail.com

+91 8308833952

Dr. L.G.Navale

Mechanical Engineering Department, DYPIET, Pimpri

²ignavale2006@yahoo.co.in

Received 5th Aug,2015

Abstract— The research area of hydrodynamic lubrication is widely diversified. The literature includes the analysis and various optimized technique of determination of static and dynamic characteristics of plain circular bearing. However these studies were unable to describe the simultaneous effect of both micropolar fluid parameters and eccentricity ratio on bearing characteristics. In the present study combined effect of micropolar parameters and eccentricity ratios are considered with wide range of variation on the bearing performance characteristics. For linear studies critical mass of journal is determined by Routh-Hurwitz stability criteria. Comparative analysis on critical values of journal mass required for both linear and nonlinear studies is carried out. Also the stability of these bearing are analyzed at various operating conditions.

Keywords— Journal Bearing, Hydrodynamic Lubrication, static characteristics, Dynamic characteristics, eccentricity, eccentricity ratio, comparative analysis.

INTRODUCTION

As per the history a theory of hydrodynamics in lubrication was introduced by Reynolds in 1886. Many numbers of researcher performed analytical and practical studies over hydrodynamic lubrication and put very important concepts and theories. Analysis of literature showed that the research area of hydrodynamic lubrication is widely diversified. The literature includes the analysis and various optimized technique of determination of static and dynamic characteristics of plain circular bearing.

The bearings have been in use for centuries but the recent developments in science and technology demands critical designs of bearings with high precision and optimized performance for the most adverse working conditions. The rapid developments in the fields of rocketry and missile technology, cryogenics, aeronautics and space engineering, nuclear engineering, electronics, computer sciences and technologies, bio-medical engineering and a lot more fields in science and technology make the aspects of designing bearings more and more challenging and innovative. Moreover, the mode, time and place of operations demand exploration of new materials, lubricants and even lubrication theories and technologies.

I. MATHEMATICAL ANALYSIS

BASIC ASSUMPTIONS

The basic assumptions in micropolar lubrication to a journal bearing include the usual lubrication assumptions in deriving Reynold's equation and the assumptions to generalize the micropolar effects.

(i) The Flow is Incompressible and steady, i.e. $\rho = \text{constant}$ and $\partial\rho/\partial t = 0$.

(ii) The flow is laminar i.e. free of vortices and turbulence.

(iii) Body forces and body couples are negligible, i.e. $FB=0$ and $CB=0$.

(iv) The variation of pressure across the film $\partial p/\partial y$ is negligibly small.

(v) The film is very thin in comparison to the length and the span of the bearing. Thus, the curvature effect of the fluid film may be ignored and the rotational velocities may be replaced by the translator velocities.

(vi) No slip occurs at the bearing surfaces.

(vii) Bearing surface are smooth, non-porous and rigid i.e. no effects of surface roughness or porosity and the surface can withstand infinite pressure and stress theoretically without having any deformation.

(viii) No fluid flow exists across the fluid film i.e. the lubrication characteristics are independent of y-direction.

(ix) The micropolar properties are also independent of y-direction. The velocity vector, the microrotational velocity vector and the fluid film pressure are given as:

$$V = [V_x(x,y,z), V_y(x,y,z), V_z(x,y,z)]$$

$$v = [v_1(x,y,z), v_2(x,y,z), v_3(x,y,z)]$$

$$p = p(x,y,z)$$

Principle of Conservation of Mass

$$\partial \rho / \partial t + \nabla (\rho V) = 0 \quad (1)$$

Principle of Conservation of Linear Momentum

$$(\lambda + 2\mu) \nabla (\nabla \cdot V) - [(2\mu + \mathcal{X})/2] \nabla * (\nabla * V) + \mathcal{X} \nabla * v - \nabla \cdot \pi + FB = \rho * DV/Dt \quad (2)$$

$$\text{Principle of Conservation of Angular Momentum } (\alpha + \beta + \gamma) \nabla (\nabla \cdot v) - \gamma \nabla * (\nabla * v) + \mathcal{X} \nabla * V - 2\mathcal{X} v + CB = \rho j Dv/Dt \quad (3)$$

Where, ρ is the mass density, V is the velocity vector, v is the micro-rotational velocity vector. π is the thermodynamic pressure and is to be replaced by the hydrodynamic film pressure, p , since, $\pi = -[\partial E / \partial \rho^{-1}] = p$. Where E is the internal energy and p is to be determined by the boundary conditions. λ and μ are the familiar viscosity coefficients of the classical fluid mechanics, while α, β and γ are the new viscosity coefficients derived as the combinational effects of the gyroviscosities for the micropolar fluid as defined by ERINGEN. \mathcal{X} is also a new viscosity coefficient for micropolar fluid, termed as spin viscosity, which establishes the link between velocity vector and the microrotational velocity vector. FB is the body force per unit mass, CB is the body couple per unit mass and j is the microinertia constant. D/Dt represents the material derivative. The constitutive equations of micropolar are

$$tk_1 = (-\pi + \lambda V_{r,1}) + (\mu - 1/2 * \mathcal{X}) (V_{k,1} + V_{1,k}) + \mathcal{X} (V_{1,k} + \eta k_1 r * v_r) \quad (4)$$

$$mk_1 = \alpha v_{r,1} + \beta v_{k,1} + \gamma v_{1,k} \quad (5)$$

Where, tk_1 and mk_1 are the stress tensor and the couple stress tensor respectively. $\eta k_1 r$ is an permutation tensor. δk_1 is Kronekar delta. The index following a prime represents the partial derivative to spatial variable $\mathcal{X}k$.

Note that for $\alpha = \beta = \gamma = \mathcal{X} = 0$ and for negligible body couple per unit mass equation (3) yields $v = 0$ and so, equation (2) reduces to the classical Navier-Stokes equation. For $\mathcal{X} = 0$ the velocity vector and the microrotational velocity vector are uncoupled and the global motion of the fluid becomes free of the microrotation and their effects.

The theoretical prediction of hydrodynamic pressures in the bearing is obtained by the solution of modified Reynolds equation satisfying the appropriate boundary conditions. The steady state and dynamic pressure profile is obtained by finite difference technique.

II. SOLUTION PROCEDURE

Journal bearing systems are analyzed by linear and nonlinear study with the help of MATLAB software incorporation of PDE toolbox. The analysis is carried out by linear and nonlinear study of journal bearing system. These studies are carried out for circular bearing geometries.

Operating conditions of journal bearing system can be varied by combination of characteristic length of the micropolar lubricant (\bar{l}_m), Coupling number (N), and eccentricity ratio. Hence with the help of these programs one can obtain results over wide range. Hence it becomes necessary to execute a program at each operating condition separately.

Solution procedure for linear analysis of a plain circular journal bearing with micropolar fluid

1. Acquire input parameters such as attitude angle (ϕ) = 60°, the initial guess for fluid film extent are specified by considering circular coordinate axis X originating from line of centers and Y axis along bearing width. Hence For present finite width bearing $X_{max}=180^\circ$, $X_{min}=0^\circ$, $Y_{max}= 2$ (since $\beta = 2$) and $Y_{min}= 0$. Characteristic length of the micropolar lubricant. (\bar{l}_m), Coupling number (N) and eccentricity ratio ($\bar{\epsilon}$) specifies the various operating conditions and it acts as variable.
2. Journal centres are located as (\bar{X}_j, \bar{Y}_j) using Cartesian co-ordinate system originated at geometric centre of bearing.
3. In order to get the solution of PDE finite difference method is employed in practice hence fluid film domain is discretized into optimum mesh size.
4. Fluid film thickness is determined at centroid of each elemental area by using thickness equation.
5. Modified Reynolds equation is solved by using PDE toolbox.
6. The pressure distribution over fluid film thickness is calculated.
7. On the basis of pressure distribution pressure gradient $\left(\frac{dp}{dx}\right)$ is determined along X axis between a mid-node on trailing edge and nearest node. If the pressure gradient $\left(\frac{dp}{dx}\right)$ becomes 'negative' i.e., termination of positive fluid pressure zone and negative pressure start buildings onwards.
8. Bearing load components along horizontal and vertical directions are calculated.
9. In the present case bearing is subjected pure radial this condition is satisfied when bearing load ratio (f_x/f_y) tends to zero. Here bearing load ratio less than 0.001 is considered as bearing subjected to pure radial load. This load ratio can be reduced to desired value by adjusting the attitude angle in iterations. In each iteration attitude angle is modified by 10° .
10. Once the attitude angle and trailing edge determined the equilibrium position of journal is located.
11. Bearing load calculated in step (8) are considered as static equilibrium forces.
12. For new displaced position of journal again instantaneous bearing load components are calculated followed by steps (4) to (6).
13. On the basis of Routh- Hurwitz stability criteria critical mass is calculated using equation.

Other dynamic characteristics such as whirl frequency and threshold speed ratios are calculated

IV ANALYSIS RESULTS

1 STATIC CHARACTERISTIC

1.1. LOAD CARRYING CAPACITY

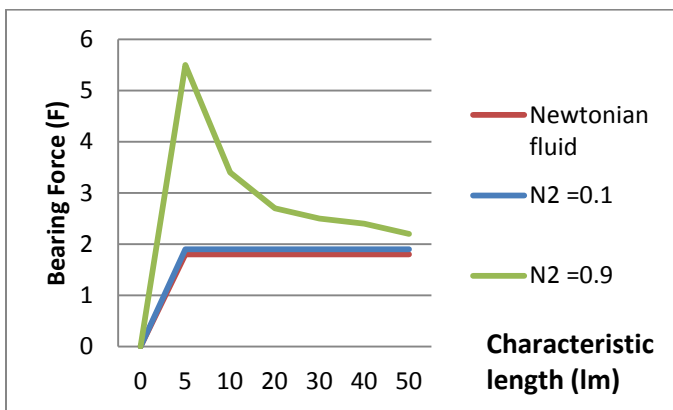


Fig.1 Variation of Bearing force as a function of non-dimensional Characteristic length (lm) at $\epsilon=0.3$

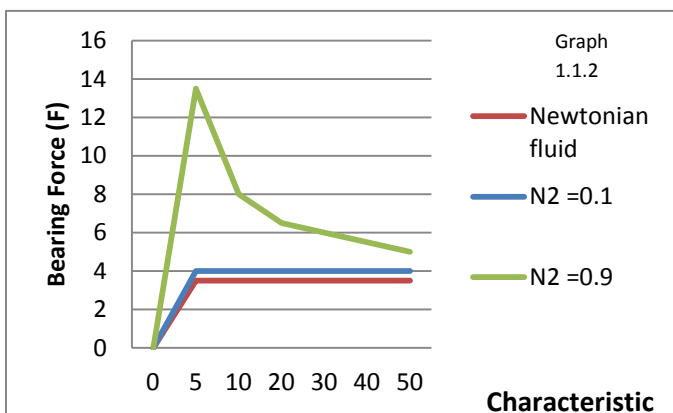


Fig.2 Variation of Bearing force as a function of non-dimensional Characteristic length (lm) at $\epsilon=0.5$

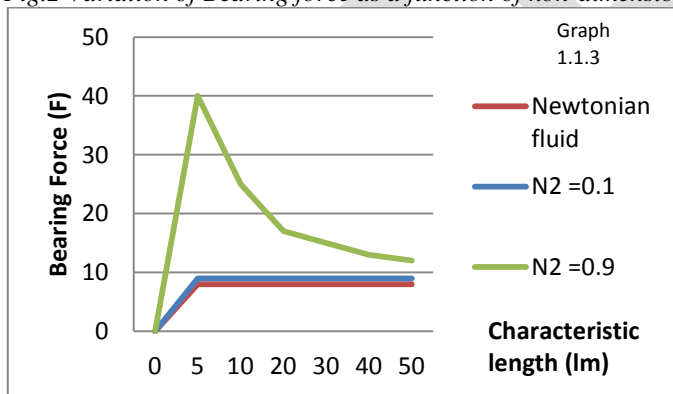


Fig.3 Variation of Bearing force as a function of non-dimensional Characteristic length (lm) at $\epsilon=0.7$

The load carrying capacity reduces as coupling number reduces and approaches to Newtonian fluid for $N2 \rightarrow 0$. It shows that for high coupling number and low characteristic length a plain circular journal bearing lubricated with micropolar fluid provides maximum load carrying capacity as compared to the Newtonian fluid.

It can be seen that for a particular value of lm and $N2$, the load carrying capacity increases for micropolar fluid as well as for Newtonian fluid with increase in eccentricity ratio. It is also been observed that the load carrying capacity is higher i.e. 4-5 times as the eccentricity ratio changes from 0.3 to 0.7 for a distinct value of lm and $N2$. The figures depict that the load capacity at any eccentricity ratio is much higher at lower value of lm and approaches to Newtonian fluid as $lm \rightarrow \infty$ or $N2 \rightarrow 0$.

1.2 ATTITUDE ANGLE (Φ)

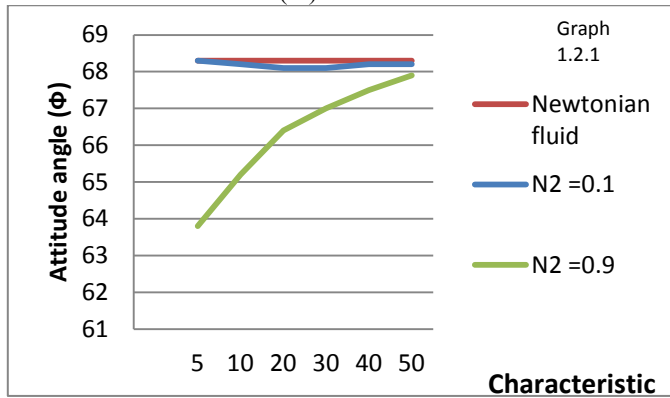


Fig.4 Variation of Attitude angle (ϕ) as a function of non-dimensional Characteristic length (l_m) at $\epsilon=0.3$

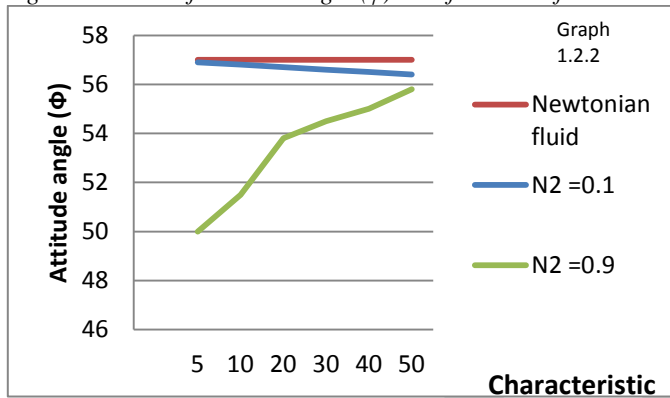


Fig.5 Variation of Attitude angle (ϕ) as a function of non-dimensional Characteristic length (l_m) at $\epsilon=0.5$

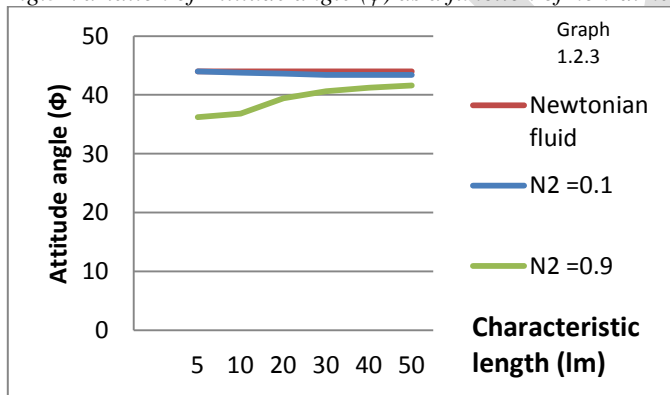


Fig.6 Variation of Attitude angle (ϕ) as a function of non-dimensional Characteristic length (l_m) at $\epsilon=0.7$

The attitude angle reduces as coupling number increases and approaches to Newtonian fluid for $N_2 \rightarrow 0$. It shows that for high coupling number and low characteristic length a plain circular journal bearing lubricated with micropolar fluid provide low attitude angle as compared to the Newtonian fluid.

It can be seen that for a particular value of l_m and N_2 , the attitude angle decreases for micropolar fluid as well as for Newtonian fluid with increase in eccentricity.

2. DYNAMIC CHARACTERISTICS

2.1 CRITICAL MASS PARAMETER (M_c)

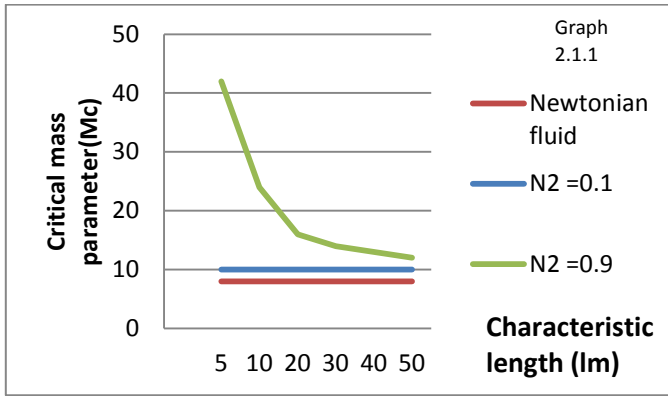


Fig. 7 Variation of Critical Mass (M_c) as a function of non-dimensional Characteristic length (l_m) at $\epsilon=0.3$

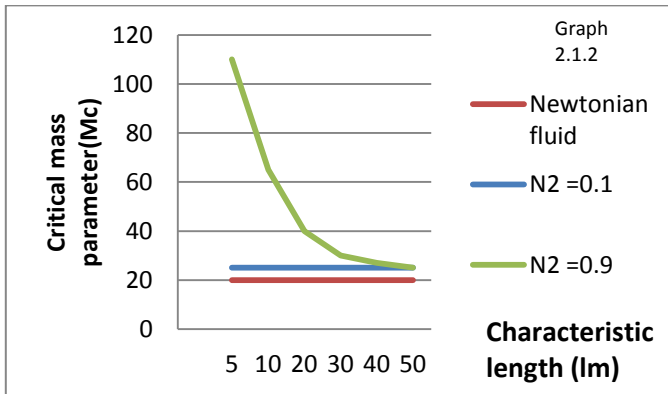


Fig. 8 Variation of Critical Mass (M_c) as a function of non-dimensional Characteristic length (l_m) at $\epsilon=0.5$

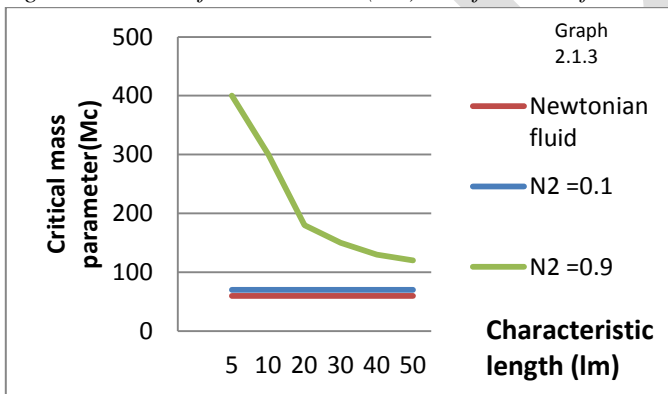


Fig. 9 Variation of Critical Mass (M_c) as a function of non-dimensional Characteristic length (l_m) at $\epsilon=0.7$

The critical mass parameter increases as N is increased. It also has been found that when $N_2 \rightarrow 0$ for any value of l_m , micropolar fluid approaches to Newtonian fluid. It can be observed from figure that critical mass decreases as increasing l_m and approaches to Newtonian fluid as l_m grows indefinitely.

2.2 WHIRL FREQUENCY RATIO

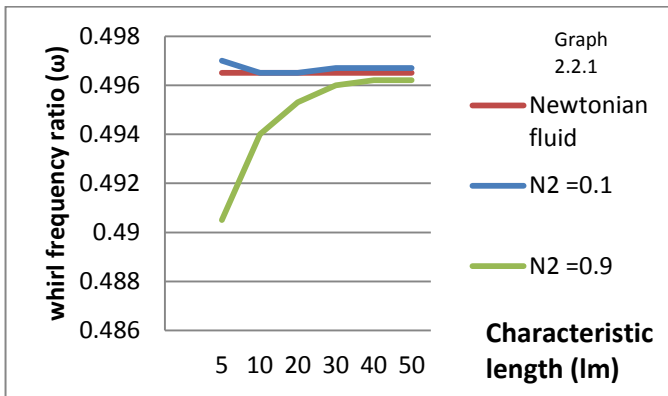


Fig.10 Variation of Whirl frequency ratio (ω) as a function of non-dimensional Characteristic length (lm) at $\epsilon=0.3$

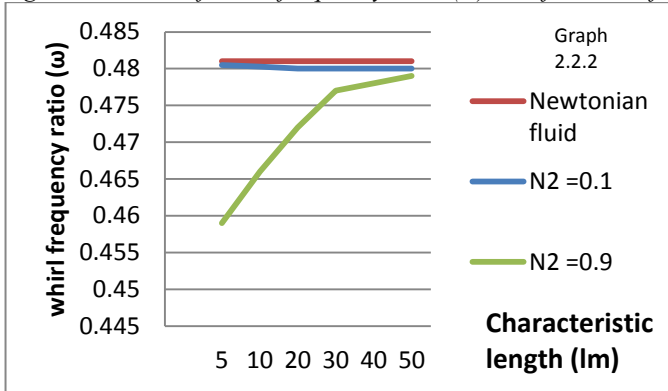


Fig. 11 Variation of Whirl frequency ratio (ω) as a function of non-dimensional Characteristic length (lm) at $\epsilon=0.5$

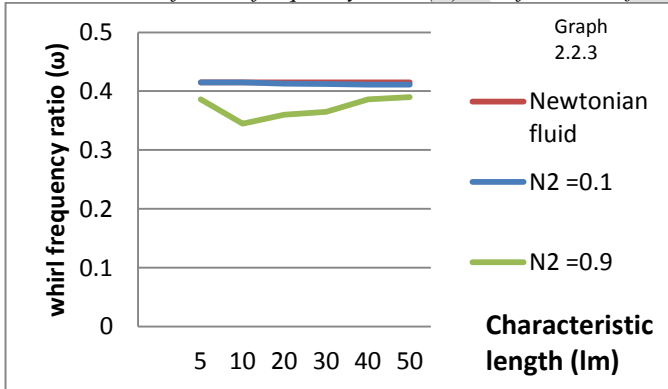


Fig. 12 Variation of Whirl frequency ratio (ω) as a function of non-dimensional Characteristic length (lm) at $\epsilon=0.7$

It observed that for a particular value of coupling number, whirl frequency ratio firstly decreases than increases with increase in lm . It clearly shows that there is a decrement in the whirl frequency ratio at small values of lm .

It can be seen that for a particular value of lm and N_2 , whirl frequency ratio decreases for micropolar fluid as well as for Newtonian fluid with increase in eccentricity ratio.

2.3 THRESHOLD SPEED

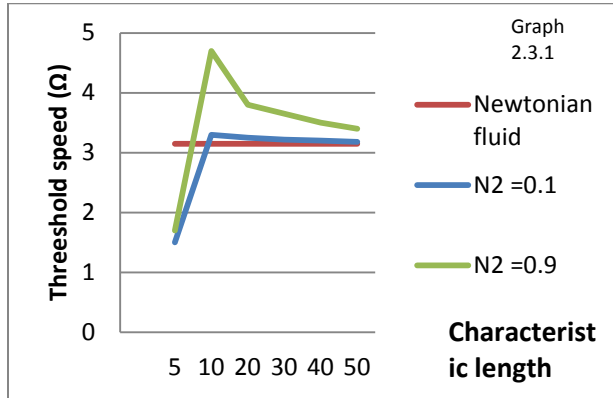


Fig. 13 Variation of Threshold Speed (Ω) as a function of non-dimensional Characteristic length (l_m) at $\epsilon=0.3$

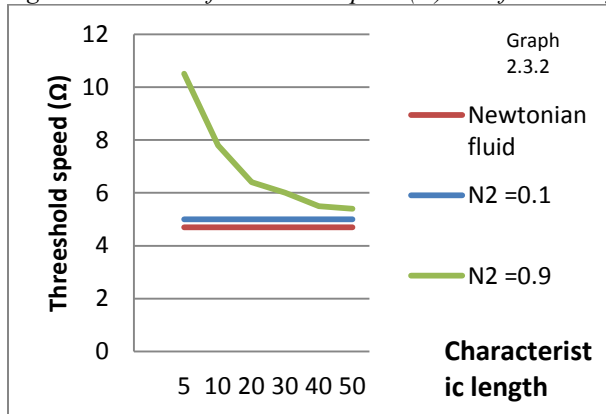


Fig. 14 Variation of Threshold Speed (Ω) as a function of non-dimensional Characteristic length (l_m) at $\epsilon=0.5$

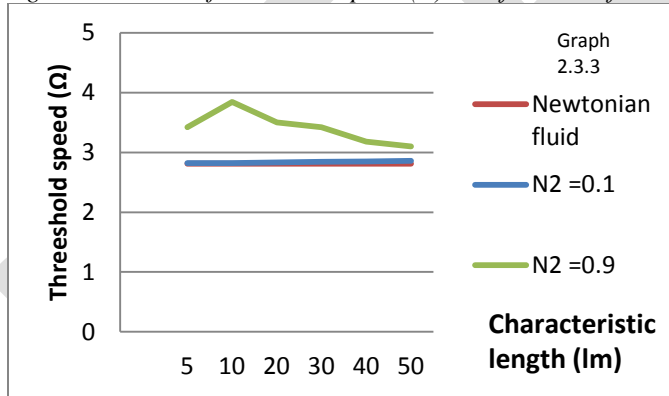


Fig. 15 Variation of Threshold Speed (Ω) as a function of non-dimensional Characteristic length (l_m) at $\epsilon=0.7$

we can see that as the coupling number decreases threshold speed decreases. It observed that for a particular value of coupling number, threshold speed increases with increase in l_m . It clearly shows that there is an augmentation in the threshold speed at small values of l_m . Curves illustrate that when l_m increases or N_2 decreases, the value of threshold speed approaches to that of the Newtonian value.

2.4 STIFFNESS COEFFICIENT

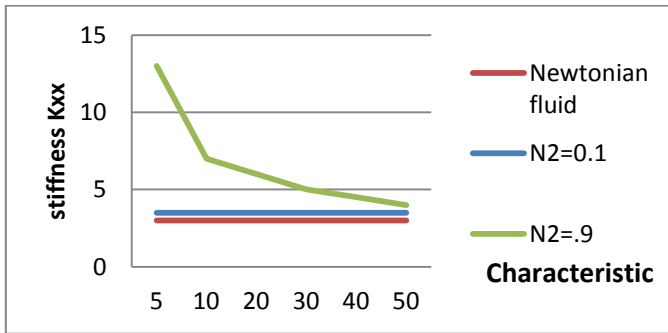


Fig.16 Variation of Stiffness (K_{xx}) as a function of non-dimensional Characteristic length (l_m) at $\epsilon = 0.3$

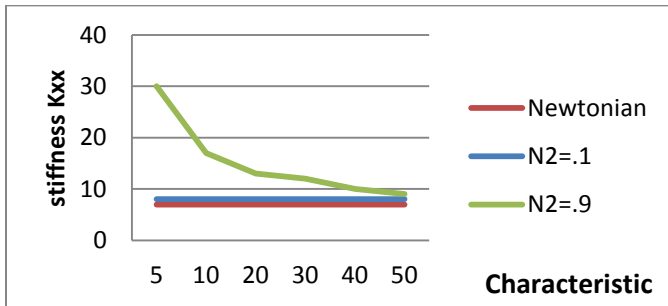


Fig.17 Variation of Stiffness (K_{xx}) as a function of non-dimensional Characteristic length (l_m) at $\epsilon = 0.5$

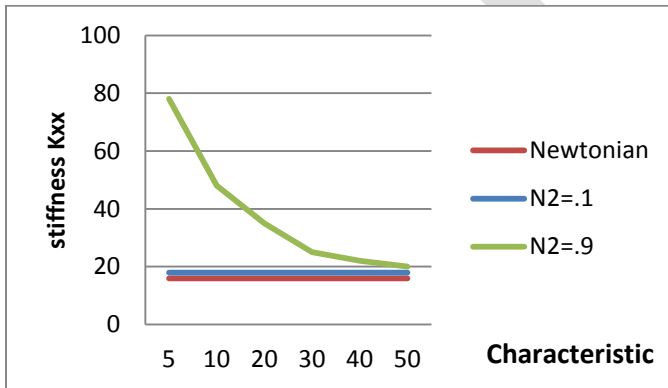


Fig.18 Variation of Stiffness (K_{xx}) as a function of non-dimensional Characteristic length (l_m) at $\epsilon = 0.7$

Figs. shows the variation of the non-dimensional components of stiffness coefficients as function of l_m for any coupling number, keeping eccentricity ratio and L/R constant at 0.3 and 2 respectively. It can be observed from the figures that at any value of l_m , the direct stiffness coefficient K_{xx} increases with increase in coupling number. For any value of coupling number, K_{xx} decreases with l_m and approaches to Newtonian fluid as l_m becomes infinitely large.

ACKNOWLEDGMENT

I am very thankful to my guide Dr. L.G.Navale, and also Head of Department Dr. Dhande, for their valuable guidance throughout my project work.

CONCLUSION

Important conclusion can be made about the use of micropolar fluid in plain circular and elliptical bearing are as follows:

1. It has been observe that load carrying capacity of both the journal bearing with micropolar lubricant at a particular eccentricity ratio increases when compared with that of bearing with Newtonian fluid.
2. The micropolar fluid approaches to Newtonian fluid as characteristic length of the micropolar fluid grows indefinitely or coupling number tends to zero.
3. The critical mass and threshold speed for bearings under micropolar fluid is increases for high coupling number and decreases when characteristic length decreases. Hence, stability of a bearing increases at high coupling number and low characteristic length.
4. The analysis predicts a lower value of critical mass for Newtonian than micropolar fluid.

REFERENCES:

- [1] Matthew Cha, Evgeny Kuzetsov, Sergei Glavatshih, "A comparative linear and nonlinear dynamic analysis of compliant cylindrical journal bearings", Mechanism and Machine theory, Feb 2013.
- [2] Qiu Zu-gan, Lu Zhang-ji, "Lubrication Theory for Micropolar fluids and its application to a Journal bearing with finite length" Applied Mathematics and Mechanics, vol 8,no.7, July 1987.
- [3] D.Sfyris, A Chasalevris, "An exact analytical solution of the Reynolds equation for the finite journal bearing lubrication", Tribology International, May 2012.
- [4] Tarun Kumar Bera, "Analysis of Steady-State Characteristics of Rough Hydrodynamic Journal Bearing Lubricated with Micro-Polar Fluids", Birbhum Institute of engineering & Technology, Suri, Birbhum, India.
- [5] Steve Pickering, "Tribology of Journal Bearing Subjected to Boundary and Mixed Lubrication", Mechanics of Contact and Lubrication, Northeastern University, 2011
- [6] R. Sinhasan, K.C. Goyal, "Transient response of a circular journal bearing lubricated with non-newtonian lubricants, Wear, 156, 1992
- [7] Eringen, "Theory of Micropolar Fluids", School of Aeronautics, Astronautics and Engineering Sciences Purdue University Lafayette, Indiana, July 1965.
- [8] B.Chetti, "Micropolar Fluids Effects on the Dynamic Characteristics of Four-lobe Journal Bearing", World Academy of Science, Engineering and Technology, Vol;5 2011.
- [9] N.P.Mehta, S.S. Rattan, Rajiv Verma, "Stability Analysis of Two Lobe Hydrodynamic Journal Bearing with Couple stress Lubricant", ARPN Journal of Engineering and Applied Science, Jan 2010.
- [10] Malcolm E. Leader, "Understanding Journal Bearings", Applied Machinery Dynamics Co.
- [11] Jaw-Ren Lin, " Linear stability analysis of rotor-bearing system: couple stress fluid model", Computers and structures, Aug 2000

Extraction of Retinal Blood Vessels from Color Fundus

Aagi A S, Radhakrishnan B
P.G Scholar, Dept of CSE, BMCE, Kollam, Kerala, India
aagi.a.s.111@gmail.com

Abstract— Retinal image analysis is an active field of research for identifying different types of diseases that affect the Retina. The extraction and analysis of retinal vasculature is an essential part of several practical applications such as detection of hypertension, Diabetic Retinopathy, stroke and cardiovascular diseases that affects eye. The proposed method consists of four stages: In the first stage we enhance the original retinal image to increase their contrast and eliminate the non uniform illumination in retinal images. The second stage involves a 2D Gabor filter which is capable of tuning to specific frequencies, thus allowing noise filtering and vessel enhancement in a single step. The next stage involves segmentation of blood vessels by an edge detection approach that separates the vascular network from the background and the final stage includes some morphological operations for obtaining better results. This proposed method may be used for determination of arteriolar to venular diameter ratio in retinal images. This process is basis for the AVR calculation i.e. for the calculation of average diameter of arteries to veins.

Keywords— Retina, Retinal vasculature, Blood vessels, Diabetic Retinopathy, Non uniform illumination, 2D Gabor filter, AVR

1. INTRODUCTION

Retinal images play vital role in several applications such as disease diagnosis and human recognition. They also play a major role in early detection of diabetics by comparing the states of the retinal blood vessels. The retinal abnormalities are commonly due to various retinopathies as well as cardiovascular diseases. Very first stages of the disease may be clinically asymptomatic and hence the early diagnosis is required to refer the patients with the high probability of retinopathy for the further diagnosis, and screen out the patients with no pathologies detected. The retinopathies such as diabetic retinopathy (DR) are identified based on the measurement of morphologic changes in retinal blood vessels.

Diabetic Retinopathy is the complication of diabetics and is a major cause of blindness. Early diagnosis and timely treatment prevent visual loss and blindness in patients with diabetes. The structure of blood vessels in the retina is affected by diabetes, hypertension, arteriosclerosis and retinopathy of prematurity through modifications in shape, width and tortuosity. The quantification of vessel features such as length, width and branching pattern, among others, can provide new insights to diagnose and stage pathologies, which affect the morphological and functional characteristics of blood vessels. However, when the vascular network is complex, or the number of images is large, manual measurements can become tiresome or even impossible. A feasible solution is the use of automated analysis, which is nowadays commonly accepted by the medical community.

In addition, the curved shape of retina and inappropriate illumination conditions during image acquisition process might lead to non uniform illumination through retinal images. Also biological characteristics, in this case changes in color of retina from person to person, raise another problem [2,3]. This paper presents an automatic approach for extraction of retinal blood vessels from the retinal vasculature. Here first we improved the contrast and quality of retinal images by using histogram equalization and Retinex approach. Contrast Limited Adaptive Histogram Equalization (CLAHE) is applied to the images for improving their contrast. Here we propose a solution to eliminate the non uniform illumination by Multi-scale Retinex with Color Restoration (MSRCR) image enhancement technique. The blood vessels are extracted by applying 2D Gabor filter. To determine the AVR extraction of edges in blood vessels are necessary. By using an edge detection approach we separated the blood vessels from the background. The retinal images are available in public database called DRIVE. Some sample images from DRIVE database can be seen in Fig.1.



Fig.1 Sample images in DRIVE database

This paper is organized as follows: In section 2 includes the related works. The proposed method is explained which includes four stages in section 3. In section 4 experimental results are discussed. Ultimately section 5 concludes the proposed work.

2. RELATED WORKS

In the past, various techniques are used to extract the blood vessels from retinal images. Kumari and Suriyanarayanan (2010) extracted the blood vessels using Wiener filter and morphological operation opening and closing. The edge of the blood vessels are detected by applying Laplacian and Gaussian operators and the thinning of blood vessel is done using morphological operator and smoothed for better clarity in the extracted blood vessel [4]. Badsha *et al.* (2013) present automatic method to extract the retinal blood vessel. The proposed method comprises several basic image processing techniques, namely edge enhancement by standard template, noise removal, thresholding, morphological operation and object classification. The proposed method has been tested on a set of retinal images [5]. Kaba *et al.* (2013) introduced an automated method to segment blood vessels in fundus retinal images. The method could be used to support a non-intrusive diagnosis in modern ophthalmology for early detection of retinal diseases, treatment evaluation or clinical study. This method combines the bias correction to correct the intensity in homogeneity of the retinal image and a matched filter to enhance the appearance of the blood vessels. The blood vessels are then extracted from the matched filter response image using the Expectation Maximization algorithm [6]. H.S. Bhadauria (2013) proposed Kirsch's templates for the extraction of blood vessel from retinal images. In this method Kirsch's edge operators are used to detect the edges by using eight filters. Kirsch templates of size 3x3 are used for the extraction of blood vessels from retinal image. More than 10 images have been tested by using this method [7].

3. PROPOSED METHOD

The extraction of retinal blood vessels such as arteries and veins is a difficult task. The detection of blood vessels is a major problem in the automatic processing of retinal images. Here we propose an efficient automated method for the extraction of blood vessels from the retinal images. Fig.2 shows the basic block diagram of the proposed system. The proposed method consists of four steps: Image enhancement, 2D Gabor convolution, edge detection and morphological processing.

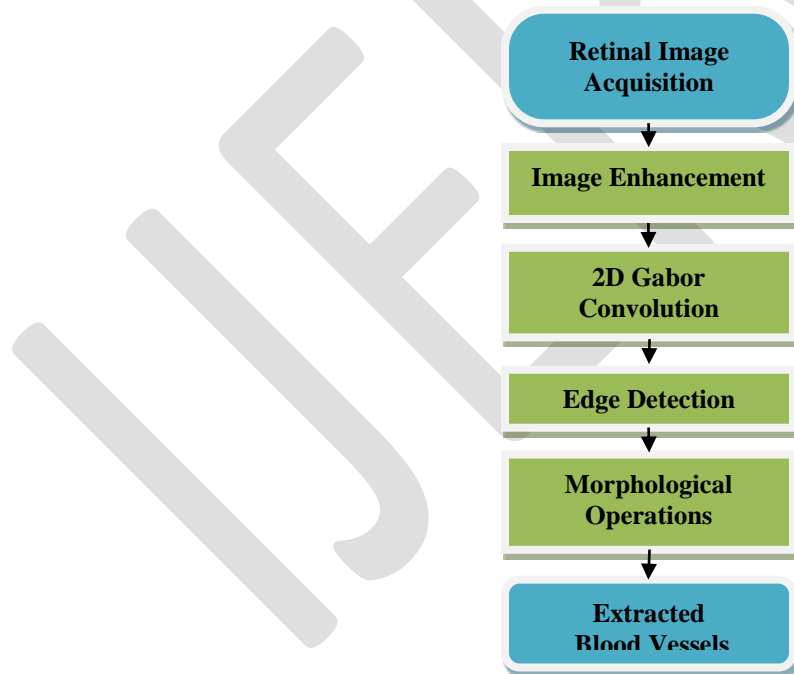


Fig.2 Block diagram of proposed system

A. Image Enhancement

It includes contrast adjustment and elimination of non-uniform illumination in retinal images. Contrast adjustment is achieved by using Contrast Limited Adaptive Histogram Equalization. Rather than entire image it operates on small regions of an image called tiles to enhance the contrast by transforming the intensity values of the image. Then histogram of the output region approximately matches the specified histogram.

Uneven illumination caused by curved shape of retina is rectified using Retinex. The idea behind Retinex theory is to approximate the illumination in image using Gaussian function and subtracting the estimation from the original image. Multi-scale retinex with color restoration (MSRCR) is used to correct the problem [8,9].

$$MSRCR_i = G[C_i\{\log I_i - \log[I_i * F_n]\} + b] \quad (1)$$

where G and b are the final gain and offset values and

$$C_i = \beta\{\log[\alpha I_i] - \log[\sum_{i=1}^s I_i]\} \quad (2)$$

where β is a gain constant and α controls the strength of the non-linearity.

The MSRCR approach is applied to each channel of RGB color space and here we use the red channel which is more obvious to differentiate arteries and veins.

B. 2D Gabor Convolution

Gabor filter is a linear filter whose impulse response is defined by a harmonic function multiplied by a Gaussian function. It is optimally localized as per the uncertainty principle in both the spatial and frequency domain. This implies Gabor filters can be highly selective in both position and frequency, thus resulting in sharper texture boundary detection. Gabor filter related segmentation method is based on filter bank model in which several filters are applied simultaneously to an input image. The filters focus on particular range of frequencies. If an input image contains two different texture areas, the local frequency differences between the areas will detect the textures in one or more filter output sub-images.

Each Gabor filter is specified by a Gabor Elementary function (GEF). GEFs can perform joint space decomposition. Gabor filters are extensively used for texture segmentation because of their good spatial and spatial-frequency localization.

Convolution filtering is commonly used for edge detection applications. Gabor function provides the optimal resolution in both time and frequency domain. It is an optimal basis for extracting the local features.

A 2-D Gabor filter is modulated by a 2D Gaussian function, which is defined as:

$$G_{\sigma, F, \theta}(x, y) = g_{\sigma}(x, y) \exp[2\pi jF(x \cos \theta + y \sin \theta)] \quad (3)$$

where

$$g_{\sigma}(x, y) = \frac{1}{2\pi\sigma^2} \exp\left[-\frac{x^2 + y^2}{2\sigma^2}\right] \quad (4)$$

where j denotes the complex number i , F is the frequency of the span-limited sinusoidal grating, θ is the orientation and σ is the scale parameter. The Gabor filter $G_{\sigma, F, \theta}$ gives a complex valued function, decomposed by $G_{\sigma, F, \theta} = G_R + jG_I$ into real and imaginary parts [10,11].

The 2D Gabor output produces a complex image of both real and imaginary parts. The Gabor transformation result is normalized to generate the output which clearly distinguishes the background and blood vessels.

C. Edge Detection

The enhanced blood vessels from background are segmented by an edge detection method. The purpose of edge detection is to significantly reduce the amount of data in an image, while preserving the structural properties. Among the edge detection methods canny edge detection algorithm is one of the most strictly defined methods that provides good and reliable detection.

Canny edge detection method uses a multi-stage algorithm to determine the blood vessel edges. It helps for the determination of Artery to Vein Ratio. The process includes 5 steps:

1. Apply Gaussian filter to smooth the image in order to remove noise.
2. Find the gradients of the image.
3. Apply non-maximum suppression to get rid of spurious response to edge detection.
4. Apply double threshold to determine potential edges.
5. Track edge by suppressing all the weak edges and not connected to strong edges.

The edges of blood vessels are segmented by using canny algorithm. The main purpose of this step is to extract the blood vessel edges from background so that the foreground blood vessels can be easily analyzed.

D. Morphological Operations

After applying canny edge detection there exist few edges which are not belonging to vessel tree because of uneven background illumination. Here we used morphological opening and dilation for reconstruction. Morphological opening is used to remove small objects from an image while preserving the shape and size of larger objects in the image. The definition of a morphological opening of an image is erosion followed by dilation, using the same structuring element for both operations.

Dilation adds pixels to the boundaries of objects in an image, while erosion removes pixels on object boundaries. The number of pixels added or removed from the objects in an image depends on the size and shape of the structuring element used to process the image. This produce a binary image in which the value of each pixel is either 1(blood vessel edge) or 0(background). Finally the extracted blood vessels having original features are obtained by multiplying it with the initial gray scale image.

4. EXPERIMENTAL RESULTS

The automatic methods described were tested on the images in DRIVE data set. The proposed method was done using MATLAB. Fig.3 shows the results of our proposed system.

In order to segment the blood vessels in the retinal image, first convolve the image with different Gabor functions. The following parameters give satisfactory results: $\theta = \{0, \frac{\pi}{6}, \frac{\pi}{4}, \frac{\pi}{3}, \frac{\pi}{2}\}$ $F = \{60,90,120\}$ and $\sigma = \{.0075, .005, .0025\}$. For canny edge detection method the effect on the test image with thresholds of 120 and 185 give better results. The edge responses are useful for measuring the AVR ratio. Also our method has an advantage over other blood vessel extraction methods and achieves better results. It corrects the non uniform illumination in retinal images to improve the accurate detection of blood vessels. Comparison of our method with other approaches gives satisfactory results. In this work we successfully extract the retinal blood vessels and obtain better results.

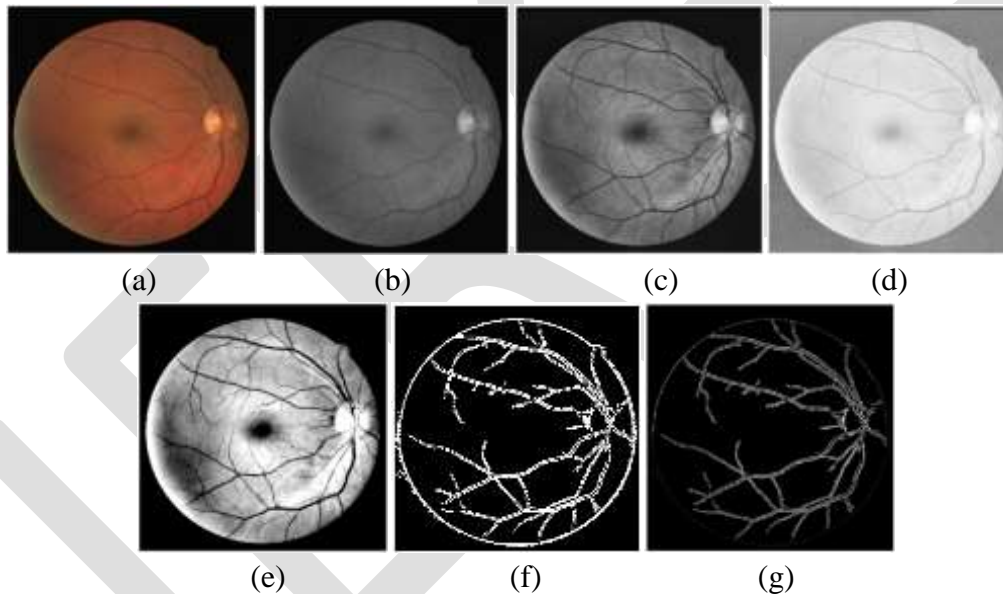


Fig.3 The results of proposed system (a) Original image (b) Gray image (c) Image after applying CLAHE (d) MSRCR in Red channel (e) 2D Gabor filter response (f) Canny response (g) Extracted blood vessels

5. CONCLUSION

This paper presents an efficient automated approach for extracting the blood vessels from retinal images. The combination of image enhancement techniques such as CLAHE and MSRCR in red channel gives better output. Segmentation of blood vessels using Gabor filter and canny edge detection is the fundamental concept. The proposed method extracts the blood vessels from the background efficiently by 2D Gabor filter and canny edge detection method. For AVR calculation blood vessel extraction is necessary. Future work will include classify arteries and veins from extracted blood vessels for calculating AVR ratio to identify different diseases that affect our eye.

REFERENCES:

- [1] Sofka M and C.V. Stewart, "Retinal Vessel Centerline Extraction Using Multiscale Matched Filters, Confidence and Edge Measures". Medical Imaging, IEEE Transactions on, 2006. 25(12): p. 1531-1546.

- [2] Youssif A.A.A, Ghalwash A.Z and Hongyu A, "A comparative evaluation of preprocessing methods for automated detection of retinal anatomy". In: Proceedings of the fifth international conference on informatics & systems (INFOS'07). 2007.
- [3] Foracchia M, Grisan E, Ruggery A, "Luminosity and contrast normalization in retinal images". *Med Image Anal*2005;9 (June (3)):179–90.
- [4] Kumari, V.V. and N. Suriyanarayanan, 2010, "Blood vessel extraction using wiener filter and morphological operation". *Int. J. Comput. Sci. Emerg. Technol.*, 1: 7-11.
- [5] Badsha, S., A.W. Reza, K.G. Tan and K. Dimiyati, 2013, "A new blood vessel extraction technique using edge enhancement and object classification". *J. Digital Imag.* DOI: 10.1007/s10278-013-9585-8
- [6] Kaba D, A.G. Salazar-Gonzalez, Y. Li, X. Liu and A. Serag, 2013, "Segmentation of retinal blood vessels using Gaussian mixture models and expectation maximization". *Proceedings of the 2nd International Conference on Health Information Science*, Mar. 25-27, Springer Berlin Heidelberg, London, UK., pp: 105-112. DOI: 10.1007/978-3-642-37899-7_9.
- [7] H.S. Bhadauria, S.S. Bisht, Annapurna Singh, "Vessels Extraction from Retinal Images". *IOSR Journal of Electronics and Communication Engineering (IOSR-JECE)* e-ISSN: 2278-2834, p-ISSN: 2278-8735. Volume 6, Issue 3 (May-Jun. 2013), PP 79-82.
- [8] Jobson D J, Rahman Z, Woodell G A, "Properties and performance of a center surround retinex". *IEEE Trans Image Process* 1997;6(3).
- [9] Jobson D J, Rahman Z, Woodell G A, "A multi-scale retinex for bridging the gap between color images and human observation of scenes". *IEEE Trans Image Process* 1997;6(3).
- [10] Soares JV, Leandro JJ, Cesar Júnior RM, Jelinek HF, Cree MJ, "Retinal vessel segmentation using the 2-D Gabor wavelet and supervised classification". *IEEE Trans Med Imag* 2006; 25(September (9)):1214–22.
- [11] Sandberg, Berta, Tony Chan, and Luminita Vese, "A level-set and Gabor-based active contour algorithm for segmenting textured images".
- [12] Nidhal Khedhair El Abbadi and Enas Hamood Al Saadi, "Blood vessels extraction using mathematical morphology". *Journal of Computer Science* 9(10):1389-1395,2013 ISSN:1549-3636

Color Filter Array Demosaicing in Bayer Pattern By The Prediction of Missing RGB

Shanu Anie Alias, Stephe Sara Philipose
P.G Scholar, Dept of CSE, BMCE, Kollam, Kerala, India
shanuanie@gmail.com

Abstract— Instead of beam splitters in digital cameras in this paper proposes an inexpensive technique using color filter arrays because it uses single sensor to capture multi color information. Single sensor digital cameras captures only one color at each pixel location and the other two color information to be interpolated is called Color Filter Array (CFA) interpolation or demosaicing. In this paper the missing green samples are first estimated, then missing red and blue samples are then estimated based on the estimated green plane. Gradient are used for extracting directional data from the input images. The Green channel interpolation is based on the directionally weighted gradient method and the directional color difference is used along with the directional data. Using the interpolated Green channel the red and blue channel get interpolated. With the completion of red and blue pixel the full color image is to be generated.

Keywords— Beam splitters, cfa interpolation, demosaicing, gradient, weighted gradient, directional data, color reconstruction.

INTRODUCTION

Demosaicing algorithm is a digital image process used to reconstruct a full color image from the incomplete color samples obtained from an image sensor overlaid with a color filter array (CFA). Also known as CFA interpolation or color reconstruction [1]. The reconstructed image is typically accurate in uniform-colored areas, but has a loss of resolution and has edge artifacts in non uniform-colored areas.

A color filter array is a mosaic of color filters in front of the image sensor. The most commonly used CFA configuration is the Bayer filter shown in Fig 1.1. This has alternating red (R) and green (G) filters for odd rows and alternating green (G) and blue (B) filters for even rows. There are twice as many green filters as red or blue ones, exploiting the human eye's higher sensitivity to green light.

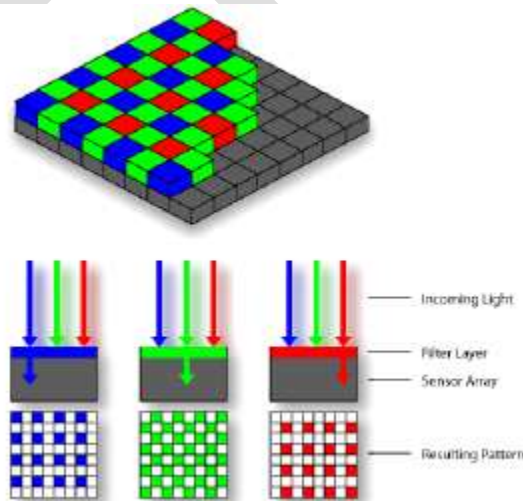


Figure 1.1 Bayer mosaic of color image

This paper is organized as follows: In section 2 includes the related works. The proposed method is explained in section 3. Ultimately section 4 concludes the proposed work.

RELATED WORKS

Nearest neighbor interpolation simply copies an adjacent pixel of the same color channel (2x2 neighborhood). It is unsuitable for any application where quality matters, but can be used for generating previews with given limited computational resources [17]

In bilinear interpolation, the red value of a non-red pixel is computed as the average of the two or four adjacent red pixels. The blue and green values are also computed in a similar way. Bilinear interpolation generates significant artifacts, especially across edges and other high-frequency content, as it doesn't take into account the correlation between the RGB values [14].

Cubic interpolation takes into account more neighbors than in algorithm no. [14] (e.g., 7x7 neighborhood). Lower weight is given to pixels which are far from the current pixel. Gradient-corrected bilinear interpolation assumes that in a luminance/chrominance decomposition, the chrominance components don't vary much across pixels. It exploits the inter-channel correlations between the different color channels and uses the gradients among one color channel, to correct the bilinearly interpolated value [15].

Smooth hue transition interpolation assumes that hue is smoothly changing across an object's surface; simple equations for the missing colours can be obtained by using the ratios between the known colours and the interpolated green values at each pixel [14]. Problem can occur when the green value is 0, so some simple normalization methods are proposed [16].

Another interesting approach is to interpolate the green channel in both directions and then to make a posteriori decision based on sum of gradients in each direction[5]. The demosaicing problem has been studied from many other angles. Glotzbach et al. proposed a frequency domain approach where they extracted high frequency components from the green channel and used them to improve red and blue channel interpolation[6]. The full range of demosaicing Gunturk et al. used the strong spectral correlation between high frequency sub bands to develop an alternating projections method [7].

Algorithms [2][3] hypothesize that the quotient of two color channels is slowly varying, following the fact that two colors occupying the same coordinate in the chromaticity plane have equal ratios between the color components. Alternatively, [4][6][10][9] assert that the differences between red, green, and blue images are slowly varying. This principle is motivated by the observation that the color channels are highly correlated. The difference image between green and red (blue) channels contains low-frequency components only. A more sophisticated color channel correlation model is explored in [7]. Moreover, [3][10][8] incorporate edge-directionality. Interpolation along an object boundary is preferable to interpolation across this boundary for most images.

PROPOSED METHOD

For extracting directional data from digital images gradients are used. Several demosaicing methods including a recent integrated gradients method proposed in [11] made use of them. In [12] demonstrated that the gradients of color difference signals could be valuable features to adaptively combine directional color difference estimates Here we use weighted gradient method using sobel mask. The modules of the proposed system framework are illustrated in Fig 2.1. The first step of the algorithm is to find the gradients along the four direction of the mosaic image, that means horizontal, vertical, right diagonal and left diagonal.

$$G_{i,j}^H = |(m(i+1, j-1) + 2 * m(i+1, j) + m(i+1, j+1)) - m(i-1, j-1) + 2 * m(i-1, j) + m(i-1, j+1)| \quad (1)$$

$$G_{i,j}^V = |(m(i-1, j+1) + 2 * m(i, j+1) + m(i+1, j+1)) - m(i-1, j-1) + 2 * m(i, j-1) + m(i+1, j-1)| \quad (2)$$

$$G_{i,j}^{rd} = |(m(i-1, j) + 2 * m(i-1, j+1) + m(i, j+1)) - m(i, j-1) + 2 * m(i+1, j-1) + m(i+1, j)| \quad (3)$$

$$G_{i,j}^{ld} = |(m(i-1, j) + 2 * m(i-1, j-1) + m(i, j-1)) - m(i+1, j) + 2 * m(i+1, j+1) + m(i, j+1)| \quad (4)$$

where H , V , rd and ld denote horizontal, vertical, right diagonal and left diagonal directions and (i, j) is the pixel location. For every pixel coordinate, we now have a true color channel value

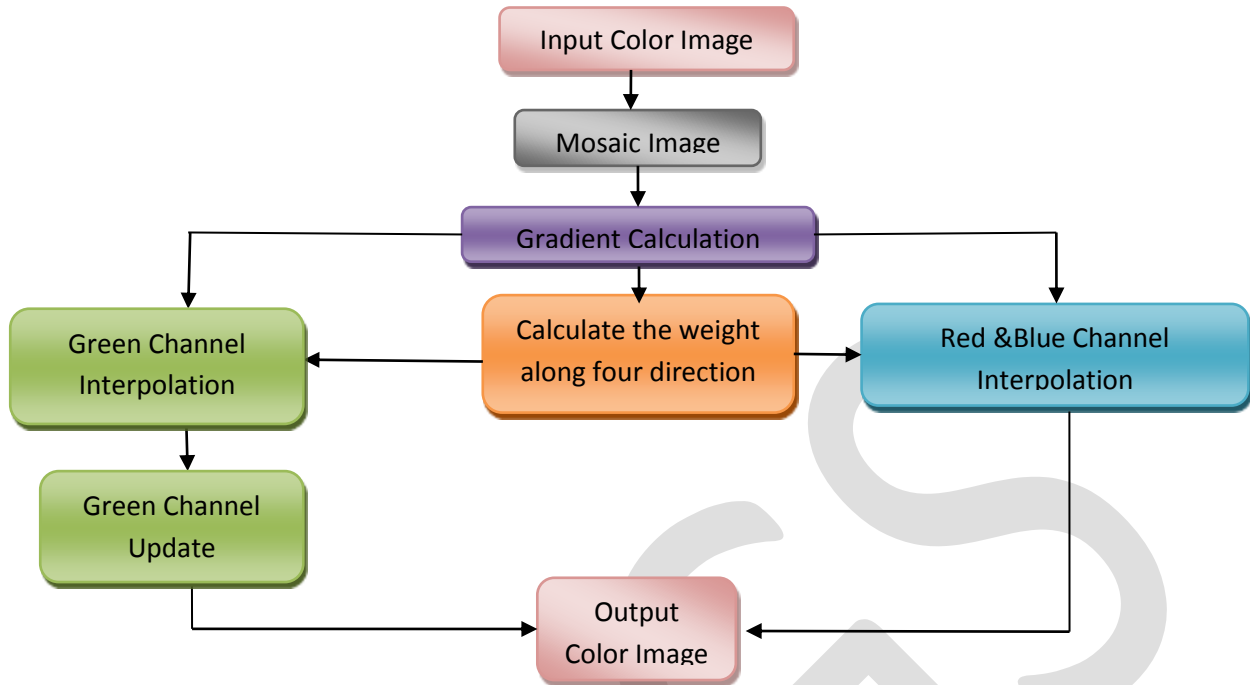


Fig.2 Block diagram of proposed system

Next Step is to find the weight along the same four direction The weights for horizontal, vertical directions, right diagonal, and left diagonal (W_H, W_V, W_{rd}, W_{ld}) are calculated by adding color gradients over a local window. For a local window size of 5 by 5, the weight for each direction is calculated as follows

$$W_H(i, j) = \left| 1 / (1 + G_{i,j}^H) \right| \quad (5)$$

$$W_V(i, j) = \left| 1 / (1 + G_{i,j}^V) \right| \quad (6)$$

$$W_{rd}(i, j) = \left| 1 / (1 + G_{i,j}^{rd}) \right| \quad (7)$$

$$W_{ld}(i, j) = \left| 1 / (1 + G_{i,j}^{ld}) \right| \quad (8)$$

Green Plane Interpolation

The next step of the algorithm is to reconstruct the green image along horizontal and vertical directions. Initial green channel interpolation section concentrates on estimating missing green pixels from known green and red pixel values using the green-red row of Bayer pattern. The same technique is used in estimating missing green pixels from known green and blue pixels[13]. Following equation is done in both red and blue planes

$$G(i, j) = \sum_{i=3}^{x-2} \sum_{j=4}^{y-2} (W_H(i, j) * (m(i, j-1) + m(i, j+1)) / 2 + W_V(i, j) * (m(i-1, j) + m(i+1, j)) / 2) / (W_H(i, j) + W_V(i, j)) \quad (9)$$

$$G(i, j) = \sum_{i=4}^{x-2} \sum_{j=3}^{y-2} (W_H(i, j) * (m(i, j-1) + m(i, j+1)) / 2 + W_V(i, j) * (m(i-1, j) + m(i+1, j)) / 2) / (W_H(i, j) + W_V(i, j)) \quad (10)$$

Green Channel Update

After green channel interpolation next is its updation this will improve the green channel results. We consider the closest four neighbours of the target pixel with each one having its own weight.

Red & Blue Channel Interpolation

After the green channel has been reconstructed, interpolate the red and blue components. The most common approach for red and blue estimation consists of interpolation of the color differences R-G, B-G instead of R and G directly. Finally, the missing blue (red) components at the red (blue) sampling positions are interpolated[13]. For the green position following equations are used

$$R(i, j) = \sum_{i=3}^{x-2} \sum_{j=3}^{y-2} (W_H(i, j) * (m(i, j-1) + m(i, j+1)) / 2) / W_H(i, j) \quad (11)$$

$$R(i, j) = \sum_{i=4}^{x-2} \sum_{j=4}^{y-2} (W_V(i, j) * (m(i-1, j) + m(i+1, j)) / 2) / W_V(i, j) \quad (12)$$

Next for the blue position equation will be

$$R(i, j) = \sum_{i=4}^{x-2} \sum_{j=3}^{y-2} (W_{rd}(i, j) * (m(i-1, j+1) + m(i+1, j-1)) / 2 + W_{ld}(i, j) * (m(i-1, j-1) + m(i+1, j+1)) / 2) / W_{rd}(i, j) + W_{ld}(i, j) \quad (13)$$

Similarly, we interpolated the blue channel. With the completion of red and blue pixel values we obtain a full color image.

CONCLUSION

This method produces better results in terms of image quality. It does not require any thresholds as it does not make any hard decisions. It is non iterative[13]. In this paper we proposed a weighted gradient method using sobel mask because of this the gradient calculation is more accurate, weight ratio will be more close to the pixel color ratio of the mosaic image and the interpolation will be more perfect.

REFERENCES:

- [1] Wikipedia, the free encyclopedia. Demosaicing, August 2010.
- [2] D. R. Cok, "Reconstruction of CCD images using template matching," *Prof. IS&T Ann. Conf./ICPS*, 1994, pp. 380-38
- [3] R. Kimmel, "Demosaicing: Image reconstruction from CCD samples," *IEEE Trans. Image Process.*, vol. 8, pp. 1221-1228, 1999.
- [4] W. T. Freeman and Polaroid Corporation, "Method and apparatus for reconstructing missing color samples," US Patent 4 774 565, 1998.
- [5] D. Menon, S. Andriani, and G. Calvagno, "Demosaicing with directional filtering and a posteriori decision," *IEEE Trans. Image Process.*, vol. 16, no. 1, pp. 132-141, Jan. 2007.
- [6] J. W. Glotzbach, R. W. Schafer, "A method of color filter array interpolation with alias cancellation properties," in *Proc. IEEE*, vol. 1. 2001, pp. 141-144.
- [7] B. K. Gunturk, Y. Altunbasak, and R. M. Mersereau, "Color plane interpolation using alternating projections," *IEEE Trans. Image Process.*, vol. 11, no. 9, pp. 997-1013, Sep. 2002.
- [8] C. A. Laroche and M. A. Prescott, "Apparatus and method for adaptively interpolating a full color image utilizing chrominance gradients," US Patent 5 373 322, 1994.
- [9] D. D. Muresan and T. W. Parks, "Optimal Recovery Demosaicing," IASTED Signal and Image Processing, Hawaii, 2002.
- [10] J. E. Adams, Jr., "Design of color filter array interpolation algorithms for digital cameras, Part 2," *IEEE Prof. Int. Conf. Image Processing*, vol. 1, 1998, pp. 488-492.
- [11] K. H. Chung and Y. H. Chan, "Low-complexity color demosaicing algorithm based on integrated gradients," *J. Electron. Imag.*, vol. 19, no. 2, pp. 021104-1-021104-15, Jun. 2010.
- [12] I. Pekkucuksen and Y. Altunbasak, "Gradient based threshold free color filter array interpolation," in *Proc. IEEE Int. Conf. Image Process.*, Sep. 2010, pp. 137-140

- [13] Ibrahim Pekkucuksen, "Multiscale Gradients-Based Color Filter Array Interpolation", IEEE TRANSACTIONS On Image Processing, Vol. 22, No. 1, January 2013
- [14] Maschal et al. Review of bayer pattern color fillter array (cfa) demosaicing with new quality assessment algorithms. Technical report, U.S. Army Research Laboratory, 2010
- [15] Henrique S. Malvar, Li wei He, and Ross Cutler. High-quality linear interpolation for demosaicing of bayer-patterned color images. In Proceedings of the IEEE International Conference on Speech, Acoustics, and Signal Processing, 2004.
- [16] R Lukac and K N Plataniotis. Normalized color-ratio modeling for CFA interpolation. IEEE Transactions on Consumer Electronics, 2004.
- [17] Rami Cohen Demosaicing Algorithms August 30, 2010

IJERGS

Compact UWB Bandnotch Antenna for UWB Applications

Muhib Ur Rahman¹

Email id: muhib462@yahoo.com

Department of Electrical Engineering, University of Engineering and Technology (UET) Peshawar, Pakistan

Abstract---In this paper, a compact UWB band notch antenna is proposed. Band notching is achieved by inserting a slot in the radiating patch. The antenna is analyzed for single band notch. The proposed antenna is operating in the frequency range of 3.4 to 10.6 GHz while its performance is not good in the WLAN band (5/6 GHz). The VSWR plot also shows that antenna has one stop band (5/6 GHz). The proposed antenna is simulated using Ansoft HFSS while its results is verified using CST Microwave studio suite. This miniature size has best matching in the UWB band because of low VSWR and advantageous radiation pattern. The ripples present in higher frequencies of the previous designed antenna has been removed by increasing the length of the ground plane. Moreover the antenna has a very compact size of (18×23 mm²) and could be easily fabricated into portable UWB devices.

Keywords ----Radiating patch, VSWR, Ripples, UWB (ultra-wide band), WLAN (wireless local area network), UWB band notch antenna.

1. Introduction

The most popular and promising technology for future short range and high speed communication is Ultra wide band (UWB). The frequency band from 3.1 to 10.6 GHz has been allocated by the Federal Communications Commission (FCC), for UWB communication applications [1].

Two subsets of UWB exist within the technology. The first one termed as direct sequence UWB (DS-UWB) and the second one is orthogonal frequency division multiple access UWB (OFDM-UWB). DS-UWB ranges from 3.1–4.85 GHz and 6.2– 9.7 GHz while OFDM-UWB ranges from 3.432 – 4.488 GHz and 6.6– 10.296 GHz. A notch band is required at 5.7 GHz for both frequency bands. Also attenuation at 10.6 GHz is needed for both frequency bands. It turns out that since the lower band is more popular in the implementation of both DS-UWB and OFDM-UWB, the mid-range stop-band is currently likely to be more useful [10].

The advantages of UWB communication are that they offer more resistance to multipath phenomenon, high data rate short range wireless communication, low complexity and low emission power [2]. The problem that encounters is that the IEEE 802.11a WLAN system operates in 5.15 to 5.825 GHz band which causes potential interference with the UWB communication. This interference can be mitigated by using a good filtering techniques. But the filtering techniques is much expensive and increases the system complexity. So by designing antenna having band notch characteristics is the most simple and economical solution [3]. There are various techniques to design band notch antennas such as etching L-shaped, E-shaped, C-shaped, arc shaped and U-shaped slots on the radiating patch [4-8]. Also there is another technique which uses parasitic strips in the printed monopole [9].

Here in this paper, We designed the UWB antenna using the work of [3]. The objective of our paper is to achieve a band notching characteristics in the designed antenna without using FR-4 substrate as it seems impractical for microstrip antennas having bandnotch more than 4 GHz. Also selecting the acceptable length of the ground plane so that no ripples may be present at higher frequencies. To achieve the desired notch band, we used a new technique of etching a slot with certain angles on the radiating patch. The optimized parameters of the slot resonator is mentioned in the table 2. The position and effect of the slot is analyzed from the surface current distributions at different frequencies. The parameters of the slots is optimized by simulations. The simulated VSWR plot shows that designed antenna operates only from 3.4 to 10.6 GHz while rejecting WLAN band in 5/6 GHz. The antenna is nearly Omni-directional and a peak gain of 4.575 dBi. The gain is suppressed in the WLAN band which is clear from the simulated gain curve. The designed antenna geometry is very simple and a very compact size which make it good to use in a portable devices.

2. Related Work:

In [3], the author designed UWB antenna having bandnotch characteristics. Also different UWB bandnotch antennas are designed by different authors such as etching L-shaped, E-shaped, C-shaped, arc shaped and U-shaped slots on the radiating patch [4-8]. These authors constructed antenna on FR-4 substrate. It seems good, however simulating and implementing antenna for more than 3 or 4 GHz frequency with FR-4 substrate isn't practical which mainly because very high loss tangent of FR-4, especially in notch

frequencies and microstrip antennas design. It can be used in planar monopole antenna, but can't be used in planar monopole antenna that has the band notch more than 4 GHz.

By observing radiation pattern of different designed antennas it will be clear that some nulls are present at higher frequencies. This is because that maximum designers select very small length of the ground plane which create ripples at higher frequencies. In some designs these nulls are due to higher order harmonics.

3. ANTENNA GEOMETRY

The geometry of the proposed antenna is shown in the Fig 1 while its parameters are listed in the table 1. The antenna is constructed on Rogers R04003 substrate with thickness (h) of 1.5mm, relative permittivity of 3.55 and $\tan\delta = 0.0027$. The antenna is fed by a 50 Ω microstrip feedline.

The dimensions of the design is listed in table and shown in the Fig 1 and 2:

Table 1: optimized parameters of the UWB antenna with band notch characteristics.

W_{sub}	L_{sub}	W_f	L_{gnd}	L_1	L_2	L_3	L_4	h	W_1
18mm	23mm	2.8mm	7.2mm	7.4mm	11.5mm	5.3mm	7.28mm	1.5mm	4mm

Table 2: optimized parameters of the slot.

L_s	L_e	α°	β°	W_e
10mm	4.75mm	65°	115°	0.45mm

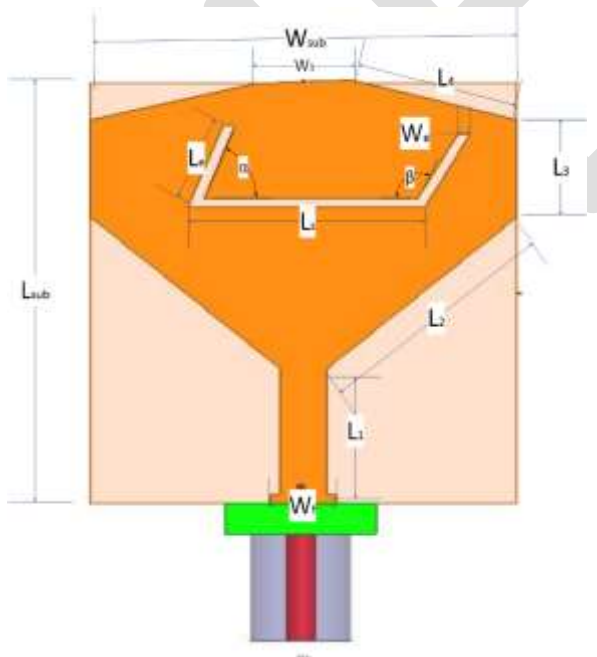


Figure 1: Front view of Designed Antenna

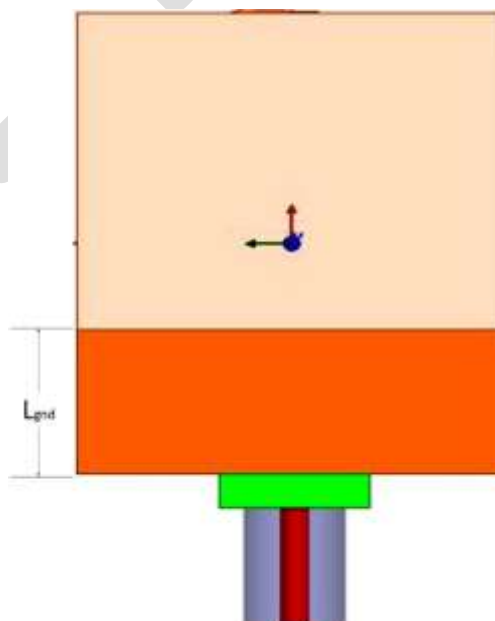


Figure 2: Back view

We inserted a slot resonator in the radiating patch of the above UWB antenna to achieve band notching. The dimensions of the slot is listed in the table 2 and shown in Fig 2. The antenna designed operate from 3.4 to 10.6 GHz while band notching characteristics at 5/6 GHz. So we have made one stop band for filtering of the WLAN signal.

4. RESULTS AND DISCUSSIONS

3.1. UWB antenna without slot-- First the antenna has been designed without slot in the radiating patch. The S_{11} plot shows that the antenna covers the entire UWB band and is matched to the transmission line from 3.4 to 10.7 GHz. The S_{11} plot without slot is shown in Fig 3. It is obvious from the plot that antenna have potential interference with the WLAN signal as it is operating in the WLAN band. The VSWR curve shows that antenna has no mismatch in UWB band as $VSWR < 2$ in the entire band and a maximum VSWR of 1.82 at 6 GHz. The VSWR plot without slot is shown in Fig 4.

3.2. UWB antenna with slot-- By inserting slot in the radiating patch, the antenna operate in the entire UWB band while rejecting WLAN signal. The geometry of slot is shown in the Fig 1. Now there is no more potential interference of the UWB and WLAN signals. The length of the notch band is calculated from the equation (1) below:

$$f_{\text{notch}} = \frac{c}{2 \times L \sqrt{\frac{\epsilon_r + 1}{2}}} \quad (1)$$

Where, L is the length of the slot resonator, ϵ_r is the relative permittivity and C is the speed of light. The length of the slot resonator is calculated from (1) while its position is analyzed from surface current distribution as shown in Fig 5. The width of the slot is optimized by simulating at different slot width as shown in Fig 3 and 4. After simulating at different slot widths we select the width of the slot as $W_e = 0.45\text{mm}$. It is cleared from the S_{11} plot and VSWR plot that the antenna has a good performance in the UWB band while notch at the WLAN band (5/6 GHz).

So, by introducing the slot of length and width discussed above in the radiating patch, the VSWR in 5/6 GHz WLAN band is greater than 2, which shows that the antenna performance is not good in this band. The antenna has been simulated using HFSS and CST microwave studio suite and the simulation results are shown in Figures.

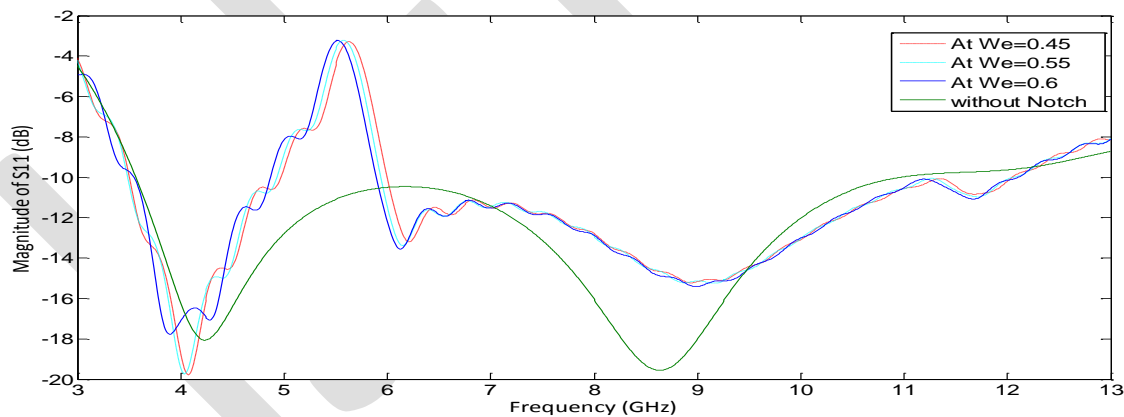


Fig 3 S_{11} vs. Frequency plots with and without Notch

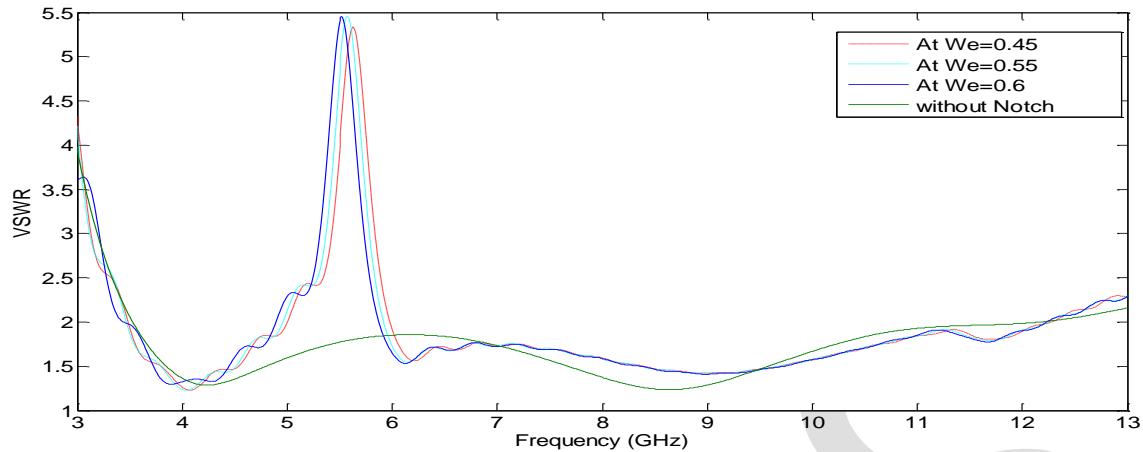


Fig 4 VSWR vs. Frequency plots with and without Notch

Surface current distribution-- Fig 5 shows the simulated current distributions on the surface of the proposed antenna at 5.5, 7.1, 8.2 and 10.1GHz. At 7.1, 8.2, and 10.1 GHz, the maximum current flows along the microstrip feed line, while low current densities around the slot. On the other hand, the surface current distribution on the antenna at 5.5 GHz is totally concentrated around the slot. So a maximum electromagnetic energy has been stored around the slot and no current flows along the microstrip feedline.

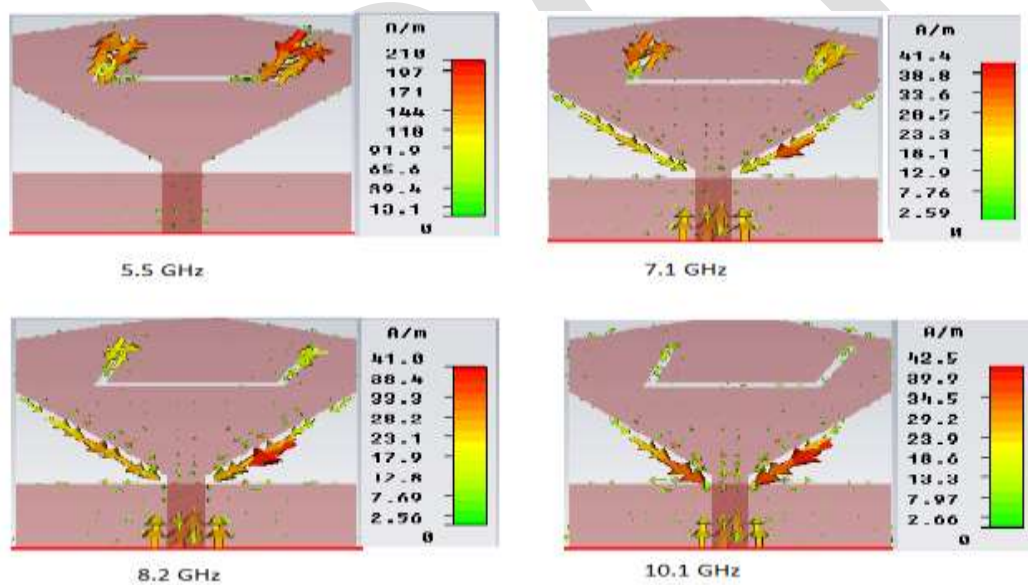


Fig 5 Simulated current distributions on the surface of the proposed antenna at different frequencies

Far field radiation pattern-- The simulated Far field of the proposed antenna at different frequencies are shown in the Fig 6. These results shows that antenna is nearly omnidirectional which make it a good candidate for UWB portable devices. These results also reveals that antenna has consistent radiation pattern throughout the band. The radiation pattern at higher frequencies are also shown in Fig 6 which shows that no ripples are present at higher frequencies. This is because that we have selected an acceptable length of the ground plane.

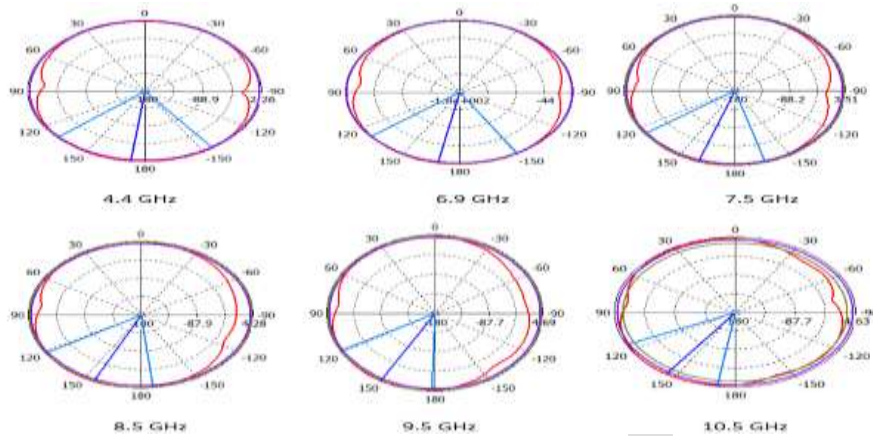


Fig 6 Radiation patterns for antenna with notches

Antenna Gain plot without notch-- The antenna gain is evaluated without notch in the radiating patch. The gain plot shows that antenna has a maximum gain of 4.5 dBi while an average gain of almost 4.3 dBi. The gain increases considerably as we move towards higher frequencies.

Antenna Gain plot with notch-- The gain plot with Notch shows that antenna gain is suppressed well in the WLAN band. The gain plot also shows that antenna performance is not good at WLAN band. The minimum gain is -1.7 dBi at 5.6 GHz which is at WLAN band. The negative gains (in dBi) indicates the destructive interference of surface currents at those frequencies leading to band-notch creation. The sharp decrease in the antenna gain is observed while moving from 5 GHz to 5.8 GHz. After this the gain increases considerably as shown in Figure 7. The maximum gain occur at 8.5 GHz which is 4.5 dBi. So the gain is also enhanced along with band notching.

Comparison of Gain with and without Notch

The Antenna gain is compared with and without notch as shown in the Fig 7. The plot clearly shows the Notch frequency band.

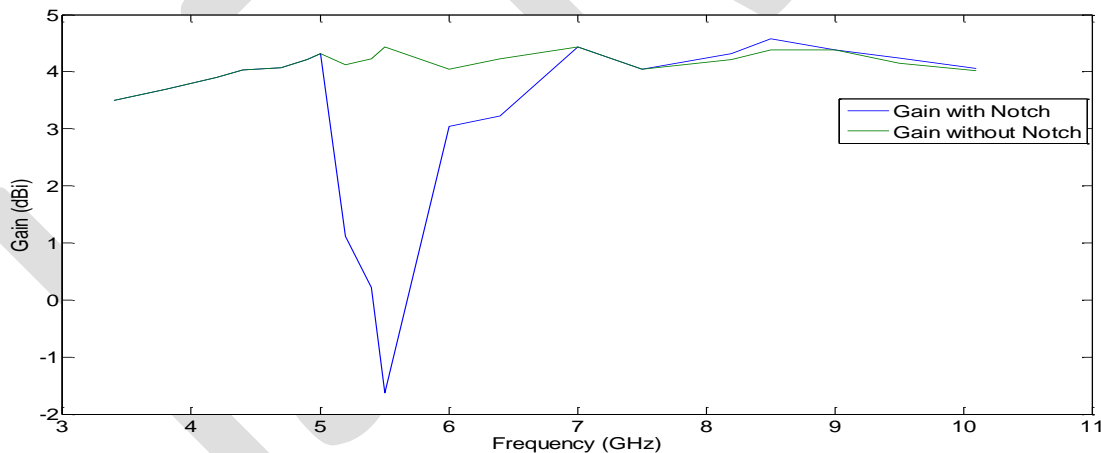


Fig 7 Antenna Gain plot with and without Notch

5. CONCLUSIONS

A compact wide band radiating patch UWB bandnotch antenna has been proposed. The potential interference between the UWB system and WLAN band has been minimized by introducing slot in the radiating patch, which rejecting the WLAN frequency band. Notching has been observed at the WLAN band which make this antenna much useful for UWB applications. This antenna work in the entire UWB band. The antenna results has been analyzed showing high average gain and nearly Omni-directional radiation pattern. The nulls at higher frequencies has been removed. The antenna provides best matching and low VSWR in the frequency band from 3 to 10.6 GHz with a band-notching effect at the frequency band from 5/6 GHz. The antenna has a very compact size of 23×18 mm² which make them to use it in the portable UWB devices without causing potential interference.

REFERENCES:

- [1] Naghshvarian Jahromi, M. (2008). Compact UWB bandnotch antenna with transmission-line-fed. *Progress In Electromagnetics Research B*, 3, 283-293.
- [2] Low, Z. N., Cheong, J. H., & Law, C. L. (2005). Low-cost PCB antenna for UWB applications. *Antennas and Wireless Propagation Letters, IEEE*, 4, 237-239.
- [3] Xu, J., Shen, D. Y., Wang, G. T., Zhang, X. H., Zhang, X. P., & Wu, K. (2012). A small UWB antenna with dual band-notched characteristics. *International Journal of Antennas and Propagation*, 2012.
- [4] Zahirul Alam, A. H. M., Islam, M. R., & Khan, S. (2008, May). Designing an UWB patch antenna with band notched by using L-shaped slot and unsymmetrical feedline. In *Electrical and Computer Engineering, 2008. CCECE 2008. Canadian Conference on* (pp. 000101-000104). IEEE.
- [5] Ali, J. K., Yassen, M. T., Hussan, M. R., & Hasan, M. F. (2012). A New Compact Ultra Wideband Printed Monopole Antenna with Reduced Ground Plane and Band Notch Characterization. *Session 3P8*, 733.
- [6] Chu, Q. X., & Yang, Y. Y. (2008). A compact ultrawideband antenna with 3.4/5.5 GHz dual band-notched characteristics. *Antennas and Propagation, IEEE Transactions on*, 56(12), 3637-3644.
- [7] Wong, K. L., Chi, Y. W., Su, C. M., & Chang, F. S. (2005). Band-notched ultra-wideband circular-disk monopole antenna with an arc-shaped slot. *Microwave and Optical Technology Letters*, 45(3), 188-191.
- [8] Cho, Y. J., Kim, K. H., Choi, D. H., sik Lee, S., & Park, S. O. (2006). A miniature UWB planar monopole antenna with 5-GHz band-rejection filter and the time-domain characteristics. *Antennas and Propagation, IEEE Transactions on*, 54(5), 1453-1460.
- [9] Kim, K. H., Cho, Y. J., Hwang, S. H., & Park, S. O. (2005). Band-notched UWB planar monopole antenna with two parasitic patches. *Electronics Letters*, 41(14), 783-785.
- [11] Jahromi, M. N., Falahati, A., & Edwards, R. M. (2011). Application of fractal binary tree slot to design and construct a dual band-notch CPW-ground-fed ultra-wide band antenna. *IET microwaves, antennas & propagation*, 5(12), 1424-1430.

Personalized Recommendation Combining User Interest and Social Circle

¹N.Latha ²Sudhakar reddy

¹M.Tech C.S Student, S.V. College Of Engineering, Tirupati, AP, India, nethaji.latha2010@gmail.com

²Principal, S.V. College Of Engineering, Tirupati, AP, India, sudhakar.n@svcolleges.edu.in

Abstract: With the advent and popularity of social network, more and more users like to share their experiences, such as ratings, reviews, and blogs. The new factors of social network like interpersonal influence and interest based on circles of friends bring opportunities and challenges for recommender system (RS) to solve the cold start and sparsity problem of datasets. Some of the social factors have been used in RS, but have not been fully considered. In this paper, three social factors, personal interest, interpersonal interest similarity, and interpersonal influence, fuse into a unified personalized recommendation model based on probabilistic matrix factorization. The factor of personal interest can make the RS recommend items to meet users' individualities, especially for experienced users. Moreover, for cold start users, the interpersonal interest similarity and interpersonal influence can enhance the intrinsic link among features in the latent space. We conduct a series of experiments on three rating datasets: Yelp, MovieLens, and Douban Movie. Experimental results show the proposed approach outperforms the existing RS approaches

Keywords: Interpersonal influence, personal interest, recommender system, social networks

I. Introduction

Recommender framework (RS) has been effectively misused to fathom data over-burden. In E-Commerce, similar to Amazon, it is imperative to taking care of mass size of data, for example, suggesting client favored things and items. Luckily, the presence of web2.0 enormously enhances client's drive on the Internet, and after that brings volume of interpersonal organizations, for example, Facebook, Twitter, Yelp, Douban, Epinions, and so on. The interpersonal relationship, particularly the friend networks, of informal communities makes it conceivable to unravel the frosty begin and sparsity problem. "Moves as one longings, chooses as you like." Just like the logo says, client's decision is dependably firmly identified with his/her own advantage. It is extremely prevalent for clients to share, transfer, and remark their most loved substance. This paper, three social components, individual interest, interpersonal interest likeness, and interpersonal impact, wire into a bound together customized suggestion model in view of probabilistic lattice factorization. The identity is meant by client thing importance of client enthusiasm to the theme of thing. To epitomize the impact of client's identity, we mine the point of thing in view of the regular thing classification labels of rating datasets. In this way, every thing is meant by a classification circulation or theme appropriation vector, which can mirror the normal for the rating datasets. In addition, we get client interest taking into account his/her rating conduct. We then allocate to the impact of client's identity in our customized suggestion model relative to their aptitude levels. Then again, the client relationship of informal organization contains two components: interpersonal impact and interpersonal interest comparability.

II Related Work

In this paper, we concentrate on probabilistic grid factorization with thought of elements of informal community. In the accompanying, we quickly survey some significant attempts to this paper, including the fundamental network factorization model [4] with no social variables, the CircleCon model [1] with the component of interpersonal trust values and the Social Contextual (ContextMF) model [2] with interpersonal impact and individual inclination.

III Implementation

Basic Matrix Factorization

To introduce various sophisticated approaches [1], [2], [3], [5], we first briefly review the basic probabilistic matrix factorization (BaseMF) approach [4], which does not take any social factors into consideration. The task of RS is to decrease the error of predicted value using R to the real rating value. Thus, the BaseMF model is trained on the observed rating data by minimizing the objective function

$$\Psi(R, U, P) = \frac{1}{2} \sum_{u,i} (R_{u,i} - \hat{R}_{u,i})^2 + \frac{\lambda}{2} (\|U\|_F^2 + \|P\|_F^2) \quad (1)$$

ContextMF Model

Jiang et al. [2] demonstrate the significance of social contextual factors (including interpersonal influence and individual preference) for item adopting on real Facebook and Twitter style datasets. The task of ContextMF model in [2] is to recommend acceptable items from sender u to receiver v . Here, the factor of interpersonal influence is similar to the trust values in CircleCon model [1]. Moreover, individual preference is mined from receiver's historical adopted items. And the interpersonal preference similarity values are represented by the matrix W . Each of the rows is normalized to unity.

The objective function of this model is

$$\begin{aligned} & \Psi(R, U, P, S^*, W^*) \\ &= \frac{1}{2} \sum_{u,j} (R_{u,j} - \hat{R}_{u,j})^2 + \frac{\lambda}{2} (\|U\|_F^2 + \|P\|_F^2) \\ &+ \frac{\beta}{2} \sum_u ((U_u - \sum_v S_{u,v}^* U_v)(U_u - \sum_v S_{u,v}^* U_v)^T) \\ &+ \frac{\gamma}{2} \sum_{u,v} (W_{u,v}^* - U_u U_v^T)^2 \end{aligned} \quad (5)$$

where the element of individual inclination is authorized by the last term in (5), which implies that client idle element U_u ought to be like his/her companions' idle element with weight of their inclination likeness in informal organization, and the rating qualities is anticipated by (1). Once the model is trained, the rating qualities can be anticipated by for any client thing sets. Other than the interpersonal impact (like the trust values in CircleCon model [1]), individual inclination is a novel element in ContextMF demonstrate, and is implemented by the last term in (5). Note that despite everything we execute the interpersonal impact as CircleCon model [1] and preclude the theme importance of things, as we additionally anticipate evaluations of things in Epinions style datasets and utilize the circle based thought in our analyses. Albeit singular inclination is proposed in this model, client inert component is still associated with his/her companions as opposed to his/her trademark. Actually, the variable of individual inclination of this model is upheld by interpersonal inclination similarity. Comparing ContextMF model, the proposed customized suggestion model has three distinctions: 1) the errand of our model is to prescribe user, regardless of sender or beneficiary, intrigued and obscure things. 2) client individual hobby is straightforwardly identified with his/her appraised things rather than join with his/her companions. 3) the variable of client enthusiasm for our model mined from client evaluated things has more impact than individual inclination in ContextMF model, on the grounds that it less demanding for the prescribed things of our model to be changed ContextMF model, because it easier for the recommended items of our model to be transformed into purchase rate than the adopted items in Facebook style social networks.

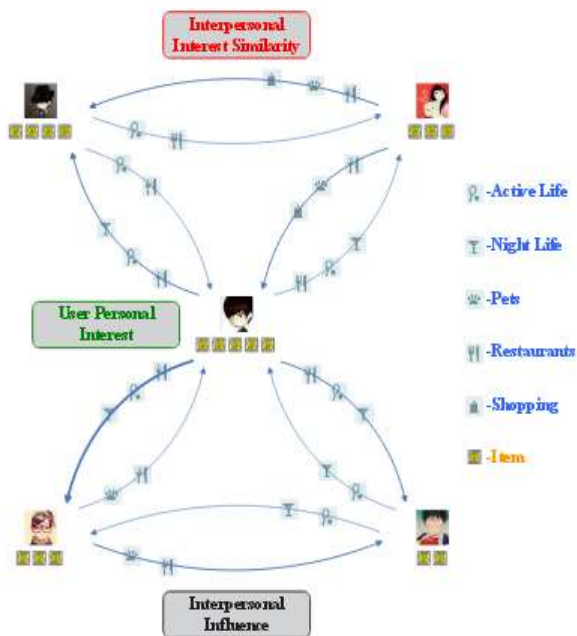


Figure 1. Three main social factors in our recommendation model, including user personal interest, interpersonal interest similarity, and interpersonal influence. The items under users are historical rating records, which can be used to mine users' personal interest. The category icon on line between two users denotes their interest similarity. And the boldness of the line between users indicates the strength of interpersonal influence.

TABEL 2
ALGORITHM OF PERSONALIZED RECOMMEN-
DATION

Algorithm of Personalized Recommendation Model
(PRM)

Initialization: $\Psi^c(0) = \Psi^c(\mathbf{U}^c(0), \mathbf{P}^c(0))$.
 Require: $0 < \epsilon < 1, t = 0$.
 while($t < 1000$)
 calculate $\frac{\partial \Psi^c(t)}{\partial \mathbf{U}^c}, \frac{\partial \Psi^c(t)}{\partial \mathbf{P}^c}$
 search optimal l
 $\mathbf{U}^c(t) = \mathbf{U}^c(t-l) - \frac{\partial \Psi^c(t)}{\partial \mathbf{U}^c}, \mathbf{P}^c(t) = \mathbf{P}^c(t-l) - \frac{\partial \Psi^c(t)}{\partial \mathbf{P}^c}$
 If ($\Psi^c(t) < \epsilon$)
 break;
 $t++$;
end

Comparative Algorithms

We conducted series of experiments to compare our personalized recommendation model (PRM) with the following existing models.

BaseMF: This model is the basic matrix factorization approach proposed in [4] without consideration of any social factors.

CircleCon: This method is proposed in [1], including

Four variants: CircleCon1, CircleCon2a, CircleCon2b, and CircleCon3. It improves the accuracy of BaseMF and SocialMF [3] by introducing the inferred trust circle of social network. And Yang et al. have demonstrated CircleCon2a, CircleCon2b, and CircleCon3 have much better performance. Thus, we just omit CircleCon1.

ContextMF: This method [2] improves the accuracy of traditional item-based collaborative filtering model in [9], influence-based model in [16], and Sorec in [17] by taking both interpersonal influence and individual preference into consideration. As stated in Section III, we train the model as (5).

IV. CONCLUSION

In this paper, a personalized recommendation approach was proposed by combining social network factors: personal interest, interpersonal interest similarity, and interpersonal influence. In particular, the personal interest denotes user's individuality of rating items, especially for the experienced users, and these factors were fused together to improve the accuracy and applicability of recommender system. We conducted extensive experiments on three large real-world social rating datasets, and showed significant improvements over existing approaches that use mixed social network information. At present, the personalized recommendation model only takes user historical rating records and interpersonal relationship of social network into consideration. In our future works, we will take user location information to recommend more personalized and real-time items.

REFERENCES:

- [1] X. -W. Yang, H. Steck, and Y. Liu. Circle-based recommendation in online social networks. KDD'12, pp. 1267-1275, Aug. 2012.
- [2] M. Jiang, P. Cui, R. Liu, Q. Yang, F. Wang, W. -W. Zhu and S. Q. Yang. Social contextual recommendation. CIKM'12, pp. 45-54, 2012.
- [3] M. Jamali and M. Ester. A matrix factorization technique with trust propagation for recommendation in social networks. In Proc. ACM conference on Recommender systems (RecSys), 2010.
- [4] R. Salakhutdinov and A. Mnih. Probabilistic matrix factorization. In NIPS 2008, 2008.
- [5] Y. Koren, R. Bell, and C. Volinsky. Matrix factorization techniques for recommender systems. Computer, pp. 30-37, Aug. 2009.
- [6] M.E. Tipping and C.M. Bishop. Probabilistic principal component analysis. Journal of the Royal Statistical Society, Series B, pp. 611-622, 1999.
- [7] G. Adomavicius, and A. Tuzhilin. Toward the next generation of recommender systems: a survey of the state-of-the-art and possible extensions. Knowledge and Data Engineering, IEEE Transactions on, pp. 734-749, Jun. 2005.

[8] R. Bell, Y. Koren, and C. Volinsky. Modeling relationships at multiple scales to improve accuracy of large recommender systems. KDD'07, pp. 95-104, 2007.

[9] B. Sarwar, G. Karypis, J. Konstan, and J. Reidl. Item-based collaborative filtering recommendation algorithms. In WWW, pp. 285-295, 2001

IJERGS

Improving Network I/O Virtualization for Cloud Computing

¹M.Srinivasulu ²T.Vijaya rao

¹M.Tech C.S Student, S.V. College Of Engineering, Tirupati, AP, India, srisravas.seenu030@gmail.com

² Assistant Professor, S.V. College Of Engineering, Tirupati, AP, India, vijayarao.t@svcolleges.edu.in

Abstract: Cloud computing is a latest technology that gives platform and software as a service. A cloud platform can be either virtualized or not. The cloud platform increases the resources availability and the flexibility of their management (allocation, migration, etc.). It also reduces the cost through hardware multiplexing and helps energy saving. Virtualization is then a more and interesting technology of cloud computing. System virtualization refers to the software and hardware techniques that allow partitioning one physical machine into multiple virtual instances that run concurrently and share the underlying physical resources and devices. Virtualization is a key technology to enable cloud computing. It enhances resource availability and offers high flexibility and cost effectiveness. In our proposed scheme allows us to dynamically tune the aggregation mechanism to achieve the best tradeoff between the packets delay and throughput. The proposed I/O virtualization model hence forth satisfies the infrastructure providers to offer cloud computing services. Here I/O virtualization model based on packet aggregation to transfer packets between the driver domain and the VMs. It will improve networking performance of VM where the access to the network device is shared through the driver domain.

Keywords: Cloud computing, I/O virtualization, driver domain, networking performance, Xen, memory latency

I. Introduction

Distributed computing is a novel ideal model that gives foundation, stage, and programming as an administration. A cloud stage can be either virtualized or not. Virtualizing the cloud stage expands the assets accessibility and the adaptability of their administration (assignment, movement, and so forth.). It additionally diminishes the expense through equipment multiplexing and helps vitality sparing. Virtualization is then a key empowering innovation of distributed computing. Framework virtualization alludes to the product and equipment systems that permit parceling one physical machine into various virtual occurrences that run simultaneously and offer the fundamental physical assets and gadgets. The virtual machine screen (VMM), likewise called hypervisor, is a product layer that displays reflections of the fundamental physical assets. It deals with the virtual machines (VM) and permits them to share the physical assets particularly the system gadget. Since the hypervisors have been initially executed to give server virtualization to backing figure escalated applications, the I/O virtualization has not been actualized on account of system concentrated applications prerequisites (high throughput, low dormancy, and so on.). At that point, current hypervisors show poor system execution because of the extra overhead brought about by the virtualization layer

To make the cloud an all the more convincing ideal model, it is vital to make the systems administration execution of the VM scale up at line rates. The goal of our proposition is to moderate the VM system execution restriction to make it conceivable to run system concentrated applications without execution debasement. The principle commitments of this work are compressed as takes after: First, we assess the systems administration execution of VM where the entrance to the system gadget is shared through the driver area. Second, we demonstrate that the memory inactivity is behind the radical corruption of the VMs throughput through profiling the significant framework parts utilization. At that point, we propose another I/O virtualization model taking into account bundle accumulation to exchange parcels between the driver space and the VMs. We indicate through exploratory assessment that the proposed instrument essentially enhances the VM throughput. Be that as it may, it acquaints an extra defer with the bundles inactivity.

II Related Work

A few examination works have been committed to

I/O execution change. Next, we will just present the most applicable related attempts to our study. If it's not too much trouble allude to the supplementary record, accessible on the web, Section 6 for more related works. LRO [14] consolidates numerous got TCP parcels and passes them as a solitary bigger bundle to the upper layer in the system. The CPU overhead is brought down and an execution change is normal. LRO permits a change from 1,000 to 1,900 Mb/s with five 1-Gb/s Intel NICs. LRO is a conglomeration component at the get side just, performed in the gadget driver, in the connection of TCP parcels gathering. On account of a virtualized framework, LRO can be utilized to exchange parcels from the NIC to the driver space. Be that as it may, the gift reuse and additionally our proposition are plans working between the driver area and the visitor spaces. XenLoop [6] is a between VM loopback channel that

empowers direct system activity between two VM in the same physical machine without the mediation of a third programming segment, for example, Dom0. At whatever point two visitor VMs inside of the same machine have a dynamic trade of system activity, they set up a bidirectional between VM information channel between them, bypassing the standard information way by means of Dom0. The transmission capacity change with XenLoop over the local net front netback ranges from an element of 1.55 to 6.19 contingent upon the exchanged message size. XenSockets [1] is a restricted correspondence channel between two VMs. It executes a between VM correspondence component in view of the Unix attachment rule.

the bundle itself is lined at the tail of the compartment. The parcels in holders remain

III Implementation

Packet Aggregation Algorithm

Give us a chance to consider the situation where bundles are exchanged from the driver area to the VM. Bundles collection is performed taking into account their MAC destination address. Upon the landing of a parcel, the holder generator module uproots its MAC header and checks whether a compartment with that same MAC destination is as of now holding up to be exchanged to the netfront. Assuming this is the case, the holder generator checks whether the aggregate size of the compartment would surpass the most extreme permitted size of the compartment in the wake of including the approaching bundle. Assuming this is the case, the compartment is exchanged to the destination through the common memory and the generator makes another holder with the same MAC header of that approaching bundle. If not, it attaches a balance of 2 bytes to the compartment in which it stores the parcel's size valuable to focus the position of the following bundle in the holder. At that point, The packets in containers remain

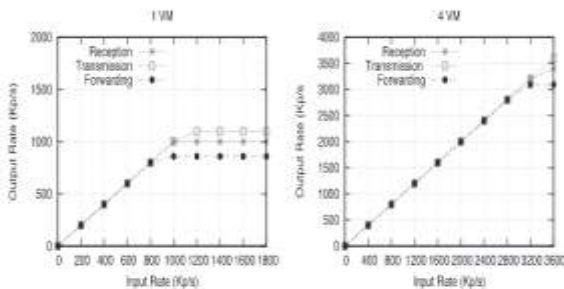


Fig. 3. Packet aggregation-based system forwarding throughput.

queuing until the container's maximum size is reached or its time-out expires. After that, the container is transferred through the memory according to the event channel mechanism. In the case where no container is available to carry the packet, the container generator creates a new container with the same MAC header of the arriving packet. This container first contains the packet's offset followed by the packet itself. More details about the aggregation mechanism are provided in Section 3.1 of the supplementary file, available online.

Hardware Bottleneck Analysis

PCI

We easily reject the hypothesis of the PCI as a bottleneck because the PCI allows the driver domain to forward packets at a rate of 800 Kp/s through a single pair of input/output ports, which is the highest rate at which packets can be forwarded through this pair.

FSB

The FSB allows to the processor to communicate with the chipset. Our platform's FSB clock frequency is of 1,333 Mhz over a 64-bits architecture. Then, the FSB bandwidth is 85.312 Gb/s. In the case of network I/O intensive applications, the FSB is mainly used to transfer packets between the processor and the main memory.

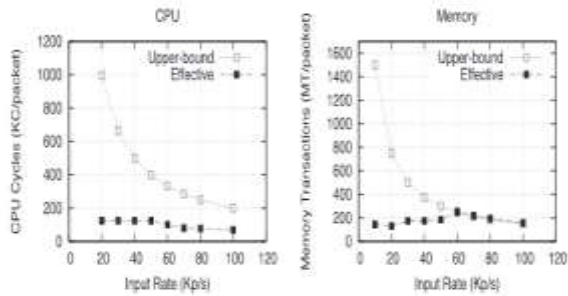


Fig. 2. Maximum and effective load on CPU and memory with one VM.

CPU
We profile the CPU cycles usage using Xenoprof [12]. Through profiling we determine the effective per packet load handled by the eight cores. Then, we compare the effective load to the upper bounds to determine whether the CPU still has room for growth. Fig. 2 shows that the effectively consumed CPU cycles remain well below the available CPU cycles expressed in Kilo Cycles per second or KC/s when the VM forwards packets at the maximum rate of 80 Kp/s. We conclude then that the system still has available CPU cycles. The CPU cannot then be the limiting factor.

IV. CONCLUSION

This results in a more efficient I/O communication. Experimental evaluation shows that the proposed packet aggregation mechanism significantly improves the networking performance. Furthermore, we studied the impact of aggregating packets on the delay. Given the additional waiting delay experienced by the packets during the aggregation operation, we proposed a new dimensioning tool to dynamically tune the aggregation mechanism to achieve the best tradeoff between the packets transmission throughput and their forwarding delay. The proposed tool is based on an analytical modeling of the system composed of the VMs, the driver domain, and the memory. The model implementation allowed us to determine the average waiting time as a function of the container size, which offers a means to guarantee a packets delay that respects the application requirements.

REFERENCES:

- [1] X. Zhang, S. McIntosh, P. Rohatgi, and J.L. Griffin, "XenSocket: A High-Throughput Interdomain Transport for Virtual Machines," Proc. ACM/ IFIP/ USENIX Int'l Conf. Middleware (Middleware '07), 2007.
- [2] M.F. Neuts, Matrix-Geometric Solutions in Stochastic Models: An Algorithmic Approach. The Johns Hopkins Press, 1981.
- [3] A. Menon, A.L. Cox, and W. Zwaenepoel, "Optimizing Network Virtualization in Xen," Proc. USENIX Ann. Technical Conf. (USENIX '06), 2006.
- [4] P. Barham, B. Dragovic, K. Fraser, S. Hand, T. Harris, A. Ho, R. Neugebauer, I. Pratt, and A. Warfield, "Xen and the Art of Virtualization," Proc. 19th ACM Symp. Operating Systems Principles (SOSP '03), Oct. 2003.
- [5] R.L. Tweedie, "Operator-Geometric Stationary Distributions for Markov Chains with Applications to Queueing Models," Advances in Applied Probability, vol. 14, pp. 368-391, 1982.
- [6] J. Wang, K. Wright, and K. Gopalan, "XenLoop: A Transparent High Performance Inter-VM Network LoopBack," Proc. ACM Symp. High Performance Parallel and Distributed Computing (HPDC '08), 2008.
- [7] X. Zhang and Y. Dong, "Optimizing Xen VMM Based on Intel Virtualization Technology," Proc. Int'l Conf. Computer Science and Software Eng., 2008.
- [8] M. Bourguiba, K. Haddadou, and G. Pujolle, "PacketAggregationBasedNetwork I/O Virtualization for Cloud Computing," Elsevier Computer Comm., vol. 35, no. 3, pp. 309-319, 2012.
- [9] K. Fraser, S. Hand, R. Neugebauer, I. Pratt, A. Warfield, and M. Williams, "Safe Hardware Access with the Xen Virtual Machine Monitor," Proc. First Workshop Operating System and Architectural Support for the On Demand IT Infrastructure (OASIS '04), 2004.

EFFECT OF PARTIAL REPLACEMENT OF COARSE AGGREGATE BY JHAMA CLASS BRICK IN CONCRETE

Mr. G. S. Patil

M.E. student

P.D.V.V.P.C.O.E., Ahmednagar.

maheshgirawale@gmail.com

Mr. P. B. Autade

Assi. Prof. Dept. of Civil. Engg.

P.D.V.V.P.C.O.E., Ahmednagar.

pankajautade@gmail.com

Abstract— Concrete is considered the world's most used construction material. Typical concrete mixtures are comprised of water, sand, cement and an aggregate of rock. This project focuses on the coarse aggregate in concrete. The other material will be used to replace the coarse aggregate of rock in typical concrete. This will include burn brick or Zama brick. This material was chosen because of their availability. The burn brick is available from brick manufacturing area. Also in brick-making, a large number of bricks are rejected due to nonconformity with the required specifications. One such major nonconformity is the distorted form of brick produced due to the uneven temperature control in the kiln. These rejected bricks can also be a potential source of coarse aggregate. This would not only make good use of the otherwise waste material but would also help alleviate disposal problems. This project presents the effects of Jhama Class Brick inclusion on the mechanical properties of concrete matrix in wet and hardened state properties. For checking mechanical properties of Jhama Class Brick bat based concrete used partially replacement Jhama class brick to coarse aggregate ratios 20%, 40%, 60% and 80% in M40 grade of concrete. It is observed that workability decreased with replacement of coarse aggregate. The Compaction factor observed as 0.92, 0.899, 0.88, 0.87 and 0.85 with varying percentage replacement of coarse aggregate by Jhama class brick bat as 0%, 20%, 40%, 60% and 80% respectively. The compressive strength of Jhama Class Brick bat based concrete used with partially replacement Jhama class brick to coarse aggregate ratios 20%, 40%, increased over conventional concrete about 6.08%, 10.02% for 3 days and 9.23%, 12.08% for 7 days and 10.02%, 11.95% for 28 days. If further increased in the percentage of replacement up to 60% and 80%, the strength was decreased by 3.73% and 8.16% respectively for 3 days and 5.69%, 9.25% for 7 days and 2.72%, 6.87% for 28 days cured cube specimen respectively. The Split Tensile and Flexural Strength of this concrete increases with 5.26%, 8.68%, and 2.74%, 4.76% respectively over plain concrete for the replacement 20% and 40% and decreased with 3.94%, 12.1% and 3.16%, 7.5% for the replacement 60% and 80%.

Keywords— Jhama class brick, Kiln, Compressive strength, Plasticizer, Jhama class Brick bat based concrete.

INTRODUCTION

Concrete is produced by mixing cement, sand, coarse aggregate and water to produced material that can be molded into almost any shape. The major volume concrete is filled with aggregate. The inclusion of aggregate in concrete reduces its drying shrinkage properties and improves many other properties such as compressive strength etc. But it is costly to transport, so local sources are needed to reduce the cost of transport, but due to geographical constraints this is not available at all places, therefore it necessitates finding other sources and alternative from local sources.

The many materials are used as a alternative source for natural coarse aggregate such as recycled low quality crushed brick, recycled coarse aggregate, coconut shell, recycled plastic aggregate, well burnt brick etc. For this work select a jhama class brick as a alternative source for course aggregate. This material was chosen because in brick making, a large number of bricks are rejected due to non conformity is the distorted form of brick produced due to high temperature control in the kiln. These rejected bricks can also be potential source of coarse aggregate. According to general definition concrete is a composite material so by taking advantage of the situation for the people, this paper presents the research that is carried out on the concrete when natural coarse aggregate is partially replaced by Jhama Class brick aggregate.

The aims of the study are:-

1. To develop a mixture proportioning process to manufacture Jhama class brick based concrete.
2. To identify and study the effect of salient parameters that affects the properties of Jhama class brick based concrete.
3. To study the short-term engineering properties of fresh and hardened Jhama class brick based concrete.

MATERIAL USED:-

A) Materials:-

a) Cement:

Cement is a fine, grey powder. It is mixed with water and materials such as sand, gravel, and crushed stone to make concrete. The cement and water form a paste that binds the other materials together as the concrete hardens. Ordinary Portland cement having 28 days compressive strength of 46 MPa (ASTM 1994) was used for preparation of all concrete cubes. By using one type of cement, the effect of varying the types of coarse aggregate in concrete is investigated.

TABLE:-I Properties of cement

Sr. No.	Characteristics	Values obtained	Standard values
1	Normal consistency	33%	
2	Initial Setting Time	48 min	Not less than 30 min.
3	Final Setting Time	240 min.	Not Greater than 600 min.
4	Sp.Gr.	3.09	
5	Fineness	4.8	

b) Fine Aggregate:

The sand used for the experimental programmed was locally procured and conformed to Indian Standard Specifications IS: 383-1970. The sand was first sieved through 4.75 mm sieve to remove any particles greater than 4.75 mm and then was washed to remove the dust.

TABLE:-II Properties of Fine Aggregate

Sr. No.	Characteristics	Value
1.	Type	Uncrushed
2.	Specific Gravity	2.68
3.	Total Water	1.02%
4.	Fineness Modulus	2.507
5.	Grading Zone	II

c) Coarse Aggregate:

The broken stone is generally used as a coarse aggregate. The nature of work decides the maximum size of the coarse aggregate. Locally available coarse aggregate having the maximum size of 20 mm was used in our work. The aggregates were washed to remove dust and dirt and were dried to surface dry condition. The aggregates were tested as per Indian Standard Specifications IS: 383-1970.

TABLE III: - Properties of Coarse Aggregate

Sr. No.	Characteristics	Value
1.	Type	Crushed
2.	Maximum Size	20 mm
3.	Specific Gravity (20mm)	2.825
4.	Total Water Absorption Absorption (20mm)	0.995%

d) Jhama Class Brick

Bricks are a versatile and durable building and construction material with good load bearing properties. Various researchers have been carried out in porosity, permeability and absorption of brick. The traditional clay bricks are manually produced by pressing clay with certain amount of sand in the wooden mould. Then the wet bricks are first dried in the sun and air and then transported to the brick kiln for subsequent burning process. The bricks are burnt up to temperature of 800-900C in the brick kiln. If the temperature in the brick kiln is uncontrolled then the bricks are burnt excessively up to the temperature 1100-1200C. Due to this the bricks are sold at cheaper rate as they become out of shape. Therefore this type of brick is known as over burnt brick. These bricks are also known as Jhama bricks.



Fig. No. I:-Jhama Class Brick Materials

These bricks, however, possess higher strength than the normal burnt clay bricks. Therefore one of the cheaper alternative for brick foundation, floors, roads etc. because of the fact that the over burnt bricks have a compact structure and hence they are sometimes found to be stronger than even the first class brick. Over burnt bricks have high compressive strength between 120 to 150 Kg/cm². However they have very poor shape. Brickwork using these bricks utilizes 40% of more mortar than traditional brickwork. However this cost is offset by the price at which over burnt bricks are available. Due to over burnt, the bricks become black and its edges also become curved. It is not used in brick work of building main wall, partition wall and some other purposes.

TABLE IV:-Comparison between Coarse Aggregate and Jhama Brick Aggregate

Properties	Coarse Aggregate	Jhama class brick bats
Aggregate Impact Value	7.24	19.35
Aggregate Crushing Value	16.85	32.2
Specific Gravity	2.83	2.67
Water Absorption	0.995%	11.08%

B) Mix Ratio:-

The mix designed was prepared according to the IS-10262:2009 recommendation for concrete mix design. 1:1.54:2.08 mix proportioning ratio was determined for targeted strength of 48 MPa For all cases 0.38 water/cement (w/c) ratio was used. And got a quantity of material for this mix ratio:-

TABLE V:-Quantity of Material per Cubic Meter of Concrete.

Material	Proportion by Weight	Weight in kg/m ³
Cement	1	375
F.A.	2.26	849.02
C.A.	3.04	1139
W/C	0.38	150 lit.

For 50kg cement, found the quantity of material

TABLE VI:-Quantity of Material per 50 kg Cement

Material	Proportion by Weight	Weight in kg/m ³
Cement	1	50
F.A.	1.54	113
C.A.	2.08	152
W/C	0.38	19 lit.

METHODOLOGY:-

GENERAL:-

This presents the details of development of the process of making Jhama class brick bat based concrete. The materials that are required for making the Jhama class brick bat based concrete, coarse aggregates, sand and the Jhama class brick coarse aggregate as per design of mix proportion M40 are clearly mentioned in a tabular format as per IS 1026-2008.

Preparation, Casting and Curing of Jhama class brick bat based Concrete:-

1. Mix Preparation:-

The batching of all the ingredients was performed by weight. The sand was air dried in the laboratory before mixing. First the surface was damped with water then all the aggregates (Natural Coarse Aggregate, Fine Aggregate and Jhama class brick coarse Aggregate) were spread on the surface area till the aggregates. After thorough mixing of aggregates cement was introduced on the ground surface and water were added slowly as per W/C ratio. The concrete was mixed for approximately three minutes after the water was added.

2. Mix Casting:-

It is found that the Jhama brick-bats based Concrete is dark in color and is cohesive. The amount of water in the mixture plays an important role on the behavior of fresh concrete. When the mixing time is long, mixtures with high water content bled and segregation of aggregates and the paste occurred. This phenomenon is usually followed by low compressive strength of hardened concrete. From the preliminary work, it was decided to observe the following standard process of mixing in all further studies,

- 1) Take the suitable proportion of the ingredients of the concrete.
- 2) Spread the fine aggregate on the ground,
- 3) After that put the coarse aggregate as well as Jhama brick-bats,
- 4) After that add the water in suitable quantity.
- 5) And continue the wet mixing for another four minutes.

Then the fresh prepared mix was casted standard cube moulds, cylinders and beams.

3. Curing:-

All the moulds were cured by immersing in a curing tank in the lab. The specimens were brought out from water approximately 24 hours before testing and kept at room temperature till testing.

• Jhama brick-bats based Concrete

Following test were conducted for this experimental work,

- a) Workability test
- b) Compressive Strength Test
- c) Split Tensile Strength Test
- d) Flexural Strength Test
- e) Mass Density Test

RESULTS AND DISCUSSION

a) Workability Test:-

To find the workability of Jhama class brick bat based concrete, used the Compaction Factor Test because the compaction factor test gives more information than the slump test. The test is a dynamic test and thus is more appropriate than static tests for highly thixotropic concrete mixtures.

TABLE VII:-Compaction Factor Test Result

Replacement in %	00	20	40	60	80
Compaction Factor	0.92	0.899	0.88	0.87	0.85

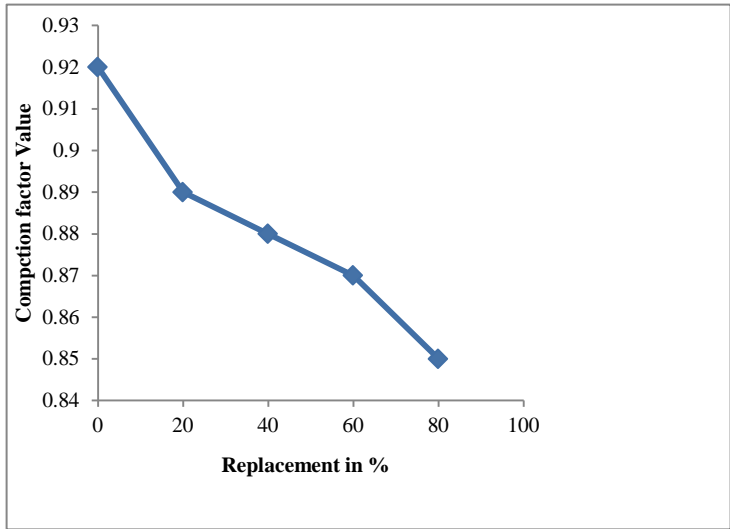


Fig. No. II:-Compaction Factor Vs Replacement

b) **Compressive Strength Test:**

Table VIII:-Compressive strength test result

Sr. No.	Replacement in %	Compressive Strength in N/mm^2		
		3Days	7 Days	28 days
1	0	13.11	28.31	37.82
2	20	13.9	30.92	41.61
3	40	14.44	31.73	42.34
4	60	12.62	26.71	36.79
5	80	12.04	25.68	35.22

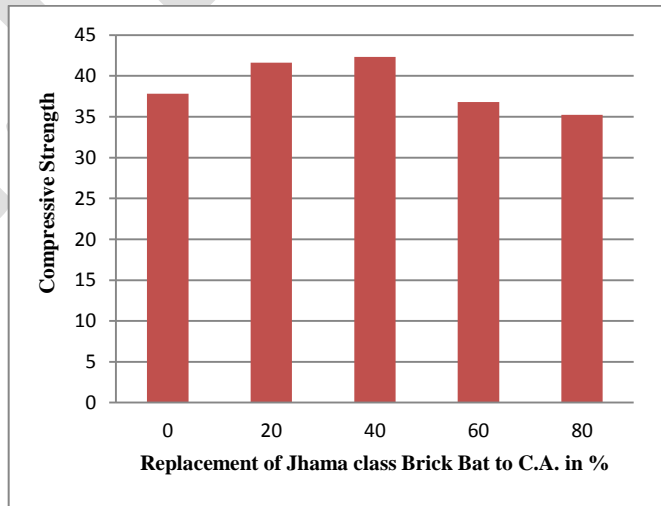


Fig. No. III:-Compressive Strength Test

c) **Split Tensile Test:**

Table IX:-Split Tensile Test Result

Sr.No.	Replacement in %	Split tensile strength in MPa
		28 Days
1	0	3.8
2	20	4
3	40	4.3
4	60	3.65
5	80	3.24

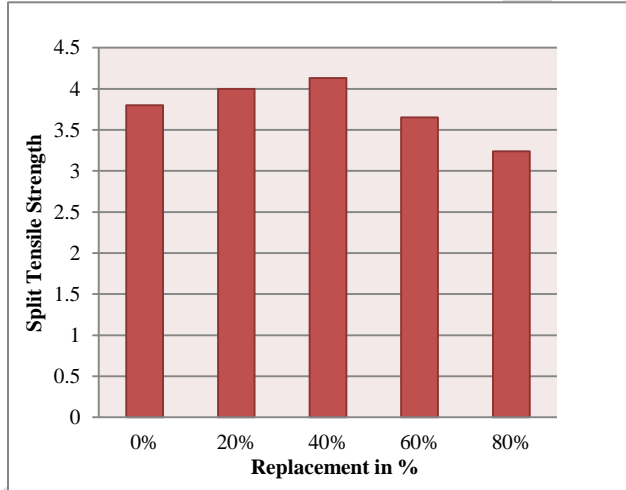


Fig. No. IV: - Split Tensile Strength Test

d) **Flexural Strength Test:**

Table X:-Flexural Test Result

Sr. No.	Replacement in %	Flexural strength in MPa
		28 Days
1	0	5.06
2	20	5.20
3	40	5.50
4	60	4.89
5	80	4.62

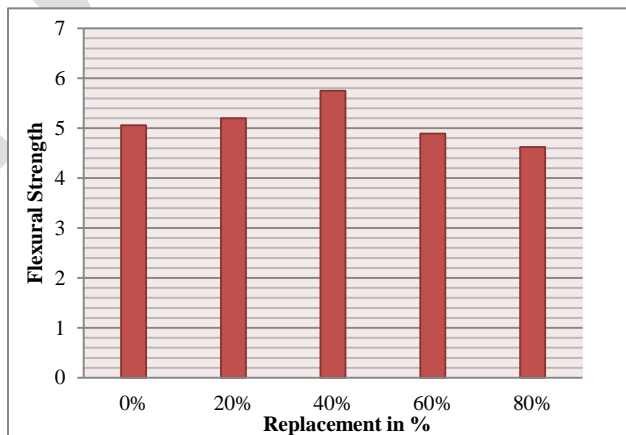
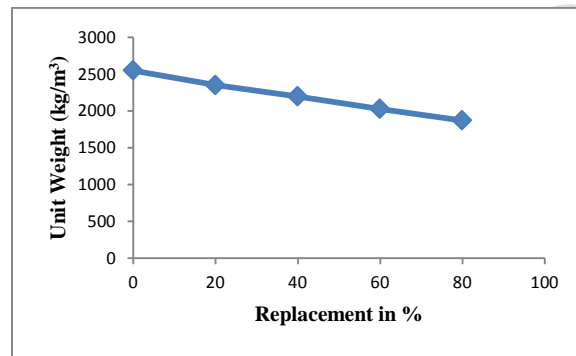


Fig. No. V: - Flexural Strength Test

e) **MASS DENSITY TEST:-**

Table VIII:-Unit Weight Test Result

Replacement in %	Unit Weight in kg/m ³
0	2548.14
20	2349.62
40	2195.55
60	2026.67
80	1869.62



CONCLUSION:-

On the basis of the result obtained during the experimental investigation, following conclusions were drawn,

1. The compaction factor decreased as the percentage of Jhama class brick increases and increased in comparison with the conventional concrete.
2. The unit weight also decreased as the percentage of Jhama class brick and decreased in comparison with the conventional concrete.
3. Concrete made by using jhama class brick as a coarse aggregate, initially it gives the higher compressive strength for the replacement 20% and 40% after that it was to decrease for 60% and 80%.
4. The compressive strength was found 6.08%, 10.02% higher than that of conventional concrete when the coarse aggregate is replaced by 20% and 40% by Jhama class brick aggregate respectively for the age of concrete 3 days.
5. The compressive strength was found 3.73%, 8.16% lower than that of conventional concrete when the coarse aggregate is replaced by 60% and 80% by Jhama class brick aggregate respectively for the age of concrete 3 days.
6. The compressive strength was found 9.23%, 12.08% higher than that of conventional concrete when the coarse aggregate is replaced by 20% and 40% by Jhama class brick aggregate respectively for the age of concrete 7 days.
7. The compressive strength was found 5.69%, 9.25% lower than that of conventional concrete when the coarse aggregate is replaced by 60% and 80% by Jhama class brick aggregate respectively for the age of concrete 7 days.
8. Compressive strength of Jhama class brick based concrete was higher by 10.02% and 11.95% than that of conventional concrete for the replacement of 20% and 40% at the age of concrete 28 days. For further increased in the percentage of replacement up to 60% and 80%, the compressive strength was decreased by 2.72% and 6.87% respectively.
9. Split Tensile strength of Jhama class brick based concrete was higher by 5.26% and 8.68% than that of conventional concrete for the replacement of 20% and 40% at the age of concrete 28 days. For further increased in the percentage of replacement up to 60% and 80%, the Split Tensile strength was decreased by 3.94% and 12.1% respectively.
10. Flexural strength of Jhama class brick based concrete was higher by 2.74% and 4.76% than that of conventional concrete for the replacement of 20% and 40% at the age of concrete 28 days. For further increased in the percentage of replacement up to 60% and 80%, the Flexural strength was decreased by 3.16% and 7.5% respectively.

REFERENCES:

1. Ahmad S.I., Roy s., (2012), "Creep behavior and its prediction for normal strength concrete made from crushed clay brick as coarse aggregate." *Journal of Material in Civil Engineering*, Vol.-24, pp.308-314.

2. Apebo N.S., Agunwamba. J. C.(2014), “ The suitability of crushed over burnt brick as coarse aggregate.”, *International Journal of Engineering Science And Innovative Technology*, Vol. 3, Issue-1
3. Bazaz J.B., Khayati M., (2012) “Properties and Performance of concrete made with recycled low quality crushed brick”, *Journal of Material in Civil Engineering*. Vol.-24., pp.330-338.
4. Chi-Sun Poon, Dixon Chan.(2005), “Effects Of Contaminants On The Properties of Concrete Paving Blocks Prepared with recycled concrete aggregate.”, *Construction And Building Materials.*, pp.164-175
5. Eldin N.N., Ahmad B., (1993), “Rubber tire Particle as concrete aggregate.”, *Journal of Material in Civil Engineering.*, Vol.-5,pp.478-496.
6. Gopinandan Roy, Jayanta pal, (2012), “Use of Brick Aggregate in Standard Concrete and Its Performance in Elevated Temperature.”, *International Journal of Engineering and Technology*, Vol. 5, No. 4
7. IS 10262-2009.
8. Khalaf F.M., Devnny A.S., (2002), “New test for porosity and water absorption of fired clay brick”, *Journal of Material in Civil Engineering*, Vol.-17, pp 456-464.
9. Khalaf F.M., Devnny A.S.,(2004), “ Recycling of demolished masonry rubble as coarse aggregate in concrete review.”, *Journal of Material in Civil Engineering.*, Vol.-16,PP.331-340.
10. Khalaf F.M., Devnny A.S.,(2005), “ Properties of new and recycled clay brick aggregate for use in concrete.”, *Journal of Material in Civil Engineering.*, Vol.-17,pp.456-464.
11. Khaldoun Rahal, (2005), “Mechanical Properties of Concrete With Recycled Coarse Aggregate”, *Building And Environmental Science*, pp 407-415.
12. Khaloo, A. R. (1994). “Properties of concrete using clinker brick as coarse aggregate.” *ACI Mater. J.*, 91(4), pp. 401–407.
13. Kulkarni S., Momin A. A., (2015), “Experimental Study on Strength Properties of Concrete using Brick Aggregates”, *International Journal of Advance Engineering and Research Development*, Vol.2, Issue-1.
14. M.M. Sabai., R. R. Mato., (2012), “Concrete block Production from Construction and Demolition Waste in Tanzania”, *Elsevier*, pp. No.9-19.
15. Mansur, M. A., Wee, T. H., and Lee, S. C. (1999). “Crushed bricks as coarse aggregate for concrete.” *ACI Mater. J.*, 96(4), pp. 478–484.
16. Mathew P., Paul T., (2013), “Recycled plastic as coarse aggregate for structural concrete.” *International Journal of Innovative Research in Science, Engineering and Technology*. Vol.2, Issue-3.
17. Mazumdar A.R., Kabir A., (2006) , “Performances of over burnt distorted brick as coarse aggregate in pavement works.”, *Journal of material in civil engineering.*, Vol.-18,pp.456-464., PP.- 18 , *Journal of Material in Civil Engineering.*, Vol.-17,pp.777-785.
18. Md. Siddikur R., Md. Bellal Hossain, (2012), “Strength behavior of recycled concrete with partial replacement of conventional aggregate.” *International journal of environment*. Vol-2., Issue-2., pp 80-86.
19. Mutuku R. N., Kabubo C. K. (2015), “Mechanical Characteristics Of Normal Concrete Partially Replaced With Crushed Clay Bricks”, *International Journal of Civil Engineering and Technology (IJCIET)*, Volume 6, Issue 1, pp. 62-75.
20. Nyok Yong Ho., Yang Pin L., (2012), “Utilization of recycled concrete aggregate in structural concrete”, *Journal of Material in Civil Engineering*, Vol.-25, pp.318-327.
21. R.V. Silva, R. K. Dhir., (2014), “Properties and composition of recycled aggregate from construction and demolition waste suitable for concrete production.” *Construction And Building Material*, pp 201-217.

HOLE DETECTION AND HEALING FOR A RoI IN WIRELESS SENSOR NETWORKS

Divya K Suku , Phini Ann Philip

PG Scholar, Department of ECE, CAARMEL Engineering College, Pathanamthitta, Kerala
Assistant Professor, Department of ECE, CAARMEL Engineering College, Pathanamthitta, Kerala

E-mail:divyasuku91@gmail.com

Abstract: Sensor technology is one of the fast growing technologies in the current scenario. And it has wide range of application also. The ability of sensors to work without being monitored by any individual is its unique quality. Wireless sensor network comprise of small sensors which have minimum communicational and computational power. Several anomalies are present in WSNs. One such problem is a hole. Area devoid of any node can be referred to as a hole. This degrades the performance of the whole network. It affects the routing capability of the network very badly. The formation of holes in a WSN is unavoidable due to the inner nature of the network. This paper deals with detecting and healing such holes in an on demand basis.

Keywords: Wireless sensor network, holes, hole detection, coverage, hole healing

INTRODUCTION

A wireless sensor network is composed of tiny sensor nodes. Each sensor node is capable of sensing some phenomenon, doing some limited data processing and communicating with each other. These tiny sensor nodes are deployed in the target field in large numbers and they collaborate to form an adhoc network capable of reporting the phenomenon to a data collection point called sink or base station. These networked sensors have many potential in civil as well as military applications that is, they are used for environmental monitoring, industrial monitoring and they are also utilized for object tracking. Sensor nodes are even used for health related applications etc.

Several anomalies can occur in wireless sensor networks that impair their desired functions such as communication and sensing. One such anomaly is a hole. Destruction of nodes causes holes. Area devoid of any node is termed as a hole. Different types of holes are present namely coverage holes, routing holes, jamming holes, black holes/sink holes etc. WSN are deployed in hostile environment and left unaltered for a relatively longer period of time. At times a group of sensors fail to carry out the network operations. Such nodes are termed as destroyed node. In sensor network we come across a type of node termed as faulty node. A faulty node is a node which gives result which significantly deviate from the results of its neighboring nodes. The emergence of holes in the network is unavoidable due to the inner nature of WSNs, random deployment, environmental factors, and external attacks. Thus, an event occurring within these holes is neither detected nor reported and, therefore, the main task of the network will not be completed. Thus, it is primordial to provide a self-organizing mechanism to detect and recover holes. This paper seeks the problem of hole detection and healing in an on demand basis.

Some of the major reason for node destruction and hole creation are:

- Power depletion: Each sensor node is equipped with power battery. Once depleted it is not an easy task to recharge the nodes.
- Physical destruction: Physical destruction of nodes due to some environmental reason cause a hole in the network.
- Existence of obstacles: An example for such a situation is a sensor node fell in a pond where its task is to monitor forest fire. This make the inactive for the purpose and a hole is created.
- Lower density regions: Nodes that fall in the lower density region acts as isolated nodes and form holes.

PROBLEM DEFINITION

There has been much researches on hole detection problem as it is one of the major problem of wireless sensor networks. In almost all process the first method id to detect the topology of the network. And it is done by many means. And also the type of the hole has to be identified. We formally define here various types of holes and their characteristics.

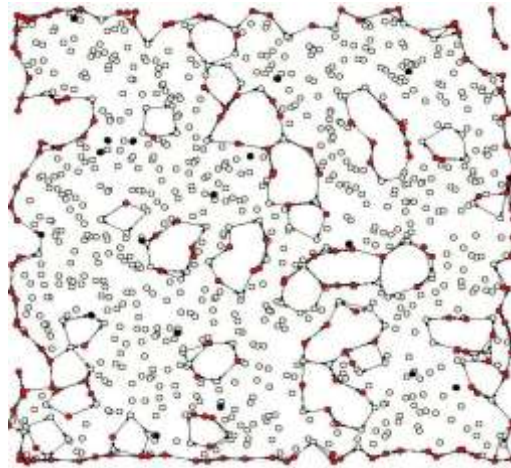


Fig.1 Holes in a WSN

1 Coverage Holes

Given a set of sensors and a target area, no coverage hole exists in the target area, if every point in that target area is covered by at least k sensors, where k is the required degree of coverage for a particular application (see Fig. 2). It is pertinent to mention that the coverage hole problem defined is dependent on application requirements. Some applications may require a higher degree of coverage of a given target area for fault tolerance/redundancy or for accurate target localization using triangulation-based positioning protocols [7] or trilateration based localization [8].

The sensing coverage of a sensor node is usually assumed uniform in all directions and is represented by unit disc model (Fig. 1). However, this idealized model is based on unrealistic assumption: perfect and same coverage in a circular disc for all the sensors. Moreover, the coverage not only depends on the sensing capability of the sensor but also on the event characteristics [9] e.g. target detection of military tanks as compared to detection of movement of soldiers depends on the nature and characteristics of event as well as the sensitivity of the sensors involved.

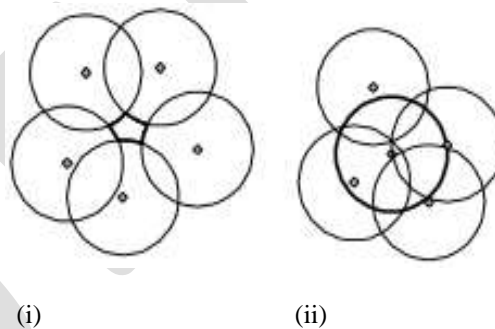


Fig.2(i). Coverage hole with unit disk sensing model (ii). Sensor with dark gray sensing circle is necessary if degree of coverage required is 2

2 Routing Holes

A routing hole consist of a region in the sensor network where either nodes are not available or the available nodes cannot participate in the actual routing of the data due to various possible reasons. These holes can be formed either due to voids in sensor deployment or because of failure of sensor nodes due to various reasons such as malfunctioning, battery depletion or an external event such as fire or structure collapse physically destroying the nodes. Routing holes can also exist due to local minimum phenomenon often faced in geographic greedy forwarding. Forwarding here is based on destination location. In Fig.3, a node x tries to forward the traffic to one of its 1-hop neighbor that is geographically closer to the destination than the node itself. This forwarding process stops when x cannot find any 1-hop neighbor closer to the destination than itself and the only route to destination requires that packet moves temporarily

farther from the destination to b or y . This special case is referred to as local minimum phenomenon and is more likely to occur whenever a routing hole is encountered.

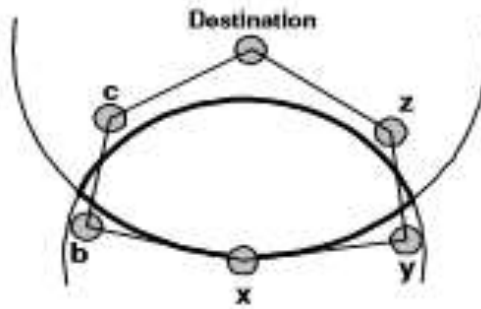


Fig.3 Local minimum phenomenon in greedy forwarding

3 Jamming Holes

An interesting scenario can occur in tracking applications when the object to be tracked is equipped with jammers capable of jamming the radio frequency being used for communication among the sensor nodes [4]. When this happens, nodes will still be able to detect the presence of the object in the area but unable to communicate the occurrence back to the sink because of the communication jamming. This zone of influence centered at the jammer is referred to as jamming hole in this paper. The jamming can be deliberate or unintentional. Unintentional jamming results when one or more of the deployed nodes malfunction and continuously transmits and occupies the wireless channel denying the facility to other neighboring nodes. In deliberate jamming an adversary is trying to impair the functionality of the sensor network by interfering with the communication ability of the sensor nodes. This adversary can be a laptop-class attacker [5] with more resources and capable of affecting a larger area of the sensor network or a mote-class attacker [5] i.e., one of the deployed nodes that has been compromised and is now acting maliciously to create a denial of service condition. Apart from communication jamming, jamming of sensing capabilities is also possible for certain kind of sensor networks e.g. consider the case of a sensor network that relies on acoustic sampling for tracking objects. If the object that is being tracked can introduce random high power acoustic noises, the sensors cannot reliably detect its presence and would be unable to report the existence of the object.

4 Sink/Black Hole/ Worm Hole

Sensor networks are highly susceptible to denial of service attacks due to their inherent characteristics i.e., low computational power, limited memory and communication bandwidth coupled with use of insecure wireless channel. A sink/black hole attack can be easily launched by an adversary node in the sensor network. The malicious node starts advertising very attractive routes to data sink. The neighbor nodes select the malicious node as the next hop for message forwarding considering it a high quality route and propagate this route to other nodes. Almost all traffic is thus attracted to the malicious node that can either drop it, selectively forward it based on some malicious filtering mechanism or change the content of the messages before relaying it. This malicious node has thus formed a sink hole with itself at the center. The sink hole is characterized by intense resource contention among neighboring nodes of the malicious node for the limited bandwidth and channel access [11]. This results in congestion and can accelerate the energy consumption of the nodes involved, leading to the formation of routing holes due to nodes failure. With sink holes forming in a sensor network, several other types of denial of service attacks are then possible [5],[11]. Worm hole is another kind of denial of service attack [12]. Here the malicious nodes, located in different part of the sensor network, create a tunnel among themselves. They start forwarding packets received at one part of the sensor network to the other end of the tunnel using a separate communication radio channel. The receiving malicious node then replays the message in other part of the network. This causes nodes located in different parts of networks to believe that they are neighbors, resulting in incorrect routing convergence.

In this paper we are working mainly on coverage holes.

RELATED WORK

There has been many such related work done on this topic. In this section we highlight the work done in order to detect holes inside the network. I.Khan et al. [2] give a detail description of work done for boundary recognition and hole detection in wireless sensor

networks. Fang et al. [4] detects holes inside the network by assuming that nodes are equipped with location awareness devices. The algorithms [10, 26, 27, 28, 29, 30, 35] under this category, use the connectivity information of sensor nodes to detect the boundary of the sensor networks and detect holes inside the wireless sensor network. These algorithms utilize the available topological information and do not make any assumptions about the geographical locations of the nodes. The algorithms [31, 32, 33] proposed under this category identify the nodes, as either inner or boundary nodes, by assuming that the node distribution in the network follows some statistical functions.

An algebraic topological method using homology theory detects single overlay coverage holes without coordinates [4], [5]. Ghrist and Muhammad [4] employed a central control algorithm that requires connectivity information for all nodes in the RoI. For N nodes, the time complexity is $O(N^5)$. For [5], it is $O(HD^2)$, where D is the maximum number of other active nodes that overlap a node's sensing area, and H is the worst-case number of redundant nodes in a large hole, with $H \geq D$. In [5], the complexity does not depend on the overall size of the network, whereas the homology algorithm encounters severe difficulties with dense networks. Additionally, the message forwarding overhead can be impractically large, since the algorithm is centralized.

Funke in [6] presented a heuristic for detecting holes based on the topology of the communication graph. The heuristic computation is not localized as it requires the computation of distance fields over the whole network.

In a more recent paper [7], Funke and Klein described a linear-time algorithm for hole detection. They require that the communication graph follows the unit disk graph model. Compared to the heuristic approach presented in [6], the algorithm does slightly worse. Furthermore, when decreasing the node density, the algorithm breaks down more and more. Wang et al. [22] proposed three different deployment protocols that relocate mobile sensors once coverage holes are detected using Voronoi diagrams. In [23], the authors proposed a scheme called Co-Fi that relocates mobile nodes to replace low energy nodes. Authors in [24] developed three hole-movement strategies for moving an existing big hole in a way that either the total energy consumption is minimized or the power consumption of sensors is balanced.

The incompleteness of previous work motivates our research presented here. Our proposed hole and border detection algorithm is distributed and lightweight, and thus more suited to the energy constrained WSNs. It does not require flooding for gathering the topology information, as is the case in [10] or synchronization among nodes.

PROPOSED METHOD

In our algorithm we propose a mechanisms to detect and heal holes. Our hole detection mechanism deals with holes of various forms and sizes. We try to alert a limited number of nodes surrounding the hole, only those nodes have the task of moving and repairing the hole. And also all the holes are not moved instead the correct path is found and the node reallocation required for that path setup is done.

While designing a hole healing algorithm there are certain important things which should be considered. How to detect the hole, estimate its size, estimate the target location for the reallocation of the node etc.

Our DHD algorithm allows us to discover holes, to compute their characteristics and to discover the network boundary. In a second phase, HEAL performs a local healing where only the nodes located at an appropriate distance from the hole will be involved in the healing process. We define an attractive force that acts from the hole center and attracts the nodes towards the hole center. At the same time, a repulsive force is defined among nodes to minimize the overlapping among them. These forces will be effective in a limited area, which we call the HHA. The proposed algorithms consist of hole detection and hole healing steps. We first discuss how to detect and heal a single hole and then we show how to deal with several holes.

The identification of holes in a wireless sensor network is of primary interest since the breakdown of sensor nodes in a larger area often indicates one of the special events to be monitored by the network in the first place (e.g. outbreak of a fire, destruction by an earthquakes etc.). This task of identifying holes is especially challenging since typical wireless sensor networks consist of lightweight, low capability nodes that are unaware of their geographic location. But there is also a secondary interest in detecting holes in a network: recently routing schemes have been proposed that do not assume knowledge of the geographic location of the network nodes but rather perform routing decisions based on the topology of the communication graph. Holes are salient features of the topology of a communication graph. In the first part of this paper we propose a simple distributed procedure to identify no des near the boundary of

the sensor field as well as near hole boundaries. Our hole detection algorithm is based purely on the topology of the communication graph, i.e. the only information available is which nodes can communicate with each other.

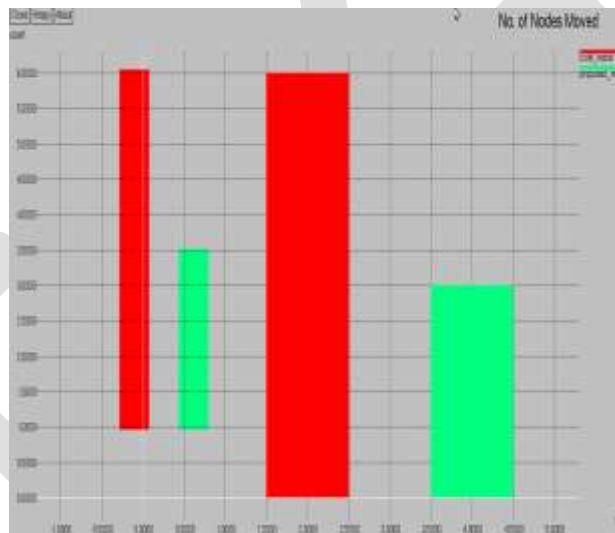
DHD is the algorithm used for the detection of the holes, it can detect multiple number of holes in WSN. DHD is a distributed and localized hole detection algorithm that operates over the Gabriel graph of the network. First we have to access the existence of a hole, which is done by identifying stuck nodes. All the nodes that are marked as stuck nodes. From this module we can identify the hole characteristics such as hole position and radius.

SIMULATION AND RESULT

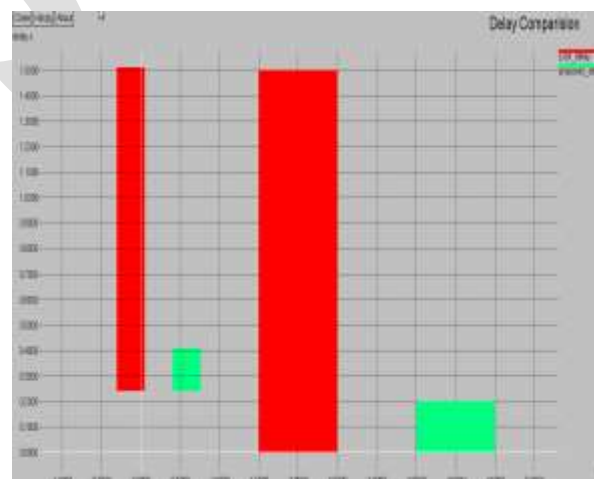
Holes are hindrance for the proper communication in the wireless sensor network. Here in this project these holes are detected automatically and healed by moving the nodes at the boundary of the hole.

We compare some performance characteristics of existing and the proposed systems. The no. of nodes moves and delay characteristics of of the proposed system with the existing technique is compared here. The results are showed in Xgraph

No. of nodes moved:The movement of nodes in the existing and proposed system is compared and examined. The Xgraph figure shown below represents this comparison.



Delay analysis:The figure below shows the delay comparison of the existing and the proposed system. The delay of the proposed system is much less than that of existing system.



CONCLUSION AND FUTURE WORK

This paper has proposed and implemented a lightweight and comprehensive two-phase protocol, HEAL, for ensuring area coverage employing a mobile WSN. The protocol uses a distributed DHD to detect holes in the network. Compared to the existing schemes, DHD has a very low complexity and deals with holes of various forms and sizes despite the nodes distribution and density. By exploiting the virtual forces concept, our approach relocates only the adequate nodes within the shortest time and at the lowest cost.

Through the performance evaluation, we validated HEAL, using different criteria and showed that it detects and heals the holes despite their number or size with less mobility in various situations. The evaluation results demonstrate that HEAL provides a cost-effective and an accurate solution for hole detection and healing in mobile WSNs. In the future, we plan to investigate the interaction between HEAL and the network layer for hole detection and healing. We are currently working on open holes located at the network boundary.

REFERENCES:

- [1] N. Ahmed, S.S. Kanhere, and S. Jha, "The Holes Problem in Wireless Sensor Networks: A Survey," SIGMOBILE Mobile Computing Comm. Rev., vol. 9, no. 2, pp. 4-18, 2005.
- [2] B. Wang, Coverage Control in Sensor Networks. Springer, 2010.
- [3] B. Kun, T. Kun, G. Naijie, L.D. Wan, and L. Xiaohu, "Topological Hole Detection in Sensor Networks with Cooperative Neighbors," Proc. Int'l Conf. Systems and Networks Comm. (ICSN '06), p. 31, 2006.
- [4] R. Ghrist and A. Muhammad, "Coverage and Hole-Detection in Sensor Networks via Homology," Proc. Fourth Int'l Symp. Information Processing in Sensor Networks (IPSN '05), pp. 254-260, Apr. 2005.
- [5] V. De Silva, R. Ghrist, and A. Muhammad, "Blind Swarms for Coverage in 2-D," Proc. Robotics: Science and Systems, pp. 335-342, June 2005.
- [6] F. Stefan, "Topological Hole Detection in Wireless Sensor Networks and its Applications," Proc. Joint Workshop on Foundations of Mobile Computing, p. 44-53, 2005.
- [7] J.W. Cai; P. Yi, Y. Tian, Y.K. Zhou, N. Liu, The Simulation and Comparison of Routing Attacks on DSR Protocol[C], WiCOM 2009, in press.
- [8] B. Sun; Y. Guan; J. Chen; U.W. Pooch, Detecting Black-hole Attack in Mobile Ad Hoc Networks[C]; 5th European Personal Mobile Communications Conference, 2003, 490-495.
- [9] A. Patcha; A. Mishra; Collaborative security architecture for black hole attack prevention in mobile ad hoc networks[C]; Radio and Wireless Conference, 2003, 75-78.
- [10] Spector, A. Z. 1989. Achieving application requirements. In Distributed Systems, S. Mullende
- [11] D. Boneh; C. Gentry; B. Lynn; H. Shacham. "Aggregate and Verifiably Encrypted Signatures from Bilinear Maps". Advances in Cryptology- EUROCRYPT'03: LNCS 2656. Berlin: SpringerVerlag, 2003. 416-432.
- [12] D.M. Shila; T. Anjali; Defending selective forwarding attacks in WMNs, IEEE International Conference on Electro/Information Technology, 2008, 96-101.
- [13] I.F. Akyildiz; X. Wang (2005). A Survey on Wireless Mesh Networks [J]. IEEE Communications Magazine, 43 (9), 23-30
- [14] D.S.J.D. Couto; D. Aguayo; J. Bicket; R. Morris, "A HighThroughput Path Metric for Multi-Hop Wireless routing," in ACM Mobicom, 2003.

[15] J.W. CAI; P. YI, Y. TIAN, Y.K. ZHOU, N. LIU, THE SIMULATION AND COMPARISON OF ROUTING ATTACKS ON DSR PROTOCOL [C], WICOM 2009, IN PRES

IJERGS

Automatic Detection of Brain Tumor Using Maximum Variance Standardization

Sreeja R, Radhakrishnan B

P.G Scholar, Dept of CSE, BMCE, Kollam, Kerala, India.

jaiharisree15@gmail.com, 9746149056

Abstract— this paper presents an automated diagnosis of brain abnormalities through the segmentation from MRI images. The main objective is to find out the difference between normal and abnormal brain. Most of the abnormalities in brain are seen in the form of tumor. The tumor has different intensity value compared to the surrounding tissue. We propose a method to find out the appropriate intensity for segmentation. We apply maximum variance standardization method to find out the appropriate intensity value for segmentation. Boundary of the abnormal region is calculated by using appropriate edge detection algorithm. Here variance is calculated from the column mean value of Input MRI image.

Keywords— Brain Tumor, MRI, Column mean, Variance, Standard Deviation, Segmentation, Average Intensity

INTRODUCTION

The National Cancer Institute (NCI) estimated that 1,658,370 new cases of cancer will be diagnosed in the United States in 2015 and 589,430 people will die from the disease. Each year in the United States, more than 35,000 people are told they have a tumor that started in the brain. American Brain Tumor Association (ABTA) clarifies this statistic further by estimating that 62,930 new cases of primary brain tumors would be diagnosed in 2010[1-3]. Image segmentation plays a critical role in all advanced image analysis applications, a key purpose of segmentation is to divide image into regions and objects that correspond to real world objects or areas, and the extent of subdivision depends on requirements of specific application. Complete segmentation of an image scene, where objects correlate with real world objects, cannot be usually achieved without inputs from the user or specific knowledge of the problem domain. Image feature selection is a significant prerequisite for most image processing algorithms, depending on these features the segmentation methods can be classified into three categories namely, thresholding, edge-based, region-based segmentation and classifier such as Hierarchical Self Organizing Map (HSOM)[9-10].

RELATED WORK

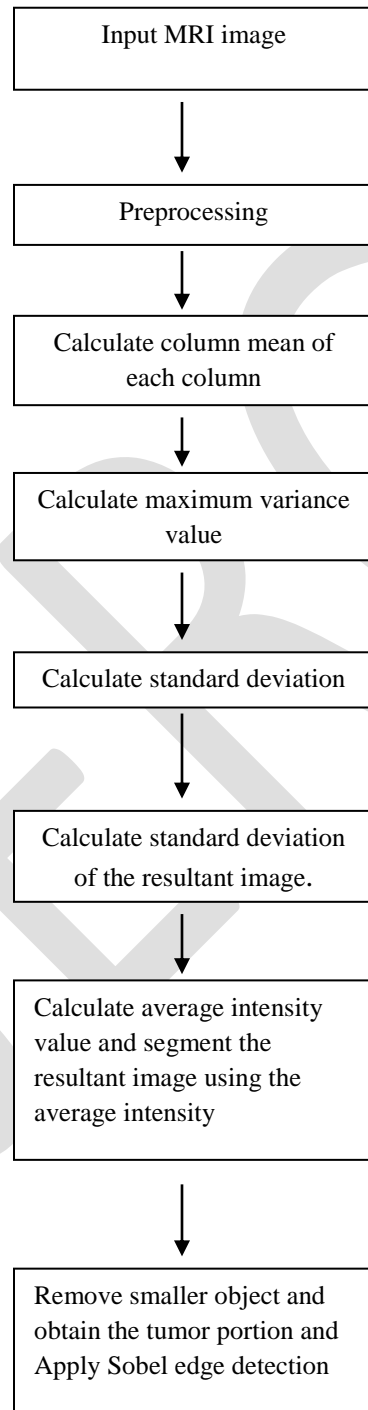
Image thresholding is the most popular segmentation method due to its intuitive properties and simple implementation [4]. Threshold selection plays a very crucial role for efficient segmentation results. Intuitively, the thresholds for multimodal histograms should be the minima between the two maxima. Some techniques sharpen the histogram peaks in image enhancement stage so as to facilitate the threshold detection. The main disadvantage of this method is the difficulty to separate object from background if the object and background are of the same intensity distribution or texture as in MRI-scans. Edge-based segmentation is described in terms of discontinuities in image attributes as Gray level, texture, color etc. These discontinuities are known as edges and are detected using edge detection operators, some of the commonly used operators are Sobel, Prewitt, Laplace, etc [5]. Segmentation resulting from edge-based method cannot be used as partial segmented output due to the presence of broken, stray, or noise edges. Advanced processing is required to obtain edges corresponding to meaningful objects. Several algorithms introduced for edge-based segmentation, the widely accepted segmentation methods are edge-image thresholding which is used to eradicate insignificant edges that occur due to factors such as noise and improper lighting conditions [5].

Edge image thresholding leads to stray edges in presence of noise where the actual edges are often missing [4]. Stray edges problem can be solved if the edge properties are determined with respect to the mutual neighbors, while presence of edge is substantiated depending on the strength of edges in local neighborhood [4]. Region-based segmentation is then used which is based on finding similarity measures to merge and split regions in an image so as to form semantic or useful division in the processed image. Self Organizing Map, SOM, as part of competitive learning neural network (CLNN) has been used to implement the vector quantization process [6-8]. The importance of SOM for vector quantization is primarily due to the similarity between the competitive learning process employed in the SOM and the vector quantization procedure. Neural units in the competitive layer need to be

approximately equal to the number of regions desired in the segmented image. It is not however, possible to determine a priori the correct number of regions in the segmented image. This is the main limitation of the conventional SOM for image segmentation.

PROPOSED WORK

In this paper we use the MRI images because the MRI images are clearer than CT images in the case of small tumor. Before the segmentation we have to prepare the image for segmentation by using some pre-processing methods.



A. Pre-processing

MRI image is converted in to grayscale image in which 0 represents black and 255 represents white. The input images may contain noises. Generally, there are two types of noises impulsive noise and Gaussian noise. So we apply median filter for removing noise. Then we apply the Gaussian filter to remove the Gaussian noise and apply adaptive filter for highlighting the edges.

B. Calculation of Column mean

For calculating the columns mean convert the pre-processed image in to double. Then calculate column mean using the following formula. An image A (i,j) and the column mean intensity of the image is obtained by summing the values of all row pixels for each column and dividing it by the number of rows.

$$I_{sum}(j) = \sum_{i=1}^M A(i, j)$$

$$\text{Columns mean (j)} = \frac{I_{sum}(j)}{\text{number of rows}}$$

Column mean is calculated for all columns. Where M is the number of row pixels.

C. Calculation of maximum variance and standard deviation

Variance is calculated for each column mean using the following formula. Usually intensity value of the tumor is relatively high with respect to its surrounding tissues. Thus, we choose the maximum variance for calculating standard deviation. Variance is calculated by using the following formula.

$$\text{Variance} = \frac{\text{sum of square of difference}}{m-1}$$

D. Calculate standard deviation

The standard deviation calculated from variance using the following formula:

$$\text{Standard Deviation} = \sqrt{\text{variance}}$$

Standard deviation is the square root of maximum variance. Thus we get a low value for the standard deviation, which indicates that they are clustered closely around the mean. The tumor intensity pixels are far away from mean so it is impossible to segment tumor tissues from surrounding tissues using standard deviation. The intensity value greater than or equal to standard deviation is set to 255 and the intensity less than standard deviation is set to 0.

$$K(i, j) = \begin{cases} 255 & \text{if } A(i, j) \geq \text{Standard Deviation} \\ 0 & \text{if } A(i, j) < \text{Standard Deviation} \end{cases}$$

E. Calculate standard deviation of the resultant image.

The standard deviation of the resultant image is recomputed as follows

$$\text{Standard Deviation}_{new} = \text{Standard Deviation}[K(i, j)]$$

The value of $\text{Standard Deviation}_{new}$ is a large value, which indicate values are far from the mean. Thus the data cover large range so we choose this value for setting the threshold value.

F. Calculate average intensity value and segment the resultant image

Using the new standard deviation an average value of intensity is calculated using the following equation.

$$I_{avg} = \frac{\sum_{i=0}^M \sum_{j=0}^N (A(i, j) | A(i, j) > \text{Standard Deviation}_{new})}{l}$$

Where, l is the total number of pixels having intensity values greater than $\text{Standard Deviation}_{new}$. The I_{avg} value is taken as a threshold value to segment the tumor from the original image. The intensity value greater than or equal to I_{avg} be set to 255 and the intensity less than I_{avg} is set to 0.

$$L(i, j) = \begin{cases} 255 & \text{if } A(i, j) \geq I_{avg} \\ 0 & \text{if } A(i, j) < I_{avg} \end{cases}$$

G. Remove smaller object and obtain the tumor portion and Apply Sobel edge detection

Label the connected component of image L (i,j) with 8 connected neighborhoods. Using regionprops function in Matlab identifies the area of the connected components. Then remove the components having an area less than the predefined value. This gives the tumor portion.

To find the boundary of the tumor Sobel edge detection is used.

$$I_x = \frac{\delta f}{\delta x} = (z_7 + 2z_8 + z_9) - (z_1 + 2z_2 + z_3)$$
$$I_y = \frac{\delta f}{\delta y} = (z_3 + 2z_6 + z_9) - (z_1 + 2z_4 + z_7)$$

Where I_x and I_y are images of same size as the original is obtained by filtering image by Sobel mask. Compute the gradient magnitude of the image that is the value of the rate of change in the direction of the gradient vector.

$$\text{Gradient Magnitude} = \sqrt{I_x^2 + I_y^2}$$

Using the gradient magnitude tumor boundary is detected.

CONCLUSION

We propose maximum variance standardization for brain tumor Detection in this work. The proposed method uses threshold based segmentation for brain tumor detection. As appropriate values of threshold are taken, the performance of the proposed detection system is high.

REFERENCES:

- [1] American Brain Tumor Association (2010). Facts and Statistics 2010 retrieved from <http://www.abta.org/sitefiles/pdflibrary>.
- [2] Central Brain Tumor Registry of the United States. (2010). CBTRUS statistical report: Primary brain and central nervous system tumors diagnosed in the United States in 2004–2006. Retrieved from <http://www.cbtrus.org/2010-NPCR-SEER/CBTRUS - WEBREPORT-Final-3-2-10.pdf>
- [3] Sidney Croul, Jessica Otte and Kamel Khalili, "Brain tumors and polyomaviruses", Journal of NeuroVirology, 9: 173–182, 2003
- [4] D. Shevad, "Multiple object segmentation and tracking in image sequence," Lamar University -Beaumont, April 2005.
- [5] R. Gonzalez and R. Woods, Digital Image Processing, 3rd Edition. Prentice Hall, 2008.
- [6] Alexander Statnikov, "Automatic cancer diagnostic decision support system for gene expression domain", Thesis, August, 2005.
- [7] M.M.Ibrahiem, E Emary and S. Ramakrishnan, "On the Application of Various Probabilistic Neural Networks in Solving Different Pattern Classification Problems," World Applied Sciences Journal, Vol. 4 No. 6, pp. 772-780, 2008.
- [8] S.Asif Hussain and M. Praveen Raju, "Neuro-Fuzzy System for Medical Image Processing" Proceedings of the Inter. Conf. on Comm. and Computational Intellig., pp.382-385, India. Dec., 2010.
- [9] D. Shevad, "Multiple object segmentation and tracking in image sequence," Lamar University -Beaumont, April 2005.
- [10] T.Logeswari and M. Karnan, "An Improved Implementation of Brain Tumor Detection Using Segmentation Based on Hierarchical Self Organizing Map", International Journal of Computer Theory and Engineering, Vol. 2, No. 4, August, 2010.

[11] Dina Aboul Dahab¹, Samy S. A. Ghoniemy², Gamal M. Selim³, International Journal of Image Processing and Visual Communication ISSN (Online)2319-1724 : Volume 1 , Issue 2 , October 2012.

[12] Pabitra Roy, Sudipta Roy, Prof. Samir Kumar Bandyopadhyay, International Journal of Advanced Research in Computer Science and Software Engineering Volume 3, Issue 11, November 2013.

IJERGS

COMPRESSION OF SENSOR DATA IN DIGITAL CAMERAS BY PREDICTION OF PRIMARY COLORS

Akshara M, Radhakrishnan B

PG Scholar, Dept of CSE, BMCE, Kollam, Kerala, India

aksharaa009@gmail.com

Abstract— The Color Filter Array is a mosaic of tiny color filters placed over the pixel sensors of an image sensor to capture color information. CFA image is divided into 4 sub images. Each sub image contains G1, G2, R and B color components. G1 is encoded by using any conventional gray scale encoding technique. G2 is predicted from encoded G1 values which produces the prediction error $e\delta G2$. Then, the G pixels are interpolated to fill in the G values at the positions of the R and B pixels. Fourth, these interpolated G pixels are subtracted from the R and B pixels, producing δR . δR is predicted from encoded G1 value, predicted G2 value and already encoded R value produces the prediction error of red. δB is predicted from encoded G1 value and from both predicted G2 and B value and also from already encoded B value produces the prediction error of blue. The error signals obtained by the prediction block are fed into an entropy encoder. The choice of predictors and weights is of course based on the direction of edges around the x. We define the edge directivity around x and take smallest two of them and they are used for the calculation of weight and then by using the weight and predictors actual value is estimated. After estimating the value of G2, R and B, three errors are calculated. These three errors are fed into an entropy encoder like Huffman encoder and they are separately encoded. Then bits per pixel and compression ratio are calculated. It can be decoded by using a Huffman decoder. From images that are outputted by Huffman decoder, mosaic image is created by inverse prediction. After applying demosaicing and color reconstruction techniques, we get the original full color image.

Keywords—Color Filter Array, JPEG-LS, Huffman encoding and decoding, Gamma correction, White balance, Bilinear interpolation, Edge directivity

INTRODUCTION

In analogue cameras images are captured in a photographic film. The film and paper needs much processing inside a darkened room to get a clear image. Digital photography doesn't need dark room, film or chemicals. Image is captured with an array of photo sensors. This array is termed as color filter array. Conventional color filter array contains 3 sensors at each pixel position to capture primary colors ie, red, blue and green. Every other colors can be made by using these three colors. In order to reduce cost and size, today's digital cameras make use of one sensor at each pixel position. The rest two colors are determined by a process called demosaicing. Among all color filter arrays, Bayer color filter array is the most popular one. Figure 1 shows Bayer color filter array[1].

G1	R1	G1	R1	G1	R1
B1	G2	B1	G2	B1	G2
G1	R1	G1	R1	G1	R1
B1	G2	B1	G2	B1	G2

Figure 1 Bayer color filter array[1]

There are several demosaicing algorithms exist for attaining high image quality [2]. Efficient interpolation algorithms exists produce images that are similar to the original image. In conventional approaches, demosaicing is performed first. After the demosaicing process, compression is performed. This increases the number of bits for compression. So the compression ratio will be low. If compression is performed first, we can achieve better compression ratio since the number of pixels used for compression is

less. So we prefer compression first scheme[3-7]. Figure 2.a shows Demosaicing first scheme and figure2.b shows compression first scheme. Image reconstruction includes color correction such as white balance, gamma correction and color correction.

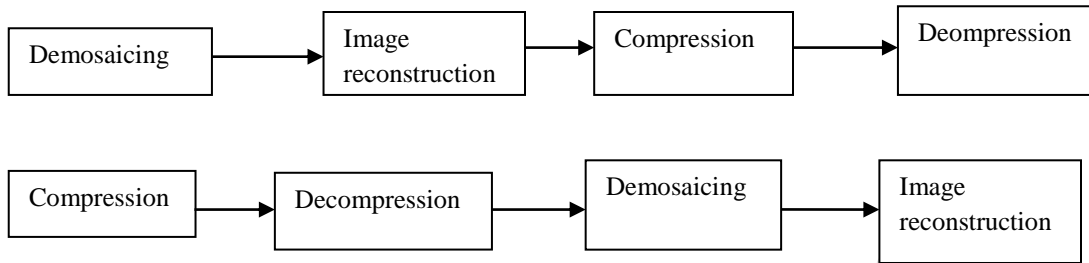


Figure 2 a) Demosaicing first scheme b) compression first scheme

In this paper a modified compression method using prediction is applied. Section 1 is proposed method, that includes compression of G1 sub image, compression of G2 sub image, compression of R and B sub images, section, error encoding, decoding and inverse prediction, bilinear interpolation and image reconstruction methods. Section 2 deals with

Proposed Method

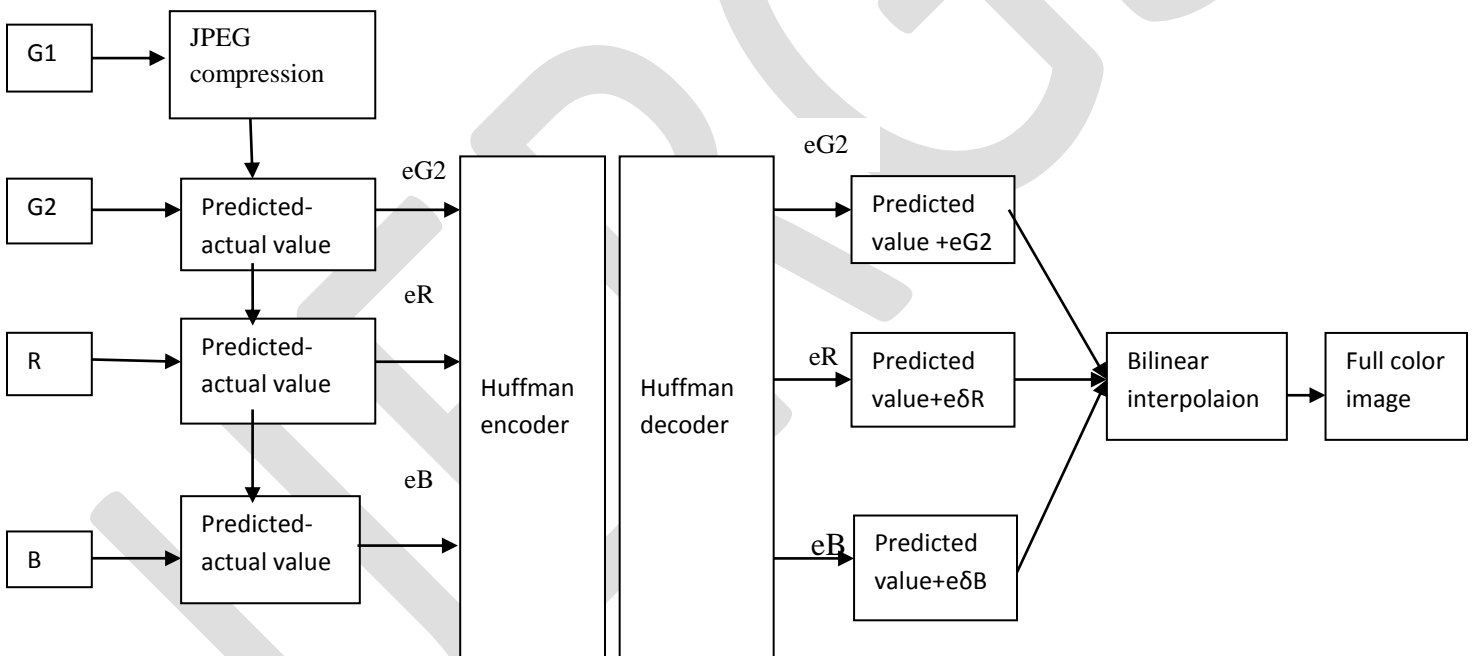


Figure 3 block diagram for lossless compression

The captured image from a camera is converted into a Bayer pattern mosaic image. From the bayer pattern, G1 sub image is separated and encoded using JPEG-LS[8] compression algorithm. Predicted G2 value is calculated from already encoded G1 sub image and pixels of already encoded G2 value. R value is calculated from already encoded G1 and G2 value and also from the already encoded pixels of red. B value is predicted from predicted values of G1, G2 and R and from already encoded pixels of B. Errors is calculated by subtracting predicted image from actual image. Errors are modeled and then compressed by Huffman encoding. Huffman decoding is performed and image is reconstructed using demosaicing technique.

1. Prediction of primary colors

G1 sub image is encoded by using jpeg compression method. This encoded value is used for predicting all other color components. Jpeg lossless compression is an efficient method for compression. The JPEG standard specifies the codec, which defines how an image is compressed into a stream of bytes and decompressed back into an image, but not the file format used to contain that stream. G2 sub image is predicted from encoded G1 sub image and also from already encoded pixels of G2 sub image. We define four predictors in four directions. Among them we take best two predictors. The predictors are:

G11	R12	G13	R14	G15	R16
B21	G22	B23	B24	B25	G26
G31	R32	G33	R34	G35	R36
B41	G42	B43	X	B44	G45
G51	R52	G53	R54	G55	R56

Fig 4 G2 predictor

$$ph = B24, pv = G42, pr = G35 + G53/2, pdl = G33 + G55/2$$

Edge directivity in these 4 directions can be calculated by the following equation.

$$Dir = \frac{\text{pixel difference in the direction of } X}{\text{difference between pixel pairs}}$$

From the all four edge directivity values, smallest and second smallest values are taken, which denote Dir1 and Dir2 respectively.

Weight can be calculated by using the equation $w1 = Dir1 + 1$ and $w2 = Dir2 + 1$

The G2 sub image can be calculated by using the equation $G2 = \frac{P1 \times w1 + P2 \times w2}{w1 + w2}$ where p1 and p2 will be the predictors in the direction of D1 and D2.

The value of Green at positions of red and blue have to be calculated. For that the same procedure used for G2 prediction is used. In order to find the real R and B values, we have to subtract the interpolated green value from the R and B values to yield δR and δB . For further prediction of red and blue colors we use δR and δB instead of R and B values. δR and δB predictions are carried out by following the same procedure that is used for G2 prediction. Firstly, four directional predictors are defined for δR and δB . After that four edge directivity values are calculated. Then final predicted value is calculated by using best two predictors and their weights for both δR and δB .

2. Error Encoding

The prediction errors for primary colors are determined by subtracting the prediction value from the actual value of image which yields three error images. These images are fed as input for Huffman encoder[10]. Huffman encoding is a lossless image compression technique. Huffman coding is well suited for gray scale image compression. Since the error images obtained are gray scale, the compression ratio is high.

3. Error decoding and inverse prediction

Error decoding is carried out by Huffman decoding algorithm. Encoded error image is fed as input for Huffman decoder. It recreates three error images. Inverse prediction is applied to the three error images and has to recreate green, red and blue sub-image. Combining these three images will create a mosaic image. Demosaicing is applied on this mosaic image to get the full color image.

4. Bilinear interpolation

Bilinear interpolation takes the closest 2×2 grid surrounding the unknown pixel. The four surrounding pixels are averaged to get the interpolated value of unknown pixel. This interpolation method yields smoother image compared to nearest neighbor interpolation method. Figure 4 shows bilinear interpolation.

5. Image reconstruction

Image reconstruction phase includes white balance, gamma correction and color correction to get a better quality full color image. Without gamma correction, the pictures captured by digital cameras will not look like original image. White balance is based

on color temperature. Digital cameras have great difficulty in auto white balance. Since this is a lossless compression method, the image obtained is an exact replica of the original image.

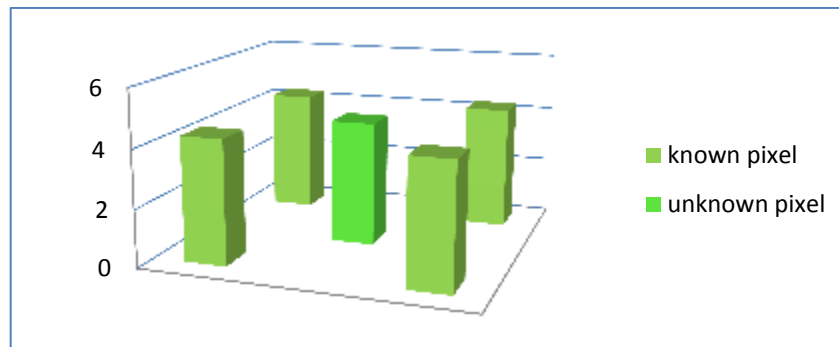


Figure 4 bilinear interpolation

PERFORMANCE EVALUATION

In the proposed method, the lossless compression algorithm is applied to figure 5a. The demosaiced image is shown in figure 5b and the final reconstructed image is shown in figure 5c. The bits per pixel value obtained for this method is 2.6550 and the compression ratio is high compared to other existing methods.



Figure 5a. Original image 5b. Decoded demosaiced image 5c. Output image

CONCLUSION

Here proposed a prediction based lossless compression method that uses primary colors such as green, blue and red. Bayer pattern is the most popular color filter array. G1 sub-image is predicted by using lossless JPEG compression algorithm. The order for predicting colors are green, red and blue respectively. Error is calculated by subtracting the predicted image from actual image. These three error images are generated for green, red and blue. These three error images are fed as input for Huffman encoder. After transmission and storage, it can be decoded using Huffman decoding algorithm. From the decoded images, we can reconstruct the mosaic image. After performing, demosaicing and image reconstruction technique, we get the full color image. This methods yields good image quality and also less bits per pixel compared to other existing methods.

REFERENCES:

- [1] B. E. Bayer, "Color imaging array," U.S. Patent 3 971 065, Jul. 1976.
- [2] B. K. Gunturk, J. W. Glotzbach, Y. Altunbasak, R. W. Schafer, and R. M. Mersereau, "Demosaicking: Color filter array interpolation," IEEE Signal Process. Mag., vol. 22, no. 1, pp. 44–54, Jan. 2005.
- [3] S. Y. Lee and A. Ortega, "A novel approach of image compression in digital cameras with a Bayer color filter array," in Proc. IEEE Int. Conf. Image Process., Oct. 2001, pp. 482–485.

- [4] R. Lukac and K. N. Plataniotis, "Single-sensor camera image compression," *IEEE Trans. Consum. Electron.*, vol. 52, no. 2, pp. 299–307, May 2006.
- [5] N. Zhang and X. L. Wu, "Lossless compression of color mosaic images," *IEEE Trans. Image Process.*, vol. 15, no. 6, pp. 1379–1388, Jun.2006.
- [6] H. S. Malvar and G. J. Sullivan, "Progressive-to-lossless compression of color-filter-array images using macropixel spectral-spatial transformation," in *Proc. DCC*, 2012, pp. 3–12.
- [7] K. H. Chung and Y. H. Chan, "A lossless compression scheme for Bayer color filter array images," *IEEE Trans. Image Process.*, vol. 17, no. 2, pp. 134–144, Feb. 2008.
- [8] Information Technology–Lossless and Near-Lossless Compression of Continuous-Tone Still Images (JPEG-LS), ISO/IEC Standard 14495-1, 1999.
- [9] K. H. Chung and Y. H. Chan, "A fast reversible compression algorithm for Bayer color filter array images," in *Proc. APSIPA*, 2009, pp. 825–888.
- [10] Shruti Porwal , Yashi Chaudhry Jitendra Joshi Manish Jain , " Data Compression Methodologies For Lossles Data And Compression Between Algorithms", In Issn 2319-5967 Volume 2, Issue 2, March 2013
- [11] www.cpn.canoneurope.com/content/education/infobak/introduction_to_digital_photography_/differences_between_analogue_and_digital.do
- [12] www.cambridgeincolour.com/tutorials/white-balance.html

Analysis of SVD Watermarked Medical Images using Fuzzy Logic

Sumit Kumar Verma[#], Er. Poonam Beniwal[#]

[#]M.Tech Scholar, ECE Department OITM, Assistant Professor
Address

sumit4390@yahoo.in, poonambeniwal249@gmail.com

Abstract— A new image watermarking scheme has been developed which combines Singular Value Decomposition and its FFT form (i.e. FFT-SVD). It consumes a lot of less resources, also it computes a larger set of data faster without effecting the quality of the original image. The proposed scheme has been simulated in MATLAB environment.

Keywords— FFT, SVD, Medical Image, Watermarking, DFT, DCT, LPF.

INTRODUCTION

In recent years the use of Internet as a platform for distribution of digital multimedia data (such as audio, video, image) has been grown. Digital data can be stored efficiently and it can be transmitted in a fast and inexpensive way through data communication networks without losing its quality. Digital data can be easily copied from original one and the copied version is similar to original data. This creates serious concerns about illegal use and manipulation of digital data. Hence copyright protection and content integrity become an important issue. Previously digital content were protected using encryption techniques but encryption alone is not sufficient to protect digital data for long time as because in encryption process digital content has to be decrypted to get the hidden information and after the decryption the digital contents are no more being encrypted and can be easily manipulated and distributed.

Therefore it leads to a creation of a new information-hiding form, called digital watermarking. In this process the copyright information is embedded into the original digital content which is to be protected from the illegal distribution. The embedded watermark should be imperceptible and it should be robust enough to survive to attacks. The hidden information may be the serial number, random number sequence, copyright information, ownership identifiers, control signals, transaction dates, text, image, or other digital formats. Watermarking is similar to steganography and some discrete features of watermarking make it popular for information/data hiding over steganography. Applications of digital watermarking incorporate copyright protection, fingerprinting, authentication, copy control, tamper detection, and data hiding applications such as broadcast monitoring.

SINGULAR VALUE DECOMPOSITION

Recently watermarking schemes based on Singular Value decomposition (SVD) have gained popularity due to its simplicity in implementation and some attractive mathematical features of SVD. The SVD for square matrices was first introduced independently by Beltrami and Jordan in 1870s and then was extended to rectangular matrices by Eckart and Young in 1936. Later, this mathematical tool demonstrated its usefulness in a variety of applications including image processing and watermarking. The important inherent properties of SVD from the view point of image processing applications which makes it popular to use are:

1. Singular Values (SVs) are stable i.e. any change to it doesn't affect the image quality.
2. SVs are able to represent inherent algebra properties of digital image.
3. SVD preserves both one-way and non-symmetric properties, which are not available using DCT or DFT transformations.
4. The size of matrices can be square or rectangular in SVD.
5. SVs are known to be invariant to some common attacks such as JPEG compression, noise addition, low pass filter (LPF), rotation, scaling and cropping. If A is an image of size $n \times n$, then SVD of A is shown as below form

$$\text{SVD}(A) = USV^T \quad (1)$$

Where U and V are orthogonal matrices, $UU^T=I$ and $VV^T=I$. Columns of U and V are called as left and right singular vectors respectively. S is a diagonal matrix of singular values σ_i , $i=1,2,\dots,n$ arranged in decreasing order and elements of S matrix are zero except diagonal elements. Therefore

$$SVD(A) = \begin{pmatrix} U_{11} & \dots & U_{1n} \\ U_{21} & \dots & U_{2n} \\ \vdots & \ddots & \vdots \\ U_{n1} & \dots & U_{nn} \end{pmatrix} \begin{pmatrix} \sigma_{11} & \dots & 0 \\ \vdots & \ddots & \vdots \\ 0 & \dots & \sigma_{nn} \end{pmatrix} \begin{pmatrix} V_{11} & \dots & V_{1n} \\ V_{21} & \dots & V_{2n} \\ \vdots & \ddots & \vdots \\ V_{n1} & \dots & V_{nn} \end{pmatrix}^T$$

$$= \sum_{i=1}^r \sigma_i u_i v_i^T$$

RESULTS

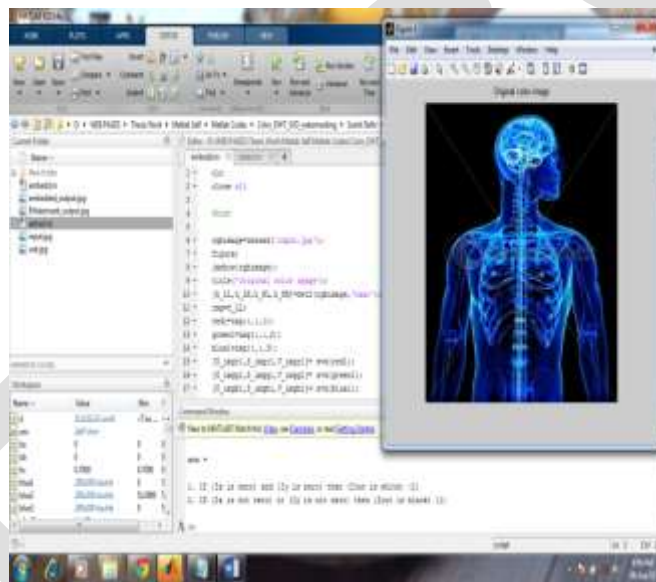


Fig-1 Original input image

The input color image of dimension 400x400 of size 60.8kb is used as an input for analysis.

INPUT IMAGES:



Image-1



Image-2



Image-3

OUTPUT IMAGES:



Output Image-1



Output Image-2



Output Image-3



Fig-2 Input watermark image

The size of the input watermark image is 38.2 kb, having dimension of 400x400

The above image is in gray scale format.

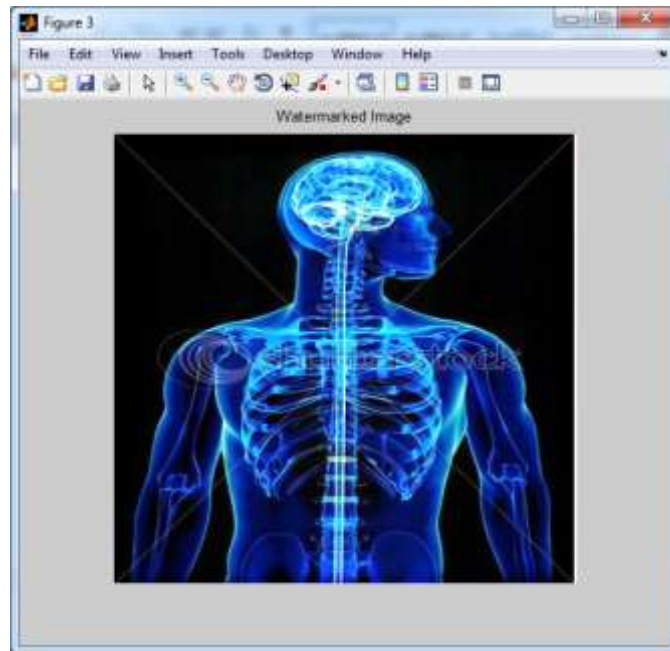


Fig-3 Input watermarked image

The output image is watermarked of the two images, almost no quality change in the image as shown above.

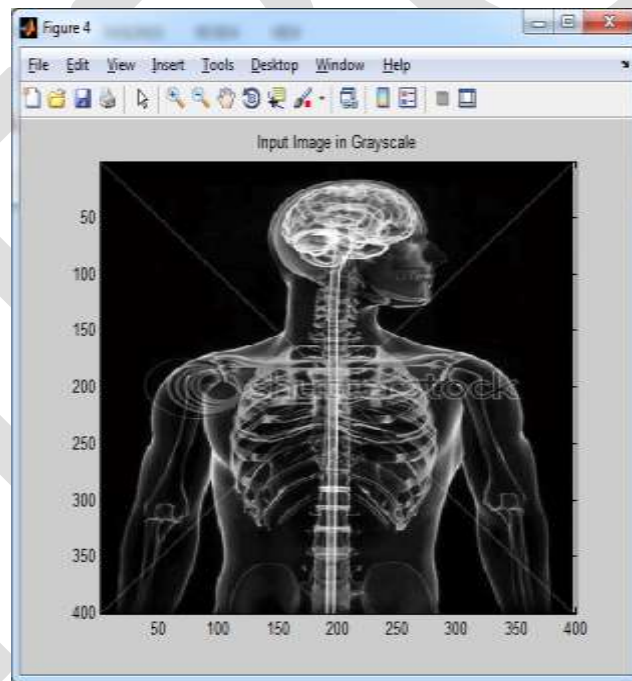


Fig-4 Image for fuzzy analysis

Input image converted in gray scale for fuzzy analysis in MATLAB

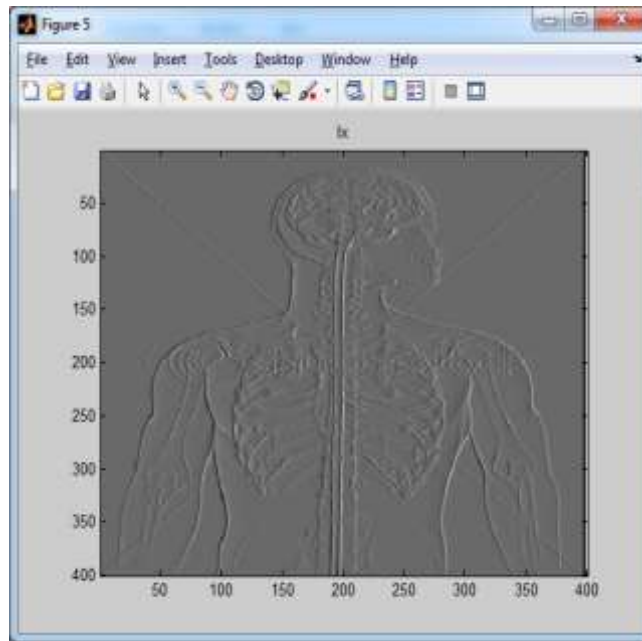


Fig-5 Fuzzy Inference System along Ix

After specifying the image gradient, Ix as the inputs of edge FIS. The output is shown as above. The fuzzy inference system present an output along vertical direction.

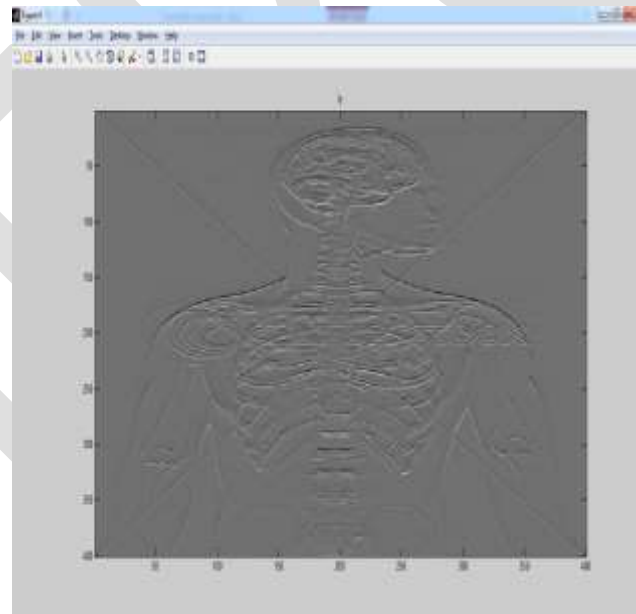


Fig-6 Fuzzy Inference System along Iy

After specifying the image gradient, Iy as the inputs of edge FIS. The output is shown as above. The fuzzy inference system present an output along horizontal direction.

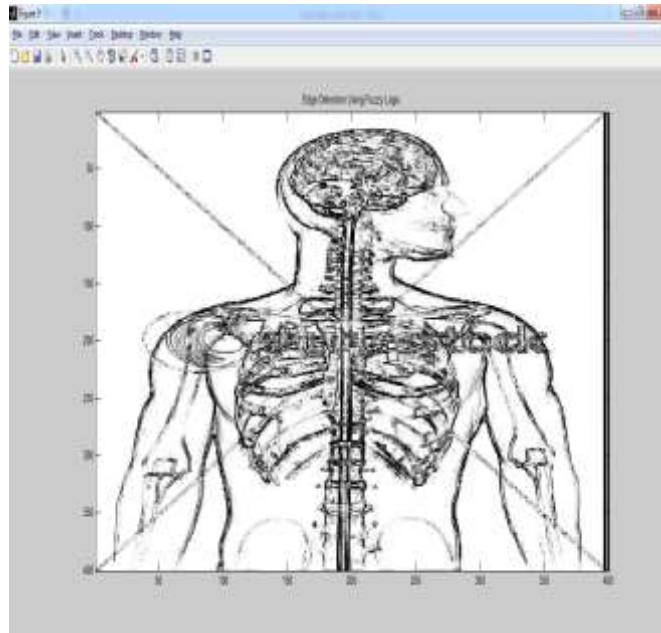


Fig-7 Edge detection using fuzzy

As we can with s_x and s_y , can change the values of w_a , w_b , w_c , b_a , b_b , and b_c to adjust the edge detector performance. The triplets specify the start, peak, and end of the triangles of the membership functions. These parameters influence the intensity of the detected edges.

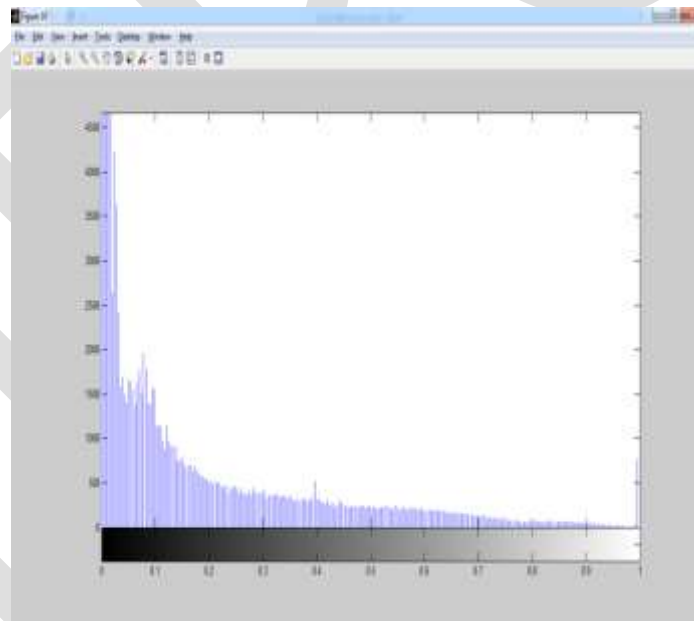


Fig-8 Histogram of the image

The histogram for the intensity image I and displays a plot of the histogram. The number of bins in the histogram is determined by the image type. If I is a grayscale image, `imhist` uses a default value of 256 bins. If I is a binary image, `imhist` uses two bins



Fig-9 Enhance the contrast of image using histogram equalization

Enhancing the contrast of image by transforming the values in an intensity image, or the values in the color map of an indexed image, so that the histogram of the output image approximately matches a specified histogram.

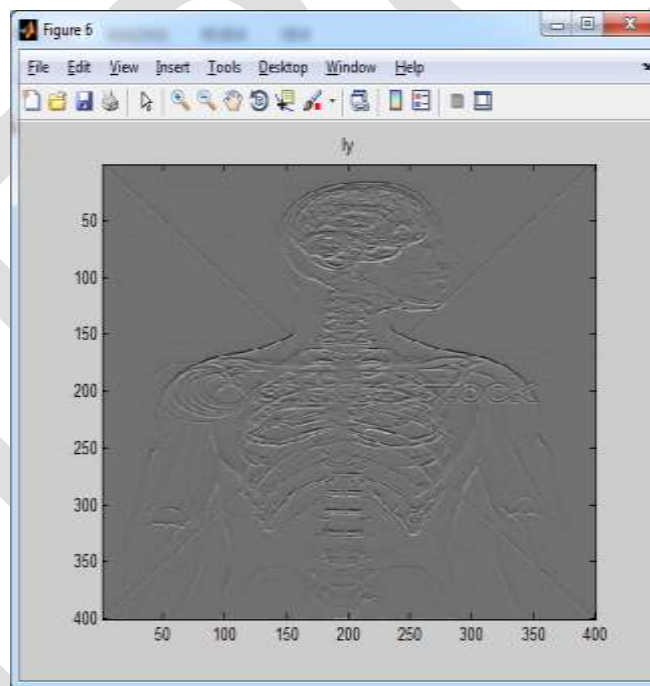


Fig-10 The output after specifying the image gradient

After specifying the image gradient, I_y as the inputs of edge FIS. The output is shown as above. The fuzzy inference system present an output along horizontal direction.

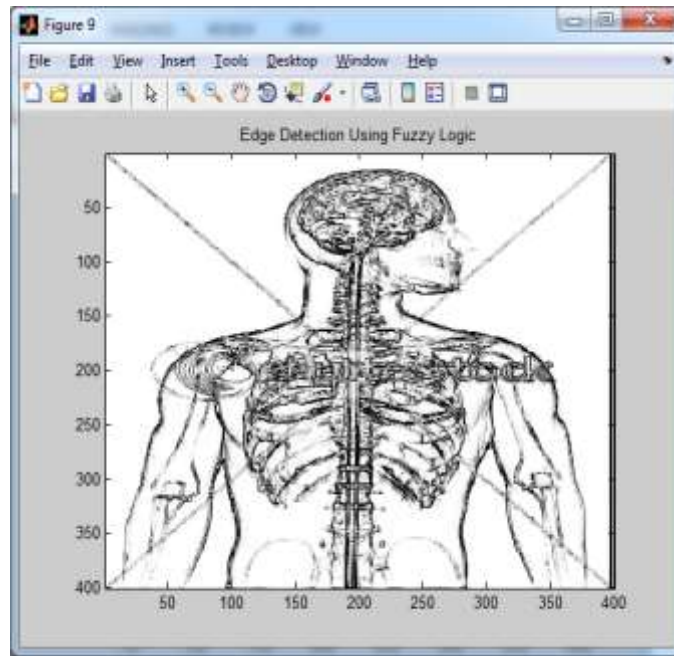


Fig-11 Evaluating fuzzy inference system (FIS)

The above result is obtained by evaluating fuzzy inference system (FIS). The output of the edge detector for each row of pixels in I using corresponding rows of I_x and I_y as inputs.

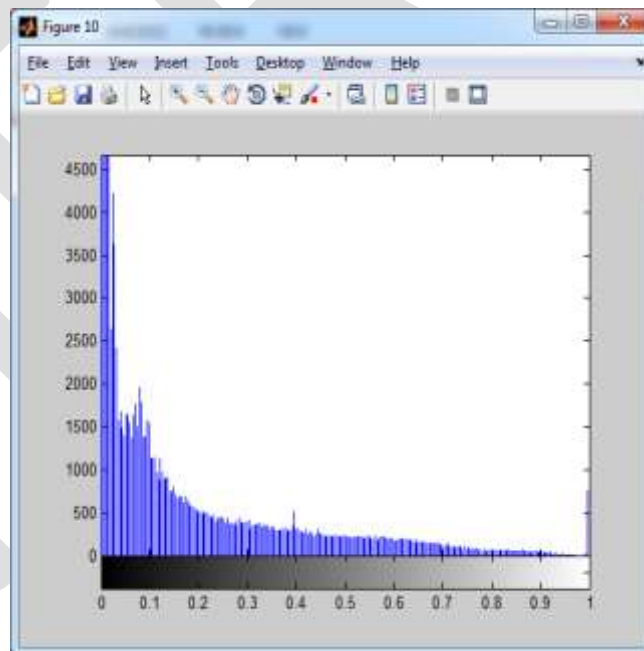


Fig-12 The histogram

The histogram is calculated by using `imhist(I)` which calculates the histogram for the intensity image I and displays a plot of the histogram. The number of bins in the histogram is determined by the image type. If I is a grayscale image, `imhist` uses a default value of 256 bins. If I is a binary image, `imhist` uses two bins.

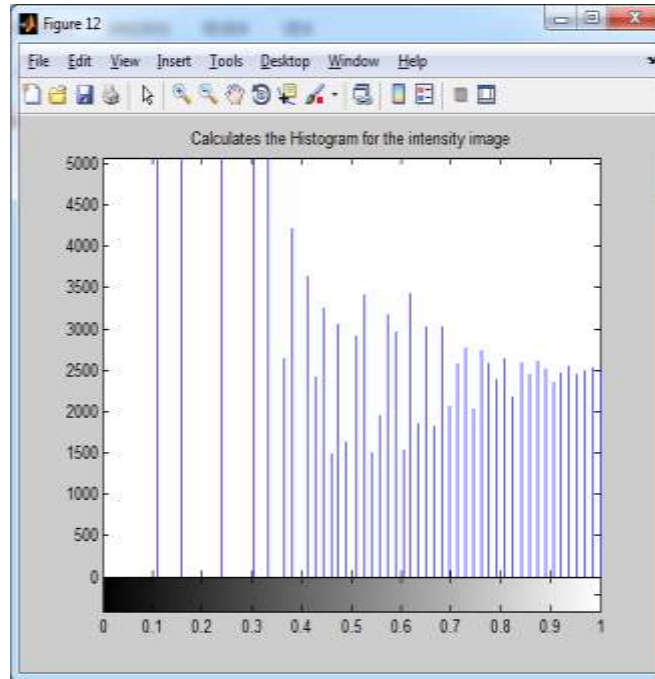


Fig-13 The histogram

The histogram is calculated by using `imhist(I)` which calculates the histogram for the intensity image I and displays a plot of the histogram. The number of bins in the histogram is determined by the image type. If I is a grayscale image, `imhist` uses a default value of 256 bins. If I is a binary image, `imhist` uses two bins. The resultant output is shown in fig 5.15 the output is of gray scale image which is used as input for fuzzy analysis.

Extraction

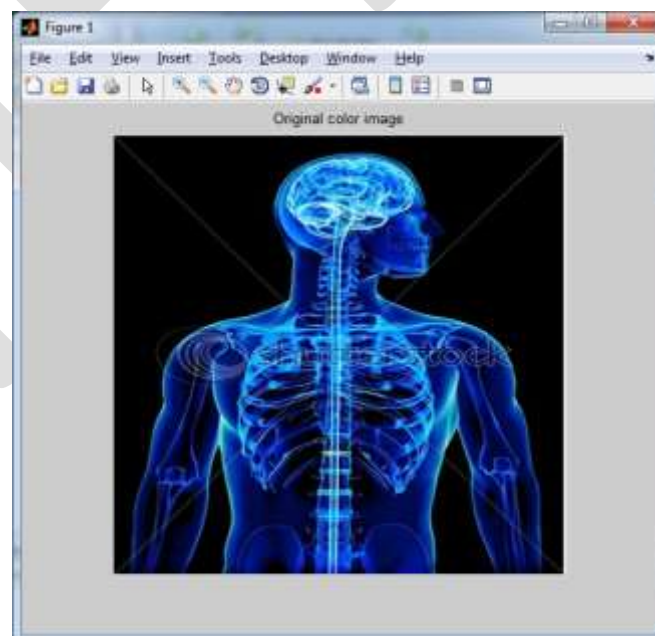


Fig-14 Input image of 60 kb in RGB format

Name	Type of	Result
Input image1	Psnr by salt and pepper	17.2630
	Snr	7.3508
	Psnr by poission noise	26.3139
	Snr	24.3904
Input image2	Psnr by salt and pepper	29.2630
	Snr	8.7508
	Psnr by poission noise	22.5100
	Snr	24.5004
Input image3		
	Psnr by salt and pepper	24.5475
	Snr	16.5092
	Psnr by poission noise	23.3003
	Snr	21.3809
Out image1	Psnr by salt and pepper	11.9375
	Snr	16.5992
	Psnr by poission noise	28.3563
	Snr	25.3829
Out image2	Psnr by salt and pepper	20.0298
	Snr	13.4650
	Psnr by poission noise	30.5171
	Snr	29.9522
Out image3	Psnr by salt and pepper	27.0200

	Snr	14.9650
	Psnr by poisson noise	10.5171
	Snr	29.9522



Fig-15 The extracted watermark, slightly change in quality, but the information is clearly visible.

The size of the image is 30kb.

CONCLUSIONS

Aiming at the medical images security problem during storage and transmission, we provides watermark method to protect it, and these method can be able to achieve integrity detection and accurate tampering localization. This method adopts image block, chaotic modulation in watermark information and encryption it. The watermark information will be embedded to original medical image. The proposed algorithms have the watermarked medical images with high and stable quality. The PSNR of the input image and the output image is almost same. This shows after decrypting the image the quality of the image is intact.

REFERENCES:

1. R. Liu and T. Tan, "A SVD-Based Watermarking Scheme for Protecting Rightful Ownership," in IEEE Transactions on Multimedia, 4(1), pp. 121-128, March 2002.
2. A. Sverdlov, S. Dexter, A. M. Eskicioglu, "Robust DCT-SVD Domain Image Watermarking for Copyright Protection: Embedding Data in all Frequencies " EUSIPCO 2005, Antalya, Turkey, September 4-8, 2005.
3. E. Ganic and A. M. Eskicioglu, "Secure DWT-SVD Domain Image Watermarking: Embedding Data in All Frequencies," ACM Multimedia and Security Workshop 2004, Magdeburg, Germany, September 20-21, 2004.
4. R. Kakarala and P.O. Ogunbona, "Signal analysis using multiresolution form of the Singular Value Decomposition", IEEE Trans. On Image processing, vol. 10, No. 5, May 2001.
5. R. Ashino, et al, "Comparing Multi resolution SVD with Other Methods for Image Compression", Proc. Fourth ISAAC Congress (York University), 2003.
6. M. Yoshikawa, et. al., "Case study on SVD multi resolution analysis", Scientific Proceedings of Riga Technical University, Series 5, Computer Science, 2005
7. B. Akhbari and S. Ghaemmaghami, "Watermarking of still images using multi resolution singular value decomposition", proceedings of International Symposium on Intelligent Signal Processing and Communication Systems, Hong Kong, pg. 325-328, Dec 2005.
8. Chih-Chin Lai, Member, IEEE, and Cheng-Chih Tsai, "Digital Image Watermarking Using Discrete Wavelet Transform and Singular Value Decomposition", IEEE Transactions on Instrumentation and Measurement, VOL. 59, NO. 11, Nov 2010.

9. S.Rastegar,F.Namazi,K. Yaghmaie,A. Aliabadian, “Hybrid watermarking algorithm based on Singular Value Decomposition & Radon Transform”, International Journal of Electronics & Communication,Elsevier,pp-658-665, Sep 2010.
10. R. Liu and T. Tan,” An SVD-based watermarking scheme for protecting rightful ownership”, IEEE Trans. Multimedia, vol. 4, no. 1, pp. 121–128, Mar. 2002
11. Li Y, Wang X, “A watermarking method combined with Radon transform and 2D wavelet transform”, Int: Proc. of the 7th world Congress on Intelligent Control and Automation, pp.4586-90, 2008.
12. S. Majumder, T. S. Das, Subir Kumar Sarkar. “BPNN and SVD based Watermarking Scheme”, International Journal of Recent Trends in Engineering [ISSN 1797-9617]DOI: 01.IJRTET 04.01.3, pg 44-47 of Volume 4 No. 1 , February 2011.
13. A. Basu, T S Das, A. Das and S.K. Sarkar, “Visual Quality Metrics For Digital Watermarking”, Journal of Materials Science Letters-Springer,2011
14. S Majumder, T S Das, S Sarkar, S K Sarkar , “SVD and lifting wavelet based fragile Image watermarking”, International journal of recent trends in engineering, Vol. 3
15. S.Majumder, M.Mishra and A.D. Singh, “A Hybrid SVD and Wavelet based Watermarking”. Proceedings of 2nd National Conference Mathematical Techniques: Emerging Paradigms for Electronics and IT Industries (MATEIT '08), pg 197-201,2008.
16. Sujata Swarnalipi, S. Majumder, T.S. Das, S.K. Sarkar, ”Binary Logo Watermarking Based on Multi resolution SVD”, International Conference on Computing and Control Engineering, Chennai, India, ISBN 978-1-4675-2248-9, April,2012

Noise Cancellation using Adaptive Filters Algorithms

Suman, Poonam Beniwal

Department of ECE, OITM, Hisar, bhariasuman13@gmail.com

Abstract— Active Noise Control (ANC) involves an electro acoustic or electromechanical system that cancels the primary (unwanted) noise based on the principle of superposition. An anti-noise signal of equal amplitude and opposite phase is generated and combined with the primary noise, resulting in the cancellation of the noise. A fundamental problem to be considered in ANC systems is the requirement of highly precise control, temporal stability and reliability. To produce high degree of attenuation, the amplitude and phase of both the primary and the secondary noise must match with the close precision. The adaptive filters are used to control the noise and it has a linear input and output characteristic. If a transfer path of the noise has nonlinear characteristics it will be difficult for the filter to generate an optimal anti-noise. In this study, we propose a algorithm, delta rule algorithm which uses non linear output function. Delta rule is used for learning complex patterns in Artificial Neural Networks. We have implemented the adaptive filters using Least Mean Square (LMS) algorithm, Recursive Least Square (RLS) algorithm and compared the results.

Keywords— ANC, LMS, RLS, delta rule, error signal, neural networks, real-time

Introduction— Active noises are real time noise and they cannot be predictable (i.e., random). The traditional way to cancel the noise, which is called passive noise control, which technique based on the use of sound absorbing materials, is effective in higher frequency noise. However, significant power of the industrial noise often occurs in the frequency range between 50-250 Hz. Here the wavelength of sound is too long, so that passive techniques are no longer cost effective because they require material that is too heavy.

Active Noise Control System is working based on the principle of superposition. The system consists of a controller for which reference about the noise is given. The controller properly scales the reference noise and the phase reverses it. The phase-reversed signal is then added to the input signal that has some noise along the original message signal so that the noise gets cancelled out. There are many methods used for ANC system include both feedback and feed-forward control. ANC is based on either feed-forward control, where a coherent reference noise input is sensed before it propagates past the secondary source, or feedback control where the active noise controller attempts to cancel the noise without the benefit of an upstream reference input. The performance of the active control system is determined largely by the signal processing algorithm and the actual acoustical implementation. Effective algorithm design requires reasonable knowledge of algorithm behaviour for the desired operating conditions. Since the active noise is random, the proper prediction of the noise cannot be possible, the controller should contain a adaptive filter part whose filter coefficients will be changing based on the error signal which is the difference between the output of the controller and the output from an unknown plant. To achieve reduction of noise in complicated multiple noise source, we must use active noise control by multiple reference channel. That is input signal to the each channel is correlated and the output also correlated.

LMS ALGORITHM— The Least Mean Square, or LMS, (Douglas and Pan, 1995) algorithm is a stochastic gradient algorithm that iterates each tap weight in the filter in the direction of the gradient of the squared amplitude of an error signal with respect to that tap weight as shown in Fig. 1. The LMS algorithm is an approximation of the steepest descent algorithm which uses an instantaneous estimate of the gradient vector.

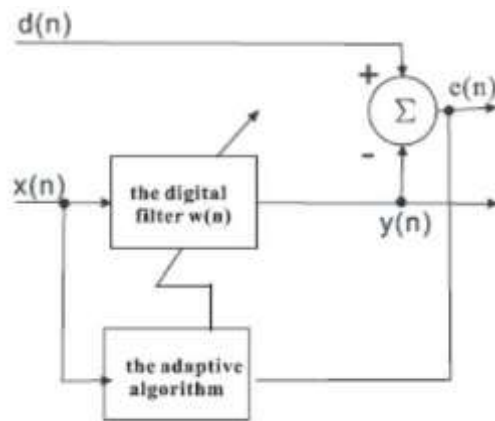


Fig. 1: Block diagram of the ANC control system using LMS algorithm

The estimate of the gradient is based on sample values of the tap input vector and an error signal. The algorithm iterates over each tap weight in the filter, moving it in the direction of the approximated gradient (Woo, 2001). Widrow et al. and Mugdha. M. Dewasthale, 2014 devised the LMS algorithm in 1959. The objective is to change (adapt) the coefficients of an FIR filter, $w(n)$, to match as closely as possible to the response of an unknown system, $p(n)$. The unknown system and the adapting filter process the same input signal $x(n)$ and have outputs $d(n)$ (also referred to as the desired signal) and $y(n)$, respectively.

The LMS algorithm basically has two processes. The first one is the filtering process and the next is adaptive process. In filtering process, the reference signal is filtered in the adaptive filter and it is combined with desired signal. The error signal is the difference of the desired signal and the output signal of the filter $w(n)$ (Glentis *et al.*, 1999). In adaptive process, the reference signal and the error signal are fed to the LMS algorithm and the weights of the filter are modified based on the LMS algorithm.

It is assumed that all the impulse responses in this study is modeled by those of finite impulse response (FIR) filters. $d(n)$ has the primary noise to be controlled and $x(n)$ is the reference about the noise.

$$d(n) = p^T(n) * x_1(n) \quad (1)$$

where $p(n)$ is the impulse response of the unknown plant and $x_1(n) = [x(n) \ x(n-1) \ x(n-M+1)]^T$

and M is the length of $p(n)$. The $y(n)$ is the output signal from the filter.

$$Y(n) = w^T(n) * x_2(n) \quad (2)$$

where $w(n) = [w(n) \ w(n-1) \ w(n-2) \ \dots \ w(n-N+1)]^T$ is the weight vector of the ANC controller with a length N and $x_2(n) = [x(n) \ x(n-1) \ x(n-N+1)]^T$.

The error signal $e(n)$ is difference of the desired signal $d(n)$ and the output of the filter $y(n)$.

$$e(n) = d(n) - y(n) \quad (3)$$

The weight of the filter $w(n)$ is updated using the following equation;

$$w(n+1) = w(n) + \mu x(n) e(n) \quad (4)$$

The termed as step size. This step size has a profound effect on the convergence behavior of the LMS algorithm. If is too small, the algorithm will take an extraordinary amount of time to converge. When is increased, the algorithm converges more quickly however, if is increased too much, the algorithm will actually diverge. A good upper bound on the value of μ is $2/3$ over the sum of the eigen values of the autocorrelation matrix of the input signal. The correction that is applied in updating the old estimate of the coefficient vector is based on the instantaneous sample value of the tap-input vector and the error signal.

The correction applied to the previous estimate consists of the product of three factors: The (scalar) step-size parameter, the error signal the correction applied to the previous estimate consists of the product of three factors: the (scalar) step-size parameter, the error signal $e(n-1)$ and the tap-m' put vector $u(n-1)$. The LMS algorithm requires approximately $20L$ iterations to converge in mean square, where L is the number of tap coefficients contained in the tapped-delay-line filter. The LMS algorithm requires $2L+1$ multiplications, increasing linearly with L .

RLS ALGORITHM— Recursive Least Square algorithm (RLS) (Kuo and Morgan, 1996) can be used with an adaptive transversal filter to provide faster convergence and smaller steady state error than the LMS algorithm (Haykin, 1996 and Upal Mahbub et al., 2012). The RLS algorithm uses the information contained in all the previous input data to estimate the inverse of the autocorrelation matrix of the input vector. It uses this estimate to properly adjust the tap weights of the filter.

In the RLS algorithm the computation of the correction utilizes all the past available information. The correction consists of the product of two factors: the true estimation error $e(n)$ and the gain vector $k(n)$. The gain vector itself consists of $P^{-1}(n)$, the inverse of the deterministic correlation matrix, multiplied by the tap-input vector $u(n)$. The major difference between the LMS and RLS algorithms is therefore the presence of P correction term of the RLS algorithm that has the effect of decorrelating the successive tap inputs, thereby making the RLS algorithm self-orthogonalizing. Because of this property, we find that the RLS algorithm is essentially independent of the eigen-value spread of the correlation matrix of the filter input. The RLS algorithm converges in mean square within less than $2L$ iterations. The rate of convergence of the RLS algorithm is therefore, in general, faster than that of the LMS algorithm by an order of magnitude. There are no approximations made in the derivation of the RLS algorithm. Accordingly, as the number of iterations approaches infinity, the least-squares estimate of the coefficient vector approaches the optimum Wiener value and correspondingly, the mean-square error approaches the minimum value possible. In other words, the RLS algorithm, in theory, exhibits zero misadjustment. The superior performance of the RLS algorithm compared to the LMS algorithm is attained at the expense of a large increase in computational complexity. The complexity of an adaptive algorithm for real-time operation is determined by two principal factors:

- The number of multiplications (with divisions counted as multiplications) per iteration and
- The precision required performing arithmetic operations. The RLS algorithm requires a total of $3L(3+L)/2$ multiplications, which increases as the square of L the number of filter coefficients. But the order of RLS algorithm can be reduced.

DELTA RULE ALGORITHM— Delta rule algorithm (Yegnarayana, 2001) is widely used in Artificial Neural Networks in pattern recognition and will be differ from the LMS algorithms in the weight update equation. The change in weight vector of the delta rule algorithm is;

$$w_i = *(d(n)-f(y(n)))(y(n))*x(n) \quad (5)$$

Where $f(y(n))$ is the output function.

The above equation is valid only for the differential output function. In LMS, the output function is linear $f(x) = x$. In this case, we are using non-linear ear output functions, which possess sigmoid nonlinearity. Since the derivative of the function is also used, the output function used should be differentiable. Two examples of sigmoid nonlinear ear function are the logistic function and the hyperbolic tangent function.

The logistic function output lies between 0 to 1. Similarly the second is hyperbolic tangent function and it is given by the output of the hyperbolic function lies between -1 to 1. is the scaling factor. Since the maximum value of the logistic function and hyperbolic tangent function is 1, the divergence of the weights is avoided. By properly choosing value of, the faster convergence can be achieved. The computational complexity of delta rule algorithm is sum of computational complexity of LMS and computations involved in the calculation of $f(x)$ and $f'(x)$ and multiplication of the function in the weight update vector. The computational complexity is not increased greatly compared to the LMS algorithm.

SIMULATION AND RESULTS— The weight update equation of LMS RLS and delta rule are (Woo, 2001), respectively. A white Gaussian noise with zero mean and unit variance is used as the reference signal. The primary path $p(n)$ is simulated by a filter of length 128.

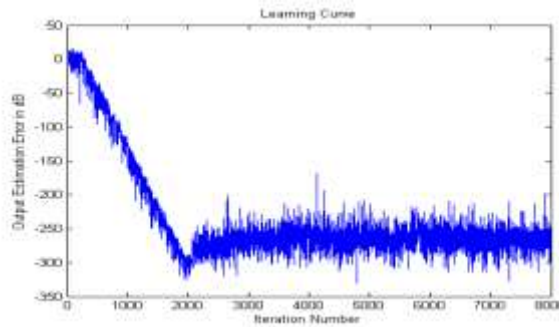


Fig. 2 Output estimation error of LMS algorithm

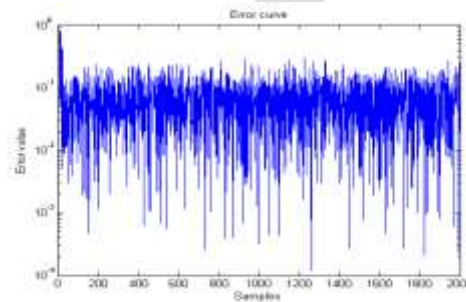


Fig. 3 Error value of RLS algorithm

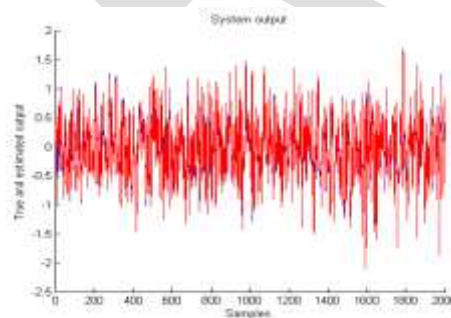


Fig. 4 True and estimated output of RLS algorithm

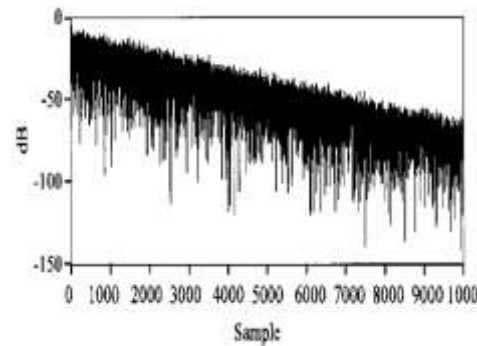


Fig. 5 Noise of delta rule algorithm

The length of $w(n)$ is chosen to be 96. The logistic function is used for the simulation of delta rule algorithm. All the weights are initialized to zero and all the results are average of 100 cycles.

All the simulations were done using MATLAB. The output estimation error of LMS algorithm is shown in the Fig. 2. The Error value of RLS algorithm is shown in the Fig. 3. The True and estimated output of RLS algorithm of RLS and noise of delta rule algorithm is shown in the Fig. 4 and 5, respectively. RLS algorithm converges very quickly than the other two algorithms and the residual noise is also less.

CONCLUSIONS— In this study, we have compared the performance of LMS, RLS and delta rule algorithm for a white Gaussian noise as reference. From the results shown in the above section, we can conclude that RLS algorithm is better in performance than both the algorithms. But the order of the complexity of the RLS algorithm is much more than the order of the complexity of the other two algorithms. The delta rule algorithm requires slightly more number of computations than the LMS algorithm and the residual noise of the delta rule algorithm is less than the residual noise of LMS algorithm. The delta rule algorithm is more efficient when both then noise reduction and computational complexity are taken in to consideration.

REFERENCES:

- [1] UPAL MAHBUB AND SHAIKH ANOWARUL FATTAH, (2012), "GRADIENT BASED ADAPTIVE FILTER ALGORITHM FOR SINGLE CHANNEL ACOUSTIC ECHO CANCELLATION IN NOISE", 2012 7TH INTERNATIONAL CONFERENCE ON ELECTRICAL AND COMPUTER ENGINEERING 20-22 DECEMBER, 2012.
- [2] MUGDHA. M. DEWASTHALE AND R. D. KHARADKAR, (2014), "IMPROVED LMS ALGORITHM WITH FIXED STEP SIZE AND FILTER LENGTH USING ADAPTIVE WEIGHT UPDATION FOR ACOUSTIC NOISE CANCELLATION", 2014 ANNUAL IEEE INDIA CONFERENCE (INDICON), PP. 1-7.
- [3] DOUGLAS, S. AND W. PAN, 1995. EXACT EXPECTATION ANALYSIS OF THE LMS ADAPTIVE FILTER, IEEE TRANS. SIGNAL PROCESS., 43: 2863-2871.
- [4] GLENTIS, G.O. K. BERBERIDIS AND S. THEODORIDIS, 1999. EFFICIENT LEAST SQUARES ADAPTIVE ALGORITHMS FOR FIR TRANSVERSAL FILTERING, IEEE SIGNAL PROCESS. MAG., 16. 4, 13-41.
- [5] HAYKIN, S., 1996. ADAPTIVE FILTER THEORY. PRENTICE HALL, 3RD EDITION.
- [6] KUO, S.M. AND D.R. MORGAN, 1996. ACTIVE NOISE CONTROL SYSTEMS-ALGORITHMS AND DSP IMPLEMENTATIONS. PP: 37.
- [7] MAEDA, Y. AND R.J.P. DE FIGUEIREDO, 1997. LEARNING RULES FOR NEURO-CONTROLLER VIA SIMULTANEOUS PERTURBATION, IEEE TRANS. ON NEURAL NETWORK, 1119/1130.
- [8] WOO, T.K., 2001. FAST HIERARCHICAL LEAST MEAN SQUARE ALGORITHM, IEEE SIGNAL PROCESS. LETT., 8: 11.
- [9] YEGNARAYANA, B., AUGUST, 2001. ARTIFICIAL NEURAL NETWORKS, PRENTICE HALL OF INDIA, PP: 124.
- [10] ZHOU D. AND DE BRUNNER V (2007), EFFICIENT ADAPTIVE NONLINEAR FILTERS FOR NONLINEAR ACTIVE NOISE CONTROL, IEEE TRANS. CIRCUITS SYST. I, REG. PAPERS, VOL. 54,3, PP. 669-681.
- [11] SICURANZA G.L. AND CARINI A (2006), PIECEWISE-LINEAR EXPANSIONS FOR NONLINEAR ACTIVE NOISE CONTROL, PROC. IEEE INT. CONF. ACOUST., SPEECH, SIGNAL PROCESSING, PP. 209-212.
- [12] AKHTAR M.T. (2007), ON ACTIVE NOISE CONTROL SYSTEMS WITH ONLINE ACOUSTIC FEEDBACK PATH MODELING, IEEE TRANSACTION ON AUDIO, SPEECH AND LANGUAGE PROCESSING, NO. 2, 593-600.

Adaptive Filters Algorithms: A Performance Comparison

Pankaj Gupta, Poonam Beniwal

Department of ECE, OITM, Hisar, pankaj.gupta181@gmail.com

Abstract— In practical application, the statistical characteristics of signal and noise are usually unknown or can't have been learned so that we hardly design fix coefficient digital filter. In allusion to this problem, the theory of the adaptive filter and adaptive noise cancellation are researched deeply. According to the Least Mean Squares (LMS) and the Recursive Least Squares (RLS) algorithms realize the design and simulation of adaptive algorithms in noise canceling, and compare and analyze the result then prove the advantage and disadvantage of two algorithms. The adaptive filter with MATLAB are simulated and the results prove its performance is better than the use of a fixed filter designed by conventional methods.

Keywords— Adaptive filters, Adaptive algorithm, RLS, LMS, Convergence Rate, Noise Vector, Simulation.

INTRODUCTION—

In the process of digital signal processing, often to deal with some unforeseen signal, noise or time-varying signals, if only by a two FIR and IIR filter of fixed coefficient cannot achieve optimal filtering[3]. Under such circumstances, we must design adaptive filters, to track the changes of signal and noise. Adaptive Filter is that it uses the filter parameters of a moment ago to automatically adjust the filter parameters of the present moment, to adapt to the statistical properties that signal and noise unknown or random change [1, 2], in order to achieve optimal filter. Based on in-depth study of adaptive filter, based on the least mean squares algorithm and recursive least squares are applied to the adaptive filter technology to the noise, and through the simulation results prove that its performance is usually much better than using conventional methods designed to filter fixed.

The so-called adaptive filter, is the use of the result of the filter parameters a moment ago, automatically adjust the filter parameters of the present moment, to adapt to the unknown signal and noise, or over time changing statistical properties, in order to achieve optimal filtering [4]. Adaptive filter has "self-regulation" and "tracking" capacities. Adaptive filter can be divided into linear and nonlinear adaptive filter. Non-linear adaptive filter has more signal processing capabilities. However, due to the non-linear adaptive filter more complicated calculations, the actual use is still the linear adaptive filter [3]. As shown in Figure.

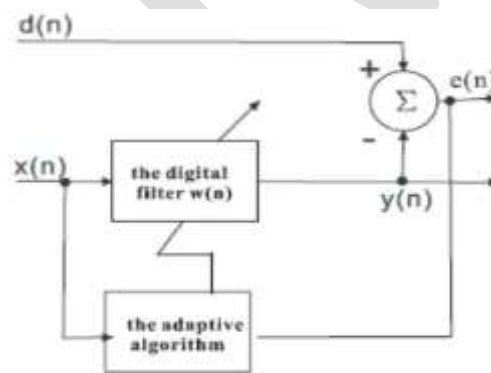


Figure 1: Adaptive filter scheme

The figure above is given the general adaptive filtering display: digital filter carries on filtering on the input signal $x(n)$, produce output signal $y(n)$. Adaptive algorithm adjusts the filter coefficient included in the vector $w(n)$, in order to let the error signal $e(n)$ to be the smallest. Error signal is the difference of useful signal $d(n)$ and the filter output $y(n)$. Therefore, adaptive filter automatically carry on a design based on the characteristic of the input signal $x(n)$ and the useful signal $d(n)$ [5]. Using this method, adaptive filter can be adapted to the environment set by these signals. When the environment changes, filter through a new set of factors, adjusts for new features[4]. The most important properties of adaptive filter is that it can work effective in unknown environment, and to track the input signal of time-varying characteristics [6]. Adaptive filter has been widely used in communications, control and many other systems. Filter out an increase noise usually means that the contaminated signal through the filter aimed to curb noise and signal relatively unchanged. This filter belongs to the scope of optimal filtering [7], the pioneering work started from Wiener, and Kalman who work to promote and strengthen. For the purpose of the filter can be fixed, and can also be adaptive. Fixed filter designers

assume that the signal characteristics of the statistical computing environment fully known, it must be based on the prior knowledge of the signal and noise. However, in most cases it is very difficult to meet the conditions; most of the practical issues must be resolved using adaptive filter. Adaptive filter is through the observation of the existing signal to understand statistical properties, which in the normal operation to adjust parameters automatically [8], to change their performance, so its design does not require of the prior knowledge of signal and noise characteristics. Adaptive filter is used for the cancellation of the noise component which is overlap with unrelated signal in the same frequency range [9].

(i) LMS Algorithm— The LMS is the most used algorithm in adaptive filtering. It is a gradient descent algorithm; it adjusts the adaptive filter taps modifying them by an amount proportional to the instantaneous estimate of the gradient of the error surface. It is represented in following equations [2].

$$y(n) = \hat{\mathbf{w}}^H(n) \cdot \mathbf{u}(n)$$

$$e(n) = d(n) - y(n)$$

$$\hat{\mathbf{w}}(n+1) = \hat{\mathbf{w}}(n) + \mu \cdot \mathbf{u}(n) \cdot e(n)$$

(ii) RLS Algorithm— The RLS algorithm performs at each instant an exact minimization of the sum of the squares of the desired signal estimation errors[3]. These are its equations: To initialize the algorithm $\mathbf{P}(n)$ should be made equal to δ^{-1} where δ is a small positive constant[2].

$$y(n) = \hat{\mathbf{w}}^H(n) \cdot \mathbf{u}(n)$$

$$\alpha(n) = d(n) - \hat{\mathbf{w}}^H(n-1) \mathbf{u}(n)$$

$$\pi(n) = \mathbf{u}^H(n) \cdot \mathbf{P}(n-1)$$

$$k(n) = \lambda + \pi(n) \cdot \mathbf{u}(n)$$

$$\mathbf{k}(n) = \frac{\mathbf{P}(n-1) \cdot \mathbf{u}(n)}{k(n)}$$

$$\hat{\mathbf{w}}(n) = \hat{\mathbf{w}}(n-1) + \mathbf{k}(n) \cdot \alpha^*(n)$$

$$\mathbf{P}'(n-1) = \mathbf{k}(n) \cdot \pi(n)$$

$$\mathbf{P}(n) = \frac{1}{\lambda} (\mathbf{P}(n-1) - \mathbf{P}'(n-1))$$

SIMULATION RESULTS—

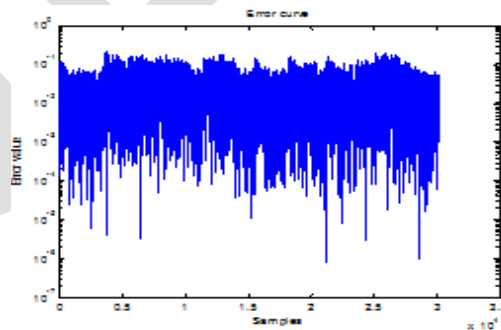


Figure 1: Error Curve

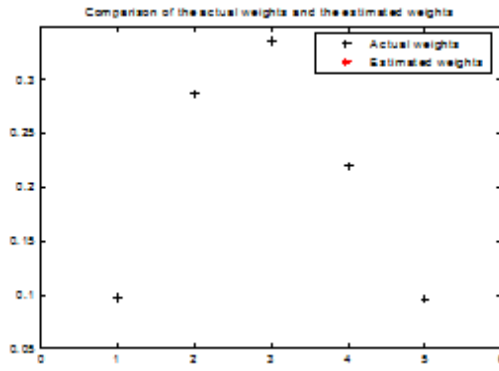


Figure 2: plot of estimated weights and filter weights

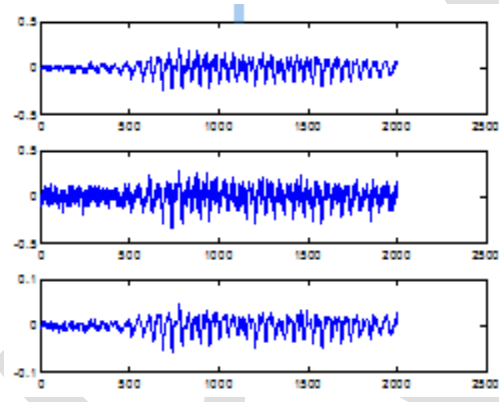


Figure 3 : Original wave , noisy wave and filtered wav

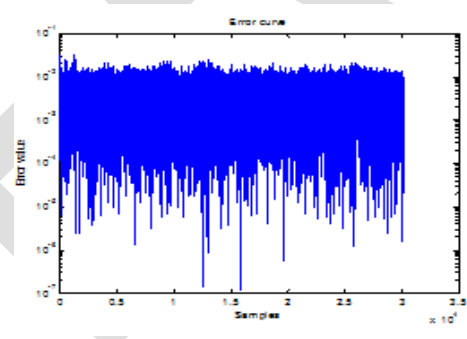


Figure 4 : Error curve

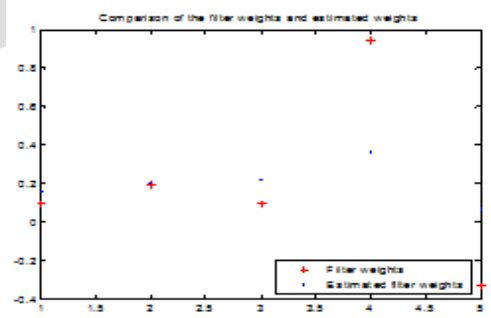


Figure 5: plot of estimated weights and filter weights

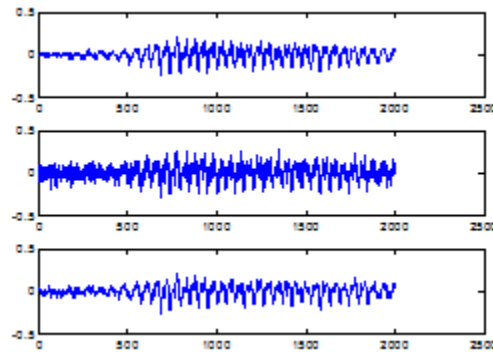


Figure 6: Original wave, noisy wave

COMPARATIVE ANALYSIS OF LMS AND RLS ALGORITHMS— The simulation results are achieved using real time speech input signal in MATLAB environment. The simulation results show that more than LMS algorithm and RLS algorithm in the area to cancel the noise has very good results, to complete the task of noise reduction. LMS filters filtering results is relatively good, the requirements length of filter is relatively short, it has a simple structure and small operation and is easy to realize hardware. But the shortcomings of LMS algorithm convergence rate is slower, but the convergence speed and noise vector there is a contradiction, accelerate the convergence speed is quicker at the same time noise vector has also increased. Convergence of the adaptive for the choices of gain constant μ is very sensitive. The noise signal and signal power when compared to larger, LMS filter output is not satisfactory, but we can step through the adjustment factor and the length of the filter method to improve. RLS algorithm filter the convergence rate is faster than the LMS algorithm, the convergence is unrelated with the spectrum of input signal, filter performance is superior to the least mean squares algorithm, but its each iteration is much larger operation than LMS. The required storage capacity is large, is not conducive to achieving a timely manner, the hardware is also relatively difficult to achieve the task of noise reduction.

CONCLUSION

Adaptive filtering is an important basis for signal processing, in recent years has developed rapidly in various fields on a wide range of applications. In addition to noise cancellation, adaptive filter the application of space is also very extensive. For example, we know areas that the system identification, adaptive equalizer, linear prediction, adaptive antenna array, and many other areas. Adaptive signal processing technology as a new subject is in depth to the direction of rapid development, especially blind adaptive signal processing and use of neural networks of non-linear.

FUTURE WORK— The application can be extended for the noise reduction in the speech for the hearing aids in the noisy environment like crowd noise, car noise, cockpit noise, aircraft noise etc. With modified RLS and LMS algorithm convergence speech can be increased as per the real time requirement fast algorithm can be developed.

REFERENCES:

- [1] A. J. URIZ ET. ALL, "IMPLEMENTATION OF A NOISE REDUCTION ALGORITHM IN A HEARING AID DEVICE BASED ON A DSPIC", IEEE LATIN AMERICA TRANSACTIONS, VOL. 11, NO. 1, FEBRUARY 2013.
- [2] ELEFThERIOU, E.; FALCONER, D. D.; "TRACKING THE PROPERTIES AND STEADY-STATE PERFORMANCE OF RLS ADAPTIVE FILTER ALGORITHMS", IEEE TRANS. ACOUST. SPEECH SIGNAL PROCESS., VOL. ASSP-34, PP. 1097-1110.
- [3] HAYKIN S., "ADAPTIVE FILTER THEORY", PRENTICE-HALL, INC.
- [4] HAYKIN, S.; SAYED, A.H.; ZEIDLER, J.R.; YEE, P.; WEI, P.C., "ADAPTIVE TRACKING OF LINEAR TIMEVARIANT SYSTEMS BY EXTENDED RLS ALGORITHMS", SIGNAL PROCESSING, IEEE TRANSACTIONS ON, VOLUME: 45 5 , PAGE(S): 1118 -1128, MAY 1997.
- [5] S.M. KUO AND D.R.MORGAN, ACTIVE NOISE CONTROL: A TUTORIAL REVIEW, PROCEEDINGS OF THE IEEE, VOLUME 87, NUMBER 6, JUNE 1999.

- [6] J.B. ALLEN, HOW DO HUMANS PROCESS AND RECOGNIZE SPEECH?, IEEE TRANSACTIONS ON SPEECH AND AUDIO PROCESSING, VOLUME 2, NO. 4, OCTOBER 1994.
- [7] W. HARRISON, J. LIM, E. SINGER, A NEW APPLICATION OF ADAPTIVE NOISE CANCELLATION, IEEE TRANS. ACOUSTIC SPEECH SIGNAL PROCESSING, VOL.34, PP. 21-27, JAN 1986.
- [8] S. I. A. SUGIYAMA, —AN ADAPTIVE NOISE CANCELLER WITH LOW SIGNAL DISTORTION FOR SPEECH CODES|| IEEE TRANS. SIGNAL PROCESSING, VOL. 47, PP. 665-674, MAR, 1999.
- [9] LIN ZHIMIN ET. ALL, “A SINGLE-CHANNEL LOUDNESS COMPENSATION METHOD FOR DIGITAL HEARING AIDS BASED ON MULTI-RESOLUTION WAVELET”, 2012 SECOND INTERNATIONAL CONFERENCE ON INSTRUMENTATION & MEASUREMENT, COMPUTER, COMMUNICATION AND CONTROL , PP 1616–1620, DECEMBER 2012.
- [10] M. A. ABD EL-FATTAH, M. I. DESSOUKY, S. M. DIAB AND F. E. ABD EL-SAMIE, “ADAPTIVE WIENER FILTERING APPROACH FOR SPEECH ENHANCEMENT”, UBIQUITOUS COMPUTING AND COMMUNICATION JOURNAL, VOL. 3 , NO. 2, PP 1- 8, APRIL 2008.
- [11] YUAN YAO, BENSHUN YI AND YONGQIANG YAO, “SPEECH ENHANCEMENT UNDER AVIATION NOISE”, INTERNATIONAL CONFERENCE ON WIRELESS COMMUNICATIONS, NETWORKING AND MOBILE COMPUTING, PP 1 - 4, SEPTEMBER 2006.
- [12] JULIE E. GREENBERG, “MODIFIED LMS ALGORITHMS FOR SPEECH PROCESSING WITH AN ADAPTIVE NOISE CANCELLER”, IEEE TRANSACTIONS ON SPEECH AND AUDIO PROCESSING, VOL.6, NO. 4, JULY 1998.

DESIGN AND FABRICATION OF COCONUT LEAVES SHREDDER

I M SANJAY KUMAR

DR. T R HEMANTH KUMAR

Product Design and Manufacturing (M.tech) Dept. of IEM

Sri Siddhartha Institute of Technology
Tumkur-05, India
Sanjaynayak51@gmail.com

Professor, Dept. of IEM
Sri Siddhartha Institute of Technology
Tumkur-05, India

trhkumar@gmail.com

Abstract- This paper presents the design and fabrication of coconut leaves shredder to obtain coconut leaves powder to prepare the vermin compost. The conventional agro-waste disposal is a traditional and oldest method of waste disposal in which agriculture wastes are dumped as it is to degrade in a particular place for decomposing. As the wastes are dumped as such, it takes more time to degrade and it causes environmental pollution. The shredder machine aims to reduce the size of agriculture waste which useful for nourishing fertilizer.

A shredder machine mainly consists of cutter, mounted on dual shaft, motor is attached at the base, smaller pulley at the motor end gives drive with the help V-belt to bigger pulley which is connected to gear. One gear will give drive to other gear, and Barrel rotates in opposite direction with the help of these gears. Shaft it rotates at 520 rpm at this time coconut leaves fed into the hopper for high rotational speed of cutter assembly coconut leaves get convert into powder

1. INTRODUCTION:

Agricultural production leaves considerable amounts of agricultural waste. Some of it is recycled into the agricultural production as fertilizer, while large amounts remain unused – and in many instances pose a disposal problem.[1]

It has been realized that large quantity of agricultural wastes remains being unutilized because handling, storage and management related difficulties. The reasons are their low bulk density, large area/volume for storage. The farmers on the field burn most of these wastes after the harvesting of crops. Thus the agricultural waste burning phenomena is being repeated every year. In order to use these wastes for some economical benefits, so the necessary of such machine was felt to utilize all kinds of agricultural waste after shredding, which could be economical and practicable.

II. LITERATURE REVIEW

Agriculture is now one of the most important sectors in the Indian economy. In order to further develop this sector technology has become one of the main components. Typically, dealing with the agriculture sector can entail difficulties relating to a number of factors. Consequently, to overcome such problems, farmers are being encouraged to adopt technology that suits their farm.

PEDAL OPERATED SHREDDER MACHINE

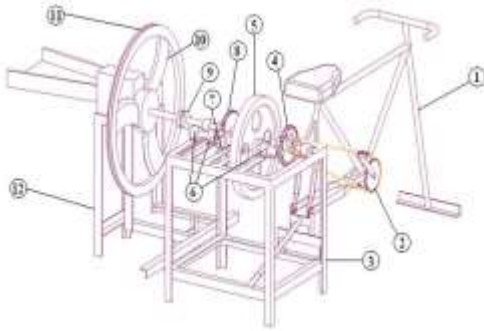


Fig1: Pedal operated shredder machine

A pedal operated shredder machine mainly required two operators one for peddling, another one for feeding purpose. ie is the main disadvantage for this machine. In this concept, the bicycle mechanism for converting and transmitting human energy through paddling to rotational kinetic energy of flywheel is hereby proposed. The energy stored in the flywheel can then use for actual cutting process. This human energy output is in the low range and the processes could be operated intermittently can be considered for utilization.[2]

Hand operated chaff cutter machine



Fig 2: Hand operated chaff cutter machine

The above figure shown is hand operated chaff cutter machine. Chaff cutters are meant for cutting all kinds of dry & green fodder into small pieces for cattle. These chaff cutters can chop the green or dry f Paddy, Grass, Groundnut etc. These machines are also useful for cutting, dry coconut leaves, Dairy Farms, and Jute Industries etc. where chopping is required. The advantages of the product are eco-friendly and maintenance is very easy.[3]

Currently available model



Fig3: Tractor PTO Model

The currently available product for cutting of coconut leaves is as shown in above figure. In the present model the outcome is in the stick form and later it must be crushed to obtain in powder form and the feeding of the coconut leaves in the existing model is of vertical type, which is difficult to feed the coconut leaves. It requires tractor PTO (Power take off shaft) machine cost also very expensive .To overcome from these problems the proposed model is developed.[4]

III.PROBLEM IDENTIFICATION AND CONCEPT DEVELOPMENT

In this project work various shredder concepts are generated and problems regarding the various coconut leaves shredder concepts are identified and selected the best concept using concept screening and concept scoring method for further progress of the project.

Concept A: Pedal Operated Shredder Machine

In this concept

SL.no	Concept-A
1	Blade material is used as MS so cutting rate are less.
2	Efficiency quite less per hour
3	It is not a user friendly
4	Human power required
5	Complicated design
6	Continuous work not possible.
7	Requires more time to cut

Concept B: Hand Operated Chaff Cutter Machine

SL.no	Concept- B
1	Low cutting rate
2	The cutter is made up of hardness steel
3	Weight of the cutter is more
4	Requires more power to cut the coconut leaves
5	There is no safety while working may get chances of accident
6	Transportation is very difficult.

Concept C: Tractor PTO Model Shredder

SL.no	Concept-C
1	Complicated design
2	It requires tractor
3	Very expensive
4	Maintainace of machine is very difficult
5	Wear and tear of blades occurs frequently
6	It requires more power
7	Wight of the machine is more

Concept D: Proposed Model

SL.no	Concept-D
1	Cutters tip are made up of tungsten carbide hence cutting rate are high.
2	Cutters having six teeth so it requires

	less time
3	Motor used single phase motor
4	Only one operator is sufficient
5	Cost of machine is less
6	Simple in design
7	Requires less power about 2 hp.
8	For safety concern protecting shield cover on belt and pulley.

Rate the concepts

A relative score of “better than” (+), “same as” (0), “Worse than” (-) is to be place in each cell of the matrix to represent how each concept in comparison to the reference concept relative to the particular criterion.

Ratings:- “better than” (+), “same as” (0), “Worse than” (-)

Rank the concepts

Table 1 . Pugh’s Chart

<u>Selection criteria</u>	<u>Concept A</u> 	<u>Concept B</u> 	<u>Concept C</u> 	<u>Concept D</u> 
Function	+	+	-	+
Cutting rate	+	+	+	+
Safety	-	+	-	-
Reliability	0	-	0	+
Cost	+	-	+	+
SUM +’S	3	3	2	4
SUM 0’S	1	0	1	0
SUM -’S	1	2	2	1
Net score	2	1	0	4
Rank	2	3	4	1

After rating all the concepts, summation of the “better than”, “same as”, “Worse than” scores and enters the sum for each category in the lower rows of the matrix. A net score is calculated by subtracting the number of “Worse than” ratings from “better than” ratings. In general, the concept with more ratings will be ranked higher and the outcome of this step is that concept “D” is ranked as “1”. So concept D is selected for the development process.

Objectives of Proposed concept:

To overcome the limitations of existing system the proposed concept minimizes certain limitations as mentioned below.

- 1 To perform different difficult jobs in the field of agriculture easily and effectively by using the new machinery.
- 2 It requires only one operator ultimately reduces the man power.
- 3 For safety concern it is user friendly.
- 4 To achieving higher rate of output in lesser time.
- 5 To reduce the adverse effects on the environment, and to use ethically justifiable production methods.

IV.PROPOSED CONCEPT:

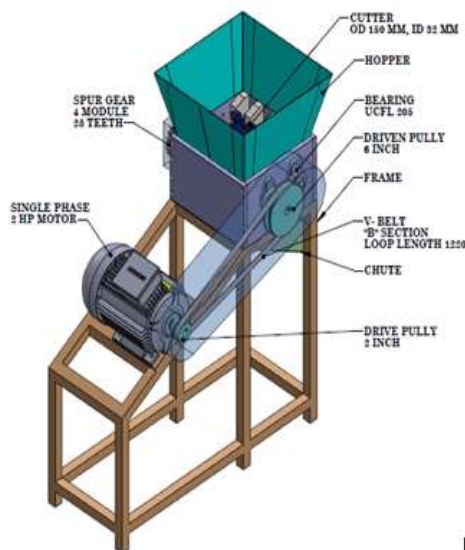


Fig4: Coconut leaves shredder.

Methodology:

The main aim of the project is to produce the small pieces of coconut leaves further it convert into manure fertilizer that will be useful for crops. The machine consists of dual shaft, Hoper, Spur gear, Frame , motor and cutter, Belt and pulley. The machine will be fabricated using mild steel frame and cutting tip of cutter made up of tungsten carbide. The machine runs in 1-phase 2hp power supply.

In this machine, the coconut dry leaves are fed, into the machine vertically through hopper. The motor is rotated at certain speed 1440 rpm. But maintain the speed ratio about 1: 3 so driven shaft rotated at 520 rpm Cutter are mounted on shaft one shaft driven by belt and pulley another shaft driven by spur gear both shaft rotated in opposite direction. Due to the high rotational force, the coconut leaves get chopped and get into powder.

GEOMETRIC 2D SOLID WORKS MODELLING

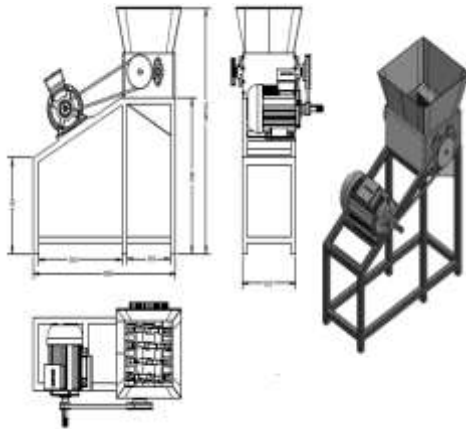


Fig 5: Proposed 2D Model

V.COMPONENTS TO BE USED FOR PROPOSED CONCEPT

PARTS	QUANTITY	MATERIALS	DESCRIPTION
Structural Frame	1	M.S	Tube=40×40 mm Thickness=2.5mm Length 86mm Breadth 320 mm Height 1030 mm
Cutter	8	Tungsten carbide and mild steel	OD 150 mm ID 32 mm Thickness=25mm 6 teeth
Motor	1	Electrical AC	Single-Phase 2hP 1440rpm
Spur gear	2	MS	OD=120mm ID=25 mm Module=4 No of Teeth=28 Thickness=25mm
Hopper	1	G.I Sheet	Length 300mm Breadth 200mm Thickness 3mm
Collecting vessel	1	G.I Sheet	Thickness 3mm Length 200 mm
Belt B-1340	1	Synthetic rubber	B1340 Length 1256 mm Thickness 11mm
Small pulley	1	Cast iron	B Section Ø 65 mm
Larger pulley	1	Cast iron	B Section Ø 150mm
Bearing	4	Cast iron	UCFL 205 D1 ID 25mm
Shaft	2	M.S	OD 32mm Length 420mm

VI. Developed Model



Fig.6: Developed model

Working principle

Working principle gives us the functionality of the proposed model. The developed model, acts as an electro mechanical which reduces the human effort as well as human intervention by utilizing the electrical motor for the cutting of leaves. The process is very much simplified as compared to the earlier processes.

The machine is first connected to the 1-phase power supply and started. Later, the dry coconut leaves are fed into the hopper. As the coconut leaves move towards the cutters assembly, this assembly rotates at the speed of 520 rpm, the coconut leaves get chopped and collected on the other side of the machine.

Advantages

- 1 This machine reduces the agro-waste and, keep the farm neat and clean
- 2 Reduces the environmental pollution
- 3 It is easily convert solid waste into small pieces.
- 4 The output of powder is good for vermin-compost and, it is a good bio fertilizer for crops.

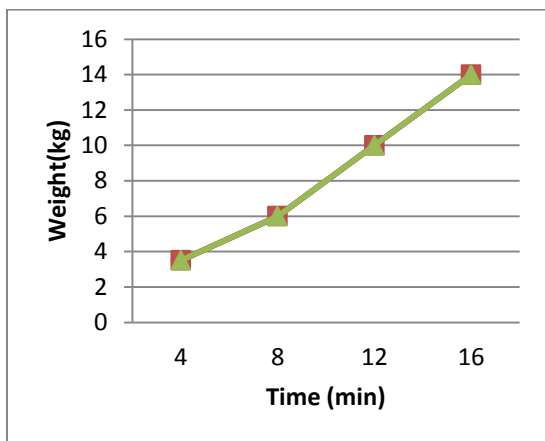
Application

- 1 The waste shredder machine can be applied not only in mass level but also small level agricultural field.

It can be used in forest industry

VII. Result

Length of leaves is five feet and number of leaves is Four



The above graph shows Time V/s kilogram. The graph clearly shows that the amount of pieces collected with respect to time. In this test 5 feet length and 4 coconut leaves are taken. The test is conducted for 4 different times. For which results are obtained, how much amount of powder collected and graph is plotted.

Conclusion

The proposed model is simple, efficient, requires less time and cost effective when compared to the existing model. In the proposed model the coconut leaves waste are shredded into machine, which is enclosed with the motor and blades made up of tungsten carbide and mild steel to obtain the outcome as small pieces about 30mm to 50 mm.

After the successful deployment of the proposed Coconut leaves cutter, the outcome of the project work is in the form of powder and further it will be used as manure fertilizer. For the different lengths

REFERENCES:

- [1] S.Nithyananth “ Design of Waste Shredder Machine” Libin Samuel et al Int. Journal of Engineering Research and Applications ISSN : 2248-9622, Vol. 4, Issue 3(Version 1), March 2014, pp.487-491
- [2]P.B.Khope and J.P.Modak“Design of experimental set-up for establishing empirical relationship for chaff cutter energized by human powered flywheel motor”Journal of Agricultural Technology 2013 Vol. 9(4): 779-791
- [3]Ajinkya S. Hande “ Methodlogy For Design and Fabrication of portable organic Waste chopping Machine To obtain comopost – A Review. Volume 1 |Issue 7 | December 2014 ISSN (online): 2349-6010 IJIRST –International Journal for Innovative Research in Science & Technology| of coconut leaves, results have been obtained and graph is plotted.
- [4] Mohamad khatib iqbal “Development of coconut leaves cutter” Vol. 3, No. 12. (June 2014) Key: citeulike:13215244.”
- [5] Y Prashanth, C Gopinath, “Design and Development of coconut fiber Extraction Machine” Department of Design, M. S. Ramaiah School of Advanced Studies, Bangalore - 560 058 Volume 13, Issue 1, April 2014
- [6]P.B.Khope, J.P.Modak“Establishing empirical relationship to predict the chaff cutting phenomenon energized by human powered flywheel motor (hpfm)”IOSR Journal of Agriculture and Veterinary Science (IOSR-JAVS) e-ISSN: 2319-2380, p-ISSN: 2319-2372. Volume 3, Issue 2 (May. - Jun. 2013), pp 35-39

IJERGS

IJERGS

IJERGS

IJERGS

IJERGS

IJERGS

APPLICATION OF VERTICAL EDGE BASED METHOD IN NUMBER PLATE EXTRACTION USING HORIZONTAL AND VERTICAL SCANNING

Silpa S Kumar, Radhakrishnan B, Raji P G
P.G Scholar, Dept of CSE, BMCE, Kollam, Kerala, India
skumarsilpa09@gmail.com

Abstract— This is a method used for car license plate detection. Firstly the Adaptive thresholding is applied for binarizing the gray scale image. Then the binarized image is enhanced by removing noise. After that, new Vertical edge based method is used to detect the number plate because of the high availability of the vertical edges in the number plate rather than the horizontal edges. Using vertical edge detection reduces the computation time. After that scan the image horizontally and vertically by pixel information are used to detect the license plate. This new Vertical edge based method to make proposed car license plate detection method faster.

Keywords— Gray scale, Binerizing, Enhance, Noise removal, Car license plate detection, Adaptive thresholding, Vertical edge based detection.

1. INTRODUCTION

The Car license plate detection and recognition system (CLPDRS) became an important area of research in image processing technology. It is mainly due to its various applications, such as the payment of parking fees, highway toll fees, traffic data collection (vehicle access control, border control) and crime prevention [1]. To identify a car, features such as model, color, and LP number can be used [2]. Among these, License plate numbers are being used to uniquely identify a car. For example in parking fee payment, number plates are used to calculate the duration of the parking. When a vehicle enters the gate, license plate is automatically recognized and stored in database. On leaving, the license plate is recognized again and compared with the stored numbers in the database. The time difference is used for calculating the parking fee.

License plates are available in various styles and colors in various countries. Every country has their own license plate format. So each country develops the CLPDRS system appropriate for the license plate format. In India the license plate containing white background with black foreground colour for private cars and for the commercial vehicle used yellow as background and black as foreground colour. The number plate start with two digit letter “state code” followed by two digit numeral followed by single letter after those four consecutive digits as the below Fig.1. From the Fig.1, 1 indicates the Country code, 2 indicate the state code, and 3 indicate the district code, 4 indicate the type of vehicle and 5 indicates the actual registration number. Locating the number plate is very challenging work in the field of image processing. The whole system mainly consists of two steps. First is to identify the position of the number plate from the particular vehicle and then segmentation of all the numbers and letters of the number plate.

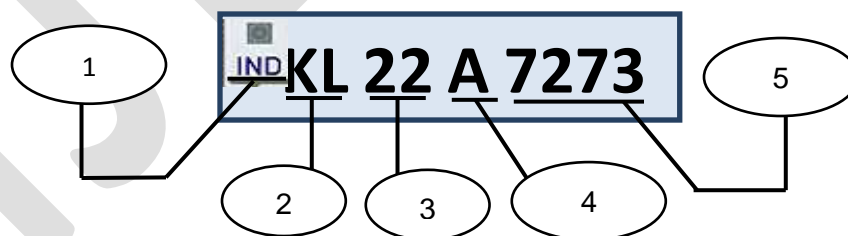


Fig.1 Sample of Indian license plate.

CLPDRS is convenient and cost efficient as it is automated. CLPDRS consists of three parts: license-plate (LP) detection (LPD), character segmentation, and character recognition. Among these, LPD is the most important part in the system because it affects the system’s accuracy. LP detection is the process of finding the region or location in an image that contains the LP. To make the license plate detection process successful and fast, many difficulties must be settled, such as the poor image quality from the uneven lighting condition, plate sizes and designs, processing time, background details and complexity and various observation angles from the vehicles and cameras [3]. To detect the region of car license plate, in the past, many techniques have been used, for example

the morphological operations [4],[5], edge extraction[6], combination of gradient features [7], salience features [8], a neural network for color [5] or grayscale [9] classification, and vector quantization [10].

Edges characterize boundaries are important techniques in image processing. Edges in images are areas with strong intensity contrasts. An edge in an image is a significant local change in the image intensity, usually associated with a discontinuity in the image intensity. Edges typically occur on the boundary between two different regions in an image. Edges can be modelled according to their intensity profiles. Edge detection refers to the process of identifying and locating sharp discontinuities in an image. The discontinuities are abrupt changes in pixel intensity which characterize boundaries of objects in a scene. So, an edge map has vastly reduced complexity, and it retains the important structure present in the original image.

Vertical edge detection is one of the most crucial steps in CLPD because it influences the whole system to correctly detect the LP [11]. Vertical edge-based CLPD is the most suitable technique to overcome some of the difficulties in the license plate detection, because of the abundance availability of vertical edges. Car license plate details always have a lot of vertical edges that can be used to generate the candidate regions for classification [12]. Historically, the most common and earliest edge detection algorithms are those based on the gradient, such as the Sobel operator [13] and the Roberts operator [3]. Sobel operator is one of the most important algorithms that has been widely used to detect the vertical edges in many CLPD methods [13].

This paper aim to propose a new and fast technique for detecting the vertical edge. It is faster than Sobel operator with an accurate performance of showing the vertical edges. Furthermore, the use of Vertical Edge based Method in CLPD would enhance the system performance. In this car-license-plate detection, the web camera is used to capture the images, and an offline process is performed to detect the plate from the whole scene image. This color input image is converted to a grayscale image, and then, Adaptive thresholding is applied on the image to constitute the binarized image. Thresholding is computed using integral image.

After thresholding, the image will only have black and white regions, and the vertical edges are extracted from these regions. Here a vertical edge detection is used to reduce the computation time of the whole car-license-plate detection method. The idea of the vertical edge detection concentrates on intersections of black–white and white–black in the black and white image. The next process is to detect the license-plate; the plate details are Scanned based on the pixel value with the help of the vertical edge detection. The image is scanned horizontally to detect candidate regions and vertically to search for the true candidate region. Finally, the true plate region is detected in the original image.

The proposed system for car license plate detection is shown in Fig.2.

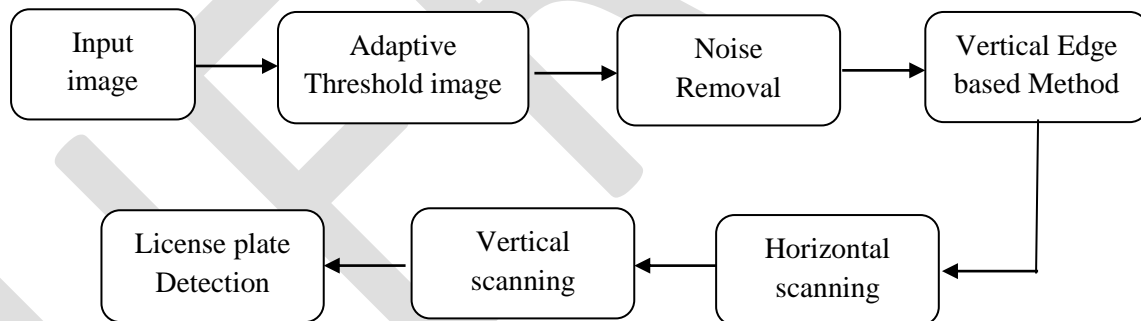


Fig.2 Block diagram of proposed system for car license plate detection.

Section II will discuss the procedures of this car license plate detection in detail. Section III draw our conclusion.

2. PROPOSED SYSTEM

Firstly an image of the car-license-plate is captured by the web camera. And this color input image is converted to a grayscale image, which enhance the speed of the car license plate detection method.

A. Adaptive Thresholding Process

This Adaptive Thresholding process is just a simple extension of Bradley and Roth's [14] and Wellner's methods [15]. The Wellner's method of quick adaptive thresholding is that pixel is compared with an approximate moving average of last S pixels, is calculated while passing through the image. If the value of the current pixel is T percent lower than the average, then it is set to white: otherwise it is set to black. Wellner uses S equal to one eighth of the image width, T equal to 0.15 to yield the best results for a verity of image. T should be the range $0.1 < T < 0.2$ in our method. The advantage of this method is the single pass through the image is required. But Wellner's algorithm depends on the scanning order of the pixels. Since the moving average is not suitable for the good

representation because the neighborhoods are not evenly distributed in all direction. So the Bradley's method used to solve the problem by using integral image. It uses the mean of local window, where local mean is computed using integral image.

Step 1: To compute integral image $I(x, y)$ from the gray scale image $g(x, y)$. To store each location of $I(x, y)$ the sum of all $g(x, y)$ terms to the left and above the pixel (x, y) . Here linear time used in the following equation for each pixel

$$I(x, y) = g(x, y) + I(x - 1, y) + I(x, y - 1) - I(x - 1, y - 1) \quad (1)$$

Step 2: The intensity summation for each local window should be computed by using two subtraction and one addition operation. The window with upper left corner $(x-(s/2), y-(s/2))$ and lower right corner $(x+(s/2), y+(s/2))$ can be computed in constant time using the following equation, s represent the local window size or length for the computed integral image, whereas s =image width/8.

$$\text{sum}_{\text{window}} = \left(I\left(x + \frac{s}{2}, y + \frac{s}{2}\right) - I\left(x + \frac{s}{2}, y - \frac{s}{2}\right) - I\left(x - \frac{s}{2}, y + \frac{s}{2}\right) + I\left(x - \frac{s}{2}, y - \frac{s}{2}\right) \right) \quad (2)$$

Step 3: Perform threshold for each pixel in an image. The gray scale image, $g(x, y)$ has the values between [0-255].

$$AT(x, y) = \begin{cases} 255, & g(x, y) \times S^2 < (1 - T) \times \text{sum}_{\text{window}} \\ 0, & \text{otherwise} \end{cases} \quad (3)$$

where $AT(x, y)$ represents the adaptive threshold value of the pixel $g(x, y)$, and S^2 represents the computed area of the local window for the selected region. The speed of this adaptive thresholding is increased by using mean and variance of local windows [16].

B. Noise Removal

In this step, while processing a binary image, the black pixel values are the background, and the white pixel values are the foreground. A 3×3 mask is used throughout all image pixels. Only black pixel values in the threshold image are tested. Once, the current pixel value located at the mask center is black, the eight-neighbor pixel values are tested. If two corresponding pixel values are white together, then the current pixel is converted to a white value as a foreground pixel value (i.e., white pixel) based on four cases. In the first case, the pixels are horizontal with an angle equal to 0° as $(-)$. In the second case, the pixels are vertical with an angle equal to 90° as $(/)$. In the third case, the pixels are inclined with an angle equal to 45° as (\backslash) . In the fourth case, the pixels are inclined with an angle equal to 135° as (\backslash) . This step is enhance the binarized image.

C. Vertical Edge Based Method

After thresholding is applied, the character region appears white and background as black. This Vertical edge based method processing these regions efficiently. It distinguish the plate details region of image particularly beginning and end of each character the plate. Therefore using this Vertical edge based method will easily detect the plate details, and the character recognition process will done faster. The idea of the Vertical edge based method concentrates on black and white pixel regions.

	0	1	2
0	$x-1, y-1$	$x-1, y$	$x-1, y+1$
1	$x, y-1$	x, y	$x, y+1$
2	$x+1, y-1$	$x+1, y$	$x+1, y+1$

Fig.3 Mask of proposed system.

A 3×3 mask is used as shown in figure 3. The center pixels located at the positions are $(0, 1)$, $(1, 1)$, $(2, 1)$. The mask is moved from left to right, if combination of black and white pixels appears in the mask then no change in center pixel value, but if the mask have all black pixels, then it changes to white. The proposed mask has the size of 3×3 . If the three pixels at location $(0, 1)$, $(1, 1)$ and $(2, 1)$ are black, then the other two columns are tested and if both or any are black, the three center pixels will be converted to white. Otherwise the second column (center pixels values) will not change. This process is repeated for the whole image. Here the three rows are checked at once. Therefore consumed time in this case is reduced.

D. Horizontal Scanning

From the Vertical Edge based Method we got a lot of vertical edges .The image is scanned from top to bottom and from left to right. This process is divided into 2 steps:

1. Count Black Pixel Availability Per Each Row: The number of black pixels in each rows are counted and stored in an array variable CountBlkPix[a], Where [a=0,1,2,3,.....height-1].
2. Divide The Image into Candidate Regions: Candidate regions are selected based on the count of black pixel values from previous step. The threshold values are used to select the rows as candidate region or not. If the CountBlkPix array value is greater than the threshold, that rows are present in candidate region.

E. Vertical Scanning

This process aims to select and extract LP from the candidate regions. The process is divided into two parts:

1. Selection Process of the LP Region:

For the candidate regions, each column will be checked one by one. If the column blackness ratio exceeds 50%, then the current column belongs to the LP region; thus, this column will be replaced by a vertical black line in the result image. Hence, each column is checked by the condition that, if $\text{BlckPix} \geq 0.5 \times \text{columnHght}$, then the current column is an element of the LP region. Here, the “BlckPix” represents the total number of black pixels per each column in the current candidate region, and the “columnHght” represents the column height of the of the candidate region. This condition with a fixed value (0.5) is used with nonblurry images. However, some pixels of the candidate regions will not be detected in case the ratio of blackness to the total length (height) of the candidate region is greater than 50%. Therefore, the condition is changed to be less than 50%, according to the ratio of the blurry level or the deformation of the LP. The condition will be modified and store in P_{RS} . The $\text{BlckPix} \geq P_{RS} \times \text{columnHght}$, where P_{RS} represents the P_{RS} factor. The P_{RS} value is reduced when the blurry level is high to highlight more important details, and it is increased when the blurry level is less. Therefore, the mathematical representation for selecting the LP region can be formulated as follows:

$$C_{\text{region}} = \begin{cases} 0, & \text{BlckPix} \geq P_{RS} \times \text{columnHght} \\ 255, & \text{otherwise} \end{cases} \quad (4)$$

where C_{region} represents the output value for the current pixel of the currently processed candidate region. If $C_{\text{region}} = 0$, consider the checked pixel as an element of the LP region; otherwise, consider it as background. The value of P_{RS} is automatically determined.

2. Making a Vote:

The columns whose top and bottom neighbors have high ratios of blackness details are given one vote. This process is done for all candidate regions. Hence, the candidate region that has the highest vote values will be the selected region as the true LP. By tracking the black vertical lines, the plate area will be detected and extracted.

3. CONCLUSION

This paper present a new and fast algorithm for detecting vertical edges, in which its performance is faster than the other existing edge detection operators. Before applying the method the image is binarized using adaptive thresholding, which makes the license plate clear. The advantages of this method is that it concentrates black pixel inside the plate and have the ability to work with blurred images for detecting vertical edges. This advantage helps to detect license plate details easily and faster than other existing methods.

REFERENCES:

- [1] S. N. Huda, K. Marzuki, Y. Rubiyah, and O. Khairuddin, “Comparison of feature extractors in license plate recognition,” in *Proc. 1st IEEE AMS*, Phuket, Thailand, 2007, pp. 502–506.
- [2] E. R. Lee, K. K. Pyeoung, and J. K. Hang, “Automatic recognition of a car license plate using color image processing,” in *Proc. IEEE Int. Conf. Image Process.*, 1994, pp. 301–305.
- [3] H. Bai and C. Liu, “A hybrid license plate extraction method based on edge statistics and morphology,” in *Proc. 17th Int. Conf. Pattern Recognit.*, Cambridge, U.K., 2004, pp. 831–834.
- [4] J.-W. Hsieh, S.-H. Yu, and Y. S. Chen, “Morphology-based license plate detection from complex scenes,” in *Proc. 16th Int. Conf. Pattern Recognit.*, Quebec City, QC, Canada, 2002, pp. 176–179.
- [5] A. A. Lensky, J. Kang-Hyun, and V. V. Gubarev, “Vehicle license plate detection using local fractal dimension and morphological analysis,” in *Proc. IEEE 1st Int. Forum Strategic Technol.*, Ulsan, Korea, 2006, pp. 47–50.38 IEEE Transactions On Vehicular Technology, Vol. 62, No. 1, January 2013.

- [6] H. Zhang, W. Jia, X. He, and Q. Wu, "A fast algorithm for license plate detection in various conditions," in *Proc. IEEE Int. Conf. Syst., Man, Cybern.*, Taipei, Taiwan, 2006, pp. 2420–2425.
- [7] S. Kim, D. Kim, Y. Ryu, and G. Kim, "A robust license-plate extraction method under complex image conditions," in *Proc. 16th Int. Conf. Pattern Recognit.*, Quebec City, QC, Canada, 2002, pp. 216–219.
- [8] Z.-X. Chen, Y.-L. Cheng, F.-L. Chang, and G.-Y. Wang, "Automatic license-plate location and recognition based on feature salience," *IEEE Trans. Veh. Technol.*, vol. 58, no. 7, pp. 3781–3785, Sep. 2009.
- [9] H. Caner, H. S. Gecim, and A. Z. Alkar, "Efficient embedded neuralnetwork- based license plate recognition system," *IEEE Trans. Veh. Technol.*, vol. 57, no. 5, pp. 2675–2683, Sep. 2008.
- [10] S. Rovetta and R. Zunino, "License-plate localization by using vector quantization," in *Proc. Int. Conf. Acous., Speech, Signal Process.*, 1999, pp. 1113–1116.
- [11] W. Jia, H. Zhang, and X. He, "Region-based license plate detection," *J. Netw. Comput. Appl.*, vol. 30, no. 4, pp. 1324–1333, Nov. 2007.
- [12] H. Bai, J. Zhu, and C. Liu, "A fast license plate extraction method on complex background," in *Proc. IEEE Int. Conf. Intell. Transp. Syst.*, 2003, pp. 985–987.
- [13] S. Thanongsak and C. Kosin, "The recognition of car license plate for automatic parking system," in *Proc. 5th Int. Symp. Signal Process. Appl.*, Brisbane, QLD, Australia, 1999, pp. 455–457.
- [14] D. Bradley and G. Roth, "Adaptive thresholding using the integral image," *J. Graph. Tools*, vol. 12, no. 2, pp. 13–21, Jun. 2007.
- [15] P. D. Wellner, "Adaptive thresholding for the DigitalDesk," Rank Xerox Ltd., Birmingham, U.K., Tech. Rep. EPC-1993-110, 1993.
- [16] F. Shafait, D. Keysers, and T. M. Breuel, "Efficient implementation of local adaptive thresholding techniques using integral images," in *Proc. Doc. Recognit. Retrieval*, 2007, pp. 681510-1–681510-6.

Optimization of Abrasive Flow Machining Parameters on Launch Vehicle Component Using Taguchi Method

Deepak Devassia¹, Dr. Shajan Kuriakose², George Oommen³

¹PG Scholar, Department of Mechanical Engineering, MA college of Engineering Kothamangalam, Kerala, India.

²Professor, Department of Mechanical Engineering, MA college of Engineering Kothamangalam, Kerala, India.

³SCI/Engr 'SF' Manager, CS&SC-CF, CSC/LPSC/ISRO, Valiyamala, Trivandrum

Email: deepakdevassia@gmail.com, +91-8943074807

Abstract— Abrasive flow machining is a non-conventional machining process which is used to polish, deburr, and radius hard to reach surfaces like intricate geometries and edges by flowing an abrasive laden viscoelastic polymer over them. Conventional methods have limitations for machining such components with complex geometries. In this process, abrasive medium flow inside the crossed holes of a launch vehicle's fluid component made of Z30C13 stainless steel. In this study, the effect of process parameters such as abrasive size, abrasive concentration and number of cycles were studied on surface roughness. Taguchi's L9 orthogonal array is preferred with three levels of parameters for experimental design without considering any interaction. The percentage contribution of each factor is found by ANOVA.

Keywords— Abrasive Flow Machining, Abrasive Size, Abrasive Concentration, Number of Cycles, Surface Roughness, Z30C13 Stainless Steel, Taguchi Method, ANOVA.

INTRODUCTION

Abrasive flow machining is a process for producing high quality surfaces that are difficult to access, especially inner profiles and is used to deburr, remove recast layer and radius surfaces. The launch vehicle fluid control components have cross holes, internal passageways, concave & convex edge blending and micro slots. Deburring and polishing of these features is difficult because of inaccessibility of tools. Manual deburring increases the risk of damaging finished surfaces. Many of the recent anomalies in control components have been attributed to loose metal particles getting entrapped on the seating surfaces. More often these particles are found to be generated from cross holes or internal passageways which are hidden from the normal vision. These particles are at many times not visible to the naked eye and can be seen only under magnification. Specialized viewing equipment's are not normally available at the shop floor to locate such type of particles. As a result machining of such components to the required finish become difficult at the shop floor. AFM is an ideal solution for precision deburring, polishing and edge radiusing of internal and external surfaces of machined components. AFM involves the use of an abrasive laden polymer which is forced to flow through the restricted flow passage with the help of the hydraulic cylinders. Abrasive action is highest in most restricted passage leading to the removal of burrs and edge polishing. The objective of the present work is to find out the set of optimum conditions for the selected control factors in order to reduce surface roughness using Taguchi's robust design methodology in abrasive flow machining of Z30C13 stainless steel.

2. LITERATURE SURVEY

Literature survey is carried out extensively to explore the various process parameters of abrasive flow machining and their effect on various output responses [1-10]. A thorough study of Taguchi's optimization and ANOVA have been conducted to optimize the process parameters of this study [11-12]. The concept of prediction of results using regression model and ANN were also studied [13]. Very few works have been carried out in the optimization of process parameters in abrasive flow machining of Z30C13 stainless steel with different controlled parameters such as abrasive size, abrasive concentration and number of cycles etc.

3. EXPERIMENTAL SETUP AND DESIGN

A two way abrasive flow machine setup has been developed for the study. The details of the machine is shown below. The work material selected is Z30C13 stainless steel.

3.1 Specification of Abrasive Flow Machine

The machine consist of a timer circuit to control the speed and direction of flow, two pneumatic cylinders which uses the power of compressed gas to reciprocate back and forth. One back and forth movement of the piston is called a cycle. The number of cycles can be adjusted by setting the timer circuit, to get desired number of cycles. The machining tests are conducted under the different conditions of abrasive size, abrasive concentration and number of cycles.



Figure No.1: Abrasive flow machine

3.2 Workpiece

The workpiece used is a launch vehicle fluid component which is made of Z30C13 stainless steel. Z30C13 is a martensitic stainless steel with 12% Chromium which is sufficient to give good corrosive resistance properties. Stress relieved and hardened conditions provide full corrosion resistance. It can resist corrosion by fresh water, atmosphere, carbonic acid, steam, gasoline, crude oil, perspiration, sterilizing solutions, etc. Typical applications are cutlery, valve parts, surgical instruments, spindles, nozzles, shafts, gears. It presents high strength after quenching and can be magnetized.



Figure No.2: CAD model of the workpiece

3.3 Abrasive Media

The abrasive media used in Abrasive Flow Machining provides the actual material removal that is polishing, deburring and edge radiusing. The abrasive media mainly consist of two parts: silicon based polymer and abrasive particles. The abrasive particle used in this study were Silicon Carbide (SiC). This particles are mixed with the polymer base to get the abrasive media.



Figure No. 3: Abrasive media

The abrasive media were developed from Vikram Sarabhai Space Center's Polymer lab of ISRO.

3.4 Design of Experiments

In this work, the optimum conditions for surface roughness in abrasive flow machining of Z30C13 stainless steel is obtained by using Taguchi robust design methodology. $L_9 (3^3)$ orthogonal array is used to conduct the experiment.

3.4.1 Selection of control factors and levels

Three process parameters with three levels are chosen as the control factors such that the levels are sufficiently far apart so that they cover wide range. The process parameter and their ranges are finalized reference from books and literature.. The three control factors selected are abrasive size (A), abrasive concentration (B) and number of cycles (C). Launch vehicle component made of Z30 C13 stainless steel were used in experimentation. The machining is performed for nine individual components. The control levels and their alternative levels are listed in Table No.1.

Table No. 1 Control Factors and Levels

Factors /Level	Abrasive size (A) (µm)	Abrasive concentration (B) (% by weight)	Number of cycles (C) (cycles/min)
1	8	30	100
2	63	40	200
3	150	50	300

3.4.2 Selection of orthogonal array

In this study, AFM parameters such as particle size, abrasive concentration and number of cycles are selected and the numbers of levels selected for each parameter are three. The Taguchi's orthogonal array method is a very effective method to deal with responses influenced by multi-variables. Compared to the conventional approach to experimentation, this method reduces the number of experiments that are required to model the response functions. The selection of Orthogonal array (OA) is based upon the number of factors and levels that are considered for doing the experiment. The degree of freedom (DOF) for each of the factor is 2 (DOF for a factor = number of levels - 1) and therefore the total DOF obtained is 8 (i.e., 4x2=8).The selected OA's degree of freedom must be greater than the total DOF of all the factors. The DOF for an OA is given by number of experiments minus 1. Hence L9 is selected for the study which has 8 degrees of freedom which is the smallest array that can be selected with the 3 level 3 factor experiment. The selected OA is presented on the following Table. 2. The Factor assignment for L₉ (3³).has been tabulated in Table No.3.

Table No.2: Standard L₉ (3⁴) O.A .

Experiment Number	Column		
	A	B	C
1	1	1	1
2	1	2	2
3	1	3	3
4	2	1	2
5	2	2	3
6	2	3	1
7	3	1	3
8	3	2	1
9	3	3	2

Table No. 3: Experimental Design

Experiment Number	Column		
	Abrasive size(A) (µm)	Abrasive concentration (B) (% by weight)	Number of cycles (C) (cycles/min)
1	8	30	100
2	8	40	200
3	8	50	300
4	63	30	200
5	63	40	300
6	63	50	100
7	150	30	300
8	150	40	100
9	150	50	200

3.4.3. Plan of experiments

The scope and objective of the present work have already been mentioned in the forgoing cases. Accordingly, the present study has been done through the following plan of experiment:

1. A two way abrasive flow machine and fixture, for positioning the workpiece while machining is developed.
2. Workpiece is made as per the required dimension by a CNC milling machine for the experiment.
3. Abrasive media is developed from Vikram Sarabhai Space Center, Trivandrum.
4. Machining parameters abrasive size, abrasive concentration and number of cycles are selected through knowledge from extensive literature survey and also in view of machine standard specifications.
5. The machining is done by filling the abrasive media inside the cylinders and by fixing the workpiece in the fixture.
6. The nine different combination of levels of the parameters are set one by one and machined .

7. Surface roughness (Ra) is measured from the internal passage of the workpiece using Taylor Hobson Talysurf

4. RESULTS AND DISCUSSION

In the experiment, the desired characteristic for surface roughness is lower the better. It means that lowest surface is desirable for better performance. The equation to find the S/N ratio for this characteristic is given below.

$$S/N = -10\log\left[\frac{1}{n}\sum_{i=1}^n (y_i^2)\right] \quad (1)$$

Where, n is the number of measurements in a trial and yi is the measured value in a trial.

The results of surface roughness values of 9 experiments and the signal to noise ratios of each set of experiment for L9 array is tabulated in Table No. 4.

Table No. 4: Experimental data for surface roughness (Ra)

Particle size (µm)	Abrasive concentration (% by weight)	No. of cycles (cycles/min)	Ra(µm)	S\N Ra
8	30	100	0.61	4.293403
8	40	200	0.57	4.882503
8	50	300	0.49	6.196078
63	30	200	0.65	3.741733
63	40	300	0.58	4.73144
63	50	100	0.57	4.882503
150	30	300	0.68	3.349822
150	40	100	0.7	3.098039
150	50	200	0.67	3.478504

Based on the analysis of S/N ratio, the optimal machining performance for the surface roughness is obtained at particle size 8 µm (level 1), abrasive concentration 50 % by weight (level 3) and number of cycles 300 cycles/min (level 3). In the analysis, particle size is shown as the most influencing parameter followed by abrasive concentration and number of cycles.

The ANOVA calculation is performed for the results obtained i.e. Surface roughness values from Table No.4. The calculations are done with the Minitab Statistical Software version 17.

Table No.5: Analysis of Variance for Surface Roughness

Source	Degrees of Freedom	Sum of squares	Mean of Squares	F ratio P	P	% of contribution
Particle size	2	0.024867	0.012433	93.25	0.011	68.41
Concentration	2	0.007400	0.003700	27.75	0.035	20.35
No. of cycles	2	0.004067	0.002033	15.25	0.062	11.10
Error	2	0.000267	0.000133			0.14
Total	8	0.036600				

Based on the ANOVA results in Table No.5, the percentage contribution of various factors to surface roughness is identified. Here, particle size is the most influencing factor followed by abrasive concentration. The percentage contribution of Particle size and Abrasive concentration towards surface roughness is 68.41% and 20.35% respectively. Also the probability level of Number of cycles is more than α (0.05) which indicates that Number of cycles has least contribution towards surface roughness. The main effects plot shows the influence of each level of factors and the SN ratio with maximum value is taken as the optimum values of surface roughness. The plot shows that surface roughness increases as particle size increases and decreases with increase in concentration and number of cycles

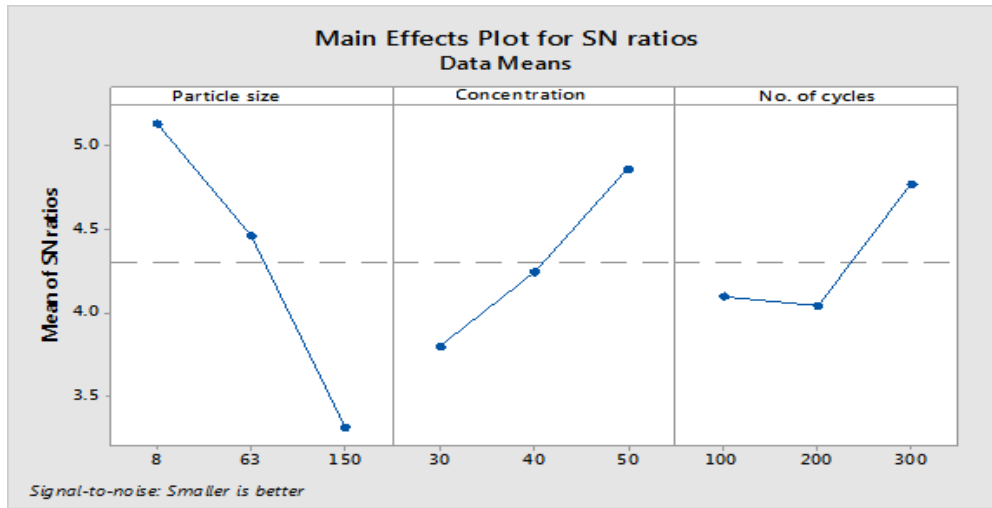


Figure No. 4: Signal to Noise Plot for Surface Roughness

4.1 Regression equation for surface roughness

The regression equation is found from the available results for predicting the surface roughness with a different combination of the process parameters.

$$\text{Surface Roughness, Ra } (\mu\text{m}) = 0.7305 + 0.000898 \text{ Particle size } (\mu\text{m}) - 0.003500 \text{ Concentration } (\% \text{ by weight}) - 0.000217 \text{ No. of cycles}$$

4.2 Confirmation Test

The confirmation test is the final step in verifying the results obtained from Taguchi's design approach. The optimal conditions are set for the significant factors and experiments are run under specified machining conditions. The results from the confirmation experiment are compared with the predicted results based on the parameters and levels tested. The predicted result is also compared with the results predicted by ANN. The optimal combination is present in the selected orthogonal array so no need of further experimenting. The validity of the regression equation is checked by taking random combination from the 27 combination, other than the 9 and predicting the roughness value of each combination by regression and ANN and experimenting with the same combination. The results are compared to validate the regression equation.

Table No.6: Experimental v/s Predicted results

LEVEL	Experimental Ra	Predicted Ra	
		by regression	by ANN
A1B3C3 (OPTIMAL)	0.49	0.497	0.49
A1B3C1	0.56	0.54	0.544
A2B3C3	0.54	0.55	0.542
A3B3C2	0.649	0.64	0.67
A1B1C3	0.58	0.58	0.59

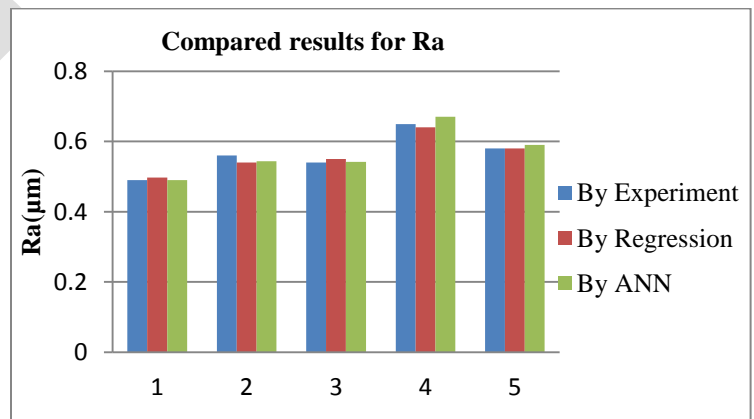


Figure No 5: Compared result for Ra

5. CONCLUSION

In this study the effect of abrasive flow machining parameters on surface roughness of Z30C13 stainless steel was studied using Taguchi's L9 orthogonal array method. From the results, it is found that, abrasive size and concentration play a significant role in AFM operation related to surface roughness. Number of cycles has no significant effect on surface roughness. Also it is found that, for

lower surface roughness the optimum levels for abrasive size, concentration and number of cycle are $8\mu\text{m}$ (level 1), 50 % by weight (level 3) and 300 cycles/min (level 3) respectively. Analysis of variance (ANOVA) is used to find the significance of the machining parameters and their contributions on surface roughness individually. Particle size is found to be the most influencing parameter on surface roughness with 68.41 % contribution followed by the concentration with 20.35 % contribution. The obtained result is used to model a regression equation. The validity of the model is found by predicting and experimenting the unknown parameter combination and comparing the result. In this study the predicted and experimented results are almost similar which shows the regression model is fit for prediction

ACKNOWLEDGMENT

The authors gratefully acknowledge the technical support and guidance provided by the Liquid Propulsion System Center of Indian Space Research Organization, Trivandrum and Carborundum Universal Limited, Kalamassery for providing the essential abrasive particles.

REFERENCES:

- [1] Ravi Gupta and Rahul Wandra "Effect and optimization of Process Parameters on surface roughness in Abrasive Flow Machining Process" IJITKM Special Issue (ICFTEM-2014), May 2014, pp. 266-273
- [2] V.K. Jain and S.G. Adsul "Experimental investigations into abrasive flow machining (AFM)" International Journal of Machine Tools & Manufacture 40 (2000) 1003–1021, November 16th, 1999
- [3] Jose Cherian and Jeoju M Issac "Effect of Process Variables in Abrasive Flow Machining" International Journal of Emerging Technology and Advanced Engineering, Volume 3, Issue 2, February 2013
- [4] Somashekhar S. Hiremath, Vidyadhar H. M and Makaram Singaperumal " A Novel Approach for Finishing Internal Complex Features Using Developed Abrasive Flow Finishing Machine" International Journal of Recent advances in Mechanical Engineering (IJMECH) Vol.2, No.4, November 2013
- [5] Przyklenk K. "Abrasive flow machining- A process for surface finishing and deburring of work pieces with a complicated shape by means of abrasive laden media", Advances in Non-Traditional Machining, PED, ASME (1986), Vol. 22 , pp. 101-110
- [6] Loveless T.R, Willams R.E and Rajurkar K. "A Study of The Effects of Abrasive Flow Finishing on Various Machined Surfaces" Journal of Material Processing Technology, 47 (1994), pp.133-151.
- [7] R.K. Jain, V.K. Jain, "Abrasive fine finishing processes - a review" International Journal for Manufacturing Science and Production (1999) 55.
- [8] Jain R K, Jain V.K, Dixit P.M; Modeling of Material Removal And Surface Roughness in Abrasive Flow Machining. International journal of Machine tool and manufacture. 30(1999) 1903-1923.
- [9] Ravi Gupta, Rahul O Vaishya, R.S Walia and P.K Kalra "Experimental Study of Process Parameters on Material Removal Mechanism in Hybrid Abrasive Flow Machining Process (AFM)" International Journal Of Scientific Research, Vol 2, Issue 6 June 2013, ISSN No 2277 – 8179
- [10] Saad Saeed Siddiqui and M Hameedullah "Abrasive flow machining performance measures on work-piece surfaces having different vent/passage considerations for media outflow" International Journal of Computer Communication and Information System Vol2. No1. ISSN: 0976–1349, Jul Dec 2010
- [11] D. Ahmadkhaniha, M. Heydarzadeh Sohi, A. Zarei-Hanzaki, S.M. Bayazid and M. Saba "Taguchi optimization of process parameters in friction stir processing of pure Mg" Journal of Magnesium and Alloys 3 (2015) 168-172, May 13th, 2015
- [12] Arshad Noor Siddiquee, Zahid A. Khan, Pankul Goel, Mukesh Kumar, Gaurav Agarwalb and Noor Zaman Khana "Optimization of Deep Drilling Process Parameters of AISI 321 Steel using Taguchi Method" 3rd International Conference on Materials Processing and Characterisation, 2014
- [13] Rajendra Darbar, D. M. Patel and Jaimin Patel "Process Parameters Optimization of FDM Process And Application Of Taguchi Approach and ANN –The Review" IJERA, ISSN: 2248-9622 Vol. 3, Issue 1, January -February 2013, pp.743-746

Diversity Analysis of Coded OFDM in Frequency Selective Channels

¹Koshy G., ²Soumya J. W.

¹PG Scholar, ²Assistant Professor,
Communication Engineering, Mahatma Gandhi University
Caarmel Engineering College, Pathanamthitta, Kerala
¹gspk.ko@gmail.com, ²soumyawills@yahoo.co.in

Abstract— For broadband wireless communication systems, Multi-Input Multi-Output (MIMO) techniques have been incorporated with Orthogonal Frequency Division Multiplexing (OFDM).. Beamforming is a multi-input multi-output technique utilizing the channel knowledge both at the transmitter and the receiver. Multiple beamforming uses more than one subchannel to improve the capacity. For frequency selective channels, to achieve Inter Symbol Interference and achieve spatial diversity combine beamforming with OFDM. Also by adding channel coding spatial diversity and multipath diversity can be achieved The diversity analysis of BICMB-OFDM-SG is limited to $R_c SL \leq 1$ where L is the number of channel taps, S is the number of parallel streams transmitted at each subcarrier and R_c is the code rate. In this paper precoding technique is employed to overcome this limitation. Also precoding provides better performance.

Keywords— MIMO systems, Beamforming, diversity methods, subcarrier multiplexing.

INTRODUCTION

High spectral efficiency and performance for a given bandwidth can be achieved by Multiple-Input Multiple-Output (MIMO) systems. In flat fading MIMO channels, single beamforming carrying only one symbol at a time achieves full diversity but spatial multiplexing without channel coding results in the loss of the full diversity order. Bit-Interleaved Coded Multiple Beamforming (BICMB) overcomes the performance degradation.

If the channel is in frequency selective fading, Orthogonal Frequency Division Multiplexing (OFDM) can be used to combat the Inter-Symbol Interference (ISI) caused by multipath propagation. Along with this for MIMO channels beamforming achieves multipath diversity and spatial diversity. Advantage of OFDM is that it has high spectral efficiency. By adding channel coding multipath diversity can be achieved. Both spatial diversity and multipath diversity can be achieved by adding channel coding. The subcarrier grouping technique is employed to provide multi-user compatibility. Bit-Interleaved Coded Multiple Beamforming Orthogonal Frequency Division Multiplexing with Subcarrier Grouping (BICMB-OFDM-SG) technique exploits these properties. For broadband wireless communication BICMB-OFDM be an important technique. In this paper, the diversity analysis of BICMB-OFDM-SG with precoding is carried out.

SYSTEM MODEL

Consider a BICMB-OFDM-SG system employing N_t transmit and N_r receive antennas, a convolutional code of code rate R_c , and transmitting S parallel data streams.

First, generate the binary message and it is encoded using convolution encoder of code rate R_c . Trellis Structure is used to create required code rate, for a high rate punctured code a perforation matrix is combined. From the information bits this generates the bit codeword c . The code word is given to bit interleaver. For burst error-correction, interleaving is widely used. Here random bit interleaver is used.

In digital communication and storage systems, to improve the performance of forward error correcting codes interleaving is used frequently. Many communication channels in now a days are not memory less. So errors typically occur in bursts rather than independently. It fails to recover the original code word, if the number of errors within a code word exceeds the error-correcting code's capability. Interleaving creates a more uniform distribution of errors by shuffling source symbols across several code words. Interleaving in multi carrier communication also provide frequency diversity e.g., to mitigate frequency-selective fading or narrowband interference.

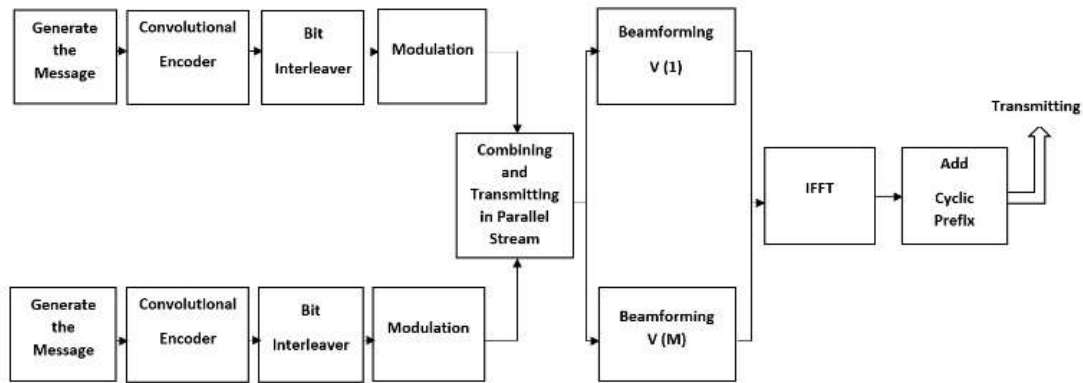


Fig. 1: Bit Interleaved Coded Multiple Beamforming with Subcarrier Grouping transmitter side

The interleaved bit sequence is then modulated, here Quadrature Amplitude Modulation (QAM) is used. Let the number of streams transmitted for each subcarrier be $S \leq \min\{N_t, N_r\}$ where N_t and N_r be the number of transmit and receive antennas. The symbol sequence is transmitted through M subcarriers. Hence, an $S \times 1$ symbol vector $x_k(m)$ is transmitted through the m^{th} subcarrier at the k^{th} time instant with $m = 1, \dots, M$. Inverse Fourier Transform is applied to the sequence. Then Cyclic Prefix is added to the sequence. The length of Cyclic Prefix (CP) is $L_{cp} \geq L$ with L denoting the number of channel taps. Cyclic prefix is employed by OFDM to combat ISI caused by multipath propagation. It is then transmitted.

Let the quasi-static flat fading MIMO channel observed at the m^{th} subcarrier be $H(m)$. The frequency selective fading MIMO channel is assumed to be Rayleigh fading channel. For each subcarrier the Singular Value Decomposition beamforming is carried out. The beamforming matrices at the m^{th} subcarrier are determined by SVD of $H(m)$,

$$H(m) = U(m)\Lambda(m)V^H(m),$$

where the $U(m)$ matrix has order of $N_r \times N_r$ and the $V(m)$ matrix of $N_t \times N_t$ are unitary, and the $N_r \times N_t$ matrix $\Lambda(m)$ is diagonal rectangular matrix. When S streams are transmitted at the same time, $U(m)$ and $V(m)$ are chosen as beamforming matrices at the receiver and transmitter at the m^{th} subcarrier, respectively. The multiplications with beamforming matrices are carried out for each subcarrier.

The system input-output relation for the m^{th} subcarrier at the k^{th} time instant is

$$y_{k,s}(m) = \lambda_s(m)x_{k,s}(m) + n_{k,s}(m)$$

with $s = 1, \dots, S$, where $y_{k,s}(m)$ and $x_{k,s}(m)$ are the s^{th} element of the $S \times 1$ received symbol vector $y_k(m)$ and the transmitted symbol vector $x_k(m)$ respectively, and $n_{k,s}(m)$ is the additive white Gaussian noise with zero mean.

In the receiver side the received data contains added white noise. Cyclic prefix is being removed from the received data. Then Fourier transform is applied to the sequence. Using the Beamforming matrix $U(m)$, information is retrieved. The data is then separated to different encoders. Each encoding section consists of QAM demodulator, Random Bit De-interleaver, and Viterbi decoder. The output obtained from the decoder is the recreated message.

Finally, the Viterbi decoder, which applies the soft-input Viterbi decoding to find the information bit sequence \hat{b} the message from the codeword \hat{c} with the minimum sum weight.

The Maximum Likelihood (ML) bit metrics at the receiver for $c_k = b \in \{0, 1\}$ as

$$\Delta(y_{k,s}(m), c_{k'}) = \min_{x \in X_{c_{k'}}^1} |y_{k,s}(m) - \lambda_s(m)x|^2$$

and makes decisions according to

$$\hat{c} = \arg \min_c \sum_{k'} \Delta(y_{k,s}(m), c_{k'})$$

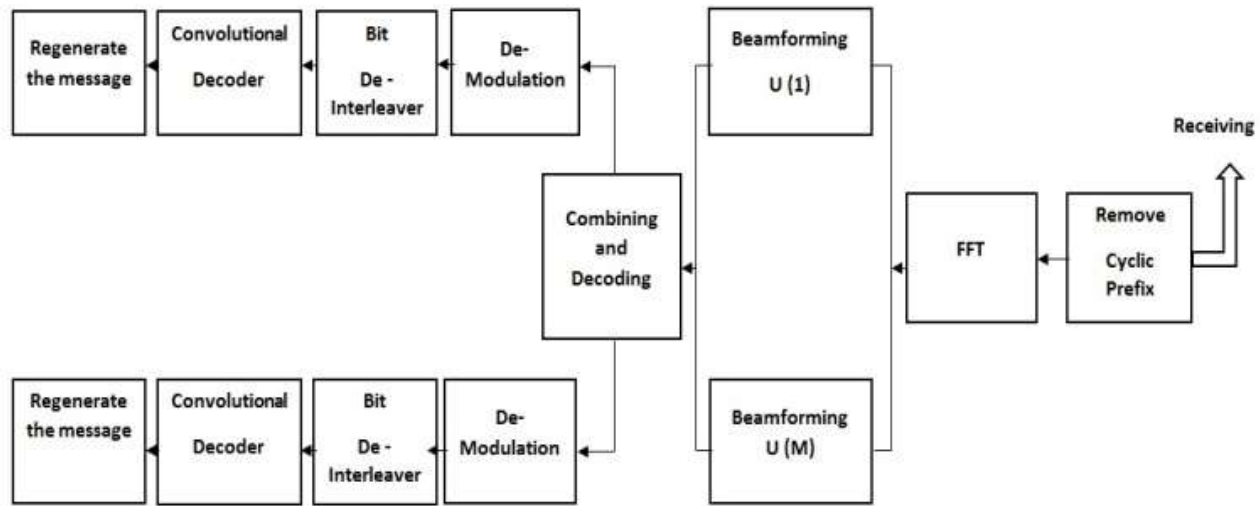


Fig. 2: Bit Interleaved Coded Multiple Beamforming with Subcarrier Grouping receiver side

In the receiver side the received data contains added white noise. Cyclic prefix is being removed from the received data. Then Fourier transform is applied to the sequence. Using the Beamforming matrix $U(m)$, information is retrieved. The data is then separated to different encoders. Each encoding section consists of QAM demodulator, Random Bit De-interleaver, and Viterbi decoder. The output obtained from the decoder is the recreated message.

Finally, the Viterbi decoder, which applies the soft-input Viterbi decoding to find the information bit sequence \hat{b} the message from the codeword \hat{c} with the minimum sum weight.

The Maximum Likelihood (ML) bit metrics at the receiver for $c_k = b \in \{0, 1\}$ as

$$\Delta(y_{k,s}(m), c_{k'}) = \min_{x \in X_{c_{k'}}} |y_{k,s}(m) - \lambda_s(m)x|^2$$

and makes decisions according to

$$\hat{c} = \arg \min_c \sum_{k'} \Delta(y_{k,s}(m), c_{k'})$$

In practice, number of subcarriers M is always much larger than number of taps L . There exists correlation among subcarriers. Due to subcarrier correlation it will cause performance degradation. Subcarrier grouping is done to overcome the performance degradation. The subcarrier grouping technique is to transmit information through multiple group of subcarriers through multiple streams. The advantages of using OFDM are multi-user interference elimination, complexity reduction and Peak-to-Average Ratio (PAR) reduction.

For $L < M$, although there exists among subcarriers some subcarriers could be uncorrelated numbers. There are $G = M/L$ groups of uncorrelated subcarriers. So transmit multiple streams of bit codewords through these G different groups of uncorrelated subcarriers

The diversity of BIMB-OFDM_SG is limited to $R_c SL \leq 1$. In the case of $R_c SL > 1$, there always exists at least an error path with no errored bits transmitted through the first subchannel of a subcarrier. Proof of the limitation is explained in [2].

BICMB-OFDM-SG WITH PRECODING

The precoding technique can be applied to each subcarrier. As compared to BICMBOFDM- SG in Fig. 1, two more precoding blocks are added along with the channel coding, bit interleaver, and modulation. At the receiver side post decoding is done. Using this precoding technique it is able to overcome the criteria BICMB-OFDM-SG of $R_cSL \leq 1$. So it provides better performance with the same transmission rate and offers multi-user compatibility.

Fig. 3 and fig. 4 represents the structure of BICMB-OFDM-SG with precoding. In MIMO antenna communications precoding is a generalization of beamforming to support multi-stream transmission.

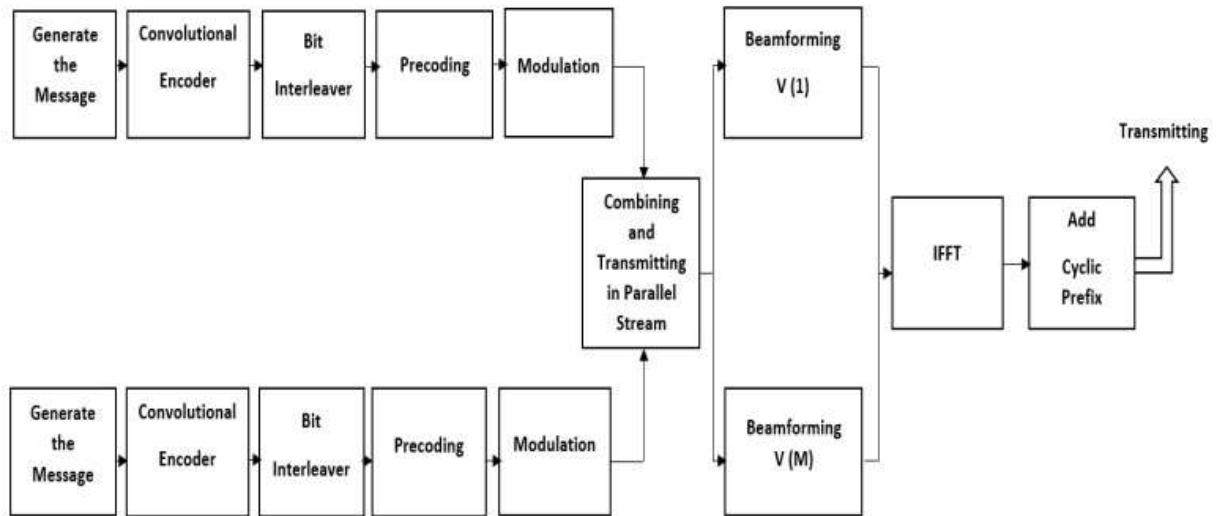


Fig.3: BICMB-OFDM_SG with precoding transmitter side

In precoding data from the interleaver is being previously coded before transmitting. The precoded data is then combined, beamformed and transmitted. At the receiving side after receiving the data, the postcoding technique is done. Information obtained after postcoding is given to demodulator, deinterleaver and decoder.

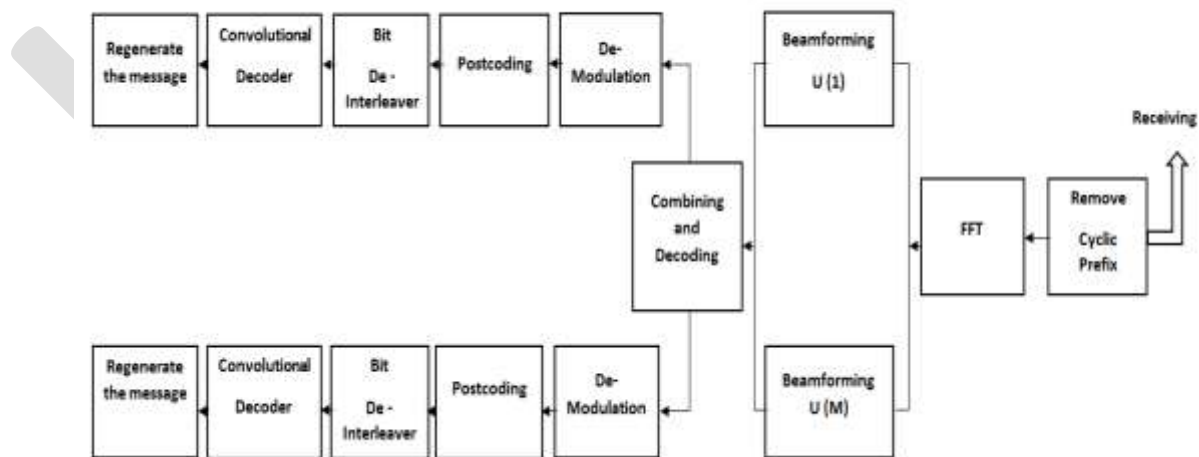


Fig. 4: BICMB-OFDM_SG with precoding receiver side

SIMULATION RESULTS

The simulation is done on MATLAB 2010. To verify the diversity analysis, $M = 64$ BICMB-OFDM-SG with $L = 1$ using 16-QAM are considered for simulations. The number of employed subchannels for each subcarrier is assumed to be the same. The generator polynomials in octal for the convolutional codes with $R_c = \frac{1}{2}$ is (5, 7) respectively. The length of CP is $L_{cp} = 8$. Different streams with $S=1$ and $S=2$ is being considered.

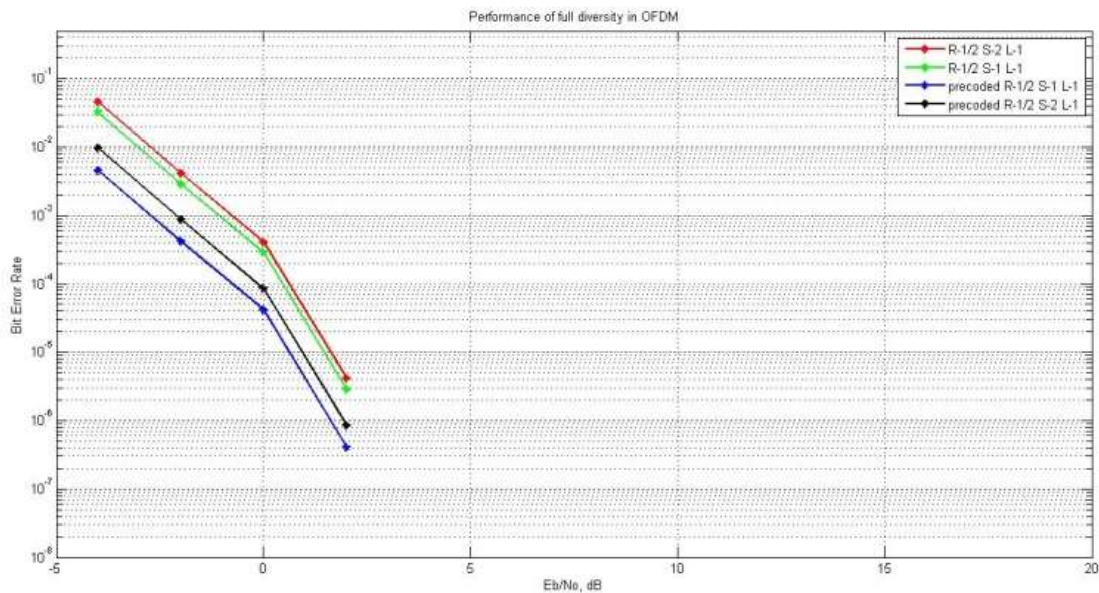


Fig. 5: BER vs. SNR for BICMB-OFDM-SG with and without precoding over equal power channel taps.

CONCLUSION

For frequency selective fading MIMO channels BICMB-OFDM-SG combines MIMO and OFDM to achieve spatial diversity, multipath diversity, spatial multiplexing, and frequency multiplexing. For broadband wireless communication it is an important technique. The comparison of BICMB-OFDM-SG and BICMB-OFDM-SG with precoding is carried out in this paper.

A sufficient and necessary condition in BICMB-OFDM-SG for achieving full diversity was $R_c S L \leq 1$. So using this precoding technique it is able to overcome the limitation and provides better result. Precoding also provide multi-user compatibility. So it is very important technique in practical application. Further improvement in diversity analysis can be done by using Low Density Parity Codes (LDPC) instead of Convolutional Codes.

REFERENCES:

- [1] L. Zheng and D. Tse, "Diversity and multiplexing: a fundamental tradeoff in multiple-antenna channels" IEEE Trans. Inf. Theory, vol. 49, no. 5, pp. 1073-1096, May 2003.
- [2] Boyu Li and Ender Ayanoglu, "Diversity Analysis of Bit-Interleaved Coded Multiple Beamforming with Orthogonal Frequency Division Multiplexing" IEEE Trans. Communications, Vol. 61, No. 9, September 2013.
- [3] E. Sengul, E. Akay, and E. Ayanoglu, "Diversity analysis of single and multiple beamforming", IEEE Trans. Commun., vol. 54, no. 6, pp. 990-993, Jun. 2006.
- [4] L. G. Ordoez, D. P. Palomar, A. Pages-Zamora, and J. R. Fonollosa, "High-SNR analytical performance of spatial multiplexing MIMO systems with CSI, IEEE Trans. Signal Process.", vol. 55, no. 11, pp. 5447-5463, Nov. 2007.
- [5] E. Akay, E. Sengul, and E. Ayanoglu, "Achieving full spatial multiplexing and full diversity in wireless communications", in Proc. 2006 IEEE WCNC, pp. 2046-2050.
- [6] Enis Akay, Ersin Sengul, and Ender Ayanoglu "Bit-interleaved coded multiple beamforming", IEEE Trans. Commun., vol. 55, no. 9, pp. 1802-1811, Sep. 2007.
- [7] N. Gresset and M. Khanfouci, "Precoded BICM design for MIMO transmit beamforming and associated low-complexity algebraic receivers", in Proc. 2008 IEEE GLOBECOM.
- [8] H. J. Park and E. Ayanoglu, "Diversity analysis of bit-interleaved coded multiple beamforming", in Proc. 2009 IEEE ICC.

- [9] Enis Akay and Ender Ayanoglu, "Full Frequency Diversity Codes for Single Input Single Output Systems" in Proc. 2004 IEEE VTC Fall, vol. 3, pp. 18701874.
- [10] Enis Akay and Ender Ayanoglu, "Achieving Full Frequency and Space Diversity in Wireless Systems via BICM, OFDM, STBC and Viterbi Decoding" IEEE Trans. Commun., vol. 54, no. 12, pp. 21642172, Dec. 2006.
- [11] E. Akay, E. Sengul, and E. Ayanoglu, "Performance analysis of beamforming for MIMO OFDM with BICM in Proc. 2005 IEEE ICC, vol. 1, pp. 613617.
- [12] Z. Wang and G. B. Giannakis, "Wireless multicarrier communications: where Fourier meets Shannon, IEEE Signal Process. Mag., vol. 17, no. 3, pp. 2948, May 2000.
- [13] D. L. Goeckel and G. Ananthaswamy, "On the design of multidimensional signal sets for OFDM systems, IEEE Trans. Commun., vol. 50, no. 3, pp. 442452, Mar. 2002.
- [14] Z. Liu, Y. Xin, and G. B. Giannakis, "Linear constellation precoding for OFDM with maximum multipath diversity and coding gains, IEEE Trans. Commun., vol. 51, no. 3, pp. 416427, Mar. 2003.
- [15] D. Haccoun and G. Begin, "High-rate punctured convolutional codes for Viterbi and sequential decoding, IEEE Trans. Commun., vol. 37, no. 11, pp. 11131125, Nov. 1989.
- [16] I. Lee, A. M. Chan, and C.-E. W. Sundberg, "Space-time bit-interleaved coded modulation for OFDM systems, IEEE Trans. Signal Process., vol. 52, no. 3, pp. 820825, Mar. 2004.
- [17] Z. Liu, Y. Xin, and G. B. Giannakis, "Space-time-frequency coded OFDM over frequency-selective fading channels, IEEE Trans. Signal Process., vol. 50, no. 10, pp. 24652476, Oct. 2002.
- [18] G. Caire, G. Taricco, and E. Biglieri, "Bit-interleaved coded modulation, IEEE Trans. Inf. Theory, vol. 44, no. 3, pp. 927946, May 1998.
- [19] B. Li and E. Ayanoglu, "Diversity analysis of bit-interleaved coded multiple Beamforming with orthogonal frequency division multiplexing, in Proc. 2013 IEEE ICC.
- [20] B. Li and E. Ayanoglu, "Diversity analysis of bit-interleaved coded multiple beam-forming with orthogonal frequency division multiplexing". arXiv: 1109.3510. Available: <http://arxiv.org>
- [21] N. Gresset, "New space-time coding techniques with bit-interleaved coded modulations,
- [22] O. Edfors, M. Sandell, J.-J. van de Beek, S. K. Wilson, and P. O. Borjesson, "OFDM channel estimation by singular value decomposition, IEEE Trans. Commun., vol. 46, no. 7, pp. 931939, Jul. 1998.
- [23] A. Edelman, "Eigenvalues and condition numbers of random matrices, Ph.D. dissertation, Massachusetts Institute of Technology, 1989.
- [24] P. J. Smith and L. M. Garth, "Distribution and characteristic functions for correlated complex Wishart matrices, J. Multivariate Analysis, vol. 98, p. 661677, Apr. 2007.
- [25] P.-H. Kuo, P. J. Smith, and L. M. Garth, "Joint density for eigenvalues of two correlated complex Wishart matrices: characterization of MIMO systems, IEEE Trans. Wireless Commun., vol. 6, no. 11, pp. 39023906, Nov. 2007.
- [26] M. Chiani, M. Z. Win, and H. Shin, "MIMO networks: the effects of interference, IEEE Trans. Inf. Theory, vol. 56, no. 1, pp. 336349, Jan. 2010.
- [27] H. J. Park and E. Ayanoglu, "An upper bound to the marginal PDF of the ordered eigenvalues of Wishart matrices and its application to MIMO diversity analysis, in Proc. 2010 IEEE ICC
- [28] A. Ghosh, J. Zhang, J. G. Andrews, and R. Muhamed, Fundamentals of LTE. Pearson Education, Inc., 2011.
- [29] Y. S. Cho, J. Kim, W. Y. Yang, and C. G. Kang, MIMO-OFDM Wireless Communications with MATLAB. Wiley-IEEE Press, 2010.
- [30] H. J. Park and E. Ayanoglu, "Constellation precoded beamforming, in Proc. 2009 IEEE GLOBECOM.
- [31] H. J. Park and E. Ayanoglu, "Bit-interleaved coded multiple beamforming with constellation precoding, in Proc. 2010 IEEE ICC.
- [32] H. J. Park, B. Li, and E. Ayanoglu, "Multiple beamforming with constellation precoding: diversity analysis and sphere decoding, in Proc. 2010 ITA.
- [33] H. J. Park, B. Li, and E. Ayanoglu, "Constellation precoded multiple beamforming, IEEE Trans. Commun., vol. 59, no. 5, pp. 12751286, May 2011.
- [34] F. Oggier, G. Rekaya, J.-C. Bel_ore, and E. Viterbo, "Perfect space-time block codes, IEEE Trans. Inf. Theory, vol. 52, no. 9, pp. 38853902, 2006.
- [35] B. Li and E. Ayanoglu, "Golden coded multiple beamforming, in Proc. 2010 IEEE GLOBE-COM.
- [36] B. Li and E. Ayanoglu, "Bit-interleaved coded multiple beamforming with perfect coding, in Proc. 2012 IEEE ICC, pp. 42464251.
- [37] B. Li and E. Ayanoglu, "Multiple beamforming with perfect coding, IEEE Trans. Commun., vol. 60, no. 6, pp. 15751586, Jun. 2012.

Strength Characteristics Of Fly Ash Activated Concrete

Palaskar Satish Muralidhar

Assi. Prof. Dept. of Civil. Engg. SCSMCOE, Nepti, A'Nagar, satishpalasakar@gmail.com, 9922955937

Abstract— Concrete is used in most of the Civil Construction work in the world. However high-energy requirement and pollution involved in the production of cement hampers the image of concrete as a sustainable material. Efforts are continuously being made to make concrete environment friendly. Fly ash activated cement concrete is a new development in the world of concrete in which cement is partially replaced by fly ash and activated by alkaline liquid to act as a binder in the concrete mix. Experimental investigation has been carried out to study effect of concentration of sodium hydroxide on compressive strength. Water and cement plus fly ash ratio of 0.45 by mass was maintained in the experimental work. The concentration of sodium hydroxide solution is varied. Cement fly ash concrete cubes of 150mm sides were cast. The curing is done for 3days, 7days, 28days, 56days and 90days at room temperature. Test result shows that the compressive strength increases with increase in concentration of sodium hydroxide, however beyond optimum concentration of sodium hydroxide compressive strength decreases.

Keywords—Concrete, Ordinary Portland Cement, Fly Ash, NaOH, Replacement, Compressive Strength, Curing, Activation

Introduction—Production of Portland cement is increasing due to the increasing demand of construction industries. Therefore the rate of production of carbon dioxide released to the atmosphere during the production of Portland cement is also increasing. Generally for each ton of Portland cement production, releases a ton of carbon dioxide to the atmosphere. The green house gas emission from the production of Portland cement is about 1.35 billion tons annually, which is about 7% of the total greenhouse gas emissions. Therefore to reduce the pollution, it is necessary to reduce or to replace the cement from concrete by other cementitious materials like fly ash, blast furnace slag, rice husk ash. Fly ash can be considered as the world's fifth largest raw material resource. An estimated 25% of fly ash in India is used for cement production, construction of roads and brick manufacture. Processed fly ash which is obtained by converting an industrial by-product into a resource material, as a component of cement, its uses helps to reduce CO₂ emission associated with concrete construction. Fly ash based concrete possesses high compressive strength, undergoes very little drying shrinkage and moderately low creep, and shows excellent resistance to sulphate and acid attack. They are not suffering from alkali-aggregate reaction and possess excellent fire resistant.

System Development— Materials used are as follows

The material used for making fly ash cement concrete specimen are low calcium dry fly ash as the source material, aggregate, cement and water. The type cement used is ordinary Portland cement of 53 grade. The ash used in this study was low calcium (ASTM class F) dry fly ash from Dirk India Pvt. Ltd. Nasik. Fly ash (P10, P63,) were obtained during the period of this study.

Fly Ash P10-Pozzocerte10 is filler ingredient, obtained by selection and processing of fly ash produced as a by-product at coal-fired electricity generating power stations. It is subjected to strict quality control.

General Information

Presentation	Coarse light weight powder
Colour	Dark grey
Bulk Weight	1.0 tonne/m ³
Fineness	60 to 85% retained on 45 micron Sieve
Package	30 kg paper bags and bulk tankers

Fly Ash P63-Pozzocrete 63 is a high efficiency class F pozzolanic material obtained by selection and processing of power station fly ashes resulting from the combustion of pulverized coal. Pozzocrete 63 is subjected to strict quality control.

General Information

Presentation	Finely divided dry powder
Colour	Light grey
Bulk Weight	Aprox. 0,90 metric ton per cubic meter
Specific density	Aprox. 2,30 metric ton per cubic meter
Size	90% < 45 micron
Particle shape	Spherical
Package	30 kg paper bags, 1 metric ton big-bags and bulk tankers

Aggregates-Local aggregate 20 mm and 12.5mm are coarse aggregate in saturated surface dry condition, were used. The coarse aggregate were crushed ballast type aggregate which are found in Deccan trap region. The fineness modulus of combined aggregate was 4.81. These size fractions are combined in fixed proportion to maintain grading complying with as per IS650: 1991.

Sand-Locally available river sand is used as fine aggregate. The sand is sieved using sieves of sizes 4.75 mm, 2.36 mm, 1.18 mm, 600 micron, 300 micron and 150 micron. The fineness modulus of combined aggregate was 3.43.

Table 3.1: Properties of Aggregates

Properties	C A I	C A II	FA(sand)
Type	Crushed angular	Crushed angular	Spherical (River sand)
Maximum Size	20mm	12.5 mm	4.75 mm
Specific Gravity	2.632	2.629	2.559
Grading	Confirming to combination of CA-I : CA-II 65 : 35		Confirming to grading zone-III
Material finer than 75 micron	Nil	Nil	1.25 %
Water Absorption	0.63%	0.804%	1.63%
Moisture Content	Nil	Nil	Nil

Manufacture Of Test Specimens

The concrete mix is prepared of proportion M (1: 1.5:3) as follows:

- 1) Material is taken on weight basis.
- 2) First aggregate is weighted to nearest gram and placed in mixing tray then sand is weighted and placed uniformly over aggregate. In the same way cement and fly ash is weighted and placed over mix of sand and aggregate.

- 3) Water cement ratio taken is 0.45. Water is then measured accurately in measuring cylinder and is uniformly poured in the mixture of cement, sand and aggregate. Care should be taken that uniformly mixing should be carried out and have uniform color.
- 4) When NaOH is used in the mix it is first mixed with water in required proportion and then it is uniformly poured in the mixture of cement, sand and aggregate.

Compressive Strength Test

Size Of Test Specimen-Test specimen cubical in shape shall be 15x15x15cm. The mould shall be 150mm size. In assembling the mould for use, the joints between the sections of mould shall be thinly coated with mould oil and a similar coating of mould oil shall be applied between the contact surfaces of the bottom of the mould and the base plate in order to ensure that no water escapes during the filling. The interior surfaces of the assembled mould shall be thinly coated with mould oil to prevent adhesion of the concrete.

Compaction-The test specimens shall be made as soon as practicable after mixing, and in such a way as to produce full compaction of the concrete with neither segregation nor excessive laitance. The concrete shall be filled into the mould in layers approximately 5 cm deep. In placing each scoopful of concrete, the scoop shall be moved around the top edge of the mould as the concrete slides from it, in order to ensure a symmetrical distribution of the concrete within the mould. Each layer shall be compacted by hand. When compacting by hand, the tamping bar shall be used and the strokes of the bar shall be distributed in a uniform manner over the cross-section of the mould. The number of strokes per layer required to produce specified conditions for cubical specimens, in no case shall the concrete be subjected to less than 35 strokes per layer for 15 cm cubes. After the top layer has been compacted, the surface of the concrete shall be finished level with the top of the mould, using a trowel, and covered with a metal plate to prevent evaporation.

Curing-The test specimens shall be stored in the laboratory at a place free from vibration, under damp matting, for 24 hours \pm ½ hour from the time of adding the water to the other ingredients. The temperature of the place of storage shall be maintained within the range of 22° to 32°C. After the period of 24 hours, they shall be marked for later identification, removed from the moulds and, unless required for testing within 24 hours, stored in clean water at a temperature of 24° to 30°C until they are transported to the testing.

Testing-Tests shall be made at the 3, 7, 28, 56, & 90 day's ages of the specimen. At least three specimens shall be made for testing at each selected age.

Procedure-Specimens stored in water shall be tested immediately on removal from the water and while they are still in the wet condition. Surface water and grit shall be wiped off the specimens and any projecting fins removed. The bearing surfaces of the testing machine shall be wiped clean and any loose sand or other material removed from the surfaces of the specimen which are to be in contact with the compression platens. In the case of cubes, the specimen shall be placed in the machine in such a manner that the load shall be applied to opposite sides of the cubes as cast, that is, not to the top and bottom. The axis of the specimen shall be carefully aligned with the centre of thrust of the spherically seated platen. No packing shall be used between the faces of the test specimen and the steel platen of the testing machine. The load shall be applied without shock and increased continuously at a rate of approximately 140 kg/sq cm/min until the resistance of the specimen to the increasing load breaks down and no greater load can be sustained. The maximum load applied to the specimen shall then be recorded and the appearance of the concrete shall be noted. The measured compressive strength of the specimen shall be calculated by dividing the maximum load applied to the specimen during the test by the cross-sectional area, calculated from the mean dimensions of the section (150X150X150mm) and shall be expressed to the nearest N per sq mm. Average of three values shall be taken as the representative of the batch provided.

Result- The details are given below

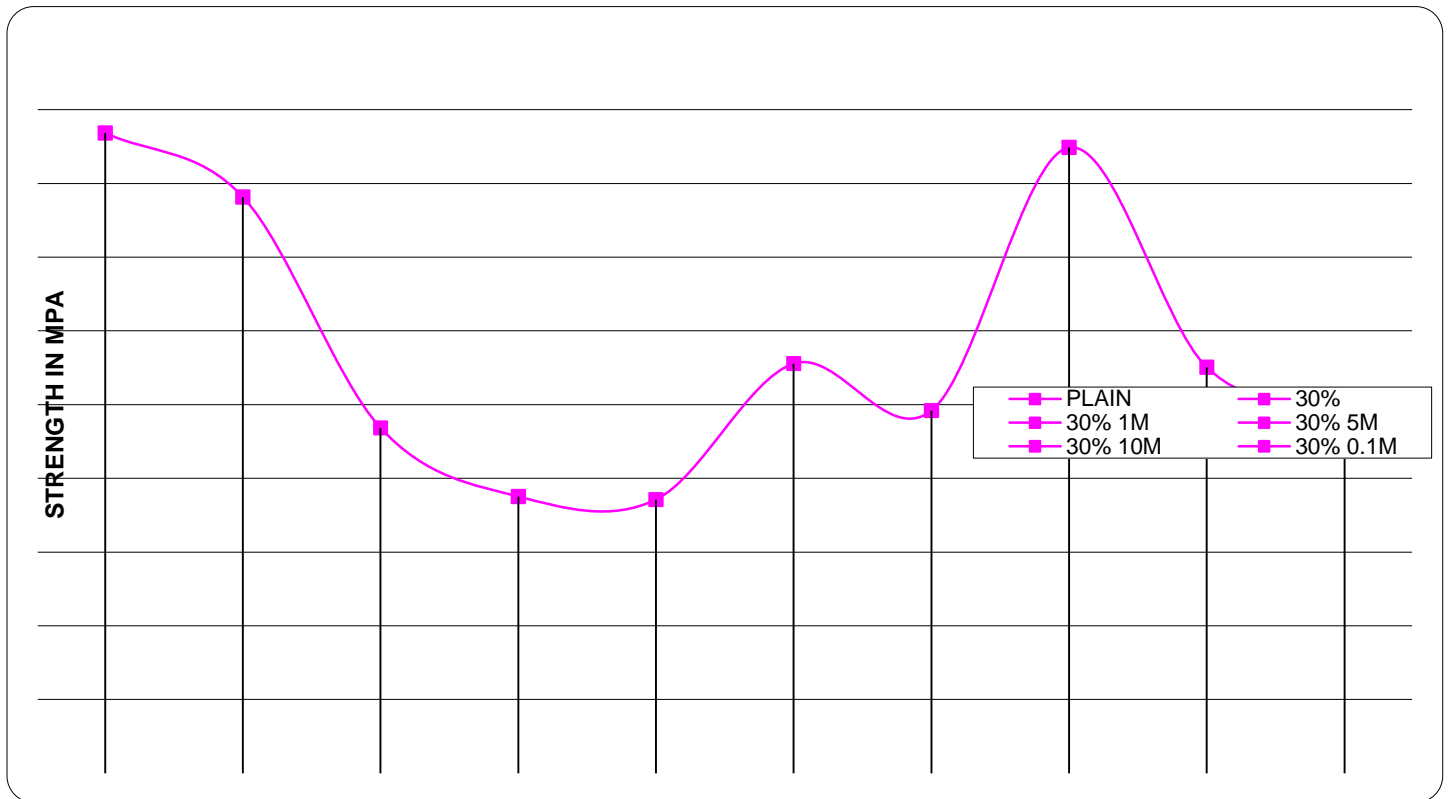


Fig.No.1. Comparison of 30% replacement of cement by P63 fly ash on Compressive strength at W/C=0.45 and varying concentration of NaOH

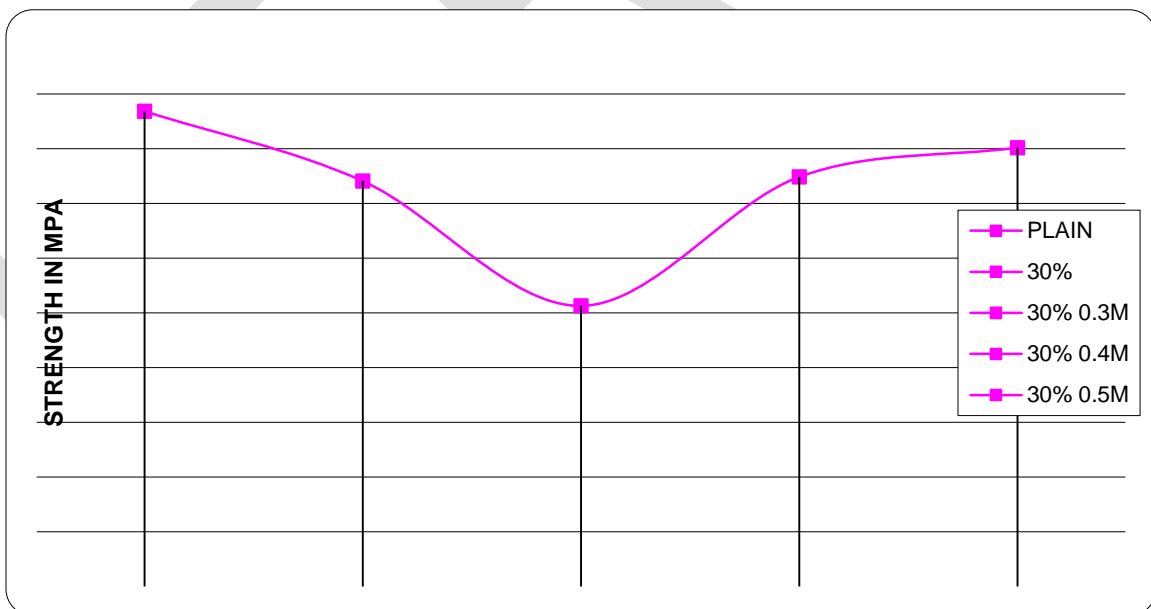


Fig.No.2 Comparison of 30% replacement of cement by P10 fly ash on Compressive strength at W/C=0.45 and varying concentration of NaOH

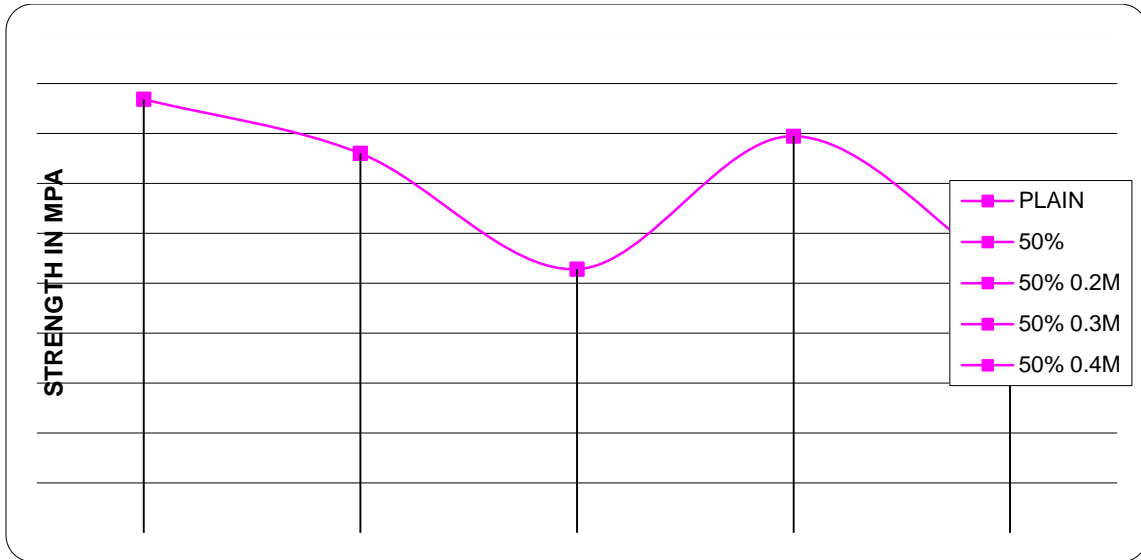


Fig.No.3 Comparison of 50% replacement of cement by P63 fly ash on Compressive strength at W/C=0.45 and varying concentration of NaOH

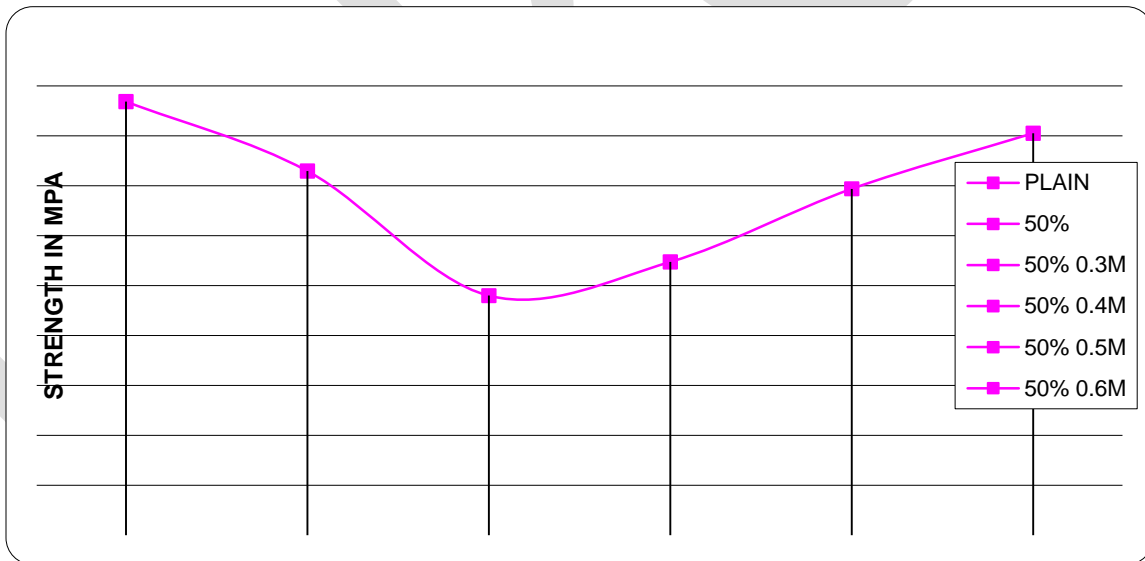


Fig.No.4. Comparison of 50% replacement of cement by P10 fly ash on Compressive strength at W/C=0.45 and varying concentration of NaOH

CONCLUSION

The conclusions drawn are summarized as follows,

1. It is observed that compressive strength decreases for P63 and P10 fly ash at 30% and 50% replacement of cement at 28 days of curing as compared to plain concrete.
2. Compressive strength for 30% replacement of cement by P63 fly ash at 56 days of curing is equal to 28 days strength of plain concrete.
3. It is observed that compressive strength for P63 and P10 fly ash at 30% and 50% replacement of cement at 28 days of curing increases with increase in concentration of NaOH upto certain level and then decreases.
4. Compressive strength for 30% replacement of cement by P63 fly ash at 28 days of curing is maximum at 0.3M NaOH and equal to 28 days strength of plain concrete.
5. Compressive strength for 50% replacement of cement by P63 fly ash at 28 days of curing is maximum at 0.3M NaOH as compared to plain concrete.
6. Compressive strength for 30% replacement of cement by P10 fly ash at 28 days of curing is maximum at 0.5M NaOH as compared to plain concrete.
7. Compressive strength for 50% replacement of cement by P10 fly ash at 28 days of curing is maximum at 0.6M NaOH as compared to plain concrete.

Conclusion must be short and precise and should reflect the work or research work you have gone through. It must have same as above in introduction paper adjustment

REFERENCES:

- [1] S. V. Patankar, S. S. Jamkar and Y. M. Ghugal “*Effect of Sodium Hydroxide on Flow and Strength of Fly ash Based Geopolymer Mortar*”, Proceedings of the International Conference on Sunrise Technologies at Dhule, 2011
- [2] M. Ahmaruzzaman, “*A review on the utilization of fly ash*”, Progress in Energy and Combustion Science, vol 36, 2010, pp. 327–363
- [3] P. J. Jawale, “*The DIRK PFA Classification Products The Design of DIRK POZZOCRETE*”, Dirk India Pvt. Ltd. Nashik, pp. 1–15
- [4] Ravindra Kumar Dhir, “*Fly ash for concrete construction in hot and aggressive environment*”, Dirk India Pvt. Ltd. Nashik, pp. 1–7
- [5] Product data sheet, Dirk India Pvt. Ltd., Nashik
- [6] A.K. Mullick, “*Performance of concrete with binary and ternary cement blends*”, The Indian Concrete Journal, January 2007, pp. 15-22
- [7] Smith Songpiriyakij King Mongkut’s, “*Alkali activated fly ash concrete*”, Institute of Technology North Bangkok, Thailand, pp. 1-4
- [8] Garcia-Lodeiro, A.Palomo, A. Fernandez-Jimenez, “*Alkali-aggregate reaction in activated fly ash system*”, Cement and Concrete Research, vol 37, 2007, pp. 175-183
- [9] P.C. Basu and S. Saraswati, “*Are existing IS codes suitable for engineering of HVFAC?*”, The Indian Concrete Journal, August 2006, pp. 17-21
- [10] Deepak Ravikumar, Sulapha Peethamparan, Narayanan Neithalath, “*Structure and strength of NaOH activated concretes containing fly ash or GGBFS as the sole binder*”, Cement and Concrete Composites, vol 32, 2010, pp. 399-410
- [11] A.K. Mullick, “*Use of fly ash in structural concrete: PartII-How much?*”, The Indian Concrete Journal, vol 79, June 2005, pp. 10-14
- [12] M.C.Nataraja, M.A.Jayaram, C.N.Raikumar, “*Inductive Classifying Artificial Network for Fly Ash Type Categorization*”, Engineering Letters, February 2007, pp. 1-10
- [13] Dr. J. D. Rathod, Dr. S. C. Patodi, “*Effect of fly ash on strength and ductility of the engineered cementitious composite*”, Proceedings of National Conference On Fly Ash/Futuristic Materials In Civil Engineering Construction For Sustainable Development, 2010, pp.1-16

- [14] S.K. Antiohos, S. Tsimas, "A novel way to upgrade the coarse part of a high calcium fly ash for reuse into cement systems", Waste Management, May 2006, pp. 1-9
- [15] Kofi Abora, Keith Quillin, Kevin A Paine, Andrew M Dunster, "effect of mix design on consistence and setting time of alkali activated concrete", Proceedings of the 11th International Conference on Non-conventional Materials and Technologies (NOCMAT 2009) 6-9 September 2009, Bath, UK, pp. 1-9
- [16] Chan-Gi Park, Jong-Whan Yoon, Wan-Young Kim, and Jong-Pil Won, "Mechanical and Durability Performance of Roller-Compacted Concrete with Fly Ash for Dam Applications", The Indian International Journal of Concrete Structures and Materials, Vol.1, December 2007, pp.57-61
- [17] M Mustafa A Bakri, H. Kamarudin, M. Bnhussain, I. Khairul Nizar, A. R Rafiza1 and Y. Zarina, "Microstructure of different NaOH molarity of fly ash based green polymeric cement", Journal of Engineering and Technology Research Vol. 3(2), February 2011, pp. 44-49
- [18] Shetty M. S., "Concrete technology- Theory and Practice", S. Chand & company, New Delhi, 1982
- [19] IS: 516, "Methods of tests for strength of concrete ", Bureau of Indian Standards, New Delhi, 1959.
- [20] IS:3812, "Specification for fly ash for used as Pozzolana and admixture", Bureau of Indian Standards, New Delhi, 1981.

Emerging trends and methods used in the field of information retrieval

Sameera Kawatkar

Kawatkar93@gmail.com

ABSTRACT- With the emerging trends in science and technology, the importance of acquiring and finding information from different sources provided by the technology is increasing tremendously. It was possible to store huge amounts of data & information as the computers became more and more advance. All the information available on the internet is made of several documents. Finding useful and relevant information from such documents was required. These documents are not always structured and organized in an efficient manner. As a result, the concept of information Retrieval (IR) emerged in the early 1950. Information retrieval finds the most relevant documents according to the inputs given up by the user. Throughout these years this concept of information retrieval has grown & advanced greatly providing easy & efficient access to many users over the internet. This article gives a brief structure of the key technologies used in the field of Information Retrieval & various ways of handling with it.

KEYWORDS: information retrieval, Boolean systems, NLP, cluster hypothesis,

MODELS AND IMPLEMENTATION OF INFORMATION RETRIEVAL SYSTEMS

In the earlier days, IR systems were regarded as the Boolean systems which allowed its users to specify their information need by a complex combination of Boolean operations like ANDs, ORs and NOTs. However there are several shortcomings of the Boolean system. The main drawback is that there is no indication of document ranking, which makes it difficult for the user to select a good search request. Also the concept of relevance ranking is not so critical in a Boolean system. As a result of these drawbacks given up by the Boolean systems, the method of ranked retrieval is now used on a commonly basis. The ranking of the documents is done by information retrieval systems considering the relevance and usefulness of a particular document for which the user had demanded a query. The information retrieval systems assign a numeric score to every document and rank them by this score. Various models have been proposed for this process. The three most used models in IR research are the vector space model, the probabilistic models, and the inference network model.

1) Vector Space Model

Vector space model is a model in information retrieval for representing the text documents. It is formally used for information retrieval, relevance ranking as well as for the filtering of the unwanted information from the required one.

In the vector space model, a document is represented as a *vector* & the text is usually represented by a vector of *terms*. These terms are nothing but typically words and phrases in a particular document. Each dimension in the vector space model corresponds to a separate term. If selected terms are words, then every word becomes an independent dimension in a vector space model. Any text can be represented by a vector in this model. If a particular term belongs to a text, then a non-zero value is given to it in the text-vector along with the dimensions corresponding to the term. Most vector based systems operate in the positive quadrant of the vector space, i.e., no term is assigned a negative value.

For assigning a numeric score to a document for a query, the vector space model measures the similarity between the query vector and the corresponding document vector. The similarity between two vectors is not inherent in the model. Typically, the angle between two vectors is used as a measure of divergence between the vectors, and cosine of the angle is used as the numeric similarity. The inner-product (or dot-product) between two vectors is also commonly used as a similarity measure as an alternative to the cosine angle.

2) Probabilistic Models

In this type of IR models the general principle which is used is that the documents in a collection should be ranked by decreasing probability of their relevance to a specific query given by the user. This is commonly regarded as the “probabilistic ranking principle (PRP)”. These Probabilistic IR models estimate the probability of relevance of documents for a query, since the exact probabilities are not available in the Information retrieval systems. This estimation is considered as the key part of the model. Most probabilistic models differ from one another due to this estimation. Maron and Kuhns proposed the initial idea of probabilistic retrieval in a paper published in 1960. Following that, many probabilistic models have been proposed, each based on a different probability estimation technique.

The probability ranking principle can be implemented as follows:

Let x be a document in the collection.

Let R represent relevance of a document w.r.t. given (fixed) query and let NR represent non-relevance.

We need to find $p(R/x)$ - probability that a retrieved document x is relevant.

$$p(R|x) = \frac{p(x|R)p(R)}{p(x)}$$

$$p(NR|x) = \frac{p(x|NR)p(NR)}{p(x)}$$

Where,

$p(R), p(NR)$: prior probability of retrieving a (non) relevant document.

$p(x/R), p(x/NR)$: probability that if a relevant (non-relevant) document is retrieved, it is x .

Now, according to Ranking Principle (Bayes' Decision Rule):

If $p(R/x) > p(NR/x)$ then x is relevant, otherwise x is not relevant

3) Inference Network Model

In this model of the Information retrieval system, document retrieval is modeled as an inference process in an inference network. Almost all the techniques used by IR systems can be implemented using this model. For the implementation of this model, a document instantiates a term with a certain strength, and the credit from multiple terms is given to a query to compute the equivalent of a numeric score for the document. The strength of instantiation of a term for a document can be considered as the *weight* of the term in

the document, and document ranking in the simplest form of this model becomes similar to ranking in the vector space model and the probabilistic models described above. The strength of instantiation of a term for a document is not defined by the model, and any formulation can be used.

QUERY MODIFICATION

In the beginning of IR, researchers concluded that it was often too hard for users to determine effective search requests. As a result, it was thought that adding different synonyms of query words to the query may improve the overall search effectiveness. Early research in the IR solely relied on a thesaurus to find synonyms for the given query. But to obtain an effective general purpose thesaurus is too costly. Due to this hindrance, researchers therefore developed techniques to automatically generate thesauri for use in query modification. There are many automatic methods which are based on analyzing word co-occurrence in the documents. Most query augmentation techniques based on automatically generated thesauri had very limited success in improving search effectiveness. This was due to the lack of query context in the augmentation process. Not all words related to a query word are meaningful in context of the query.

In 1965 Rocchio proposed a method using relevance feedback for query modification. Relevance feedback was basically designed by the fact that it is easy for users to judge some documents as relevant or non-relevant for their respective query.

By using such relevance judgments, the system is then automatically able to generate a better query for further searching process. The user is told to judge the relevance of the top few documents retrieved by the system. Later, based on these judgments, the system modifies the query and thereby issues a completely new query for finding more relevant documents from the collection. Relevance feedback has thus proved to work quite effectively across test collections.

Many New techniques to do meaningful query expansion in absence of any user feedback were developed in 1990. Most efficient and commonly used of all these is the “pseudo-feedback”, which is regarded as a variant of relevance feedback. Considering that the top few documents retrieved by an IR system mostly fall under the general query topic, we can thus select the most appropriate related terms from these documents which will yield useful new terms irrespective of document relevance. In pseudo-feedback method, the starting few documents in the information retrieval system that are retrieved for the initial user query are said to be “relevant”, and thus performs relevance feedback to generate a new query. As a result, this expanded new query can then be used to rank the documents for presentation to the user. This concept of Pseudo feedback has therefore shown to be a very effective technique, especially for short user queries.

OTHER TECHNIQUES AND APPLICATIONS:

Along with the typical information retrieval models, many other techniques have been developed and have thereby succeeded in their own distinct ways. Following are few of them:

- 1) **Cluster hypothesis:** It basically deals with separating the information into different appropriate clusters. After analyzing them, we can then conclude that the documents which fall under same cluster have a similar relevance for a given query. Document clustering techniques are still regarded as huge and an active area of research recently. If we consider in terms of classification, we can say that if the points fall in the same cluster, they are most likely to be of the same class. There can also be multiple clusters forming a single class.
- 2) **Natural Language Processing (NLP):** It is has also considered as a tool to enhance retrieval effectiveness.

Natural language processing (NLP) deals with the application of computational models to text or speech data. Automatic (machine) translation between languages; dialogue systems, are the areas that come under NLP. These applications allow a human to interact with a machine using a natural language; and information extraction. Here the goal is to transform unstructured text into structured (database) representations which can further be searched and browsed in flexible ways by the different users handling it. These applications of NLP technologies are therefore having a dramatic impact on the way people interact with computers, with each other through the use of different languages, and also on the way people access the vast amount of information and data over the internet.

CONCLUSION

From the above described advanced techniques and developments in the field of information retrieval , we can thus say that it has improved tremendously in a positive manner, and made information discovery more easier and thereby faster. The task of finding information from the documents can be effectively done using these statistical techniques. These techniques developed in the field of information retrieval are being used in many other everyday used areas as well. For example; junk-email filters, web search engines, news clipping services. With the amount of information made available on the internet increasing exponentially, information retrieval is definitely going to be a boon for huge number of users in the future.

REFERENCES:

1. www.google.com
2. www.wikipedia.com
3. www.researchbible.com
4. Books from various subjects

Design and couple field analysis of Aircraft disc brake rotor

Anudeep.B, Naga Sunil.B

Asst.prof in RGM CET, deepnitw@gmail.com, 9063012368

Abstract— A brake is a device by means of which artificial frictional resistance is applied to moving machine member, in order to stop the motion of a machine. Braking is a process which converts the kinetic energy of the vehicle into mechanical energy which must be dissipated in the form of heat. Here, the 3D model of aircraft disc brake rotor was created by using CATIA V5R20 with particular dimensions. The structural and thermal analysis of aircraft disc rotor was done in ANSYS 14.5. The materials used for aircraft disc rotor are aluminium metal matrix and ceramic coating. The main aim of this project is validate the mathematical result with ansys results. The maximum stress developed is 26.87MPa for aluminium metal matrix composite (AMMC) and 21.47MPa for ceramic coated aircraft disc brake rotor. Finally, the analysis suggests that Mechanical and thermal properties of aluminium alloy may be improved through the addition of ceramic coatings on the surface which in contact with the brake pad.

Keywords— Aircraft disc brake rotor, Catia V5R20, Ansys 14.5, aluminium metal matrix composite (AMMC), ceramic coating, von-mises stress, total deformation.

INTRODUCTION

Very early aircraft have no brake system to slow and stop the aircraft while it is on the ground. Instead, they rely on slow speeds, soft airfield surfaces, and the friction developed by the tail skid to reduce speed during ground operation. Brake systems designed for aircraft became common after World War I as the speed and complexity of aircraft increased and the use of smooth, paved runway surfaces proliferated. All modern aircraft are equipped with brakes. Their proper functioning is relied upon for safe operation of the aircraft on the ground. The brakes slow the aircraft and stop it in a reasonable amount of time. They hold the aircraft stationary during engine run-up and, in many cases, steer the aircraft during taxi. On most aircraft, each of the main wheels is equipped with a brake unit. The nose wheel or tail wheel does not have a brake.



Fig 1: Aircraft disc brake and exploded view

In the typical brake system, mechanical and/or hydraulic linkages to the rudder pedals allow the pilot to control the brakes. Pushing on the top of the right rudder pedal activates the brake on the right main wheel(s) and pushing on the top of the left rudder pedal operates the brake on the left main wheel(s). The basic operation of brakes involves converting the kinetic energy of motion into heat energy through the creation of friction. A great amount of heat is developed and forces on the brake system components are demanding. Proper adjustment, inspection, and maintenance of the brakes are essential for effective operation.

Table 2: Properties of zirconia-based ceramic coating (MgZrO₃)

Property	Value
Density(Kg/m ³)	5600
Young's modulus (Pa)	4.60E+10
Poisson ratio	0.2
Bulk modulus (Pa)	2.56E+10
Shear modulus (Pa)	1.92E+10
Thermal conductivity(W/mK)	0.8

AIRCRAFT DISC BRAKE ROTOR DATA:

- Mass of the aircraft vehicle = 57749 kg
- Initial velocity (u) = 69.44m/s
- Vehicle speed at the end of the braking application (v) = 0 m/s
- Brake rotor diameter = 0.3m
- Axle weight distribution 30% on each side (γ)=0.3
- Percentage of kinetic energy that disc absorbs (90%) $k=0.9$
- Acceleration due to gravity $g = 9.81\text{m/s}^2$
- Coefficient of friction for dry pavement $\mu=0.7$

MODELING OF AIRCRAFT DISC BRAKE ROTOR IN CATIA V5R20

The solid modeling of the aircraft disc brake was made with the help of CAD tools CATIA v5 as shown in Figure 1. By using the following dimensions, we can prepare the aircraft disc brake. Fig 1 and 2 shows the 2d model and CATIA 3D model of aircraft disc brake with the particular dimensions.

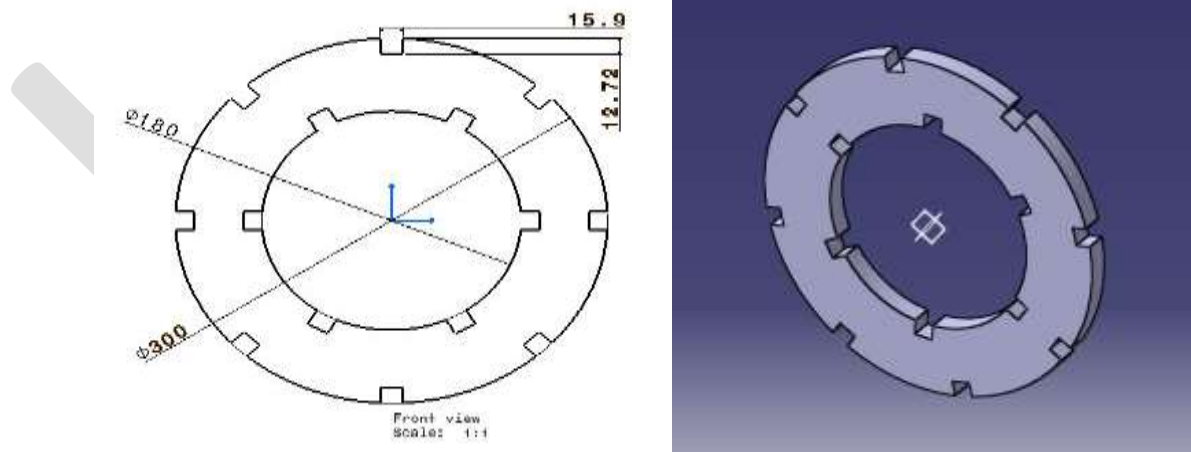


Fig 3: Aircraft disc rotor 2D and 3D model

MATHEMATICAL CALCULATIONS:

Energy generated during braking

$$KE = k \frac{1}{2} \gamma \frac{m(u-v)^2}{2}$$

$$KE = 0.9 \times 0.5 \times 0.3 \times 57749 \times \frac{(69.44 - 0)^2}{2}$$

$$KE = 18796096.47 \text{ joules}$$

Braking Power: Braking power during continued braking is obtained by differentiating energy with respect to time (t=65sec).

$$P_b = \frac{K.E}{t} = \frac{18796096.47}{65} = 289170.71 \text{ watts}$$

Calculate the Heat Flux (Q): Heat Flux is defined as the amount of heat transferred per unit area per unit time, from or to a surface.

$$Q = \frac{P_b}{A}$$

$$A = \frac{\pi}{4} \times (D^2 - d^2) = \frac{\pi}{4} \times (0.3^2 - 0.18^2)$$

$$A = 0.04523 \text{ m}^2$$

$$Q = \frac{289170.71}{0.04523} = 6393338.82 \text{ W/m}^2$$

ANALYTICAL TEMPERATURE RISE CALCULATIONS

Single stop temperature rise is the temperature rise due to single braking condition.

$$T_{max} = \frac{0.527 \times q \times \sqrt{t}}{\sqrt{\rho c k}} + T_{amb}$$

T_{max} = maximum disc temperature ($^{\circ}\text{C}$)

q = Heat flux (W/m^2)

t = Break on time (sec)

ρ = Density of disc brake material (Kg/m^3)

C = Brake disc specific heat capacity (J/Kg/K)

K = Brake disc thermal conductivity (W/mK)

T_{amb} = Ambient temperature ($^{\circ}\text{C}$)

$$T_{max} = \frac{0.527 \times 6393338.82 \times \sqrt{65}}{\sqrt{2670 \times 910 \times 250}} + 20^{\circ}\text{C} \quad T_{max} = 1122.17^{\circ}\text{C}$$

Fade Stop Temperature Rise: The temperature rise after repeated stopping can also be approximated, although so many variables exist it is suggested this is only used for basic optimization work.

$$\Delta T = \frac{Pt}{\rho cv}$$

Where: ΔT = Average temperature increase per stop ($^{\circ}\text{C}$)

P = Average power (Watts)

t = time taking to take maximum temperature rise when brake applied

ρ = Density of disc brake material (Kg/m³)

C = Brake disc specific heat capacity (J/Kg/K)

V = Disc volume (m³)

$$\Delta T = \frac{289170.71 \times 4}{2670 \times 910 \times 0.04523 \times 0.019}$$
$$\Delta T = 553.96 \text{ } ^\circ\text{C}$$

The compressive stresses ' σ ' developed in the surface of a disc from sudden temperature increases is

$$\sigma = \frac{E}{1 - 2\mu} \times \alpha \times \Delta T$$

$$\sigma = \frac{71 \times 10^9}{1 - (2 \times 0.33)} \times 0.22 \times 10^{-6} \times 553.96$$

Compressive stresses $\sigma = 25.04 \text{ MPa}$

INTRODUCTION TO ANSYS

ANSYS is general-purpose finite element analysis (FEA) software package. Finite Element Analysis is a numerical method of deconstructing a complex system into very small pieces (of user-designated size) called elements. The software implements equations that govern the behaviour of these elements and solves them all; creating a comprehensive explanation of how the system acts as a whole. These results then can be presented in tabulated, or graphical forms. This type of analysis is typically used for the design and optimization of a system far too complex to analyze by hand. Systems that may fit into this category are too complex due to their geometry, scale, or governing equations.

Coupled-field analysis of AMMC aircraft disc brake rotor in ANSYS 14.5

1. First, Prepared aircraft disc brake model in CATIA V5 and Save as this part as IGES for Exporting into Ansys Workbench 14.5 Environment. Import .IGES Model in ANSYS Workbench Simulation Module.

2. Apply Material for aircraft disc brake

Material Details: Aluminium Metal Matrix composite (Table 1) material and coated with ceramic coating (Table2)

The zirconia-based ceramic coatings are used as thermal barrier coatings owing to their low conductivity and their relatively high coefficients of thermal expansion, which reduce the detrimental interfacial stresses.

3. Mesh the aircraft disc brake

4. Define boundary condition for Analysis Boundary conditions play an important role in finite element calculation here, rotor supports are fixed. Pressure 13MPa and rotational velocity 60 rad/sec

5. Define type of Analysis for both AMMC and ceramic material (MgZrO₃)

Type of Analysis:-Static Structural and steady state thermal

6. Apply the pressure on aircraft disc brake

7. Run the Analysis

8. Get the Results

Structural analysis of AMMC aircraft disc brake rotor: A static analysis calculates the effects of steady loading conditions on a structure, while ignoring inertia and damping effects, such as those caused by time varying loads. A static analysis can, however.

Include steady inertia loads (such as gravity and rotational velocity), and time varying loads that can be approximated as static equivalent loads. Static analysis determines the displacements, stresses, strains and forces in structures and components caused by loads that do not induce significant inertia and damping effect. Steady loading and response conditions are assumed; that is, the loads and structures response are assumed to vary slowly with respect to time.

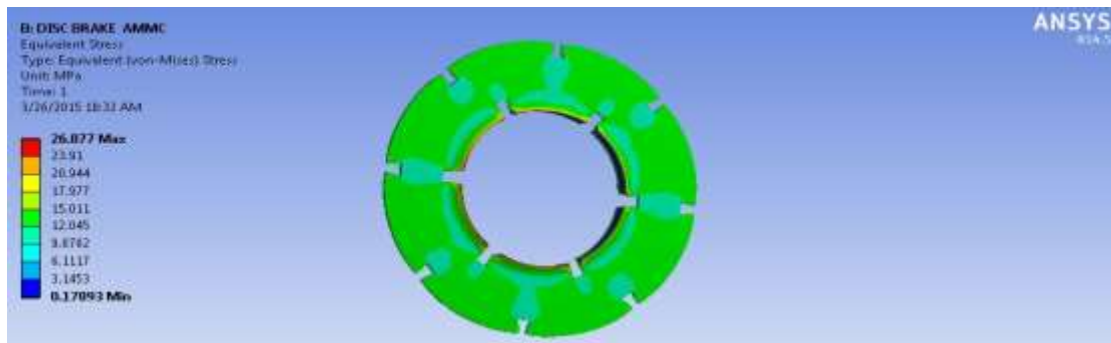


Fig 3: Von-Mises stresses of AMMC aircraft disc brake rotor

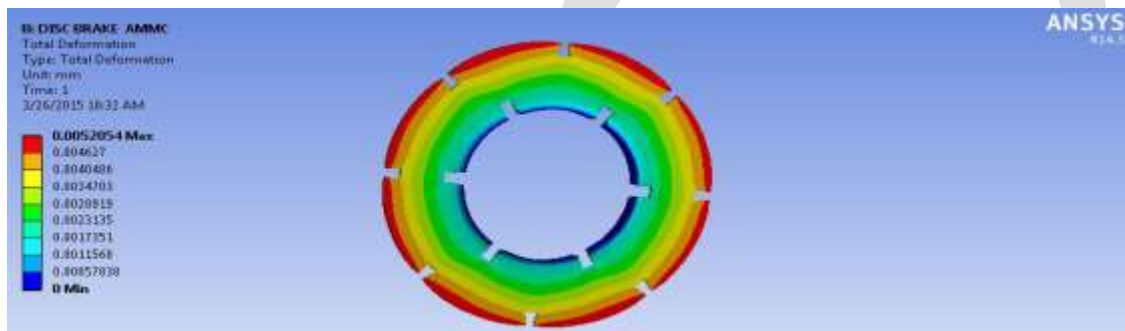


Fig 4: Total deformation of AMMC aircraft disc brake

Steady state thermal analysis of AMMC aircraft disc brake: The analysis is a coupled type analysis as the thermal analysis is done and the residual thermal stress are imported to the static structural analysis. For thermal analysis, boundary condition, convection heat coefficient is applied along with the heat flow throughout the body, and then it is solved in terms of temperature and heat flux. The thermal stress is imported to static structural analysis. The boundary condition and loading condition were set following conditions for testing purpose in one automotive manufacturing company. The boundary conditions were defined by fixing all the surfaces. The force is applied to the patch where the brake pad touches the instant when brake is applied. It is solved in terms of total deformation, equivalent stress and equivalent strain.

Structural analysis of aircraft disc brake rotor with ceramic coating (MgZrO₃):

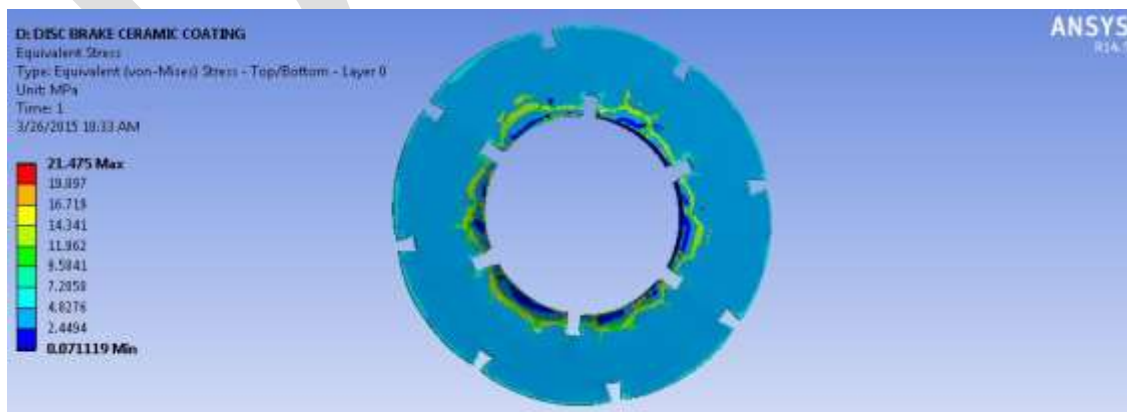


Fig 6: Von-Mises stresses of ceramic coated aircraft disc brake

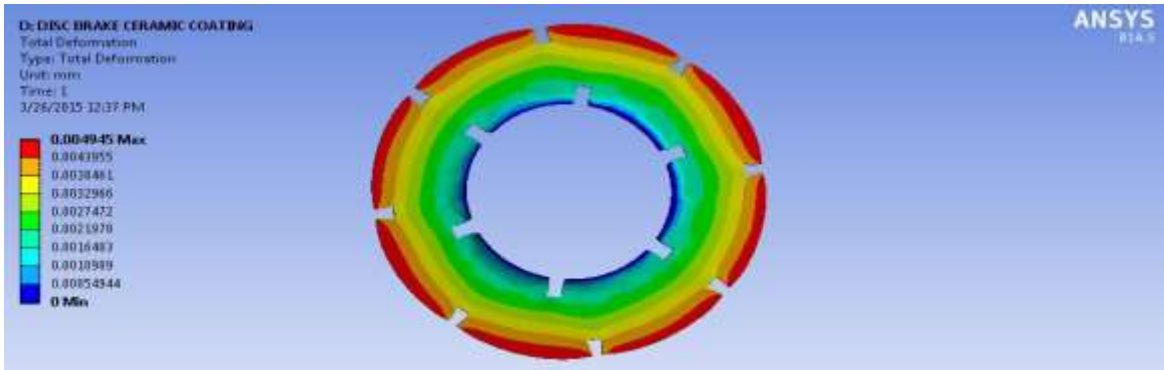


Fig 7: Total deformation of ceramic coated aircraft disc brake

Steady state thermal analysis of Aircraft disc brake with ceramic coating (MgZrO3):

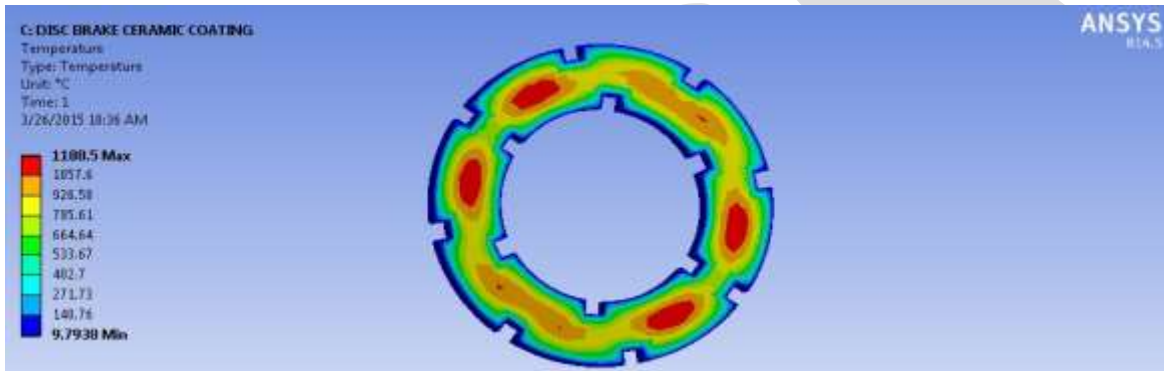


Fig 8: Temperature distribution on ceramic coated aircraft disc brake

COMPARISON THE RESULTS OF AIRCRAFT DISC BRAKE:

Table 3: Comparison of analytical and FEM results of AMMC

Table 4: Comparison of AMMC and ceramic coated disc brakes

Property	AMMC	Ceramic coated
Von misses stress (Mpa)	26.87	21.475
Total deformation(mm)	0.0052	0.0049
Maximum temperature (°C)	1166.2	1188.5

CONCLUSION

- In this aircraft disc

Property	Analytical	FEM
Von misses stress (Mpa)	25.04	26.87
Maximum temperature (°C)	1122.7	1166.2

research, the rotor model was

created by CATIA V5 R20 software. Then, the model created by CATIA was imported to ANSYS software.

- Validation is done through finite element solver with the initial model and checked that maximum stress and displacement are within control.
- Above Results Shows that FEA Results Conformal matches with the theoretical calculation so we can say that FEA is a good tool to reduce time consuming theoretical Work.
- The maximum temperature 1166.2°c appears at the brake padding surface as shown in the fig5. The maximum stress 26.87MPa appears at the edge of fixed supports as shown in fig3.
- From coupled field analysis of ceramic coated disc brake, it is observed that the maximum temperature 1188.5°C appears at the padding area and the maximum stress (21.47MPa) developed at the supports of edges.
- From table 4, we observed that by using of ceramic coating less deformation was developed compared to AMMC.
- From table 4, we observed that by using of ceramic coating less von misses stress was developed compared to AMMC.
- Finally, the analysis suggests that Mechanical and thermal properties of aluminium alloy may be improved through the addition of ceramic coatings on the surface which in contact with the brake pad.

REFERENCES:

- [1] Artus.S, Cocquemot, Staroswiecki.M, Hayat. S, Covo.C , (2004) , “Temperature Estimation of CHV Brake Discs using an Energy Balance Approach”, IEEE Intelligent Transportatlon Systems Conference, Washington, D.C., USA,pp-390-395.
- [2] Artus.S, Cocquemot, Staroswiecki.M, Hayat. S, Covo.C,(2005), “CHV's brake discs temperature estimation: results in open road Tests”, Proceedings of the 8th International IEEE Conference on Intelligent Transportation Systems Vienna, Austria.
- [3] Li Yuren , Liu Weigu, Tian Guanglai, Wei Hanbing , Xue Jing, (2009), “The Finite Element Model of Transient Temperature Field of Airplane Brake Disks with Rough Surface Profile”, Proceedings of the IEEE International Conference on Automation and Logistics,pp-41-44.
- [4] Mugeo Dong, Sok Won Kim, Nam-Ku, “Thermophysical Properties of Automotive Brake Disk Materials”, Department of Physics, University of Ulsan pp-680 – 749.
- [5] Fei Gao1, Gang Xiao, Yuanming Zhang, (2009), “Semi-similarity design of motorcycle-hydraulicdisk brake: strategy and Application”, pp-576-579.
- [6] Guangqiang Wu, Lin He ,Xianjie Meng, (2009), “Numerical Study on the Vibration Characteristics of Automobile Brake Disk and Pad”, IEEE transactions, pp-1798-1802.

A HIGH STEP UP RESONANT BOOST CONVERTER USING ZCS WITH PUSH-PULL TOPOLOGY

Maheswarreddy.K , PG Scholar. Suresh.K , Assistant Professor

Department of EEE, R.G.M College of engineering, Kurnool (D), Andhra Pradesh, India

Maheswarreddy.power@gmail.com, karasani.suresh@gmail.com.

Abstract— This dissertation proposes a push-pull boost power factor corrector (PFC). It is composed of two boost converters with a coupled inductor. The two identical modules can share the output power and increase the power capability up to the medium power level applications. The main advantage is coupling the two independent boost inductors into a single magnetic core to substantially reduce the circuit volume and the cost without degrading the conversion efficiency too much, which are the important targets of the modern switching power supply design. The interleaved operations of the switches with a cut-in-half duty cycle can reduce the conduction losses of the switches as well as both the turns and diameters of the inductor windings, which help more to the reduction of the circuit volume. Moreover, the operating frequency of the core, and thus the frequency of the two-phase inductor current ripple, is double that of the switching frequency. Also the ripple current at the input side and the output capacitor size are reduced. The power factor and the power density are improved.

Keywords— push pull topology, coupled inductor, quasi resonant converter

INTRODUCTION

Generally boost converter topology is the most commonly used technique to improve the power factor. It is always necessary to reach power factor as unity a cost effective solution can be obtained for greater than 0.95. In this proposed system we are using the push-pull technique to boost up the voltage level up to 380V dc for an input of 110 V ac supply.

A push-pull converter is a type of DC-to-DC converter that uses a transformer to change the voltage of a DC power supply. The proposed system having the capable of operating three modes of operation they are Continuous Conduction Mode, Discontinuous Conduction Mode and Transition Mode.

Even though Continuous Conduction Mode best suitable for high power applications the inductor value in this mode is high and in case of Discontinuous Conduction Mode the input harmonics level is high. But in case of transition mode the inductor value is moderate and useful for medium power applications so this mode is used for the proposed topology.

Derived from 2 TM boost converters with the interleaved operations, the power rating is increased and the input current and output current are shared equally with lower current ripples. Therefore, the total harmonic distortion (THD) of input current and the output capacitance can be reduced. However, the need of two inductors with two independent cores increases the circuit volume.

In this paper, a push-pull boost PFC composed of two interleaved TM boost PFCs and a coupled inductor is proposed and a single magnetic core is used. The two identical modules can share the output power and promote the power capability up to the medium-power-level applications.

In addition to this coupling of the two distributed boost inductors into a one magnetic core automatically reduces the circuit volume, which is the important goal of the development of switching power supply today. The interleaved operations of the switches act like a push-pull converter. The difference is that the operating frequency of the core is getting double of the switching frequency,

which means that not only the circuit size is reduced and also the operating frequency of the core is getting double of the switching frequency.

The same distributions of the input current and output current, the proposed topology with a cut-in 0.5 duty cycle can reduce the conduction losses of the switches on both the turns and diameters of the inductor windings

It is also maintains the advantages of a TM boost PFC, such as QR valley switching on the switch and zero-current switching (ZCS) of the output diode, to reduce the switching losses and improve the conversion efficiency.

MATLAB/SIMULINK used for the proposed system to simulate for an universal line voltage of 110v ac, a 380-V output dc voltage and a 100-W output power in order to verify its feasibility.

CIRCUIT TOPOLOGY

Fig 1 shows block diagram for push-pull Quasi Resonant converter. Here the power conversion occurs in three segments. In the first segment single phase AC supply is fed to the rectifier, to convert AC to DC. The output from the rectifier is modulated sin wave. This modulated sin wave is given to the quasi resonant converter. Using quasi resonant converter the voltage has been boosted. Then it is given to the load

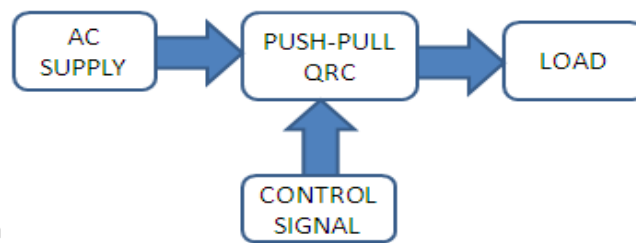


Fig.1. Block diagram of push-pull Quasi Resonant converter

A. Circuit Diagram Of Push-Pull Quasi resonant Converter

The circuit diagram for push- pull quasi resonant converter is shown in fig below. First we are converting ac voltage into dc voltage by using rectifier. The output from the rectifier is modulated sin wave then this supply is given to the push pull quasi resonant converter. This quasi resonant converter boost up the voltage to 380V. The proposed topology is operated by transition mode with constant on time and variable frequency.

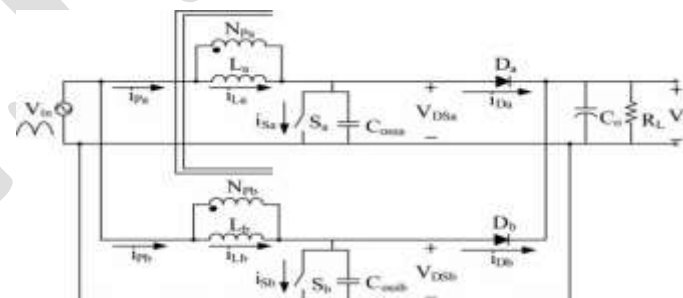


Fig.2.push pull quasi resonant converter

The proposed topology consists of two modules. Module A consists of the switch S_a , the winding N_{p_a} , the inductor L_a , and the output diode D_a . Module B consists of the switch S_b , the winding N_{p_b} , the inductor L_b , and the output diode D_b . These two modules

have a common output capacitor C_o . L_a and L_b are 2 coupled windings wound on the same magnetic core. Theoretically; the same turns of these two windings will lead to the same inductances To analyze the operating principles, there are some assumptions listed as follows.

1) The conducting resistances of S_a and S_b are ideally zero. The conduction time interval is DT_s , where D is the duty Cycle and T_s will be the switching period.

2) The forward voltages of D_a and D_b are ideally zero.

3) The magnetic core for manufacturing L_a and L_b is perfectly Coupled without leakage inductance. In addition, The turns of the windings N_{Pa} and N_{Pb} will be same. Therefore, L_a and L_b are also matched

OPERATION MODES IN QUASI-RESONANT CONVERTER

The operating modes of the proposed topology are analyzed as follows

A. Mode 1 operation: $t_0 < t < t_1$

Referring to Fig4, in module A S_a conducts Thus, the voltage across N_{Pa} equals to the rectified line- voltage. The inductor current i_{L_a} increases linearly and D_a is reverse-biased. In module B, S_b is turned OFF. The voltage across N_{Pa} is coupled to N_{Pb} . Hence, the voltage across N_{Pb} is also V_{in} , and the dotted terminal is positive. L_b stores energy as L_a does. The inductor current i_{L_b} increases linearly and flows into the non dotted terminal of N_{Pb} . By the coupling effect, this current flows into the dotted node of N_{Pa} . Since the voltage across S_b is zero, D_b is also reverse-biased. C_o supplies the energy to the load. The constant turn-on time of S_a is decided by the management of the controller depending on the rectified line-in voltage V_{in} . This is the initial mode of operation.

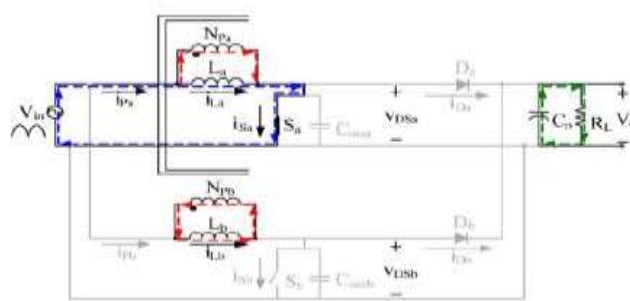


Fig.3. Module A S_a ON, module B S_b OFF

B. Mode 2 operation: $t_1 < t < t_2$

As shown in Fig. 5, in module A, S_a is turned OFF. D_a conducts for i_{L_a} to flow continuously. L_a releases its energy to C_o and the load. The voltage across N_p is $(V_o - V_{in})$ and the dotted terminal is negative. In module B, S_b is still turned OFF the voltage across N_{Pa} is coupled to N_{Pb} . Hence, the voltage across N_{Pb} is also $(V_o - V_{in})$, and the dotted node is negative. D_b is thus forward-biased to carry the continuous i_{L_b} . L_b is also releases its energy to C_o and the load. Both i_{L_a} and i_{L_b} are decreasing linearly. This state ends until L_a and L_b release their energies completely, and i_{L_a} and i_{L_b} decrease to zero. in this mode we are boosting the voltage.

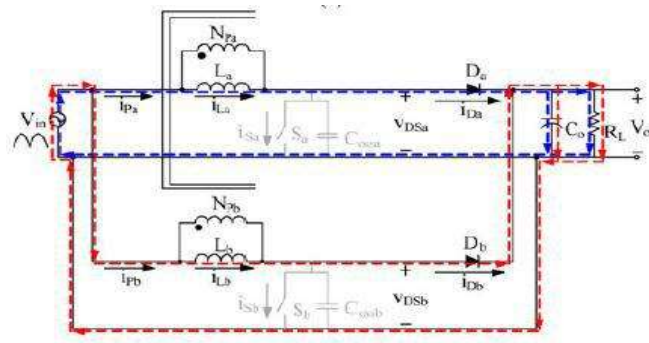


Fig .4.Module A S_a OFF Module B S_b OFF

C. Mode 3 operation: $t_2 < t < t_3$

As shown in Fig. 6, in module A, S_a keeps turned OFF. At t_2 , D_a is turned OFF with ZCS since i_{La} decreases to zero naturally. Similarly, in module B, S_b is still turned OFF. D_b is turned OFF with ZCS at t_2 since i_{Lb} decreases to zero naturally, too. In this interval, C_o supplies the energy to the load. At the same time, in module A, the series resonant loop formed by V_{in} , the parallel connection of L_a and L_b , and the output capacitor switch S_a , C_{ossa} , starts to resonate. Similarly, in module B, the series resonant loop formed by V_{in} , the parallel connection of L_a and L_b , and the output capacitance of the switch S_b , C_{ossb} , begins to resonate. Therefore, v_{Dsa} and v_{Dsb} decrease simultaneously. This mode is helpful to increasing the power factor.

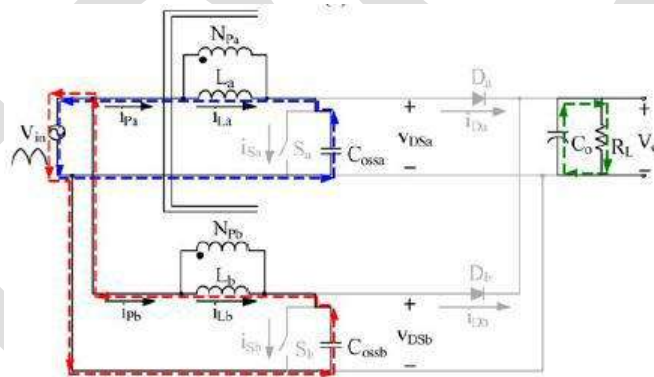


Fig.5.Module A S_a OFF & Module B S_b OFF

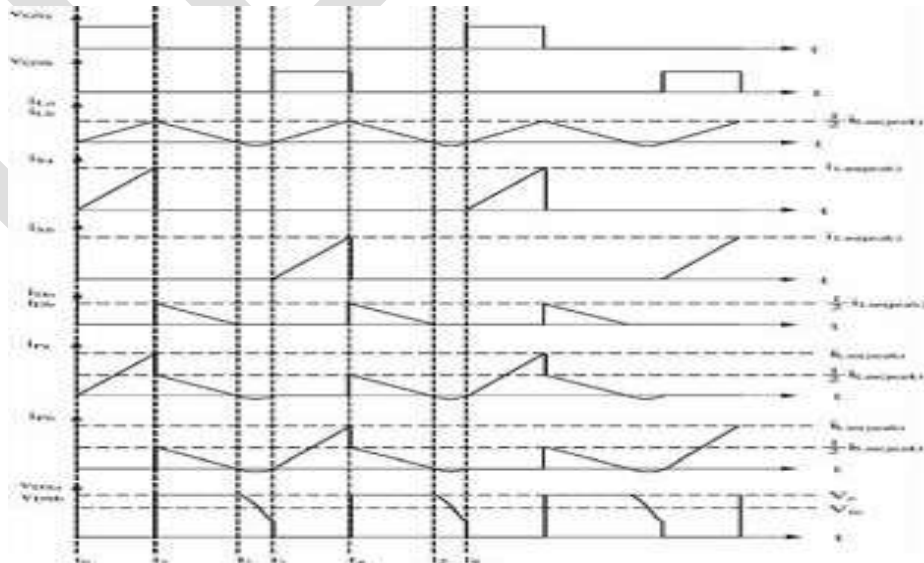


Fig.6.Key wave forms for proposed topology

SIMULATOIN RESULTS

MATLAB/SIMULINK is used for the simulation studies. Fig 7 shows the simulation circuit of push pull quasi-resonant converter with input voltage of 110V AC the corresponding output voltage is 380 dc, $P_o=100W$. The Efficiency of the converter and input current distortion is shown in fig 12 and fig 13.

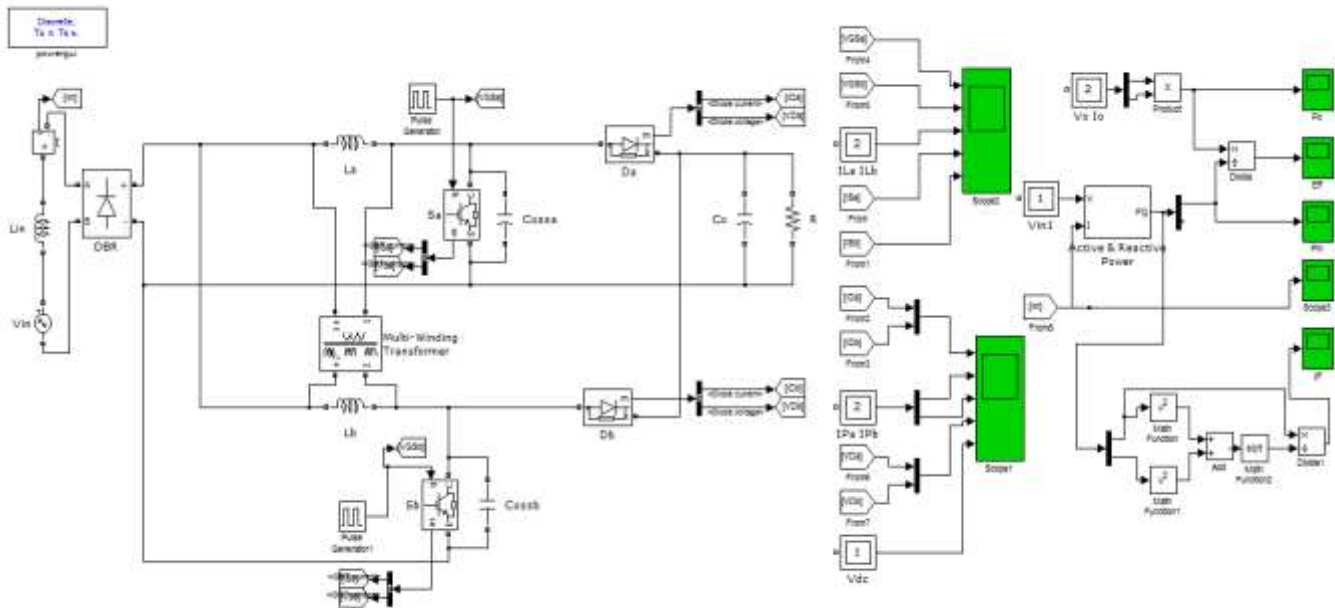


Fig.7.Simulation circuit of push pull quasi resonant converter

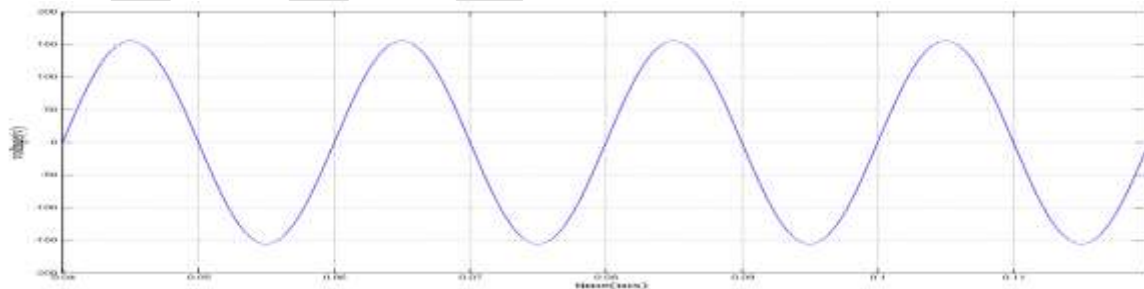


Fig.8.Input voltage of the converter 110 Vac

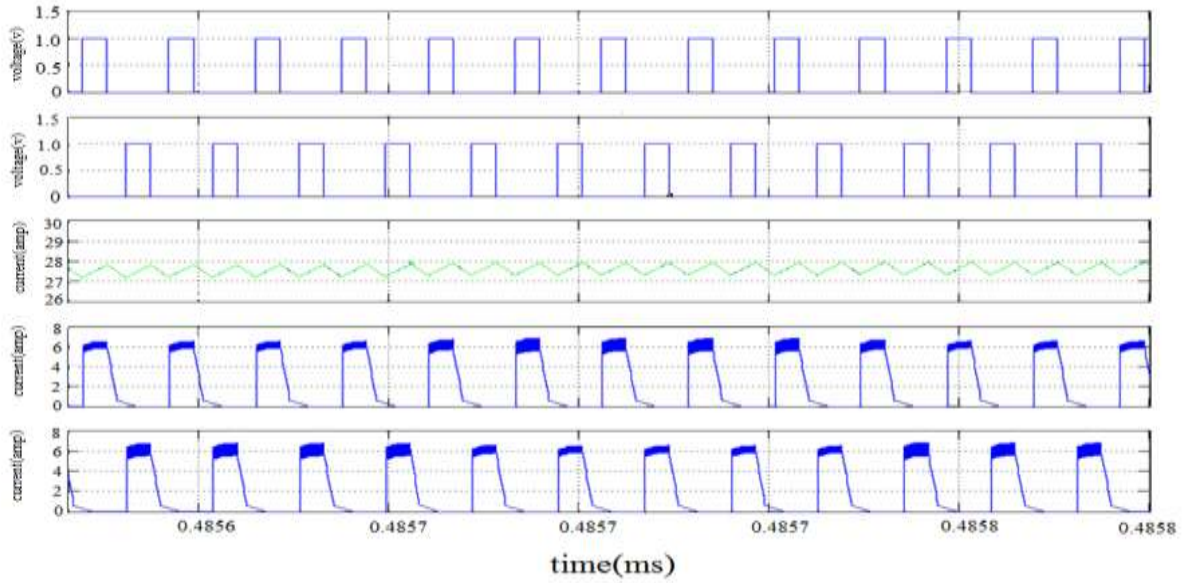


Fig.9. Gate pulses V_{GSa} & V_{GSb} , Inductor currents I_{La} & I_{Lb} , Switches currents I_{Sa} & I_{Sb}

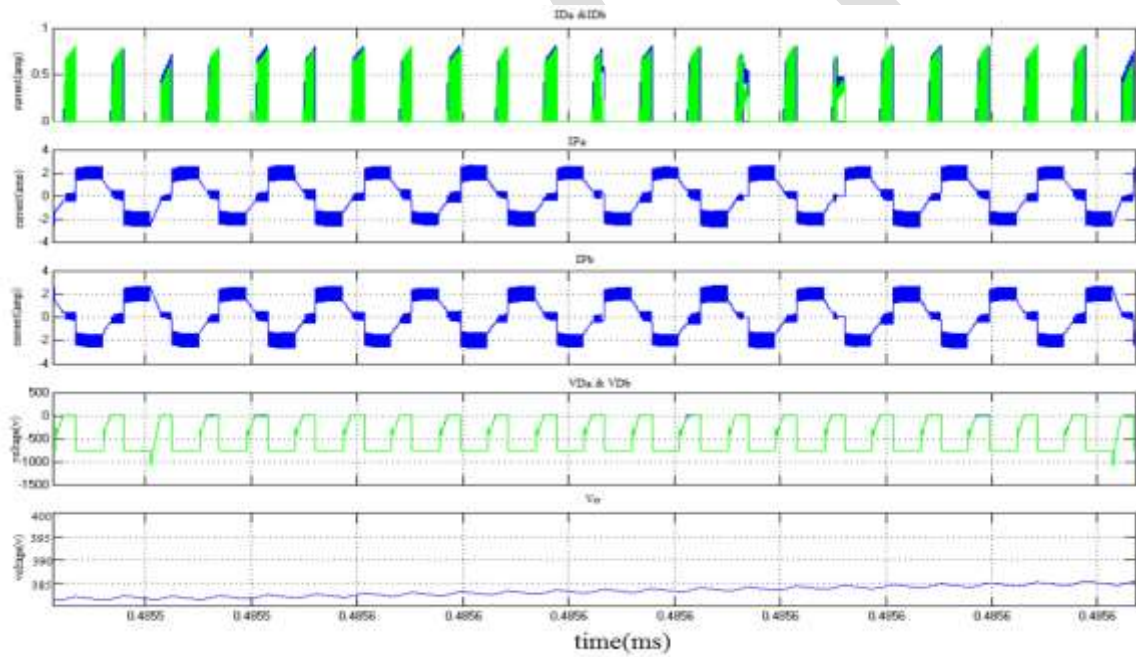


Fig.10. Diode currents I_{Da} & I_{Db} , Winding currents I_{Pa} & I_{Pb} , Voltage across switches V_{Da} & V_{Db} , Output voltage V_o

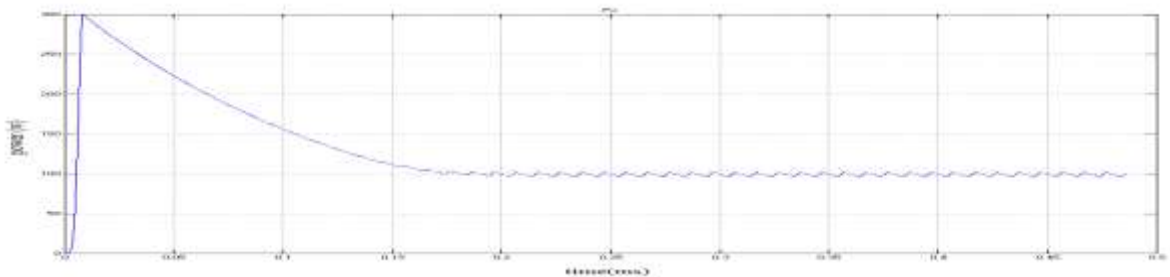


Fig.11. output power 100W

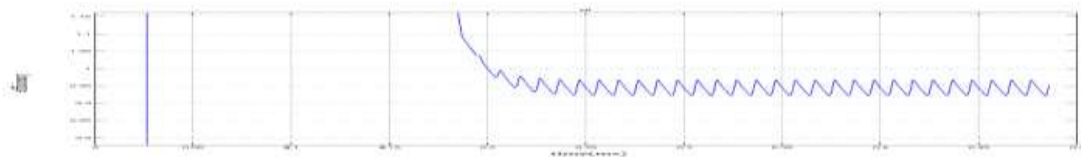


Fig.12. Efficiency of the converter

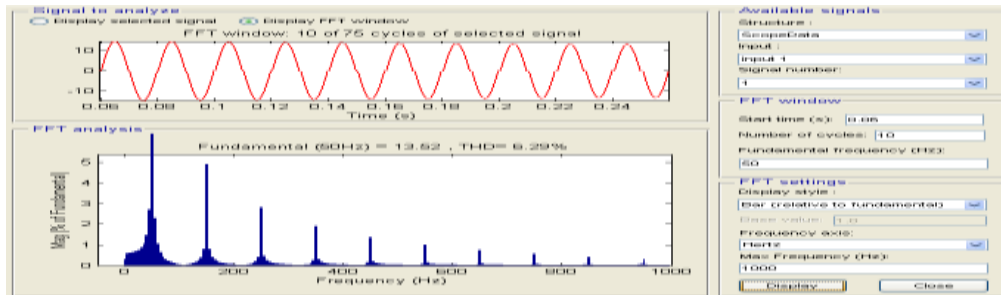


Fig.13. Input currents THD

LOAD	EFFICIENCY	THD	P.F
50	93.2%	7.01%	0.9
100	95.2%	6.24%	0.912
150	96.3%	4.63%	0.99
200	97.3%	3.22%	0.993

Table 1 : Efficiencies, P.F, and THD values at different load levels measured under 110 V_{ac}

LOAD	EFFICIENCY	THD	P.F
50	92.1%	1.12%	0.9224
100	96.2%	6.36%	0.95
150	98.1%	10.43%	0.98
200	98.2%	7.62%	0.995

Table 2 : Efficiencies, P.F, and THD values at different load levels measured under 220 V_{ac}

CONCLUSION

In this paper, a novel of push pull quasi resonant converter techniques for Boost PFC is simulated in order to boost up the voltage level and improve the power factor. Simulation has been done using MATLAB/SIMULINK for an input voltage of 110V AC and power output 100w for 380dc output voltage. In the systems we are gaining the power factor nearby unity

REFERENCES:

- [1] K. Yao, X. Ruan, X. Mao, and Z. Ye, —Reducing storage capacitor of a DCM boost PFC converter, *IEEE Trans. Power Electron.*, vol. 27, no. 1, pp. 151–160, Jan. 2012.
- [2] X. Zhang and J.W. Spencer, —Analysis of boost PFC converters operating in the discontinuous conduction mode, *IEEE Trans. Power Electron.*, vol. 26, no. 12, pp. 3621–3628, Dec. 2011.
- [3] B. Su, J. Zhang, and Z. Lu, —Totem-pole boost bridgeless PFC rectifier with simple zero-current detection and full-range ZVS operating at the boundary of DCM/CCM, *IEEE Trans. Power Electron.*, vol. 26, no. 2, pp. 427–435, Feb. 2011.
- [4] B. Akin and H. Bodur, —A new single-phase soft-switching power factor correction converter, *IEEE Trans. Power Electron.*, vol. 26, no. 2, pp. 436–443, Feb. 2011.
- [5] Y.-S. Roh, Y.-J. Moon, J.-C. Gong, and C. Yoo, —Active power factor correction (PFC) circuit with resistor free zero-current detection, *IEEE Trans. Power Electron.*, vol. 26, no. 2, pp. 630–637, Feb. 2011.
- [6] Y.-T. Chen, S. Shiu, and R. Liang, —Analysis and design of a zero-voltage switching and zero-current-switching interleaved boost converter, *IEEE Trans. Power Electron.*, vol. 27, no. 1, pp. 161–173, Jan. 2012.
- [7] H. Hsia, H.-Y. Tsai, D. Chen, M. Lee, and C.-S. Huang, —Interleaved active-clamping converter with ZVS/ZCS features, *IEEE Trans. Power Electron.*, vol. 26, no. 1, pp. 29–37, Jan. 2011.
- [8] S. Dwari and L. Parsa, —An efficient high-step-up interleaved DC–DC converter with a common active clamp, *IEEE Trans. Power Electron.*, vol. 26, no. 1, pp. 66–78, Jan. 2011.
- [9] Y.-C. Hsieh, M.-R. Chen, and H.-L. Cheng, —An interleaved flyback converter featured with zero-voltage transition, *IEEE Trans. Power Electron.*, vol. 26, no. 1, pp. 79–84, Jan. 2011.
- [10] R.-L. Lin, C.-C. Hsu, and S.-K. Changchien, —Interleaved four-phase buckbased current source with center-tapped energy-recovery scheme for electrical discharge machining, *IEEE Trans. Power Electron.*, vol. 26, no. 1, pp. 110–118, Jan. 2011.
- [11] W. Li and X. He, —A family of isolated interleaved boost and buck converters with winding-cross-coupled inductors, *IEEE Trans. Power Electron.*, vol. 23, no. 6, pp. 3164–3173, Nov. 2008.
- [12] L. Huber, B. T. Irving, and M.M. Jovanovic, —Open-loop control methods for interleaved DCM/CCM boundary boost PFC converters, *IEEE Trans. Power Electron.*, vol. 23, no. 4, pp. 1649–1657, Jul. 2008.
- [13] *IEEE Trans. Power Electron.*, vol. 23, no. 4, pp. 1649–1657, Jul. 2008

An Automatic Method for Segmenting Lungs

Jithy John, Rainu Boben
P.G Scholar, Dept of CSE, BMCE, Kollam, Kerala, India
jithyjohn90@gmail.com

Abstract— Image segmentation is an important task for image understanding and analysis. Image segmentation can be applied in medical field such as diagnosing the diseases. In recent times, Computed Tomography (CT) is the most effectively method used for detecting lung cancer and other types of diseases associated with lung. Segmentation of lung is an analysis the lung deeply and checks for whether it contains any diseases or not. Nodule is an early stage of lung cancer i.e., mass in the lung. Lung segmentation is complex due to presence of juxta-pleural nodule and blood vessels. So this drawback is overcome by a fully automated method of lung segmentation is used. In this paper, segmentation scheme consist of three stages: pre-processing, lung extraction, lung identification. The goal of pre-processing is reduce the noise from CT image of lung. Second stage is lung extraction for removing fat, tissues and artifacts of patients. Third stage is lung identification for detecting lung by using Fuzzy C Means algorithm and also removes the airways. This method is mostly used for identifying the lung nodules as well as other diseases.

KEYWORDS— LUNG, IMAGE SEGMENTATION, FUZZY C MEANS, JUXTAPLEURAL, NODULE, BLOOD VESSELS, COMPUTED TOMOGRAPHY

1. INTRODUCTION

Image segmentation is an important image processing step, and it is used everywhere if we want to analyze what is inside the image. Image segmentation; basically provide the meaningful objects of the image [1]. In recent years image segmentation has been extensively applied in medical field for diagnosing the diseases. In case of medical image segmentation the aim is to: study anatomical structure, identify Region of Interest i.e. locate tumor, lesion and other abnormalities, measure tissue volume to measure growth of tumor (also decrease in size of tumor with treatment), help in treatment planning prior to radiation therapy; in radiation dose calculation, measuring tumor volume and its response to therapy, detection of micro calcification on mammograms automated classification of blood cells, studying brain development, image registration, etc [2].

Medical imaging techniques often use anatomic structures as a 'guide' to perform segmentation tasks. Such techniques typically require some form of expert human supervision to provide accurate and consistent identification of anatomic structures of interest. Automatic segmentation of medical images is a difficult task as medical images are complex in nature and rarely have any simple linear feature. Further, the output of segmentation algorithm is affected due to partial volume effect, intensity inhomogeneity, presence of artifacts, and closeness in gray level of different soft tissue. Artifacts present in MR and CT images can be divided into three categories on the basis of image processing technique needed to rectify them: artifacts needing appropriate filtering technique, artifacts needing appropriate image restoration techniques for example motion artifacts and artifacts needing specific algorithm are; partial volume, intensity inhomogeneity.

One of the medical imaging segmentation is lung segmentation. The lungs are a pair of spongy, air-filled organs located on either side of the chest (thorax). A pulmonary nodule is a small round or oval-shaped growth in the lung. It is sometimes also called a spot on the lung or a coin lesion. Pulmonary nodules are generally smaller than 3 centimeters in diameter. If the growth is larger than that, it is known as a pulmonary mass. A mass is more likely to represent a cancer than is a nodule. Computed Tomography (CT) based Computer-Aided Detection (CAD) is the most commonly used diagnosis technique due to its high sensitivity of small pulmonary nodules and flexible representation of the human thorax.

CT or Computer Axial Tomography, uses special X-ray tube to obtain image data from different angles around the body, and then uses computer processing of the data to show a cross-section of body tissues and organs. Some of the basic ideas underlying CT are reconstruction from projections that means that the patient data is getting measured at many positions and angles. CT modalities can show various types of tissues, lung, soft tissue and bones, and using specialized equipment and expertise to create and interpret CT scans of the body, radiologists can more easily diagnose tumor, cancer or other lesion, and to measure its size, precise location, and the extent of the tumor's involvement with other nearby tissue. The images received from a CT scanner can reveal some soft tissue and other structures that cannot even be seen in conventional X-rays. Computerized Tomography scan an image provides detailed, cross sectional views of all types of tissues in the human body. It is used for diagnosing various cancers like lung, liver etc and also measure

size, location of tumor and extent of damage to the nearby tissues [12]. CT images shows very small as well as neighboring tissues such as muscle and blood vessels. Fig.1 shows CT image of lung.

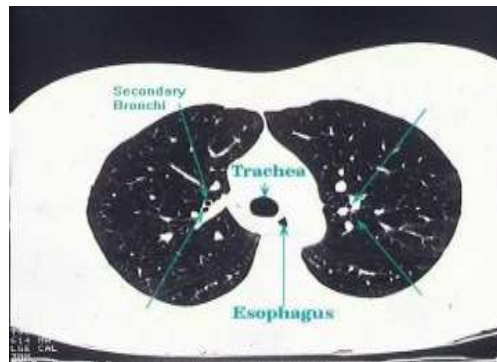


Fig.1 CT scan image of lung

In this paper, propose automated lung segmentation in CT images for deeply analyzing any diseases in the lung. This method is beginning with preprocessing by using anisotropic filter for remove noise without blurring edges and then extracts the lung parenchyma and airways region from CT image. The lung region is identified by using Fuzzy C Means clustering.

This paper is organized as follows: In section 2 includes the related works. The proposed method is explained which includes 3 stages in section 3. Ultimately section 4 concludes the proposed work.

2. RELATED WORKS

In the past, various techniques are used to segment the lung. Manual segmentation of lung images is extremely times consuming for users, labor intensive and prone to human errors [3]. Armato et al. showed that 5–17% of the lung nodules in their test data were missed due to the inaccurate pre-processing segmentation, depending on whether or not the segmentation algorithm was adapted specifically to the nodule detection task [4].

Pu et al. proposed an adaptive border marching algorithm (ABM) to correct the lung boundary. The problem with ABM is that the border marching with fixed threshold may fail in some slices. For example, the lung lobe containing juxtaleural nodule needs a smaller threshold while the lung lobe without juxtaleural nodule and containing convex region requires higher threshold [5].

Giger et al. presented the computerized detection of pulmonary nodules on CT scans. The rolling ball algorithm (RBA) is one of the early used methods to ameliorate the lung contour that is determined by thresholding. The rolling ball is a circular filter with a predefined radius [3]. A rolling ball algorithm was applied to the lung contours segmented by thresholding to avoid the loss of the juxtaleural nodules. The extremely varied sizes of juxtaleural nodules, it is difficult to select a proper rolling ball radius that is suitable for all juxtaleural nodules [4].

Sluimer et al propose a segmentation-by-registration scheme is used to segment and correct the lung boundary. This type of methods works well on the lungs even containing (substantial) pathologic abnormalities. But the creation of a model used in registration is not a trivial issue due to the high density pathologies in varying degrees of severity [6]. Although radiologists are able to identify the lung boundary slice by slice, it is extremely time-consuming and prone to intra- and inter-observer variability [7].

3. PROPOSED METHOD

Segmentation of lung is very difficult due to some fat, bone, tissues and other artifact. So this drawback is rectified by an automated lung segmentation is proposed.

In proposed system consists of three main stages: Image pre-processing, Lung extraction, Lung identification. Fig 2 shows the overview of proposed system.

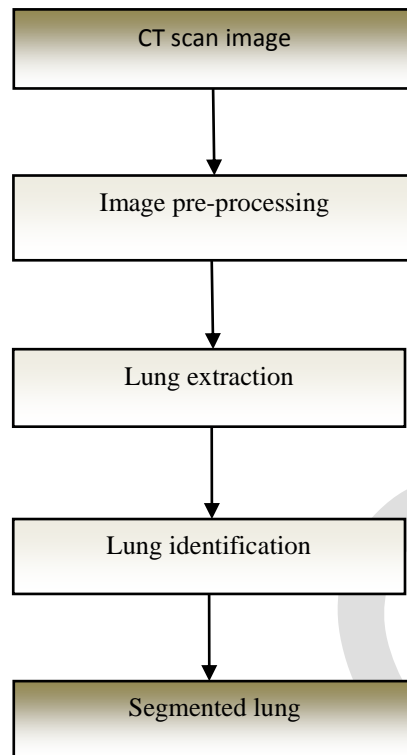


Fig.2 Overview of Proposed System

A. Image Pre-Processing

The first step was to convert the image to gray scale. So by converting the image to gray scale, the processing time is reduced and a faster algorithm is produced [2]. The goal of pre-processing is to reduce image noise. Nonlinear anisotropic diffusion filtering is an implicit edge detection step into the filtering process. This encourages intra-region smoothing and preserves the inter-region edge [9, 11].

B. Lung Extraction

In CT scan image contain two kinds of voxels. One is body voxels (high intensity pixels) such as ribs, fat and chest wall structures and another voxels is non-body voxels (low intensity pixels) such as air-filled region. Each voxels have CT number or Hounsfield unit [HU]. The Hounsfield unit (HU) scale is a linear transformation of the linear attenuation coefficient of the original attenuation coefficient. CT number is quantitative scale for describing radio-density. Radio-density of air at STP is -1000HU, lung tissue range from -910HU to -500HU and chest wall, blood vessels, bone which have above -500HU. Fig 3 shows values of Hounsfield values or CT number of each region in CT scan image. The main goal of this step is removal of chest wall, bone, fat for future segmentation. This is achieved by generating histogram of CT image and calculates threshold value by taking mean value of two peaks for Binarize the images. Binary image are generated from input gray-level CT image by select threshold from histogram of lung, a better method than the conventional thresholding algorithm, in which the threshold is simply chosen as the minimum between the two maxima of the gray level histogram. The image histogram is initially divided into two parts using a starting threshold value, which can be for example half the maximum of the dynamic range of the current image, or the conventional threshold value just described. The background removed image contains holes in Lung lobe; those are either nodules or vessels. It is important to include them in the Lung lobe region. These holes are filled using the hole filling morphological operators. Fig 4 shows the histogram of pixels in CT images in which fats, bone and muscles have high HU value than lung parenchyma and airway.

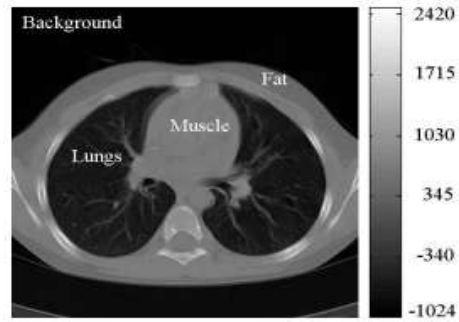


Fig.3 HU values of CT image

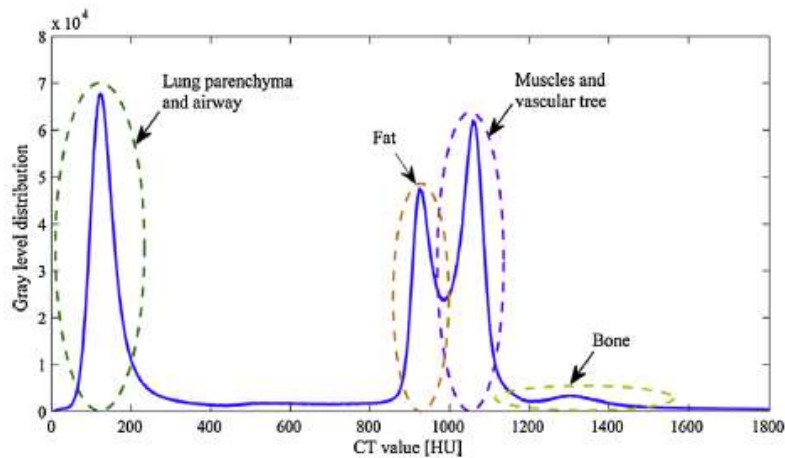


Fig.4 Histogram of pixels in CT images

C. Lung Identification

1. Lung parenchyma and airways are detection

In hard clustering, data is divided into distinct clusters, where each data element belongs to exactly one cluster. In fuzzy clustering, data elements can belong to more than one cluster, and associated with each element is a set of membership levels. These indicate the strength of the association between that data element and a particular cluster. Fuzzy clustering is a process of assigning these membership levels, and then using them to assign data elements to one or more clusters [10].

Fuzzy segmentation has been favored over hard segmentation in some medical image applications since partial volume effects and image noise reduce the accuracy of hard segmentation. To cope with the limits of hard segmentation, a fuzzy c-means (FCM) clustering method [11] is employed to classify pixels into several tissue categories.

In FCM method, a set of tissue classes is first determined. Each pixel is then classified by its membership values of tissue classes according to its intensity. Each tissue class has a centroid. FCM can be written as the minimization of the weighted inter-class sum of the squared error objective function J_{FCM}

$$J_{FCM} = \sum_{c=1}^C \sum_{j=1}^J u_{jc}^2 \|I_j - v_c\|^2 \quad (1)$$

where v_c is the centroid of class c and C is the total number of tissue classes; u_{jc} is the membership value of pixel j for class c and requires $u_{jc} \in [0,1]$ subject to $\sum_{c=1}^C u_{jc} = 1$; J is the total number pixels in the image and I_j is the image intensity at the position j .

The objective function is minimized when a large membership is assigned to pixel close to the centroid of a class and a small membership value is assigned to a pixel far away from the centroid. This is a nonlinear problem and can be solved iteratively. During each iteration, a new set of membership functions and class centroids are computed. The following steps describe the FCM method:

1. Set the initial values for class centroids, $v_c, c = 1, \dots, C$.
2. Compute the membership values

$$u_{jc} = \frac{\|I_j - v_c\|^{-2}}{\sum_{i=1}^C \|I_j - v_i\|^{-2}} \quad (2)$$

3. Compute the new centroid for each class

$$v_c = \frac{\sum_{j=1}^J u_{jc}^2 I_j}{\sum_{j=1}^J u_{jc}^2} \quad (3)$$

4. Repeat steps (2) and (3) until the algorithm converges. Convergence is reached when the maximum changes over all centroid between two iterations are less than a predefined small threshold value $\epsilon(0.001$ in current algorithm).

2. Large Airways Elimination

After detecting lung parenchyma region, next step to remove the main trachea and bronchus by region growing algorithm [11, 13]. A seed pixel is selected from centroid location of trachea region. Then compare between seed pixel and neighboring pixel if it is similar, then grows seed pixels towards to boundary of lung. This procedure continues until the stopping criterion is reached.

3. Left and Right Lung Separation

After the large airways elimination, then analyze the remaining connected components slice by slice [10]. This results either in one (both left and right lungs merge together) or two (both two lungs are separated) by using erosion [8]. Erosion is the dual of dilation. The erosion of object X with a structuring element SE is denoted as:

$$Y = X \ominus d . SE \quad (4)$$

Also here the structuring element is defined by the connectivity, which can be 4 or 8- connected for 2D images. If the central pixel in the 3×3 neighborhood is an object pixel and at least one of the pixels in the neighborhood is a non-object pixel, the central pixel becomes a non-object pixel.

The juxtapleural nodules tend to be excluded from the lung segmentation result in the previous step due to its density that is similar with thorax; moreover, high density pulmonary vessels are also ruled out from segmentation result which gives rise to indentations and salience in the lung boundary near the mediastinum. By using Gaussian filter this problems can be solved [11].

Finally, the output image is segmented image of lung. This output can be used for further analysis as well as finding pathologies of lung.

4. CONCLUSION

This paper presents an efficient automated approach for segmenting lung on CT images. Automated segmentation of lung on CT image is more accuracy than manual segmentation of lung as well as easy to segment and studying deeply each part of segmented images. The CT images are preprocessing, extracted and identification. The first is preprocessing by using anisotropic filter. The advantages of anisotropic filter are to remove the noise without blurring edges. It also smoothes intra-region and preserve inter-region. The second stage is lung extraction which helps us to remove artifacts for further segmentation. The third stage is lung identification in which lung is extracted for deeply analysis by using FCM. Future work will be correcting the lung contour and detected the lung nodule.

REFERENCES:

- [1] Sujata Saini and Komal Arora, "A Study Analysis on the Different Image Segmentation Techniques", International Journal of Information & Computation Technology, Volume 4, Number 14 (2014), pp. 1445- 1452.
- [2] Nihad Mesanovic , Mislav Grgic , Haris Huseinagic," Automatic CT Image Segmentation of the Lungs with Region Growing Algorithm".
- [3] Shicheng Hu, Kesen Bi, Quanxu Ge, Mingchao Li, Xin Xie and Xin Xiang, "Curvature-Based Correction Algorithm For Automatic Lung Segmentation On Chest CT Images", Journal of Biological Systems, Vol. 22, No. 1 (2014) 1-28.
- [4] S.G. Armato, M.L. Giger, C.J. Moran, J.T. Blackburn, K. Doi, H. MacMahon, "Computerized detection of pulmonary nodules on CT scans", Radiographics 19 (5)(1999) 1303-1311.

- [5] J. Pu, J. Roos, C.A. Yi, S. Napel, G.D. Rubin, D.S. Paik, "Adaptive border marching algorithm: automatic lung segmentation on chest CT images", *Comput. Med. Imaging Graph.* 32 (6) (2008) 452–462.
- [6] I. Sluimer, M. Prokop, B. van Ginneken, "Toward automated segmentation of the pathological lung in CT", *IEEE Trans. Med. Imaging* 24 (8) (2005) 1025–1038.
- [7] Q. Li, F. Li, K. Suzuki, J. Shiraishi, H. Abe, R. Engelmann, Y. Nie, H. MacMahon, K. Doi, "Computer-aided diagnosis in thoracic CT", *Seminars in Ultrasound, CT, MRI* 26 (5) (2005) 357–363.
- [8] S. Hu, E.A. Hoffman, J.M. Reinhardt, "Automatic lung segmentation for accurate quantitation of volumetric X-ray CT images", *IEEE Trans. Med. Imaging* 20 (6) (2001) 490–498.
- [9] P. Perona, J. Malik, "Scale-space and edge detection using anisotropic diffusion", *IEEE Trans. Pattern Anal. Mach. Intell.* 12 (7) (1990) 629–639.
- [10] S. Sivakumar, C. Chandrasekar, "Lungs image segmentation through weighted FCM", *IEEE International Conference on Recent Advances in Computing and Software Systems*, 2012, pp. 109–113.
- [11] Shengjun Zhou, Yuanzhi Cheng, Shinichi Tamura, "Automated lung segmentation and smoothing techniques for inclusion of juxtapleural nodules and pulmonary vessels on chest CT images", *Biomedical Signal Processing and Control* 13 (2014) 62–70.
- [12] MN Prasad, MS Brown, S Ahmad, F Abtin, J Allen, "Automatic segmentation of lung parenchyma based on curvature of ribs using HRCT images in scleroderma studies", *Medical Imaging*, Vol. 6915, (2008).
- M. Sonka, V. Hlavac, R. Boyle, *Image Processing, Analysis, and Machine Vision*, Brooks/Cole Publishing, Pacific Grove, CA, 1999

INTEGRATED MICROBIAL-VERMIFILTRATION TECHNIQUE FOR AYURVEDIC INDUSTRIAL EFFLUENTS

Divya C Das, Mary Joseph, Deepak Varghese
Department of Biotechnology, MET'S school of engineering,
maryjcherayath@gmail.com,
Phone No: 9567284363

Abstract— Sustainable, effective and cheapest method of effluent treatment is yet to be reality especially for industrial waste water. Many of the existing methods resulted in several environmental problems. So this paper, mainly focuses on the development of treatment method for Ayurvedic liquid effluents by integrating microbial pre-treatment and vermifiltration. Firstly, Ayurvedic effluent was pretreated with a microbial consortium and later fed to a vermifiltration unit. Organic wastes, heavy metals and solids are ingested and absorbed through earthworm's body wall and degraded which was found to remove BOD, COD, total dissolved solids (TDS) and the total suspended solids (TSS) from wastewater. There was no sludge formation in the process and odor free. The final vermifiltered water exhibited a significant reduction in COD by 98.03%, BOD by 98.43%, TSS by 95.8% TDS by 78.66% and oil & grease by 92.58%. The resultant water was clean and disinfected enough to be reused for irrigation.

Keywords: Vermifiltration, Earthworms, Biofilter, Effluent, Odor-free process, Microbial pre-treatment, Irrigation

INTRODUCTION

Human relationship with the environment has been found to change from industrial revolution to the present day. Industrial effluents create a lot of environmental impacts by its uncontrolled discharge which is a great concern in developing countries like India since environmental preservation adds to its economy. Even though industries are needed to fulfil diverse necessities of man, the huge amount of harmful wastes leads to undesirable consequences. Presently, linear waste water disposal systems are followed in ETPs by using the activated sludge method [3]. Environmental regulations insist on zero discharge waste water treatment systems, thereby the refinement of conventional treatment technologies and implementation of new technologies for waste water treatment to meet stringent water quality criteria is made mandatory. [7].

In developing countries, about 80% of the world population use traditional herbal medicines to treat diseases. Herbal medicines and other finished herbal products contain active ingredients from plants or other plant materials. India has a glorious tradition in the field of herbal medicine [8]. Presently, Ayurveda medicines are used to treat different kinds of diseases and are being popular day by day. Herbal pharmaceutical companies generate huge volume of biodegradable wastewater during processing and production. Herbal pharmaceutical wastewater is moderately strong with COD and BOD concentration and can be discharged only after proper treatment [18]. Plant based raw materials are used in preparation of Ayurveda medicines. Condenser waste from evaporators, chemical waste, spent liquors from fermentation operations, sewage, laboratory and floor washing waste contributes to the organic and inorganic matter in Ayurvedic waste water.

Vermifilter, a low- cost sustainable technology has an immense potential for decentralization in rural areas over conventional systems[10]. Vermifiltration, also known by the term lumbrifiltration, is an extension of vermicomposting for solid waste management [4]. Dissolved and suspended solids get trapped in the vermifilter bed. They are processed by complex biodegradation by passive absorption through the body wall of the earthworms and microbes immobilized in the gut area of the earthworms. Aerobic and anaerobic microbes in the soil also promotes the degradation of organic and inorganic matter [11]. The two processes-microbial process and vermi-process were found to work simultaneously in the treatment of domestic as well as industrial wastewater [9]. The resulting effluent becomes highly nutritious and can be reused for irrigation purpose.

In the present paper, pretreatment of the Ayurvedic effluent with enzyme producing strains were studied.

MATERIALS

Eisenia fetida earthworms were collected from the composting units of Kerala Agricultural University (KAU), Mannuthy. Bedding material consisting of straw, cow dung, vegetable scraps was used after suitable sterilization in the upper most layer of vermicompost.

METHODS

COLLECTION, STORAGE AND PHYSICO CHEMICAL ANALYSIS OF INDUSTRIAL EFFLUENT:

Liquid effluents were collected from Ayurveda Industry. To minimize the potential of volatilization or biodegradation between sampling and analysis, the samples were kept cool as possible without freezing. Samples were cooled with ice or in a refrigeration system set at 4°C. Initial values of BOD, COD, TSS, TDS, Oil and grease, Total nitrogen, Total phosphorous, Sulphate, Chromium, Nickel, Copper present in the liquid effluents were determined.

ISOLATION OF ENZYME PRODUCING STRAINS:

Protease and lipase producing strains were isolated from the effluent by standard plating techniques [13]. A protease (*Bacillus sp.*) and lipase (*Bacillus sp.*) producing was selected from the isolated strains. Antagonism of the two strains were checked by T-streak technique on Nutrient Agar plate. A bacterial consortium was prepared using the selected strains by mixing 5ml of each overnight grown strains in 20ml of nutrient broth [14].

REMOVAL OF OIL CONTENT OF THE EFFLUENT:

Broken brick pieces of varying size were filled inside the column of diameter 6.3 cm. The effluent was passed through the column at a minimum flow rate of 0.025 LPS. The process was repeated for 3 times [1].

PRE-TREATMENT OF THE EFFLUENT:

The experiments were conducted on a lab scale, in the college laboratory. 100ml of Ayurvedic effluent was taken in three 500ml conical flasks each. Each conical flasks was inoculated with protease producing strain (*Bacillus sp.*), lipase producing strain (*Bacillus sp.*), and consortium (Mixture of protease and lipase producing strains) with 1 ml of overnight cultures and incubated at 37°C at 100rpm for 24 hours. Effect of pre-treatment of effluent with consortium and selected strains on reduction of BOD and COD was studied.

EFFECT OF TIME ON PRE-TREATMENT OF THE EFFLUENT:

100ml of Ayurvedic effluent was taken in three 500ml conical flasks each. Each conical flasks was inoculated with protease producing strain (*Bacillus sp.*), lipase producing strain (*Bacillus sp.*), and consortium (Mixture of protease and lipase producing strains) with 1ml of overnight cultures. Influence of time on pretreatment of effluent was determined by incubating the conical flasks at 37°C at 100rpm for 24, 48 and 72 hours respectively and reduction of BOD and COD were studied.

PREPARATION OF A LAB SCALE VERMIFILTER SETUP:

A lab scale vermifilter setup consist of smooth walled cylindrical plastic tank of 26cm length and 17cm diameter. Lower section resembles a trickling filter consisting of successive layers of pebbles, bricks, gravel, and fine sand laid from bottom to top. The upper bedding material of VF tank was prepared using cow dung and straw as standard bedding materials, and colonies of selected earthworms (Table 1 and 2). For uniform effluent discharge, reservoir with a distribution system was used (fig.1). The treated water was collected at the bottom from the outlet pipe [15].

Serial no.	Parameters estimated	Values
1	Area of the vermi filter system	0.044 m ²
2	Volume of the soil profile in the vermi bed	3.97*10 ⁻⁴ m ³
3	Porosity of the vermi bed	42.5%
4	Moisture content of the vermi bed	77.40%
5	Temperature of the system	32 °C
6	Volumetric flow rate	9.3 L/hr.
7	Hydraulic loading rate (HLR)	0.211 m/hr.
8	Minimum hydraulic retention time (HRT)	2 hrs.

Table 1: Design parameters of vermifilter set up

Layers (from bottom to top)	Size range (cm)	Thickness (cm)
Pebbles	1-2	4
Brick	0.05-2	3
Gravel	0.5-1	5
Sand	16-20mm mesh	6
Scraps, cow dung, earthworms	1.5 kg	7

Table 2: Size and thickness of layers



Fig.1: Lab scale setup of vermifilter

VERMIFILTRATION OF RAW EFFLUENT:

The reservoir was filled with 1L of raw effluent without pre-treatment, and was uniformly distributed at a flow rate of 9.3 L/hr to the surface of the vermifilter set up. The entire system was retained for 2hrs. After 2 hrs the treated water was collected at the bottom outlet. The entire set up was allowed to remain to convert the bedding material into humified vermi compost. The treated water collected at the bottom outlet was checked for its BOD, COD, Oil and grease content [16].

VERMIFILTRATION OF PRE-TREATED EFFLUENT:

2L of raw effluent was pretreated with individual enzyme producing strains and consortium at 37°C for 72 hours with agitation (100 rpm). The reservoir was filled with 1L of pretreated effluent, and was uniformly distributed at a flow rate of 9.3 L/hr to the surface of the vermifilter set up. The entire system was retained for 2hrs. After 2 hrs the treated water was collected at the bottom outlet. The entire set up was allowed to remain to convert the bedding material into humified vermi compost. The trickled water was collected at the bottom outlet and checked for its BOD, COD, Oil and grease content [16].

STUDY OF THE EFFECT OF ENZYME PRODUCING MICROBIAL STRAINS IN THE PRE-TREATED EFFLUENT ON THE EARTHWORMS IN THE VERMIFILTER:

The microbial count in the pre-treated effluent before and after vermifiltration was determined by standard plate count method [13]. The effluent samples before and after vermifiltration were serially diluted and spread plated on Nutrient agar medium. The number of desired colonies of enzyme producing strains were counted. The amount of biomass and number of earthworms before and after vermifiltration were also determined. The above results were analyzed to derive the relationship between the microbial strains and earthworm population. The above procedure was done for protease pre-treated, lipase pre-treated and consortium pre-treated effluents.

RESULTS AND DISCUSSIONS

PHYSICO-CHEMICAL ANALYSIS OF AYURVEDIC EFFLUENT

Ayurvedic effluent was turbid, oily and blackish in color. The characteristics of Ayurvedic effluent is given below in Table no.3

PARAMETERS TESTED	Value (mg/l)
pH	6.23
Total Dissolved Solids	2010
Total Suspended Solids	3020
BOD	3880
COD	7000
Oil & Grease	64.7
Total Phosphorous	55.62
Total Nitrogen	327.55
Sulphate	247.66
Chromium	<0.01
Nickel	<0.01
Copper	<0.01

Table 3: Results of physico-chemical analysis of Ayurvedic effluent

REMOVAL OF OIL AND GREASE FROM THE EFFLUENT

The experiment was carried out using the process of adsorption in which Laterite brick material was used as the adsorbent. The raw effluent was passed at a minimum flow rate of 0.025 LPS through the column containing broken brick pieces. The process was repeated for 3 times. The results proved that Laterite was a powerful adsorbent medium. It can be adopted at the source to remove oil and grease [1]. The process resulted in significant reduction of oil and grease from 64.7 mg/l to 7.76±0.2 mg/l with 88±0.25% reduction (Table .4)

Oil and grease Content in raw effluent (mg/l)	Oil and grease content after passage though the column (mg/l)	Percentage Reduction (%)
64.7	7.76±0.2	88±0.25

Table 4: Results of oil removal

PRE-TREATMENT OF THE EFFLUENT:

Ayurvedic effluent was inoculated with protease producing strain (*Bacillus sp*), lipase producing strain (*Bacillus sp*), and consortium (mixture of protease and lipase producing strains) incubated at 37°C at 100rpm in rotary shaker for 72hours. Reduction of BOD and COD by microbial pretreatment was studied in detail and given in table 5 and fig. 2 & 3. Protease and lipase action helps in degradation of proteins and lipids present in the effluent and make it readily available for consumption by microbes and earthworms. Bio management of liquid effluent with enzymes and microbes resulted in significant reduction of organic matter and thereby reducing the BOD load for the vermifiltration process.

EFFECT OF TIME ON PRE-TREATMENT OF EFFLUENT

Ayurvedic effluent was incubated at 37°C at 100rpm in rotary shaker for 24, 48 and 72 hours respectively with protease producing strain (*Bacillus sp*), lipase producing strain (*Bacillus sp*), and consortium (mixture of protease and lipase producing strains). Thus the effect of time on reduction of BOD and COD by pretreatment was studied in detail and has given in table 5 and fig. 2 & 3. In our study, pretreatment with consortium at 72 hours gave the maximum reduction of BOD by 96.1% and COD by 97% which shows increase in contact time with enzymes and microbes decreased the BOD and COD. Agitation at 100 rpm had a significant effect on the growth and activity of the enzyme producing microbes, for the reduction of organic content in the effluent which indicates the oxygen requirement in microbial pretreatment (fig 4& 5).

Time (hrs)	BOD (mg/l)			COD (mg/l)		
	Protease Treatment	Lipase Treatment	Consortium Treatment	Protease Treatment	Lipase Treatment	Consortium Treatment
24	390±2.0	423±4.0	313±3.7	545±2.5	806±2.5	475±3.0
48	324±4.0	393±2.6	264±2.5	426±2.6	751±1.5	386±3.0
72	210±8.5	294±3.0	151±3.5	355±3.0	645±2.5	208±2.0

Table 5: Results of optimization of time for pre-treatment

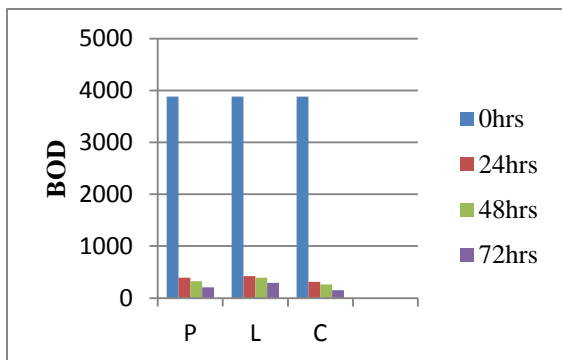


Fig.2: Role of time in BOD removal.

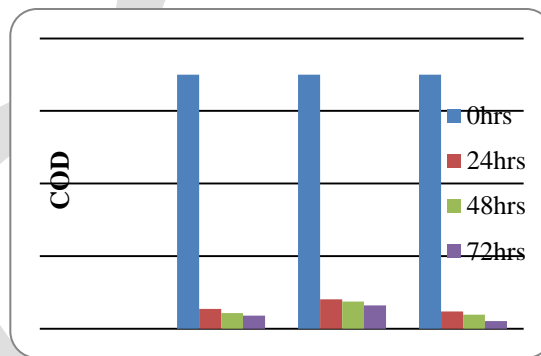


Fig.3: Role of time in COD removal.

EFFECT OF PRETREATMENT ON VERMIFILTRATION

Vermifiltration of raw effluent without pretreatment showed reduction of BOD by 91.95%, COD by 93.23 % and oil & grease by 87.17% (Table 6 & fig 4). 2L of raw effluent was pretreated with individual enzyme producing strains and consortium at 37°C for 72 hours with agitation at 100 rpm and was uniformly distributed to the surface of the vermifilter set up. The trickled water was collected at the bottom outlet and checked for its BOD, COD, Oil and grease content. The maximum reduction of BOD by 98.43% COD by 98.03% and oil & grease by 92.58% was found in the effluent after vermifiltration process with consortium treatment (Table 6& fig 4). Synergistic action of enzymes, microbes and earthworms lead to considerable reduction of BOD, COD and oil & grease. Studies have shown the gut of endogenic earthworms like *Eisenia fetida* having microbes with cellulolytic activity. The cellulases helps to degrade the cellulose present in the Ayurvedic effluents thereby reducing the BOD and COD [17].

Parameters (mg/l)	Vermi filtered Raw effluent	Vermi filtered Protease pre-treated effluent	Vermi filtered Lipase pre-treated effluent	Vermi filtered consortium pre-treated Effluent
BOD	312.33±4.5	153.33±4.1	167±4.3	61.00±3.2
COD	473.66±4.7	263.00±6.5	374.6±4.5	137.66±2.5
OIL&GREASE	8.4±2.0	8.06±0.2	7.53±0.4	4.8±0.2

Table 6: Results of vermifiltration of pre-treated Ayurvedic effluent

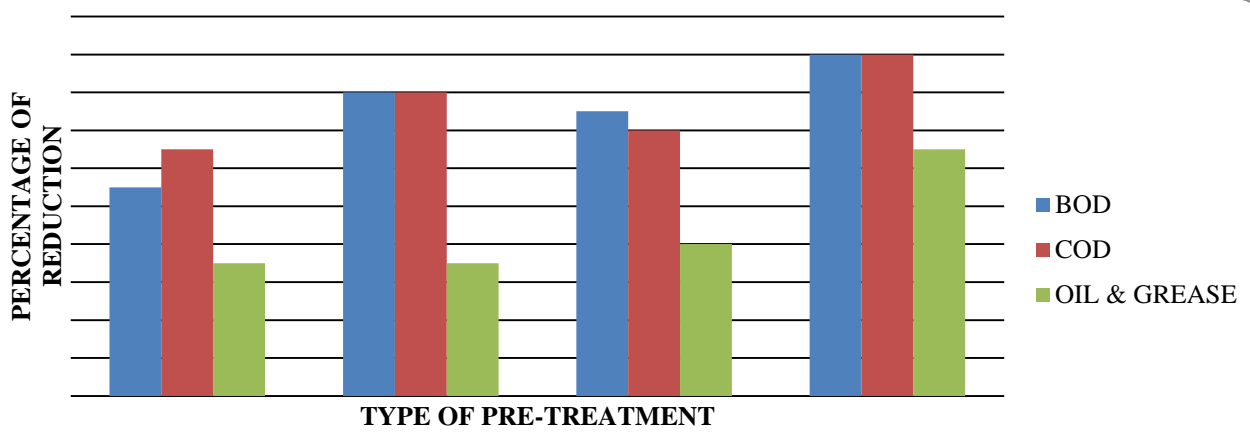


Fig.4: Results for Vermifiltration of pre-treated Ayurvedic effluent

STUDY OF THE EFFECT OF ENZYME PRODUCING MICROBIAL STRAINS ON GROWTH OF EARTHWORMS

Treatment	Number of bacterial colonies in the effluent (CFU) (10 ⁻⁹ dilution)	
	Before Vermifiltration	After Vermifiltration
Raw effluent	6.26±0.03	6.83±0.62
Protease pre-treated	10±0.15	12±0.04
Lipase pre-treated	10.48±0.12	11.04±0.02
Consortium pre-treated	14.3±0.05	15.5±0.07

Table 7: No. of bacterial colonies in the effluent (10⁻⁹ dilution) before and after vermifiltration

Treatment	Biomass of adult earthworms (g)	
	Before Vermifiltration	After Vermifiltration
Protease pretreated	18.35±0.3	23.77±0.05
Lipase pretreated	18.54±0.04	22.48±0.25
Consortium pretreated	18.31 ±0.12	23.64±0.32

Table 8. Biomass of adult earthworms in the pre-treated effluent before and after vermifiltration

Treatment	Biomass of young earthworms (g)	
	Before Vermifiltration	After Vermifiltration
Protease pretreated	9.9±0.25	11.02±0.06
Lipase pretreated	9.85± 0.03	10.70±0.2
Consortium pretreated	10.4±0.09	11.45±0.54

Table 9: Biomass of Young earthworms in the pre-treated effluent before and after vermifiltration

From the above data it was found that for protease, lipase and consortium pre-treatment, the number of bacterial colonies in the pre-treated effluent, remained almost consistent before and after vermifiltration. Number and biomass of earthworms in the vermifilter set up were also found to increase after the vermifiltration process. Increase in the number of earthworms and consistent bacterial count indicated that there was no negative effect on the growth of the desired enzyme producing microbes and earthworms. This proves that the water does not contain harmful compounds and is considerably safe to discharge for irrigational purposes.

IRRIGATIONAL WATER QUALITY CRITERIA OF FINAL DISCHARGED EFFLUENT

The effluent obtained after vermifiltration of the consortium pre-treatment was further analyzed for its biosafety and irrigational water quality criteria (Table 10).

Parameters (mg/l)	Qty in treated effluent (mg/l)	Max. permissible limit in irrigation water (mg/l)
pH	6.2±1.5	6-8.5
BOD	61±3.2	80
COD	137±2.5	150
TSS	130±.007	250
TDS	429±.03	2100
Sulphates	136±.03	1000
Chromium	<0.01	0.1
Copper	<0.01	0.2
Nickel	<0.01	0.2
Total nitrogen	18±.009	30
Total phosphorous	26±.05	50

Table 10: Irrigational water quality criteria of final discharged effluent

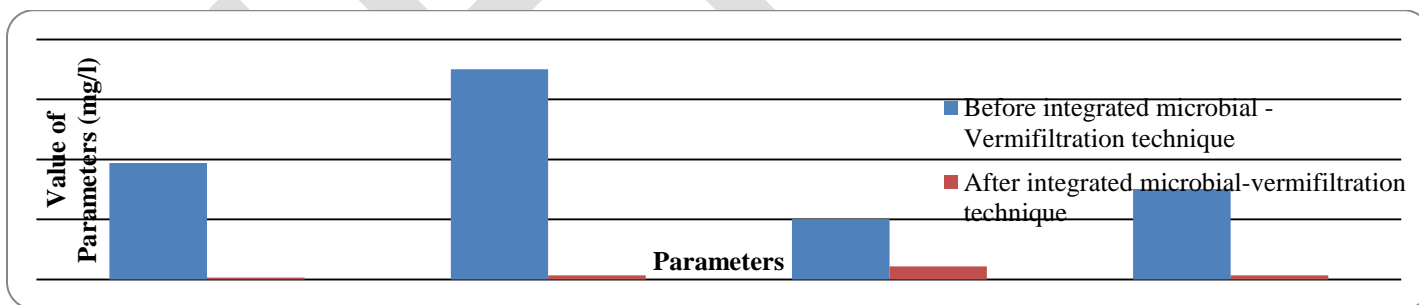


Fig.5: Results of effluent before and after integrated microbial- vermifiltration technique

VARIATION IN PH VALUE OF TREATED WASTE WATER

Results indicate that the pH value of both raw effluent and treated effluent have an average value of 6.2.

REMOVAL OF TOTAL SUSPENDED SOLIDS

Results showed that the microbes and earthworms can significantly remove the suspended solids from the wastewater by over 95%.

REMOVAL OF TOTAL DISSOLVED SOLID

Total suspended solids (TSS) and total dissolved solids (TDS) showed drastic reduction during integrated microbial-vermifiltration process. The total reduction in TDS content was about 75% in vermifiltration unit with pretreatment. Results thus clearly suggested the capability of earthworms to remove solid fractions of wastewater during integrated microbial -vermifiltration processes.

REMOVAL OF BIOCHEMICAL OXYGEN DEMAND (BOD)

BOD indicates the organic load of wastewater. The BOD load in effluents vermifiltration unit with pretreatment was significantly lower than initial levels and integrated microbial -vermifiltration showed more removal efficiency. Results show that the earthworms can remove BOD load by over 98.43%.

REMOVAL OF CHEMICAL OXYGEN DEMAND (COD)

Results showed that the average COD removed from the wastewater by vermifiltration with pretreatment is over 98.03% indicating degradation of several chemicals by enzymes in the gut of earthworms which is not usually degraded by microbial pretreatment.

CONCLUSION

Integrated microbial- Vermifiltration technique for the treatment of ayurveda liquid effluent was developed. It is a decentralized and cost effective method which can be applied to treat both domestic and industrial waste water treatment. A huge reduction in various effluent parameters like BOD, COD, TSS, TDS, Oil & grease, was observed. Presence of heavy metals in Ayurvedic effluent is almost zero. Vermifiltration of the effluent pre-treated using the bacterial consortium at optimum conditions showed maximum reduction in the above mentioned parameters. Treated effluent well suited the irrigational water quality criteria.

REFERENCES:

- [1] Ajith Hebbar H, Jayantha K. S (2013), Oil and Grease Removal from Wastewater Using Laterite as an Adsorbent Material. Volume 3, Issue 5, 2250-2459.
- [2] Bouché MB, Qiu JP (1998). Concrete contributions of earthworms in the environmental study. *Doc. Pédzoool. Intégréol.* 3: 225-252.
- [3] Buyukgungor H, Gurel L (2009). The role of biotechnology on the treatment of wastes. *African Journal of Biotechnology* 8 (25), 7253 – 7262.
- [4] Ghatnekar, S. D., Kavian, M. F., Sharma, S. M., Ghatnekar, S. S., Ghatnekar, G. S., & Ghatnekar, A. V. (2010). Application of Vermi filter-based Effluent Treatment Plant (Pilot scale) for Biomanagement of Liquid Effluents from the Gelatine Industry. *Dynamic Soil, Dynamic Plant Vol 4 Special Issue 1*, 83-88.
- [5] *Indian J.Environmental Protection*, vol 27, No.6, June 2007.
- [6] Kharwade A.M. and Khedikar I. P. (2011). Laboratory scale studies on domestic grey water through vermifilter and non-vermifilter. *Journal of Engineering Research and Studies*, 2 (4): 35-39
- [7] Kumar L, Rajan R, Sabumon PC (2008). Development of an ecologically sustainable waste water treatment system. *Water Science and Technology* 58(1), 7-12.
- [8] Nandy, T.; Kaul, S. N.; Szpyrcowicz, L. (1998). Treatment of herbal pharmaceutical wastewater with energy recovery. *International Journal of Environmental Studies*. Vol 54, 83-105.
- [9] Sinha R. K., Bharambe G. and Chaudhari U (2008). Sewage treatment by vermifiltration with synchronous treatment of sludge by earthworms: a low cost sustainable technology over conventional system with potential for decentralization. *The Environmentalist*, 28, 409-420.
- [10] Taylor M, Clarke WP, Greenfield PF (2003). The treatment of domestic wastewater using small-scale vermicompost filter beds. *Ecol. Eng.* Vol 21: 197-203.
- [11] Tomar, P., & Suthar, S. (2011). Urban wastewater treatment using vermi- biofiltration system. *Desalination* Vol 28 no.2, 95-103.
- [12] Wang, S., Yang, J., Lou, S., & Yang, J. (2010). Wastewater treatment performance of a vermifilter enhancement by a converter sla-coal cinder filter. *Ecological Engineering* Vol 36, 489-494.
- [13] Benson, H. J. *Microbiological Applications* 8th Edition. New York: McGraw Hill, 2002. Fig. 21-1. Pg. 87. Bacterial Population Counts. ICBN# 0-07-231889-9.

- [14] Payel Sarkar, Andrew Roysten Rai and Shilpi Ghosh (2013), Degradation of Aromatic Petroleum Hydrocarbons (Btex) By A Solvent Tolerant Bacterial Consortium. Vol 7, ISSN 1982 – 3932.
- [15] A.Merly Xavier, A.Logeswari, S.Mano, Dr.M.Thirumarimurugan, Dr.T.Kannadasan (2013), Vermiculture For The Treatment Of Diary Effluents. Vol 1, ISSN : 2320 – 5083.
- [16] Standard Methods For the Examination of Water and Wastewater (2005).
- [17] Fujii K, Ikeda K, Yoshida S (2012) Isolation and characterization of aerobic microorganisms with cellulolytic activity in the gut of endogeic earthworms. Int Microbiol. Sep; 15(3):121-30.
- [18] Atul P. Vanerkar, , Abhay B. Fulke, Satish K. Lokhande, Manisha D. Giripunje, and Shanta Satyanarayan (2015), Recycling and treatment of herbal pharmaceutical wastewater using *Scenedesmus quadricuada*, Current Science, Vol. 108, No. 5

Advanced High Speed Frequency to Voltage Converter for Industrial Controllers.

Ayyaj .I .Nadaf 1, Dr. P. P. Shaha2, Dr. M. K. Bhanarkar3
Department of Electronics, Shivaji University, Kolhapur1,3 ,
Department of Electronics, Devchand College, Nipani2
ayyaz.nadaf@gmail.com.

Abstract— This paper presents utilization of on chip Pulse Width Modulation (PWM) for generating analog voltage. Industrial controllers or PLC requires digital to analog converters for process control. Many industrial devices like Variable Frequency Drive (VFD) work on standard analog input 0 to 10v. To communicate DAC modules and PLC special protocol are involved. It leads to time latency to get analog output. This paper represents without any protocol single digital output pin of PLC to give frequency to DAC module. This module converts those ranges of frequency signal to calibrated PWM to get analog output with low pass filter. With this module one can get analog voltage in standard range of 0 to 10v with ripple less than 0.1V. For This module can work in range of 1 kHz to 10 kHz.

Keywords— DAC, LOW PASS FILTER, PLC, PWM, PROTOCOL, VFD.

INTRODUCTION

IN Automated industry there are lots of process variable need to be controlled so as to get process under control. Simply saying there are lots of continuous signals need to monitor and control. Continuous actuators are major parts of the process. Today's continuous actuators are able to work on multiple standards like 4-20 mA, -10v to +10V DC, 0 to 10V DC. It is necessary to create interface between digital controllers and actuators. Industrial controller like PLC has capability to generate frequency signal. It's a need to create an interface can accept those frequency signals from PLC and generate 0 to 10V DC analog output. This analog output signal can then easily feed to industrial devices like VFD, PID controller etc.

In a typical PWM signal, the base frequency is fixed, but the pulse width is a variable or fixed. The pulse width is directly proportional to the amplitude of the original unmodulated signal. In other words, in a PWM signal, the frequency of the waveform is a constant while the duty cycle varies according to the amplitude of the original signal. A simple low pass filter is used to generate an output voltage directly proportional to the average time spent in the high level.

RESEARCH PROBLEM

Many industrial devices work on standard analog input 0 to 10v. To communicate DAC modules and PLC special protocol are involved. It leads to time latency to get analog output. DAC using R-2R ladder requires more power, more no of components, uses more no of bits to achieve good resolution. Potentiometric DACs have excellent linearity but they are much expensive and available with limited no of bits. All these methods involve reference power supply.

RELATED WORK

1.4V 13 μ W 83dB DR CT- $\Sigma\Delta$ modulator with Dual-Slope quantizer and PWM DAC for bipotential signal acquisition. This paper presents the implementation and measurements of a novel ultra-low power low voltage multi-bit continuous-time sigma-delta (CT- $\Sigma\Delta$) modulator, whose quantizer and feedback DACs operate in the time domain [1]. A low power successive approximation A/D converter based on PWM technique, this paper introduces a new architecture for a simple, practical and high precision conversion and analysis with Fourier transform method [2]. An AC voltage standard based on a PWM based DAC. This paper describes a new AC voltage standard which uses a traceable DC voltage standard as an input and produces an AC output at an equivalent RMS voltage to 1 μ V/V uncertainty [3].

PWM BASED DAC APPROACH

Industrial controller requires converting of digital to analog signal with minimum settling time, less bulky system, and accurate result without investing in much cost in new modules. Some advantages of PWM based DAC systems are

- Single pin requirement from the microcontroller GPIO pins.
- Extremely low external component requirement, without severe precision requirement.
- Output resistance that is independent of input.

$$[\text{ScaleCount}] = \left[\frac{\text{ScaleMaxVa lue}}{\text{Digital Input Max Count}} \right] \times \text{Digital Input}$$

As the scaling factor is a constant for a given DAC implementation, it can be precomputed and stored for use. e.g. In 8 bit PWM max count can be given is 255. In this case we need to read input frequency by means of timer, this is the digital count. For measuring of input frequency max up to 100 kHz. Timer need to select must have time base of 0.01 mS.

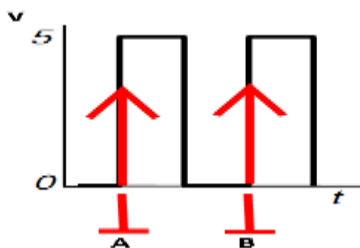


Figure 1: Input frequency signal.

Here to measure frequency of input signal; it is necessary to start timer at first rising edge A and stop timer at second rising edge B. Frequency of input signal is reciprocal of timing count difference between B and A multiplied by time base for timer. This digital input is must be calibrated for full scale 100% duty cycle. For example digital count of input frequency is 46015; max count possible with 16 bit variable register is 64536. If duty cycles register is 8 bit so for 100% duty cycle count should be 255. Therefore

$$[\text{ScaleCount}] = \left[\frac{255}{65536} \right] \times \text{Digital Input}$$

$$[\text{Scale Count}] = 0.003890 \times \text{Digital Input.}$$

0.003890 is precomputed constant based on calibration factors.

Scale Count is same to Duty Cycle count.

$$\text{Duty Cycle} = [0.003890] \times 46015.$$

Duty Cycle= 179; it is 70% of total 100% duty ratio.

The PWM/DAC approach is not new, but performance limitations have historically confined its use to low-resolution, low-bandwidth applications. The performance of the method relates directly to the ability of the low pass filter to remove the high frequency components of the PWM signal. Use of filter with too low a cut-off frequency, and DAC bandwidth suffers. Use a filter with too high a cut-off frequency DAC resolution suffers but one way to improve both of these problems is to increase the frequency of the PWM.

dac resolution:

$$A_o = \left[\frac{D_i}{2^N} \right] \times \text{Ref}$$

Where:

A_o = Analog output.

D_i = Digital input as a duty cycle count.

N = Number of digital input bits (resolution)

Ref = Reference Value (full scale).

Band width of the desired signal should be $F_{BW} \leq [F_{PWM}]$. If F_{BW} is selected such that, $F_{BW} = F_{PWM}$ then the external low pass filter should be a brick wall type filter. Brick-wall type analog filter are very difficult and expensive to build. So, for practical purpose, the external low pass filter, that has much smaller cut-off bandwidth than PWM bandwidth, should be used as shown in figure below[6].

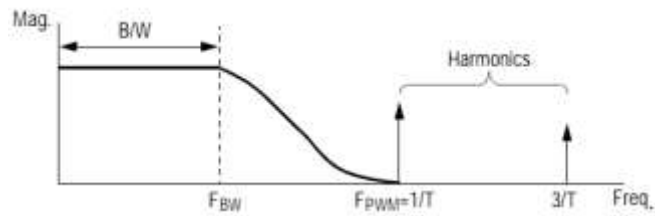


Figure 2: Bandwidth of Low Pass filter.

The 2nd order low-pass filter offers 40 dB/decade of stop band roll off, which is a two-fold improvement over the 1st order filter. The transfer function is given by the equation.

$$\frac{V_{out}(s)}{V_{in}(s)} = \frac{\omega_n^2}{s^2 + 2\zeta\omega_n s + \omega_n^2}$$

Where ω_n is the undamped natural frequency in units of (rad/s) and ζ is the non-dimensional damping ratio. It is straightforward to show that the filter bandwidth is BW [7].

$$BW = \omega_n \left[(1 - 2\zeta^2) + \sqrt{4\zeta^4 - 4\zeta^2 + 2} \right]^{1/2}$$

MODELING AND SIMULATION

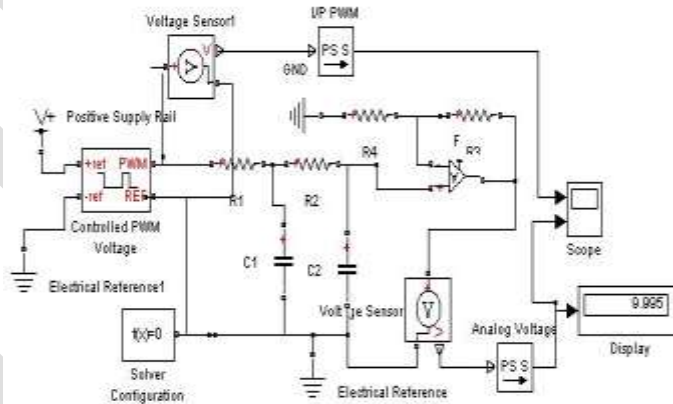
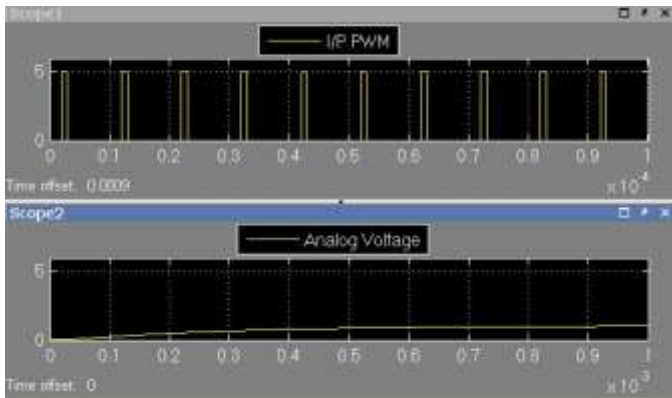


Figure 3: Simulation of DAC.

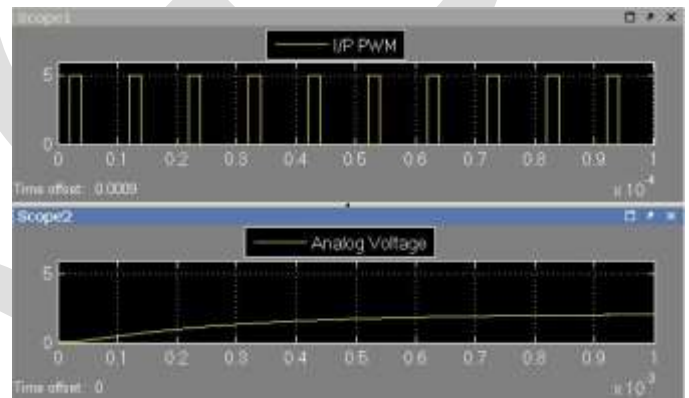
RESULTS:-

Sr. no	% Duty Cycle	Analog Voltage V
1	10	1.023
2	20	2.046
3	30	3.068
4	40	4.091
5	50	5.113
6	60	6.135
7	70	7.157
8	80	8.178
9	90	9.199
10	100	9.995

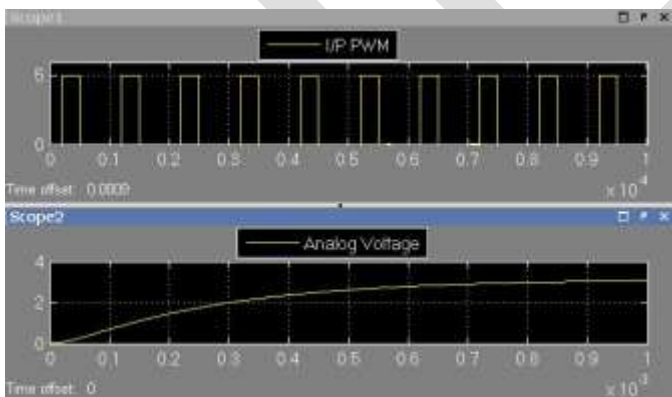
Wave forms for each % Duty Cycle



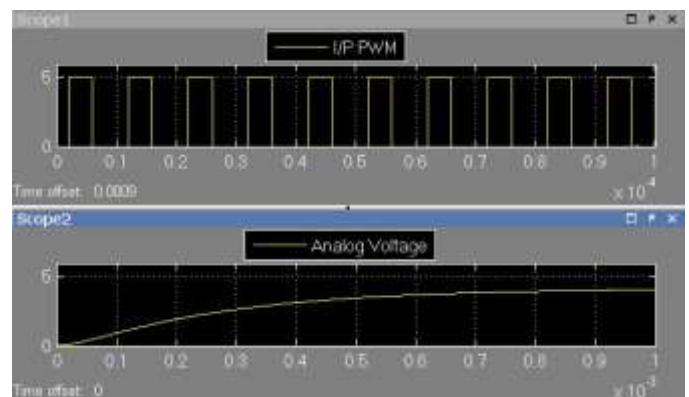
Duty Cycle =10 %, analog voltage 1.023 V.



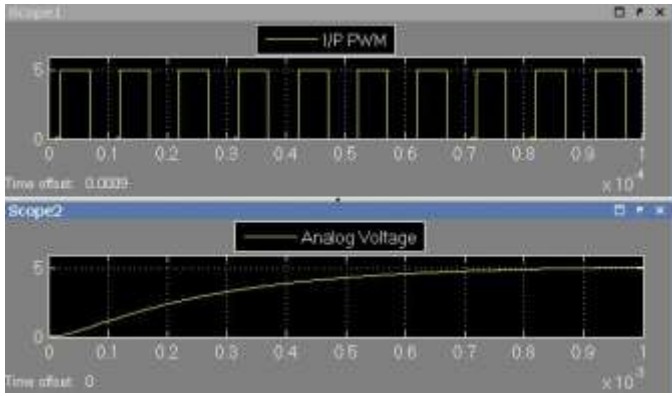
Duty Cycle =20 %, analog voltage 2.046 V.



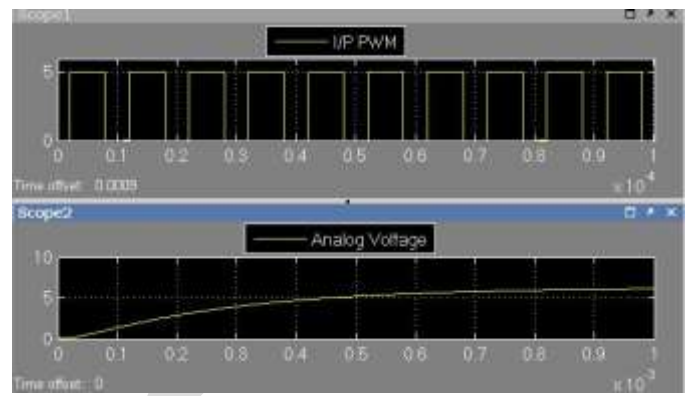
Duty Cycle =30 %, analog voltage 3.068 V.



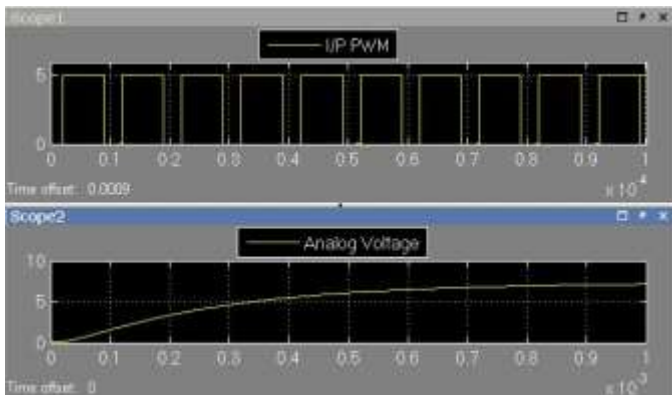
Duty Cycle =40 %, analog voltage 4.091 V



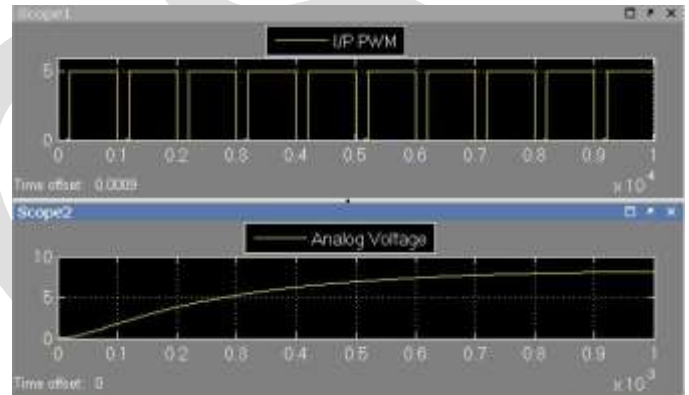
Duty Cycle =50 % , analog voltage 5.113 V.



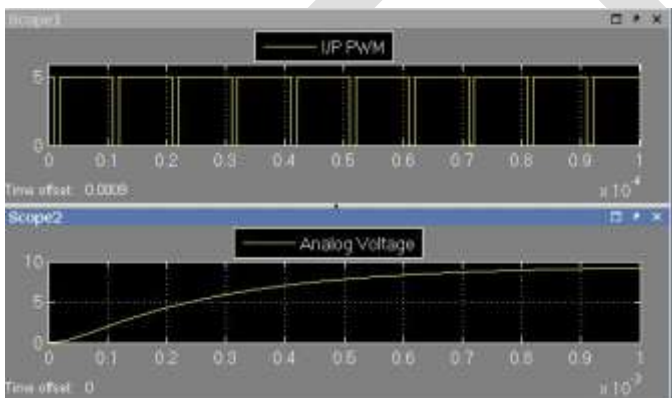
Duty Cycle =60 % , analog voltage 6.135 V.



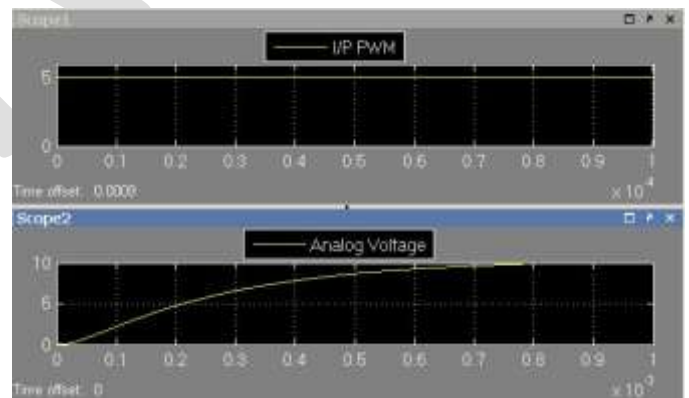
Duty Cycle =70 % , analog voltage 7.157 V.



Duty Cycle =80 % , analog voltage 8.178 V.



Duty Cycle =90 % , analog voltage 9.119 V.



Duty Cycle =100 % , analog voltage 9.995 V.

MATERIALS

The simulation model is developed under Matlab 7.0 With Dell XPS m1210 machine core 2 duo processor and 1 GB Ram on windows 7 platforms. Actual circuit is built with PIC18f4550 microcontroller having high speed PWM facility. Optoisolator PC817 is used for PLC and Module isolation. Ladder program written for Mitsubishi FX-2N PLC used with Gx Developer.

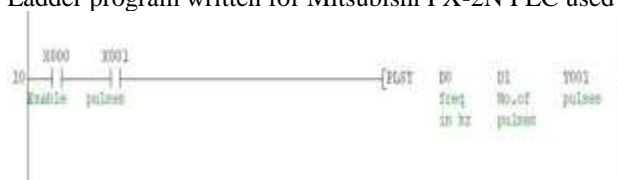


Figure 4: Ladder to generate frequency signal.

REFERENCES:

- [1] Cannillo, F. ; Imec, Leuven, Belgium ; Prefasi, E. ; Hernandez, L. ; Pun, E. "1.4V 13 μ W 83dB DR CT- $\Sigma\Delta$ modulator with Dual-Slope quantizer and PWM DAC for biopotential signal acquisition" ESSCIRC (ESSCIRC), 2011ESSCIRC (ESSCIRC), 2011 12-16 Sept. 2011.PP 267 – 270.
- [2] Della Colletta, G. ; Grupo de Microeletronica, Univ. Fed. de Eng. de Itajuba-UNIFEI, Itajuba, Brazil ; Ferreira, L.H.C. ; Pimenta, T.C. "A low power Successive Approximation A/D converter based on PWM technique" Circuits and Systems (LASCAS), 2012 IEEE Third Latin American Symposium on Feb. 29 2012-March 2 2012. PP 1 – 4.
- [3] Wright, P.S. ; Nat. Phys. Lab., Teddington, UK ; Pickering, J.R. "An AC voltage standard based on a PWM DAC" Instrumentation and Measurement, IEEE Transactions on (Volume:48 , Issue: 2) PP 457 – 461.
- [4] Chun Wei Lin ; Department of Electronic Engineering, National Yunlin University of Science & Technology, 64002, Taiwan ; Sheng Feng Lin "A BIST scheme for testing DAC" Electrical Engineering/Electronics, Computer, Telecommunications and Information Technology (ECTI-CON), 2012 9th International Conference on 16-18 May 2012, pages 1-4.
- [5] Wang Yan-wei ; Inst. of Wood Ind., Chinese Acad. of Forestry, Beijing, China ; Cheng Fang ; Zhou Yu-cheng ; Xu Jia-he "Analysis of double-T filter used for PWM circuit to D/A converter" Control and Decision Conference (CCDC), 2012 on 23-25 May 2012 pages 2752 – 2756.
- [6] Andy Britton "Digital Filters for Analogue Engineers" June 2010.
- [7] Digital to Analog Converter by Douglas A. Mercer ('77) Fellow Analog Devices Inc. Wilmington, MA USA (doug.mercer@analog.com)RPI IEEE Student Chapter October22, 2008.
- [8] D/A Conversion Using PWM and R-2R Ladders to Generate Sine and DTMF Waveforms Authors: Rob Stein and John Day Microchip Technology Inc.
- [9] Using PWM Output as a Digital-to-Analog Converter on a TMS320C240 DSP application note.
- [10] AVR131: Using the AVR's High-speed PWM avr application note.
- [11] Chwan-Hwa Wu, Senior Member, IEEE, J. David Irwin, Fellow, IEEE, and Fa Foster Dai, Senior Member, IEEE "Enabling Multimedia Applications for Factory Automation" IEEE TRANSACTIONS ON INDUSTRIAL ELECTRONICS, VOL. 48, NO. 5, OCTOBER 2001.
- [12] Songchar Jiang "Wireless Communications and a Priority Access Protocol for Multiple Mobile Terminals in Factory Automation" IEEE TRANSACTIONS ON ROBOTICS AND AUTOMATION, VOL. 14, NO. 1, FEBRUARY 1998.
- [13] Adnan Salihbegovic , Vlatko Marinković , Zoran Cico , Elvedin Karavdić b, Nina Delic ETF Sarajevo, Bosnia and Herzegovina b Bosna-S Oil Services Company, Bosnia and Herzegovina "Web based multilayered distributed SCADA/HMI system in refinery application" Computer Standards & Interfaces 31 (2009) 599–612.

AN EFFICIENT TECHNIQUE FOR THE REMOVAL OF RANDOM VALUED IMPULSE NOISE IN DIGITAL IMAGES

Aswathy Mohan T C, Prof Radhakrishnan B Prof BijiKumar R

P.G Scholar, Dept of CSE, BMCE, Kollam, Kerala, India

aswathymohantc@gmail.com,8281925024

Abstract— Digital image processing is important in many areas. Noise removal in digital images is important in many fields. In this paper we propose an efficient method for the removal of random valued impulse noise. Here using a detection process and a filtering process. Detection process detects the noisy pixels by using the absolute difference and median filter for filtering.

Keywords — Fixed value Impulse Noise, Random Value Impulse Noise, Peak Signal to Noise Ratio, Threshold, Median Filter Mean Square Error, Noise Detector

1. INTRODUCTION

Digital image processing has important in many areas such as digital telecommunication, remote sensing, robotics, graphic printing, and medical imaging, defense and security applications[1]. During the transmission and acquisition, images are corrupted by the different type of noise. Because of the noise, quality of image is reduced and other features like edge sharpness and pattern recognition are also badly affected. There may be different types of noise like Gaussian type noise, impulse type noise, shot noise. The impulse noise that affects the contents of the image[2]. Impulse noise is normally produced as a result of various reasons, including electromagnetic interference, errors and scratches on recording disks, and erroneous synchronization in digital recording and communication equipment. It also occurs during image acquisition, transmission due to malfunctioning of pixel elements in the camera sensors, faulty memory locations, and timing errors in analog-to-digital conversion and bit errors during transmission.

Noise may be modeled as impulse noise or salt and pepper noise. The pixels corrupted by any of the fixed valued impulse noise (0 or 255). The corrupted pixels take either 0(black) or 255 (white) with equal probability distribution. For images corrupted with impulse noise, the noisy image 'u⁰' is related to the original image 'u' by

$$u^0(i, j) = \begin{cases} n(i, j), & \text{with probability } p \\ u(i, j), & \text{with probability } (1 - p) \end{cases} \quad (1)$$

where n(i,j) is the noisy pixels with probability p. For noise free image, p=0.

Impulse noise is characterized by replacing a portion of an image pixel with noise values, leaving the remainder unchanged. An important characteristic of this type of noise is that only part of the pixels are corrupted and the rest are noise free. The impulse noise has generally two types: fixed value impulse noise[3] and random value impulse noise. The fixed value impulse noise is also known as salt and pepper noise which can be either 0 or 255 (0 for black and 255 for white). It is generally reflected by pixels having minimum and value in gray scale image. The random value impulse noise is random in nature can have any value between 0 and 255 and it is very difficult to remove this noise. To remove the effect of noise, we have several algorithms but removal of noise and restoration of original image causes blurring the edges of image. Impulse noise causes random black and white dots on the image so impulse noise reduction is very important phenomena of image processing. The basic idea of image de-noising has two parts:

1. Detection
2. Filtering

Detection of noise determines that the image is corrupted by noise or not, and noise removal part remove the noise from the image while preserving the other important detail of image. Filters are better option to remove the noise from the image because their implementation is very easy. The filters can be divided in two types: linear filter and non-linear filter. Linear filters are like average filter or called averaging low pass filter. But linear filter tends to blur edges and other details of image, which may reduce the accuracy of output[2]. On the other hand non-linear type filter like median filter has better results than linear filter because median filter remove the impulse noise without edge blurring[1]. The standard median filter[3] mostly used because of its good performance and preservation of image details. A median filter is an example of a non-linear filter and it is very good at preserving image detail.

The following three steps are used to calculate median:

1. Process every pixel in the image one by one.
2. Select the size of filtering window and sort the all pixels of window in order based upon their intensities.
3. Replace the central pixel with the median value of sorted pixels.

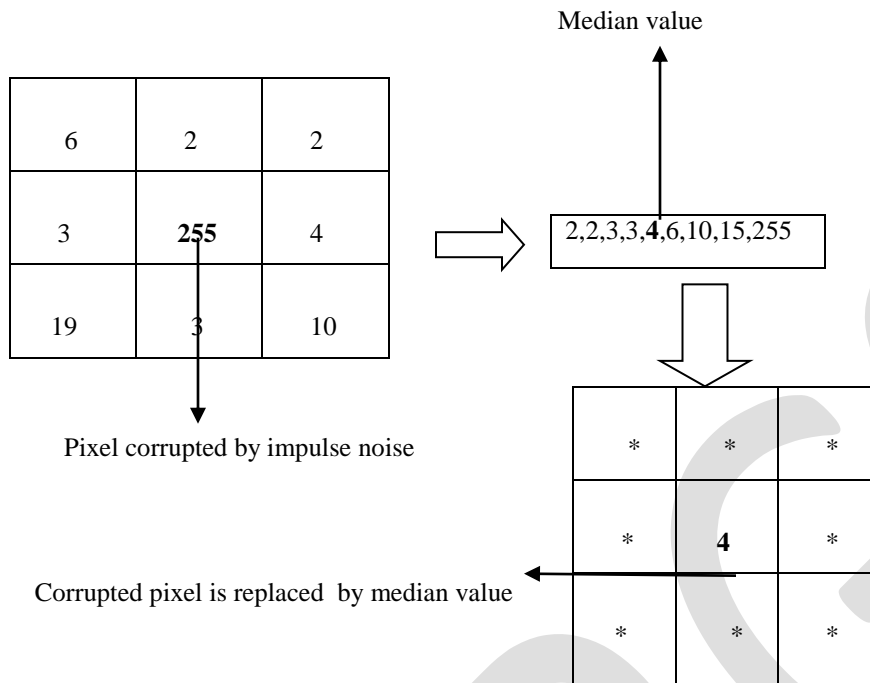


Fig.1.Evaluation of Standard Median Filter

The center value is taken for odd number of pixels and for even number of pixels calculates the mean of center pixels. The performance of median filter also depends on the size of window of filter. Smaller window preserve the details but it will cause the reduction in noise suppression. Larger window has great noise reduction capability but image details (edges, corners, fine lines) preservation is limited. With the improvement in the standard median filters, there were so many filters has designed like weighted median filter[4], centre weighted median filter[5] , adaptive median filter[6], rank order median filter[7] . In SDROM [8] method, for removing IN the nature of the filtering operation is conditioned on a state variable defined as the output of a classifier that operates on the differences between the input pixel and the remaining rank-ordered pixels in a sliding window. Different median filters uses different sorting algorithm [2] like merge sort, quick sort, heap sort to sort the elements in the window. Whether the pixel is noisy or noiseless can be identified in the detection phase, so that only noisy pixel will be replaced by the median value and noiseless pixel will be unaffected. This technique reduce the processing time and also improve the quality of image.

2.PROPOSED METHOD

The proposed methodology is divided into 2 phases. In the first phase, a 9x9 window which includes the center pixel and its neighboring pixels .ie, total 81 elements is considered. Then the absolute difference in the intensity of the center pixel and each neighbouring pixel is calculated

$$\text{ie, AbsoluteDifference(AD)} = |I_{\text{center pixel}} - I_{\text{neighboring pixel}}| \quad (2)$$

Then mean of the five smallest AbsoluteDifference values are taken

$$\text{ie, Mean} = \frac{1}{5} \sum_1^5 AD \quad (3)$$

If the Mean is greater than the threshold value, the tested pixel is considered as noisy and suppressed by using Standard Median Filter.

The proposed architecture is given below,

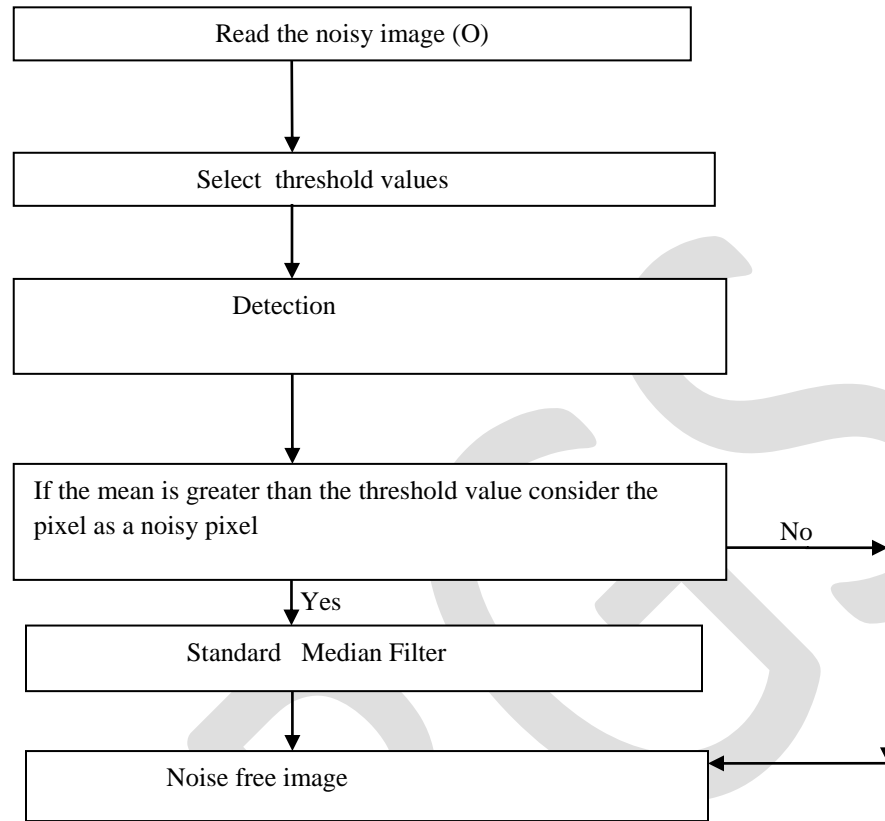


Fig.2. Flow chart of proposed method

A. Selection of Threshold

The threshold values used must be selected based on the previous knowledge or experimental results of different digital images and is inversely proportional to noise density. Three different threshold values are used to get better results[15].

B. Evaluation Metrics

Our main aim is to obtain an output image that is close to the original image. This can be done by comparing the Peak Signal to Noise Ratio (PSNR) values of both the output image and the original image. To measure the quality of restored image, Mean square error (MSE) and peak signal-to-noise ratio (PSNR) quality measure is used.

1. Mean square error (MSE)

The mean square error or MSE[2] of an estimator is one of many ways to quantify the difference between values implied by an estimator and the true values of the quantity being estimated. The MSE of the restored image is given by

$$MSE = \frac{1}{mn} \sum_{i_1=1}^m \sum_{i_2=1}^n |u(i_1, i_2) - I(i_1, i_2)|^2 \quad (4)$$

2. Peak Signal to Noise Ratio (PSNR)

The Peak Signal-to-Noise Ratio (PSNR) is an important metric to measure the objective dissimilarity of the filtered output from the original uncorrupted image[15].

$$PSNR = 10 \log_{10} \frac{(255)^2}{MSE} \text{ (dB)} \quad (5)$$

C.Experimental results



Results of different methods included in comparison for test image Lena with 80% of random-valued impulse noise. (a)Original image (b) Gray scale image (c) Noisy Image (d) WMF(e) CWMF(f) AMF(g) ROMF (h) SDRM (i) PA

D.Tabulation

In order to analyze the various de-noising methods quantitatively, TABLE 1 shows the Peak Signal-to-Noise Ratio (PSNR) of the various de-noising methods. PSNR does not always reflect the actual human perception of image quality because it is based on the log ratio of the signal to noise. TABLE 1 shows the comparison of PSNR values for restored image of Lena image affected by impulse noise with different noise ratios for different de-noising methods.

Table 1
 Comparison of PSNR values for restored image of Lena image affected by impulse noise with different noise ratios for different de-noising methods.

Noise Ratio	Peak signal to noise ratio					
	WMF	CWMF	AMF	ROMF	SDROM	PA
10%	31.9535	28.7013	30.3484	30.3565	29.9640	31.5089
20%	27.0922	26.4133	25.8988	27.2061	27.0950	28.0955
30%	23.3156	22.8368	22.3629	22.9127	23.8967	25.5397
40%	19.3500	19.6114	19.0939	19.9864	20.8678	22.7452
50%	16.9189	17.1028	16.8717	17.3967	18.2817	20.5162
60%	15.2140	14.9498	14.9014	15.3538	16.0753	19.2017
70%	13.6335	13.3965	13.4848	13.8791	14.2011	17.7907
80%	12.4300	12.0779	12.3467	12.8804	13.0436	16.7176

The de-noising method consists of both detection and filtering schemes. In TABLE 1, the filtering method used is the standard median filter and the detection schemes used are WMF (Weighted Median Filter), CWMF (Center Weighted Median Filter), Adaptive Median Filter(AMF), ROMF (Rank Ordered Median Filter), and SDROM (Signal Dependent Rank Ordered Median Filter) and the PA (Proposed Algorithm) respectively. The restored images using these de-noising methods for the Lena image with different impulse noise ratios 10%, 30%, 50%, 70% and 80% are analyzed. The highest PSNR value among the PSNR values of denoised Lena image obtained for different de-noising methods is highlighted by bold digits. The restored images using these de-noising methods for the Lena image with different impulse noise ratios 10%, 30%, 50%, 70% and 80% are analyzed.

3.CONCLUSION

Several methods have been proposed for restoration of images contaminated by random valued impulse noise, which includes the detection and filtering which are done separately on the images. Some existing methods provide good results for low noise density images whereas only a few provide good results for high noise rates. These methods are more time consuming and may result in execution complexity. Suppose if the original image itself contains more number of noise added pixels, then the existing filters fail to distinguish the original pixel from the corrupted one. The main advantage of the proposed method is that it effectively removes Random Value Impulse Noise from images and it gives better image compared to other filters in case of high noise density.

REFERENCES:

- [1] R. C. Gonzalez and R. E. Woods, Digital Image Processing. Englewood Cliffs,NJ: Prentice-Hall, 2002
- [2] Vikas Gupta, Madhu shandilya “Image De-noising by Dual Threshold Median Filtering for Random Valued Impulse Noise” Nirma University International Conference On Engineering,nuicone-2012,06-08 DECEMBER 2012
- [3] Zhu Youlian, Huang Cheng, “An Improved Median Filtering Algorithm Combined with Average Filtering”, IEEE, 2011 Third International Conference on Measuring Technology and Mechatronics Automation, 6-7 Jan. 2011, pp.420-423
- [4] WANG Chang-you, YANG Fu-ping, GONG Hui, “A new kind of adaptive weighted median filter algorithm”, 2010 I.J.C on Computer Application and System Modeling (ICASM 2010).

- [5] T.-C. Lin, P.-T. Yu, , “A new adaptive center weighted median filter for suppressing impulsive noise in images”, *Information Sciences* 177 (2007)1073–1087
- [6] H. Hwang and R. A. “Adaptive Median Filters:New Algorithms and Results”Haddad *IEEE Transactions on image processing*, Vol. 4, No. 4, April 1995
- [7] James C. Church, Yixin Chen, and Stephen V. Rice “A Spatial Median Filter for Noise Removal in Digital Images”,*Southeast-con*,2008
- [8] Abreu E, Lightstone M, Mitra SK, Arakawa K. “A new efficient approach for the removal of impulse noise from highly corrupted images”., *IEEE Trans ImageProcess* 1996;5(6):1012–25.
- [9] Eng HL, Ma KK. “Noise adaptive soft-switching median filter”. *IEEE Trans Image Process* 2001;10(2):242–51.
- [10] Paul ME, Bruce KC. “Language algorithms for digital signal processing”. Prentice Hall; 1991
- [11] Chen T, Wu HR. “Adaptive impulse detection using center-weighted median filters”. *IEEE Signal Process Lett* 2001;8(1):1–3.
- [12] Wang Z, Zhang D. “Progressive switching median filter for the removal of impulse noise from highly corrupted images”. *IEEE Trans Circuits Syst* 1999;46(1):78–80.
- [13] Kuykin D, Khryashchev V, Apalkov I.” Modified progressive switched median filter for image enhancement. In: *Proc of I.C on computer graphics and vision*”. 2009. p. 303–4.
- [14] Sun T, Neuvo Y. “Detail-preserving median based filters in image processing”.*Pattern Recognit Lett* 1994;15(4):341–7.
- [15] Ilke Turkmen,”A new method to remove random valued impulse noise”. *Int.J.Electron.*2013

WHITE BLOOD CELL NUCLEUS AND CYTOPLASM EXTRACTION USING MATHEMATICAL OPERATIONS

Alfiya Jabbar

PG Scholar, Dept of CSE, BMCE, Kollam, Kerala, India

alfiya.jbr@gmail.com

Abstract- An automatic image segmentation system can make the inspection procedure of blood smear much faster. The most important step of such system is the White Blood Cell segmentation. In this mainly focus on nucleus segmentation thereby classifying whether it is grouped or single one. Then extract the cytoplasm of the White Blood Cells. Inorder to segment the nucleus from the whole body by using a combination of automatic contrast stretching supported by image arithmetic operation and minimum filter.

Index Terms- Image segmentation, Mathematical operation, White Blood Cells, Leukemia diagnosis, Contrast stretching, Minimum filter, Morphological operation.

1. INTRODUCTION

Blood is composed of Red blood cells, White blood cells and platelets. As White blood cell count is more compared to Red blood cells then it is the indication of Leukemia. There are different types of diseases related to blood system and the instruments which are used in the diagnosis of diseases are very costly, thus identification of white blood cells count that provides useful information to doctors in diagnosis different kind of disease in the blood system. Generally white blood cells are called leukocytes which protect against the foreign material and the infectious diseases and red blood cells are called erythrocytes which deliver oxygen to body tissues.

WBC is mainly classified as granulocytes and agranulocytes. There are three types of granulocytes namely neutrophils, eosinophils, and basophils. As seen under a microscope, the granules in these white blood cells are apparent when stained. There are two types of agranulocytes, also known as nongranular leukocytes: lymphocytes and monocytes. These white blood cells appear to have no obvious granules. Agranulocytes typically have a large nucleus due to the lack of noticeable cytoplasmic granules. White blood cells are produced by bone marrow within bone. Some white blood cells mature in the lymph nodes, spleen, or thymus gland. The life span of mature leukocytes ranges from about a few hours to several days. Blood cell production is often regulated by body structures such as the lymph nodes, spleen, liver, and kidneys. During times of infection or injury, more white blood cells are produced and are present in the blood. A blood test known as a WBC or white blood cell count is used to measure the number of white blood cells in the blood. Normally, there are between 4,300-10,800 white blood cells present per microliter of blood. A low WBC count may be due to disease, radiation exposure, or bone marrow deficiency. A high WBC count may indicate the presence of an infectious or inflammatory disease, anemia, leukemia, stress, or tissue damage.

When hematologists conduct blood tests, these experts uses two most common types of analyzing tools for diagnosing and screening blood smears: Complete Blood Count (CBC), Differential Blood Count (DBC). CBC machine uses an instrument called a "Cytometer" which is useful in the blood lab for counting the blood cells and components for each sample taken from patients.

Differential blood counting machines operate by sampling human blood and drawing a small amount of blood through narrow tubing. Inside this tubing there are sensors that count the number of each blood cell type, which are going through the tube. The drawbacks of this process are that the DBC sensors need occasional calibration, the maintenance cost is high, and the DBC might misclassify some cells.

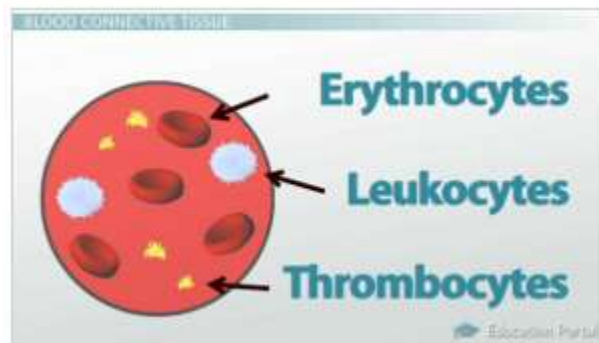


Fig.1 Blood Components

In this paper, first we make the copy of input image so as the first copy is contrast stretched and second copy is histogram equalized. Then through arithmetic operations nucleus are extracted. Then check whether the extracted nucleus is grouped or single. Finally cytoplasm are extracted from each nucleus. The grouped and single nucleus are identified depending upon the area.

2. RESEARCH METHODOLOGY

In this paper for segmentation of white blood cell nucleus mathematical morphing and some mathematical operations have been used.

A. *Mathematical operation*

In this section, we focus on the arithmetic operation on the image like addition and subtraction for highlighting the white blood cell components, removing the components which are not the white blood cells and brightening all the components in the image except the cell nucleus.

The addition of two images is performed straightforwardly in a single pass. The output pixel values are given by:

$$Q(I,j) = p_1(I,j) + p_2(I,j) \quad (1)$$

Or if it is simply desired to add a constant value C to a single image then:

$$Q(I,j) = p_1(I,j) + C \quad (2)$$

If the pixel values in the input images are actually vectors rather than the scalar values then the individual components are simply added separately to produce the output value. Addition is when you add the corresponding color channels of the images to each other. Each color component is a number between 0 and 255, so if the sum of the two colors becomes higher than 255, it has to be truncated to 255 again, by taking the minimum of the result and 255. Copy paste this into the arithmetic loop and run it to see the result of the sum the two photos. Subtraction works in a similar way, but now you have to truncate negative results to 0.

B. *Mathematical morphing*

In this section, we focus on image morphing which remove the unwanted components like platelets from the image. In some research mathematical morphing is used as the final step for smoothing the region of interest. Erosion, dilation, closing and opening are the basic operations. The opening and closing operations are derived from the erosion and dilation of morphing. Closing removes the small holes. Erosion will allow thicker lines to get skinny and detect the hole inside the letter “o”. Dilation is the dual operation of the erosion. Opening essentially removes the outer tiny “hairline” leaks.

3. PROPOSED METHOD

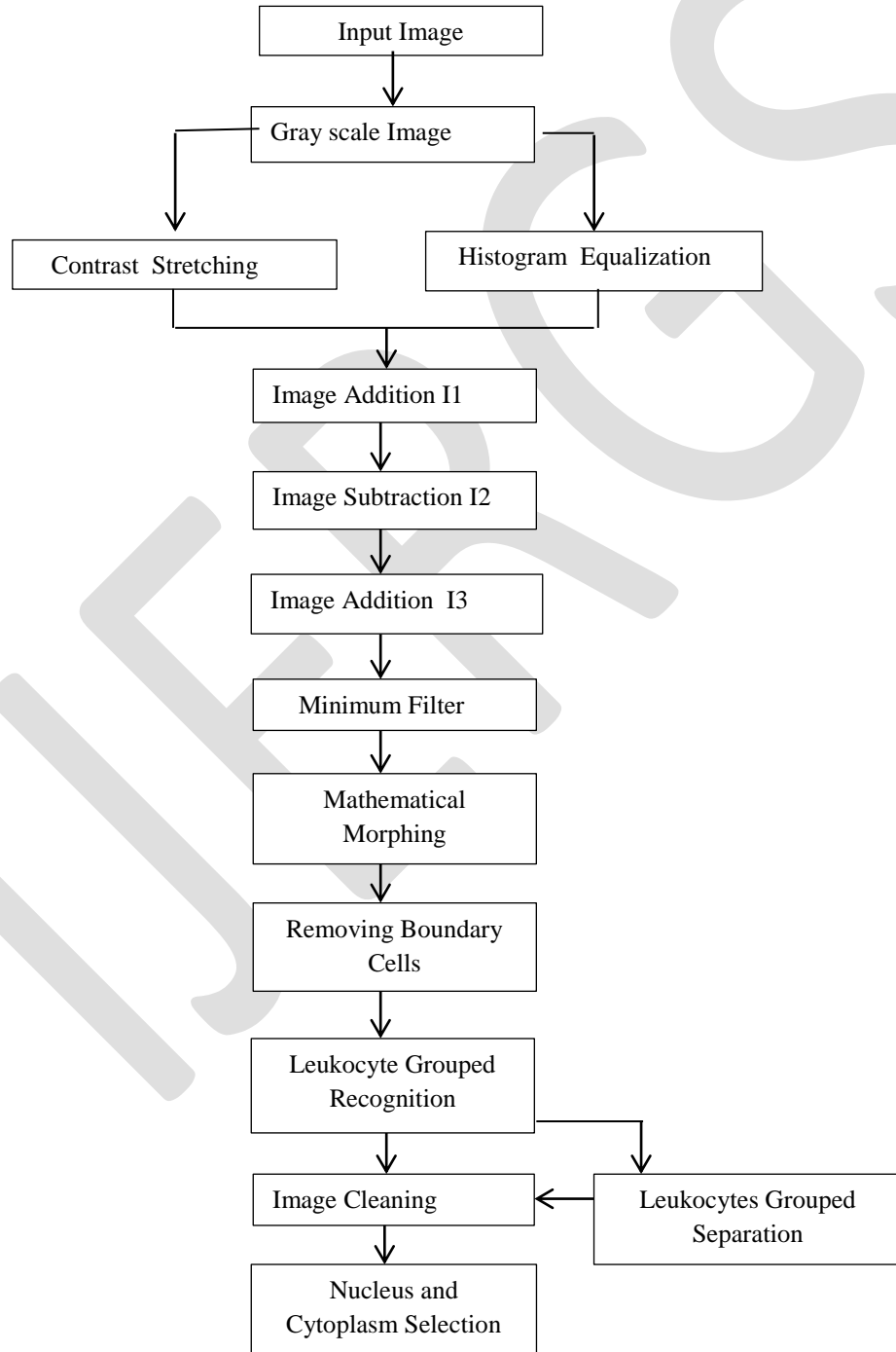


Fig.2 Proposed Method Schema

Firstly, all the images are converted into grayscale images, so that the nucleus part of the cell will be darker. The identification of white blood cell nucleus is based on the contrast stretching, histogram equalization and image arithmetic. After converting the original image into grayscale image, make two copies of the image. First image is contrast stretched and second image undergoes histogram equalization. Then addition operation is applied on these two copies referred as I1.

$$I1(I,j) = L(I,j)+H(I,j) \quad (3)$$

I1 is then subtracted from histogram equalized image to get R2.

$$I2(I,j) = I1(I,j)-H(I,j) \quad (4)$$

Then I1 and I2 are get added to get I3.

$$I3(I,j) = I1(I,j)+I2(I,j) \quad (5)$$

After applying mathematical operation we apply 3-by-3 minimum filter in order to reduce the noise present in the image I3. Then apply mathematical closing operation so that holes present in the segmented image will be filled. From the nucleus segmented image, remove the objects which are on the boundary of the image. After getting the leukocyte image, recognize whether the leukocytes are grouped or not. Then image cleaning is done. Thereby we can select the nucleus and cytoplasm from the image.

4. CONCLUSION

The prominent fact of automatic blood cell recognition and analysis is the ability to find all the nucleated cell in the image and remove all the remaining components. This paper introduces the automatic white blood cell localization by using mathematical operations and morphological operations for segmentation. In this research, we firstly apply mathematical operation for segmenting the white blood cells. Then minimum filter is applied to avoid the noise content in the image. Finally apply the morphological closing operation in order to fill the holes in the image. This research introduces a method for white blood cell nucleus and cytoplasm identification and segmentation as a first step towards a fully automated system for diagnosis of different kind of diseases and classification using peripheral blood microscopic image. White blood cell segmentation is the key procedure in the automatic leukemia diagnosis system.

REFERENCES:

1. P.S.Hiremath, Parashuram Bannigidad and Sai Greta, "Automated Identification and Classification of White Blood Cells (Leukocytes) in Digital Microscopic Images", IJCA Special Issue on "Recent Trends in Image Processing and Pattern Recognition" RTIPPR, pp. 59-63, 2010.
2. Anjali Gautam, H.S. Bhadauria, Annapurna Singh, "White Blood Nucleus Segmentation Using an Automated Thresholding and Mathematical Morphing".
3. S. Chinwaraphat, A. Sanpanich, C. Pintavirooj, M. Sangworasil, and P. Tosranon, "A Modified Fuzzy Clustering For White Blood Cell Segmentation", The 3rd International Symposium on Biomedical Engineering (ISBME), pp. 356-359, 2008.
4. Naveed Abbas and Dzulkipli Mohamad., "Automatic Color Nuclei Segmentation of Leukocytes for Acute Leukemia".
5. Hongmin Cai, Zhong Yang, Xinhua Cao. "A New Iterative Triclass Thresholding Technique in Image Segmentation".
6. Lorenzo Putzu, Cecilia Di Ruberto "White Blood Cells Identification and Classification from Leukemic Blood Image" IWBBIO, pp.99-106, 2013.
7. Stanislav Mirčić and Nikola Jorgovanović, Automatic Classification of Leukocytes, Journal Of Automatic Control, University Of Belgrade, Vol 16, pp. 29-32, 2006 ©.

8. Nipon Theera-Umpon, "Patch-Based White Blood Cell Nucleus Segmentation Using Fuzzy Clustering", ECTI Transactions on Electrical Engg., Electronics, and Communications Vol.3, No.1, pp. 15-19, February 2005.
9. Ms. Minal D. Joshi¹, Prof. A.H.Karode², Prof. S.R.Suralkar, "Detection Of Acute Leukemia Using White Blood Cells Segmentation Based On Blood Samples".
10. Juma Al-Muhairy, Yousef Al-Assai. "Automatic White Blood Cell Segmentation Based On Image Processing".
11. Leyza Baldo Dorini Rodrigo Minetto Neucimar Jeronimo Leite, "White blood cell segmentation using morphological operators and scale-space analysis".
12. Leyza Baldo Dorini, Rodrigo Minetto, and Neucimar Jeronimo Leite "Semiautomatic White Blood Cell Segmentation Based on Multiscale Analysis" IEEE Journal of Biomedical and Health Informatics, Vol. 17, No. 1, pp. 250-256, January 2013.

Relay Selection for Bidirectional Wireless Networks With Outdated CSI Using Weight Factor

Fathima A., Kiran Krishnan

PG Scholar, Department of ECE, CAARMEL Engineering College, Pathanamthitta, Kerala
Assistant Professor, Department of ECE, CAARMEL Engineering College, Pathanamthitta, Kerala

Email:fathimaa2015@gmail.com

Abstract: The Most researches on relay selection (RS) in bidirectional relay network typically assume perfect channel state information (CSI). However, outdated CSI, which is caused by the time-variation of channel, cannot be ignored in the practical system, and the performance of the conventional bidirectional RS scheme degrades greatly with outdated CSI. In this paper, to improve the performance of RS with outdated CSI, we propose a weighted bidirectional RS scheme, in which a deterministic weight factor decided by the correlation coefficient of outdated CSI, is introduced in the selection process. The outage probability bound of the weighted bidirectional RS is derived and verified, along with the asymptotic expression in high signal-to-noise ratio (SNR). Based on the analytical expressions, the optimal weight factor and the optimal power allocation scheme in minimizing the outage probability are obtained. Simulation results reveal that when the CSI is outdated, the diversity order reduces from full diversity to one. Furthermore, the weighted bidirectional RS scheme with the optimal weight factor yields a significant performance gain over the conventional bidirectional RS scheme, especially in high SNR.

Keywords: Relay selection, amplify-and-forward, outdated channel state information.

INTRODUCTION

In bidirectional relay communications two sources exchange information through the intermediate relays, and different transmission schemes of bidirectional relay have been proposed in [1], [2]. An amplify-and-forward (AF) based network coding scheme, named as analog network coding (ANC), was proposed in [2]. In that the exchange of information between two sources occupies two phases, and thus the spectral efficiency get improved [2]. Relay selection (RS) technique in bidirectional relay communications has been researched, due to its ability to achieve full diversity with only one relay [3]–[7]. Performing RS, the best relay is firstly selected before the subsequent data transmission, according to the predefined RS scheme. In [6], an optimal RS scheme in minimizing the average symbol error rate (SER) was proposed and analyzed, and the optimal power allocation scheme in minimizing the asymptotic SER was provided. The diversity order for various RS schemes of bidirectional RS was studied in [7], and it revealed that all the RS schemes can achieve full diversity when the channel state information (CSI) is perfect.

In this paper, to improve the performance of RS with outdated CSI, the weighted bidirectional RS scheme is proposed and analyzed in this paper. To compensate the performance loss caused by the outdated CSI, a novel weighted bidirectional RS scheme is proposed by introducing the weight factor in the selection process. The outage probability bound of the weighted bidirectional RS scheme with outdated CSI is derived and verified, along with the asymptotic expression in high signal-to-noise ratio (SNR). According to the analytical expressions, the optimal weight factor and the optimal power allocation scheme in minimizing the outage probability are also obtained. The expression of the optimal weight factor reveals that the factor is decided by the correlation coefficient of outdated CSI, the number of relays, and the channel variances. Simulation results reveal that once the CSI is outdated, the diversity order reduces from full diversity to one. Furthermore, the outage probability of the weighted bidirectional RS with the optimal weight factor can achieve the considerable performance gain over the conventional bidirectional RS, specifically in high SNR.

RELATED WORK

Most previous researches on RS in bidirectional relay network typically assume perfect CSI. In the conventional bidirectional RS scheme, the effect of correlation coefficients of outdated CSI has not been considered in the selection process. Outdated CSI, caused by the time-variation of channel, cannot be ignored in the practical system, and it makes the selected relay not the best for the data transmission. The impact of outdated CSI has been discussed in one-way relay and two-way relay. In [11], [12], the expressions of SER and outage probability for one-way AF RS were achieved, and the partial RS and opportunistic RS were both considered with

outdated CSI. The impact of outdated CSI on the one-way decode-and-forward (DF) RS was analyzed in [13]. In [14], the two-way network with one relay and multiple users was studied, and the effect of outdated CSI on user selection was researched. In [15], the performance of SER was analyzed in the bidirectional AF relay, when the CSI is outdated. Compared with the conventional RS scheme with outdated CSI, the proposed weighted RS scheme is revised by introducing the deterministic weight factor in the selection process. The outage probability bound of the weighted RS scheme with outdated CSI is derived and verified, along with the asymptotic expression in high signal-to-noise ratio (SNR).

SYSTEM MODEL

As presented in Fig. 1, the system investigated in this paper is a bidirectional AF relay network, in which two sources $S_j, j = 1, 2$, exchange information through N relays $R_i, i = 1, \dots, N$, and each communication node is equipped with a single half-duplex antenna. The transmit powers of each source and each relay are denoted by P_s and P_r , respectively. The direct link between the two sources does not exist due to the shadowing effect, and the channel coefficients between S_j and R_i are reciprocal, denoted by h_{ij} . All the channel coefficients follow independent complex-Gaussian distribution with zero mean and variance of σ_j^2

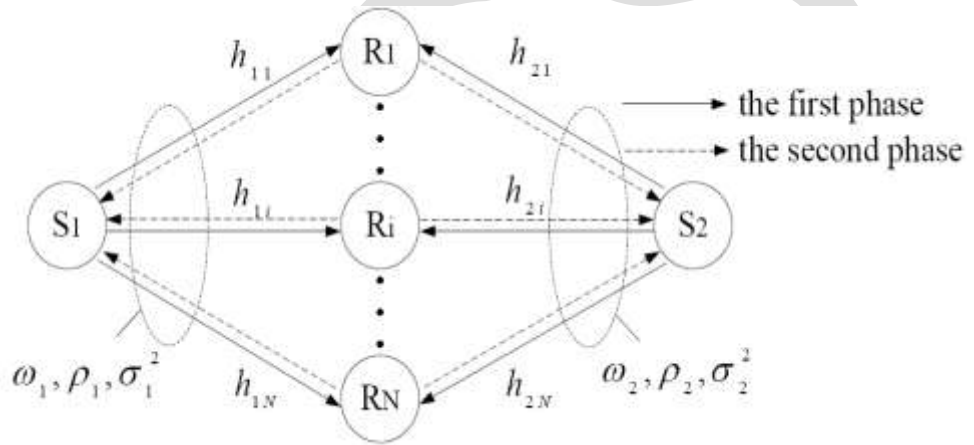


Fig 1: System model

A. Instantaneous Received SNR at the Sources

Considering the transmission via R_i , the data transmission process of bidirectional AF relay is divided into two phases when adopting the ANC. At the first phase, the sources simultaneously send their respective information to R_i . The received signal at R_i is expressed as $r_i = \sqrt{P_s}h_{1i}s_1 + \sqrt{P_s}h_{2i}s_2 + n_{ri}$, where s_j denotes the modulated symbols transmitted by S_j with the average power normalized, and n_{ri} is the additive white Gaussian noise (AWGN) at R_i , which has zero mean and variance of σ_n^2 . At the second phase, R_i amplifies the received signal and forwards it back to the sources. The signal generated by R_i is $t_i = \sqrt{P_r}\beta_i r_i$, where β_i is the variable-gain factor [12]. The received signal at S_j is $y_j = h_{t,ji}t_i + n_{sj}$, where n_{sj} is the AWGN at S_j . The instantaneous received signal-to-noise ratio (SNR) at S_j via R_i is

$$\gamma_{ji} = \frac{\psi_s \psi_r |h_{ji}|^2 |h_{\bar{j}i}|^2}{(\psi_s + \psi_r) |h_{ji}|^2 + \psi_s |h_{\bar{j}i}|^2 + 1}$$

where $\psi_s = P_s/\sigma_n^2, \psi_r = P_r/\sigma_n^2$

In high SNR, the expression can be further simplified, i.e.,

$$\gamma_{ji} \approx \frac{\psi_r |h_{ji}|^2 \psi_h |h_{\bar{j}i}|^2}{\psi_r |h_{ji}|^2 + \psi_h |h_{\bar{j}i}|^2}$$

where $\psi_h = \frac{\psi_s \psi_r}{(\psi_s + \psi_r)}$.

B. Relay Selection Schemes

The outage probability of bidirectional RS is defined as

$$P_{out}(R) = \Pr \left\{ \min \left[\frac{1}{2} \log_2 (1 + \gamma_{1k}), \frac{1}{2} \log_2 (1 + \gamma_{2k}) \right] < R \right\}$$

where k is the index of the selected relay, R is the target rate, and γ_{jk} is the received SNR at S_j via the selected relay R_k . The pre-log factor is 1/2, because the transmission from one source to the other occupies two phases. Due to the monotony of the log function, the outage probability is re-expressed as

$$P_{out}(R) = \Pr [\min (\gamma_{1k}, \gamma_{2k}) < 2^{2R} - 1].$$

Therefore, the optimal RS scheme of bidirectional relay in minimizing the outage probability is

$$k = \arg \max_{i=1, \dots, N} \min (\gamma_{1i}, \gamma_{2i})$$

where k is the index of the selected relay. The value of k is equivalent to

$$k = \arg \max_i \min \{ |h_{1i}|^2, |h_{2i}|^2 \}$$

Due to the time-variation of channel, h_{ji} gets outdated. Hence we replace value with \hat{h}_{ji} thus the equation of k becomes

$$k = \arg \max_i \min \{ |\hat{h}_{1i}|^2, |\hat{h}_{2i}|^2 \}$$

Now we are introducing weights to the equation, ω_1 and ω_2 . Then the above equation becomes

$$k = \arg \max_{i=1, \dots, N} \min \{ \omega_1 |\hat{h}_{1i}|^2, \omega_2 |\hat{h}_{2i}|^2 \}$$

Due to the symmetry among different relay links, the RS scheme is equivalent to

$$k = \arg \max_{i=1, \dots, N} \min \{ |\hat{h}_{1i}|^2, \omega |\hat{h}_{2i}|^2 \}$$

where $\omega \triangleq \omega_2 / \omega_1$ i.e., only the ratio of ω_2 and ω_1 has impact on the system performance.

Therefore, the conventional bidirectional RS scheme can be treated as the special case of the proposed weighted bidirectional RS scheme, when $\omega = 1$. Accordingly, in the following, we analyze the outage probability of the weighted bidirectional RS scheme, as a function of the weight factor ω . Then, the optimal weight factor ω_{opt} in minimizing the outage probability is obtained. The following results will reveal that the weighted bidirectional RS with the optimal weight factor ω_{opt} will have lower outage probability than the conventional bidirectional RS, i.e., $\omega = 1$.

SIMULATION RESULTS

In this section, Monte-Carlo simulations are provided to validate the preceding analysis and to highlight the performance of the weighted bidirectional RS with outdated CSI. Without loss of generality, we assume the target rate $R = 0.1$ bps/Hz, the total average SNR is denoted by $\psi = 2\psi_s + \psi_r$. In Fig. 2, the outage probabilities of the conventional bidirectional RS, i.e., $\omega = 1$, and the weighted bidirectional RS, i.e., $\omega = \omega_{opt}$, versus the average SNR are studied. In Fig. 2, the impact of outdated CSI is studied when the number of relays $N = 4$ and the system structure is symmetric, i.e., the channel variances and the Doppler spreads $fd_1T_d = fd_2T_d = fdT_d$. Due to the previous analysis, the optimal weight factor $\omega_{opt} = 1$, and thus the conventional bidirectional RS is equivalent to the optimal weighted bidirectional RS. Moreover, different lines are provided under different $f_d T_d$ means CSI is severely outdated,

whereas smaller $f_d T_d$ means CSI is slightly outdated, and especially $f_d T_d = 0$ means CSI is perfect. In Fig. 3, it is shown when there is no relay used for transfer of packets between two nodes in a bidirectional wireless network. The direct bidirectional data transfer between the nodes. In this case due to noise and other impairments in the channel connecting two nodes, the data quality will degrade and will contain a lot of errors. Since the network is bidirectional the symbol from one node will be mixed with symbol from other node. But in case of using a number of relays we can select the best one that provides maximum efficiency to the bidirectional networks.

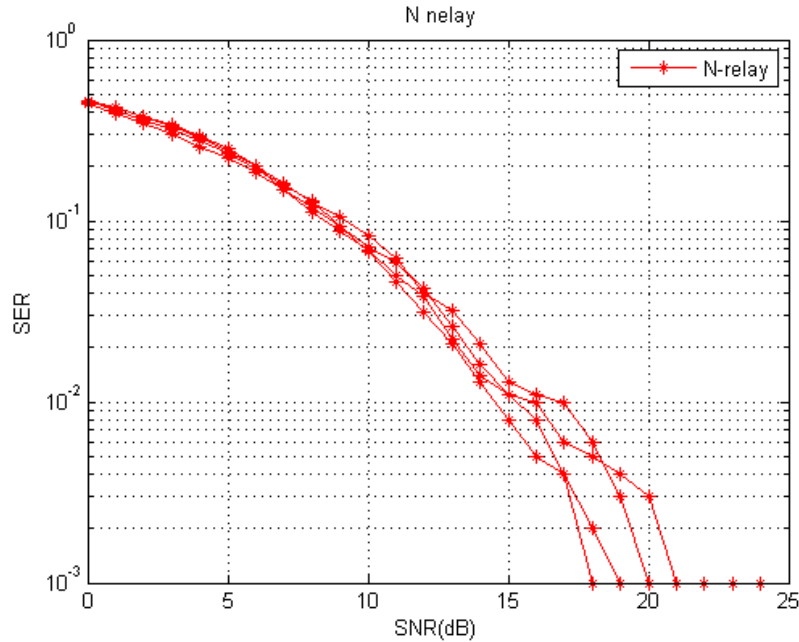


Fig 2: The outage probability with outdated CSI, when N = 4

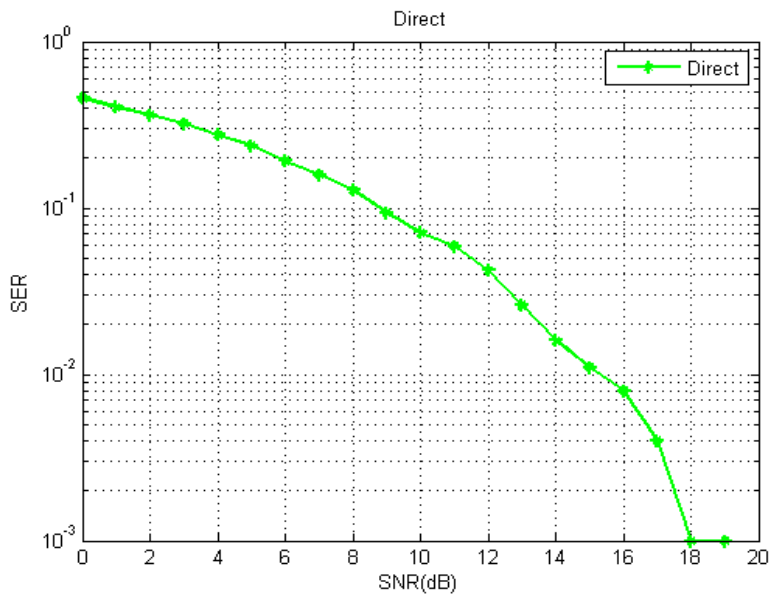


Fig 3: The outage probability with outdated CSI in direct data transfer

In Fig. 4., the best relay for communication is selected based on the weight factors. According to the analytical expressions, the optimal weight factor and the optimal power allocation scheme in minimizing the outage probability are also obtained. The expression of the optimal weight factor reveals that the factor is decided by the correlation coefficient of outdated CSI, the number of relays, and

the channel variances. Therefore, the conventional bidirectional RS scheme can be treated as the special case of the proposed weighted bidirectional RS scheme, when $\omega = 1$. Accordingly, in the following, we analyze the outage probability of the weighted bidirectional RS scheme, as a function of the weight factor. Then, the optimal weight factor ω_{opt} in minimizing the outage probability is obtained. The following results will reveal that the weighted bidirectional RS with the optimal weight factor ω_{opt} will has lower outage probability than the conventional bidirectional RS, i.e., $\omega = 1$.

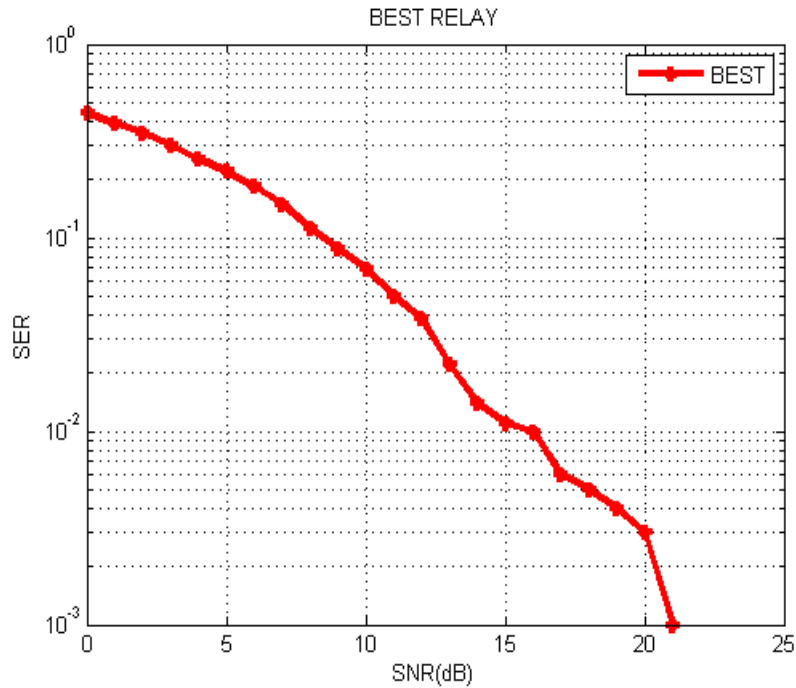


Fig 4: The outage probability with outdated CSI for the best relay among the 4.

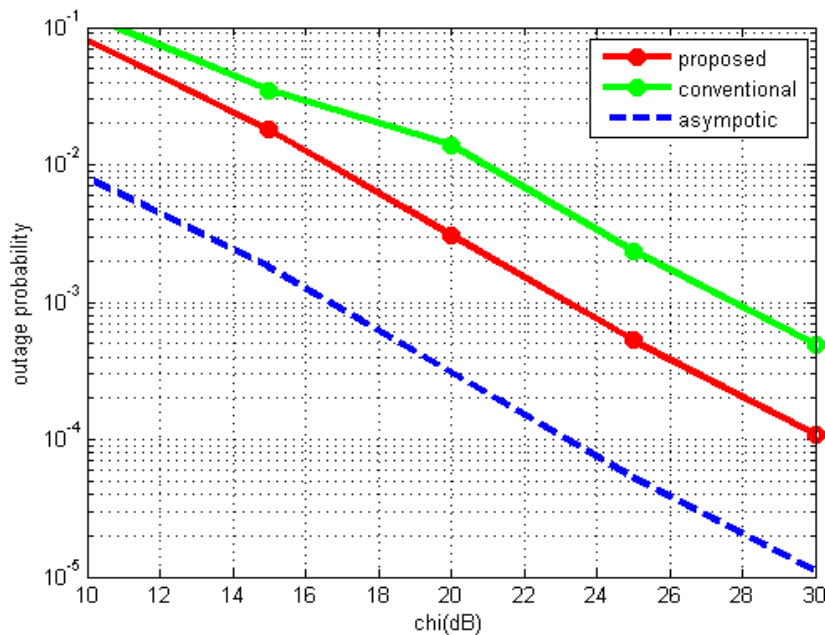


Fig 5: Outage probability with outdated CSI, when the doppler spread are different

In Fig. 5, the graph shows the outage probability with doppler spread for proposed scheme and conventional scheme. As doppler spread increases the outage probability decreases. This is because the CSI value depends on the value of doppler spread. When doppler spread is high that means the CSI is severely outdated, whereas smaller doppler spread means CSI is slightly outdated, and especially doppler spread is zero means CSI is perfect. However, increasing the number of relays N can still lower the outage probability, because the coding gain, i.e., the shift of the curve in SNR gets improved. From the figure we can see that the weighted bidirectional RS yields the significant performance gain over the conventional bidirectional RS. Specifically, the bidirectional RS are further compared when the number of relays $N=4$. The situation of different channel variances when the Doppler spreads are same. The figure verifies the analytical expressions when the system structure is asymmetric. The figure shows that even if doppler spreads are equal, $\omega = 1$ is still not the optimal due to the difference of channel variances. The figure also reveals that although the weighted bidirectional RS cannot improve the diversity order, it can improve the coding gain, and the gain grows larger when increasing the number of relays N or increasing the average SNR.

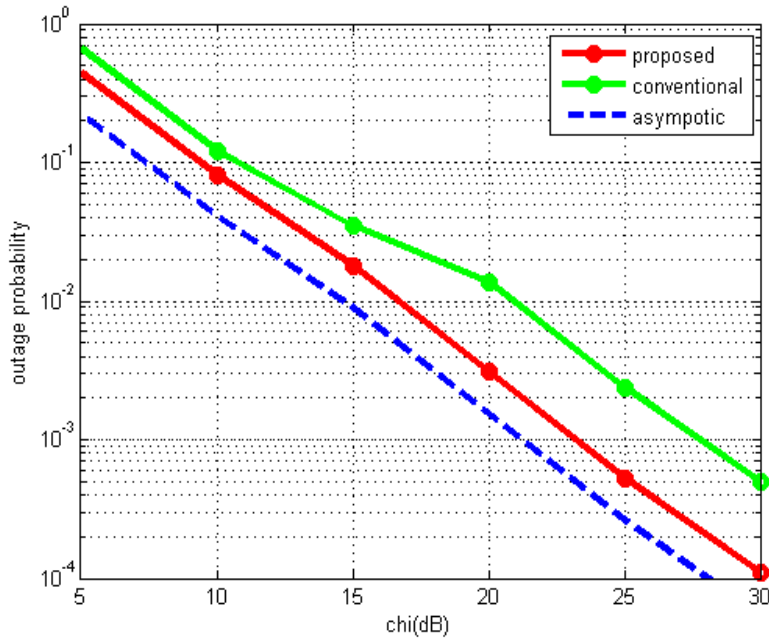


Fig 6: Outage probability with outdated CSI, when the channel variances are different

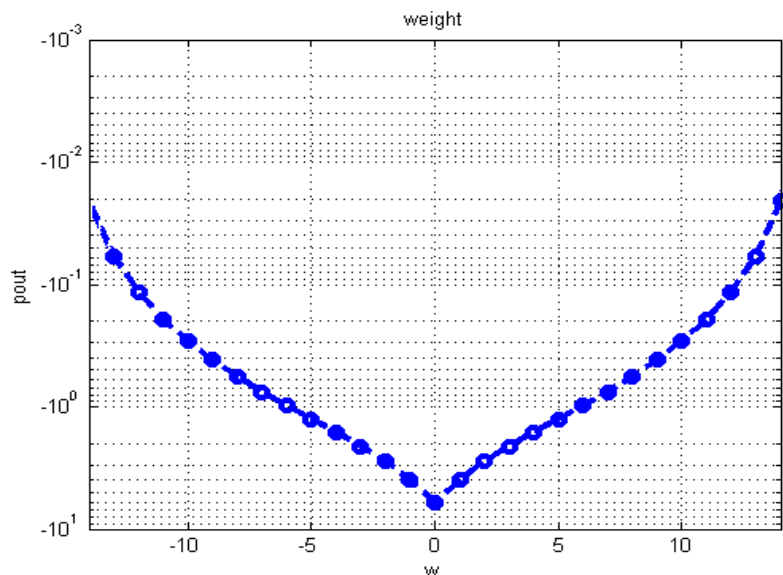


Fig 7: The impact of weight factor on outage probability

In Fig. 7, the effect of the weight factor on the simulated outage probabilities are investigated. This figure reveals that there exists the optimal weight factor in minimizing the outage probability; when the number of relays N increases, the curve around ρ_{opt} becomes steeper, and thus the performance gain of the weighted bidirectional RS scheme gets improved, which explains the phenomenon that increasing N results in larger performance gain. From Fig. 7, we can also verify that the optimal weight factor obtained by the simulated outage probability matches with that obtained by the analytical lower bound.

CONCLUSION

In this paper, we analyzed the impact of outdated CSI on the performance of bidirectional AF RS. The weighted bidirectional RS was proposed to improve the performance of RS with outdated CSI. The outage probability bound of the proposed RS scheme was obtained and verified, along with the asymptotic outage probability. Based on the analytical expressions, the optimal weight factor and the optimal power allocation scheme in minimizing the outage probability were achieved. The optimal weight factor is mainly decided by the number of relays, the correlation coefficients of outdated CSI, and the channel variances. Nevertheless, the optimal power allocation scheme has no relationship with these parameters. Furthermore, the analytical and simulation results reveal that when the CSI is outdated, the diversity order reduces from full diversity to one. However, the weighted bidirectional RS with the optimal weight factor outperforms the conventional bidirectional RS, when the system structure is asymmetric. In the future work we will be proposing SNR based relay selection for Fading Channels. In this based on the SNR of the received signal at the destination, the destination decides whether relaying is needed or not by comparing received SNR with a threshold SNR.

REFERENCES:

- [1] S. Zhang and S.-C. Liew, Channel coding and decoding in a relay system operated with physical-layer network coding, *IEEE J. Sel. Areas Commun.*, vol. 27, no. 5, pp.788796, Jun. 2009.
- [2] P. Popovski and H. Yomo, Wireless network coding by amplify-and forward for bi-directional traffic flows, *IEEE Commun. Lett.*, vol. 11, no. 1, pp. 1618, Jan. 2007.
- [3] Z. Ding and K. K. Leung, Impact of imperfect channel state information on bi-directional communications with relay selection, *IEEE Trans. Signal Process.*, vol. 59, no. 11, pp. 56575662, Nov. 2011.
- [4] L. Fan, X. Lei, P. Fan, and R. Q. Hu, Outage Probability Analysis and Power Allocation for Two-Way Relay Networks with User Selection and Outdated Channel State Information, *IEEE Commun. Lett.*, vol. 16, no. 9, pp. 14421445, Sep. 2012.
- [5] Y. Li, R. H. Y. Louie, and B. Vucetic, Relay selection with network coding in two-way relay channels, *IEEE Trans. Veh. Technol.*, vol. 59, no. 9, pp. 44894499, Nov. 2010.
- [6] L. Song, Relay selection for two-way relaying with amplify-and-forward protocols, *IEEE Trans. Veh. Technol.*, vol. 60, no. 4, pp. 19541959, May 2011.
- [7] P. K. Upadhyay and S. Prakriya, Performance of two-way opportunistic relaying with analog network coding over Nakagami-m fading, *IEEE Trans. Veh. Technol.*, vol. 60, no. 4, pp. 19651971, May 2011.
- [8] D. S. Michalopoulos, H. A. Suraweera, G. K. Karagiannidis, and R. Schober, Amplify-and- forward relay selection with outdated channel estimates, *IEEE Trans. Commun.*, vol. 60, no. 5, pp. 12781290, May 2012.
- [9] H. Cui, R. Zhang, L. Song, and B. Jiao, Relay selection for bidirectional AF relay network with outdated CSI, *IEEE Trans. Veh. Technol.*, vol. 62, no. 9, pp. 43574365, Nov. 2013.
- [10] H. Cui, L. Song, and B. Jiao, Weighted amplify-and-forward relay selection with outdated channel state information, *IEEE Wireless Commun. Lett.*, vol. 2, no. 6, pp. 651654, Dec.

A New Approach To Graph Based Object Classification On Images

Sandhya S Krishnan, Kavitha V K
P.G Scholar, Dept of CSE, BMCE, Kollam, Kerala, India
Sandhya4parvathy@gmail.com

Abstract: The main idea of graph based image modeling is that the regions of the image, which contain similar properties, are denoted by graph vertices, and the relations between different regions are denoted by graph edges. The vertex and edge attributes usually describe the characteristics of that region and the relation between regions respectively. A simple approach to keep the structural and topological information of an image is to use digital image representation techniques; for instance, quad trees, etc. By modeling images as graphs, the task of image classification becomes one of classifying graphs. Quad trees have been used for representing images in the form of trees. In this paper we propose an algorithm that discovers the subgraphs present in a graph represented by a stream of labeled nodes and edges. Our algorithm is efficient and is easily tuned by the user to produce interesting patterns from various kinds of graph data.

Keywords: Graph, Vertex, Edge, Attribute, Digital image representation, Quad tree, Subgraph

1. INTRODUCTION

Data in multiple domains can be naturally modeled as graphs [1] since graphs are general and powerful data structures that can be used to represent diverse types of objects. Several authors have developed graph-based techniques and methods for satisfying the need of converting large volumes of data into useful information [2]. The frequent approximate subgraph (FAS) discovery is an example of such techniques [3,4,5]. These techniques have become important topics in mining tasks where the mined patterns are detected taking into account distortions in the data.

It is common to model complex data with the help of graphs consisting of nodes and edges that are often labeled to store additional information. Representing these data in the form of a graph can help visualise relationships between entities which are convoluted when captured in relational tables. Graph mining ranges from indexing graphs, finding frequent patterns, finding inexact matches, graph partitioning and so on. The subgraphs are categorized into various classes, and the approaches of graph based data mining strongly depend on the targeted class.

Graph invariants provide an important mathematical criterion to efficiently reduce the search space of the targeted graph structures in some approaches. Furthermore, the mining measures define the characteristics of the patterns to be mined similar to conventional data mining. Knowledge Discovery in Databases (KDD) is a systematic and automatic process to analyse and discover hidden knowledge (or patterns) from databases. The general process of KDD commences with the acquisition of relevant data, followed by preprocessing, feature extraction, patterns discovery and finally communication of the identified patterns to the user. A large number of different techniques have been developed to perform KDD. The work described in this paper is focused on classification, specifically the classification of image data (the term image mining will be used throughout this paper to indicate the application of data mining techniques to image data, and the term image classification to indicate the application of classification techniques to image data).

The basic outline of this paper is as follows. Section 2 provides some basic concepts and related works. The graph-based image representation is presented in Section 3. The framework for image classification is explained in Section 4 and the experimental results in a real image collection are discussed in Section 5. Finally, conclusions of the research and some ideas about future directions are exposed in Section 6.

2 BACKGROUND

In this section, we start by providing the background knowledge and notation used in the following sections.

2.1 Basic Concepts

This work is focused on simple undirected labeled graphs; henceforth, when we refer to graph we assume this type of graph. Before presenting their formal definition, we will define the domain of labels.

Definition 1 (labeled graph) A labeled graph can be represented as $G = (V, E, L_V, L_E, u)$, where V is a set whose elements are called vertices, $E \subseteq V \times V$ is a set of edges; L_V and L_E are vertex and edge labels respectively.

Definition 2 (sub graph) Let $G_1 = (V_1, E_1, L_{V_1}, L_{E_1}, u_1)$ and $G_2 = (V_2, E_2, L_{V_2}, L_{E_2}, u_2)$ be two graphs, we say that G_1 is a subgraph of G_2 iff $V_1 \subseteq V_2$, $\forall u \in V_1$, $u_1(u) = u_2(u)$, and $E_1 \subseteq E_2$, and $\forall (u,v) \in E_1$, $u_1(u,v) = u_2(u,v)$. In this case, we use the notation $G_1 \subseteq G_2$. G_2 is also a super graph of G_1 .

Definition 3 (Adjacency Matrix) Adjacency Matrix is a 2D array of size $V \times V$ where V is the number of vertices in a graph. Let the 2D array be $adj[i][j]$, a slot $adj[i][j] = 1$ indicates that there is an edge from vertex i to vertex j . Adjacency matrix for undirected graph is always symmetric.

2.2 Related work

Graph classification has received lots of attention because of its wide range of applicability to real-world data such as biological data, chemical compound data, and semi structured data to name a few. In most of these approaches a graph is represented using various descriptors and a classification model is built using statistical or machine learning techniques. Karypis et al. [6] use similar approach by generating frequent sub structure based descriptors using a frequent subgraph mining algorithm and selecting the best substructures to define the feature vectors, which is subsequently used by Support Vector Machine (SVM) classifiers to build the classification model.

Han et al. [7] showed that frequent closed graphs based descriptor space is a better approach than the frequent subgraphs based descriptors, and it generates typically lower dimensional feature vectors. A number of methods have been proposed in recent years using cyclic patterns [8], acyclic, path and tree fragments [9] to define the descriptor space and to generate features. With this feature based representation any classification technique can be used for the classification task.

3. PROPOSED FRAMEWORK

We take a graph based approach to object classification. Let $G=(V,E)$ be an undirected graph with vertices V and edges E . Generally speaking, image mining aims to discover implicit patterns among image databases. The fundamental issue of image mining is how to use low-level (primitive) representations to extract high-level hidden patterns with efficiency and effectiveness. Representing images as graphs can maintain the structural information of images.

There are a number of techniques for graph based image representation. The main idea of graph based image representation is that the regions of the image, which contain similar properties, are denoted by graph nodes, and the relations between different regions are denoted by graph edges. The node and edge attributes usually describe the characteristics of that region and the relation between regions respectively. The flowchart of the Graph based image classification framework is illustrated in Figure 1.

A quad-tree [10] is a widely used tree structure for representing images. The fundamental idea behind the quad-tree is that any image can be divided into four quadrants. Each quadrant can be further split into four equal-sized sub quadrants (NW, NE, SW and SE), and so on. The quad-tree decomposition is based on recursively subdividing the sub-images until the imposed limit is met. In this paper, we use a quad-tree to represent each image.

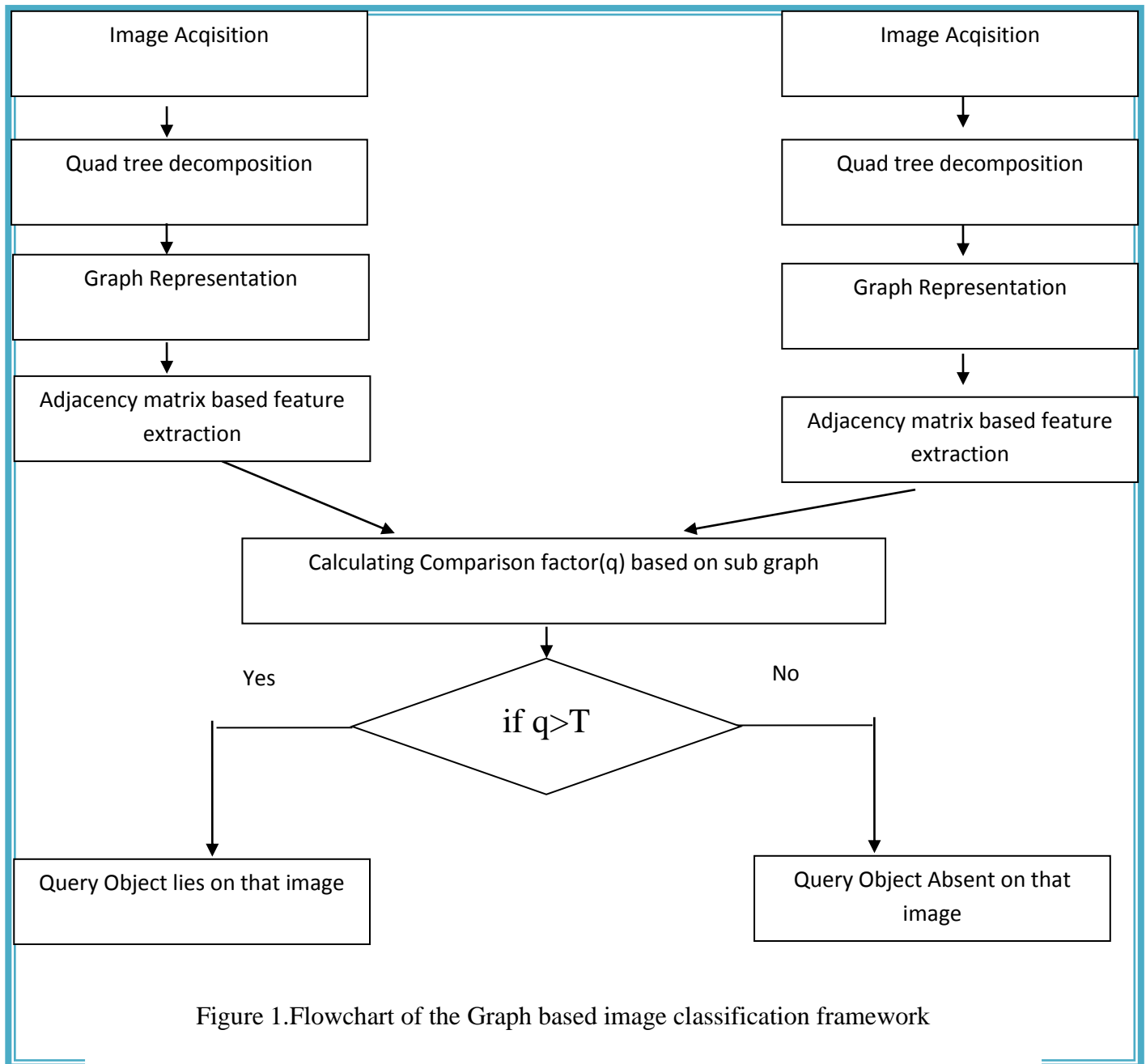


Figure 1. Flowchart of the Graph based image classification framework

The algorithm mainly comprises of the following steps:

- Initial step is the Quad tree decomposition of the acquired image .
- After that the graph is constructed based on the Adjacency matrix(adj[][]). An entry $adj[i][j]= 1$ in the respective matrix indicates that there is an edge from vertex i to vertex j . Otherwise the entry is 0.
- Calculation of comparison factor(q) based on the subgraph is the decision making step.
- If the comparison factor(q)>threshold(T) then the Object lies on that image, else the Object is absent on that image.

4. EXPERIMENTAL RESULTS

The graph based Object classification method is tested on the acquired sample image and Figure 2 shows the output of the proposed system. In subgraph mining the goal is to develop algorithms to discover frequently occurring subgraphs in the graph database. Although there are many efficient and scalable frequent pattern mining algorithms exist for itemset mining and sequence mining, our method achieve an efficient and scalable algorithm for subgraph mining.

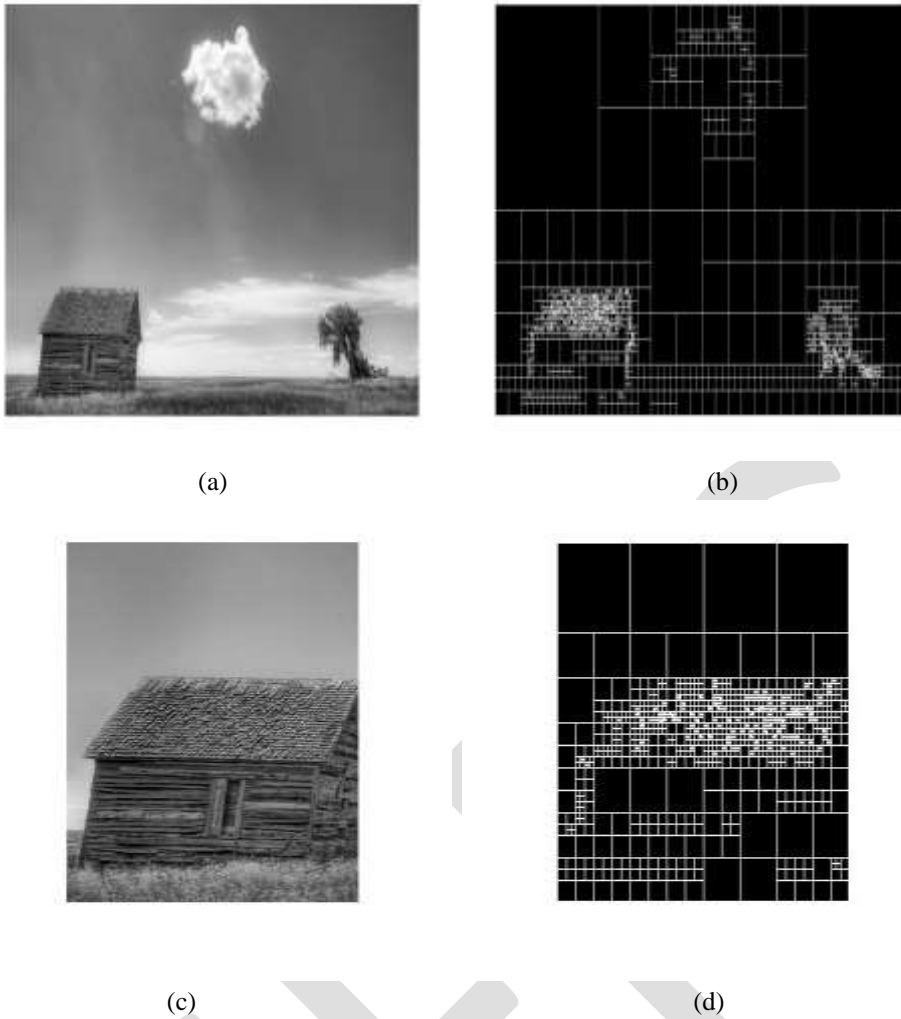


Figure 2.(a) Original image, (b) Quad tree of the Original image, (c) Query image, (d) Quad tree of the Query image

5. CONCLUSION

This paper presents an efficient approach for graph based Object Classification on Images. We presented an algorithm to find the pattern present in an image. We have shown how the proposed method finds relevant pattern using the comparison factor of the image. Future work will focus on making the presented approach more meaningful for the underlying application in which complex object can be classified.

REFERENCES:

[1] J. Friedman, T. Hastie, and Robert Tibshirani. Additive logistic regression: A statistical view of boosting. *The Annals of Statistics*, 38(2):337–374, April 2000.

[2] A. Berger. The Improved Iterative Scaling Algorithm: A gentle Introduction. Technical report, Carnegie Mellon University, 1997. 374

- [3] A.L. Berger, V.J. Della Pietra, and S.A. Della Pietra. Maximum Entropy Approach for Natural Language Processing. *Computational Linguistics*.22(1) P: 39 – 71,1996.
- [4] H. Mannila, and P. Smyth. Prediction with Local Patterns using Cross-Entropy. *In Proc. of the fifth ACM SIGKDD*, P: 357 – 361, ISBN:1-58113-143-7, 1999.
- [5] K. Nigam, J. Lafferty, and A. Maccallum. Using Maximum Entropy for Text Classification. *IJCAI-99 Workshop on Machine Learning for Information*, 1999.
- [6] M. Deshpande, M. Kuramochi, Nikil Wale, and G. Karypis, Frequent Substructure-Based Approaches for Classifying Chemical Compounds, *IEEE Transactions on Knowledge and Data Engineering*, vol. 17, no. 8, pp.1036-1050, Aug., 2005.
- [7] C. Liu, X. Yan, H. Yu, J. Han, and P. S. Yu. Mining Behavior Graphs for Backtrace of Noncrashing Bugs. *In Proc. of SIAM Int. Conf. on Data Mining (SDM'05)*, 2005.
- [8] T. Horvath, T. Grtner, and S. Wrobel. Cyclic pattern kernels for predictive graph mining. *In Proc. of the 10th ACM SIGKDD international conference on Knowledge discovery and data mining*, pages 158-167, 2004
- [9] N. Wale and G. Karypis. Acyclic Subgraph-based Descriptor Spaces for Chemical Compound Retrieval and Classification. *In Proc of IEEE International Conference on Data Mining (ICDM)*, 2006.
- [10] R.A. Finkel, J.L. Bentley, Quad trees: a data structure for retrieval on composite keys, *Acta Informatica* 4 (1974) 1–9.
- [11] Y. Jia, J. Zhang, J. Huan, An efficient graph-mining method for complicated and noisy data with real-world applications, *Knowledge and Information Systems* 28 (2011) 423–447.
- [12] C. Jiang, F. Coenen, Graph-based image classification by weighting scheme, in: *Proceedings of the Artificial Intelligence*, Springer, Heidelberg, 2008, pp. 63– 76.
- [13] C. Jiang, F. Coenen, R. Sanderson, M. Zito, Text classification using graph mining-based feature extraction, *Knowledge-Based Systems* 23 (2010) 302–308.
- [14] C. Jiang, F. Coenen, M. Zito, Frequent sub-graph mining on edge weighted graphs, in: *Proceedings of the 12th international conference on Data warehousing and knowledge discovery*, Springer-Verlag, Berlin, Heidelberg, 2010, pp. 77–88.
- [15] A. Jiménez, F. Berzal, J.C.C. Talavera, Frequent tree pattern mining: a survey, *Intelligence Data Analysis* 14 (2010) 603–622. *Statics of Large Networks*, 2008.

Autonomous Connectivity Using Mesh Networks

Parvathy Ajay, Bibin Varghese Kurien

PG Scholar, Department of ECE, CAARMEL Engineering College, Pathanamthitta, Kerala
Assistant Professor, Department of ECE, CAARMEL Engineering College, Pathanamthitta, Kerala

Email:parvathyajay91@gmail.com

Abstract: Mobile ad hoc networks (MANETs) are ideal for situations where a fixed infrastructure is unavailable or infeasible. The growth in wireless communication technologies attracts a considerable amount of attention in mobile ad-hoc networks. Since mobile hosts in an ad-hoc network usually move freely, the topology of the network changes dynamically and disconnection occurs frequently. These characteristics make a mobile ad-hoc network be likely to be separated into several disconnected partitions, and the data accessibility is hence reduced. Today's MANETs, however, may suffer from network partitioning. This limitation makes MANETs unsuitable for applications such as crisis management and battlefield communications, in which team members might need to work in groups scattered in the application terrain. In such applications, intergroup communication is crucial to the team collaboration. To address this weakness, we introduce in this paper a new class of ad-hoc network called Autonomous Mobile Mesh Network (AMMNET). Unlike conventional mesh networks, the mobile mesh nodes of an AMMNET are capable of following the mesh clients in the application terrain, and organizing themselves into a suitable network topology to ensure good connectivity for both intra- and intergroup. We propose HEF algorithm for the cluster head selection.

Keywords: Mobile mesh networks, dynamic topology deployment, client tracking, HEF algorithm, mesh client.

INTRODUCTION

MANETs are among the most popularly studied network communication technologies. In such an environment, no communication infrastructure is required. The mobile nodes also play the role of the routers, helping to forward data packets to their destinations via multiple-hop relay. This type of network is suitable for situations where a fixed infrastructure is unavailable or infeasible. One great challenge in designing robust MANETs is to minimize network partitions. As autonomous mobile users move about in a MANET, the network topology may change rapidly and unpredictably over time; and portions of the network may intermittently become partitioned. This condition is undesirable, particularly for mission-critical applications such as crisis management and battlefield communications. We address this challenging problem in this paper by proposing a new class of robust mobile ad hoc network called Autonomous Mobile Mesh Networks (AMMNET).

In a standard wireless mesh network, stationary mesh nodes provide routing and relay capabilities. They form a mesh-like wireless network that allows mobile mesh clients to communicate with each other through multi hop communications. When a mesh node fails, it can simply be replaced by a new one; and the mesh network will recognize the new mesh node and automatically reconfigure itself. The proposed AMMNET has the following additional advantage. The mobility of the mesh clients is confined to the fixed area serviced by a standard wireless mesh network due to the stationary mesh nodes. In contrast, an AMMNET is a wireless mesh network with autonomous mobile mesh nodes. In addition to the standard routing and relay functionality, these mobile mesh nodes move with their mesh clients, and have the intelligence to dynamically adapt the network topology to provide optimal service. In particular, an AMMNET tries to prevent network partitioning to ensure connectivity for all its users. This property makes AMMNET a highly robust MANET.

RELATED WORK

We classify the works related to AMMNET into three categories: 1) stationary wireless mesh networks: AMMNET is a new type of mesh networks, but supports dynamic topology adaptation, 2) sensor covering: the techniques for sensor covering is related to the design of covering mobile clients in AMMNET, and 3) location tracking: tracking mobile clients in AMMNET is an application of location tracking. In the last few years, stationary wireless mesh networks have been developed to enable last-mile wireless broadband access [1]. Past work on stationary mesh networks focuses on routing traffic in a mesh topology to best utilize the network capacity [2]. Some literatures further study how to utilize non overlapping channels [3], [5], [6] and explicitly control the network topology [7], [8] to improve the network capacity of a stationary mesh. Our work builds on the concept of such a stationary mesh-based infrastructure, and extends it to enable communication among partitioned mobile clients. We improve the security inside the network. We study dynamic deployment of an AMMNET in this work, and leave utilizing non overlapping channels to improve network capacity as our future study. A self-deployment protocol is proposed in [9] to enable randomly scattered sensors to automatically move to the target planned positions. Instead of deploying stationary sensor nodes to cover the entire monitoring field, an alternative is proposed in [10], to use mobile mules to move around different monitoring areas and gather data along the traversed paths performance of sensor covering.

AUTONOMOUS MOBILE MESH NETWORK

Similar to stationary wireless mesh networks, an AMMNET is a mesh-based infrastructure that forwards data for mobile clients. A client can connect to any nearby mesh node, which helps relay data to the destination mesh node via multi hop forwarding. For ease of description, in this paper we use the terms “mesh node” and “router” interchangeably. Like stationary wireless mesh networks, where routers are deployed in fixed locations, routers in an AMMNET can forward data for mobile clients along the routing paths built by any existing ad hoc routing protocols, for example, AODV. Unlike stationary wireless mesh networks, where routers are deployed at fixed locations, routers in an AMMNET are mobile platforms with autonomous movement capability [11]. They are equipped with positioning devices such as GPS, to provide navigational aid while tracking mobile clients. Clients are not required to know their locations, and only need to periodically probe beacon messages. Once mesh nodes receive the beacon messages, they can detect the clients within its transmission range. With this capability, mesh nodes can continuously monitor the mobility pattern of the clients, and move with them to provide them seamless connectivity.

Our design considers applications where clients follow group mobility patterns [12] to move toward different directions in smaller groups. That is, the clients belonging to the same group have similar movement characteristics. However, different groups of clients might move in different directions, as illustrated in Fig. 1. The group mobility model has been verified as a realistic mobility model [13] and applied to many practical scenarios, such as campus networks [14] and ad hoc networks [15], [16]. Our goal is to dynamically allocate a finite number of mesh nodes to cover as many mobile clients as possible, while maintaining the connectivity between the groups of clients. Even though we describe the operation of AMMNET using the group mobility model, AMMNET can actually support a more general mobility model, where clients might move independently. In an extreme case, each client can be thought of as a group that contains only one user, and the design of AMMNET can still be applied to support connectivity for those independent clients.

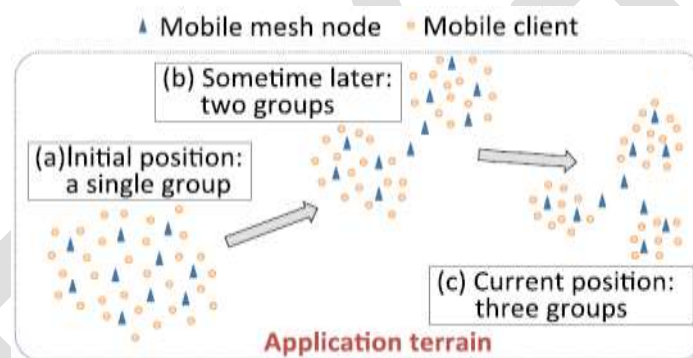


Fig 1: Topology Adaptation

Cluster Head Selection

To reduce the work load, we are dividing our project into small modules, they are given as below.

1. Grid sensor network deployment
2. Cluster formation
 - a. Collecting grid information
 - b. Energy calculation
3. Cluster head changes

Grid sensor network deployment

In sensor network, we can deploy the sensor in two types. One is random deployment and optimal grid deployment. Whenever we used random deployment, the network will get many of the problems like as coverage problem, energy reduction problem and interferences. To avoid this many problems we are going to use optimal grid sensor deployment. Grid sensor network deployment is nothing but deployment of sensor in fixed and optimally calculated sensor placement in certain distance. Using grid sensor deployment we can improve the coverage area and also we can avoid the high cost.

Cluster Formation

Cluster formation is the process of grouping sensor devices by collecting the grid location information and gathering energy information. In our paper, we are using the grid sensor deployment, so we are defining cluster formation will be done within the grid. So initially we are calculating the each and every node location information and energy of the node. We are initializing the network with same energy level so initial cluster head selection is done randomly. And remaining node in that grid is joining with that cluster head.

Cluster head changes

In sensor network, if we forming the clustering mean we can improve the network life time is possible but the constant cluster head mean that particular node will lose more energy. To avoid this problem we need to use cluster head changes. There is the different cluster head changing algorithm is available like as LEACH. In that algorithm cluster head changes will be in random manner, so that may chances to reduce the some particular node energy. To avoid this problem we are using the HEF algorithm.

Each and every second calculated energy is going to store in energy list, whenever cluster head duration is over then we are comparing energy of each and every node in that list. And which one having high energy in that list we are selecting that node as the cluster head for that period.

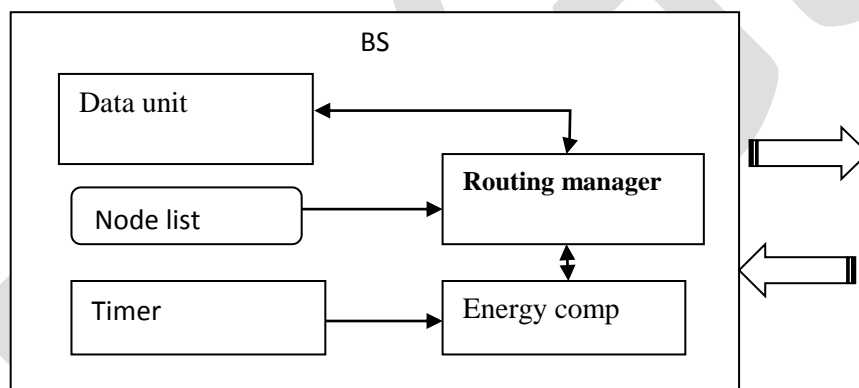


Fig 2: Energy comparison

In our paper, we are considering only the communication part; we are not implementing any sensing part. The data unit is used to generate the data. Each and every node has the energy unit. Energy unit has the current energy level. Routing manager controls the all events such as sending, receiving and data transmission. In base station, node has the node list and energy comparison unit and data unit. Data unit collects all info. Energy comparison unit compare the energy level and gives high remaining energy node name. Routing manger will selects CH by HEF. And timer used for trigger the event to compare the energy level. In our method we reduced the changes for repeated node as cluster head, in our model high energy node only going to act as CH so energy loss is less.

HEF(High Energy First)

In this HEF (High Energy First) is employed for electing cluster head. This algorithmic program selected the best ranking residual energy node as cluster head. HEF may be a centralized cluster choice algorithmic program. It also can be enforced during a distributed manner by suggests that of synchronization approach. The interactions and operations between parts in HEF algorithmic program area unit as follows:

1. HEF selects the cluster head in step with the residual energy of every device node. Then the "setup" message (with cluster ID) is distributed to the cluster heads of alternative clusters.
2. The cluster head broadcasts the "set up" message to all or any the neighboring device nodes to hitch this cluster.
3. When receiving these messages regular nodes send the "join" message to the corresponding cluster head. Then those regular nodes are related to this cluster.

4. Every cluster head acknowledges the commitment and sends TDMA schedule to regular nodes.
5. The device nodes perform sensing, process and communication tasks co-operatively at their corresponding clock cycle. The energy data is additionally transmitted at this clock cycle.
6. The cluster head transmits all collected data to sink node or base station.

Simulation Results

This can be achieved by network simulator 2. Here the tool command language (TCL) is used.

Number of nodes - 50

In intra group communication

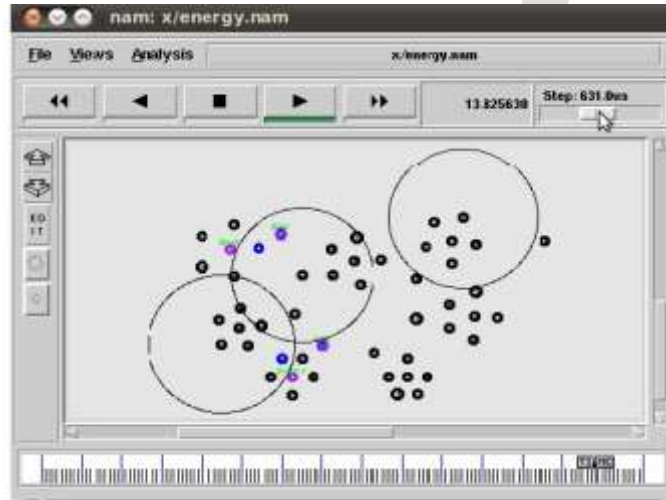


Fig 3: Cluster head selection and data transfer

Energy loss and Delay

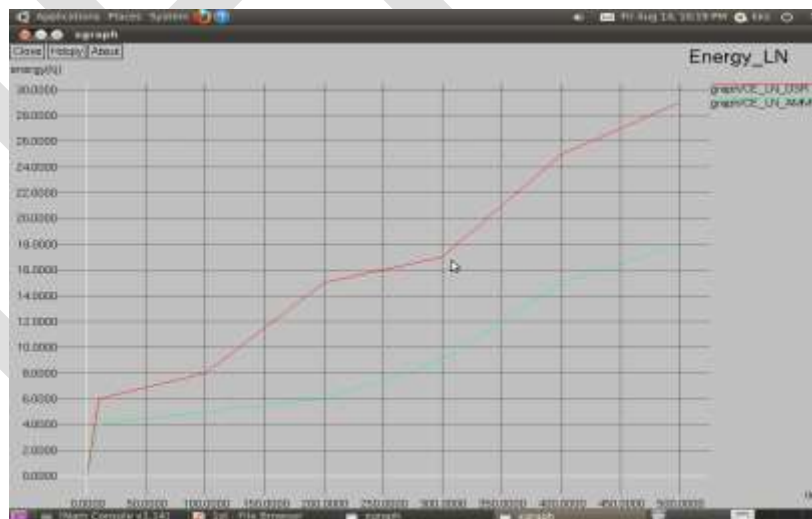


Fig 4: Energy loss

In this scenario (Fig 4. Energy loss) shows that energy loss is less in proposed method. Fig 5 shows that delay in proposed method is less than that of the previous method.

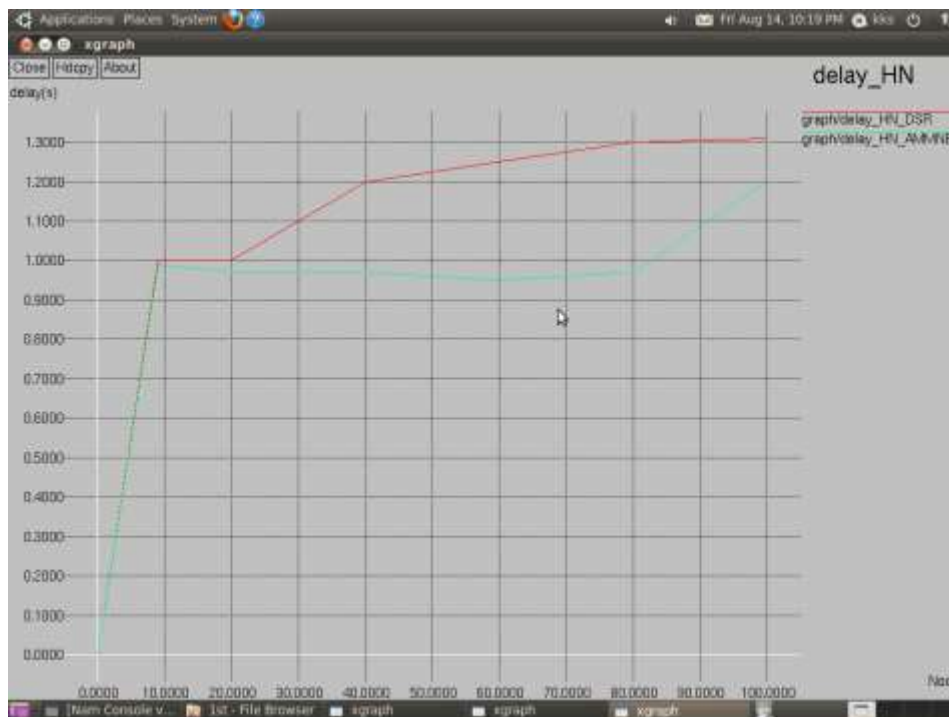


Fig 6: Delay

Conclusion

In our project we improved network life time compare than previous method, in previous model there may be chances to repeated node may act as cluster head so energy loss of that certain node is high. But in our method we reduced the changes for repeated node as cluster head, in our model high energy node only going to act as CH so energy loss is less. In this work we not considered any security level in our future work we can consider security by double encryption of message in the source node and at the cluster head .

REFERENCES:

- [1] F. Akyildiz, X. Wang, and W. Wang, "Wireless Mesh Networks A Survey," Computer Networks, vol. 47, no. 4, pp. 445-487, 2005.
- [2] R. Draves, J. Padhye, and B. Zill, "Comparison of Routing Metrics for Static Multi-Hop Wireless Networks," Proc. ACM SIGCOMM, 2004.
- [3] M. Alicherry, R. Bhatia, and L.E. Li, "Joint Channel Assignment and Routing for Throughput Optimization in Multi-Radio Wireless Mesh Networks," Proc.ACM MobiCom, 2005S. Zhou, J. Gong, Z. Yang, Z. Niu, P. Yang, Green mobile access network with dynamic base station energy saving, 2009 ACM Mobicom
- [4] K.N. Ramachandran, E.M. Belding, K.C. Almeroth, and M.M. Buddhikot, "Interference-Aware Channel Assignment in Multi-Radio Wireless Mesh Networks," Proc. IEEE INFOCOM, 2006.
- [5] J. Tang, G. Xue, and W. Zhang, "Interference-Aware Topology Control and QoS Routing in Multi-Channel Wireless Mesh Networks," Proc. ACM MobiHoc, 2005.
- [6] A. Naveed, S. Kanhere, and S. Jha, "Topology Control and Channel Assignment in Multi-Radio Multi-Channel Wireless Mesh Networks," Proc. IEEE Int'l Conf. Mobile Adhoc and Sensor Systems (MASS), 2007.

- [7] S. Meguerdichian, F. Koushanfar, M. Potkonjak, and M. Srivastava, "Coverage Problems in Wireless Ad-Hoc Sensor Networks," Proc. IEEE INFOCOM, 2001.
- [8] C.-F. Huang and Y.-C. Tseng, "The Coverage Problem in a Wireless Sensor Network," Mobile Networks and Applications, vol. 10, pp. 519-528, Aug. 2005
- [9] Y. Bejeran, "Simple and Efficient k-Coverage Verification without Location Information," Proc. IEEE INFOCOM, 2008.
- [10] X. Wang, G. Xing, Y. Zhang, C. Lu, R. Pless, and C. Gill, "Integrated Coverage and Connectivity Configuration in Wireless Sensor Networks," Proc. ACM First Int'l Conf. Embedded Networked Sensor Systems (SenSys), 2003
- [11] "Quadrocopter LLC," <http://quadrocopter.us/>, 2013.
- [12] R. Roy, Handbook of Mobility Models and Mobile Ad Hoc Networks. Springer, 2010.
- [13] Y.-C. Chen, E. Rosensweig, J. Kurose, and D. Towsley, "Group Detection in Mobility Traces," Proc. Sixth Int'l Wireless Comm. And Mobile Computing Conf. (IWCMC '10), 2010.
- [14] T. Camp, J. Boleng, and V. Davies, "A Survey of Mobility Models for Ad Hoc Network Research," Wireless Comm. and Mobile Computing, vol. 2, no. 5, pp. 483-502, 2002.
- [15] X. Hong, M. Gerla, G. Pei, and C. Chiang, "A Group Mobility Model for Ad Hoc Wireless Networks," Proc. Second ACM Int'l Workshop Modeling, Analysis and Simulation of Wireless and Mobile Systems (MSWiM '99), 1999.
- [16] K. Blakely and B. Lowekamp, "A Structured Group Mobility Model for the Simulation of Mobile Ad Hoc Networks," Proc. Second Int'l Workshop Mobility Management & Wireless Access Protocols (MobiWac), 2004.

FPGA-Based Finger Vein Recognition System for Personal Verification

Mrunali Jadhav, Priya M. Nerkar

Student, Assistant Professor, 15.mrunal@gmail.com, priyamnerkar@gmail.com, 9011833349

Abstract— In today's society with the rapid growth in the field of electronic information technology and its simultaneous deployment in every field, the personal verification is a critical key problem. Due to this fact, the biometric authentication has gaining popularity as it provides a high security and reliable approach for personal authentication. Finger vein biometric is advantageous over other types of biometric systems because it has low forgery rate, aliveness detection as well as stable over long period of time. The paper presents the implementation of image processing algorithm and Feature extraction process in MATLAB. And for final authentication the template matching is carried out on Field Programmable Gate Array (FPGA) for fast recognition. The system is prototyped on Papilio one 500k FPGA board which has Xilinx Spartan 3E chip inside. The performance of the proposed system is evaluated by the time required to verify one input finger vein sample and Precision.

Keywords— Biometric, finger vein recognition, feature extraction, FPGA, Papilio one, MATLAB, Precision

INTRODUCTION

The personal information can be protected in the form of biometrics. The traditional authentication systems like identity card or password can be easily stolen or acquired by unauthorized person [1]. All these traditional authentication systems are gradually replaced by biometric systems like fingerprints, iris recognition, palm print and veins. The biometric authentication system is chosen over conventional authentication system because of their distinctiveness and highly secured nature.

Out of these biometric systems, finger vein biometric is one of the emerging techniques. In this type of biometric system the vascular pattern under one's skin is utilized as a unique feature for authentication. Veins are hidden underneath the skin surface and are mostly invisible to human eye, they are not prone to external distortion and also the vein patterns are much harder to replicate as compared to other biometric traits. Vein patterns are unique for each individual and are stable over a long period of time. Because of its uniqueness, stability and high resistance to criminal attacks, vein pattern is more reliable biological feature for a secure biometric authentication system [5][2].

The Biometric system is often implemented in an untrusted environment that uses an insecure and non-reliable central server for the storage of the biometric templates [9]. This can be the source of biometric information leakage. The solution to this problems is given by recent development in vein authentication by hardware implementation of the system [12][7][11][18]. It provides secure information storage and tamper resistance, hence it provides the protection from physical and software attacks. The finger-vein biometric system for personal authentication is promising in security and convenience point of view. The comparison between different biometric systems is as shown in Table 1 [4], I=insufficient, N=normal, G=good.

Table 1 Comparison of Major Biometrics Method

Bio-metric	Anti-forgery	Accuracy	Speed	Enrolment rate	Resistance	cost
Finger print	I	N	N	I	I	G
Iris	N	G	N	N	I	I
Face	N	I	N	N	G	I
Voice	N	I	N	N	G	N
Vein	G	G	G	N	N	N

This paper presents preliminary requirement for the implementation of finger vein recognition system on FPGA. It includes image preprocessing and feature extraction processes on finger vein images in MATLAB which is required for developing Biometric recognition system on FPGA. According to best of our knowledge the implementation of the entire preprocessing module, feature extraction and matching on FPGA is very challenging and also it will be very time consuming process. The solution to this is proposed in this work by performing all preprocessing task and feature extraction in MATLAB and final template matching in FPGA. By doing this the speed of authentication is quite good. Also the system is cost effective.

RELATED WORK

A lot of work has been carried out in this field of biometric using finger veins for authentication and also for variety of applications on different platforms. In this section review of some prior work on finger vein biometric security system is discussed.

David Mulyono et al. in [2] introduced a preliminary process to enhance the image quality that worsen by the light effect and some noise produced by the web camera while acquisition, then vein pattern segmentation by adaptive thresholding and matched using improved template matching algorithm. The final result shows that by applying some appropriate process the vein image with not that much good quality can be used for personal identification as long as the veins are clear.

In [16] D. Wang et al. and M. Subramani et al. in [4] presented highly secured and reliable user identification mechanism using vein biometric technology for consumer electronics devices. Radon transforms and singular value decomposition method is used for feature extraction process and classification using a normalized distance measure.

N. Mahri et al. in [17] presented an algorithm for vein recognition with less complexity in the image preprocessing phase, where vein pattern extraction is not included in the authentication process. Phase only correlation is applied at the matching stage. In this technique, matching is by using phase component of 2D-DFT of an image. This technique is reliable, robust and doing less job in pattern extraction.

V. Ramya et al. in [8] introduced a novel design for personal authentication and for vehicle security using finger vein recognition system. Wavelet transform is used for feature point extraction using HAAR mother wavelet. The attracting feature of HAAR transform includes fast implementation and able to analyze the local features. The authors have presented hardware implementation of finger vein recognition system for vehicle security application, a vehicle set up consist of embedded main board module which has AT89C51 microcontroller and communication module consisting of LCD display, alarm and GSM. Purpose of this module is to alert the authorized vehicle user.

Zhi Liu et al. in [12] proposed a real-time embedded finger vein recognition system for authentication on mobile devices. The system is implemented on a DSP platform. The results proved that the system has low computational complexity and low power consumption, thus qualified for authentication on mobile devices.

M. Khalil-Hani et al. in [18] proposed an embedded system implementation of finger vein biometric on FPGA. The system is prototyped on Altera Stratix-II FPGA hardware board with Nios2-Linux operating system running at 100 MHz. In this authentication system, feature extraction is based on minutiae extracted from vein pattern images while biometric matching is based on modified Hausdorff distance technique. The system gives high performance and optimum accuracy by an embedded system implementation on FPGA.

From the prior literature it is observed that the hardware based approach is cost effective and gives high performance. Also such systems can be used for variety of applications.

OVERVIEW OF THE SYSTEM

The proposed system consists of three modules: Image acquisition module, human communication module (PC) and FPGA board. The figure 1 shows the functional block diagram of the proposed work. The image acquisition module is used to collect the finger vein images for processing. The human communication module (PC) is used to perform basic image processing algorithms like RGB to gray scaling, edge detection and also feature extraction process in MATLAB. This preprocessing is required to prepare finger vein images for further processing. This human communication module (PC) is used to display the recognition results and also to receive inputs from image acquisition module. After pre-processing and feature extraction processes, the template matching is done on FPGA for final authentication.

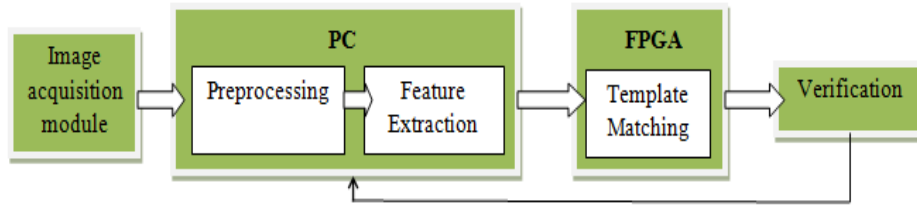


Figure 1 Functional block diagram of proposed work

The proposed finger vein recognition system consists of two stages: enrollment stage and verification stage[12]. The enrollment stage starts with pre-processing of the input finger vein images. For the verification stage after pre-processing and feature extraction process feature templates are generated. The input finger-vein image is matched with the corresponding template after its features are extracted and authentication is done for genuine or imposter user. Figure 2 shows the flowchart of the proposed system.

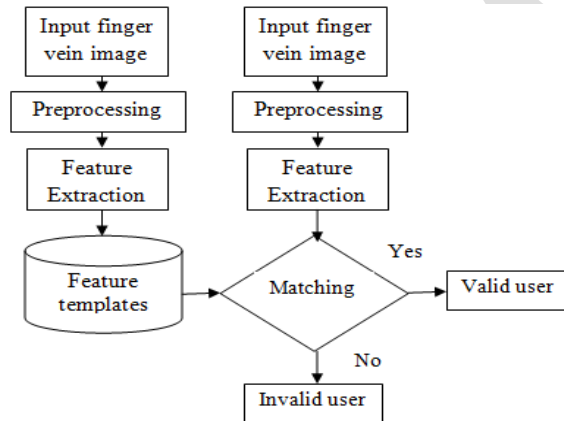


Figure 2 Flowchart of finger-vein authentication system

METHODOLOGY

In this section the step by step description for finger vein authentication is discussed, which includes image acquisition of finger vein image, different preprocessing techniques on vein image, feature extraction and matching process for final authentication.

A) Image acquisition

Image acquisition is of two types off-line and online. On-line images are the images which are taken in real time and off-line images means the images which are taken from already created database. The images in real time can be obtained by normal web camera or by designing a finger-vein imaging device based on light transmission for more distinct imaging.

In the proposed work the off-line finger vein images are used for human identification. Figure 3 shows some images from the used database.

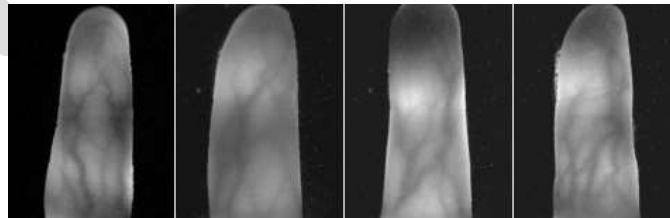


Figure 3 Database images

B) Pre-processing

In image-based biometric systems like finger vein system, a number of pre-processing tasks are required prior to enhance the image quality, some of these tasks are contrast, brightness, edge information, noise removal, sharpen image, etc., furthermore, to produce a better quality of image that will be used for later stage as an input image and assuring that more relevant information can be detected for authentication. A finger vein based authentication system mainly consists of following pre-processing stages and they are RGB to grayscale conversion, Gaussian blurring and edge detection.

In RGB to grayscale conversion color image is converted into grayscale. In the grayscale digital image the value of each pixel is a single sample means it carries only intensity information. Images of this sort are known as black-and-white, which are composed of shades of gray, varying from black at the weakest intensity to white at the strongest.

The formula for RGB to grayscale conversion is as stated below:

$$\text{GRAY} = 0.299 * r + 0.587 * g + 0.114 * b \quad (1)$$

The unwanted noise in the finger vein image is removed using Gaussian blur [4][8]. This blurring is also called smoothing. In this process blurring of an image is carried out by using Gaussian function typically to reduce image noise and image detail. As we are performing all the preprocessing operations in MATLAB, so this smoothing of an image is performed by calling *fspecial* function. This function has two argument *hsize* and *sigma*, where *hsize* specifies the number of rows or columns in the function means it gives size of the filter and *sigma* is a standard deviation of the Gaussian with units in pixels. The size of the *hsize* and *sigma* depends upon how much we want to smooth it. In the proposed work the size of these two arguments are taken as [5 5] and 2 respectively.

After this noise removal, the edges are detected by using canny operator in MATLAB. A canny operator with locally adaptive threshold is used to get the single pixel edge of the finger.

C) Feature Extraction

Feature extraction is most important step in this authentication process. It is a special form of dimensionality reduction. It is a transformation of input data into the set of features. In the proposed work for this feature extraction process the canny edge detection method is used for feature extraction process. Extraction of features such as edges and curves from an image is useful for final authentication. Edges are important features in an image, they represents significant local intensity changes.

An image is viewed as a function. For a given pixel values i, j ; we have an intensity $I(i, j)$. While extracting features there may be chance that operator will return non-zero values in regions where there is no edge. So, thresholding can be used which minimizes false positives and only pick local maxima. Final edges are determined by suppressing all edges that are not connected to a very strong edge. After this feature extraction process, the template database is generated which is used for final authentication in matching process. The canny edge detection algorithm used for this process runs in following steps as shown in figure 4 and figure 5 shows the result of extracted features from the finger vein image.



Figure 4 canny edge detection algorithm



Figure 5 Feature extraction

D) Matching

After features are extracted from the vein image the matching stage measures the similarity or dissimilarity between the input finger vein image features and the previously enrolled ones in the database. Template matching is performed on FPGA, where input image and the image in the database which is generated after extracting features are compared. A standard threshold value is set for authentication purpose. During this template matching process, the error sum is generated. When this error sum is above the threshold value then the message will be displayed that the user is invalid; and if this error sum is less than threshold value then it is a valid user. In this way authentication takes place. Figure 5 shows the authentication of a valid user. Similarly, the result for invalid user will be generated with generation of error rate during template matching. This final authentication will be displayed on PC in MATLAB GUI.



Figure 5 Authentication for valid user

RESULTS AND DISCUSSION

The performance metric used for the final authentication process is precision. Precision is a measure of exactness or quality. It is a probability that a randomly selected data is relevant. It is given by the equation as below

$$\text{Precision} = \frac{\text{no. of correctly identified images}}{\text{total no. of correct images}} \quad (2)$$

In the proposed work, total no of images taken are 20, out of which 16 users have enrolled in database. Out of these 16, 14 users are correctly identified and 2 are not may be because of some noise present in the image. For classification task, the terms True Positives (TP) and False Positives (FP) are the two outcomes which are considered.

Table 2 For classification task

	Identified	Not identified
Correct(relevant)	14 (TP)	2 (FP)

From the above table, the precision is calculated as shown below.

$$\text{Precision} = \frac{TP}{TP+FP} = \frac{14}{14+2} = \frac{14}{16} = 0.875 \quad (3)$$

From this analysis, it is observed that the precision of the template matching stage for the proposed system is calculated about 87.5% is. Also the platform used for template matching stage is papilio one 500k FPGA board which is very easy for implementing the logic for different algorithms according to the users interest and it is a very cost effective solution. Because of this the overall cost of the system is reduced.

CONCLUSION

In this paper, the hardware based approach for personal authentication is given based on finger vein patterns. The algorithms required for authentication are discussed in detail. These processes are required to prepare image for further processing and perform final authentication on FPGA. This authentication process uses predefined vein images from the database. This hardware system of finger vein authentication system on FPGA can be used for variety of application. The results for feature extraction and matching process are also discussed. From the analysis, it is observed that the recognition time means the time taken to match one sample of finger vein is about 41 seconds.

Also for performance evaluation of the proposed system, precision is one of the parameter considered. Precision is a probability that randomly selected input images are matched perfectly. For the proposed system the precision we get is about 87.5%.

The performance of the system can be improved by designing imaging device to acquire high quality finger vein images.

REFERENCES:

- [1] A. K. Jain, S. Pankanti, S. Prabhakar, H. Lin and A. Ross, "Biometric: a grand challenge" Proceedings of 17th International Conference on Pattern Recognition (ICPR) vol 2, pp 935-942, 2004.
- [2] David Mulyono, "A study of finger vein biometric for personal identification" IEEE Proceedings of the International Symposium Biometrics and Security technologies, pages 134-141, 2008.
- [3] H. Lee, S. Lee, T. Kim, and Hyokyung Bahn, "Secure user identification for consumer electronics devices," IEEE Transactions on Consumer Electronics, vol.54, no.4, pp.1798-1802, Nov. 2008.
- [4] M.Subramani, "Highly secure and reliable user identification based on finger vein patterns" Double Blind Peer Reviewed International Research Journal, 11, 2011.
- [5] Kumar, A., Zhou, Y.B, "Human identification using finger images", IEEE Transactions on Image Process, 21(4): 2228–2244, 2012.
- [6] Jinfeng Yang, Yihua Shi, "Towards Finger Vein Image Restoration and Enhancement for Finger Vein Recognition", Elsevier, Information Sciences 33-52, 2014.
- [7] V.Ramya and P.Vijay kumar, "A novel design of finger vein recognition for personal authentication and vehicle security" Journal of Theoretical and Applied Information Technology, 65, 2014
- [8] K. Amruthavally, "An embedded real-time finger-vein recognition system for security levels" International journal of Engineering Research and General Science, 1, 2013.
- [9] S. L. Yang, K. Sakiyama, and I. M. Verbauwhede, "A compact and efficient fingerprint verification system for secure embedded devices," in Conference Record of the Thirty-Seventh Asilomar Conference on Signals, Systems and Computers, pp. 2058- 2062, 2003.
- [10] Jinfeng Yang, Yihua Shi, "Finger Vein ROI Localization and Vein ridge Enhancement", Elsevier, Pattern Recognition Letters 33, 1569-579, 2012.
- [11] Y.H. Lee, Khalil-Hani, Rabia Bakhteri, "FPGA-based Finger vein Biometric system with Adaptive illumination for better image acquisition", International Symposium on Computer Applications and Industrial Electronics (ISCAIE 2012), December 3-4, 2012.
- [12] Zhi Liu and Shangling Song, "An embedded real-time finger-vein recognition system for mobile devices" IEEE Transactions on Consumer Electronics, 58(2), 2012.
- [13] Song, W., Kim, T., Kim, H.C., Choi, J.H., Kong, H. J., Lee, S.R., "A finger-vein verification system using mean curvature", Pattern Recognition Letter, 32 (11):1541-1547, 2011.
- [14] Wu, J. D., Liu, C.T., "Finger-vein pattern identification using principal component analysis and the neural network technique", Expert Systems with Applications, 38(5): 5423-5427, 2011.
- [15] Yang, X. Li, "Efficient finger vein localization and recognition", in: International Conference on Pattern Recognition, IEEE, pp.1148–1151, 2010.
- [16] D. Wang , J. Li, and G. Memik, "User identification based on finger vein patterns for consumer electronics devices", IEEE Transactions on Consumer Electronics, vol. 56, no. 2, pp. 799-804, 2010.
- [17] Nurhafizah Mahri, "Finger vein recognition algorithm using phase only correlation" IEEE, 2010.
- [18] M. Khalil-Hani and P.C. Eng., "FPGA-based embedded system implementation of finger vein biometrics" IEEE Symposium on Industrial Electronics and Applications, 2010.
- [19] Zhi Liu, Yilong Yin, Hongjun Wang, Shangling Song, Qingli Li, "Finger vein recognition with manifold learning" Journal of Network and Computer Applications 33, 275–282, 2010.
- [20] Rongyang Xiao, Gongping Yang, Yilong Yin, and Lu Yang, "A Novel Matching Strategy for Finger Vein Recognition" Springer-Verlag Berlin Heidelberg, pp. 364–371, 2013.
- [21] Mrunali jadhav, Priya M. RavaleNerkar, "A Biometric System for Person Authentication Based on Finger Vein Patterns on FPGA", International Journal of Advanced Research in Electrical, Electronics and Instrumentation Engineering, Vol. 4, Issue 6, June 2015.

EFFICIENT KEYWORD SEARCH ON LARGE RDF DATA USING OPTIMIZATION TECHNIQUE

Leya Zacharias¹, Neema George²

Department of Computer Science and Engineering, Mahatma Gandhi University, Mangalam College of Engineering, Kerala

Email id: leyaaza@yahoo.com

9496736469

Abstract- Now a day's keyword search in data mining is very emerging topic. Latest keyword search techniques on Semantic Web are moving away from shallow, information retrieval-style approaches that merely find "keyword matches" towards more interpretive approaches that attempt to induce structure from keyword queries. Exploiting identity links among RDF resources allows applications to efficiently integrate data. Keys can be very useful to discover these identity links. A set of properties is considered as a key when its values uniquely identify resources. However, these keys are usually not available. The approaches that attempt to automatically discover keys can easily be overwhelmed by the size of the data and require clean data. By using summarization algorithm the RDF data can be summarized. Here searching is done with optimization technique, so the result is accurate and efficient and also time complexity can be reduced. Unlike other techniques, our search algorithms always return correct results. For making the searching more efficient and get the accurate result within the time bound genetic algorithm is used.

Keywords— Keyword search, RDF data, Genetic algorithm.

INTRODUCTION

Data mining becomes an essential research area in the field of computer science, as it helps much more in keyword searching. In recent day's more and more data is provided in RDF format. Storing large amounts of RDF data and efficiently processing queries on these types of data is becoming very crucial. But it is not always necessary that they will provide the appropriate result that they are actually looking for. Now a day's more and more data is provided in RDF format, storing large amounts of RDF data and efficiently processing queries on such data is becoming crucial. But it is not always necessary that they get the appropriate result that they searching for.

The amount of data published on the Semantic Web has grown at increasing rates in the recent years. This is mainly happened due to the activities of the Linked Data community and the adoption of RDF by major web publishers. The number of data to be managed is stretching the scalability limitations of triple stores that are conventionally used to manage Semantic Web data. In the same time, the Semantic Web is increasingly reaching end users who need efficient and effective access to large subsets of this data. These type of end users prefer simple, but ambiguous natural language queries over highly selective, formal graph queries in SPARQL, the query language of triple stores. In a web search scenario, formulating SPARQL queries may not be feasible altogether due to the heterogeneity of data.

The RDF (Resource Description Framework) is the de-facto standard for data representation on the Web. It is no surprise that we are inundated with large amounts of rapidly growing RDF data from disparate domains. For example, the Linked Open Data (LOD) initiative integrates billions of entities from hundreds of sources. Just one of these sources, the DBpedia dataset, explains more than 3:64 million things using more than 1 billion RDF triples; and it contains numerous keywords. The Resource Description Framework (RDF) may be understood as a common purpose, schema-flexible model for explaining meta data and graph-shaped information. RDF represents information in the form of statements (triples or quads). Every triple connotes an edge between two nodes in a graph. The quad position can be used to give statements identity or to place statements within a named graph. RDF gives some basic concepts used to model information - statements are composed of a subject (a URI or a Blank Node), a predicate (always a URI), an object (a URI, Blank Node, or Literal value), and a context (a URI or a Blank Node). URIs are used to identity a particular resource, whereas Literal values describe constants such as character strings and may carry either a language code or data.

Keyword-based queries over semi-structured data are an important function of modern information management. When this information is available as Linked Data, it can be abstracted as a graph. Generally speaking, the end results of queries over this type of data are sub-structures of the graph that contain the keywords searched in the nodes. The task of indexing and finding the individual nodes containing those keywords is relatively inexpensive and has well-established tools available for it.

Ascertaining the connections between those selected nodes is a decomposable problem. This involves expensive and time-consuming graph explorations. More than that it must be solved on-the-fly at query processing time. The scale at which those interrogations must be solved grows as more and more data is made accessible to the Web of Data. Over and above that, to address the possibility of merging databases in the future, and to execute queries that include databases that had originally different schemes. Those queries must trust only on the most basic format of the Linked Data model, the subject-predicate-object format.

First and most important objective is to evidence the related work done in keyword search. This is worth noting that it does not aim at surveying this field. As an alternative, it aims at giving the full picture of the evolution of keyword searching, initiated by the field of IR, and then adopted by the fields of web and databases. This is how each field has contributed to each other and in keyword searching severally. This way, the demands and trends of each research period can be identified and assessed, together with the research problems that each area has faced. The very next objective of the dissertation is to advance the state-of-the-art research in keyword search over RDF data. To this goal, the contributions of this dissertation lay on the design, implementation, and evaluation of a system supporting keyword searching over RDF data. The third and endmost objective is to shed light on the evaluation of systems and techniques targeting at keyword search over structured and semi structured data. Keyword search provide only an approximate description of the information items to be retrieved. Hence, the correctness of the retrieval cannot be formally verified, as it is the case with query languages, such as SQL. Alternatively, retrieval effectiveness is measured by user perception and experience.

The efforts of this work are twofold:

1. Provide a mechanism to store sizable RDF graphs in a distributed way. we developed a mechanism that partition and summarize (shards) the RDF graph and persist data in separate, distributed data stores.
2. Provide a measurable keyword-based search mechanism for RDF graphs. We use optimization processing mechanism to provide a scalable result to the task of building keyword indexes for RDF datasets.

The rest of the paper is organized as follows: in Section 1, we describe the related works. In Section 2, we present the search using genetic algorithm. In Section 3, reports extensive experimental results to support the proposed searching using genetic algorithm. Finally, in Section 4, we summarize the present study and draw some conclusions.

I. RELATED WORK

Conventional keyword search engines are limited to a specific information model and cannot easily get used to unstructured, semi-structured or structured data. This paper projected an effective and merging keyword search method, called EASE[6], for indexing and querying large collections of heterogeneous data. To fulfill high efficiency in processing keyword queries, we first model unstructured, semi-structured and structured data as graphs. After that summarize the graphs and create graph indices as an alternative of using traditional inverted indices. This proposed an extensive inverted index to facilitate keyword-based search. After all this present a novel ranking mechanism for enhancing search effectiveness. It have conducted an extensive experimental study using real datasets. The final results show that EASE achieves both high search efficiency and high perfection, and outperforms the existing approaches drastically.

Query dispensation over graph-structured information is enjoying a growing number of applications. A top-k keyword search query on a graph and the top k answers according to some ranking criteria [2]. Here each answer is a substructure of the graph containing all query key-words. Present techniques for supporting such queries on general graphs suffer from several drawbacks. For example poor worst-case performance, not taking full benefit of indexes, and high memory requirements. To deal with these problems, it proposed BLINKS, a bi-level indexing and query processing scheme for top-k keyword search on graphs. BLINKS are follows a search strategy with provable performance bounds, while additionally exploiting a bi-level index for pruning and accelerating the search. To minimize the index space, BLINKS partitions a data graph into blocks: The bi level index stores summary information at the block level to initiate and guide search among blocks, and more detailed information for each block to accelerate search within blocks.

Applications in which bare text coexists with structured information are enveloping. Commercial relational database management systems (RDBMSs) generally provide querying capabilities for text attributes that incorporate state-of-the-art information retrieval (IR) relevance ranking strategies. But this search functionality requires that queries specify the exact column or columns against which a given list of keywords is to be matched [5]. This necessity can be cumbersome and unbendable from a user point of view. Perfect answers to a keyword query might require to be “assembled” –in perhaps unpredicted ways– by joining tuples from multiple relations. This inspection has stimulated recent research on free-form keyword search over RDBMSs. This paper adapts IR-style document-relevance ranking strategies to the problem of processing free-form keyword queries over RDBMSs. This query model can handle problems with both AND and OR semantics. The same exploits the sophisticated single-column text-search functionality often available in commercial RDBMSs. It develops query-processing measures that are constructed on a crucial characteristic of IR-style keyword search: only the few most relevant matches –according to some definition of “relevance”– are generally of interest. As a result, rather than computing all matches for a keyword query, which leads to inefficient executions, this techniques focus on the top-k matches for the query, for moderate values of k.

With the mounting volume of text information stored in relational databases, there is a huge demand for RDBMS to support keyword queries over text data [4]. As a search result this often assembled from multiple relational tables, traditional IR-style ranking and query evaluation methods cannot be applied directly. In this paper we will study the effectiveness and the efficiency issues of answering top-k keyword query in relational database systems. This will propose a latest ranking formula by adapting existing IR techniques based on a natural notion of virtual document. Compared with prior approaches, this new ranking method is very simple but effective. And all these agree with human perceptions. It studied effective query processing mechanism for the new ranking method, and propose algorithms that have minimal accesses to the database. It carried out extensive experiments on large-scale real data-bases using two popular RDBMSs. These results demonstrate strategic progress to the alternative approaches in terms of retrieval effectiveness and efficiency.

Design a scalable and exact solution that handles practical RDF data sets with tens of millions of triples. To address the scalability issues, our solution builds a new, succinct and efficient summary from the underlying RDF graph based on its types. Given a keyword search query, we use the outline [1] to prune the search space, leading to much better efficiency compared to a baseline solution. To sum up, our contributions we identify and address limitations in the existing, state-of-the-art methods for keyword search in RDF data. This shows that these limitations could lead to incomplete and incorrect answers in real RDF data sets. But we propose a new, correct baseline solution based on the backward search idea. Develop efficient algorithms to summarize the structure of RDF data, based on the types in RDF graphs, and use it to speed up the search is more scalable and lends significant pruning power without sacrificing the soundness of the result. The conclusion is light-weight and updatable. Also by applying optimization algorithm to the search result we will gain most appropriate and efficient result. Optimization here is check with genetic algorithm

Proposed algorithm

To find the keyword on large RDF first convert the RDF data set to RDF graph. Apply partitioning algorithm [1] and Summerization algorithm [1] to the RDF graph. By this result searching is done here searching is done with Genetic algorithm. By applying GA, result will be more perfect and also time complexity can be reduced.

Genetic algorithm is based on principles of development and natural selection. It is a search technique used in computing to find true or fairly accurate solutions to optimization and search problems. Genetic Algorithms are guided by analogy of natural behavior. They make use with a population of “individuals”, each representing a possible solution. The majority conferred individuals are given opportunities to “reproduce”, by “cross breeding” with other individuals in the population. The new generation thus produced contains mellower proportion of the description owned by the good members of former generations. The well projected GA will converge to optimal solution of the problem.

Parameters in Genetic Algorithm

There are many parameters to consider for the application of GA. Given below are certain parameters and methodology that are discussing

Representation of a Chromosome

A chromosome represent a path which includes the given search keyword.

Evaluation of fitness function

The fitness functions is the shortest path problem to find the weight of the path and thus find the shortest path.

Initialization

Initialization is the phase of genetic algorithm in which individual genomes are chosen from a large scale group for later breeding.

Crossover

The stage at which the chromosome is broken depends on the randomly selected crossover point. It is based on exchange between two fixed length chromosomes.

Mutation

When selection gets over and crossover, a new population full of individuals will emerge. This operator randomly alters genes to partially shift the search to new locations. Mutation also randomly selected operators are taken.

Selection

A practical variant of the genetic process of constructing a new population is to allow the best organism from the present generation to carry over the next, unaltered. This will make sure the quality of the genetic algorithm will not decrease from one generation to next. Individual solutions are selected through a *fitness-based* process. Most functions are stochastic and designed so that a small proportion of less weight solutions are selected.

Reproduction

The very next step is to generate a second generation population of solutions from those selected by way of genetic operators - crossover or mutation.

II. PSEUDO CODE

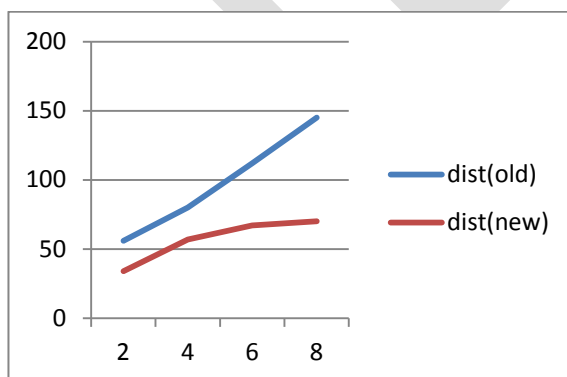
ALGORITHM

1. Initialization - Create an initial population. This population is usually randomly created and can be any desired size, from only a few individuals to thousands. Here the initial population is the number of nodes that matching the keyword and foaming a path with the keyword. All should be fully connected from that minimum path should considered as the best solution. Here fully connected best m solution is taken as the initial population.
2. Evaluation – Each and every member of the population is then evaluated and we calculate a 'fitness' for that individual. The fitness value is computed by how well it fits with our desired requirements. Here best is chosen with the best path that have the lesser weight, weight is calculated by $best = 7 * (m - (\text{number of selected nodes})) / m$, where m be the total number of solution
3. Selection - We want to be constantly improving our populations overall fitness. Selection helps us to do this by discarding the bad designs and only keeping the best individuals in the population. There are a few different selection process but the basic idea is the same, make it more likely that fitter individuals will be selected for our next generation. in the selection process 2m solution are generated, first m solution is copied from the initialization process, "for i=1 to m choose randomly selected two solution and find best in the two "these should be repeated for m times and thus 2m solution should be generated.
4. Crossover - During crossover we generate new individuals by combining aspects of our selected individuals. The hope is that by combining certain traits from two or more individuals we will create an even 'fitter' offspring which will inherit the best traits. In the crossover section first best m solution is chosen from the selection process, next m solution is generated by " for i=1 to m "choose randomly selected two solution apply a randomly selected crossover operation to the two solution and generate a new solution""
5. Mutation - We need to add a little bit randomness into our populations' genetics else every combination of solutions we can create would be in our initial population. Mutation typically works by making very small changes at random to an individual. In the mutation section first best m solution is chosen from the crossover process, next m solution is generated by " for i=1 to m "choose randomly selected two solution apply a randomly selected mutation operation to the two solution and generate a new solution""
6. And repeat! - Now we have our next generation we can start again from step two until we reach a best solution.

III. SIMULATION RESULTS

The section assess the performance of the proposed Searching in the RDF data using Genetic algorithm. Experiments are conducted on a desktop computer with Intel Core2 Duo Processor with Windows8 operating system along with 2GB RAM. The algorithms were introduced in java. MySQL is used as a backend. Any real life RDF datasets can be used for the experimental evaluations. The search result using genetic algorithm is compared with the old search algorithm result it shows that searching using genetic algorithm gives the most accurate result. Also compared with time complexity it also shows that the new one is taking lesser time with best results.

The figure shows the new one give the most perfect result compared to the old one, and also second figure shows time complexity regarding the new and old one. This shows the better performance.



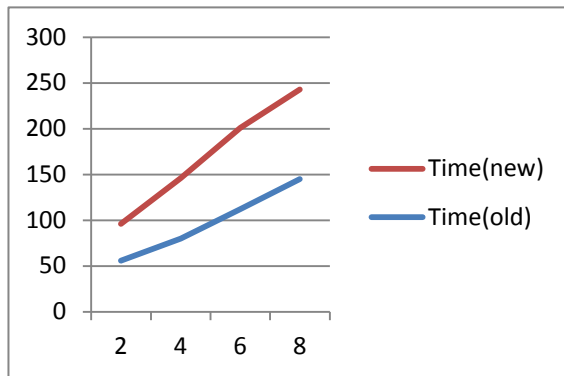


Fig : Performance Evaluation

IV. CONCLUSION

The most important research areas in data mining are searching in RDF data set which is useful in web search areas, which is important when considering to the semantic web concept. While using genetic algorithm for searching improves the searching quality and also better performance regarding to the old one. The main benefit and advantage of using genetic algorithm is it provides better accuracy and time complexity can be reduced compared to the old one. Keyword search now days we know the most important research area. The end results are analyzed based on the algorithm and dataset selected.

V. ACKNOWLEDGEMENT

The first author would like to thanks all those people, who guided and supported. Without their valuable guidance and support, this task was not possible and also likes to thank colleagues for their discussions and suggestions.

REFERENCES:

- [1] Wangchao Le, Feifei Li, AnastasiosKementsietsidis, and SongyunDuan, "Scalable Keyword Search on Large RDF Data" iee transactions on knowledge and data engineering, VOL. 26, NO. 11, NOVEMBER 2014
- [2] H. He, H. Wang, J. Yang, and P. S. Yu, "BLINKS: Ranked Keyword Searches on Graphs," in Proceedings of the 2007 ACM SIGMOD International Conference on Management of Data, ser. SIGMOD '07, June2007, pp. 305–316.
- [3] Y. Chen, W. Wang, Z. Liu, and X. Lin, "Keyword Search on Structured and Semi-Structured Data," Proc. ACM Int'l Conf. Management of Data (SIGMOD), 2009.
- [4] Y. Luo, W. Wang, and X. Lin, "SPARK: A Keyword Search Engine on Relational Databases," Proc. IEEE 24th Int'l Conf. Data Eng. (ICDE), 2008.
- [5] V. Hristidis, L. Gravano, and Y. Papakonstantinou, "Efficient IRStyle Keyword Search Over Relational Databases," Proc. 29th Int'l Conf. Very Large Data Bases (VLDB), 2003.
- [6] G. Li, B.C. Ooi, J. Feng, J. Wang, and L. Zhou, "Ease: Efficient and Adaptive keyword Search on Unstructured, Semi-structured and Structured Data," Proc. ACM SIGMOD Int'l Conf. Management of Data, 2008.
- [7] Y. Chen, W. Wang, and Z. Liu, "Keyword-Based Search and Exploration on Databases," Proc. 27th Int'l Conf. Data Eng. (ICDE), 2011.
- [8] A. Aggarwal and J.S. Vitter, "The Input/output Complexity of Sorting and Related Problems," Comm. ACM, vol. 31, no. 9, pp. 1116-1127, 1988.
- [9] G. Bhalotia, A. Hulgeri, C. Nakhe, S. Chakrabarti, and S.Sudarshan, "Keyword Searching and Browsing in Databases Using Banks," Proc. 18th Int'l Conf. Data Eng. (ICDE), 2002.
- [10] J. Broekstra et al., "Sesame: A Generic Architecture for Storing and Querying RDF and RDF Schema," Proc. First Int'l Semantic Web Conf. The Semantic Web (ISWC), 2002.
- [11] H. Fu and K. Anyanwu, "Effectively Interpreting Keyword Queries on RDF Databases with a Rear View," Proc. 10th Int'l Conf. Semantic Web (ISWC), 2011.
- [12] Y. Guo, Z. Pan, and J. Heflin, "LUBM: A benchmark for OWL Knowledge Base Systems," J. Web Semantics, vol. 3, pp. 158-182, 2005.
- [13] C. Weiss, P. Karras, and A. Bernstein, "Hexastore: Sextuple Indexing for Semantic Web Data Management," Proc. VLDB Endowment, vol. 1, pp. 1008-1019, 2008.
- [14] B.B. Dalvi, M. Kshirsagar, and S. Sudarshan, "Keyword Search on External Memory Data Graphs," Proc. VLDB Endowment, vol. 1, pp. 1189-1204, 2008

CASE STUDY ON LIVE STREAMING SOCIAL MEDIA DATA INTO SAP HANA PERFORM TEXT ANALYSIS AND CLUSTERING

Thakur Navneetha Singh (M.tech Scholar)

Vasavi college of Engineering, t.neetusingh@gmail.com

Abstract— The main objective of this project is to feed the real-time data feeds from social media (twitter) and this data then can be used to perform the text analytics for sentiment analysis and as well as perform Segmentation using SAP HANA clustering. In this case study I am going to focus on how to access real-time social media information using Twitter. Based on our interested trend that we want to analyze , we pull out the specific tweets in real-time using Twitter API, then process and loaded this data into a SAP HANA database. To talk with the Twitter API and load the data into SAP HANA , We can make use node.js which is a free open source Google Chrome run-time. Here In this case study i have used SAP HANA instance hosted in cloud but one can also use the SAP HANA database will be hosted on the developer trail edition of the SAP HANA Cloud Platform. This project is done by using SAP HANA (in memory database platform) and Its Predictive Analysis Library algorithms in a practical approach. Once the data has been loaded we will perform further analysis. Sentiment Analysis is performed by finding whether people are tweeting positive or negative statements. Then different types of tweeters can then be grouped and segmented by estimating the influence of tweeter using the Predictive Analysis Library. For example, we can determine who is influential due to a high number of followers and re-tweets and then group the influential tweeters who are expressing negative thoughts about a product together. We can then target that group with an educational outreach program. But as a case study here I am not going to focus on a particular product because its upto the user requirement who want to focus on which kind of data from social media. So here as I am just focusing on how to feed the real-time data feeds from social media (twitter) and how this data , then can be used to perform the text analytics for sentiment analysis and as well as Segmentation using SAP HANA clustering as an example I focus on tweets related to entrepreneur 2015.

Keywords— Live Streaming , Twitter Streaming, real-time data , SAP HANA, Sentiment Analysis, Clustering, Automated Predictive Library, PAL - Predictive Analysis Library.

INTRODUCTION

I am going to access some real time social media information (example twitter) so we are going to get information on specific tweets that we want to look for and pull those out in real time from twitter API, Process those tweets and load that tweets in real time to HANA database.

HANA database will be hosted on cloud platform in Linux SUSE or trial HANA cloud platform Developer edition can be used by registering for it. Then once we load data in HANA database we can do further analysis on it say for example sentiment analysis to understand what people are saying, liking or not liking whatever product or service tweets that we want to analyze. Then we may want to segment or group different types of persons (twitter users) based on their tweets. There may be people who may be saying many negative things about the products or service and there may be some influential since lot of people may follow and retweets , we then target such people take decision accordingly educate them etc. So we do some predictive analysis in order to segment groups sending similar kinds of tweets together by using SAP Predictive Analytics Library.

We can connect to SAP HANA Database hosted in cloud through eclipse IDE where we install and configure SAP HANA studio. Then using this HANA studio we access HANA database and do operations required such as SQL operation or modeling etc using SQL editor from HANA studio.

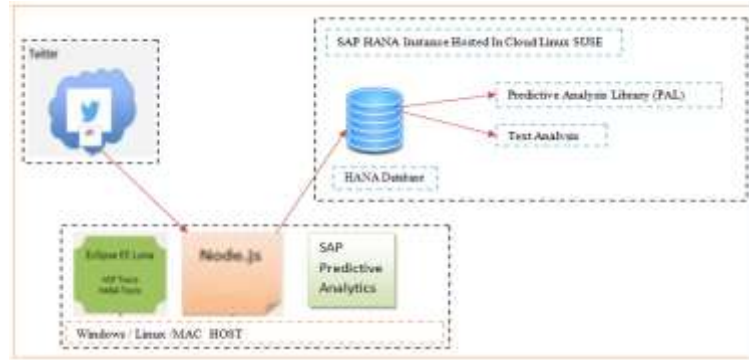


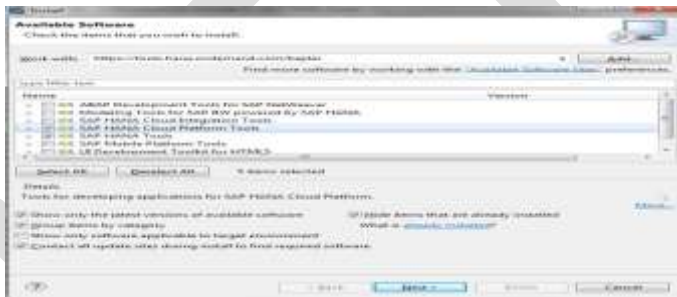
fig: Architecture of Live Streaming into SAP HANA

PROCEDURE TO PERFORM REAL TIME DATA LOAD INTO SAP HANA

Prior to start with the this case study of loading data into SAP HANA one should installed HANA database in LINUX SUSE or Register at hanatrial.ondemand.com for the trial HANA cloud platform for developer and create HANA XS instance. Once on successful hosting of HANA Database follow the below steps to load data in to sap hana in real time from social media:

STEP 1: INSTALL SAP HANA CLOUD PLATFORM TOOLS

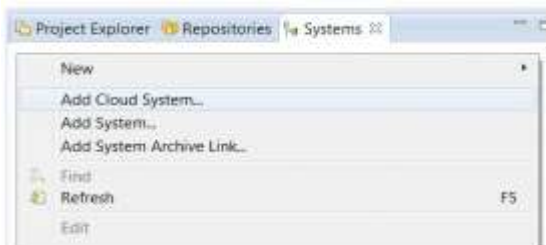
1. Open HANA Studio i.e Eclipse IDE.
2. Go to Help - Install New Software
3. Depending on Eclipse version, enter one of the following URLs:
For Eclipse Kepler (4.3) - <https://tools.hana.ondemand.com/kepler>
For Eclipse Luna (4.4) - <https://tools.hana.ondemand.com/luna>
4. Select "SAP HANA Tools" and "SAP HANA Cloud Platform Tools".



5. Click Next...Next and finally Finish. You will need to restart the HANA Studio.

STEP 2: CONNECT TO HANA INSTANCE FROM HANA STUDIO

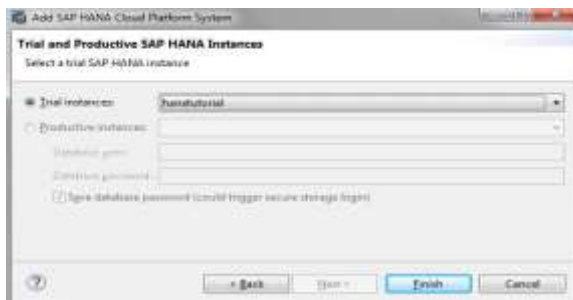
1. Open HANA Studio.
2. In System view, right click and select "Add Cloud System".



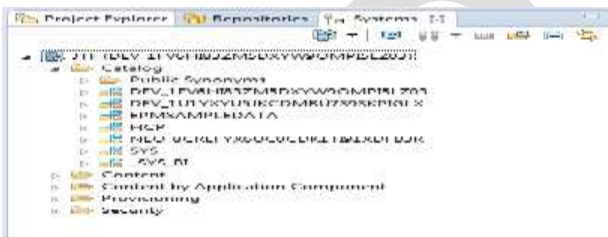
3. Enter Account Name, User Name and Password. To know more about Account Name and User Name, refer to the article [Free Access to SAP HANA Cloud](#) a Account Dashboard



4. Select the HANA Instance that you have created in step [Free Access to SAP HANA Cloud](#) à Create a trial SAP HANA Instance.



5. Click on Finish and HANA Cloud system will be added.



STEP 3: REGISTER AT TWITTER

We can find the information about the twitter steaming API's under documentation at <https://dev.twitter.com>.



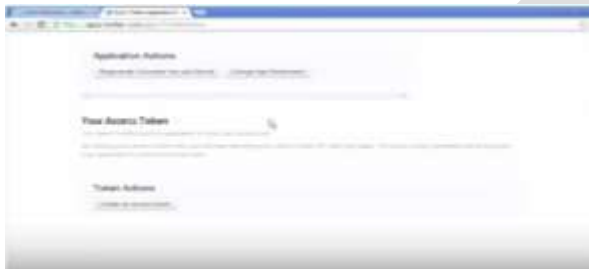
If you don't already have an account then register at twitter i.e apps.twitter.com where we get the following keys using which we can connect to twitter and fetch data:



Click on Create New App and fill the application details and accept the agreement and hit create application. Once the application is created then you will find the page as below, note down the consumer key you see under application settings.



Click on Keys And Access Tokens tabs , scroll down and click create my access token button.



Now **get Access Token**: This access token can be used to make API requests on your own account's behalf. Do not share your access token secret with anyone.

- Access Token , Access Token Secret , Access Level Read and write and Owner

Note down all the keys under application settings and access token.

STEP 4: CREATE TABLE DEFINITION IN SAP HANA

Create Table in HANA where you want to store the data that we capture from live streaming using the sql command as shown below:

```
--EntrepreneurTweets--
CREATE COLUMN TABLE "Entrepreneur2015Tweets" (
  "id" VARCHAR(256) NOT NULL,
  "created" TIMESTAMP,
  "text" NVARCHAR(256),
  "lang" VARCHAR(256),
  "user" VARCHAR(256),
  "replyUser" VARCHAR(256),
  "retweetedUser" VARCHAR(256),
  "lat" DOUBLE,
  "lon" DOUBLE,
  PRIMARY KEY ("id")
);
```

STEP 5: DOWNLOAD NODE.JS

Download the node.js from the this location <https://github.com/saphanaacademy/Live3HCP>.

STEP 6: SETUP NODE.JS

1. In browser enter <https://nodejs.org>.
2. Click on install and follow the steps as shown in below screen shots.

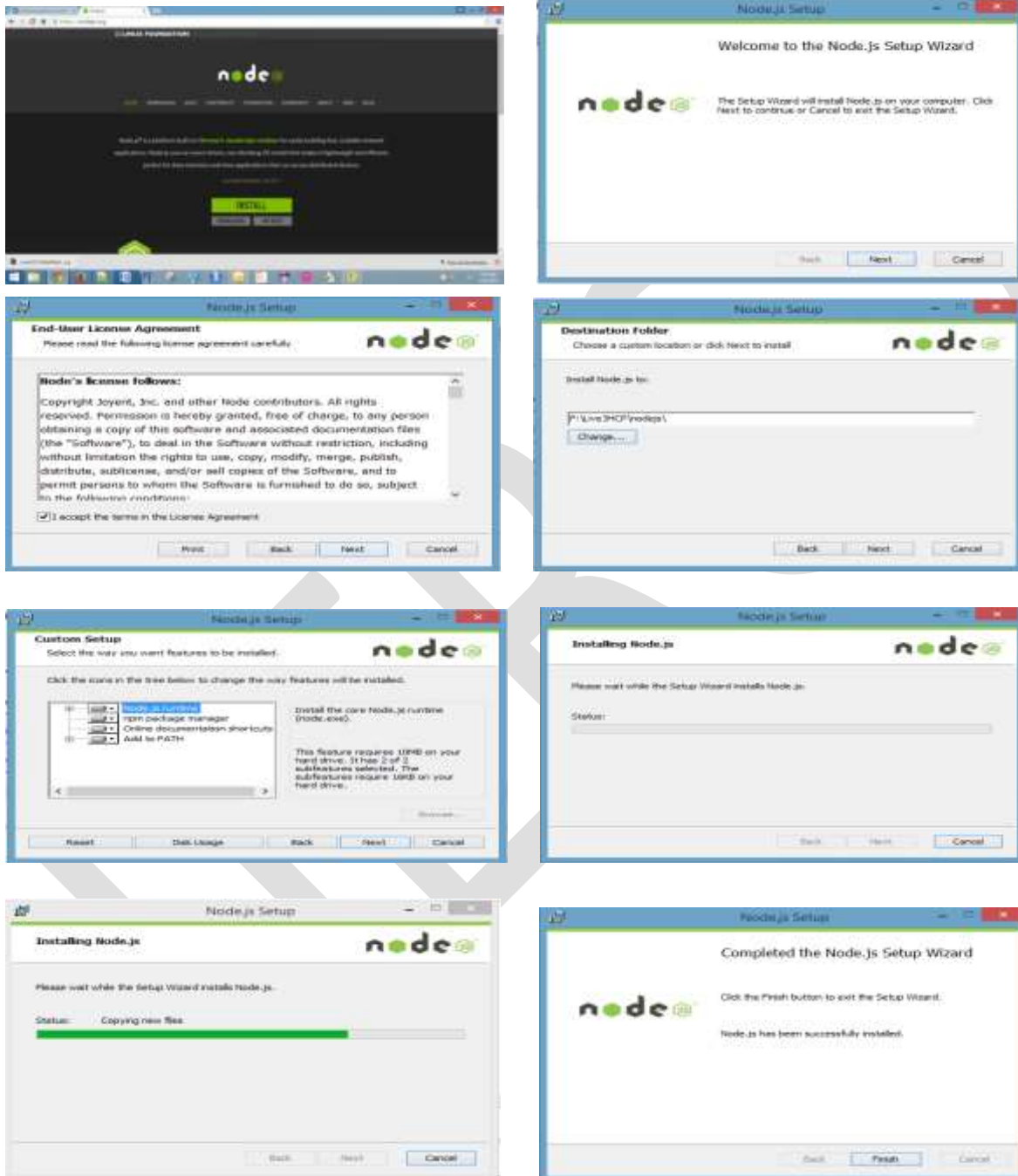


fig: representing different screenshots of node.js installation process

To test that node.js is install properly enter : `node -v` in command prompt

Open a web browser (Chrome in Philip's demonstration) and navigate to the application by entering localhost:8888 (port number). "Cannot GET/" will be displayed because we didn't specify a URL. Entering localhost:8888/do/start will display "Nothing to track" as we have yet to specify what we want to track. To track anything you want on Twitter (e.g. company name, product, service) enter **localhost:8888/do/start?track=entrepreneur2015** (here instead of entrepreneur2015 mention the keyword that you wish to track)



fig : Start application

Once app started: we can see trace of records or tweets that got inserted in tweets table in command prompt.

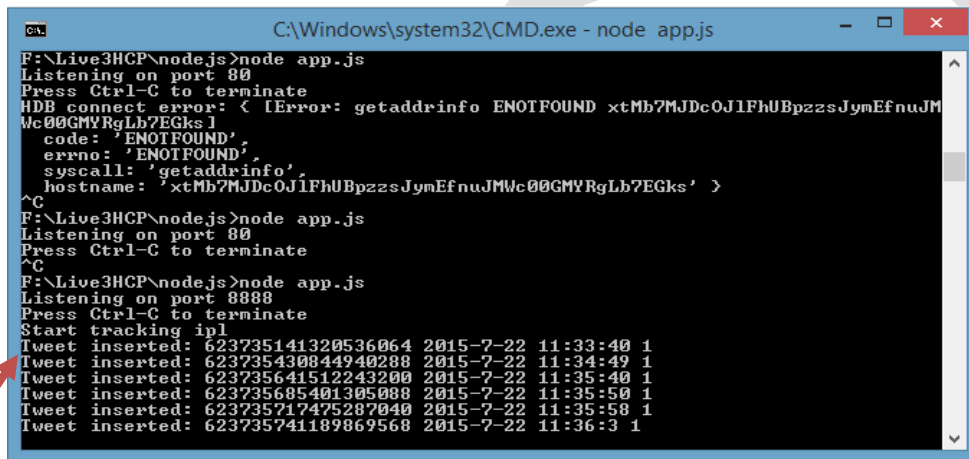


fig: real-time tweets fetching and loading in HANA table

STEP 10: CHECK THE DATA LOAD INTO HANA TABLE CREATED IN STEP 2

Now go to hana studio and check that the table that we create in step 2 i.e tweets get loaded with the data. In HANA Studio Right click on the tweets table and click data preview (or) from sql editor run the select command as : **SELECT * FROM TWEETS;**

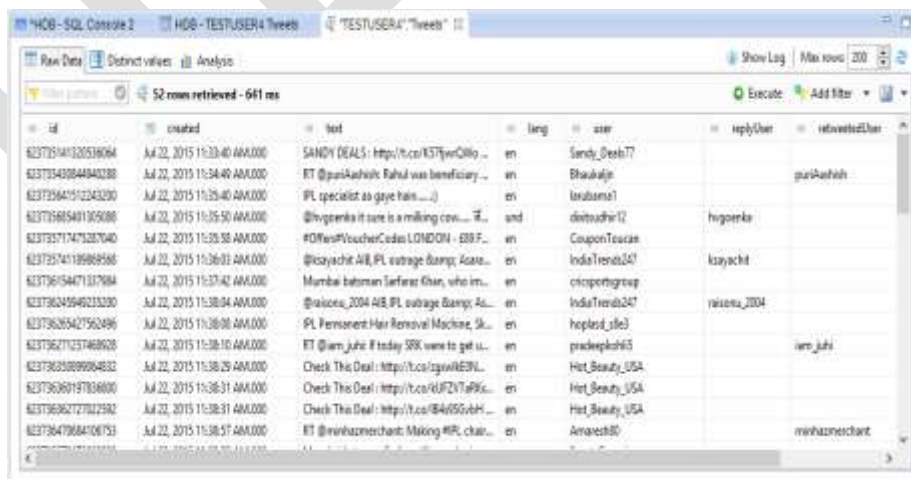


fig: Tweets Data Populated in HANA Table.

STEP 11: STOP APPLICATION

Unless we stop the application tweets will be loaded in real-time from twitter to tweets table in HANA. So in order to stop streaming the data we need to stop the application then only it stops loading data in tweets table in HANA. To stop application in the web browser if you enter **localhost:8888/do/stop** then no more Tweets will be loaded into SAP HANA.



fig : Stop application

STEP 12: PERFORM TEXT ANALYSIS FOR SENTIMENT ANALYSIS

Performing Text analysis SAP HANA allow us to identify the sentiment of persons sending tweets - for example strong positive, weak positive, weak negative, or strong negative sentiment. As we have loaded real-time Twitter data into our SAP HANA table we can view the actual text of each individual tweet. Now from sql editor of hana studio create Text Index using below code and make sure that you set the proper schema in your current session. To set schema set schema name.

```
-- CREATE TEXT ANALYSIS INDEX ON EntrepreneurTweets--  
CREATE FULLTEXT INDEX "Entrepreneur2015tweets" ON "Entrepreneur2015Tweets"("text")  
    CONFIGURATION 'EXTRACTION_CORE_VOICEOFCUSTOMER'  
    LANGUAGE COLUMN "lang"  
    LANGUAGE DETECTION ('EN', 'FR', 'DE', 'ES', 'ZH')  
    TEXT ANALYSIS ON  
    ;
```

The above code will create a full Text Index on the text column of the Tweets table. The index will be called tweets. A configuration will be set to extract the core voice of customer for the sentiment analysis part of the text analysis. The SQL specifies the language of each Tweet via the Language column of the Tweets table and also determines what languages we will do the sentiment analysis on. Sentiment analysis can be done on Tweets in the following languages English, German, French, Spanish, and Chinese. The final line of code actually turns on the text analysis. Highlight the code and click the run button to execute it. Now for all of the available data as well as for any new rows that are added in HANA table Tweets, a new table will be created automatically that will be logically seen as an index.

Overview of \$TA_Tweets Text Index: Newly created text index called \$TA_Tweets will appear in list of tables. To preview the data right click on the \$TA_Tweets table and select data preview we will see some important columns. These include TA_RULE, a column that confirms that entity extraction is occurring. The TA_TOKEN lists the piece of information that the text analysis is performed on. TA_TYPE shows what type of text analysis is it and what has been extracted. Examples include location, social media and sentiment. The text index determines the five types of sentiment a Tweet can have. For example the word "Grand" is determined to be strong positive sentiment and "Disappointed" is determined to be weak negative sentiment. Some words are labeled ambiguous and could be considered profane such as "loser."

STEP 13: CALCULATE AND CREATE INFLUENCE AND STANCE VIEW IN HANA STUDIO

This section explains how to create a view that contains scoring for each Twitter user based on their influence and stance (attitude).

Twitter Influence Index :The influence score reflects a Tweeter’s influence based on the number of retweets and replies their Tweets have garnered.Tweets table notes the Twitter handles of users who have retweeted and replied to each individual Tweet. People are considered more influential if their Tweets are replied to and retweeted than if they are the ones who retweet and reply to others’ Tweets. Taking the total number of Tweets that you retweet and reply to and subtracting it from the total amount your personal Tweets have been retweet and replied to gives a numeric index reflecting your individual Twitter influence.

Twitter Influence = (# of times your Tweets that have been retweeted + # of times your Tweets that have been replied to) - (# of Tweets you’ve retweeted + # of Tweet you’ve replied to)

Establish a User’s Stance: Stance is based on sentiment analysis. Open the \$TA_Tweets table created in the prior. Open the Analysis tab and left click on the TA_TYPE in the String folder and choose to add it as a filter. Choose to filter on Strong Positive Sentiment.

Drag TA_TOKEN as the Labels axis and id(Count) as the Values axis. Then choose Tag Cloud as your Analytic and you will get an indication of what words are used to represent Strong Positive sentiment. We can also choose Weak Positive, Weak Negative, and Strong Negative as TA_TYPE to see the words that are classified as those particular sentiments.

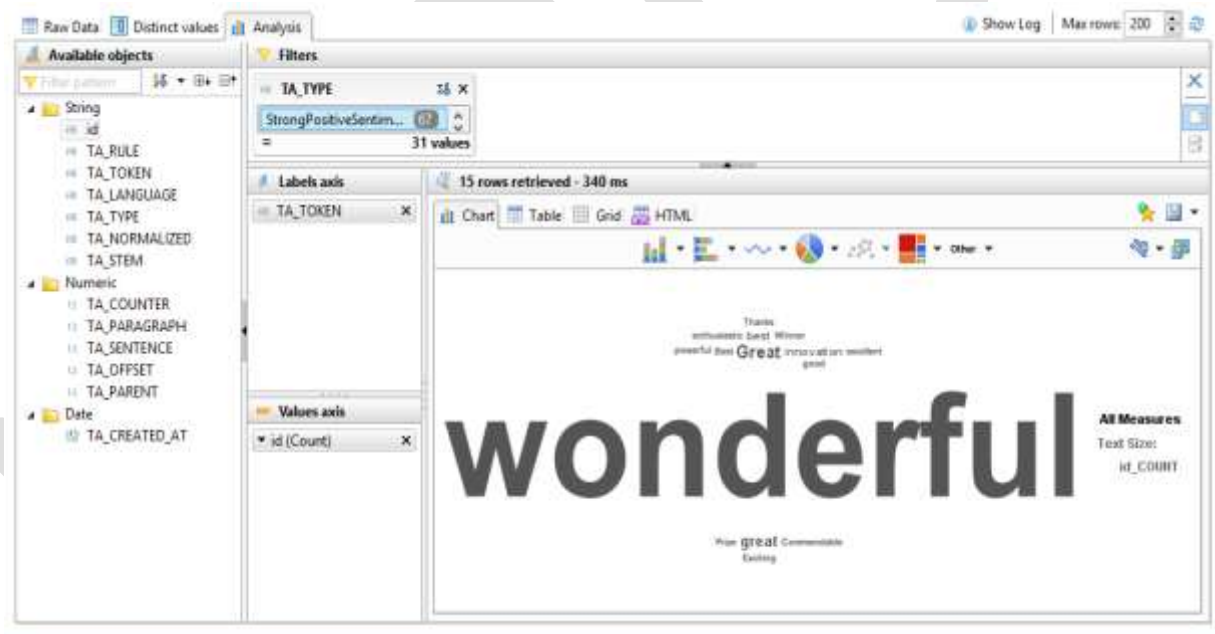


fig :Text Analysis Results

So we can add up the occurrence of the words categorized into the different sentiments for a particular user, assign those sentiment categories particular numeric values and then subtract the weak total from the strong total to get an overall indicator of a user’s stance (attitude).

Overview of SQL View Code – Influence Score

This code will create a view that will process the influence and stance calculations described above. To showcase part of the code Philip runs the four lines before the last of code (see below). Running that returns a count of the number of retweets each Tweeter has.

```
54 LEFT JOIN (  
55 SELECT "user", COUNT(*) AS RSC  
56 FROM "Tweets"  
57 WHERE "replyUser" != ''  
58 GROUP BY "user"  
59 ) rsc ON rsc."user" = t."user"  
60 LEFT JOIN (  
61 SELECT "user", COUNT(*) AS RTSC  
62 FROM "Tweets"  
63 WHERE "retweetedUser" != ''  
64 GROUP BY "user"  
65 ) rtsc ON rtsc."user" = t."user"  
66  
67
```

The section of code of above this highlighted part counts the number of replies in a similar manner. Both parts of this code are straight forward SQL select group bys. This SQL only looks at data within the time that it has been collected. The code also looks at the number times a user has been retweeted and the number of replies. So we must run these four subqueries and join the results together. We need to ensure that we capture all of the user because many user may not have preformed one of those four Twitter actions.

At the top of the code, the case statement will determine the influence score by adding together the number of received retweet (if retweets is missing then it's set to zero so propagation of missing values isn't returned) and replies and then subtracting the number of sent retweets and replies. Using a select from distinct will ensure we capture all of the Tweepers irrespective if they have used retweets or replies.

```
6 -- CREATE TWEETERS VIEW WITH INFLUENCE & STANCE SCORES  
7 CREATE VIEW "Tweepers" AS  
8 SELECT t."user",  
9 CAST(  
10 (CASE WHEN SP IS NULL THEN 0 ELSE SP * 5 END)  
11 + (CASE WHEN WP IS NULL THEN 0 ELSE WP * 2 END)  
12 - (CASE WHEN WN IS NULL THEN 0 ELSE WN * 2 END)  
13 - (CASE WHEN SN IS NULL THEN 0 ELSE SN * 5 END)  
14 AS INT) AS "stance",  
15 CAST(  
16 ((CASE WHEN RRC IS NULL THEN 0 ELSE RRC END) + (CASE WHEN RTRC IS NULL THEN 0 ELSE RTRC END)  
17 - ((CASE WHEN RBC IS NULL THEN 0 ELSE RBC END) + (CASE WHEN RTSC IS NULL THEN 0 ELSE RTSC EN  
18 AS INT) AS "influence"  
19 FROM (SELECT DISTINCT "user" FROM "Tweets") t
```

Overview of SQL View Code – Stance Score

For the stance we will run a query that will pull out the number of StrongPositive, WeakPositive, StrongNegative and WeakNegative sentiments tweeted by an individual user. Instead of having a row for each sentiment per user we transpose that data into four individual columns for each user.

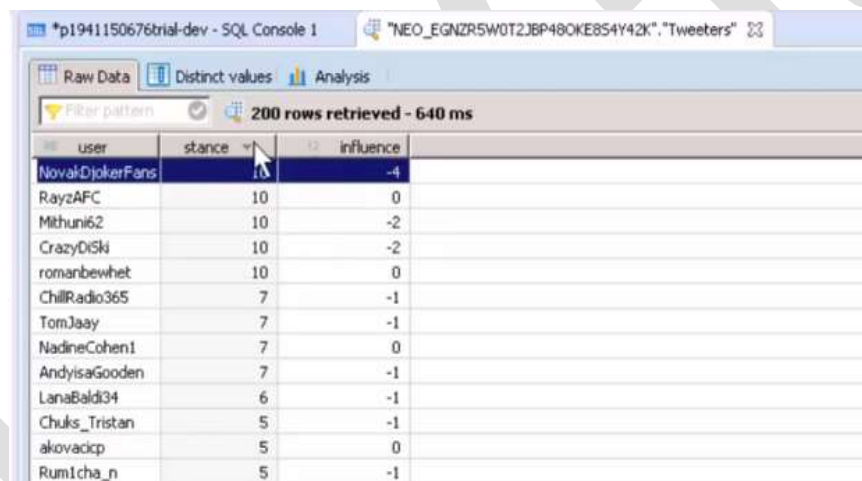
```
23 LEFT JOIN (  
24 SELECT "id",  
25 SUM(CASE TA_TYPE WHEN 'StrongPositiveSentiment' THEN "total" END) AS SP,  
26 SUM(CASE TA_TYPE WHEN 'WeakPositiveSentiment' THEN "total" END) AS WP,  
27 SUM(CASE TA_TYPE WHEN 'WeakNegativeSentiment' THEN "total" END) AS WN,  
28 SUM(CASE TA_TYPE WHEN 'StrongNegativeSentiment' THEN "total" END) AS SN  
29 FROM (  
30 SELECT "id", TA_TYPE, COUNT(*) AS "total"  
31 FROM "TA_tweets"  
32 WHERE TA_TYPE = 'StrongPositiveSentiment' OR  
33 TA_TYPE = 'WeakPositiveSentiment' OR  
34 TA_TYPE = 'WeakNegativeSentiment' OR  
35 TA_TYPE = 'StrongNegativeSentiment'  
36 GROUP BY "id", TA_TYPE  
37 )  
38 GROUP BY "id"  
39 ) i ON t."id" = i."id"  
40 GROUP BY "user"
```

Finally we will join that data together and apply a stance ratio. We have given Strong Positive a score of 5, Weak Positive a score of 2, Weak Negative a score of 2, and Strong Negative a score of 5. We will add up those scores and then subtract the overall negative value from the overall positive value to get a stance score.

```
8 SELECT t."user",
9 CAST (
10 (CASE WHEN SP IS NULL THEN 0 ELSE SP * 5 END)
11 + (CASE WHEN WP IS NULL THEN 0 ELSE WP * 2 END)
12 - (CASE WHEN WN IS NULL THEN 0 ELSE WN * 2 END)
13 - (CASE WHEN SN IS NULL THEN 0 ELSE SN * 5 END)
14 AS INT) AS "stance",
```

Running the Code to Create the Stance and Influence View

Newly created Tweepers view appear in the list of views right click on the Tweepers view and select data preview .Then we can see the data containing three columns user stance and influence score for every Tweeter. For example a user could have a very positive stance but a very low influencer score. This information is incredibly useful as we can now group together users with similar influences and stances.



user	stance	influence
NovakDjokerFans	10	-4
RayzAFC	10	0
Mithun62	10	-2
CrazyDiSkI	10	-2
romanbewhet	10	0
ChillRadio365	7	-1
TomJaay	7	-1
NadineCohen1	7	0
AndyisaGooden	7	-1
LanaBald34	6	-1
Chuks_Tristan	5	-1
akovadicip	5	0
RumIcha_n	5	-1

fig: User influence and stance

STEP 14: PERFORM SEGMENTATION

This section explains how the SAP HANA predictive analysis library (PAL) can be used to cluster similar Tweepers together based on their influence and stance scores.

Reading through the SAP HANA PAL documentation is vital for getting a full understanding of the myriad capabilities PAL offers. PAL is embedded data mining algorithms in the SAP HANA engine (where the data actually resides).Back in Eclipse do a data preview on the Tweepers table we just created. This Tweepers table will be the input table for the predictive analysis. Our id will be the Twitter users' handles and our inputs will be the stance and influence scores. Here i have used k-means clustering algorithm of PAL to perform segmentation.

Running the Code and Examining the Tables : To actually run the clustering is rather simple. First the results tables must be empty and then the stored procedure must be called. The input table/view is the Twitter view, which will send real-time data straight into the

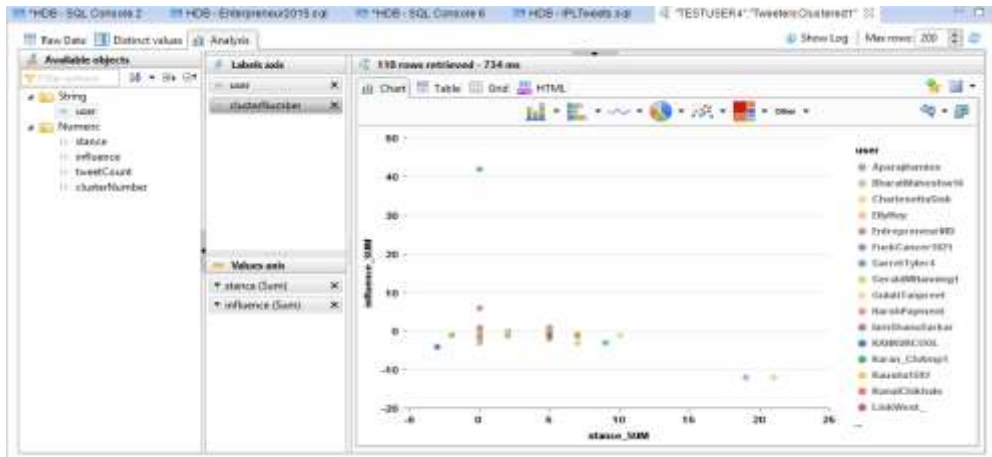


fig: User segmentation results

COMPLETE PAL PROCEDURE CODE TO PERFORM SEGEMENTATION USING K-MEANS

```
CALL"SYS".AFLLANG_WRAPPER_PROCEDURE_DROP('TESTUSER4', 'ENTERPRENEUR_CLUSTER_PROCEDURE');
CALL"SYS".AFLLANG_WRAPPER_PROCEDURE_CREATE('AFLPAL', 'KMEANS', 'TESTUSER4', 'ENTERPRENEUR_CLUSTER_PROCEDURE', PAL_SIGNATURE_TBL);
```

---TESTING---

- **CREATE PARAMETER TABLE**

```
CREATE COLUMN TABLE PAL_PARAMS1 LIKE PAL_T_PARAMS1;
INSERT INTO PAL_PARAMS1 VALUES ('THREAD_NUMBER', 2, null, null);
INSERT INTO PAL_PARAMS1 VALUES ('GROUP_NUMBER_MIN', 3, null, null);
INSERT INTO PAL_PARAMS1 VALUES ('GROUP_NUMBER_MAX', 6, null, null);
INSERT INTO PAL_PARAMS1 VALUES ('INIT_TYPE', 4, null, null);
INSERT INTO PAL_PARAMS1 VALUES ('DISTANCE_LEVEL', 2, null, null);
INSERT INTO PAL_PARAMS1 VALUES ('MAX_ITERATION', 100, null, null);
INSERT INTO PAL_PARAMS1 VALUES ('EXIT_THRESHOLD', null, 1.0E-6, null);
INSERT INTO PAL_PARAMS1 VALUES ('NORMALIZATION', 0, null, null);
```

- **CREATE OUTPUT TABLES**

```
CREATE COLUMN TABLE PAL_RESULTS1 LIKE PAL_T_RESULTS1;
CREATE COLUMN TABLE PAL_CENTERS1 LIKE PAL_T_CENTERS1;
```

- **CREATE VIEWS FOR ODATA**

```
CREATE VIEW "TweetersClustered" AS
SELECT s.*, t."tweetCount", c."clusterNumber" + 1 AS "clusterNumber" FROM "EntrepreneurTweeters" s INNER JOIN (
```

```
SELECT "user", COUNT(*) AS "tweetCount"  
FROM "Entrepreneur2015Tweets" GROUP BY "user") t ON t."user" = s."user" INNER JOIN "PAL_RESULTS1" c ON  
c."user" = s."user" ;
```

```
CREATE VIEW "CLUSTERS1" AS SELECT c."CLUSTERNUMBER" + 1 AS "CLUSTERNUMBER", c."STANCE", c."INFLUENCE",  
T."USERS"
```

```
FROM "PAL_CENTERS1" c INNER JOIN ( SELECT "clusterNumber", COUNT(*) as "users" FROM "PAL_RESULTS1"  
GROUP BY "clusterNumber" ) t ON t."clusterNumber" = c."clusterNumber";
```

- **RUNTIME CALL THE PAL PROCEDURE CREATED**

```
TRUNCATE TABLE PAL_RESULTS1;  
TRUNCATE TABLE PAL_CENTERS1;
```

```
CALLTESTUSER4."ENTERPRENEUR_CLUSTER_PROCEDURE"("EntrepreneurTweeters",PAL_PARAMS1,  
PAL_RESULTS1, PAL_CENTERS1) WITH OVERVIEW;
```

CONCLUSION

We can make use of the power of in memory database HANA and can perform predictive analysis to take business decisions using the APL library of HANA or we can also use SAP Predictive Analytics software. This was just a sample case study explaining how live Streaming data from social sites to HANA can be performed and depending on our business requirements we can perform the analysis accordingly.

REFERENCES:

- [1] <http://saphanatutorial.com/>
- [2] http://help.sap.com/hana/sap_hana_studio_installation_update_guide_en.pdf
- [2] <http://scn.sap.com/community/predictive-analytics/blog/2015/03/02/what-is-the-sap-automated-predictive-library-apl-for-sap-hana>
- [3] <http://scn.sap.com/community/hana-in-memory/blog/2015/02/19/how-to-install-the-automated-predictive-library-in-sap-hana>
- [4] <http://scn.sap.com/community/hana-in-memory/blog/2015/03/17/introducing-the-sap-automated-predictive-library>
- [5] https://help.sap.com/hana/SAP_HANA_Predictive_Analysis_Library_PAL_en.pdf
- [6] <http://scn.sap.com/community/hana-in-memory/blog/2015/03/17/introducing-the-sap-automated-predictive-library>
- [7] <http://scn.sap.com/docs/DOC-59928>
- [8] <http://scn.sap.com/community/predictive-analytics/blog/2015/03/02/what-is-the-sap-automated-predictive-library-apl-for-sap-hana>
- [9] https://hcp.sap.com/content/dam/website/saphana/en_us/Technology%20Documents/SPS09/SAP%20HANA%20SPS%2009%20-%20Smart%20Data%20Streaming.pdf

[10] <http://saphanatutorial.com/sap-hana-text-analysis-using-twitter-data/>

[11] <http://scn.sap.com/community/developer-center/hana/blog/2015/04/09/text-analysis-in-sap-hana-integrate-with-twitter-api>

[12] <https://scn.sap.com/thread/3495915>

[13] <http://scn.sap.com/community/developer-center/hana/blog/2014/09/10/sap-hana-twitter--find-your-leads>

[14] https://hcp.sap.com/content/dam/website/saphana/en_us/Technology%20Documents/SPS09/SAP%20HANA%20SPS%2009%20-%20Smart%20Data%20Streaming.pdf

[15] <http://scn.sap.com/community/developer-center/cloud-platform/blog/2015/02/06/live3--sap-hana-cloud-platform-tutorials-for-advanced-real-time-social-media-analytics>

Ergonomic Bicycle for Ladies

Asso. Prof. Pradeep M. Ingole^[1], Dr. Ajay U. Awate^[2], Mukund Manas^[3]

Associate Professor, PRMITR, Badnera^[1]

Professor, PRMITR, Badnera,^[2]

Assistant Professor, KJCOEM, Pune.^[3]

Mob. no.: +91-08793604439

E-mail_id: mukund.manas@gmail.com

Abstract— Proper fit is vital for cycling performance, efficiency, comfort and injury prevention. Study reveals that bicycle is generally male favored. It struggles in popularity with females despite the fact that cycling is a good exercise. There is a small but significant difference between male and female anatomy. Due to so, they have different requirements, taste, specifications than the males. This paper emphasizes principal difference between male and female anatomy. It highlights the basic physiological factors, differences of females and their comfort during cycling. Thus, proposing brief study on “The Ergonomic bicycle for Ladies”, taking into account their peculiar anatomy. Here, we are introducing conceptual, new anthropometrically designed seat, frame, handle, tires etc. in bicycle to make it popular for the gender. Hence, an attempt has been made to make cycling more comfortable and popular.

Keywords— Anatomy, pelvis, saddle, anthropometry, hip, stem, Ergonomics, comfort, androgynous, silhouette, Dutch type

Posture, Tracking type cycling posture.

INTRODUCTION

Bicycle is a pedal driven, human- powered vehicle with two wheels attached to a frame, one behind the other. It has evolved significantly in this technological era. Comfort, a combination of physical and psychological factors, is now a dominating issue in design. It is still the best means for transportation. A surprising issue has been observed in case of cycling. All teenagers around eleven years use bicycle. There is no real issue of gender. But as we proceed from eleven to nineteen years and further, female cyclist decrease sharply to almost zero percentage. Particularly in India, a women (age above 23 years above) is hardly seen on bicycle. So concentrating on the phenomenon we are highlighting the proper reasoning behind the problem. Here, evaluating modifications to make bicycle more popular among ladies. Incorporating these points and redesigning bicycle for females. In the article below, we define these aspects one by one.

DIFFERENCE BETWEEN MALE AND FEMALE ANATOMY

The bicycle available is designed on the basis of human anatomy dominated by the male perception. However, the anatomy of female changes slowly and drastically from twelve years. It is this time that female organ starts to develop. This anatomy is the characteristics of the female which is distinctly different from males. Due to these changes their requirement as per their anthropometry, changes from the males. Hence the designed cycle is less comfortable for the female gender. As a result, cycling is less popular in them, despite the fact that cycling is a good exercise.

The other side of the coin is that the female anatomy can range all the way from the marked characters of female to the androgynous figure (does not strongly show in male and female direction).

Male and Female anatomy are seldom so different that even a skeleton (or certain parts of it) betrays their sex.

On a vertical axis there is no real difference. Other than height proportion, joints don't move up or down. The variations are almost entirely on the horizontal axis, i.e. in width of certain parts of the body. Below, designates the various differences between male and female anthropometry.

1. Hip and Shoulders

Most and foremost is the shoulder, Hips and the hip to shoulder ratio. So as to sustain fetus during pregnancy the women has broader Pelvis bone than men. Secondly, there is development and projection of the mammary gland or the female breast.

These two adjustment effect is seen on the entire female body abdomen. As a result, in women, hip is the broadest part and then the chest. This is shown in the figure:-1.1(a) and Figure:-. 1.1 (b). So, female silhouette is broader at the shoulder, narrow at the waist and broadest at the Thighs, giving an hourglass figure as shown in figure: - 1.1(a) and (b).This projections are seen in the width as well. Their breast and buttock tends to bulge outwards as shown in the figure: - 1.1(a)

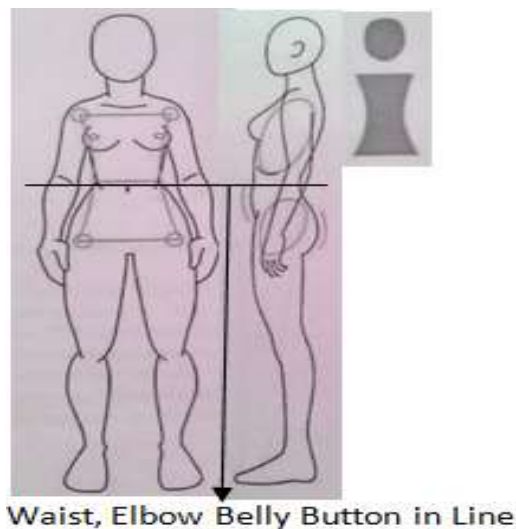


Figure: - 1.1(a) Female body domain

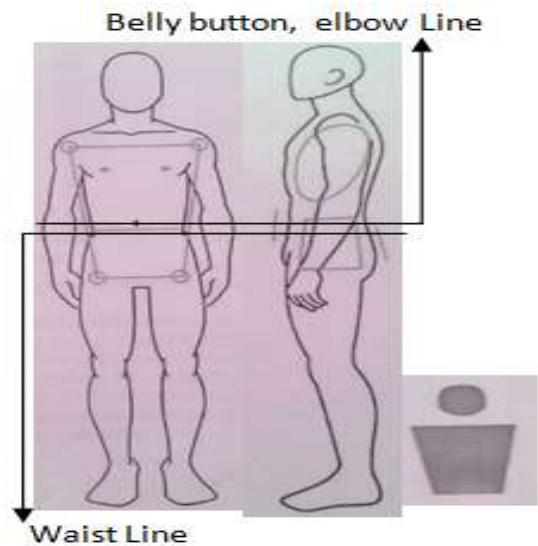


Figure: - 1.1(b) Male body domain

For males, the broadest part is shoulder and its slants linearly, as we descend towards belly. This slant is disturbed by pelvis, giving a trapeze shape. This is shown in figure: - 1.1 (b)

2. Joints:-

Figure: - 1.2 shows rough bone structure of male and females. Three noticeable differences are observed.

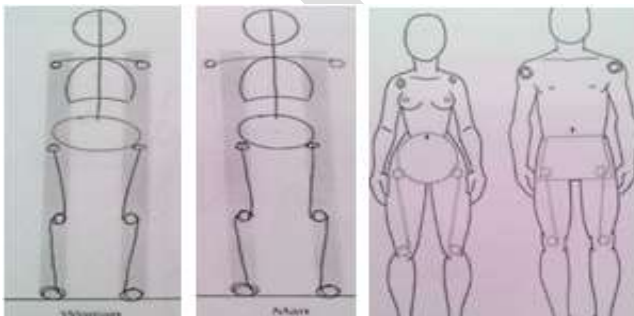


Figure: - 1.2 Bone line of male and female

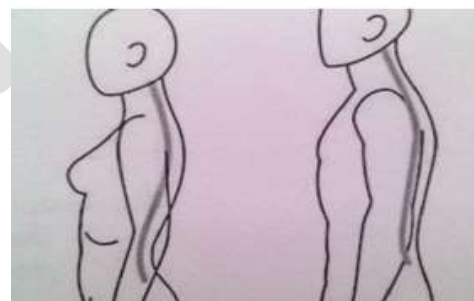


Figure: - 1.3 Vertebra of the male and female

Firstly, the males shoulder joints falls outside the body contour. As such the arms of male hang naturally away from the body. Thus, their natural posture of arm is away from the body. The female arm-sockets are attached inside the body structure shown in figure: - 1.2. The arm, forearm, tends to rest on the body contour. Hence female natural posture of the arm lies near the body unlike males.

Secondly, in males thigh is less tapered as compared to females. This is shown in figure: - 1.2, the right one.

It's the broadened pelvis bone in female makes thigh taper in, much more to join knees. Much inclined foreleg bone is other outcome of female broadened pelvis. The hips joint jut out visibly in the female body.

Thirdly, in males the belly button and elbow are in line but are offset with waist. But in ladies, the belly button, elbow and waist lie in same line. This is shown in the figure:-1.2

3. Vertebral column

The women back bone and the male back bone position is shown in figure: -1.3 from figure it's clear that female vertebra is more "S" shaped than males for pelvis support. Hence, their back-bone is more sensitive than males.

4. Other Minor differences

Besides these points stated above, there are minor properties that is sensitive to gender. However they are subjected to great variations. These points are discussed one by one as follows:-

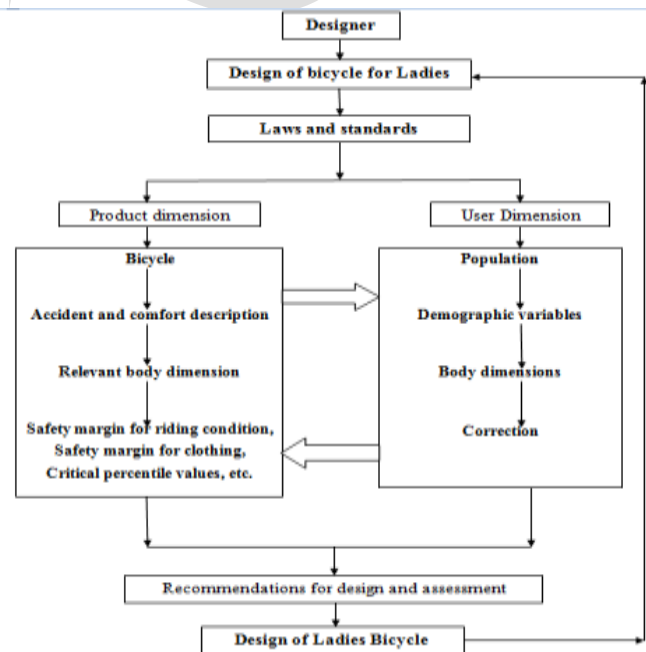
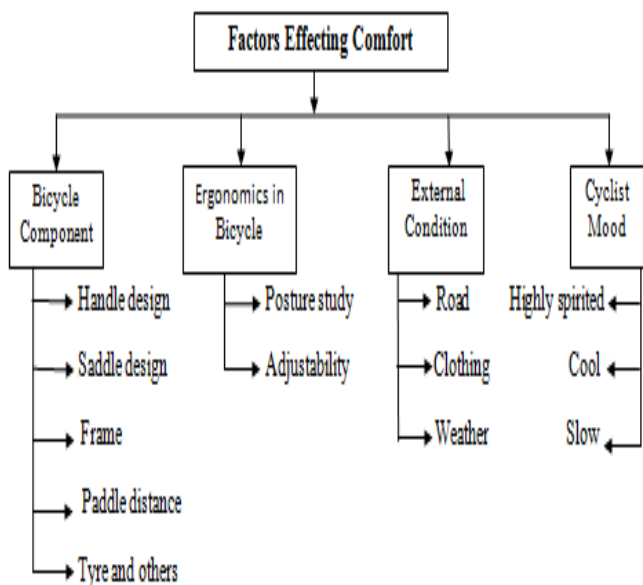
- Women body part soft rounded shapes. She stores more fat under skin as compared to males. The males body are on the other hand harsher and angular
- Palm, hands and sole of the foot are shorter than the males. Palm, hands and sole are half the face as shown in the figure.
- Women generally prefer long hairs.

Chart: - 1.2 is simplified over –view of the design process for ladies bicycle according to Molenbroek. It states the step by step design procedure of the ladies cycle.

Table: - 1.1 states the strategy involved during ladies cycle design. The first stage is the laws and standard specification which is directly picked according to the Steenbekkers and Snyder laws. We have discussed the anthropometric details of women with respect to males in the above section. Now, going for the design specifications, one by one according to the data observed.

Table: - 1.1 Design step of Ergonomic bicycle for ladies.

Chart: - 1.2 Basic principal design of Bicycle for ladies



DESIGN OF LADY BICYCLE FOR MORE COMFORT

Factors affecting the comfort of the lady rider are delt one by one below. Table:-1.2 The External factors (Road, clothing, weather, etc.) and the cyclist mood (sporty, cool fatigue mood etc.) are taken as constant in our analysis. Here, concentrating on bicycle components and ergonomic factors of female cycling in the current paper.

1. Ergonomic design in bicycle for ladies comfort

It is very important to have proper distance between the saddle and handle of a cyclist. This distance varies with individual anthropometric dimensions of ladies. Thus two component of adjustment is being proposed. It is vital for proper fit. They are:-

- (a) Horizontal distance between Saddle and handle.
- (b) Vertical distance between Saddle and handle.

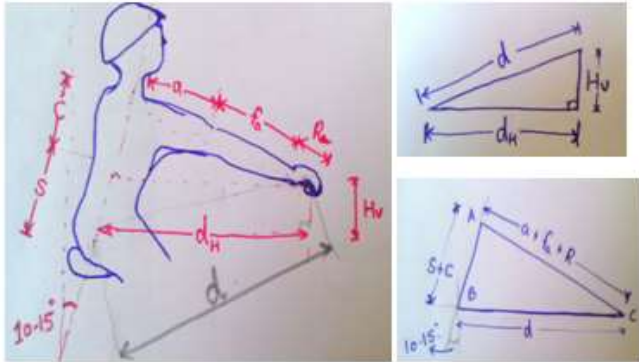


Figure:-1.4 Male favored posture while cycling

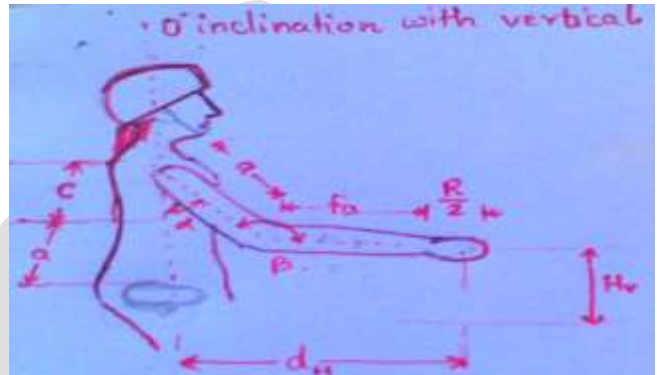


Figure:-1.5 Female favored posture while cycling

Figure:-1.4 and Figure: -1.5 clearly describes the favored posture by different gender while cycling. For the females, the body is erect and arms are closer to the body.

From the figure:-1.5 by simple geometry we have

(a) Horizontal distance between Saddle and handle:-

$$d_H = a \sin \alpha + F_a + R/2$$

(b) Vertical distance between Saddle and handle:-

$$H_v = c + a - a \cos \alpha$$

Set of 20 female data s been taken as stated in the graph below. On their taste and favoring, we have designed the bicycle handle bar. Design stated is based on the ergonomic posture stated above. They are:-

1. Distance between Saddle and handle bar- horizontally = 575mm
2. Distance between Saddle and handle bar- vertically = 195 mm
3. Horizontal distance of adjustable Handle Bar rod = 375mm
4. Handle rod diameter = 30mm
5. Handle rod adjustability –

- a). Angular adjustability
- b). Horizontal adjustability
- c). Vertical adjustability through stem.

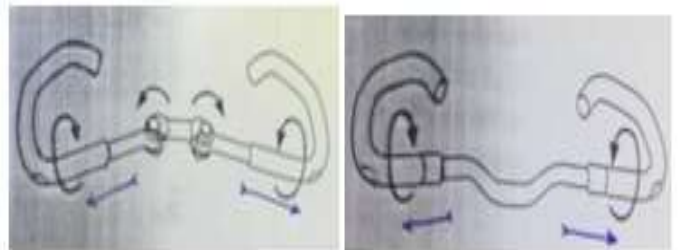


Figure:-1.6 Proposed adjustment

6. Wrist angle = 170°

7. Bend angle = 0° .

Instrument Used for measurement



Figure: - 1.7(a)



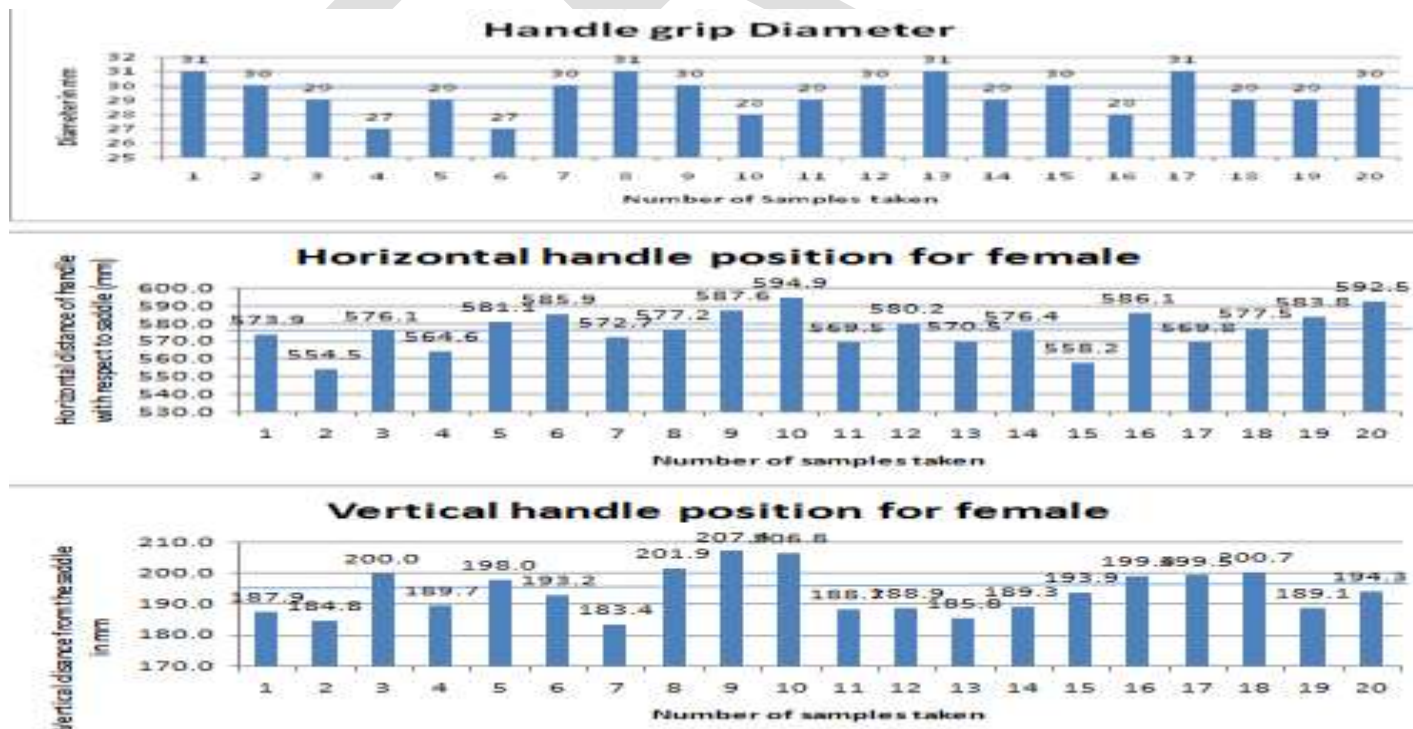
Figure: - 1.7(b)



Figure: - 1.8

The design stated above, clearly depicts the peculiar dimensions of handle bar distinct from market available. Also there is clear difference between the handle choices of ladies with respect to males. The posture comfort clearly depicts the “City” type posture. However, handlebar is subjected to stem change as shown in figure: - 1.8. The four butterfly screw and nuts adjust various handle grips as shown in figure 1.8. Prototype handle bar adjusts various sets of adjustable handle grip. It can simply be done by unscrewing the butterfly nut, de-attaching former bar and attaching the next handle bar grip to screw the four nuts.

The figure: - 1.7(a) and figure: - 1.7 (b) shows the measuring angle bar, for the dimensioning the posture angle and grip width. Figure:-1.7(a) is the part of figure: - 1.7 (b). It is intentionally tapered for grip diameter measurement. The table 4.1 and 4.2 are recorded using these measuring instruments and prototype. Set of 20 samples of the data has been taken using these instruments which is shown in the Graph: -1.3 below.



Graph: - 1.3

2. Bicycle components design favoring the females

Designing of saddle

1. Saddle Inclination:-



Figure:-1.9 Saddle with nose and saddle without nose

The saddle tilt that is “too nose up” will put additional pressure on the front soft tissues part. This usually causes a slouched posture on the bike.

A saddle that is too “nose down” will result in slide forward on the saddle and make you sit on the wrong part of the saddle. The sit bones will no longer provide adequate support and more weight will be placed on the hands, causing numbness and hand pain.

The saddle on a road bike should be either level, for a more upright rider, or slightly nose down— just a few degrees down from horizontal —for a more forward riding position. On a time taking trial cycling, the saddle should be more nose down as the pelvis is rotated more forward at the front of the bike. A seat post with adjustable angles allows you to find that ideal tilt. Many posts have saddle clamps with notches that often leave you with the choice of being either too nose up or too nose down.

The inclination of the seat must be in range 5 deg., nose down as per handle design. The inclined normal reactions of the body will apply more weight component on the pedal. On the other hand higher inclination will cause more force exertion on the arm. Thus a balanced inclination is must.

2. Saddle Height:-

Secondly, but most important is the saddle height. It determines the cycling height of rider. It should neither be too large nor too low. Also the height should favor all the positioning of the leg for paddling as well as the hand for proper handling. All such conditions is addressed one after the other.



Figure: - 1.10

Position Too High or Too low:-

The saddle that is too high will take rider's weight off the pedals and exert more weight on the saddle. It will also cause rider hips to rock, causing side to side movement and chafing.

The saddle too low will cause jamming of the leg, causing ineffective cycling force to peddle force.

Position Too Far Back or Too Front:-

The position too front will cause more folding and cramped feeling. But weight component will be on the pedal, causing forceful cycling.

Moving the seat forward so that the knees are over the pedal axis, changing the pedaling angle, usually, improves saddle comfort.

3. Shape of the saddle:-

The conventional seat used is flat rake like structure. It fails to confer the buttock ache for long ride. Figure below gives the detailed new modification seen in seat. The front round section is replaced by flat gel nose. Several engraving is provided to have better buttock contact causing less irritation. Hole at the centre or at end in provided for better air circulation at the buttock.



Figure: - 1.11 Types of modern designed comfortable saddle seat.

4. Anatomically favored lady cyclist posture on cycle:-



Figure: - 1.12 (a)

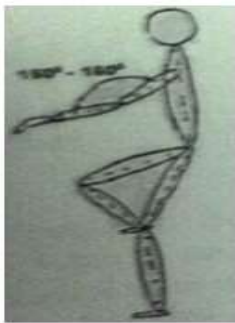
Figure: - 1.12 (b)



Figure - 1.12 (c)

Posture of lady cyclist: - a. Dutch type position (most popular) b. Tracking position for ladies c. Front view position of handle reach.

Considering these factors in mind proposing the general postural structure of women during cycling, shown in figure:-1.12. As stated above, we can now clearly see the difference of Posture favored during cycling. The male backbone is inclined to about 10 deg. and arm of almost straight. Female arm are close to the body and inclined 150° to 160° . This is shown in the figure:-1.12(a) figure:- 1.12 (b) and the difference is shown in the figure: - 1.13.



Female posture



Male Posture



Figure: - 1.14



Figure: - 1.15

Figure: - 1.13

Handle design

After posture study shown in the figure above only two types of handlebar is proposed here. Firstly, most popular, the “Classic Bike Handle Bar”, in Figure: - 1.14 upper and Figure:-1.12(a). Secondly, less popular “City Bike Handle bar” Figure:- 1.6 bottom and Figure:-1.12(b).

Frame design

The conventional frame of the bicycle as shown in the figure:-1.15. Particularly for the ladies, this frame is most suitable. It makes easy a climb and decent on the cycle. Woman clothing such as “sari” and skirts makes easy access in the frame. Beside these it makes easy control at the start and stop.

Paddle distance

The paddle distance is another critical factor. The paddling distance should be such that at the top the angle of the leg should be more than 68° . At the bottom position it should be greater than 170° . This posture is shown in the figure:-1.13.

Tyre and others

- The choice of broad and streamline tiers are left by the rider for its nature of use. Out of four grades of tire size, she can choose any one.
- Chin cover in must.
- Material more popular is carbon fiber other than steel

REFERENCES:

- [1] Lambros laios, John Giannatsis, “Ergonomic Evaluation and redesign of children of children bicycle based on anthropometric data”, Applied Ergonomics 2009
- [2] S.C. Jirapure, M.W.Andure, S.W. Mohod, “ Ergonomic Design of a bicycle – A bike of rural people
- [3] Joachim Vanwalleghem, Fredrik Mortier, Ives De Baere, Mia Loccuier, Wim Van Paepegem, Design of an instrumented bicycle for evaluation of bicycle dynamics and its relation with the cyclist comfort.
- [4] Jason K Moore, Mont hubbard, A.L. Sehwab, J.D.G. Kooijman, Dale L. Peterson, ”Statics of bicycle rider motion”.

- [5] K Mallikarjun, Sumer Singh, Manas Ranjan Mishra. “ Design of bicycle for Indian children Focusing on Aesthetic and Ergonomics”.
- [6] P.C.M Donkers, H.M. Toussaint, J.F.M Molenbroek, and L.P.A Steenbekkers, “Recommendations for the assessment and design of young children’s bicycles on the basis of anthropometric data”.
- [7] F.S Ayachi, J.Dorey,C. Guastavino, “Identifying factors of bicycle comfort: An online survey with enthusiast cyclists.
- [8] Dominic Krumm, Stephan Odenwald, Development of a dynamometer to measure grip forces at a bicycle handlebar.

IJERGS

SKIN COLOR DETECTION AND BACKGROUND SUBTRACTION FUSION FOR HAND GESTURE SEGMENTATION

Yogesh B.Dongare, Prof.Ramesh Patole
G.H.Raisoni College of Engineering & Management,Chass,Ahmednagar, India.
yogesh.dongare05@gmail.com
rameshpatole@gmail.com

ABSTRACT

Hand gestures recognition play a important role in Human Computer Interaction(HCI). They serve as primary interaction tools for gesture based computer control. The present work is a part of vision based hand gesture recognition system for Human Computer Interaction. Here we have proposed an algorithm with the fusion of skin color model and background subtraction that gives robust output in the presence of drastic illumination changes. In this we paper we compare different methodologies of hand segmentation approaches for gesture recognition systems. This study is a first step towards development of a reliable, efficient and robust gesture recognition system with high detection rate for better performance of system on Android mobile device.

Keywords: hand gesture detection, appearance based segmentation, skin color detection, background subtraction;

INTRODUCTION

As computers become more usefull in society, facilitates natural human-computer interaction (HCI) have a very positive impact on their use [1].By using various improvements in the image acquisition and image processing technology, hand gestures become a significant,growing and popular tool in human computer interaction (HCI) systems [2].This hand gesture recognition is a field of research with growing applications in different area of research. The applications where we can use this techniques are Sign language recognition, Virtual reality, Robotics, Gesture-to speech, Television control, Smart room interactions and medical interactions [3]. The goal of gesture recognition system is the rendering of the semantics that the hand(s) location, posture of hand, or gesture information conveys.

Segmentation of gestures is the separation of hand gestures from a continuous image sequences containing gestures [2]. Hand segmentation is the key and major task to the analysis of gesture and detection of a gesture. A static gestures is a specially hand configuration and pose and this is represented by a single image. A dynamic gesture are the moving gestures, represented by a sequence of images [3]. Quality of the gesture segmentation in real time affects the rate of recognition of gestures. Effective use of various information of images such as color, motion, geometric information are the key of the study [2].For the detection of static gestures (i.e. postures), a general classifier or a template-matcher are used. Hand detection an be done in various ways such as pixel based [4], shape based [5], 3d model based [6], motion based [7] parameters. However, dynamic hand gestures have a temporal characteristics and requires techniques that can handle this dimension like Dynamic Time Warping, Time Delay Neural Network, Finite State Machines, and Advanced Hidden Markov Models (HMM) [1]. Hand tracking can be done by using template based, optimal estimation, particle filtering and camshift algorithms [1].

Segmentation can be mainly done through two major mostly used technologies for human computer interaction are contact based devices and vision based devices. Contact based device method is the old traditional technique for modeling of Gesture. The user signs by using gloves and the system will perform functions through sensing apparatus like wires, accelerometers and multi touch based detectors [8]. This is a 3d model which gives a direct measurement of hand position, joint angle and orientations [3]. Limitations are the system can detect and recognize only single hand gestures. Experiencing all these, the contact based devices will not provide much acceptability in hand gesture recognition, so that vision based devices have been introduced for taking images for gesture recognition in human computer interaction [1].

Vision based techniques are simple to use, easiest and affordable to implement human computer interaction in real-time. Contact based devices are user cooperative for user,precise and flexible to use and configure, on the other hand ,Vision based devices are flexible to use and healthy [1]. The two major types of vision based hand gesture representation are 3D model based methods and appearance based methods. The 3D model based method is advantageous that it updates the different model parameters while checking the matches of transition in temporal model, which leads to proper hand gesture recognition and representation, though making it computationally important with requirement of dedicated hardware [9]. Appearance based hand gesture representation has

color based model, silhouette geometry model and motion based model. Appearance based hand gesture representation methods are classified into two subcategories, 2D static model based methods and motion based methods [3]. The generalized block diagram of appearance based static approach is as shown in the fig 1.

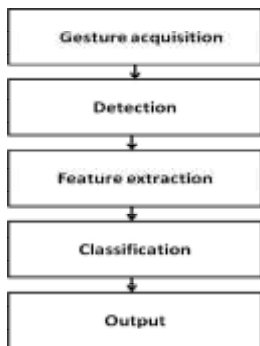


Fig 1: Appearance based Approach

The device camera is used for the purpose of collecting images or video frame for the process of image or gesture acquisition. Hand Detection contains Segmentation and Edge Detection steps. After performing segmentation of the hand gestures, an edge traversal algorithm is used on the contour of segmented hand for removing noise from unwanted background. Feature Extraction is used to calculate particular features because of that is variation in the image data. Features that are not useful are discarded. Classifier is used to identify the hand gesture from the alphabets of the sign language used [2]. Generally, if there is large vocabulary then recognition task becomes complex.

Below discussion will explain the Appearance based segmentation, current difference and skin color fusion algorithm, comparison with previous algorithms and Conclusion.

APPEARANCE BASED SEGMENTATION

In Gesturer Localization, the person who is performing the gestures is extracted from the rest of the visual image scene [7]. Appearance based static method includes finding target region from the intensity image that includes data descriptive of a hand. These methods utilize several types of visual features like skin color, shape, motion and anatomical models of hands for detection of human hand motion and gestures[10] Various gray-level segmentation techniques, such as use of single threshold value, adaptive thresholding, P-tile method, edge pixel method, iterative method and use of fuzzy set are available for hand segmentation[11]. Thresholding technique is applicable for simple hand images in the static, uniform backgrounds.

Clustering technique is also used at initial stages [5]. Initially this algorithm locates k clusters in the image. Each pixel in the image is grouped to the nearest cluster; clusters are moved to the average of their class values. This process is repeated until the stopping condition is met [5]. The time complexity of this algorithm is very less but false detection rate is high.

Color based segmentation generally rely on histogram matching, look up table approach and skin pixel data training through various color space [7]. Several color spaces have been proposed including RGB, normalized RGB [2], HSV [12], YCbCr [2], YUV [13], etc. Color spaces that separate luminance component from the chrominance component are preferred. This is due to the fact that by employing chromaticity-dependent components of color only, some degree of robustness to illumination changes and shadows can be achieved [1].

Burande et al. [14] implemented Blobs analysis technique for skin color detection under complex background. In this technique, several skin colored blobs are formed by making connected components and hand region is detected.

The major drawback of color based segmentation is color of human skin varies greatly across human races or even between individuals of the same race. In general, color segmentation can be confused by background objects that have a color distribution similar to human skin. Background subtraction can be done to overcome this problem. However, background subtraction is typically based on the assumption that the camera system does not move with respect to a static background. The difference in luminance of pixels from two successive images is close to zero for pixels of the background [15].

Segmentation handles the challenges of vision based system such as skin color detection, complex background removal and variable lighting condition. Efficient segmentation is the key of success towards any gesture recognition.

CURRENT APPROACH

Our current approach is a fusion of skin color and background segmentation. Face and hand of signer were successfully detected by using skin color segmentation. False detection of skin region in the uncontrolled background also occurs due to light variation. So background subtraction was used to find the difference between the hand gesture image and the background object.

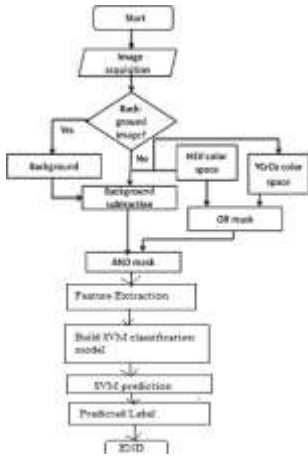


Fig 2: Flowchart of proposed algorithm

I. Background subtraction:

In gesture making only position of the hands of gesturer will change, where as background and other body parts remain almost static. In image acquisition, background image ($bgr(x,y)$) without hand gesture is taken initially. The new image taken is considered as foreground image ($fgr(x,y)$). To isolate the gesture ($gst(x,y)$) from image, difference principle is applied.

$$gst_i(x,y) = fgr_i(x,y) - bgr(x,y) \quad (1)$$

Difference foreground gesture obtained is converted into binary image setting appropriate threshold. As the background is not perfectly static, noise part is added. To obtain clean hand image, this technique is combined with skin detection. To remove this noise, connected component analysis is applied, and to fill the holes in hand if any region filling is applied and to obtain clear edges morphological processing is applied.

II. Skin detection in HSV and YCrCb color space:

Every color image is composed of three planes namely hue (H), saturation (S) and value (V). To extract the hand from the image, foreground image is decomposed into H, S and V planes. The following threshold is imposed on each plane to extract skin regions like hand, head and the rest body parts.

$$\begin{aligned} 0.05 < H < 0.17 \\ 0.1 < S < 0.3 \\ 0.09 < V < 0.15 \end{aligned} \quad (2)$$

In YCbCr color space, every color image is decomposed into Yellow (Y), Chromium blue (Cb) and Chromium red (Cr) planes. Threshold is applied in YCbCr color space as shown below.

$$\begin{aligned} 76 < Cb < 128 \\ 132 < Cr < 172 \end{aligned} \quad (3)$$

Results obtained from two color spaces are converted into binary images and added to maximize the skin color detection. Finally results obtained from background subtraction and skin color models are multiplied to eliminate the body parts other than hand. If the

background is in the range of skin color, false detection is eliminated to a considerable manner. Region filling and morphological processing are done to enhance the gesture image.

III. Experimental Results:

In accordance with the established background subtraction of equation (1), the binary gesture image is obtained. The background and foreground images are shown in the fig 3(a) and (b).



Fig 3 a) Foreground image a) Difference image b) Color space segmented image c) Hand gesture image

Hand gesture area detected contained some interference region caused due to clothes. Biggest blob analysis is implemented to obtain hand region as shown in the fig 3(c).

The skin color detection method in HSV and YCrCb color spaces is used to make skin color segmentation on the foreground image in correspond to equations (2) and (3). The hand region is highlighted after skin color detection as shown in fig 3(d). The two images of background subtraction and skin segmentation were multiplied. Region filling and morphological operations were performed to enhance the image. Then the hand gesture image is obtained as shown in fig 3(e).

COMPARISON WITH PREVIOUS APPROACHES:

All the above discussed Appearance based approaches are implemented on different platform and are compared with our technique. The results of segmentation methods implemented are shown in the table (1). Compared with the previous approaches, our proposed algorithm is illumination invariant, skin color and shadow insensitive. It is applicable to even skin color backgrounds to obtain data descriptive of hand to a considerable extent.

Approach	Implementation	Characteristics
Dynamic thresholding(gray level segmentation)[11]	 <p>Fig 4: a)Input Image (from web) b)Segmented Image</p>	Single posture, uniform background, non-real time.
Clustering technique(LAB color space) [5]	 <p>Fig 5: a)Input Image (from web) b)Segmented Image</p>	Single posture, uniform background, skin color sensitive, non-real time.
Skin modeling (YIQ and YUV color spaces)[13]	 <p>Fig 6: a)Input Image b)Segmented Image</p>	Illumination invariant and applicable to complex background, but sensitive to skin color.

<p>Blob analysis(YCBCR color space [2,14])</p>	 <p>Fig 7: a)Input Image b)Segmented Image</p>	<p>Applicable to complex background, but depth dependent. False detection rate is high.</p>
<p>Background subtraction[15]</p>	 <p>Fig 8: a)Background Image b)Foreground Image c)Segmented Image</p>	<p>Applicable to static complex background , but illumination variant and shadow sensitive.</p>
<p>Proposed approach</p>	 <p>Fig 9: a)Background Image b)Foreground Image c)Segmented Image</p>	<p>Illumination invariant, skin color insensitive, low false detection rate. Applicable to complex but static backgrounds.</p>

Table 1: Implementation of Segmentation Approaches

CONCLUSION

Hand gesture segmentation is the most important step in the gesture recognition systems. Segmentation process has direct impact on balancing accuracy-performance-usefulness trade-off of recognition systems. The algorithm we implemented is robust with respect to drastic illumination changes and cluttered backgrounds. The proposed algorithm fails if the hand region overlaps the face. In future the focus would be on improving the algorithm to avoid false detections if the hand is overlapped with face. This is merely the first step towards implementation of effective gesture recognition system. Further the project will be extended to recognize the detected gestures.

REFERENCES

- [1] S Rautaray, A Agarwal. "Vision Based Hand Gesture Recognition for Human Computer Interaction: A Survey". Springer Science & Business Media Dordrecht 2012.
- [2] makant Yadav. "Fusion of Information from Data-Gloves and a Camera for Hand Gesture Recognition", M.Tech thesis, 2011.
- [3] I Pavlovic, R Sharma, T S Huang. "Visual Interpretation of Hand Gestures for Human Computer Interaction: A Review", IEEE Transactions on Pattern Analysis and Machine Intelligence, Vol. 19, No. 7, 1997.
- Viola, M Jones. "Robust Real-Time Object Detection", IEEE Workshop on Statistical and Computational Theories of Vision, Vancouver, 2001.
- [4] Panwar, P S Mehra. "Hand Gesture Recognition for Human Computer Interaction", Proceedings of IEEE International Conference on Image Information Processing (ICIIP 2011), Wagnaghat, India, November 2011.
- [5] Rehg, T Kanade. "Visual Tracking of High DoF Articulated Structures: An Application to Human Hand Tracking," European Conference on Computer Vision and Image Understanding: 35-46, 1994.
- [6] Howe, F Wong, A Chekima, "Comparison of Hand Segmentation Methodologies for Hand Gesture Recognition", IEEE-978-4244-2328-6, 2008.

[7]

Karam. "A Framework for Research and Design of Gesture-Based Human Computer Interactions", PhD Thesis, University of Southampton, 2006.

[8]

Bourke, J O' Brien , G Lyons. "Evaluation of a Threshold-Based Tri-Axial Accelerometer Fall Detection Algorithm", Gait & Posture 26(2):194–199, 2007.

[9]

A Ibraheem, R Z Khan. "Vision Based Gesture Recognition Using Neural Networks Approaches: A Review", International Journal of Human Computer Interaction (IJHCI), Malaysia, Vol. 3(1), 2012.

[10]

Stergiopoulou, N Papamarkos. "Hand Gesture Recognition using a Neural Network Shape Fitting Technique". Elsevier Engineering Applications of Artificial Intelligence 22, 11411158, 2009.

[11]

M Hasan, P K Mishra. "HSV brightness factor matching for gesture recognition system". International Journal of Image Processing (IJIP), vol. 4(5), 2010.

[12]

Metaxas. "Sign Language and Human Activity Recognition". CVPR Workshop on Gesture Recognition, June 2011.

[13]

Burande, R Tugnayat, N Choudhary. "Advanced Recognition Techniques for Human Computer Interaction", IEEE, Vol 2 pp., 480483, 2010.

X Zabulis, H Baltzakis and A Argyros. "Vision Based Hand Gesture Recognition for HumanComputer Interaction"

Design of Low Voltage Low Dropout Regulator

Yogeshree Patil, Prof. S.N. Kulkarni

yogeshree.patil07@gmail.com, hod_etc@dypic.in

Dr. D. Y. Patil School of engineering,pune.

Abstract-

A low voltage low dropout regulator provides an output voltage near about 0.8V by giving input voltage of 1V, with 45nm CMOS technology. The LDO consist of Operational Transconductance Amplifier which works as error amplifier with current splitting technique to boost gain. The power MOS Mp is used for low voltage and low dropout voltage. The output variation is 12mV for current of 0-100mA. The proposed LDO operates over wide range of frequency and provides power supply rejection more than 60 dB at 100 KHz. The simulation of proposed LDO in Advance design system tool.

Keywords: low dropout regulator, fast transient response, high power supply rejection, small area etc.

INTRODUCTION

Low dropout regulators (LDOs) are widely used in power management integrated circuits and systems [1] [2]. Because it provides stable DC voltage whose input and output voltage difference is low. The dropout voltage means the input/output differential voltage where control loop starts regulating [3]. The regulator provides stable DC voltage and acceptable level particularly for product that are operated by portable battery like cameras, hand phones, and laptop. Now a day's study and research on power management technique for different application has been increases [4]. Power management improves the power efficiency of devices resulting in prolong battery life cycle and operating time for the device.

Voltage Regulator can be classified as Low Dropout (LDO) linear Regulator, switching regulator and switch capacitor regulator and each regulator has its own characteristics and application. The low dropout regulators have some good characteristics indeed, but they also have some problems in their implementations such as PSR and transient response etc.[5]. Regulating performances, quiescent current, operating voltages are the important characteristics to be considered during designing LDO. The other specifications are drop-out voltage, load regulation, line regulation, output voltage variation, output capacitor and ESR range and input/output voltage range. so to improve performance of low dropout regulator, a new technique is presented to design a high performance LDO with fast load transient response, high power supply rejection ratio, small quiescent current, good load Regulation and precise over current protection. Bandwidth is also another important specification in voltage regulator design. The higher the bandwidth of a regulator, the more rapidly it can react to changes in input and power supply and stay the output voltage constant. High bandwidth improves the power supply rejection ratio (PSRR) of the regulator, which is a measure of how well the regulator attenuates noise on the power supply. The better the power supply rejection, the less the output voltage changes in response to fluctuations in the supply.

From the precise review of related work and published literature, it is observed that many researchers has designed low dropout regulator using different technique. Some researchers focused on improving transient response [2] [6] [7] or some focused on enhancing power supply rejection ratio [8] [9] or both of the regulators. In [2] [7] they proposed regulators any a large driving current or else additional circuits which consume significant I_Q . In [10] they proposed low dropout regulator design in 90nm which provides 0.85V output voltage by applying 1V input voltage and provides high PSRR and fast transient response.

DESIGN CONSIDERATIONS

Many factors must be considered when designing a Low dropout regulator. Reducing power consumption is for all time advantageous, specially with portable consumer electronics. Less power consumption allows the device's battery to last longer, means the user needs to charge the battery less often. Efficiency is determined by the dropout voltage. Dropout voltage means the difference among the unregulated supply voltage and regulated output voltage. Lowering the dropout voltage can lower the necessary voltage of the unregulated power supply, which lowers the power consumption of the regulator. A less power-hungry device uses a smaller battery and better portability.

Portability of regulator improves by decreasing area. the devices which consist of more than one voltage regulators has many benefits from a voltage regulator design which requires smaller area, because in house circuitry can be made smaller and easier to bring around. Because of small area more devices are fixed into one wafer, which reduces cost of manufacturing.

Bandwidth is one of the important specification of LDO design. If the bandwidth of regulator is high, it reacts more quickly to change in input voltage and power supply and keeps output voltage constant. Power supply rejection ratio (PSRR) of the regulator can be improves by keeping higher bandwidth, which attenuates noise on the power supply. The enhanced the power supply rejection,

the less the output voltage changes in response to fluctuations in the supply. The PSRR can be categorized by the magnitude of attenuation as well as the range of frequencies over which the attenuation occurs. Typically PSRR is greatest at low frequencies.

Another factor to consider in LDO regulator design is stability. The Low dropout regulator provides a constant voltage to other components, a regulator prone to oscillation is not advantageous. Stability of regulator varies with output current and load capacitance i.e. load condition, which can be partly specified or unknown, a regulator design that has good phase margin for a wide range of output loads is best. Associated with stability is load regulation, the percentage change in output voltage in response to a change in the output current.

CIRCUIT REALIZATION AND SIMULATION RESULTS

The proposed LDO regulator optimizes the four parameters i. e. low-voltage operation while achieving a fast transient response, low I_Q and high PSR and small area. The schematic of proposed LDO shown in fig1. The Operational Transconductance Amplifier (OTA) which works as Error Amplifier (EA). EA is composed of M_{EA1} - M_{EA9} . OTA type error amplifier does not requires compensation capacitor and it operates at minimum voltage $V_{DD, min} = V_{th} + 2V_{ov} (\leq 1 V)$. EA contains low input offset voltage to achieve an accurate output. The Impedance at node v_X and v_Y is set low to sustain the system stability by push the non dominant pole p_X to high frequency. Full swing is achieved at node v_G using M_{EA7} , M_{EA9} . The use of M_{EA7} and M_{EA9} reduces the size of MP power transistor. Hence it reduces the circuit area and gate capacitance. MP drives on sufficient slew rate using EA output. The Gain of the EA is given as:

$$\begin{aligned}
 A_{EA0} &= g_{m2} \times A \times (r_{O7} || r_{O9}) \\
 &\approx g_{m2} \times A \times r_{O9} \\
 &= (2I_{d2}/V_{OV2}) \times A \times 1/(\lambda_9 \times A \times Id2) \\
 &= 2/ (V_{OV2} \times \lambda_9) \dots \dots \dots (1)
 \end{aligned}$$

Where I_{d2} =Bias Current, V_{OV2} =Overdrive voltage of M_{EA2} A =current ration b/w first and second stage of EA. The gain of EA in eq 1 is low for fast transient response therefore there has been used the current splitting technique to increase the gain. The gain is increased using sufficient g_{m2} and increasing r_{O9} . The Power MOS Mp is used because of its low voltage and low dropout voltage requirements. The Increased gain using g_{m2} and r_{O9} increased the PSR. The replica of power noise created on gate terminal is used to cancel out the power noise at source terminal of Power MOS. There is applied two equivalent transistor M_{EA4} and M_{EA5} b/w I_{EATA} and Ground to attenuate power supply noise at node v_X and v_Y . First stage of the EA also contains M_{ta1} - M_{ta8} which reduces the Slew time of power MOS gate terminal by increasing the charging and discharging current during the load transient. M_P , M_{ta3} and M_{ta8} are biased in cutoff region to avoid high I_Q and breaking point of perfect replication at gate terminal of these transistors. V_{out} and V_{FB} feedback voltage changes because of large load change. This Feedback voltage variation is amplified. The v_{FB} variation is then amplified by the output variation detector of the transient accelerator, generating v_{X1} and v_{Y1} as follows:

$$\begin{cases}
 \frac{v_{Y1}}{v_{FB}} \approx -g_{m2} \times \left(\frac{1}{g_{m5}}\right) \times g_{m,ta2} \times (r_{O,ta1} || r_{O,ta2}) \\
 \frac{v_{X1}}{v_{FB}} \approx -g_{m2} \times \left(\frac{1}{g_{m4}}\right) \times g_{m,ta6} \times \frac{(W/L)_{M_{ta5}}}{(W/L)_{M_{ta4}}} \times (r_{O,ta5} || r_{O,ta7})
 \end{cases} \quad (2)$$

Where $g_{m, ij} = i_{a6}, i_{a2}, r_{O, ij} = i_{a1}, i_{a2}, i_{a5}, i_{a7}$, and $(W/L)_{M_{ij}} = i_{a5}, i_{a4}$ represent the transconductance, output resistance, and aspect ratio of the corresponding transistors, respectively. v_{X1} and v_{Y1} turn on the M_{t8} if the load current increases otherwise M_{ta3} . As V_{out} reaches its final value M_{ta3} and M_{ta8} turned off.

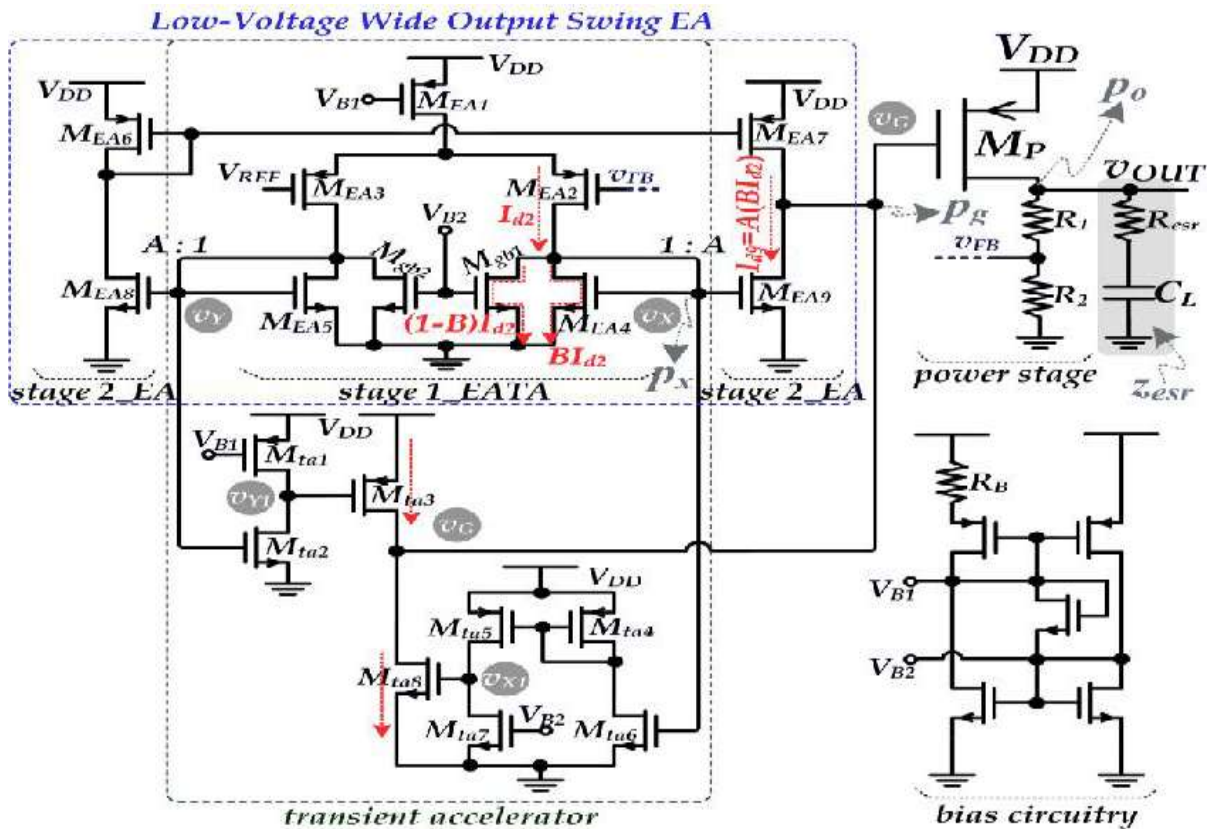


fig 1. Schematic of the proposed LDO regulator.

The proposed LDO is designed in 45 nm CMOS process. The LDO is able to operate at 1V, which covers a wide range of the battery voltage. The proposed LDO provides dropout voltage near about 200mV. It gives near about 0.8 V output voltage which is shown fig2.

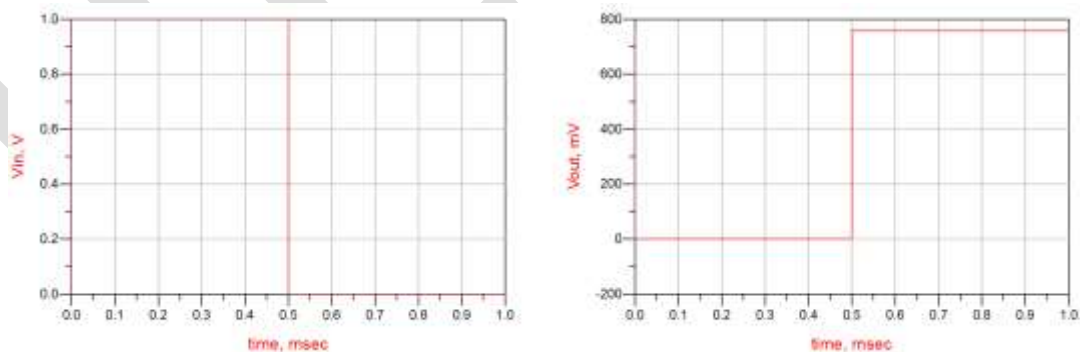


Fig2: Output Voltage waveform

The input voltage is 1 V and the values of R_1 and R_2 can be adjusted to generate any regulated output level between 0.85 and 0.5 V. The maximum I_Q is $60 \mu\text{A}$, achieving a 99.94% current efficiency. The C_L used for measurement is $1 \mu\text{F}$ with a R_{esr} of 1Ω . Fig. 3 shows the measured waveforms of the load transient test where the load current is switched between 0 and 100 mA within $10 \mu\text{s}$. The input/output voltage V_{DD} and V_{OUT} is set to $\{1 \text{ V}, 0.85 \text{ V}\}$ and $\{1 \text{ V}, 0.5 \text{ V}\}$, respectively.

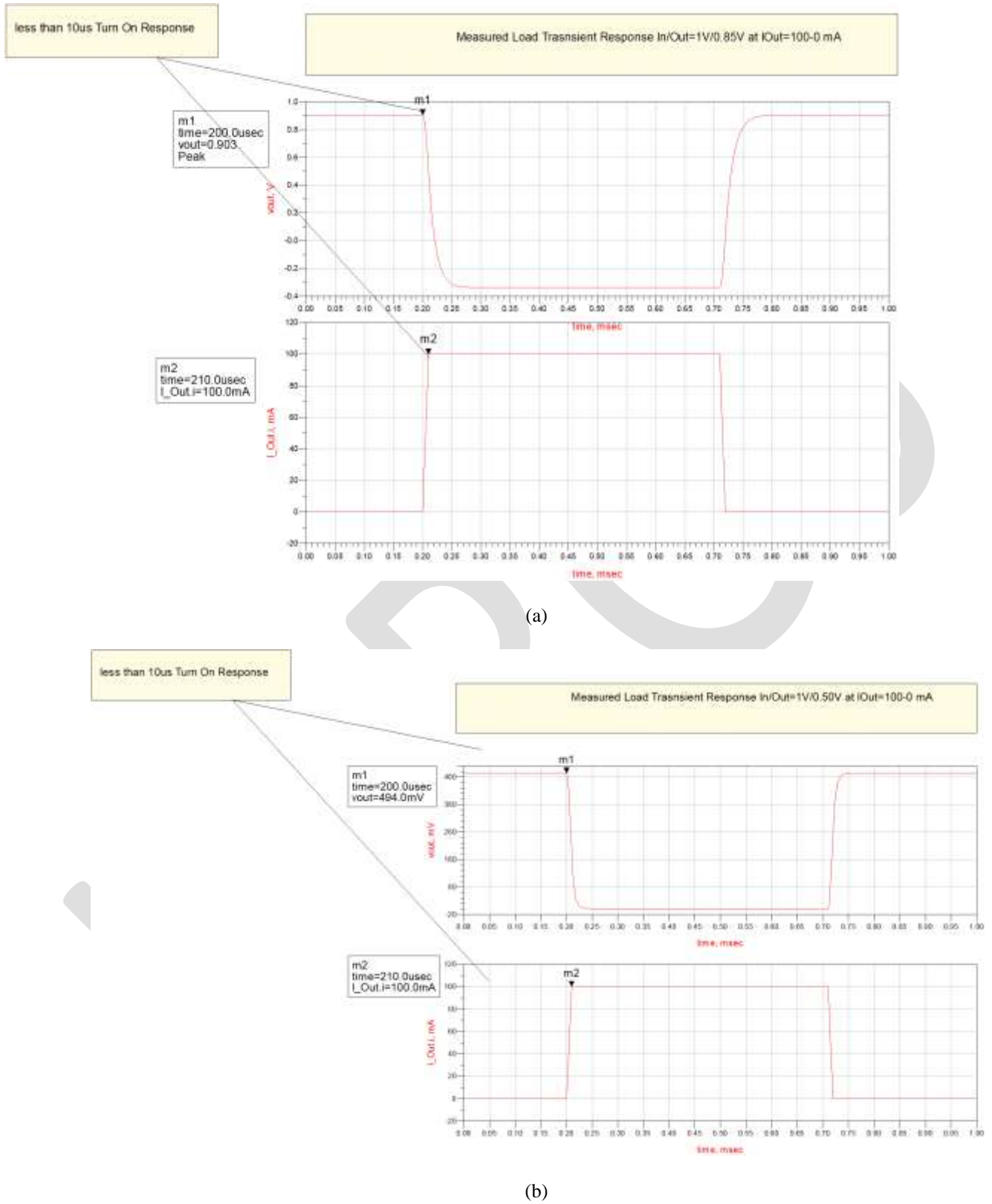


Fig 3. Load Transient Response (a) LDO Load Transient Response at 0.8V output
(b) LDO Load Transient Response at 0.5V output

The PSR performance is also measured when the test conditions are $V_{DD} = 1\text{ V}$, $V_{OUT} = 0.85\text{ V}$, and $I_{OUT} = 100\text{ mA}$ and the measured result is shown in Fig. 4. The proposed LDO regulator achieves a PSR more than 60 dB at low frequencies whereas the roll off frequency is 100 kHz.

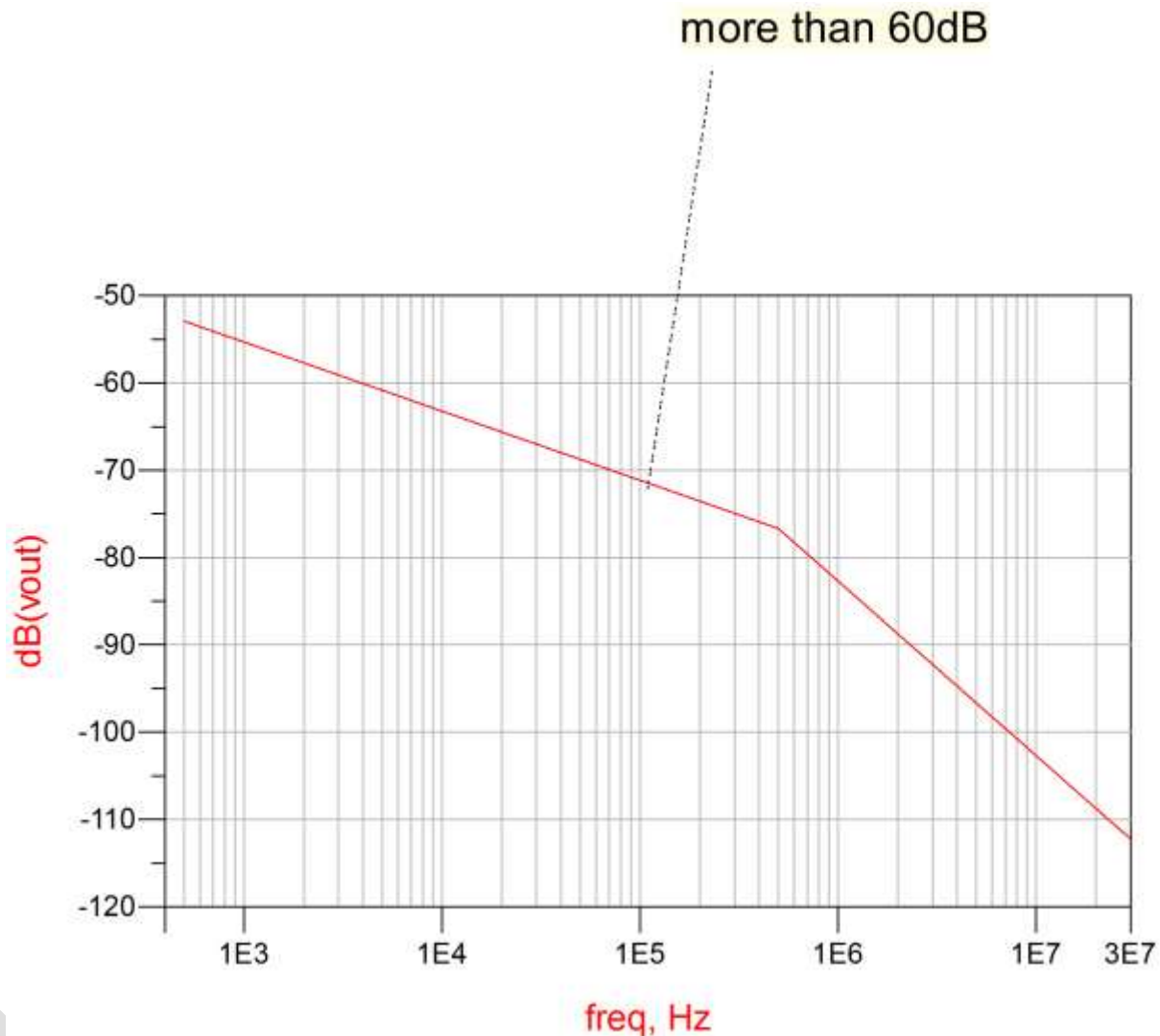


Fig 4 LDO Load PSR at $I_{out}=100\text{mA}$

CONCLUSION

In this paper presented an LDO regulator with a simple OTA-type EA plus an adaptive transient accelerator, which can achieve operation below 1 V, fast transient response, low I_Q , and high PSR under a wide range of operating conditions. The proposed LDO regulator was designed using a 45 nm CMOS process to convert an input of 1 V to an output near about 0.8V, while achieving a PSR more than 60 dB with a 0–100-kHz frequency range. The output variation is 12mV for current of 0-100mA. The experimental results verified the feasibility of the proposed LDO regulator.

REFERENCES:

[1] Ka Nang Leung , Mok, P.K.T.,” A capacitor-free CMOS low-dropout regulator with damping-factor-control frequency compensation”, IEEE J. Solid-State Circuits, 38(10), 1691-1702, sep 2003.

- [2] P. Hazucha, T. Karnik, B. A. Bloechel, C. Parsons, D. Finan, and S. Borkar, "Area-efficient linear regulator with ultra-fast load regulation," *IEEE J. Solid-State Circuits*, vol. 40, no. 4, pp. 993–940, Apr. 2005.
- [3] G. A. Rincon-Mora, "Current efficient, low voltage, low drop-out regulators," Ph.D. dissertation, Elect. Comp. Eng. Dept., Georgia Inst. of Technology, Atlanta, 1996.
- [4] Chenchang, Z., Wing-Hung, K., "An Output-Capacitor-Free Adaptively Biased Low-Dropout Regulator with Subthreshold Undershoot-Reduction for SoC", *IEEE Transaction on Circuits and Systems*, may 2012.
- [5] Cheng, W. Y., Yueh, H. C., Liu, B. D., "A low dropout voltage regulator with programmable output", *Proceedings of the 4th IEEE Conference on Industrial Electronics and Applications*, May 2009.
- [6] M. Al-Shyoukh, H. Lee, and R. Perez, "A transient-enhanced low- quiescent current low-dropout regulator with buffer impedance attenuation," *IEEE J. Solid-State Circuits*, vol. 42, no. 8, pp. 1732–1742, Aug. 2007.
- [7] Y.-H. Lam and W.-H. Ki, "A 0.9 V 0.35 μm adaptively biased CMOS LDO regulator with fast transient response," in *Proc. IEEE Int. Solid- State Circuits Conf.*, Feb. 2008, pp. 442–443, 626.
- [8] C. Zhan and W.-H. Ki, "An adaptively biased low-dropout regulator with transient enhancement," in *Proc. Asia South Pacific Design Autom. Conf.*, 2011, pp. 117–118.
- [9] A. P. Patel and G. A. Rincon-Mora, "High Power-Supply-Rejection (PSR) Current-Mode Low-Dropout (LDO) Regulator," *IEEE Trans. Circuits Syst. II, Exp. Briefs*, vol. 57, no. 11, pp. 868–873, Nov. 2010.
- [10] Chung-hsun Huang, member ,IEEE Ying-Ting Ma, And Wei-Chen Liao, "Design of a low voltage low dropout regulator" *IEEE TRANSACTIONS ON VERY LARGE SCALE INTEGRATION (VLSI) SYSTEMS*, VOL. 22, NO. 6, JUNE 2014.
- [11] Robert J. Milliken, Jose Silva-Martínez, Senior Member, IEEE, and Edgar Sánchez-Sinencio, Fellow, IEEE, ' Full On-Chip CMOS Low-Dropout Voltage Regulator', *IEEE Transactions On Circuits And Systems—I: Regular Papers*, Vol. 54, No. 9, September 2007.
- [12] Yogeshree Patil, S. N. Kulkarni, " Design and analysis of Low Voltage Low Dropout Regulator", *International Journal of Science Technology and Engineering*, vol. 1, No. 10, April 2015.

Shadow Processing Method of High Resolution Remote Sensing Image Using IOBA Matching

Arya S Raj, Kavitha V K

P.G Scholar, Dept of CSE, BMCE, Kollam, Kerala, India

aryasraj13@gmail.com

Abstract— Shadows in remotely sensed images create difficulties in many applications; thus, they should be effectively detected prior to further processing. In accordance with the characteristics of high resolution color remote sensing images, we put forward a Shadow Processing Method of High Resolution Remote Sensing Image Using IOBA Matching with shape information preserved in color aerial images for solving problems caused by cast shadows. In this method, suspected shadows are extracted according to the statistical features of the images. Furthermore, some dark objects which could be mistaken for shadows are ruled out. Once the shadows are detected they are classified and a non-shadow area around each shadow termed as outer buffer area is estimated using IOBA matching. The mean and variance of these outer buffer areas are used to compensate the shadow regions. Experiments show that the new method can accurately detect shadows from urban high-resolution remote sensing images and can effectively restore shadows with a rate of over 85%.

Keywords — Shadow, Remote Sensing Image, Inner Buffer Area, Outer Buffer Area, IOBA matching, Shadow Detection, Shadow Removal.

INTRODUCTION

In the process of requirement of high resolution remote sensing image, shadows are casted by buildings especially present in urban environments. Shadows can be used to detect buildings and estimate the heights of the buildings [1]. But during the progress of remote sensing images, the shadows have adverse impact on the image. They cause loss of information for the surface under the shadows as well as difficulties for image interpretation, image matching, change detection and other applications. The motivation for this research is to remove the big shadow regions in images, so that objects covered by shadows can be easily extracted for applications.

Many effective algorithms have been proposed for shadow detection. Existing shadow detection methods can be roughly categorized into two groups [9,4]: model-based methods and shadow-feature-based methods. The first group uses prior information such as scene, moving targets, and camera altitude to construct shadow models [5], [6]. This group of methods is often used in some specific scene conditions such as aerial image analysis and video monitoring. The second group of methods identifies shadow areas with information such as gray scale, brightness, saturation, and texture.

An improved algorithm exists that combines the two methods [3]. First, the shadow areas are estimated according to the space coordinates of buildings calculated from digital surface models and the altitude and azimuth of the sun. Then, to accurately identify a shadow, the threshold value is obtained from the estimated grayscale value of the shadow areas. However, information such as scene and camera altitude is not usually readily available. Consequently, most shadow detection algorithms are based on shadow features. For example, the shadow region appears as a low grayscale value in the image, and the threshold is chosen between two peaks in the grayscale histogram of the image data to separate the shadow from the nonshadow region [2]. An illuminant invariance model has been used to detect shadows; this method can obtain a comparatively complete shadow outline from a complex scene and derive the shadow-free image by using certain neutral interface reflecting assumptions [7]. In a related study, images are converted into different invariant color spaces (HSV, HCV, YIQ, and YCbCr) to obtain shadows with Otsu's algorithm [8]. This can effectively get rid of the false shadows created by vegetation in certain invariant spaces. Based on that work, a successive thresholding scheme was proposed to detect shadows [9]. To avoid the false shadows of dark objects such as vegetation and moist soil, the normalized difference vegetation index [10], and the normalized saturation-value difference index area considered [11].

A variety of image enhancement methods have been proposed for shadow removal, such as histogram matching [2], gamma correction [13], linear correlation correction (LCC) [2], [13], and restoration of the color invariance model [8]. In a related study [13], several enhancement methods were analyzed to recover shadows, namely, gamma correction, LCC, and histogram matching. Inspired by this related analysis, a better approach was developed, based on a linear relationship between shadow classes and the corresponding

nonshadow classes [12]. In addition, a paired-region-based approach is employed to detect and remove the shadows in a single image by calculating the difference between the shadow and nonshadow regions of the same type [14]. Aside from the aforementioned methods, shadows can be retrieved using multisource data. For example, shadow pixels can be identified from the region of interest in an image and from another image obtained at a different time. Then, nonshadow pixels of the corresponding region are used to replace the shadow pixels. This latter approach is useful in low-resolution images [2].

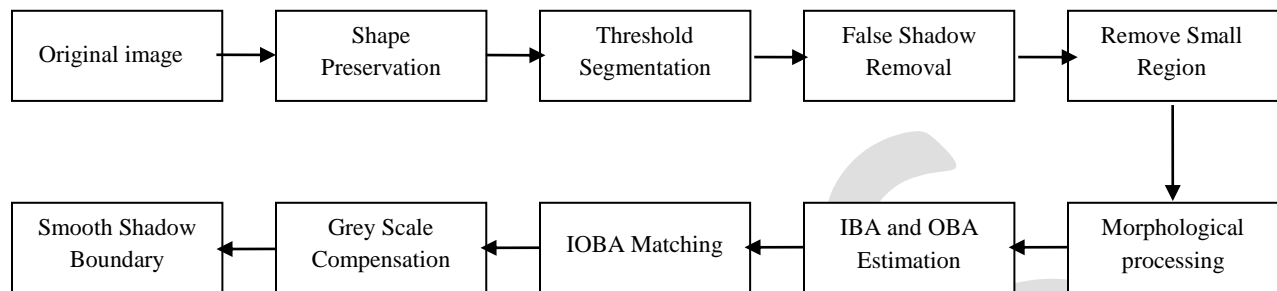


Fig.1 Flowchart of Shadow Processing Method of High Resolution Remote Sensing Image Using IOBA Matching

Due to the shortcomings of pixel-level shadow detection, in this study, we propose a new technique: a Shadow Processing Method of High Resolution Remote Sensing Image Using IOBA Matching. First, apply sobel operation for shape preservation, and then suspected shadows are detected with the threshold method of image segmentation. Next, the false shadows are ruled out (i.e., vegetation region). Then the shadow regions after removing the small regions are processed through mathematical morphology closed operation. This will allow only the real shadows to be detected in subsequent steps.

Shadow removal employs a series of steps. First we extract the inner and outer buffer area of each independent shadow region. Homogeneous sections are obtained through IOBA sectional matching. Finally, using the homogeneous sections, the mean and variance of the outer homogeneous sections is used to compensate the shadow region. The proposed method for shadow detection and removal is shown in Fig. 1.

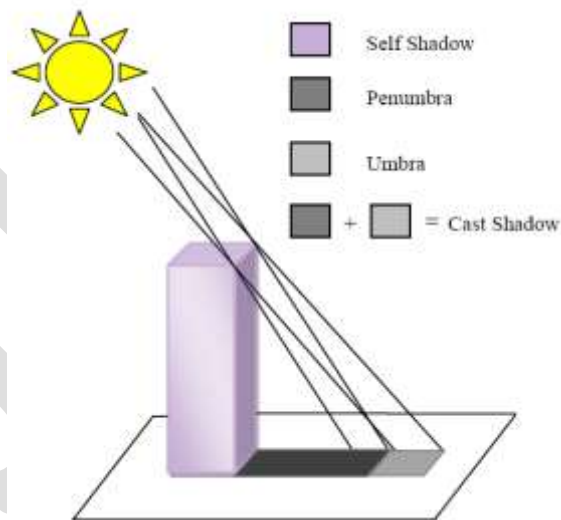


Fig. 2 Principle of shadow formation

PROPOSED METHOD

Shadows could be defined as the parts of the scene that is not directly illuminated by a light source due to an obstructing object or objects. A typical shadow could be divided into 2 different types. One type is denoted as self shadow where the shadow region is on the object itself. The other type is cast shadow for which the shadow region is on the background or on another objects. The cast shadow is usually further divided into 2 parts, umbra and penumbra. The umbra is created because the direct light has been completely blocked, while the penumbra is created by something partly blocking the direct light, as shown in Fig. 2. In remote sensing image we mainly focus only on the shadows in the cast shadow area. The proposed method consists of the following steps:

A. Shape Preservation

The shape preservation process is an option for providing additional shape information of the shadow-casting cultural features. The component is used in finding the boundaries and shapes of cultural features and dark regions, including shadows in which luminance is obstructed. A Sobel operator is applied on the gray component for shape preserved threshold segmentation,

B. Threshold Segmentation

For shadow detection, a properly set threshold can separate image into non-shadowed regions and shadow regions without too many pixels being misclassified [2]. Researchers have used several different methods to find the threshold to accurately separate shadow and non-shadow areas. Bimodal histogram splitting provides a feasible way to find the threshold for shadow detection, and the mean of the two peaks is adopted as the threshold [2]. Attain the threshold according to the histogram of the original image and then find the suspected shadow objects by comparing the threshold and grayscale average of each object obtained in segmentation. Chose the grayscale value with the minimum frequency in the neighborhood of the mean of the two peaks as the threshold, as shown in

$$G_q = \frac{1}{2} (G_m + G_s) \quad (1)$$

$$h(T) = \text{Min}\{h(G_q - \varepsilon), h(G_q + \varepsilon)\} \quad (2)$$

In the equations, G_m is the average grayscale value of an image; G_s stands for the left peak of the shadow in the histogram; T is the threshold; ε represents the neighborhood of T , where $T \in [G_q - \varepsilon, G_q + \varepsilon]$; and $h(I)$ is the frequency of I , where $I = 0, 1, \dots, 255$. To avoid the influence of abnormal information, 2% of the pixels on the left and right sides of the histogram are not included.

C. False Shadow Removal

Dark objects may be included in the suspected shadows, so more accurate shadow detection results are needed to eliminate these dark objects. Rayleigh scattering results in a smaller grayscale difference between a shadow area and a non-shadow area in the blue (B) waveband than in the red (R) and green (G) wavebands. Consequently, for the majority of shadows, the grayscale average at the blue waveband G_b is slightly larger than the grayscale average at the green waveband G_g . Also, the properties of green vegetation itself make G_g significantly larger than G_b , so false shadows from vegetation can be ruled out by comparing the G_b and G_g of all suspected shadows.

D. Remove Small Region

After initial image segmentation, an area of every independent decomposed region is computed. If it is lower than threshold value, it can be considered as surface features with low-light level in non-shadowed region and it is ruled out from shadow region.

E. Morphological processing

But in this case, cavity may appear because of extensive surface features with high-light level within shadow regions. Shadow regions after segmentation are processed through mathematical morphology closed operation.

F. IBA and OBA Estimation

Outer Buffer area (OBA) of each shadow region is the non shadow area around that connected shadow component. Thus, after determining the connected component, the Inner and Outer Buffer Area of each connected shadow components is computed using morphological dilation or erosion operation and image subtraction operation as follows:

$$I_{dilated,k} = (I_k \oplus B_{square}) \quad (3)$$

$$I_{eroded,k} = (I_k \ominus B_{square}) \quad (4)$$

The dilation operation will expand the shadow boundaries and the erosion operation will contract the shadow boundaries. B_{square} is a square structuring element. The size of the structuring element will decide the size of Inner and Outer Buffer Area. In this paper a 3x3 square structuring element is used.

$$I_{OBA,k} = (I_{dilated,k} - I_k) \quad (5)$$

$$I_{IBA,k} = (I_{eroded,k} - I_k) \quad (6)$$

where $k = 1, 2, \dots, m$ and m represent the sets of connected components or m different shadows in the image. m can have the value one or greater than one, depending on the number of shadows..

G. IOBA Matching

To recover the shadow areas in an image, we use a shadow removal method based on IOBA matching. There is a large probability that both shadow and non-shadow areas in close range on both sides of the shadow boundary belong to the same type of object. The Buffer Area (BA) in the shadow area is marked as Inner Buffer Area (IBA); Buffer Area (BA) in the non-shadow area is marked as Outer Buffer Area (OBA). When the correlation between IBA and OBA is close enough, there is a large probability that this location belongs to the same type of object. That is, similarity matching needs to be applied to the inner and outer buffer area section by section to rule out the two kinds of non-homogeneous sections.

To rule out the non-homogeneous sections, the inner and outer buffer area is divided into average sections with the same standard, and then, the similarity of each buffer area is calculated section by section. If the variance between inner and outer buffer area at a section is small, it means that the shade and light fluctuation features of the buffer area pair at this section are consistent. If consistent, then this buffer area pair belongs to the same type of object, with different illuminations, and thus is considered to be matching. If the variance between inner and outer buffer area at a section is large, then some abnormal parts representing some different types of objects exist in this section; therefore, these outer buffer area parts should be ruled out, as shown in Fig. 3.

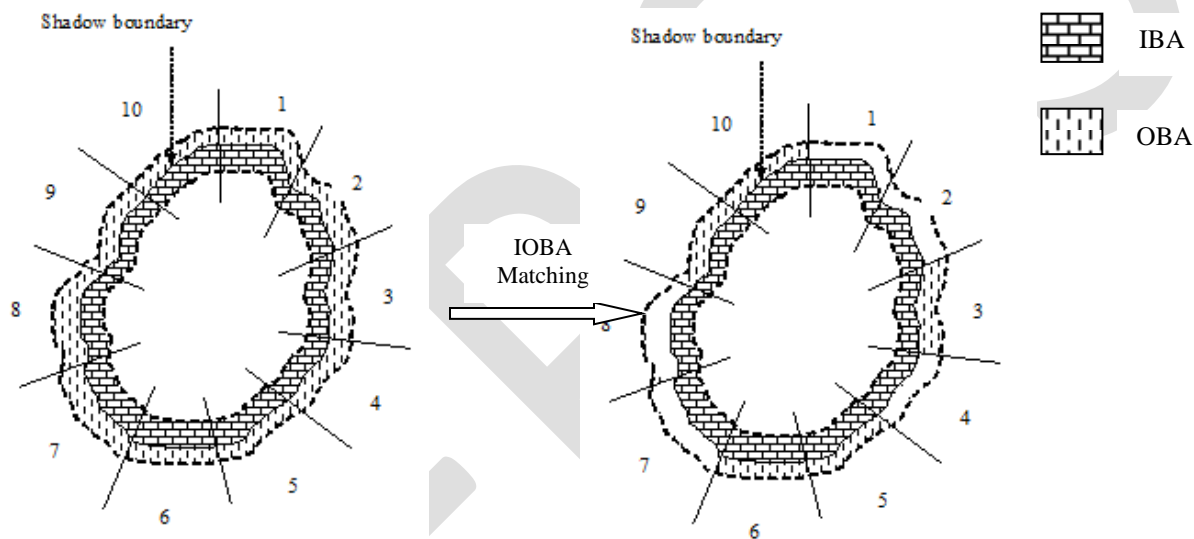


Fig. 3 Diagram of IOBA matching

H. Grey Scale Compensation

Shadows are removed, with the homogeneous sections (section - 3, 4, 5, 6, 9, 10) obtained by IOBA matching, using the following transformation function. That is, the mean and variance of outer buffer area after IOBA matching and mean and variance of shadow region is used to compensate the shadow region.

$$I'_k = \mu_{OBA',k} + \frac{I_k - \mu_k}{\sigma_k} * \sigma_{OBA',k} \quad (7)$$

where $k = 1, 2, \dots, m$. I'_k is the compensated value of the shadow pixel. $\mu_{OBA',k}$ and $\sigma_{OBA',k}$ are the mean and variance of the outer buffer area after IOBA matching. μ_k and σ_k the mean and variance of the corresponding shadow region. The resulting image is shadow free image.

I. Smooth Shadow Boundary

After processing mentioned above, an obvious boundary-line appears between shadow regions and clear surface feature regions. Fig. 4 can explain the reason of this phenomenon. Fig. 4 left is a typical boundary-line, vertical line means shadow regions boundary. Fig. 4 the right one is shadow boundary after processing. It is observed that a sudden gray change due to transition zone appears on shadow boundary. This is a strong boundary effect. To reduce this effect, a median filtering along shadow boundary could be in progress after grey scale compensation, so that transition of shadow regions to non-shadowed regions could be in progress.

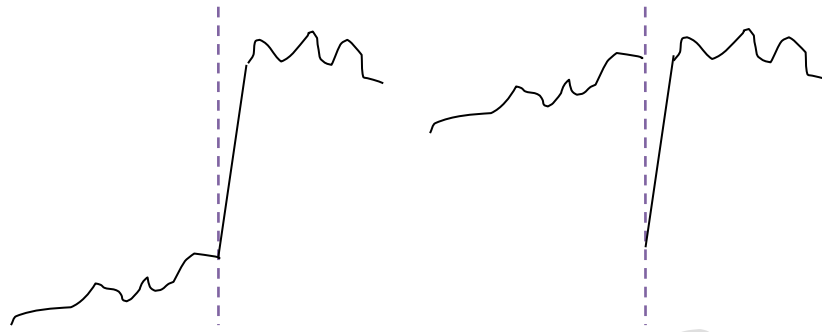


Fig. 4 Boundary regions before and after grey scale compensation

EXPERIMENTAL RESULTS

In order to test the validity of this method, a remote sensing image is used. Fig.3 shows the results of our proposed system. The accuracy of shadow detection can be seen from the fact that roads and vegetation regions are not detected as shadows, though they have similar characteristics as shadows. In the process of shadow removal on the high resolution remote sensing image, information in shadow regions should be tried to restore while information in non-shadowed regions should be tried to reserve.

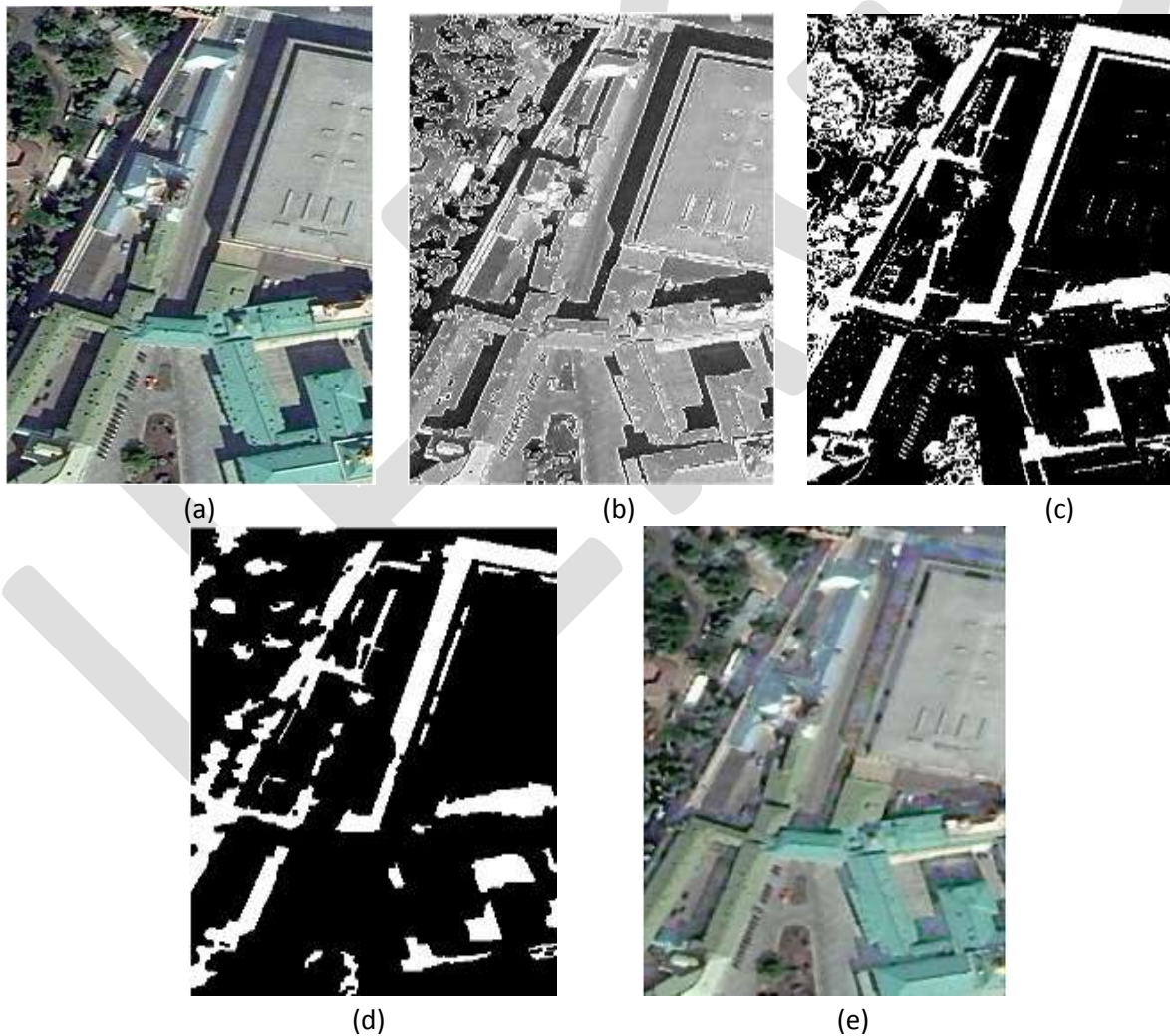


Fig.3 The results of proposed system (a) Original Image (b) Segmentation Result (c) Result of Shadow Detection (d) Result of Shadow Detection after False Shadow Removal (e) Recovered Image

CONCLUSION

This paper put forward a systematic and effective method for shadow detection and removal in a single high-resolution remote sensing image. In order to get a shadow detection result, image segmentation considering shadows is applied first. It classifies shadow and non-shadow region using threshold segmentation and false shadows are ruled out. After the homogeneous sections are obtained using IOBA matching, the mean and variance value of the outer buffer area around each shadow region is used to compensate the shadow region.

REFERENCES:

- [1] T. Kim, T. Javzandulam, and T.-Y. Lee, "Semiautomatic reconstruction of building height and footprints from single satellite images," in *Proc. IGARSS*, Jul. 2007, vol. 2, pp. 4737–4740.
- [2] P.M. Dare, "Shadow analysis in high-resolution satellite imagery of urban areas," *Photogramm. Eng. Remote Sens.*, vol. 71, no. 2, pp. 169–177, 2005.
- [3] Y. Li, P. Gong, and T. Sasagawa, "Integrated shadow removal based on photogrammetry and image analysis," *Int. J. Remote Sens.*, vol. 26, no. 18, pp. 3911–3929, 2005.
- [4] J. Yoon, C. Koch, and T. J. Ellis, "ShadowFlash: An approach for shadow removal in an active illumination environment," in *Proc. 13th BMVC*, Cardiff, U.K., Sep. 2–5, 2002, pp. 636–645.
- [5] R. B. Irvin and D. M. McKeown, Jr, "Methods for exploiting the relationship between buildings and their shadows in aerial imagery," *IEEE Trans. Syst., Man, Cybern.*, vol. 19, no. 6, pp. 1564–1575, Dec. 1989.
- [6] Y. Li, T. Sasagawa, and P. Gong, "A system of the shadow detection and shadow removal for high resolution city aerial photo," in *Proc. ISPRS Congr. Comm.*, 2004, vol. 35, pp. 802–807, Part B3.
- [7] E. Salvador, A. Cavallaro, and T. Ebrahimi, "Shadow identification and classification using invariant color models," in *Proc. IEEE Int. Conf. Acoust., Speech, Signal Process.*, 2001, vol. 3, pp. 1545–1548.
- [8] V. J. D. Tsai, "A comparative study on shadow compensation of color aerial images in invariant color models," *IEEE Trans. Geosci. Remote Sens.*, vol. 44, no. 6, pp. 1661–1671, Jun. 2006.
- [9] K.-L. Chung, Y.-R. Lin, and Y.-H. Huang, "Efficient shadow detection of color aerial images based on successive thresholding scheme," *IEEE Trans. Geosci. Remote Sens.*, vol. 47, no. 2, pp. 671–682, Feb. 2009.
- [10] D. Cai, M. Li, Z. Bao *et al.*, "Study on shadow detection method on high resolution remote sensing image based on HIS space transformation and NDVI index," in *Proc. 18th Int. Conf. Geoinformat.*, Jun. 2010, pp. 1–4.
- [11] [15] H. Ma, Q. Qin, and X. Shen, "Shadow segmentation and compensation in high resolution satellite images," in *Proc. IEEE IGARSS*, Jul. 2008, vol. 2, pp. 1036–1039.
- [12] L. Lorenzi, F. Melgani, and G. Mercier, "A complete processing chain for shadow detection and reconstruction in VHR images," *IEEE Trans. Geosci. Remote Sens.*, vol. 50, no. 9, pp. 3440–3452, 2012.
- [13] P. Sarabandi, F. Yamazaki, M. Matsuoka *et al.*, "Shadow detection and radiometric restoration in satellite high resolution images," in *Proc. IEEE IGARSS*, Sep. 2004, vol. 6, pp. 3744–3747.
- [14] R. Guo, Q. Dai, and D. Hoiem, "Single-image shadow detection and removal using paired regions," in *Proc. IEEE Conf. Comput. Vis. Pattern Recog.*, 2011, pp. 2033–2040.
- [15] Zhouwei Zhang and Fen Chen "A Shadow Processing Method of High Spatial Resolution Remote Sensing Image" 3rd International Congress on Image and Signal Processing, 2010
- [16] Krishna Kant Singh, Kirat Pal and M.J.Nigam, "Shadow Detection and Removal from Remote Sensing Images Using NDI and Morphological Operators," *International Journal of Computer Applications* (0975 – 8887) Volume 42– No.10, March 2012.

Priority And Lifetime Based Packet Scheduling Scheme In Wireless Sensor Networks

Deepthy Skariah, Eva George

PG Scholar, Department of ECE, CAARMEL Engineering College, Pathanamthitta, Kerala
Assistant Professor, Department of ECE, CAARMEL Engineering College, Pathanamthitta, Kerala

Email:deepthyskariah15@gmail.com

Abstract: A wireless sensor network (WSN) is a computer network consisting of spatially distributed autonomous devices using sensors to cooperatively monitor physical or environmental conditions such as temperature, sound, vibration, pressure, motion or pollutants, at different locations. The development of wireless sensor networks was originally motivated by military applications i.e. battlefield surveillance. However, wireless sensor networks are now used in many civilian application areas, including environment and habitat monitoring, healthcare applications, home automation, and traffic control. Scheduling different types of packets, such as real-time and non-real-time data packets, at sensor nodes with resource constraints in Wireless Sensor Networks (WSN) is of vital importance to reduce sensors energy consumptions and end-to-end data transmission delays.

Most of the existing packet scheduling mechanisms of the wireless sensor network use First Come First Served (FCFS) non pre-emptive priority and pre-emptive priority scheduling algorithms. The above algorithms have high processing overhead and also long end-to-end data transmission delay. In FCFS concept the data packet which is entering the node first will go out first from the node, and the packet which will enter last will leave at last. But in FCFS scheduling of real time data packets coming to the node have to wait for a long time period. In non pre-emptive priority scheduling algorithm there is starvation of real time data packets because once the processor enters the running state, it will not allow remove until it is completed, so there is starvation of real time data packets. In pre-emptive scheduling, starvation of non-real time data packets, due to continuous arrival of real time data. Therefore the data packets are to be schedule in multilevel queue. But the multilevel queue scheduling scheme is not suitable for dynamic inputs, and hence the scheme is designed for dynamically change in the inputs. The Dynamic Multilevel Priority (DMP) packet scheduling is the scheme for dynamically changes in the inputs. In this scheme each node except the last level of the virtual hierarchy in the zone based topology of wireless sensor network has three levels of priority queues. Real time data packets are placed into highest priority queue and can preempt the data packets in the other queues. Non real time data packets are placed into other two queues based on threshold of their estimated processing time. The leaf node have two queues, one for real time data packet and another for non real time data packet since they do not receive data from other nodes and thus reduces end to end delay. This scheme reduces the average waiting time and end to end delay of data packets.

Keywords: Wireless sensor network, packet scheduling, pre-emptive priority scheduling, non-pre-emptive priority scheduling, real-time, non-real-time, data waiting time, FCFS.

INTRODUCTION

A wireless sensor network (WSN) is a computer network which consists of spatially distributed autonomous devices using sensors to look after physical or environmental conditions like temperature, vibration, sound, pressure, motion or pollutants in various locations. Military applications gave motivation for the development of wireless sensor networks i.e. in battlefield. Now a days wireless sensor networks are used in many civilian applications, healthcare applications, home automation and in traffic control. Scheduling is the most widely used concept in WSNs because it determines the order of transmission of number of data packets based on their data priority and transmission deadline. For instance, real time data packets are given the highest priority when compared to that of non-real time data packets. Some of the available or existing scheduling mechanisms in wireless sensor networks are First Come First Serve, Preemptive Priority and Non preemptive Priority algorithms. The major drawbacks of using these algorithms are that the end-to-end transmission delay will be more and processing overhead will be high. Dynamic refers to the system which is active and undergoes progress frequently. Multilevel priority indicates that instead of single queue, multiple queues are used to assign different priorities to the incoming packet. Packet scheduling is the process used to select which packet to be serviced or which to be dropped based on the priority such as real time packet and non-real time packet. Packet scheduling can guarantee quality of service and improve transmission rate in wireless sensor networks. The proposed scheme Dynamic Multilevel Priority (DMP) packet scheduling is for the processes where the inputs changes dynamically. In this scheme, zone based topology is used where the nodes are organized in virtual hierarchy. All the nodes except the last level has three different levels of priority queues. Real time data packets are placed into

highest priority queue and can preempt the data packets in the other queues. The leaf node has only two queues. One is for real time data packets and other is for non-real time data packets because it will not receive any data from lower level nodes. Hence this scheme reduces average waiting time and end-to-end transmission delay.

RELATED WORK

The existing task scheduling algorithm are based on several factors such as Deadline: - Packet scheduling schemes can be classified based on the deadline of arrival of data packets to the base station (BS), which are as follows First Come First Served (FCFS): Most existing WSN applications use First Come First Served (FCFS) schedulers that process data in the order of their arrival times at the ready queue. In FCFS, data that arrive late at the intermediate nodes of the network from the distant leaf nodes require a lot of time to be delivered to base station (BS) but data from nearby neighbouring nodes take less time to be processed at the intermediate nodes. In FCFS, many data packets arrive late and thus, experience long waiting times.

A. Deadline

First Come First Serve: This may be the simplest way for a scheduler to schedule the packets. In fact, FCFS does not consider the QoS parameters of each packets, it just sends the packets according to the order of their arrival time. Thus, the QoS guarantee provided by FCFS is in general weak and highly depends on the traffic characteristic of flows. For example, if there are some flows which have very bursty traffic, under the discipline of FCFS, a packet will very likely be blocked for a long time by packets burst which arrives before it. In the worst case, the unfairness between different flows cannot be bounded, and the QoS cannot be no longer guaranteed. However, since FCFS has the advantage of simple to implement, it is still adopted in many communication networks, especially the networks providing best effort services. If some level of QoS is required, then more sophisticated scheduling algorithm is needed.

Earliest Deadline First (EDF): For networks providing real-time services such as multimedia applications, earliest deadline first (EDF) is one of the most well-known scheduling algorithms. The concept behind EDF is straightforward. It essentially schedules the packets in a greedy manner which always picks the packets with the closest deadline. Compare with strict priority discipline, we can regard EDF as a scheduling algorithm which provides time-dependent priority to each eligible packet.

Packet Type: - Packet scheduling schemes can be classified based on the types of data packets, which are as follows.

Real-time packet scheduling: Packets at sensor nodes should be scheduled based on their types and priorities. Real-time data packets are considered as the highest priority packets among all data packets in the ready queue. Hence, they are processed with the highest priority and delivered to the BS with a minimum possible end-to-end delay.

Non-real-time packet scheduling: Non-real time packets have lower priority than real-time tasks. They are hence delivered to BS either using first come first serve or shortest job first basis when no real-time packet exists at the ready queue of a sensor node. These packets can be intuitively preempted by real-time packets.

Priority: Packet scheduling schemes can be classified based on the priority of data packets that are sensed at different sensor nodes
Non-preemptive: In non-preemptive priority packet scheduling, when a packet t1 starts execution, task t1 carries on even if a higher priority packet t2 than the currently running packet t1 arrives at the ready queue. Thus t2 has to wait in the ready queue until the execution of t1 is complete.

Preemptive: In preemptive priority packet scheduling, higher priority packets are processed first and can preempt lower priority packets by saving the context of lower priority packets if they are already running.

Number of Queue: - Packet scheduling schemes can also be classified based on the number of levels in the ready queue of a sensor node. These are as follows.

Single Queue: Each sensor node has a single ready queue. All types of data packets enter the ready queue and are scheduled based on different criteria: type, priority, size, etc. Single queue scheduling has a high starvation rate.

Multi-level Queue: Each node has two or more queues. Data packets are placed into the different queues according to their priorities and types. Thus, scheduling has two phases: (i) Allocating tasks among different queues, (ii) scheduling packets in each queue. The number of queues at a node depends on the level of the node in the network. For instance, a node at the lowest level or a leaf node has a minimum number of queues whilst a node at the upper levels has more queues to reduce end-to-end data transmission delay and balance network energy consumptions. Figure 1 illustrates the main concept behind multi-level queue scheduling algorithms.

ASSUMPTIONS

The following assumptions are made to design and implement DMP packet scheduling scheme

- Data traffic comprises only real-time and non-real-time data, e.g., real-time health data sensed by body sensors and non-real-time temperature data.
- All data packets (real-time and non-real-time) are of same size
- Sensors are time synchronized.
- No data aggregation is performed at intermediate nodes for real time data.
- Nodes are considered located at different levels based on the number of hop counts from BS.
- Timeslots are allocated to nodes at different levels using TDMA scheme, e.g., nodes at the lowest level, l_k are assigned timeslot 1. Details of timeslot allocation are explained in the “Terminologies” subsection.
- The ready queue at each node has maximum three levels or sections for real-time data (pr1) non-real-time remote data (pr2) and non-real-time local data (pr3).
- The length of data queues is variable. For instance, the length of real-time data queue (pr1) is assumed to be smaller than that of non-real-time data queues (pr2 and pr3). However, the length of the non-real-time pr2 and pr3 queues are same.
- DMP scheduling scheme uses a multichannel MAC protocol to send multiple packets simultaneously.

TERMINOLOGIES

In this section, we define the following terminologies and factors that are used in designing the DMP packet scheduling scheme.

Protocol Used

The Zone Routing Protocol (ZRP) aims to address the problems by combining the best properties of both approaches. ZRP can be classed as a hybrid reactive/proactive routing protocol. ZRP reduces the proactive scope to a zone centred on each node. In a limited zone, the maintenance of routing information is easier. Further, the amount of routing information that is never used is minimized. Still, nodes farther away can be reached with reactive routing. Despite the use of zones, ZRP has a flat view over the network. In this way, the organizational overhead related to hierarchical protocols can be avoided. First hybrid routing protocol with both a proactive and a reactive routing component. IARP periodically computes the route to all intra zone nodes (nodes that are within the routing zone of a node) and maintains this information in a data structure called IARP routing table. In order to know about a node's direct neighbours and possible link failures, IARP depends on a neighbour Discovery Protocol (NDP) provided by the MAC layer. IERP is a family of reactive routing protocols like DSR or AODV that offer enhanced route discovery and route maintenance services based on local connectivity monitored by IARP. For route discovery by IERP, the notion border casting is introduced.

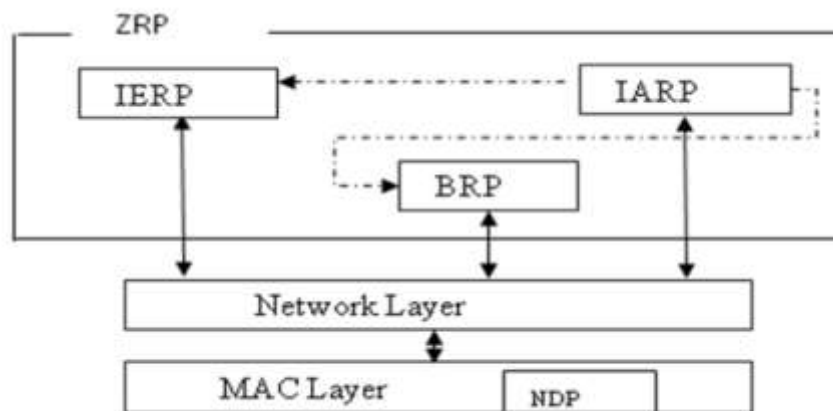


Fig 1: ZRP Architecture

In a zone based routing protocol, each zone is identified by a zone head (ZH) and nodes follow a hierarchical structure, based on the number of hops they are distant from the base station (BS). For instance, nodes in zones that are one hop and two hops away from the BS are considered to be at level 1 and level 2, respectively. Each zone is also divided into a number of small squares in such a way that if a sensor node exists in square S1, it covers all neighbouring squares. Thus, this protocol reduces the probability of having any sensing hole in the network even if the neighbouring squares of a node do not have any sensor node.

PROPOSED DYNAMIC MULTILEVEL PRIORITY PACKET SCHEDULING SCHEME

In non-preemptive packet scheduling schemes real-time data packets have to wait for completing the transmissions of other non-real-time data packets. On the other hand, in preemptive priority scheduling, lower-priority data packets can be placed into starvation for continuous arrival of higher priority data. In the multilevel queue scheduling algorithm [], each node at the lowest level has a single task queue considering that it has only local data to process. However, local data can also be real-time or non-real time and should be thus processed according to their priorities. Otherwise, emergency real-time data traffic may experience long queuing delays till they could be processed. Thus, we propose a Dynamic Multilevel Priority (DMP) packet scheduling scheme that ensures a trade off between priority and fairness.

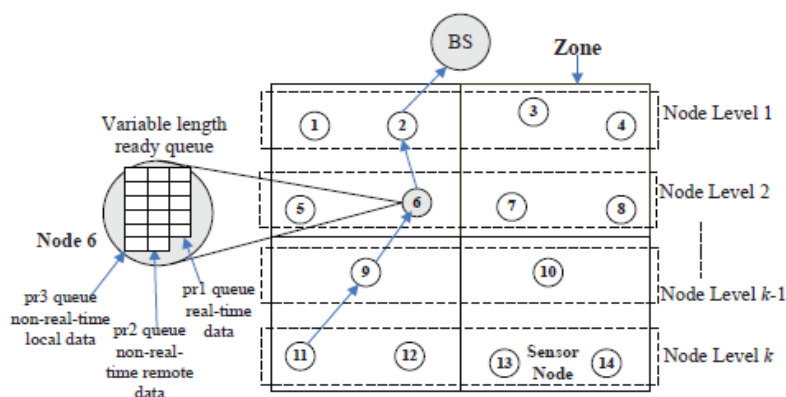


Fig 2: Dynamic Multilevel priority scheduling scheme

Among many network design issues, such as routing protocols and data aggregation, that reduce sensor energy consumption and data transmission delay, packet scheduling (interchangeably use as task scheduling) at sensor nodes is highly important since it ensures delivery of different types of data packets based on their priority and fairness with a minimum latency. For instance, data sensed for real-time we propose a Dynamic Multilevel Priority (DMP) packet scheduling scheme for WSNs in which sensor nodes are virtually organized into a hierarchical structure. Nodes that have the same hop distance from the BS are considered to be located at the same hierarchical level. We consider a network then divide it into zones. Each zone has a zone head which is used for routing. Zone head are used for routing data to the destination i.e. to the base station. Data are transmitted with the help of zone head. Other member nodes are not used for routing. They only transmit data to their zone head within the zone. Within a zone data are sending through Intra-zone routing and outside the zone data are sending through inter-zone routing.

WORKING PRINCIPLE

The proposed scheduling scheme assumes that nodes are virtually organized following a hierarchical structure. Nodes that are at the same hop distance from the base station (BS) are considered to be located at the same level as shown in figure 5.1. Data packets of nodes at different levels are processed using the Time-Division Multiplexing Access (TDMA) scheme. For instance, nodes that are located at the lowest level and the second lowest level can be allocated timeslots 1 and 2, respectively. We consider three-level of queues, that is, the maximum number of levels in the ready queue of a node is three: priority 1 (pr1), priority 2 (pr2), and priority 3 (pr3) queues. Real-time data packets go to pr1, the highest priority queue, and are processed using FCFS. Non-real-time data packets that arrive from sensor nodes at lower levels go to pr2, the second highest priority queue. Finally, non-real time data packets that are sensed at a local node go to pr3, the lowest priority queue as shown in below figure 3.2. The possible reasons for choosing maximum three queues are to process (i) real-time pr1 tasks with the highest priority to achieve the overall goal of WSNs, (ii) non real-time pr2 tasks to achieve the minimum average task waiting time and also to balance the end to end delay by giving higher priority to remote data packets, (iii) non-real-time pr3 tasks with lower priority to achieve fairness by preempting pr2 tasks if pr3 tasks wait a number of consecutive timeslots.

In the proposed scheme, queue sizes differ based on the application requirements. Since preemptive priority scheduling incurs overhead due to the context storage and switching in re- source constraint sensor networks, the size of the ready queue for preemptive priority schedulers is expected to be smaller than that of the preemptable priority schedulers. The idea behind this is that the highest-

priority real-time/emergency tasks rarely occur. They are thus placed in the preemptive priority task queue (pr1 queue) and can preempt the currently running tasks. Since these processes are small in number, the number of preemptions will be a few. On the other hand, non-real-time packets that arrive from the sensor nodes at lower level are placed in the preemptable priority queue (pr2 queue). The processing of these data packets can be preempted by the highest priority real-time tasks and also after a certain time period if tasks at the lower priority pr3 queue do not get processed due to the continuous arrival of higher priority data packets. Real time packets are usually processed in FCFS fashion. Each packet has an ID, which consists of two parts, namely level ID and node ID. When two equal priority packets arrive at the ready queue at the same time, the data packet which is generated at the lower level will have higher priority. This phenomenon reduces the end-to-end delay of the lower level tasks to reach the BS. For two tasks of the same level, the smaller task (i.e., in terms of data size) will have higher priority. Moreover, it is expected that when a node x senses and receives data from lower-level nodes, it is able to process and forward most data within its allocated timeslot; hence, the probability that the ready queue at a node becomes full and drops packets is low. However, if any data remains in the ready queue of node x during its allocated timeslot, that data will be transmitted in the next allocated timeslot. Timeslots at each level are not fixed. They are rather calculated based on the data sensing period, data transmission rate, and CPU speed. They are increased as the levels progress through BS. However, if there is any real-time or emergency response data at a particular level, the time required to transmit that data will be short and will not increase at the upper levels since there is no data aggregation.

The remaining time of a timeslot of nodes at a particular level will be used to process data packets at other queues. Since the probability of having real-time emergency data is low, it is expected that this scenario would not degrade the system performance. Instead, it may improve the perceived Quality of Service (QoS) by delivering real-time data fast. Moreover, if any node x at a particular level completes its task before the expiration of its allocated timeslot, node x goes to sleep by turning its radio off for the sake of energy efficiency.

METHODOLOGY OF THE PROPOSED SYSTEM

Methodology of the proposed system requires the following parameters

A. Network Initialization

In the network design the nodes 'n' are deployed randomly in the networks. The node which is in the centre of the network is chosen as the base station. And the communication range of the node is set to 250m. Area where the nodes are deployed is divided into number of zones and for each zone, zone head is chosen.

B. Packet Classification

Packets are classified based on the priority levels. Packet scheduling at sensor nodes is highly important since it ensures delivery of different types of data packets based on their priority and fairness with a minimum latency. For instance, data sensed for real-time applications have higher priority than data sensed for non-real-time applications. The processing of data packets available at a sensor node and also reduces energy consumptions

C. Task Scheduling

Allocation is done for task schedulers. Based on the priority queue packets are scheduled. Real time packets which are given the higher priority are scheduled using FCFS. Non real time packets with other two lower priorities are processed using SJF

D. Performance Evaluation

Evaluating the performance of this system gives positive results on minimum average waiting time and reduction in end-to-end delay while transmission. We compare results obtained from DMPPS with that of FCFS and obtain simulation results.

SIMULATION RESULTS

The simulation model is implemented using the NS2 programming language. It is used to evaluate the performance of the proposed DMP packet scheduling scheme, comparing it against the FCFS, and Multilevel Queue scheduling schemes. The comparison is made in terms of average packet waiting time, and end-to-end data transmission delay. The number of simulated zones varies from 4 to 12 zones. Nodes are distributed uniformly over the zones. The ready queue of each node can hold a maximum of 50 tasks. Each task has a Type ID that identifies its type. For instance, type 0 is considered to be a real-time task. Data packets are placed into the ready queue based on the processing time of the task. Moreover, each packet has a hop count number that is assigned randomly, and the packet with the highest hop count number is placed into the highest-priority queue. We run the simulation both for a specific number of zones, and levels in the network until data from a node in each zone or level reach BS. Simulation results are presented for both real-time data and all types of data traffic.

Here the nodes are assigned priorities that is 0 and 1. Priority 0 means highest priority and 1 means lower priority. Packets originating from these nodes will have respective priorities. When packet 0 arrives at a node it will check the priority of the packets. The packet having priority 0 is forwarded first to the destination (BS).

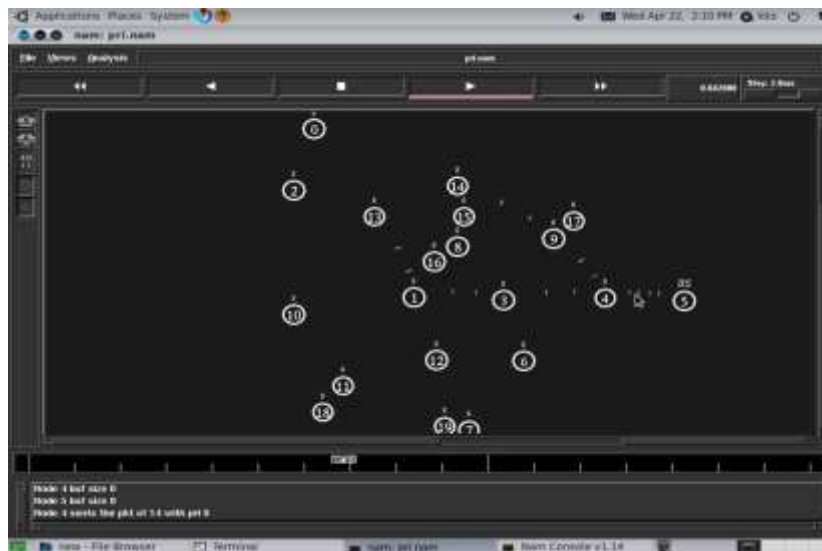


Fig 3: DMP Packet scheduling

In the DMP task scheduling approach, the source of a data packet is used to define the priority of data packets other than real-time. The priority of non-real time data packet will be more if it is sensed at remote node rather than the current sending node. Moreover, when no real-time tasks are available, pr3 tasks can preempt pr2 tasks if they are in starvation for a long time. This allows the processing of different types of tasks with fairness. The memory is also dynamically allocated to three queues and the size of the highest-priority queue is usually smaller than the two other queues since pr1 real-time tasks do not occur frequently compared to non-real-time tasks. As the memory capacity of a sensor node is limited, this also balances memory usages. Moreover, tasks are mostly non-real-time and are processed in the pr2 and pr3 queues. Non-real-time tasks that a node x receives from the lower level nodes are known as non-real time remote tasks and processed with higher priority (pr2) than the non-real-time local tasks that x senses. Thus, non-real time remote tasks incur less average waiting time. In addition, the average waiting time will not be affected for real-time tasks that are processed using FCFS scheduling, since these real-time tasks occur infrequently with a short processing time.

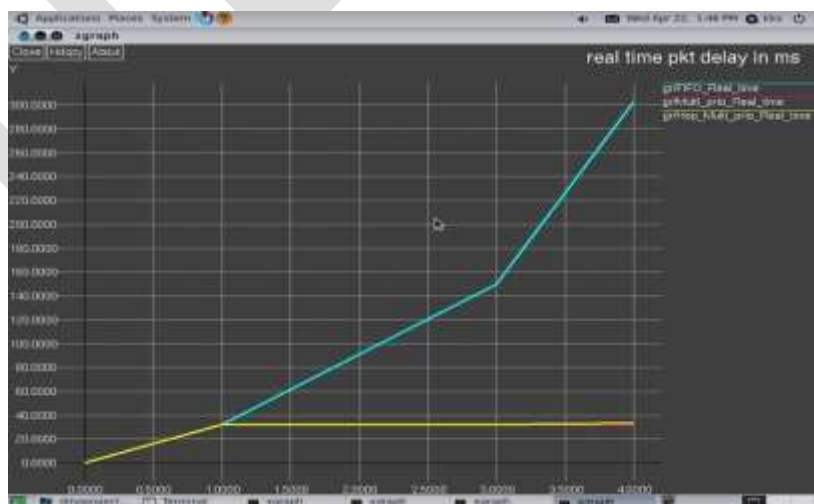


Fig 4: Real time packet delay comparison

The figure shows the comparison between the real time packet delays of DMP packet scheduling scheme, comparing it against the FCFS, and Multilevel Queue scheduling schemes.

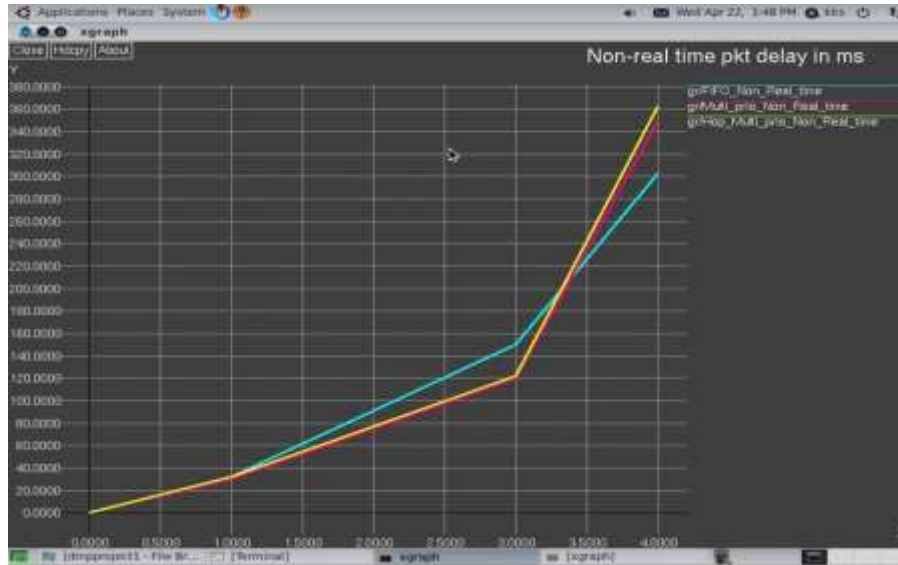


Fig 5: Non Real time packet delay comparison

The figure shows the comparison between the non-real time packet delays of DMP packet scheduling scheme, comparing it against the FCFS, and Multilevel Queue scheduling schemes.



Fig 6: Life time based packet scheduling

Here packets are assigned priorities according to their life time. Packets having shorter life time will be given higher priority than the packet having longer life time. The aim of life time based packet scheduling is to deliver the data packet before the expiration of its life time.

Figure 7 shows that in networks dead packets causes congestion. The dead packets are the packets whose life time has been expired.

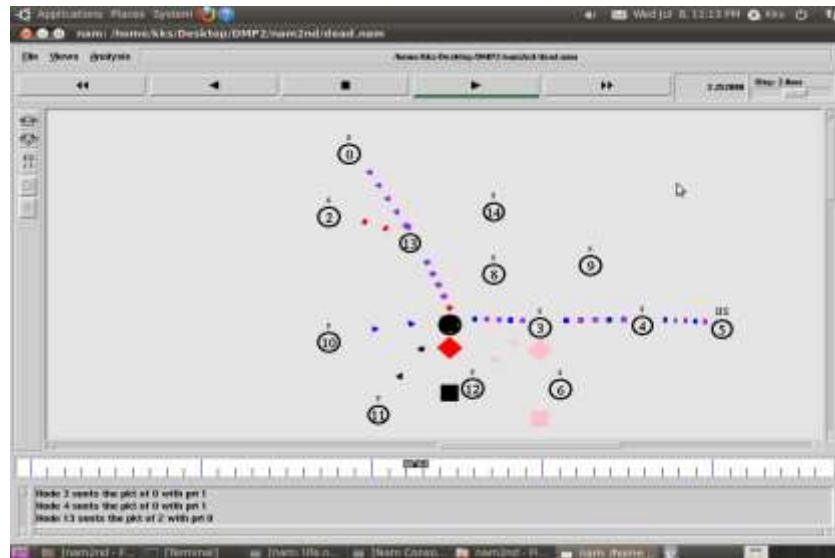


Fig 7: Dead packet dropping

CONCLUSION

We have discussed the hybrid Zone Routing Protocol in this paper, which is the combination of reactive and proactive routing protocols and have advantages of both type of protocols. The ZRP protocol is suitable for large networks and is not an independent protocol but rather a routing framework. It is especially well adapted to large networks and diverse mobility patterns and also we propose a Dynamic Multilevel Priority (DMP) packet scheduling scheme for Wireless Sensor Networks (WSNs). The scheme uses three-level of priority queues to schedule data packets based on their types and priorities. It ensures minimum end-to-end data transmission for the highest priority data while exhibiting acceptable fairness towards lowest-priority data. Experimental results show that the proposed DMP packet scheduling scheme has better performance than the existing FCFS and Multilevel Queue Scheduler in terms of the average task waiting time and end- to-end delay.

Also here we are scheduling the packets base on life time, which ensures that the delivery of data packets before the expiration of its life time. Dead packet dropping reduces the network congestion and makes this scheduling most suited for real time applications.

REFERENCES:

- [1] B. Nazir and H. Hasbullah, "Dynamic sleep scheduling for minimizing delay in wireless sensor network," in Proc. 2011 Saudi International Electron., Communications Photon. Conf., pp. 1–5
- [2] P. Guo, T. Jiang, Q. Zhang, and K. Zhang, "Sleep scheduling for critical event monitoring in wireless sensor networks," IEEE Trans. Parallel Distrib. Syst., vol. 23, no. 2, pp. 345–352, Feb. 2012.
- [3] O. Khader, A. Willig, and A. Wolisz, "Distributed wakeup scheduling scheme for supporting periodic traffic in wsns," in Proc. 2009 European Wireless Conf., pp. 287–292.
- [4] Y. H. Wang, Y. L. Wu, and K. F. Huang, "A power saving sleep scheduling based on transmission power control for wireless sensor networks," in Proc. 2011 International Conf. Ubi-Media Computer, pp. 19–24.
- [5] Nidal Nasser, Lutful Karim, and Tarik Taleb "Dynamic Multilevel Priority Packet Scheduling Scheme for Wireless Sensor Network", IEEE Transactions On Wireless Communications, VOL. 12, NO. 4, APRIL 2013, pp. 1448-1459.

- [6] Ali Sharifkhani, and Norman C. Beaulieu, "A Mobile-Sink-Based Packet Transmission Scheduling Algorithm for Dense Wireless Sensor Networks", IEEE Transactions On Vehicular Technology, VOL. 58, NO. 5, JUNE 2009, pp. 2509-2518.
- [7] Nilesh Khude, Anurag Kumar, Aditya Karnik, "Time and Energy Complexity of Distributed Computation of a Class of Functions in Wireless Sensor Networks", IEEE Transactions On Mobile Computing, VOL. 7, NO. 5, MAY 2008, pp. 617-631.
- [8] Xiaoling Zhang, Wei Liang, Haibin Yu, Xisheng Feng, "Reliable transmission scheduling for multi-channel wireless sensor networks with low-cost channel estimation", IET Communications, ISSN1, 2013, Vol. 7, pp. 71-81.
- [9] F. Liu, C. Tsui, and Y. J. Zhang, "Joint routing and sleep scheduling for lifetime maximization of wireless sensor networks," IEEE Trans. Wireless Communication, vol. 9, no. 7, pp. 2258-2267, July 2010.
- [10] J.Liu, N.Guo, and S. He, "An energy-aware coverage based node scheduling scheme for wireless sensor networks," in Proc. 2008 International Conf. Young Comput. Scientists, pp. 462-468.
- [11] S. Paul, S. Nandi, and I. Singh, "A dynamic balanced-energy sleep scheduling scheme in heterogeneous wireless sensor network," in Proc. 2008 IEEE International Conf. Netw., pp. 1-6, 2008.
- [12] O. Khader, A. Willig, and A. Wolisz, "Distributed wakeup scheduling scheme for supporting periodic traffic in wsns," in Proc. 2009 European Wireless Conf., pp. 287-292

Excellent Code Dissemination Protocol using Multi-objective Optimization in WSN

Saniya Elza Dominic, Gayathri.R.Krishna

MG university, Saniya.prakkadan@gmail.com, 9447124870

Abstract— Wireless reprogramming is a difficult technique for software deployment in wireless sensor networks (WSNs). Code dissemination is a basic building block to enable wireless reprogramming. Here present ECD, an Excellent Code Dissemination protocol leveraging 1-hop link quality information based on the TinyOS platform. Compared to previous works, ECD has three main features. First, it supports dynamically configurable packet sizes. By increasing the packet size for high PHY rate radios, it improves the transmission efficiency. Second, it has a precise sender selection algorithm to mitigate transmission collisions and transmissions over poor links. Third, it has a simple impact-based backoff timer design to shorten the time spent in coordinating multiple eligible senders so that the largest impact sender is most likely to transmit. These features is incorporated into multi objective optimization (MOPs) approach using Genetic algorithm (GA) to further reduce delay due to best sender selection. Results show that ECD-MOP outperforms other protocols, in terms of completion time.

Keywords— Dissemination, Delay, Genetic algorithm, Link quality, Multi objective optimization, Reprogramming, Wireless sensor network.

I. INTRODUCTION

Recent development in microelectronic mechanical systems and wireless communication technologies have fostered the rapid development of networked embedded systems like wireless sensor networks (WSNs) [1], [23]. A wireless sensor network (WSN) consists of a number of nodes used for monitoring purposes which pass the information collected via the network to a main location.

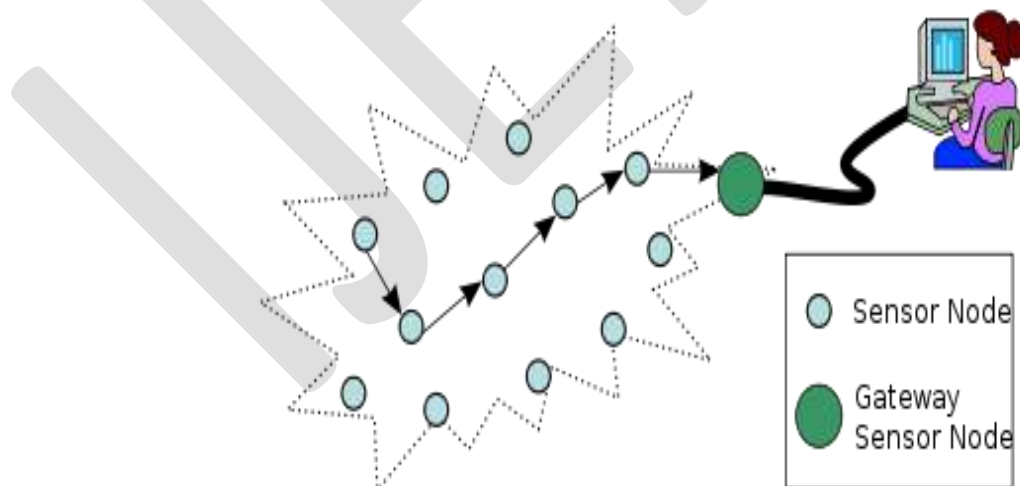


Fig.1. Example of a wireless sensor network

WSN applications often need to be changed after deployment for a variety of reason, reconfiguring a set of parameters, changing tasks of individual nodes, and patching security holes. Many large-scale WSNs [12], however, are deployed in environments

where physically collecting previously deployed nodes is either very difficult or infeasible. Wireless reprogramming is a crucial technique to address such challenges.

Code dissemination is a basic building block for wireless reprogramming [4], [21]. Existing code dissemination protocols (represented by Deluge [6] and MNP [7]) adopt several key techniques to ensure high reliability and performance. First, they exchange control-plane messages for high reliability [6], [7], and [21]. Second, they segment a large code object into fixed-sized pages for pipelining [6], [7]. The page transmission time and inter-page negotiation time (which involves exchanges of control-plane messages) are therefore two major contributors to the overall completion time.

However, existing protocol designs exhibit their inefficiency in two main areas. First, the data throughput Efficiency--the ratio between the network throughput and PHY data rate degrades rapidly as the PHY rate increases. For example, given the packet size of approximately 36 bytes in both Deluge and MNP (both were originally designed for the 19.2 Kbps CC1000 radio), the efficiency ratio for the current 250 Kbps CC2420 radio is only 14.3 percent. Second, the current sender selection algorithm in MNP [7] (for addressing the broadcast storm problem [14]) does not consider link quality information and needs multiple rounds of message exchanges, resulting in transmission redundancy and long completion time. To address the first issue, here increase the packet size to improve the transmission efficiency for high PHY rate radios. However, it would be inappropriate to fix the packet size to its maximum allowable size as a fixed packet size may not be appropriate for all platforms under every conditions [3]. Therefore, we support dynamically configurable packet sizes in design.

To overcome the second issue, leverages 1-hop neighbors' link quality information learned over the air to improve the sender selection accuracy. Here dynamically estimate the impacts of senders by considering both uncovered neighbours (i.e., neighbors that do not receive an entire page) and the link qualities to those neighbors. A node's transmission is considered more effective if the node has more uncovered neighbours with good link qualities. Taking link qualities help to put minimum weight on senders with poor link qualities to their neighbors. This is especially important when large packets are transmitted over the air. The basic idea is to prioritize sender transmissions so that the best sender with the largest impact is most likely to transmit.

Here an impact-based backoff timer design is used to shorten the time spent in coordinating multiple eligible senders so that the largest impact sender is most likely to transmit. To further reduce delay due to accurate sender selection, Here incorporate Multi objective based optimization using genetic algorithm. Genetic algorithm is known as a global heuristic algorithm, a genetic algorithm generates an optimal solution through generating different individuals. Focused fitness function is one of procedures of the algorithm.

II. RELATED WORKS

Deluge [6] is perhaps the most popular code dissemination protocol used for reliable code updates. Hui et al. gave Deluge which is a reliable data dissemination protocol for propagating large data objects (by dividing those to fixed sized pages) from one source node to other nodes over a multi-hop, wireless sensor network [6]. Dissemination of large data objects i.e. program images poses many issues like large size of programs, toleration of varying node densities and ensuring complete reliability in transfer etc.

Deluge achieves reliability in unpredictable wireless environments and robustness when node densities can vary by factors of a thousand or more. This protocol is based on Trickle algorithm. Here each and every node follows a set of strictly local rules to achieve data dissemination in the network. A node at regular intervals advertises the most recent version of the data item it has to whichever nodes that can hear its broadcast. Consider B receives an advertisement from an older node A, and then B will respond with the information that it has. From the information received, A determines which portion of the data items need updating and requests them from any neighbour that advertises the availability of the needed data, including B. Nodes receiving these requests then broadcast any requested data. Thus nodes advertise newly received data in order to propagate it further to other nodes. A problem in Deluge is that when a sender receives requests from receivers, it will start transmitting data packets after a specified timeout. Multiple senders in a neighborhood start transmitting concurrently, causing collisions.

Sandeep et al. proposed a multihop network reprogramming protocol (MNP) [7]. It provides a reliable service to propagate new program code to all sensor nodes in the network. The main aim of this dissemination protocol is to ensure reliable, low memory usage and fast data dissemination. It is based on a sender selection protocol in which source nodes compete with each other based on the number of distinct requests they have received. In each neighbourhood, a source node sends out program codes to multiple receivers. When the receivers get the whole program image at their side, they become source nodes, and send the code into their

neighbourhood. But here there can be issues of collisions. This is solved by selecting a suitable sensor node based on some parameters maintained by the nodes and some advertisement and download messages exchanged by the nodes. It is like a greedy algorithm. Pipelining can be used in this protocol to enable faster data propagation in the case of larger networks. To do pipelining, programs are divided into segments, each of which contains a fixed number of packets. Once a sensor node receives all the segments of a program, it can reboot with the new program. This continues till all the nodes are hence updated.

Compared to the above two works, our system has two main differences. First, a dynamically configurable packet sizes to support large packets to improve the dissemination performance. Second, employs an accurate and fast sender. Sprinkler [13] uses the localization service at each node to construct a connected dominating set (CDS). It uses TDMA to schedule packet transmissions among the CDS nodes to reduce energy consumption by minimizing packet transmissions. ECD mitigate the problem by limiting the number of concurrent transmitters in a neighborhood via dynamic sender selection.. Sprinkler, employs a TDMA-based approach. Sprinkler assumes a unit disk radio model. Nodes can be assigned the same time slot (and can concurrently transmit) only when the distance is sufficiently large. However, whether there are collisions in practice depends on whether the unit disk radio model is accurate enough as well as whether the model keeps unchanged over time.

CF [22] is a recent work that exploits spatial link correlation to mitigate ACK overhead. ECD vary with CF in three aspects. First, CF is used for flooding a single packet while ECD is used for disseminating large code objects consisting of multiple pages and packets. CF does not assure a 100 percent reliability while ECD employs handshake and negotiation to achieve 100 percent reliability. Second, the basic rule for sender selection are the same for both protocols, i.e., choosing the sender which can cover the most number of uncovered (i.e., not yet received) receivers in a neighborhood. The techniques used in both protocols, however, are different. CF relies on ACKs and exploits link correlation to estimate the expected number of uncovered nodes while ECD relies on NAKs (i.e., REQ messages) and the link qualities to estimate the expected number of uncovered receivers. Third, both protocols rely on backoff timers to prioritize the transmissions. In CF the backoff period is simply calculated as the reciprocal of the impact. In ECD, the backoff period is more carefully optimized by minimizing the probabilities of “priority inversion” and transmission collisions.

III. MOTIVATION

This section identifies the need to incorporate a more accurate sender selection algorithm.

Sender Selection

Sender selection is a well studied technique to reduce contentions and collisions in broadcast protocols. The basic principle in these algorithms is to select the best sender for forwarding the data while avoiding simultaneous transmissions from other neighboring nodes. This includes two main aspects. First, an precise metric should be used to estimate senders' impacts. Second, efficient mechanisms should be designed to coordinate transmissions of eligible senders so that the largest impact sender is most likely to transmit.

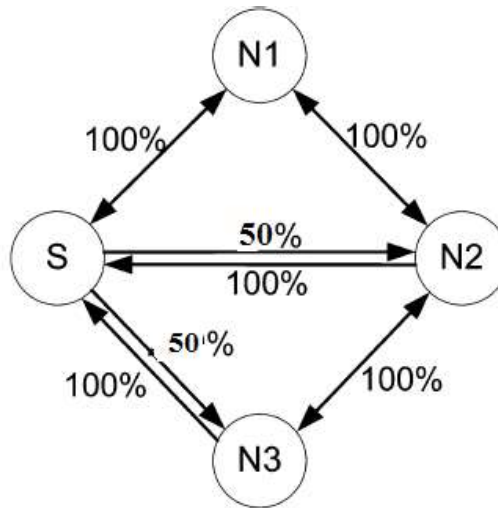


Fig. 2 Example of sender selection.

Fig. 2 shows the benefits of our accurate sender selection algorithm. Assume S is the source node and there are 20 packets per page. In Fig. 2, indicate the link qualities by the figures above the edges. For example, the link quality from S to N2 is 50 percent while the reverse link quality is 100 percent. Therefore, S can directly communicate with N1, N2, N3. However, the link qualities are different. Since the link quality from S to N1 is 100 percent, after S's transmission of a page, N1 can receive all the packets. On the other hand, since the link qualities from S to N2 and N3 are 50 percent, N2 and N3 can thus receive 50% packets. With MNP's approach, S will still be the next sender because it will receive the most number of requests. Hence, in MNP, 80 transmissions are needed for S to cover all N1, N2, N3. ECD considers link qualities. By one round of page transmission, S cannot cover one receiver whereas N1 can cover N2. Therefore, N1 will be the sender (covering N2 by one page transmission), followed by N2 being the next sender (covering N3 by one page transmission). These cause delay in ECD. Because higher link quality data reaches slower than lower link quality data. Through higher link quality link more data will transmit than lower. This cause extra delay.

Impact Estimation

MNP's sender selection algorithm may spend too many transmissions on poor links. It can be avoided in our protocol design. Here ECD estimate the number of uncovered nodes and the outbound link qualities to them. To calculate the number of uncovered nodes, use the REQ messages sent by uncovered nodes when missing packets are detected. There are two differences between ECD's REQ mechanism and Deluge's REQ mechanism. First, one or more eligible senders overhear the REQ message and may be responsible for sending requested packets in the REQ message that is not destined for them. This makes the set of eligible senders so that ECD select the best one. Second, it is to be note that in Deluge [6], REQ messages may be suppressed if another REQ message for the same page is overheard. This mechanism, however, will lead to biased estimation in protocol design. Because of this reason, in ECD, the uncovered nodes send REQ messages unless there is an ongoing page transmission.

The ability to accurately estimate wireless link quality is critical to the performance of routing protocols. Link quality estimation has been an important research topic in the wireless sensor networking community and researchers have developed a large number of different methods to estimate link quality. Link quality prediction is an important approach to solve this problem. Here ECD estimate the link quality based on the past knowledge and information, link quality prediction is essential for routing decisions for future data transmission

IV. MULTI OBJECTIVE OPTIMIZATION FORMULATION

Although substantial amount of search in optimization is conducted with regards to single objective problems, optimization problems with multi conflicting objectives are inevitable in many topics specially engineering applications. Two main methods have been proposed by scientist for solving multi-objective optimization problems: 1) Classical method, 2) Evolutionary algorithms. Classical methods are able to reach one optimal solution at each run, while evolutionary algorithms are based on a population of solutions which will hopefully lead to a number of optimal solutions at every generation. The evolutionary algorithm method which

had shown benefits over the classical approach can be categorized into various categories. Genetic Algorithm is one of the methods that imitate the evolution of genes and chromosomes.

The aim is to develop a fast and efficient multi-objective optimization technique by using GA (Genetic Algorithm) method, in order to solve multi-objective optimization problems with constraints. When only one objective function involves in the problem, it is called single objective optimization, however in most real world problems more than one objective function is required to be optimized, and therefore these problems are named multi-objective optimization. This paper tries to reduce delay to maximize the performance and reduce cost of routing using optimization technique.

The characteristic of evolutionary methods which use a population of solutions that evolve in each generation is well suited for multi-objective optimization problems. Since one of the main goals of MOOP solvers is to find a set of non-dominated solutions with the minimum distance to Pareto-front, evolutionary algorithms can generate a set of non-dominated solutions in each generation. The first goal in multi-objective optimization is achieved by a proper fitness assignment strategy and a careful reproduction operator. Diversity in the Pareto-set can be obtained by designing a suitable selection operator.

Consider a decision-maker who wishes to optimize K objectives such that the objectives are non-commensurable and the decision-maker has no clear preference of the objectives relative to each other. Without loss of generality, all objectives are of the minimization type. A minimization type objective can be converted to a maximization type by multiplying negative one. A minimization multi-objective decision problem with K objectives is defined as follows: Given an n -dimensional decision variable vector $\mathbf{x} = \{x_1, \dots, x_n\}$ in the solution space \mathbf{X} , find a vector \mathbf{x}^* that minimizes a given set of K objective $z(\mathbf{x}^*) = \{z_1(\mathbf{x}^*), \dots, z_K(\mathbf{x}^*)\}$ [23]. The solution space \mathbf{X} is generally restricted by a series of constraints, such as $g_j(\mathbf{x}^*) = b_j$ for $j = 1, \dots, m$, and bounds on the decision variables [23].

In many real-life situations, objectives under consideration conflict with each other. Hence, optimizing value \mathbf{x} with respect to a single objective often results in unexpected results with respect to the other objectives. Therefore, a best multi-objective solution that simultaneously optimizes each objective function is almost impossible. A best solution to a multi-objective problem is to find a set of solutions, each of which satisfies the objectives at a normal level without dominating one over another solution.

If all objective functions are for minimization, a good solution \mathbf{x} is said to dominate another good solution \mathbf{y} ($\mathbf{x} > \mathbf{y}$), if and only if, $z_i(\mathbf{x}) \leq z_i(\mathbf{y})$ for $i = 1, \dots, K$ and $z_j(\mathbf{x}) < z_j(\mathbf{y})$ for at least one objective function j . A resultant solution is said to be *Pareto optimal* if it is not dominated by any other solution in the solution space. A Pareto optimal solution cannot be further changed with any aspect to any other objective without worsening at least one other objective. The set of all feasible non-dominated solutions in \mathbf{X} is referred to as the *Pareto optimal set* [21].

The final goal of a multi-objective optimization algorithm is to find solutions in the Pareto optimal set. However, finding such a Pareto optimal set, for many multi-objective problems, is practically not possible due to its bigger size. In addition, especially for combinatorial optimization problems, proof of solution optimality is computationally infeasible. Therefore, a way to multi-objective optimization is to investigate a set of solutions that represent the Pareto optimal set as well as possible.

Genetic Algorithm

The concept of GA was developed by Holland and his colleagues in the 1960s and 1970s. GA was inspired by the evolutionist theory explaining the origin of species. In nature, weak and unfit species within environment are faced with extinction by natural selection [22]. The fit ones have greater opportunity to pass their genes to future generations via reproduction. Species carrying the right combination in their genes become dominant in their population. In long process, of evolution, random changes may occur in genes. If these changes provide additional benefit in the challenge for survival, new species develop from the old ones.

In GA terminology, a solution vector $\mathbf{x} \in \mathbf{X}$ is called an individual or a *chromosome*. Chromosomes are made of number of units called *genes* [22]. Each gene controls one or more features of the chromosome. In the implementation of GA by Holland, genes are assumed to be binary digits. In later implementations, more varied gene types have been introduced. A mapping mechanism between the solution space and the chromosomes is required. This mapping is called an encoding. GA operates with a collection of chromosomes, called a *population*. The population is randomly initialized. As the search evolves, the population contains fitter and fitter solutions, and eventually it converges, result is a single dominated solution. Holland also presented a proof of convergence (the schema theorem) to the global optimum where chromosomes are binary vectors.

GA uses two operators to generate new solutions from existing ones: *crossover* and *mutation*. The crossover operator is the mostly used operator of GA. In crossover, two chromosomes, called *parents*, are joined together to form new chromosomes, called *offspring*. The parents are selected among already existing chromosomes in the population pool with preference towards fitness

so that offspring is expected to get a good genes which make the parents fitter. By repeatedly applying the crossover operator, genes of best chromosomes are expected to appear more frequently in the population, which leads to convergence to an overall good solution.

The mutation operator introduces sudden and random changes into characteristics of chromosomes. Mutation is generally applied at the gene. In GA implementations, the mutation rate (probability of changing the properties of a gene) is very low and depends on the length of the chromosome. Therefore, the new chromosome produced by mutation will not have a greater difference from the original one. Mutation plays a crucial role in GA.

Reproduction involves selection of chromosomes for the next generation. In the most general case, the fitness of an individual determines the probability of its survival for the next generation. There are varies selection procedures in GA depending on how the fitness values are used. Proportional selection, ranking, and tournament selection are the most popular selection procedures. The procedure of a generic GA is given as follows:

- Step 1:* Set $t=1$. Randomly generate N solutions to form the first population, P_1 . Evaluate the fitness of solutions in P_1 .
- Step 2: Crossover:* Develop an offspring population N_t as follows:
 - 2.1. Choose two solutions x and y from P_t based on the fitness values.
 - 2.2. Using a crossover operator, generate offspring and add them to N_t .
- Step 3: Mutation:* Mutate each solution $x \in N_t$ with a predefined mutation rate.
- Step 4: Fitness assignment:* Evaluate and assign a fitness value to each solution $x \in N_t$ based on its objective function value and infeasibility.
- Step 5: Selection:* Select N solutions from N_t based on their fitness and copy them to P_{t+1} .
- Step 6:* If the stopping criterion is satisfied, stop the search and return to the current population, else, set $t=t+1$ go to Step 2.

Multi-objective GA

Being a population-based approach, Genetic algorithm is mostly opted to solve multi-objective optimization problems. A single-objective GA can be modified to find a set of multiple non-dominated solutions in a single run. The ability of GA to simultaneously search different regions of a solution space makes it possible to find a diverse set of solutions for difficult problems. In addition, most multi-objective GA do not require the user to prioritize, scale, or weigh objectives. Therefore, GA has been the most popular heuristic approach to multi-objective design and optimization problems. Jones et al. reported that 90% of the approaches to multi-objective optimization aimed to approximate the true Pareto front for the underlying problem.

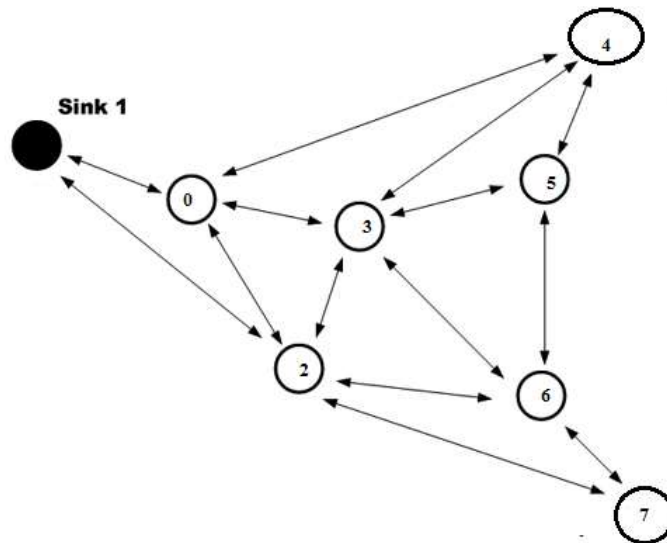


Fig. 3 Code dissemination nodes

Here in a network, select 1 as sink node to propagate code dissemination. Based on ECD-MOP each node under goes initialization, selection, mutation and crossover. This process goes for 48 rounds. Until best solution is obtained. Solution so obtained in ECD-MOP has least delay and Fast completion time.

0	1	2	3	4	5	6	Rand1	Rand2	Rank
4	6	10	6	10	1,2	0	0	0	4.330275...
4	2,0,6	10	4	10	1,2,3	4	0	0	2.632520...
4	6,0,3,2	4	6	10	3	0,4	0	0	4.888888...
4	2,6,0,3	10,4	4,6	10	2,1,3	4	0	0	2.885527...
4	6,3	10	4	10	2,3	4	0	0	2.708333...
4	0,2	4,10	6	10	3	0,4	0	0	4.888888...
4	3	10	4	10	2,3,1	0	0	0	3.266666...
4	0,3	10,4	4,6	10	1	4,0	0	0	4.745896...
4	6,3,2,0	10	4,6	10	2,3	4	0	0	2.618861...
4	3,6,2	10	6	10	2,3,1	0	0	0	4.662015...

Fig.4 Initialization phase on above code dissemination node

The above table shows how initialisation is done on each node. After initialisation, selection is next phase. For each node select combination. Then crossover and mutation is done. This is continued in several rounds. Finally obtain best solution.

Performance Evaluation

In this section, we evaluate the performance of ECD with multi objective optimization using GA through one’s simulation. Here first describe our performance metrics and simulation scenarios. Then evaluate the system performance with given scenarios and parameters. Finally, done comparisons between our ECD and ECD-MOP. The results confirm that ECD-MOP (multi objective optimization) have fast completion time, less delay.

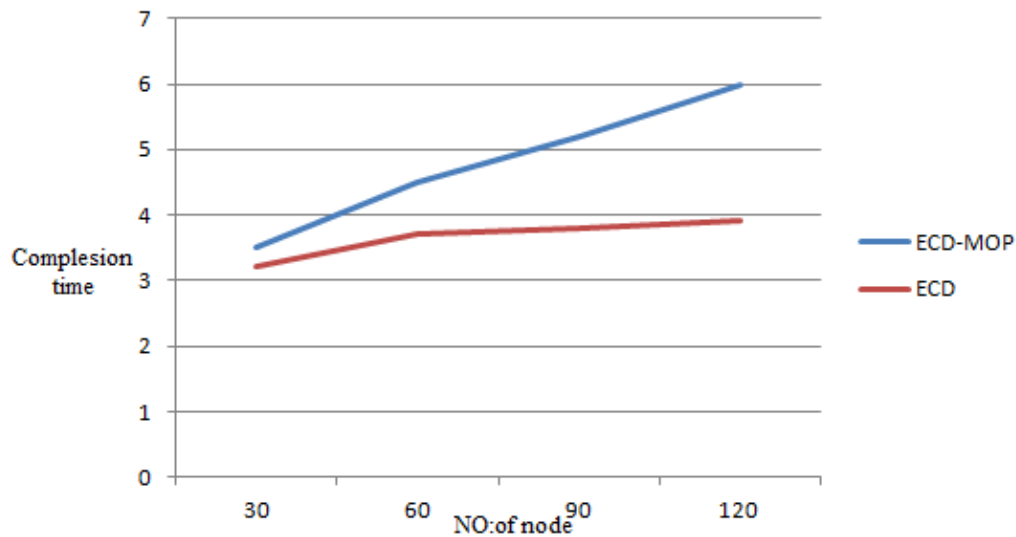


Fig .5 Performance evaluations on completion time

ACKNOWLEDGMENT

The first author would like to thanks all those people, who guided and supported. Without their valuable guidance and support, this task was not possible and also likes to thank colleagues for their discussions and suggestions.

CONCLUSION

Here present ECD, an Excellent Code Dissemination protocol for wireless sensor networks. Compared to prior works, ECD has three main features. First, it supports dynamically configurable packet sizes. By increasing the packet size for high PHY rate radios, it significantly improves the transmission efficiency. Second, it has an accurate and best sender selection algorithm to mitigate transmission collisions and transmissions over poor links. Third, ECD has a simple impact-based backoff timer design to shorten the time spent in coordinating multiple eligible senders so that the largest impact sender is most likely to transmit. In order to further reduce delay and overhead due to best sender selection, here incorporate multi objective optimization technique using Genetic Algorithm (ECD-MOP). This will provide a solution which has less delay and Fast completion time.

REFERENCES:

- [1] I.F. Akyildiz, W. Su, Y. Sankarasubramaniam, and E. Cayirci, "Wireless Sensor Networks: A Survey," *Comput. Netw.*, vol. 38, no. 4, pp. 393-422, Mar. 2002.
- [2] W. Dong, C. Chen, X. Liu, J. Bu, and Y. Liu, "Performance of Bulk Data Dissemination in Wireless Sensor Networks," in *Proc. IEEE/ACM Int'l. Conf. DCOSS*, 2009, pp. 356-369.
- [3] W. Dong, X. Liu, C. Chen, Y. He, G. Chen, Y. Liu, and J. Bu, "DPLC: Dynamic Packet Length Control in Wireless Sensor Networks," in *Proc. IEEE INFOCOM*, 2010, pp. 1-9.
- [4] W. Dong, Y. Liu, X. Wu, L. Gu, and C. Chen, "Elon: Enabling Efficient and Long-Term Reprogramming for Wireless Sensor Networks," in *Proc. ACM SIGMETRICS*, 2010, pp. 49-60.
- [5] M. Heusse, F. Rousseau, R. Cuillier, and A. Duda, "Idle Sense: An Optimal Access Method for High Throughput and Fairness in Rate Diverse Wireless LANs," in *Proc. ACM SIGCOMM*, 2005, pp. 121-132.
- [6] J.W. Hui and D. Culler, "The Dynamic Behavior of a Data Dissemination Protocol for Network Programming at Scale," in *Proc. ACM SenSys*, 2004, pp. 81-94.
- [7] S. Kulkarni and L. Wang, "Energy-Efficient Multihop Reprogramming for Sensor Networks," *ACM Trans. Sens. Netw.*, vol. 5, no. 2, p. 16, Mar. 2009.
- [8] P. Levis, N. Lee, M. Welsh, and D. Culler, "TOSSIM: Accurate and Scalable Simulation of Entire TinyOS Applications," in *Proc. ACM SenSys*, 2003, pp. 126-137.
- [9] P. Levis, N. Patel, D. Culler, and S. Shenker, "Trickle: A Self-Regulating Algorithm for Code Propagation and Maintenance in Wireless Sensor Networks," in *Proc. USENIX Symp. NSDI*, 2004, p. 2.
- [10] Y. Liu, Y. He, M. Li, J. Wang, K. Liu, L. Mo, W. Dong, Z. Yang, M. Xi, and J. Zhao, "Does Wireless Sensor Network Scale? A Measurement Study on GreenOrbs," in *Proc. IEEE INFOCOM*, 2011, pp. 873-881.
- [11] W. Lou and J. Wu, "Towards Broadcast Reliability in Mobile Ad Hoc Networks with Double Coverage," *IEEE Trans. Mobile Comput.*, vol. 6, no. 2, pp. 148-163, Feb. 2007.
- [12] L. Mo, Y. He, Y. Liu, J. Zhao, S. Tang, X.-Y. Li, and G. Dai, "Canopy Closure Estimates with GreenOrbs: Sustainable Sensing in the Forest," in *Proc. ACM SenSys*, 2009, pp. 99-112.
- [13] V. Naik, A. Arora, P. Sinha, and H. Zhang, "Sprinkler: A Reliable and Energy Efficient Data Dissemination Service for Wireless Embedded Devices," in *Proc. IEEE RTSS*, 2005, p. 286.
- [14] S.-Y. Ni, Y.-C. Tseng, Y.-S. Chen, and J.-P. Sheu, "The Broadcast Storm Problem in a Mobile Ad Hoc Networks," in *Proc. ACM MobiCom*, 1999, pp. 151-162.
- [15] Y. Sankarasubramaniam, I.F. Akyildiz, and S.W. McLaughlin, "Energy Efficiency Based Packet Size Optimization in Wireless Sensor Networks," in *Proc. IEEE Int'l. Workshop Sens. Netw. Protocols Appl.*, 2003, pp. 1-8.
- [16] S. Sen, N. Santhapuri, R.R. Choudhury, and S. Nelakuditi, "AccuRate: Constellation Based Rate Estimation in Wireless Networks," in *Proc. USENIX Symp. NSDI*, 2010, p. 12.

- [17] K. Srinivasan, P. Dutta, A. Tavakoli, and P. Levis, "Understanding the Causes of Packet Delivery Success and Failure in Dense Wireless Sensor Networks," Stanford Univ., Stanford, CA, USA, 2006, Tech. Rep. SING-06-00.
- [18] F. Stann, J. Heidemann, R. Shroff, and M.Z. Murtaza, "RBP: Robust Broadcast Propagation in Wireless Networks," in Proc. ACM SenSys, 2006, pp. 85-98.
- [19] TinyOS TEP 124: The Link Estimation Exchange Protocol (LEEP). [Online]. Available: <http://www.tinyos.net/tinyos-2.x/doc/html/tep124.html>
- [20] M. Vutukuru, H. Balakrishnan, and K. Jamieson, "Cross-Layer Wireless Bit Rate Adaptation," in Proc. ACM SIGCOMM, 2009, pp. 3-14.
- [21] <http://www.sciencedirect.com/science/article/pii/S0951832005002012>
- [22] <http://www.ijscce.org/attachments/File/v3i2/B1423053213.pdf>
- [23] <http://www.researchgate.net/publication/269330296>

Correlation-Based Feature Subset Selection for Privacy Preserving Data Mining

Jintu Ann John¹, Neethu Maria John²

Department of Computer Science and Engineering, Mahatma Gandhi University, Mangalam College of Engineering

Email id: jintuannjohn@gmail.com

9747825486

Abstract— In recent year's privacy preservation in data mining has become an important issue. The main aim is to protect the sensitive information in data while extracting knowledge from large amount of data. The data from different sources have to collaborate effectively while maximizing the utility of collected information. With the advance of the information age, data collection and data analysis have exploded both in size and complexity. The attempt to extract important patterns and trends from the vast data sets has led to a challenging field called Data Mining. When a complete data set is available, various statistical, machine learning and modeling techniques can be applied to analyze the data. Usually, data are distributed across multiple sites. The data warehousing approach has been used to mine distributed databases. It is used to collect data from all the participating sites and are stored at a centralized warehouse. However, many data owners are unwilling to share their data with others due to privacy and confidentiality concerns. So it is a limitation to perform mutually beneficial data mining tasks. To overcome this Privacy-Preserving Data Mining has emerged. The research of Privacy-Preserving Data Mining is aimed at bridging the gap between collaborative data mining and data confidentiality. It involves many areas such as statistics, computer sciences, and social sciences. The existing cryptographic techniques for privacy preservation are not very effective for providing privacy preservation on large scale datasets. So random decision trees are used to generate equivalent and accurate models with much smaller costs. The server sends data to multiple clients after doing dataset partitioning. In this paper the dataset is partitioned based on the correlation between the features. This method is more accurate than the existing vertical partitioning of dataset.

Keywords— Data mining; privacy preserving data mining; feature subset selection; feature clustering; Random Decision Tree; homomorphic encryption; security.

INTRODUCTION

Data mining is the process of mining information from large databases. Building and applying any data mining model generally assumes that the underlying data is freely accessible. But it is true. Privacy and security factors may limit the sharing or centralization of data. Privacy-preserving data mining has emerged as an effective method to solve this problem [2]. Distributed solutions have been proposed that can preserve privacy while still enabling data mining. Privacy preservation means, Protecting specific individual values, breaking the link between values and the individual they apply to, protecting source, etc. This paper aims for a high standard of privacy: Not only individual entities are protected, but to the extent feasible even the schema are protected from disclosure.

The server sends data to multiple clients. The distributed data have to be protected. The data should be send only after the partitioning of dataset. The dataset partitioning is done according to the correlation between the features. The similar features are belongs to the same class and forms the clusters. Then construct Random Decision Tree for each clusters. The Random Decision Tree[1] approach is more accurate and efficient than existing cryptographic techniques.

Feature selection involves identifying a subset of the most useful features that produces compatible results as the original entire set of features. A feature selection algorithm may be evaluated from both the efficiency and effectiveness points of view. While the efficiency concerns the time required to find a subset of features, the effectiveness is related to the quality of the subset of features.

The Correlation-Based Feature Subset Selection algorithm works in four steps.

- The irrelevant features are removed.
- Construct Minimum Spanning Tree using Prim's Algorithm.
- Features are divided into clusters.
- The most representative feature that is strongly related to target classes is selected from each cluster to form a subset of features.

Features in different clusters are relatively independent. The features belongs to a particular cluster are similar. To ensure the efficiency of Correlation-Based Feature Subset Selection algorithm, we adopt the efficient minimum-spanning tree (MST) clustering method. After the partitioning of dataset construct Random decision tree. Random decision tree algorithm constructs multiple decision trees randomly. When constructing each tree, the algorithm picks a remaining feature randomly at each node expansion without any purity function check. A categorical feature (such as gender) is considered remaining if the same categorical feature has not been chosen previously in a particular decision path starting from the root of tree to the current node. Once a categorical feature is chosen, it is useless to pick it again on the same decision path because every example in the same path will have the same value (either male or female). However, a continuous feature (such as income) can be chosen more than once in the same decision path. Each time the continuous feature is chosen, a random threshold is selected.

A Random decision tree stops growing any deeper if one of the following conditions is met:

- A node becomes empty or there are no more examples to split in the current node.
- The depth of tree exceeds some limits.
- Each node of the tree records class distributions.

Then apply Homomorphic encryption to the leaf nodes of RDT. This is done for providing more privacy and security. Homomorphic encryption is a form of encryption that allows computations to be carried out on ciphertext, thus generating an encrypted result, which, when decrypted matches the result of operations performed on the plain text.

The rest of the paper is organized as follows: in Section 1, we describe the related works. In Section 2, we present the Correlation-based feature subset selection algorithm. In Section 3, reports extensive experimental results to support the proposed Correlation-Based Feature Subset Selection algorithm. Finally, in Section 4, we summarize the present study and draw some conclusions.

II RELATED WORK

In [1], the privacy preserving data mining is done by generating Random Decision Tree framework. Here, the dataset partitioning is done by vertical and horizontal partitioning of dataset. In both cases, according to the slowest machine the time delay takes place. So when a new slowest machine came the time increases. Privacy and security concerns can prevent sharing of data, derailing data mining projects. Distributed knowledge discovery, if done correctly, can alleviate this problem. In this paper, we tackle the problem of classification. We introduce a generalized privacy preserving variant of the ID3 algorithm for vertically partitioned data [6] distributed over two or more parties. A completely random decision tree algorithm [2] that achieves much higher accuracy than the single best hypothesis and is comparable to boosted or bagged multiple best hypotheses. The advantage of multiple random tree is its training efficiency as well as minimal memory requirement. Data is distributed in various sites that need to be mined in a secure manner without revealing anything except the results of mining. Privacy-preserving horizontal distributed classification techniques [7] where multiple sites collaborate and broadcast the mining results. However in the process, no information about either the data maintained in the sites or data obtained during computation is divulged. Two protocols are presented to construct a Privacy Preserving Naïve Bayesian classifier using the Pailler's homomorphic encryption techniques.

Advances in computer networking and database technologies have enabled the collection and storage of large quantities of data, also the freedom and transparency of information flow on the Internet has heightened concerns of privacy. Nowadays the scenario of one centralized database that maintains all the data is difficult to achieve due to different reasons including physical, geographical restrictions and size of the data itself. The data is normally maintained by more than one organization, each of which aims at keeping its information stored in the databases privately, thus, privacy-preserving techniques and protocols are designed to perform data mining on distributed data when privacy is highly concerned. Cluster analysis [13] is a frequently used data mining task which aims at decomposing or partitioning a usually multivariate data set into groups such that the data objects in one group are most similar to each other. It focuses on arbitrarily partitioned data [8] which is a generalization of horizontally partitioned data and vertically partitioned

data along with Shamir's Secret Sharing Schemes which was designed with the goal of achieving complete privacy for secure computation and communication between different parties.

Distributed clustering algorithm DK-Means is developed, which improves the K-Means algorithm, that is, the site in the clustering process does not require transferring large amounts of data objects, only needs to send the clustering centers as well as the total number of clusters of data objects, which reduces data traffic of the distributed clustering process so as to improve operating efficiency. This strategy [4] would be applied on the database into two different parties, recursively produce k cluster centers from each of the party, and then merge these 2k centers into the k final centers.

III PROPOSED ALGORITHM

A. Correlation-Based Feature Subset Selection Algorithm

The proposed method can be able to identify and remove the irrelevant and redundant information. Good feature subsets contain features that are highly correlated with the class, yet uncorrelated with each other.

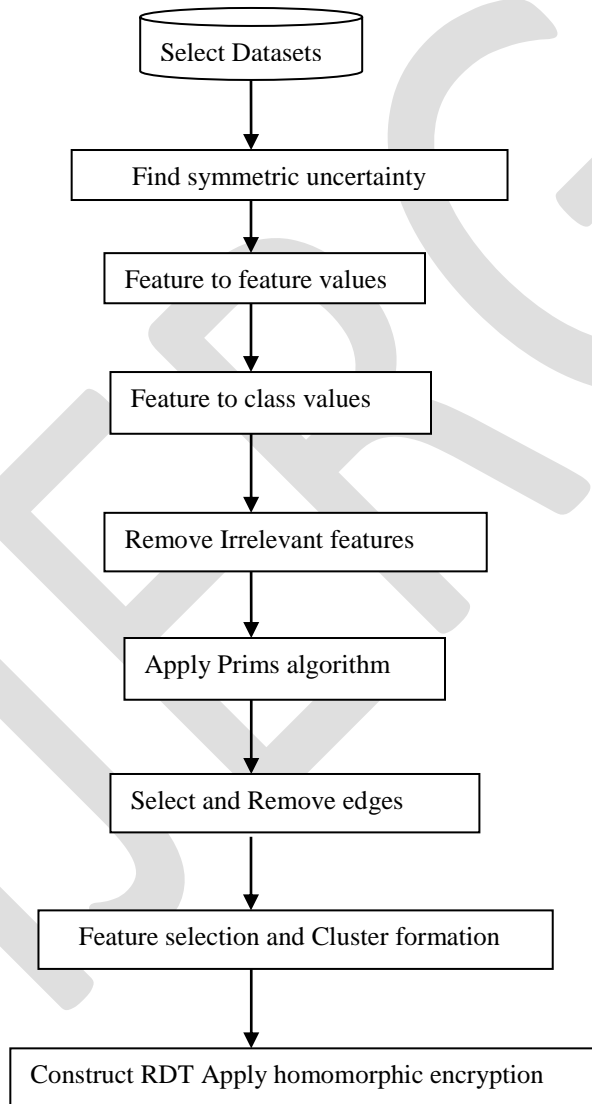


Fig 1: Framework for Correlation-Based Feature Subset Selection Algorithm

The irrelevant feature removal is straightforward once the right relevance measure is defined or selected. In our proposed algorithm, redundant feature elimination can be done by:

- 1) the construction of the minimum spanning tree from a weighted complete graph;
- 2) the partitioning of the MST into a forest with each tree representing a cluster;
- 3) the selection of representative features from the clusters.

The symmetric uncertainty can be defined as:

$$SU(A,B) = \frac{2*Gain(A|B)}{H(A)+H(B)}$$

Where,

- 1.H(A) is the entropy of a discrete random variable A.

$$H(A) = -\sum_{a \in A} p(a) \log_2 p(a)$$

p(a) is the prior probabilities for all values.

- 2.Gain(A|B) is the amount by which the entropy of B decreases.

$$\begin{aligned} Gain(A|B) &= H(A) - H(A|B) \\ &= H(B) - H(B|A) \end{aligned}$$

H(A|B) is the conditional entropy.

IV PSEUDO CODE

- Step 1:Removes Irrelevant features.
- Step 2:Construct Minimum Spanning Tree.
- Step 3:Using Prims Algorithm to generate the minimum Spanning Tree.
- Step 4:Tree partition.
- Step 5:Remove redundant edges.
- Step 6:Select representative features.
- Step 7:Cluster formation.

	P1		P2		
	Oulook	temperature	Humidity	windy	play
P1	Sunny	hot	High	weak	no
	Sunny	hot	High	strong	no
	Overcast	hot	High	weak	no
	Rainy	mild	High	weak	no
	Rainy	cool	Normal	strong	no
	Overcast	cool	Normal	strong	yes
P2	Sunny	mild	High	weak	no
	Sunny	cool	Normal	weak	yes
	Rainy	mild	Normal	weak	yes
	Sunny	mild	Normal	strong	yes
	Overcast	mild	High	strong	yes
	Rainy	mild	High	strong	no

Table 1: Sample weather dataset

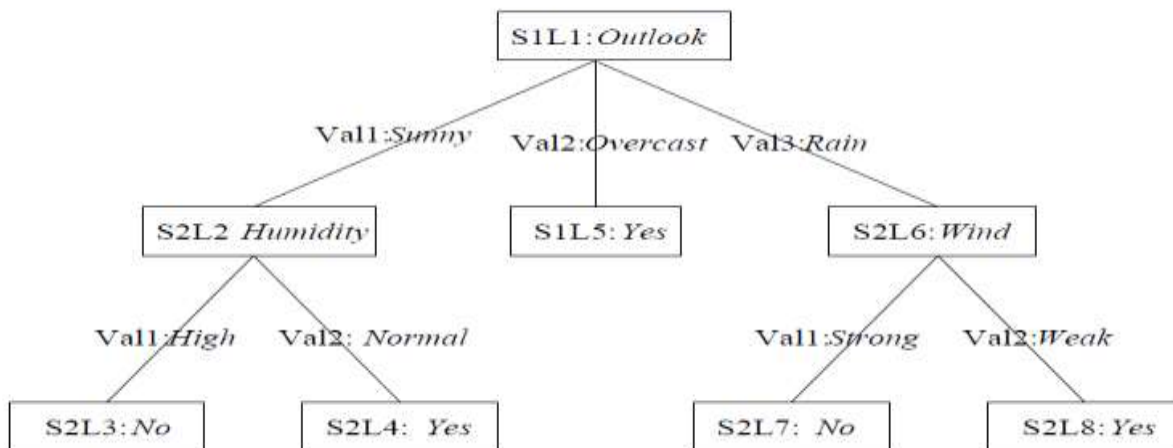


Fig 2: Random Decision Tree for weather dataset.

V SIMULATION RESULTS

The proposed method is more accurate than the existing method. In vertical partitioning of dataset is partitioned vertically. The dataset partitioning is not based on any factor. It is partitioned vertically without considering any facts. But in the proposed system the dataset is partitioned based on the similarity of the features. The more correlated features are belongs to the same class. Then if there are

redundant features it should have to eliminate. Then clusters are formed. The features in each cluster are highly correlated. But the clusters are not similar to each other.

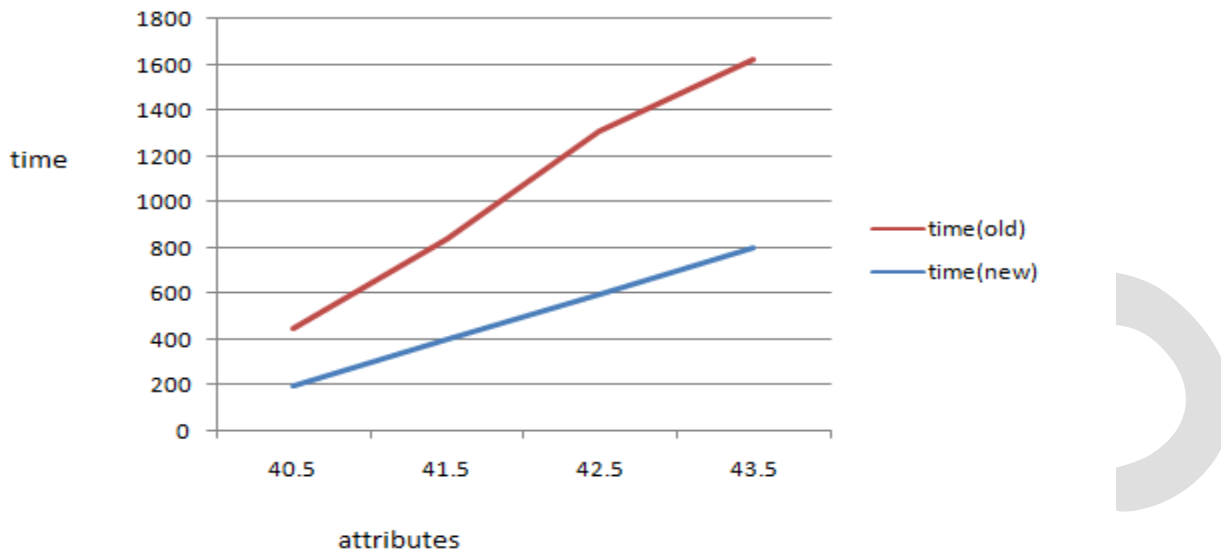


Fig 3: Performance Evaluation

VI CONCLUSION

In this paper, we have presented a novel correlation-based feature subset selection algorithm for high dimensional data. The algorithm involves 1) removing irrelevant features, 2) constructing a minimum spanning tree, and 3) selecting representative features. Then generates the clusters. The dataset partitioning based on this approach is more efficient and accurate than the existing vertical partitioning. In the proposed algorithm, a cluster consists of features. Then construct Random Decision Tree based on these clusters. Since RDTs can be used to generate equivalent, accurate and better models with much smaller cost, we have proposed distributed privacy-preserving RDTs. Our approach leverages the fact that randomness in structure can provide strong privacy with less computation. Then apply homomorphic encryption to provide more security. The RDT algorithm scales linearly with data set size, and requires significantly less time than existing cryptographic approaches.

REFERENCES:

- [1] Jaideep Vaidya, Basit Shafiq, Wei Fan, Danish Mehmood, and David Lorenzi, "A Random Decision Tree Framework for Privacy Preserving Data Mining", IEEE Transactions On Dependable And Secure Computing, Vol. 11, No. 5, September/October 2014
- [2] J. Vaidya, C. Clifton, and M. Zhu, "Privacy-Preserving Data Mining", Advances in Information Security first ed., vol. 19, Springer-Verlag, 2005.
- [3] W. Fan, H. Wang, P.S. Yu, and S. Ma, "Is Random Model Better? On Its Accuracy and Efficiency," Proc. Third IEEE Int'l Conf. Data Mining (ICDM '03), pp. 51-58, 2003
- [4] G. Jagannathan and R. Wright, "Privacy-preserving distributed k-means clustering over arbitrarily partitioned data", In 11th KDD, pages 593-599, 2005.
- [5] W. Du and Z. Zhan, "Building Decision Tree Classifier on Private Data," Proc. IEEE Int'l Conf. Data Mining Workshop on Privacy, Security, and Data Mining, pp. 1-8, Dec. 2002.

- [6] J. Vaidya, C. Clifton, M. Kantarcioglu, and A.S. Patterson, "Privacy-Preserving Decision Trees over Vertically Partitioned Data," *ACM Trans. Knowledge Discovery from Data*, vol. 2, no. 3, pp. 1-27, 2008.
- [7] M. Kantarcioglu and C. Clifton, "Privacy-Preserving Distributed Mining of Association Rules on Horizontally Partitioned Data," *IEEE Trans. Knowledge and Data Eng.*, vol. 16, no. 9, pp. 1026-1037, Sept. 2004.
- [8] G. Jagannathan and R.N. Wright, "Privacy-Preserving Distributed k-Means Clustering over Arbitrarily Partitioned Data," *Proc. ACM SIGKDD Int'l Conf. Knowledge Discovery and Data Mining*, pp. 593-599, Aug. 2005.
- [9] H. Kargupta, S. Datta, Q. Wang, and K. Sivakumar, "On the Privacy Preserving Properties of Random Data Perturbation Techniques," *Proc. Third IEEE Int'l Conf. Data Mining (ICDM '03)*, Nov. 2003.
- [10] J. Souza, "Feature Selection with a General Hybrid Algorithm," PhD dissertation, Univ. of Ottawa, 2004.
- [11] L. Yu and H. Liu, "Efficient Feature Selection via Analysis of Relevance and Redundancy," *J. Machine Learning Research*, vol. 10, no. 5, pp. 1205-1224, 2004.
- [12] C. Sha, X. Qiu, and A. Zhou, "Feature Selection Based on a New Dependency Measure," *Proc. Fifth Int'l Conf. Fuzzy Systems and Knowledge Discovery*, vol. 1, pp. 266-270, 2008.
- [13] I.S. Dhillon, S. Mallela, and R. Kumar, "A Divisive Information Theoretic Feature Clustering Algorithm for Text Classification," *J. Machine Learning Research*, vol. 3, pp. 1265-1287, 2003.
- [14] M. Dash and H. Liu, "Consistency-Based Search in Feature Selection," *Artificial Intelligence*, vol. 151, nos. 1/2, pp. 155-176, 2003.

II. RATCHETS AND RATCHETS GEARING

A *ratchet* is a form of gear in which the teeth are cut for one-way operation or to transmit intermittent motion. The ratchet wheel is used widely in machinery and many mechanisms. Ratchet-wheel teeth can be either on the perimeter of a disk or on the inner edge of a ring.

The *pawl*, which engages the ratchet teeth, is a beam member pivoted at one end, the other end being shaped to fit the ratchet-tooth flank.

Ratchet Gear Design. In the design of ratchet gearing, the teeth must be designed so that the pawl will remain in engagement under ratchet-wheel loading. In ratchet gear systems, the pawl will either push the ratchet wheel or the ratchet wheel will push on the pawl and/or the pawl will pull the ratchet wheel or the ratchet wheel will pull on the pawl. See Figs. 8.1a and b for the four variations of ratchet and pawl action. In the figure, F indicates the origin and direction of the force and R indicates the reaction direction.

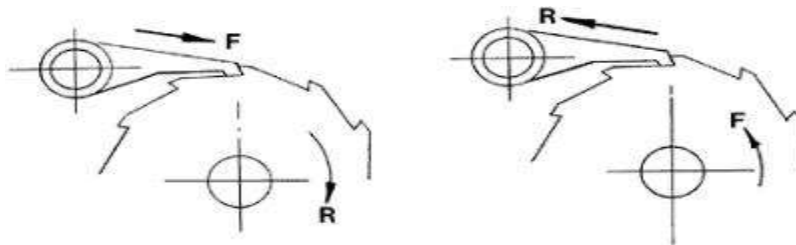


Figure 2: Variation of ratchet and pawl action (F = force; R = reaction).

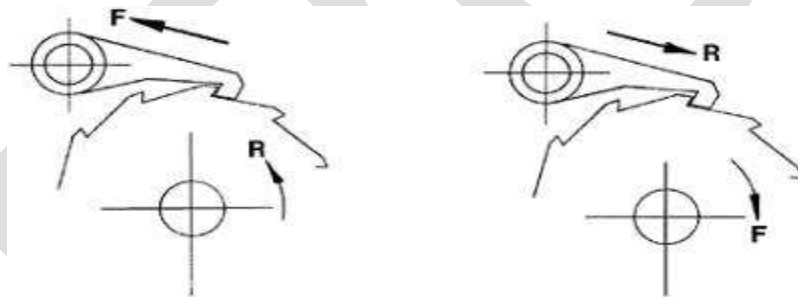


Figure 3: Variation of ratchet and pawl action (F = force; R = reaction).

Tooth geometry for case I in Fig. 8.1a is shown in Fig. 8.2. A line perpendicular to the face of the ratchet-wheel tooth must pass between the centers of the ratchet wheel.

II. PROPERTIES OF MATERIALS

- **Part Name : Ratchet Pawl**
- **Material Name: C20 (Steel Forging)**
 - 1) Tensile Strength : 425 MPa
 - 2) Poisson Ratio: 0.27 – 0.30
 - 3) Modulus of elasticity (E) : 190 - 210 GPa
 - 4) Specific Heat Capacity: 0.46
 - 5) Density : 7.85 g/cm³
 - 6) Thermal conductivity : 58.6 W/m.k
 - 7) Bulk modulus : 140 MPa
 - 8) Yield strength : 360 MPa
 - 9) Hardness :156 HB
 - 10) Shear modulus :80 MPa

- **Part Name : Ratchet wheel**

- **Material Name: EN9 (Normalize)**

- 1) Tensile Strength : 700 MPa
- 2) Yield Strength : 355 MPa
- 3) Elongation % : 13%
- 4) Modulus of elasticity (E) : $206 \times 10^3 \text{ N/mm}^2$
- 5) Density : 7800 kg/m
- 6) Hardness : 201 to 255 HB

III. RAPR MECHANISM DESCRIPTION

The RaPR mechanism described in this work was designed with the following design criteria as constraints: the ratchet wheel should advance one and only one tooth per actuation pulse; the ratchet wheel driver and restraint mechanism will be in a planar arrangement; the ratchet mechanism should operate on as little space of the ratchet wheel as possible; stand-alone spring elements and complicated assemblies should be minimized or eliminated; moving parts should be balanced about their pivot points; the aspect ratio of parts will be 10:1 or less; the device must be able to be actuated by a stator electromagnet; the driver mechanism will act as the rotor to the electromagnet stator by completing a magnetic circuit; the ratchet wheel will have 36 teeth; no lubricants will be considered for friction reduction; the ratchet mechanism will be designed such that it can be fabricated using micro wire EDM.

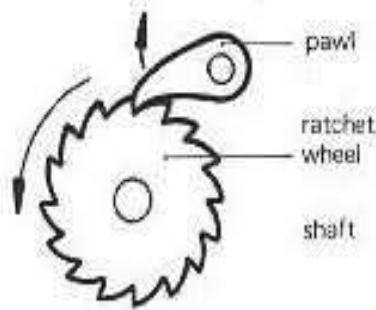


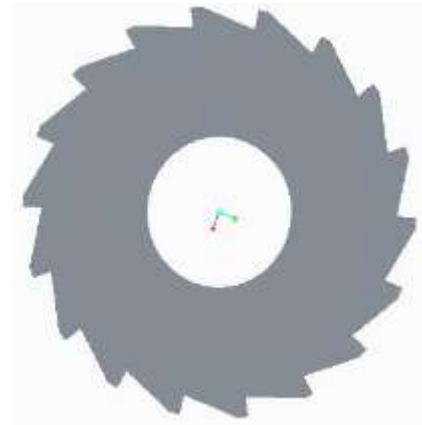
Fig.4.Ratchet pawl mechanism

IV.MODELLING WITH CREO

Following is the modeling of the existing model:



(a)

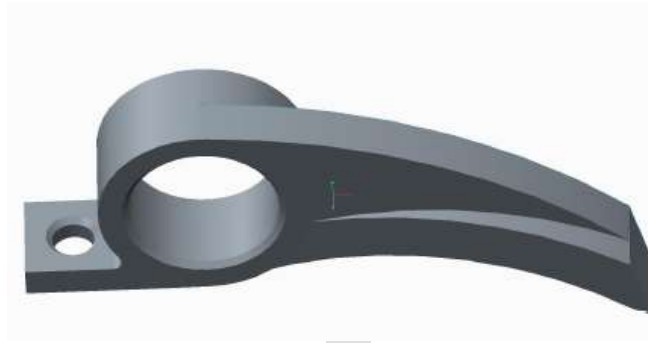


(b)

Fig.5.Ratchet wheel



(b)

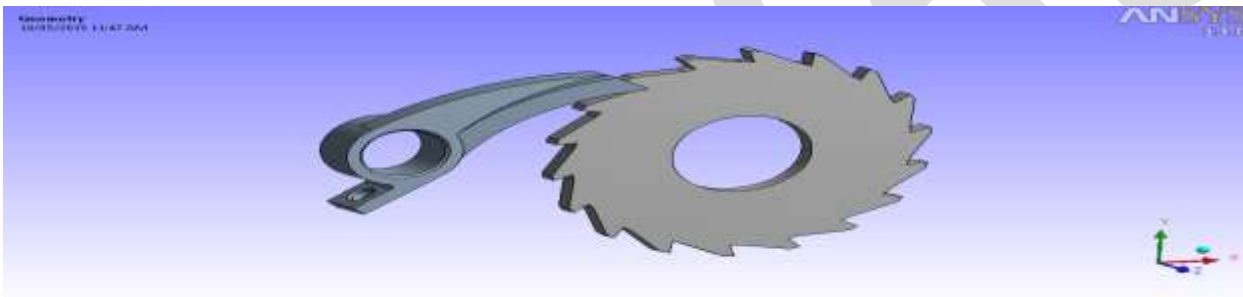


(d)

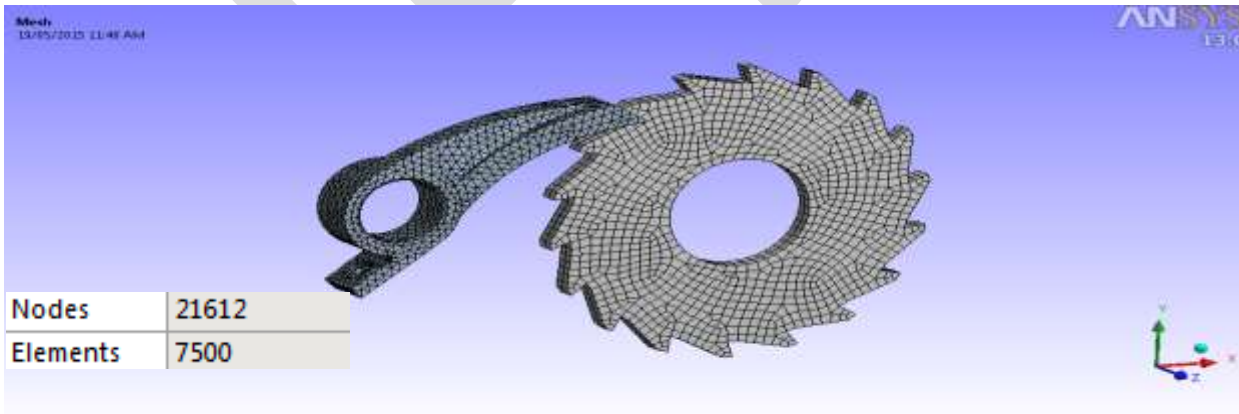
Fig.6.Pawl

FINITE ELEMENT ANALYSIS OF THE ABOVE PARTS OF EXISTING MODEL THROUGH ANSYS

Geometry

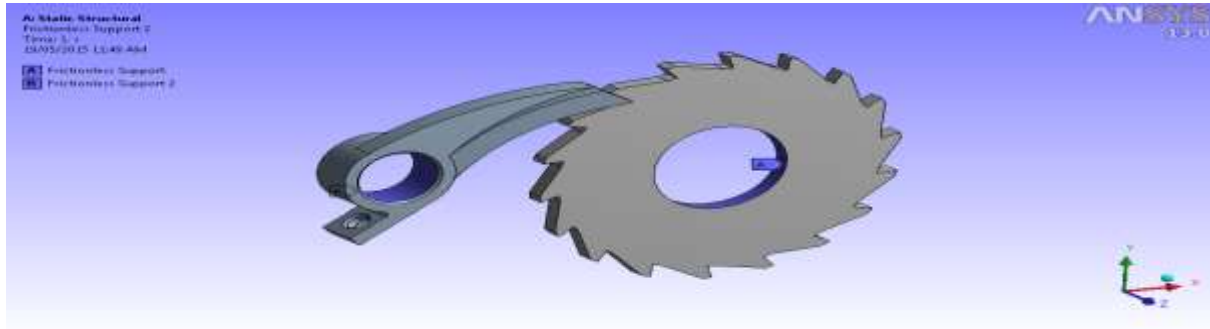


Meshing

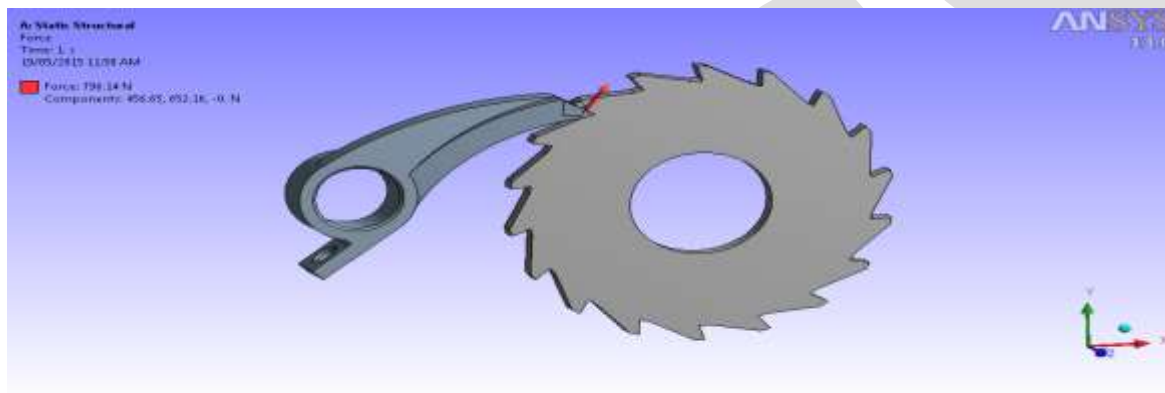


BOUNDARY CONDITION

Frictionless Support

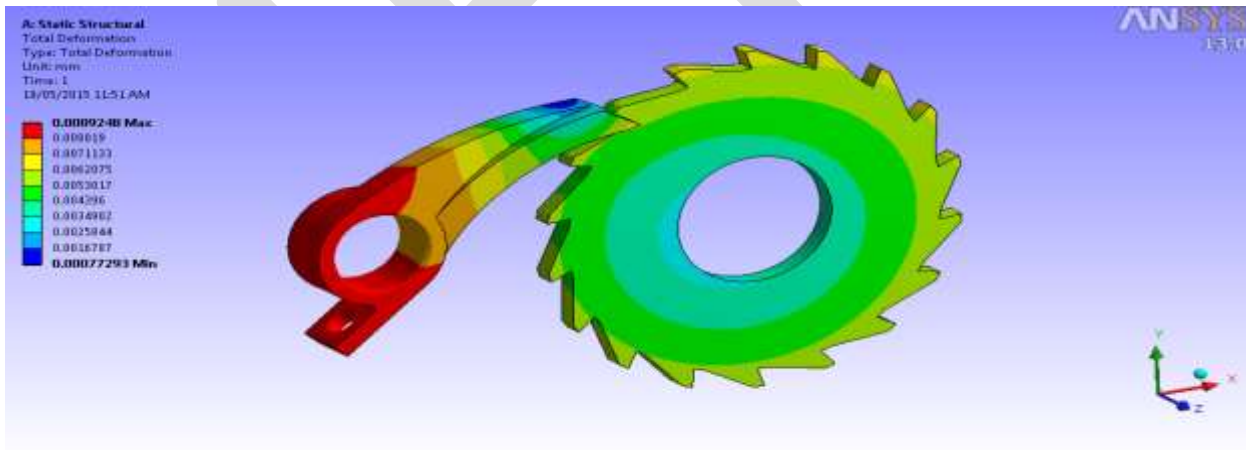


Force

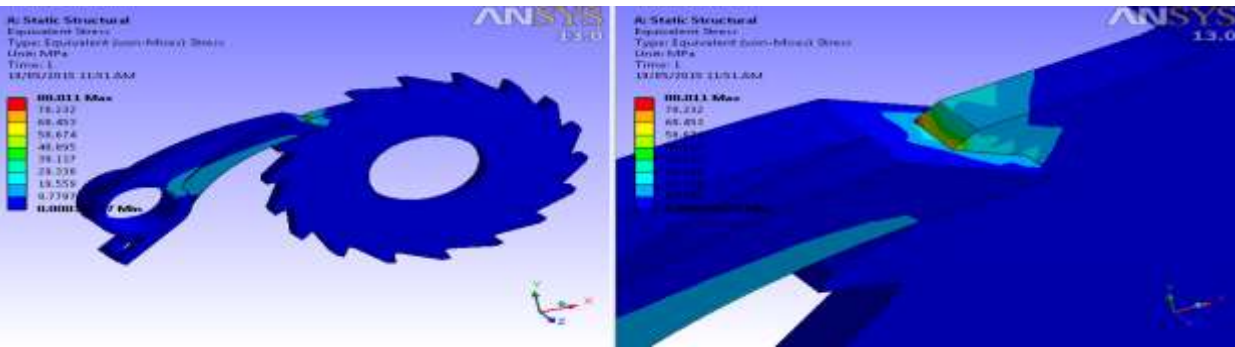


RESULTS

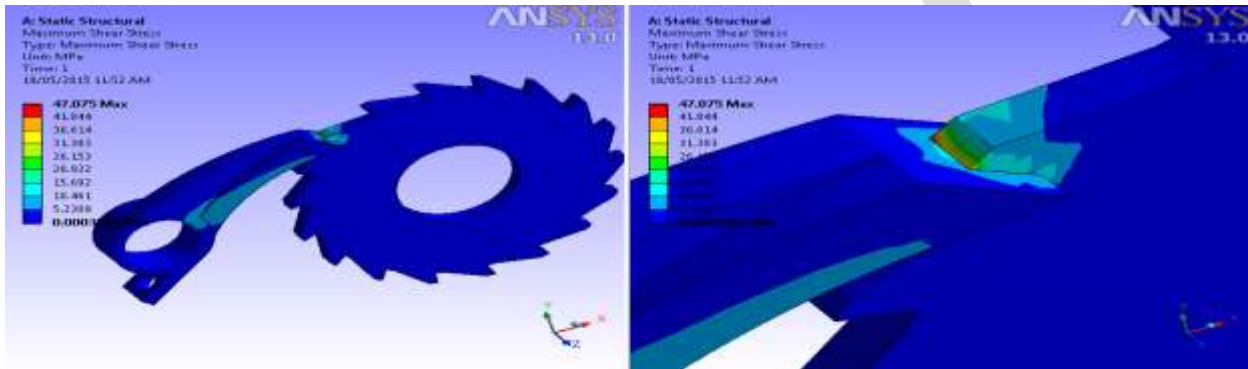
Total Deformation



Von-Mises Stress



Max Shear Stress



CONCLUSION

The RaPR mechanism design was able to adequately fulfil the design specifications.. The ANSYS results shown that maximum shear stress and principle stresses are nominal stresses on ratchet mechanism

REFERENCES:

- [1] V. P. Bondaletov, "Pawl Motion in Free-Running Ratchet Gear at High Ratchet Speeds", *ISSN 1068-798X, Russian Engineering Research*, 2008, Vol. 28, No. 9, pp. 845–848.
- [2] J. A. Kennedy, L. L. Howell, "The Ratchet and Pawl Ring (RaPR) Mechanism", *12th IFToMM World Congress, Besançon (France), June 18-21, 2007*.
- [3] V. P. Bondaletov, V. I. Medvedev, and A. V. Petrov, "Extending the Life of Free Wheel Ratchet Mechanisms by Backup of the Working Components", *ISSN 1068_798X, Russian Engineering Research*, 2010, Vol. 30, No. 12, pp. 1208–

SWITCHED INDUCTOR Z SOURCE HALF BRIDGE CONVERTER

Anilkumar K K , Babu Thomas, Rajan P Thomas

P. G Student, anil.mahadeva@gmail.com, +91-8907304077

Abstract— Applying an Switched Impedance network into a half-bridge converter, a novel Switched Inductor Z-source half-bridge converter is presented. This Switched Inductor Z-source half-bridge converter can solve the problems of the shoot-through and limited voltage. Also the boost ability of the converter is also improved compared to conventional z source converter. Furthermore, it can generate a broader range of output voltage values and much more kinds of waveforms, such as the varied positive or negative output voltages and the varied time ratio between positive and negative voltages, which are particularly desirable for some special power supplies, like the electrochemical power supply. Finally, the proposed converter is simulated in MATLAB/SimulinkR2010a, and the simulation results can verify the effectiveness of the proposed converter

Keywords— Half-bridge converter, limited Voltage, shoot-through, Switched Inductor Z-source, electrochemical power supply, Switched Impedance, boost ability

INTRODUCTION

Conventional half-bridge converters have their switches in series, as shown in Fig. 1, with which the shoot-through can occur [1], which means that the strong current flowing through the switches makes them break down. Moreover, the ac output voltage is limited below the dc voltage, which is named the limited voltage problem, because, in practice, ac output voltage is sometimes desirable to be higher than the dc voltage. Furthermore, an unbalanced midpoint of input capacitors in conventional half-bridge converters leads to large ripples [2], [3], making the system unstable.

In half-bridge VSI, where two large capacitors are required to provide a neutral point N, such that each capacitor maintains a constant voltage $\frac{V_i}{2}$. Because the current harmonics injected by the operation of the inverter are low-order harmonics, a set of large capacitors (C+ and C-) is required. Figure 1.1 shows the power topology of a half-bridge VSI. It is clear that both switches S1 and S2 cannot be on simultaneously because a short circuit across the dc link voltage source V_i would be produced. In order to avoid the short circuit across the dc bus and the undefined ac output voltage condition, the modulating technique should always ensure that at any instant either the top or the bottom switch of the inverter leg is on.

Here, a switched inductor Z-source half-bridge converter is proposed, in which, instead of putting two LC Z-networks a switched inductor Z Source network is used to couple with the capacitors. It can generate a much broader range of output voltages and more abundant wave- forms than the conventional Z-source converter. It is also remarked that it has higher efficiency than conventional half-bridge converters, where an additional dc-dc boost converter is needed to obtain such desired outputs. The switched inductor Z-source converter can generate boost- buck voltage, minimize component count, increase efficiency, and reduce cost and For applications where over drive is desirable and the available dc voltage is limited, an additional dc-dc boost converter is needed to obtain a desired ac output. The additional power converter stage increases system cost and lowers efficiency.

A typical application of the switched inductor Z-source half-bridge converter is in the electrochemical power supply, whose output voltages are requested to be varied, including varied positive or negative output voltages and the varied time ratio between positive and negative voltages. These characteristics, desired in electrochemical power supply, are the very ones of the proposed converter.

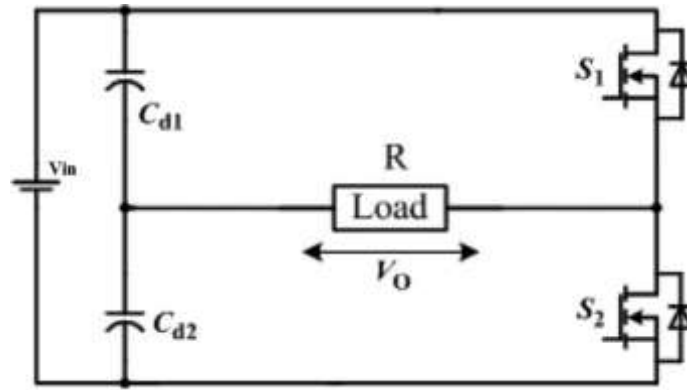


Figure.1 : Conventional half-bridge converter

SYSTEM DESIGN AND ANALYSIS

The proposed converter is depicted in Fig. 2, in which switched inductor Z source converter consisting of four inductors L_1, L_2, L_3, L_4 and capacitors C_1 and C_2 integrated to conventional half bridge converter, consisting of capacitors C_{d1} and C_{d2} , switches S_1 and S_2 , and diode D, which is used to prevent the current from flowing back to the source. There in, the use of the inductors in the Z-network is to avoid strong current in the circuit when the switches are in the shoot-through state.

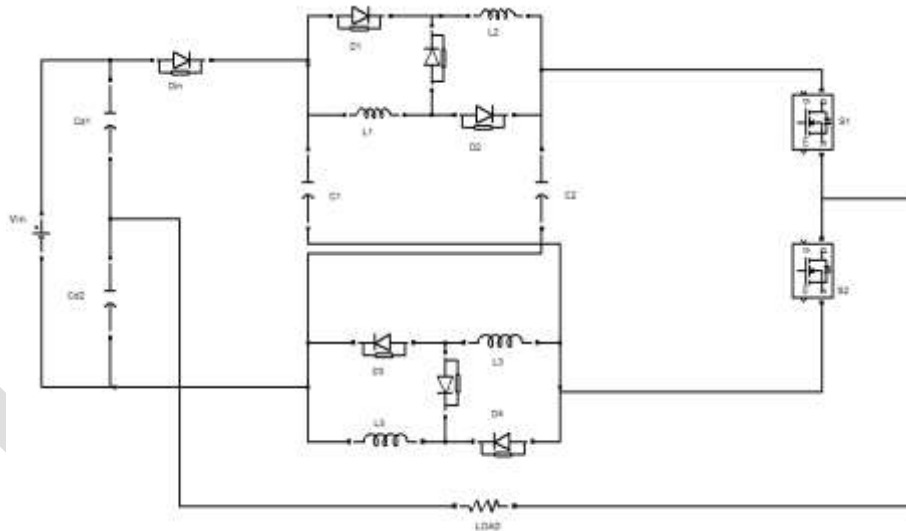


Figure. 2: Switched Inductor Z Source Converter

The proposed converter performs differently in two cases: $D_1 + D_2 \leq 1$ and $D_1 + D_2 > 1$.

A. Case. 1: $D_1 + D_2 \leq 1$

In this case, S_1 and S_2 are not switched on at the same time; then, the circuit is in the non-shoot-through state. There are three modes corresponding to the states of the switches. In the first mode, Fig. 2.2(a) shows an equivalent circuit for the mode when the S_1 is on and S_2 is off, in which the current flows out of the source, through the diode, the Z-network, and S_1 , and then back to the source. The arrows indicate the current directions. In the second mode, Fig. 2.2(b) shows an equivalent circuit of that when S_1 and S_2 are off, in which the current also flows out of the source, through the diode and the Z-network, and back to the source; there is no output here. In the third mode, Fig. 2.2(c) shows an equivalent circuit of that when S_2 is on and S_1 is off, in which the diode suffers a negative voltage and, thus, turns off. The current flows out of the source, through the load, S_2 , and the Z-network, and then back to the source. Furthermore, the current direction is also indicated. The operation process for this case is similar to the traditional one for half-bridge converters, which is not detailed here.

B. Case 2: $D_1 + D_2 > 1$

In this case, the behaviour of the switches in the circuit leads to three modes within a switch period T , which correspond to three linear equivalent circuits: Mode 1, when S_1 and S_2 are on; Mode 2, when S_1 is on and S_2 is off; and Mode 3, when S_1 is off and S_2 is on.

Denote t_0 as the beginning of one period, t_1 as the mode transition instant from mode 1 to mode 2, i.e., $t_1 = t_0 + (D_2 + D_1 - 1)T$, t_2 as the mode transition instant from mode 2 to mode 3, i.e., $t_2 = t_1 + (1 - D_2)T$, and $t_3 = T$ as the end of the period. In the steady state of the converter, its operation process in a switch period is analysed in the following, and the output voltage v_o will be deduced in each mode.

Mode 1: $t \in [t_0, t_1]$

As shown in Fig.3, in loops 1 and 2, capacitors C_1 and C_2 discharge the energy to inductors L_1 and L_2 , L_3 and L_4 thereafter, i_{L1} , i_{L2} , i_{L3} and i_{L4} increases. Thus, all inductors store the energy, and one has

$$\begin{aligned} V_{L1} = V_{L2} &= V_{C1} \\ V_{L3} = V_{L4} &= V_{C2} \end{aligned} \quad (1)$$

where i_{L1} , i_{L2} , i_{L3} and i_{L4} , V_{L1} , V_{L2} , V_{C1} , and V_{C2} are the currents of L_1 , L_2 , L_3 and L_4 and the voltages of L_1 , L_2 , L_3 and L_4 , C_1 and C_2 respectively. The voltage of diode D is $-(V_{C1} + V_{C2} - V_d)$, so D undertakes negative voltage stress and, thus, turns off. The energy of C_2 is delivered to the load R_L and C_{d2} through the C_2 - R_L - C_{d2} loop, so C_{d2} charges and C_{d1} discharges.

In terms of the C_2 - R_L - C_{d2} loop, the output voltage of the converter read

$$V_o = V_{C2} - V_{C_{d2}} \quad (2)$$

Where $V_{C_{d2}}$ is the voltage of C_{d2} .

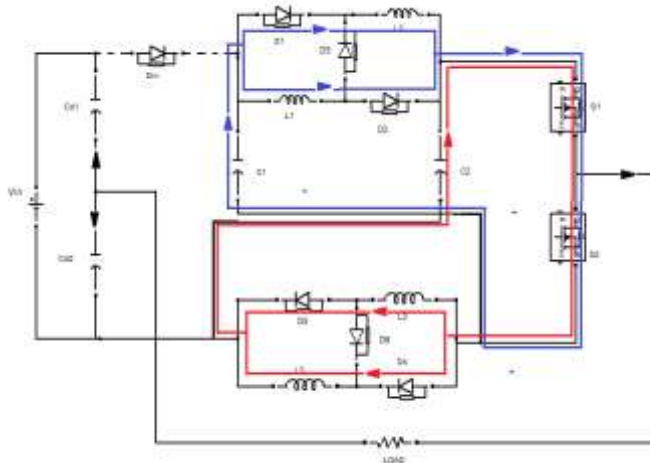


Figure3. Mode 1 Operation

Mode 2: $t \in [t_1, t_2]$

As shown in Fig.4, S_1 is on, and S_2 is off. In loop 1, the source V_d and L_1 and L_2 discharge the energy to C_2 , so that V_{C2} increases. In loop 2, the source V_d and L_3 and L_4 discharge the energy to C_1 ; thereafter, V_{C1} increases. Then, the energy of C_2 is delivered to the load R_L and C_{d2} through the C_2 - R_L - C_{d2} loop, so C_{d2} charges and C_{d1} discharges. From loop 1,

$$V_{L1} = V_d - V_{C2} \quad (3)$$

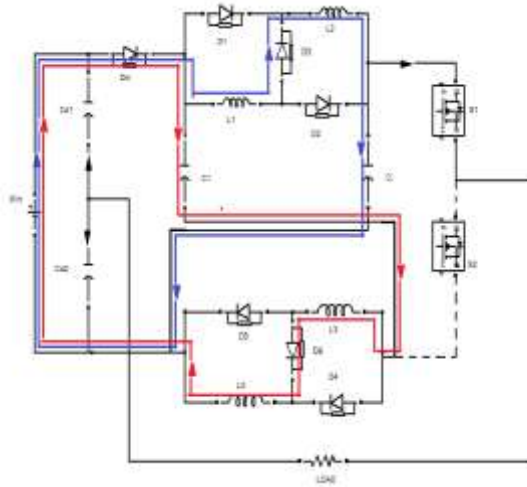


Figure. 4: Mode 2 Operation

Mode 3: $t \in [t_2, t_3]$

In Fig. 5, S_1 is off, and S_2 is on. In loop 1, the source V_d , L_1 and L_2 discharge the energy to C_2 ; thus, V_{C2} increases. Similarly, in loop 2, V_d , L_3 and L_4 discharge the energy to C_1 ; thus, V_{C1} increases. The energy of L_2 and C_{d2} is delivered to R_L through the L_2 - C_{d2} - R_L loop, so C_{d2} discharges and C_{d1} charges.

In terms of loop 1, one has the same equation as (3). In terms of the V_d -D- C_1 - R_L - C_{d2} loop, the output voltage is

$$v_0 = -(v_{Cd2} + v_{C1} - V_d) \quad (4)$$

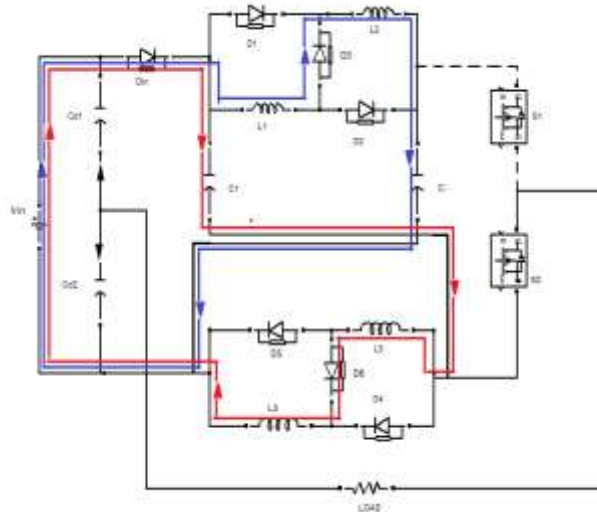


Figure. 5: Mode 3 Operation

Fig. 9 : Inductor Current

Fig. 9 shows the inductor current. All the inductor have the same current waveforms. Voltage across the switches is shown in Fig. 10. Both the switches have the same voltage waveform.

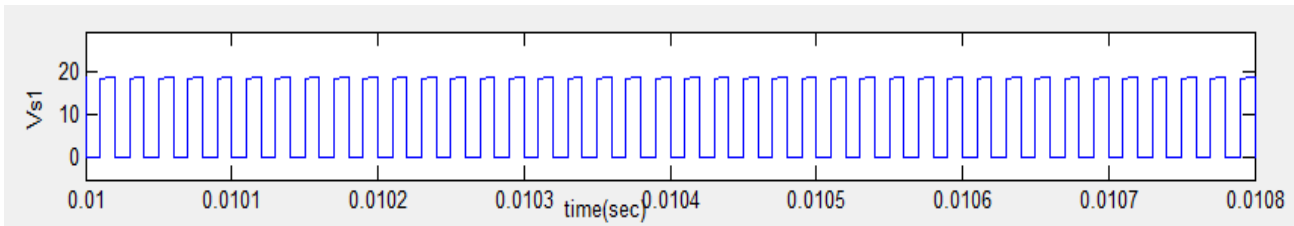
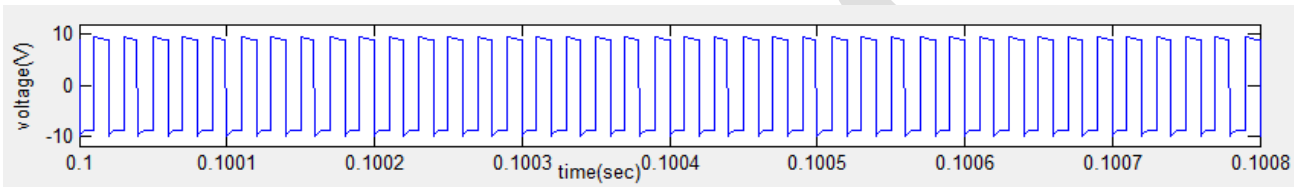
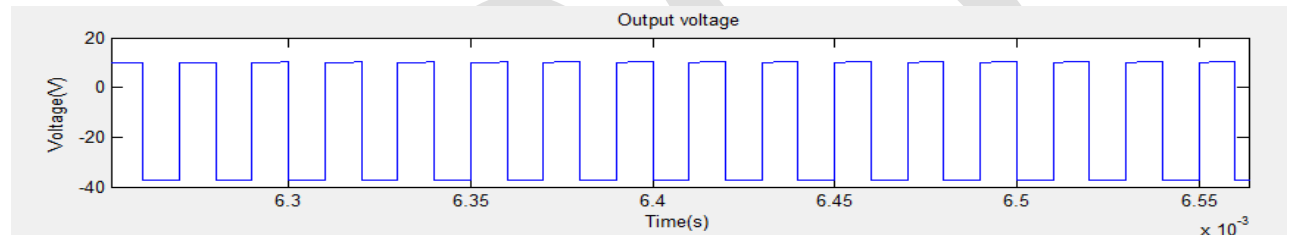


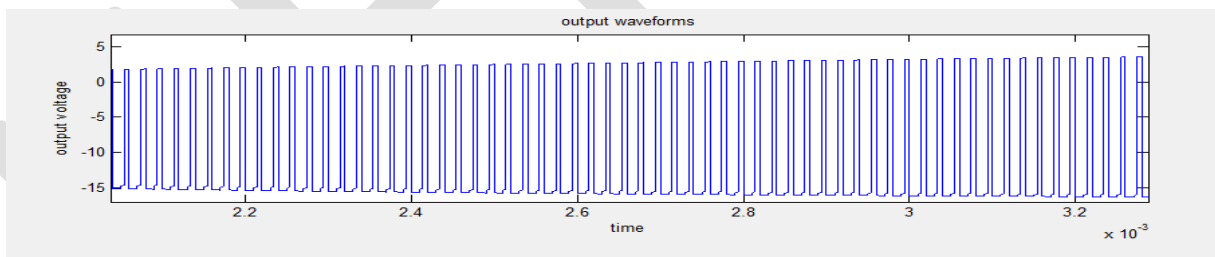
Fig. 10 : Voltage Across Switch



(a)



(b)



(c)

Fig. 11: (a) (b) (c) Output Voltage Waveforms For Various Duty Cycles

Fig. 11 shows the output voltage waveforms for different duty cycles. Thus, by varying the duty cycle, the positive and negative peak and also the time period can be varied

CONCLUSION

This paper propose a novel Z-source half-bridge converter that can output buck– boost voltages. Different from the Z-source converter, it needs only switched inductor Z-network between the input capacitors and the switches. From the simulation it is known that the proposed inverter can provide a strong boost ability to overcome the limitations of the classical Z-source converter.

The converter produces output voltage waveforms with varied positive and negative peaks and with varied time periods. Moreover, the converter has been analyzed in two different states, including the shoot-through and non-shoot-through states. Furthermore, the feature of the proposed converter owning abundant outputs under an appropriate control is very desirable for requirements of the electrochemical power supply.

REFERENCES:

- [1] B. Zhao, Q. G. Yu, Z. W. Leng, and X. Y. Chen, "Switched Z- source isolated bidirectional DC-DC converter and its phase- shifting shootthrough bivariate coordinated control strategy," *IEEE Trans. Ind. Electron.*, vol. 59, no. 12, pp. 4657-4670,
- [2] Y. C. Hung, F. S. Shyu, C. J. Lin, and Y. S. Lai, "New voltage balance technique for capacitors of symmetrical half-bridge converter with current mode control," in *Proc. PEDS*, 2003, pp. 365-369.
- [3] Z. Liu, B. Liu, S. Duan, Y. Kang, and K. N. J. Soon, "A novel DC capacitor voltage balance control method for cascade multilevel STATCOM," *IEEE Trans. Power Electron.*, vol. 27, no. 1, pp. 14-27, Jan. 2012.
- A. Faruk Bakan , Ismail Aksoy, "Loss Analysis of Half Bridge Converter in High Current and Low Power Applications" World Academy of Science, Engineering and Technology, 2013
- [4] F. Z. Peng, "Z-source inverter", *IEEE TRANSACTIONS ON INDUSTRY APPLICATIONS*, VOL. 39, NO. MARCH/APRIL 2003
- [5] B. M. Ge, Q. Lei, W. Qian, and F. Z. Peang, "A family of Z- Source matrix converters," *IEEE Trans. Ind. Electron.*, vol. 59, no. 1, pp. 35-46, Jan. 2012.
- [6] S. M. Dehghan, M. Mohamadian, A. Yazdian, and F. Ashrafzadeh, "A dual-input-dual-output Z-source inverter," *IEEE Trans. Power Electron.*, vol. 25, no. 2, pp. 360-368, Feb. 2010.
- [7] Eduardo I. Ortiz Rivera, Member Luis A. Rodríguez , "The Z- Source Converter as an Introduction to Power Electronics and Undergraduate Research", 37th ASEE/IEEE Frontiers in Education Conference
- [8] Minh-Khai Nguyen, Young-Cheol Lim, Geum-Bae Cho, "Switched-Inductor Quasi-Z-Source Inverter", *IEEE TRANSACTIONS ON POWER ELECTRONICS*, VOL. 26, NO. 11, NOVEMBER 2011
- [9] P. C. Loh, F. Blaabjerg, and C. P. Wong, "Comparative evaluation of pulsewidth modulation strategies for Z-source neutral-point-clamped inverter," *IEEE Trans. Power Electron.*, vol. 22, no. 3, pp. 1005-1013, May 2007.
- [10] W. M. Zhang, M. H. Deng, Y. Q. Pei, and Z. A. Wang, "Design and optimization of high current power supply for electrochemistry," in *Proc. IPEC*, 2010, pp. 86-91.
- [11] X. Hu, Z. Y. Ling, X. H. He, and S. S. Chen, "Controlling transmission spectra of photonic crystals under electrochemical oxidization of aluminum," *J. Electrochem. Soc.*, vol. 156, no. 5, pp. C176-C179, 2009.

Optimized Solution for Denial-of-Service Attacks in Bloom-Filter-Based Forwarding

Anisha Sarah Mathew¹, Mitha Rachel Jose²

Department of Computer Science and Engineering, Mahatma Gandhi University, Mangalam College of Engineering, Kerala

Email id: anmathew00@gmail.com

9961617089

Abstract— Today, the Internet is an essential part of everyday life and many important and crucial services like banking, shopping, transport, health, and communication are partly or completely dependent on the Internet. Also it was originally designed for openness and scalability without much concern for security. Unfortunately, it is not possible to reliably determine the source of received IP packets, as the protocol does not provide authentication of the packet based on the source address field, can be easily pirated. Furthermore the Internet routing infrastructure also does not keep information about forwarded packets. Malicious users can exploit these design weaknesses of the internet to degrade its operation. Denial of Service attacks is launched by large number of compromised host to interrupt the services of legitimate users. Bloom Filter resolves current problem in the network such as routing table growth, multicast scalability and denial of service attack. Based on the information stored in the packet header as a filter, nodes will forward the packet. But it has a several problems like false positive issues, high memory and time usage. In order to overcome these problems, an algorithm called simulated annealing has been used, which results in the efficient detection of denial of service attacks in bloom filter forwarding.

Keywords— Bloom Filter, DoS, Network security, Simulated Annealing.

I. INTRODUCTION

Security is a fundamental component of every network design. A security policy defines what people can and can't do with network components and resources. Most security issues focus on the connection of the corporate network to the Internet and related issues such as viruses transmitted via electronic mail and intrusion from hackers. For secure communication to take place desirable security aspects such as confidentiality, authentication, message integrity and non repudiation is to be considered.

Classes of attack might include passive monitoring of communications, active network attacks, close-in attacks, exploitation by insiders and attacks through the service provider. A system must be able to limit damage and recover rapidly when attacks occur. Denial of Service is an attempt to flood an online service or computer resource by an attacker [13] with unwanted traffic in order to prevent it from functioning efficiently or reliably (Yuval et al., 2010). A number of sites are affected by such attacks, thus DoS attacks can be limited or completely eliminated by performing a change in packet forwarding logic in such a way that it will not affect Internet Protocol(IP) or other layers in TCP/IP protocol stack [12]. The Denial of Service attack incorporated multiple compromised machines and resources at a time to attack a sole target.

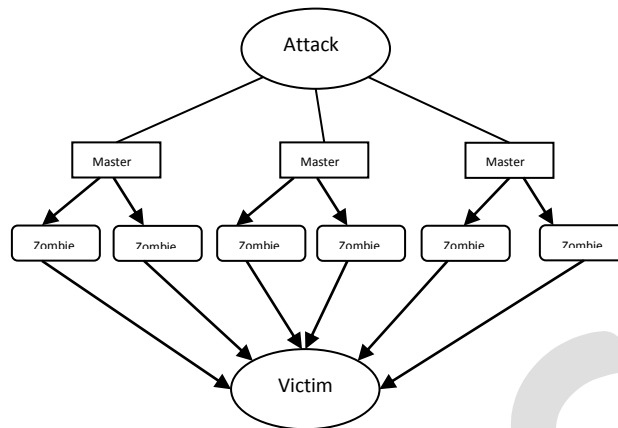


Fig. 1. Denial of Service Attack

A number of solutions are available as defence against the DoS attack however none can be a solution in standalone form and for longer time. Solutions include hop count filtering , Router base solution, Stack Pi, Push back router based defence , differential packet filtering , trace back through marking , trace back using entropy variations [4] and by using bloom filter technique. By using bloom filter technique [11] , computation capability of a machine enhances, access time of different files reduces. A Bloom Filter [4] is an ingenious randomized data structure for concisely representing a set in order to support approximate membership queries. The advantage of using bloom filter technique is as follows : Very little state and signalling required, native multicast support, no global addressing, path not revealed, no routing tables and lookups required.

In the existing system, it explains the intentional creation of routing loops and their anomalies by reverse engineering[1] the secret link identifiers with the help of a distributed adversary. It also explains how bloom filter forwarding are vulnerable to a form of packet injection that enables distributed flooding attacks by botnets [14] . It shows an attack against bloom filter discovery [5] in which a subscriber [15] prevents others from unsubscribing. The main drawback of the existing system is the rise of false positive result and absence of an accurate result.

In the proposed system, it defines that Bloom filter forwarding which prevents denial of service attacks in an optimized manner. This is done by using simulated annealing. Thus an optimized data analysis takes place. In the existing system, tree structure and connectivity data structures are used, instead of that, here graph is used. Hence time complexity and memory usage also reduces.

The rest of the paper is structured as follows : Section II gives an overview of the previous work on DoS preventive measures , Section III presents the Optimized solution for the DoS attacks in bloom filter forwarding , Section IV presents the experimental results and Section V concludes the paper.

II. Related work

Self-Routing Denial-of-Service Resistant Capabilities Using Inpacket Bloom Filters: Bloom-filter-based source-routing architecture which is resistant to Distributed Denial-of-Service attacks. This approach is based on forwarding identifiers that act simultaneously as path designators, i.e. define which path the packet [2] should take, and as capabilities, i.e. effectively allowing the forwarding nodes along the path to enforce a security policy where only explicitly authorized packets[10] are forwarded. The compact representation is based on a small Bloom filter whose candidate elements (i.e. link names) are dynamically computed at packet forwarding time using a loosely synchronized time-based shared secret and additional in-packet flow information (e.g., invariant packet contents).

Implementing zFilter based forwarding node on a NetFPGA: In this paper, it describes about the NetFPGA based forwarding node implementation for this new, IP-less, forwarding fabric. The implementation requires removing the traditional IP forwarding implementation, and replacing it with the Bloom-filter matching techniques for making the forwarding decisions. [6].

Secure in-packet Bloom Filter forwarding on the NetFPGA: In packet Bloom-Filter allows one to forward source-routed packets with minimal forwarding tables; the Bloom-Filter [1] is encoded with the identities of the links through which the packet needs to be forwarded if the link identities [7] are made content dependent. In this paper, it describes about the early implementation and testing of an in-packet Bloom filters forwarding node that implements cryptographically computed link identifiers.

Forwarding anomalies in Bloom filter based multicast: Several recently proposed multicast protocols use in-packet Bloom filters to encode multicast trees [5]. These mechanisms are highly scalable because no per-flow state is required in the routers and because

routing decisions can be made efficiently by simply checking for the presence of outbound links [16] in the filter. This paper explores such anomalies, namely (1) packets storms, (2) forwarding loops and (3) flow duplication. This paper proposes stateless solution that increases the robustness and the scalability of Bloom filter-based multicast protocols [8]. In particular, it shows that the parameters of the filter need to be varied to guarantee the stability of the packet forwarding, and which presents a bit permutation technique that effectively prevents both accidental and maliciously created anomalies. The solution to avoid such anomalies [9], the context of Bloom-Cast is proposed, which is a source-specific inter-domain multicast protocol, which uses analytical methods and simulations [3].

III. PROPOSED ALGORITHM

In this paper, we have presented a new solution for the DoS attacks in bloom filter forwarding. This done by using simulated annealing algorithm. Local Optimum is found each time and thus an accurate result is obtained with reduced false positive value. The system architecture is as shown below in Fig.2.

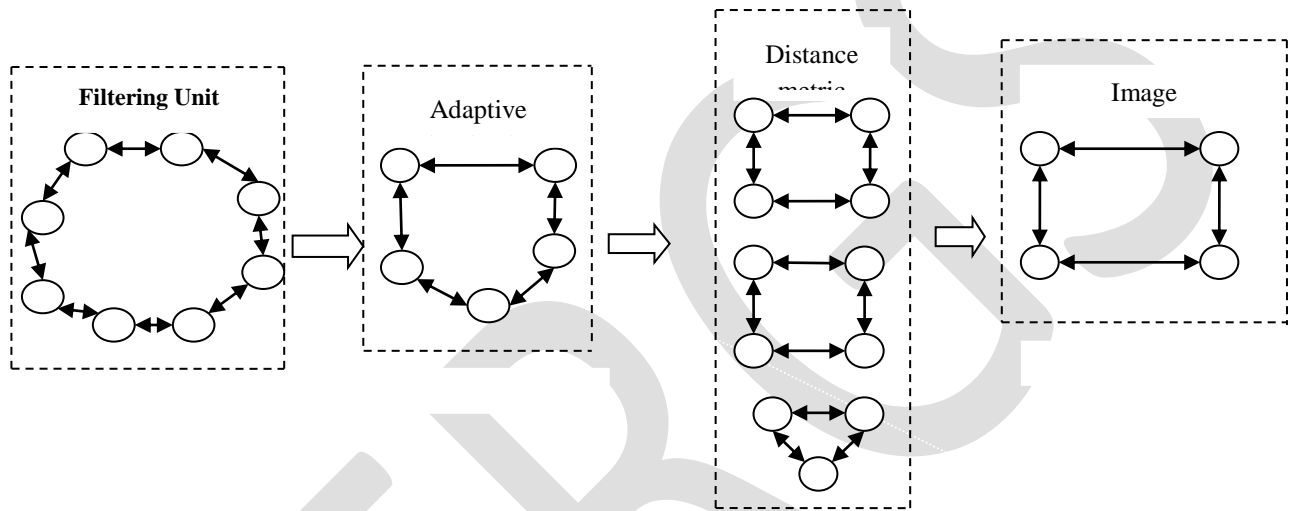


Fig.2. Detection of DoS using Simulated Annealing

Every incoming packet is received and it forms a graph; each node in the graph contains the sender, destination, data length and time details. Incoming packets are captured. The packets form graph, which is bidirectional, hence it takes less time and memory usage. A threshold is determined. Weight of each edge is found out. Highest weight of each node is found out. Thus the edges above the threshold value is considered. The different cycles among those edges are found out. From the above cycle obtained the attacker will be detected. For the result to be obtained in an optimized way, simulated annealing algorithm is used. Thus a local optimum is found out. An initial threshold value is set, based on that threshold value, local optimum is found out. Later access the threshold value for finding more optimized value until it reaches the stopping criteria.

In Optimized Bloom Filter Forwarding, there are mainly six phases: Packet Capturing Module, Attacker Module, Server Module, Filtering Module, Monitoring Module and Detection module.

A. Packet Capturing Module

The incoming packets are captured. These packets are filtered, monitored and detected to find whether it is an attacker group.

B. Attacker Module

Client machine acts as the attacker. Attacker attempts to make a machine or network resource unavailable to its intended [users](#), such as to temporarily or indefinitely interrupt or suspend [services](#) of a [host](#) connected to the [Internet](#). Thus it results in complete shutdown of the target services.

C. Server Module

Server machine is the target machine to which packets are to be sent. Attacker tries to disrupt the network, preventing legitimate packets from getting through to their destination.

D. Filtering Module

The filtering unit captures the packet moving in and out of the network. Filtering unit is meant for providing protection against flooding attacks using real internet dataset.

E. Monitoring Module

The monitor's main task is to record the state (open, in progress, established) of any incoming session, information that will be utilized during the detection phase. Furthermore, it should be stressed that a single tracking memory solution can only be used as an indication of an attack, whereas the proposed monitor's information can be used, among others, for identifying malicious messages.

F. Detection Module

This unit is concerned with the detection of the threats or the malware. The detection is based on factors like number of port scans, unusually frequent logins and signups, high rate of packets send to a single port. There is a threshold associated with each of them described. This threshold value is automatically generated by applying a simulated annealing algorithm over the past history of traffic flows present in the database. The packet with fingerprints or signatures with values of the above given parameters exceeding their respective threshold will be classified as an attack. According to the unusual behavioural patterns like continuous port scans, unlimited connection request to the same IP or multiple packets destined to the same interface, extremely large number of packets with urgent pointer set, session hijacking etc, the attacks are detected.

Optimized Bloom Filter Forwarding consists of following steps:

1. Packet Capturing: Incoming packets are captured. These are represented as graph data structure , which is bidirectional hence time complexity reduces and memory usage reduces.
2. Abnormal node Calculation : Each node is considered , those node with edges more than 2 is selected. Those nodes are considered as attackers. This form an attacker group.
3. Detection of unusual cycles : To the attacker group , simulated annealing is applied and thus an optimized solution is obtained.
4. Detecting attacker groups : By applying simulated annealing False positiveness is limited with high accuracy.

While packet capturing takes place, packet analyzer intercepts and logs traffic passing over a digital [network](#) or part of a network. As [data streams](#) flow across the network, the sniffer captures each [packet](#) and, if needed, decodes the packet's raw data, showing the values of various fields in the packet, and analyzes its content according to the appropriate [RFC](#) or other specifications. False positiveness is the event of detecting a legitimate user or application as a threat. Increase in the false positiveness causes degradation in the overall performance factor of the detection system. By applying simulated annealing algorithm, the threshold value assigned such that all the packet flows exceeding that threshold value will be declared as an attack. This will reduce the false positiveness of the detection system when compared to the previous works.

IV. EXPERIMENTAL RESULTS

The performance of the proposed scheme is compare with the old scheme with respect to time complexity and memory usage. The Experiment is done on the basis of the memory usage when compared to our present system and the existing system. The figure 3 shows that memory usage decreases in our present system.

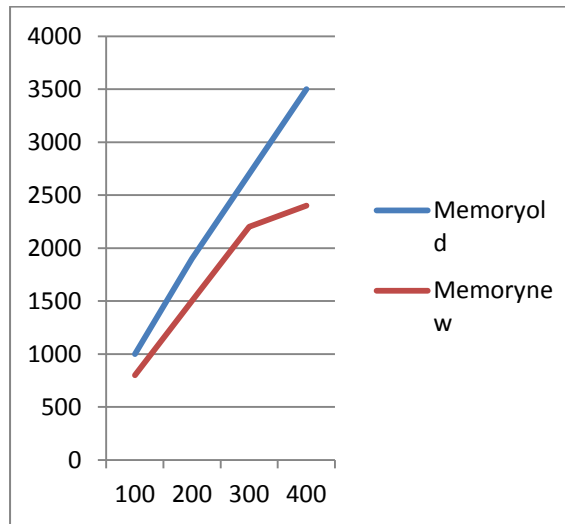


Fig 3 : Memory usage

The figure 4 shows that time taken decreases in our present system compared to the existing system due to the usage of graphs instead of trees.

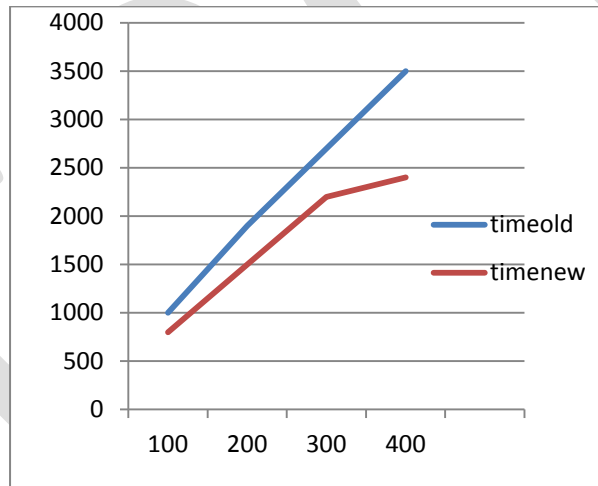


Fig 4: Time usage

V. CONCLUSION

DoS attacks can target tangible system resources, such as computational resources (bandwidth, disk space, processor time); configuration information (routing information, etc.); state information (for example, unsolicited TCP session resetting). This causes degradation in the overall performance factor of the detection system. The system presents how the denial of service attack is detected and prevented in bloom filter forwarding. In the present system, data analysis takes place using Simulated Annealing. Thus an optimized solution is obtained which result in less false positiveness and high accuracy.

ACKNOWLEDGMENT

I would like to acknowledge my project guide Ms Mitha Rachel Jose for her valuable support and useful guidance. I thank my friends and my family for being there with me.

REFERENCES:

- [1] Markku Antikainen, Tuomas Aura, and Mikko Särelä, "Denial of Service Attacks in Bloom-Filter-Based Forwarding," *IEEE/ACM Transactions on Networking*, vol. 22, no. 5, October 2014
- [2] S. Ratnasamy, A. Ermolinskiy, and S. Shenker, "Revisiting IP multicast," *Comput. Commun. Rev.*, vol. 36, no. 4, pp. 15–26, 2006.
- [3] C. Rothenberg, P. Jokela, P. Nikander, M. Särelä, and J. Ylitalo, "Self-routing denial-of-service resistant capabilities using in-packet Bloom filters," in *Proc. Eur. Conf. Comput. Netw. Defense*, 2009, pp. 46–51.
- [4] P. Jokela, A. Zahemszky, C. Esteve Rothenberg, S. Arianfar, and P. Nikander, "LIPSIN: Line speed publish/subscribe inter-networking," in *Proc. ACM SIGCOMM*, 2009, pp. 195–206.
- [5] M. Särelä, C. E. Rothenberg, T. Aura, A. Zahemszky, P. Nikander, and J. Ott, "Forwarding anomalies in Bloom filter based multicast," in *Proc. 30th IEEE INFOCOM*, 2011, pp. 2399–2407.
- [6] C. Macapuna, C. Rothenberg, and M. Magalhães, "In-packet Bloom filter based data center networking with distributed OpenFlow controllers," in *Proc. IEEE GLOBECOM Workshops*, Dec. 2010, pp. 584–588.
- [7] C. Rothenberg, C. Macapuna, F. Verdi, M. Magalhães, and A. Zahemszky, "Data center networking with in-packet Bloom filters," in *Proc. 28th SBRC*, Gramado, Brazil, 2010, pp. 553–566.
- [8] A. Zahemszky, P. Jokela, M. Särelä, S. Ruponen, J. Kempf, and P. Nikander, "MPSS: Multiprotocol stateless switching," in *Proc. IEEE INFOCOM Workshops*, 2010, pp. 1–6.
- [9] J. Keinänen, P. Jokela, and K. Slavov, "Implementing zFilter based forwarding node on a NetFPGA," in *Proc. NetFPGA Dev. Workshop*, 2009, pp. 1–8.
- [10] A. Ghani and P. Nikander, "Secure in-packet Bloom filter forwarding on the NetFPGA," in *Proc. 1st Eur. NetFPGA Dev. Workshop*, 2010, pp. 1–7.
- [11] B. H. Bloom, "Space/time trade-offs in hash coding with allowable errors," *Commun. ACM*, vol. 13, pp. 422–426, Jul. 1970.
- [12] M. Särelä, "BloomCasting for publish/subscribe networks," Ph.D. dissertation, Aalto Univ., Espoo, Finland, 2011.
- [13] R. Lee, Z. Shi, and X. Yang, "Efficient permutation instructions for fast software cryptography," *IEEE Micro.*, vol. 21, no. 6, pp. 56–69, Nov.–Dec. 2002.
- [14] T. Anderson, T. Roscoe, and D. Wetherall, "Preventing Internet denial-of-service with capabilities," *Comput. Commun. Rev.*, vol. 34, no. 1, pp. 39–44, 2004.

- [15] D. Mazières, M. Kaminsky, M. F. Kaashoek, and E. Witchel, “Separating key management from file system security,” *Oper. Syst. Rev.* vol. 33, pp. 124–139, Dec. 1999.
- [16] D. Lagutin, “Securing the Internet with digital signatures,” Ph.D. dissertation, School of Science and Technology, Aalto University, Espoo, Finland, 2010.

IJERGS

Double Boost SEPIC AC-DC Converter

Sona P¹, Kavitha Issac², Beena M Varghese³

¹ Student, Electrical and Electronics Engineering, Mar Athanasius College of Engineering, Kerala, India

² Asst. Professor, Electrical and Electronics Engineering, Mar Athanasius College of Engineering, Kerala, India

³ Asso. Professor, Electrical and Electronics Engineering, Mar Athanasius College of Engineering, Kerala, India

Abstract- In this paper, a new single phase dual output ac-dc bridgeless double boost SEPIC (IDBS) converter is proposed which is a high step up converter. The absence of bridge rectifier in the proposed rectifier and the conduction of one semiconductor switch in the current flowing path during each switching cycle result in less conduction losses and improves efficiency. The proposed topology is designed to operate to achieve nearly a unity power factor and low total harmonic distortion (THD) of the input current. The DCM operation gives advantages such as zero-current turn-on in the power switches and simple control circuitry. The proposed topology gives better performance than modified bridgeless SEPIC rectifier in terms of efficiency, total harmonic distortion (THD), and power factor.. A design example for a 500-W/600 V dc with 120 V input voltage is provided. The proposed circuit is simulated in Matlab 2010a which ensures the feasibility of the converter

Key Words: AC - DC power converter, PFC Correction, High step-up converter, SEPIC Converter, Switched Capacitor, DCM, Double boost converter

1. INTRODUCTION

The demand for clean energy is increasing day by day and thus power supplies with active power factor correction (PFC) techniques are becoming necessary for many types of electronic equipment. They are designed to meet harmonic regulations and standards, such as the IEC 61000-3-2 [1]. Full bridge power supplies with active power factor correction (PFC) techniques cannot provide a high voltage gain and also they suffers from the fact that three semiconductor switches conducts at any instant of time.

In response to these concerns, considerable research efforts have been directed toward the development of efficient bridgeless PFC circuit topologies. A bridgeless PFC circuit allows the current to flow through a minimum number of switching devices compared to the conventional PFC circuit. The bridgeless boost rectifier has the drawbacks that the input-output isolation cannot easily be implemented, the startup inrush current is high, and there is a lack of current limiting during overload conditions. The boost converter operating in discontinuous current mode (DCM) can offer a number of advantages such as inherent PFC function, simple control, soft turn-on of the main switch, and reduced diode reversed-recovery losses. However, the DCM operation requires a boost inductor since it must switch extremely high peak ripple currents and voltages. As a result, a more robust input filter must be employed to suppress the high-frequency components of the pulsating input current, which increases the overall weight and cost of the rectifier.

A SEPIC converter is a less popular topology for PFC converter design because the control can be complex, due to its 2 pairs of un-damped complex poles, compared with other FC converters, such as the boost converter, fly-back converter. The advantage of the SEPIC converter is that its output voltage is not necessarily limited by its input voltage range. This property means that the output voltage can be higher or lower than input voltage. SEPIC converter offers easy implementation of magnetic coupling which results in reduction of input current ripple and low inrush current [3]. But Sepic converters suffer from higher switch voltage stresses. This increases the cost and conduction losses of the converter]. Converters uses switched-capacitor and voltage multiplier cell technique

which results in increase in the voltage gain as well as reduce the voltage stress across the power switch [10-12]. The use of switched capacitors can significantly extend the voltage gain, minimize the input current ripple and doubles the transferable power.

In this paper, a bridgeless dual output double boost AC - DC converter utilizing switched capacitor technology without extreme duty-cycle operation is introduced. This is achieved by integrating a Double boost Sepic DC - DC converter with a PFC correction circuit. We can have two outputs from the converter, actual output and the capacitor of the modified circuit provides another output. The Double Boost converter is selected due to its high step-up capability and the Sepic converter is selected due to its capability of providing low input current ripple. Hence, the Double Boost Sepic ac -dc converter allows the duty cycle to be extended further and makes the proposed converter more suitable for high step-up voltage applications. In addition, the proposed converter maintains the key advantages of the conventional boost and Sepic converters.

2. DOUBLE BOOST SEPIC AC-DC PFC CONVERTER

The basic circuit diagram of a bridgeless SEPIC double boost PFC Rectifier with voltage multiplier is illustrated in the figure 1. The bridgeless configuration will reduce the conduction losses since the diode bridge is removed, as a result the overall efficiency will increase. The voltage multiplier will result in high gain. The proposed circuit consists of two SEPIC circuits with switched capacitor configuration that consists of diodes and capacitors connected in a symmetrical configuration. Each configuration will operate in a half-line cycle. Moreover, the symmetrical operation of the converter simplifies the control signals for switches Q_1 and Q_2 which drives the circuitry.

The proposed topology shown in Figure 1 has a practical drawbacks of lack of limiting large inrush current flowing through inductors and switches. Therefore, special measures are taken to limit inrush current in the circuit and it should be necessary to ensure soft start of the system and to protect the circuit components from damage.

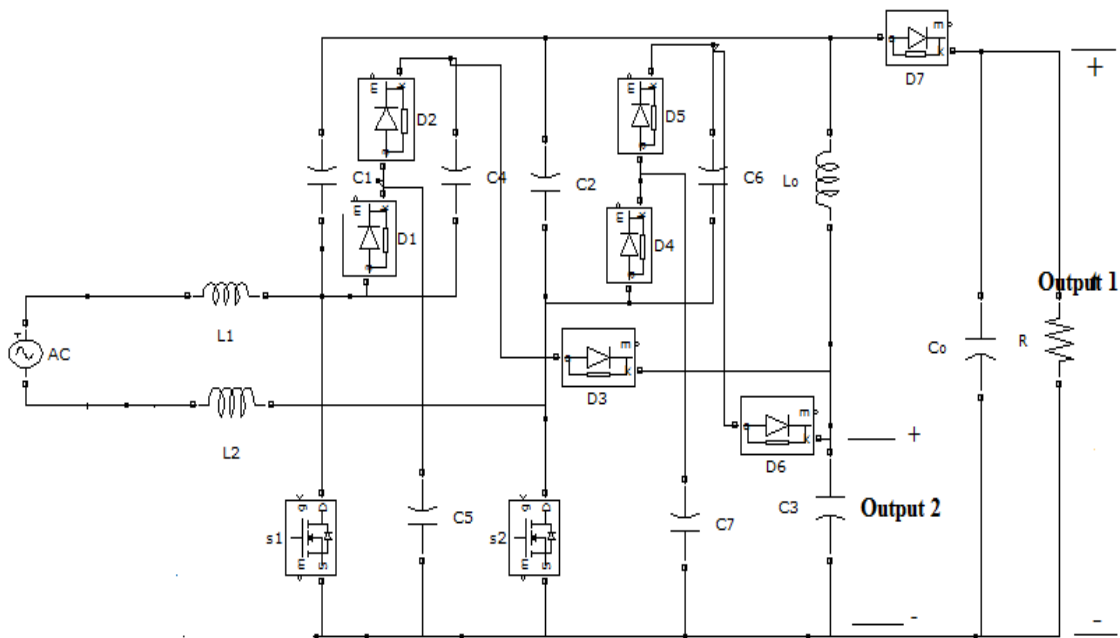


Fig. 1: Circuit diagram of the double boost SEPIC AC – DC PFC converter

2.1 Principle of Operation and Analysis

The proposed circuit consists of two symmetrical configurations as illustrated in figure 2. The circuit is analysed for the positive half line cycle and negative half line cycle. Accordingly, the circuit operation in one T_s can be divided into two stages as shown in

Figure 2(a) and (b). The circuit operation during one switching period T_s in a positive half-line period can be divided into two distinct operating modes, as shown in Figure 4 and figure 5, and it can be described as follows. Figure 3 shows its ideal key waveforms. The operational modes are described briefly as follows.

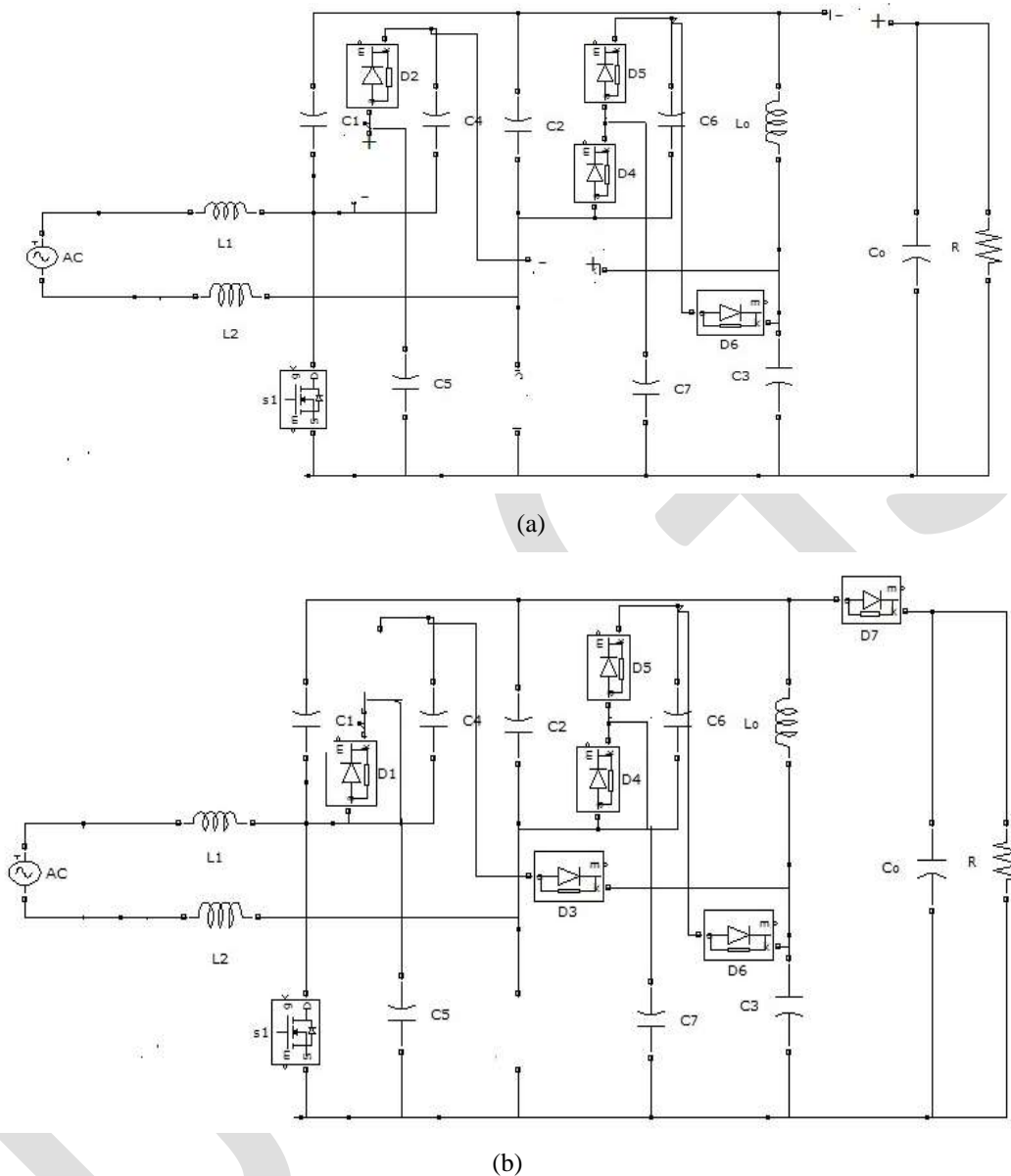


Fig 2: Topological stages of the converter of fig 1. (a)Switch ON topology, (b) Switch OFF topology

Mode 1

During the positive half cycle, the power switch Q_1 operates. When it is turned on, inductor L_1 stores energy and simultaneously diode D_2 is turned on. Diode D_1 is reversed-biased by the capacitor voltage V_{C1} , while diodes D_3 and D_7 are turned off by the negative voltage $(V_{C1} - V_{C3})$ and $(V_{C4} - V_0)$ across them, respectively. In this stage, the currents through the two inductors increases linearly at a rate proportional to the input voltage V_{in} . Capacitor C_4 charges capacitor C_5 while capacitor C_1 is being charged by inductor $L_0(i_{L_0})$. This mode lasts till the voltage across capacitor C_4 and C_5 are equal, while the difference between the capacitors' voltages V_{C1} and V_{C3} must equal to the input voltage, i.e.,

$$V_{C4} = V_{C5} \text{ -----(1)}$$

$$V_{in} = V_{C1} - V_{C3} \text{ -----(2)}$$

At the end of this interval, the switch is turned-off initiating the next subinterval.

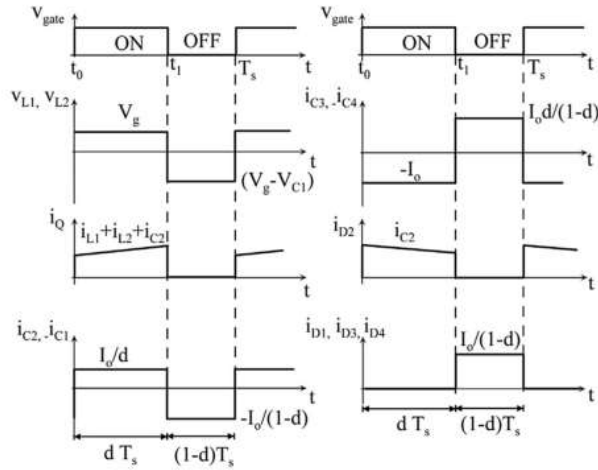


Fig 3: Theoretical Waveforms

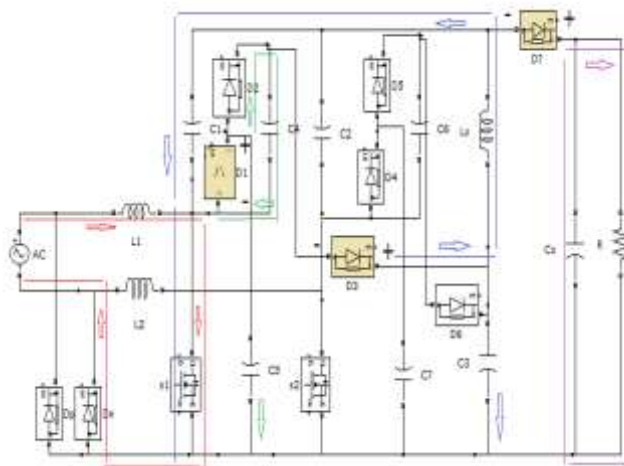


Fig. 4: Current flow path of the double boost SEPIC AC – DC PFC converter during Mode 1

Mode 2

When the switch Q_1 is turned off, Diodes D_1, D_3, D_7 are turned on simultaneously providing a path for the input and output inductor currents. Diode D_2 is reverse biased by the voltage V_{C4} . In this stage, the inductors currents i_{L1} and i_{L0} decreases linearly at a rate proportional to the voltage $(V_{in} - V_{C5})$ and $(V_{C3}-V_o)$, respectively. Capacitors C_1 and C_3 are being charged by the currents $(i_{L1} + i_{C4} + i_{C1})$ and $(i_{D3} - i_{L2})$, respectively. During this stage, the output Capacitor C_o and the load R_L are being charged by the current $(i_{L0} + i_{C1})$. Referring to Figure 5, the following relations must hold:

$$V_o = V_{C3} + V_{C1} - V_{C4} \text{-----(3)}$$

$$V_{C3} = 2V_{C5} \text{-----(4)}$$

$$\Delta Q = i_{L3} DT \text{ -----(11)}$$

$$\Delta V_C = i_{L3} DT/C \text{ -----(12)}$$

Assuming 5% ripples in output voltage and $i_{L3} = i_o$

Solving we get

$$C_1 - C_7 = 22 \mu F, L_1, L_2 = 10mH$$

3. SIMULATION DIAGRAM & RESULTS

The proposed circuit "Double Boost SEPIC AC – DC PFC converter" has been modelled and simulated in Matlab/ Simulink 2010a. The components values obtained from the design equations for an input voltage of 120V are used.

Table -1: Simulation Parameters

Parameters	Value
Input voltage	120 V
Output Voltage	700V, 600V
Inductors L_1, L_2, L_3	10mH, 180uH
Capacitors $C_1 - C_7$	50μH
Output Capacitor, C_o	1000μH
Switching frequency	50kHz
Grid frequency	50Hz
Duty cycle	37%

The input voltage is set to 120V and both switches operates with a frequency of 50 kHz and duty cycle 37% . Simulation waveforms coincide with the theoretical operating waveforms.

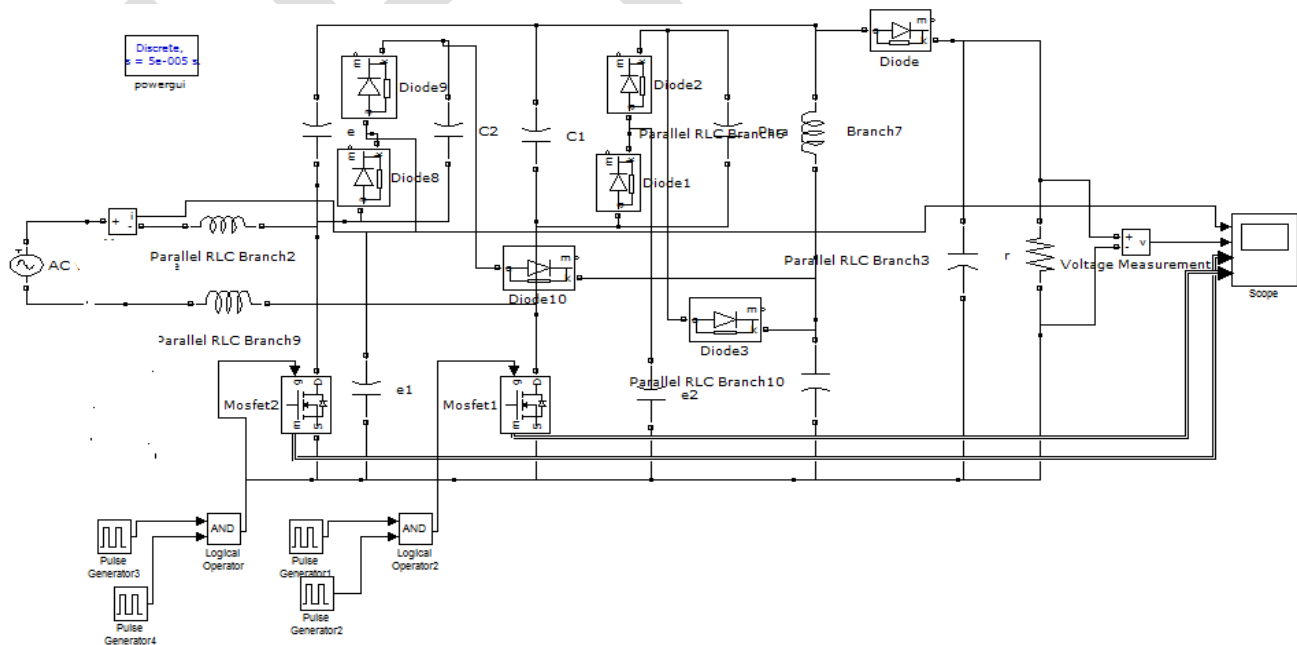


Fig 6: Simulink Diagram of bridgeless PFC Double boost SEPIC Rectifier

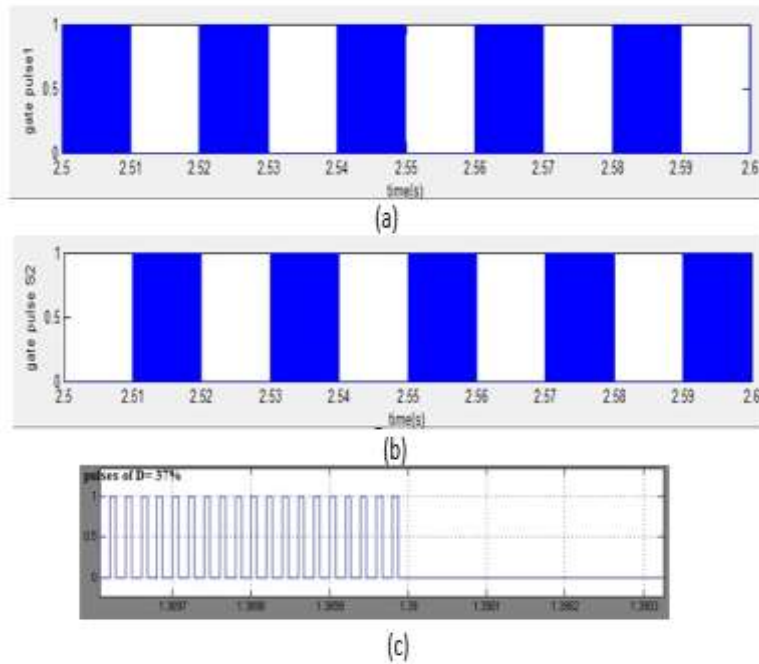


Fig 7: Simulated waveforms of (a) gate pulses for Q1 (b) gate pulses for Q2
(c) magnified portion of pulses with Duty cycle = 37%

The simulated waveforms of input voltage and current and output voltage and current are shown in the fig 8 and 9 respectively.

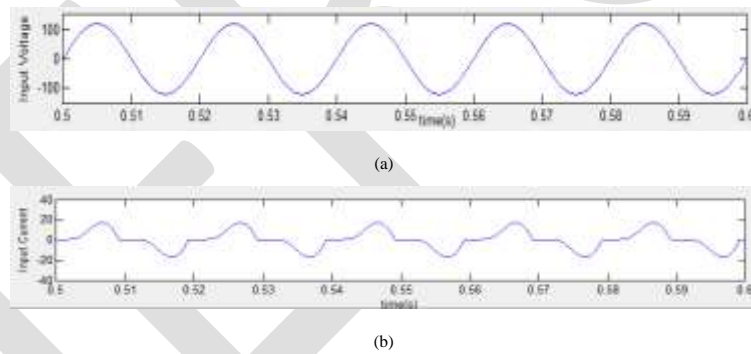


Fig 8: Simulated waveforms (a) Input voltage (b) Input current

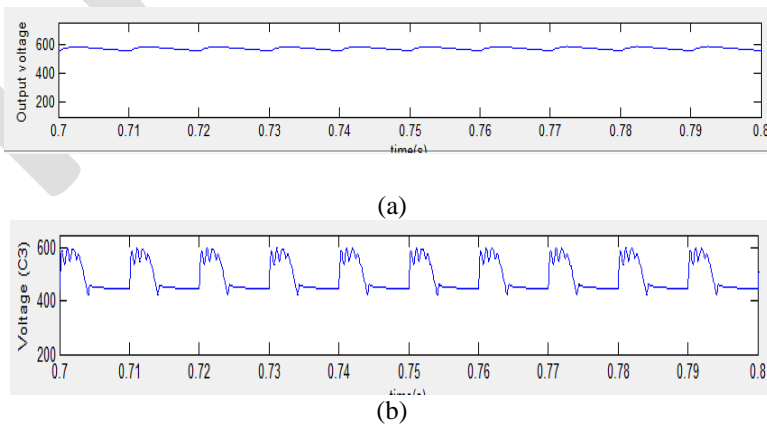


Fig 9: Simulated waveforms (a) Output voltage 1 (b) Output voltage 2

The current through inductors L_1 and L_2 rises and falls with respect to the switching pulses are shown in figure 7.

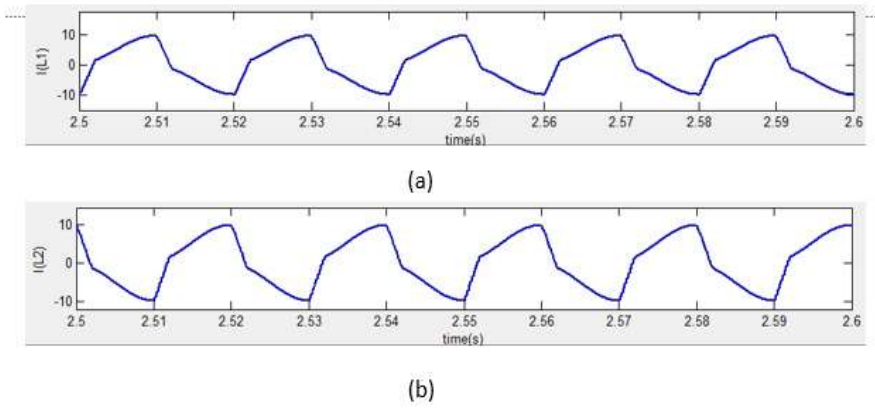
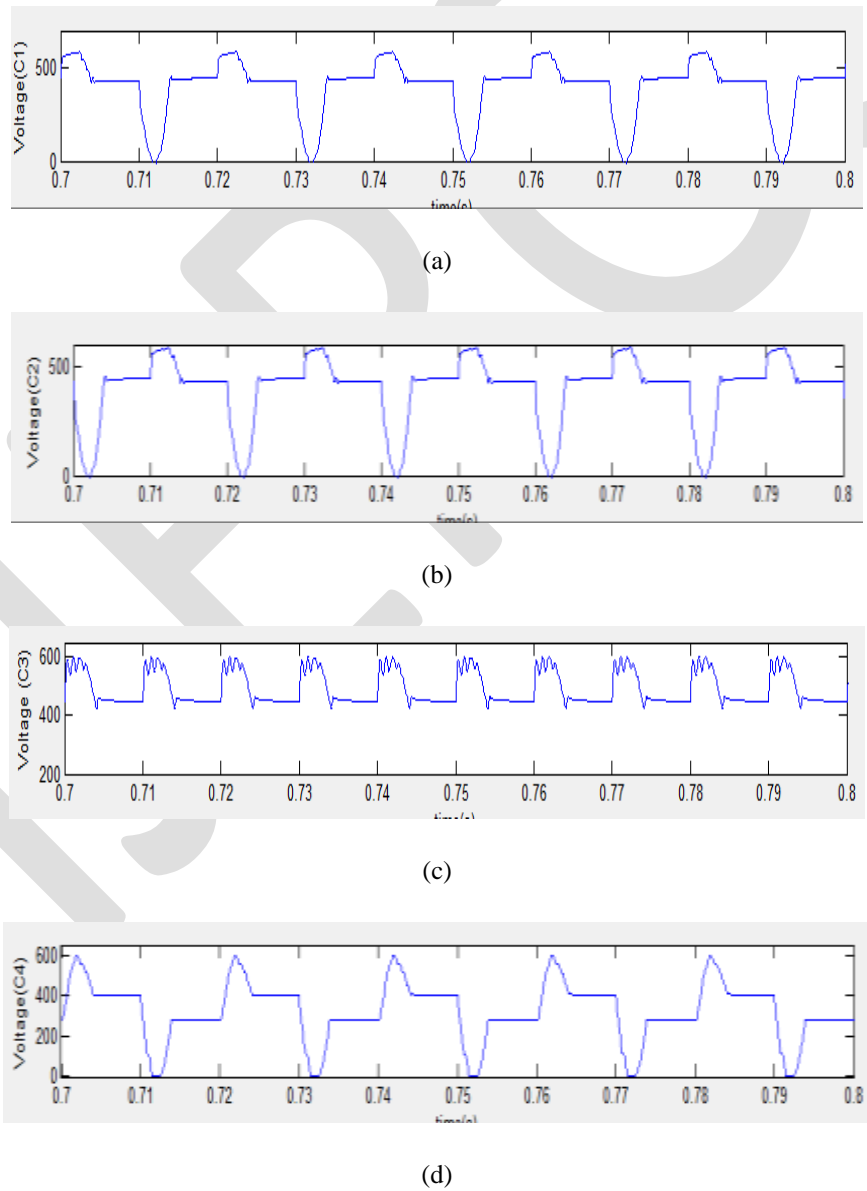


Fig 14: Simulated waveforms of (a) Inductor current L_1 (b) Inductor current L_2



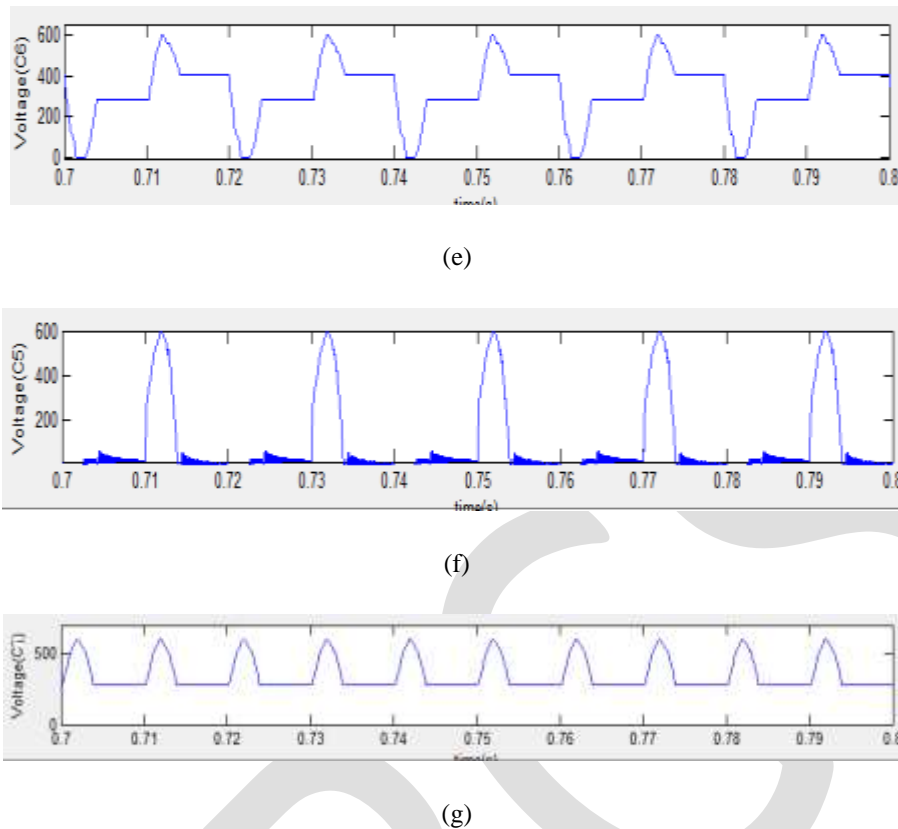


Fig 14: Simulated waveforms of Voltages across (a) C_1 (b) C_2 (c) C_3 (d) C_4 (e) C_6 (f) C_5 (g) C_7 (h)

4. CONCLUSIONS

A new topology based on double boost SEPIC has been presented and simulated in Matlab/Simulink 2010a which ensures the performance of the converter. The proposed topology has a higher efficiency than the full bridge topology due to its bridgeless nature. The proposed converter is operated at high switching frequencies to reduce input current ripple. Hence, the overall advantages will be higher efficiency, reduced size and weight, simpler structure and control. The two power switches in the proposed topology can be driven by the same control signal, which significantly simplifies the control circuitry. The THD of the converter is reduced to 10% and a 0.95 power factor is obtained by the proposed converter. The proposed integration technique can be easily extended together power converters to meet the demand for a wide range of voltages.

REFERENCES

- [1] Hussain S, Dylan Dah-Chuan Lu, Amirmaser Yazdani, Bin Wu "An Efficient Single Switch Quasi-Active PFC Converter With Continuous Input Current and Low DC-Bus Voltage Stress", *IEEE Transactions on Industrial Electronics*, Vol. 61, No. 4, April 2014.
- [2] Fariborz Musavi, Wilson Eberle, William G Dunford "A Phase Shifted Semi Bridgeless Boost Power Factor Corrected Converter for Plug in Hybrid Electric Vehicle Battery Chargers", *IEEE Trans. Power Electron.*, 2010, 25, (6), pp. 15651575
- [3] Luo, F.L., Ye, H, "Positive output multiple-lift push-pull switched capacitor Luo converters", *IJMTA*, Vol- 1, No.2 Jan 2013.
- [4] Denizer N Martins, Andersen, G.K., Blaabjerg, F, "Three Phase Rectifier using a Sepic DC - DC Converter in Continuous conduction mode for Power Factor Correction", *IEEE Trans. Ind. Electron.*, 53, (1), pp. 2632711, 2009
- [5] Carlos Gabriel Bianchin, Roger Gules "High Power Factor Rectifier Using The Modified Sepic Converter Operating in Discontinuous Conduction Mode", *IEEE Transactions on Power Electronics*, Vol. 18, Issue. 10, pp. 272-287, Dec 2014.

- [6] Ahmed M. Al Gabri, Esam H. Ismail "Bridgeless PFC Modified SEPIC Rectifier with Extended Gain for Universal Input Voltage Applications ", *IEEE Transactions on Power Electronics*, Vol. 30, Issue. 8, pp. 4272-4282, March 2015.
- [7] M. Mahdavi and H. Farzanehfard, "Bridgeless SEPIC PFC Rectifier With Reduced Components and Conduction Losses", *IEEE Transactions on Industrial Electronics*, Vol. 58, No. 9, pp.4153-4160, September 2011.
- [8] R. W. Erickson and D. Maksimovic, Fundamentals of Power Electronics, 2nd ed, *New York Kluwer Academic Publishers, 2004*.
- [9] A. A. Fardoun, E. H. Ismail, A.J. Sabzali and M. A. Al-Safar, New Efficient Bridgeless Cuk Rectifiers for PFC Applications, *IEEE Transactions on Power Electronics*, Vol. 27, No. 7, pp. 3292-3301, July 2012.
- [10] Mohammed Mahadavi , Hosein Farzanehfard, "Zero-voltage transition bridgeless single-ended primary inductance converter power factor correction rectifier" , *IET Power Electron* 2014 , Vol 7, Issue 4, pp 895 – 902.
- [11] Yu Tang, Ting Wang, Yaohua He, "A Switched Capacitor Based Active Network Converter with High Voltage Gain" *IEEE Transactions on Power Electronics* , vol. 3, no. 8, pp. December 2013
- [12] Yu Tang, Ting Wang, Dongjin Fu, "Multicell Switched Inductor/ Switched Capacitor combined Active Network Converters" *Industrial Electronics and Applications (ICIEA)*, 2014 IEEE 9th Conference on June 2014

Image Forgeries Detection by Color Illumination Approach

Mrs. Bhavana S¹ Manoj.Kumar²

¹Department of Computer Science and Engineering, VTU RO Kalaburagi, India

²Department of Computer Science and Engineering, VTU RO Kalaburagi, India

sg.bhavana@vtu.ac.in¹

mkmanoj604@gmail.com²

Abstract—In recent days, photographs have been used as evidence in courts. Photographers are able to create composites of analog pictures, this process is very time consuming and requires expert knowledge. Today, Powerful digital image editing software makes image modifications straightforward. This undermines our trust in photographs. In this paper, one of the most common forms of photographic manipulation, known as image composition or splicing is analysed .A forgery detection method that exploits subtle inconsistencies in the color of the illumination of images. The proposed approach is machine-learning based and requires minimal user interaction. The technique is applicable to images containing two or more people and requires no expert interaction for the tampering decision. Here, the existing work can be extended by using advanced face detection method using skin tone information and edges . A lighting insensitive face detection method based upon the edge and skin tone information of the input color image is proposed. From these illuminant estimates, we extract texture- and edge-based features which are then provided to a machine-learning approach for automatic decision-making.

Index Terms—Color constancy, illuminant color, image forensics, machine learning, spliced image detection, texture and edge descriptors.

INTRODUCTION

Digital image processing is the use of computer algorithms to perform image processing on digital images. As a subcategory or field of digital signal processing, digital image processing has many advantages over analog image processing. It allows a much wider range of algorithms to be applied to the input data and can avoid problems such as the build-up of noise and signal distortion during processing. Since images are defined over two dimensions (perhaps more) digital image processing may be modelled in the form of multidimensional systems.



Figure 1: Spliced image containing peoples that look authentic subjectively

The set of image forensic tools can be roughly grouped into five categories: 1) pixel based techniques that detect statistical anomalies introduced at the pixel level; 2) format-based techniques that leverage the statistical correlations introduced by a specific lossy compression scheme; 3) camera-based techniques that exploit artifacts introduced by the camera lens, sensor, or on-chip postprocessing; 4) physically based techniques that explicitly model and detect anomalies in the three-dimensional interaction between physical objects, light, and the camera; and 5) geometric based techniques that make measurements of objects in the world and their positions relative to the camera. Therefore, just before thinking of taking vital actions upon a questionable image, one must be able to detect that an image has been altered. Image composition (or splicing) is one of the most common image manipulation operations. One such example is shown in Fig. 1, in which the girl on the right is inserted. Although this image shows a harmless manipulation case, but several more controversial cases were reported, e.g., the 2011 Benetton Un- Hate advertising campaign¹ or the diplomatically delicate case in which an Egyptian state-run newspaper published a manipulated photograph of Egypt's former president, Hosni Mubarak, at the front, rather than the back, of a group of leaders meeting for peace talks².

While checking the authenticity of an image, forensic investigators use all available sources of tampering evidence. Among other telltale signs, illumination inconsistencies are potentially effective for splicing detection: from the viewpoint of a manipulator, proper adjustment of the illumination conditions is hard to achieve when creating a composite image.

In this spirit, Riess and Angelopoulou proposed to analyze illuminant color estimates from local image regions. Unfortunately, the interpretation of their resulting so-called *illuminant maps* is left to human experts. But in real it turns out, this decision is, in practice, often more challenging than it seems. Reason, relying on human visual assessment can be misleading, as the human visual system is quite inept at judging illumination environments in pictures. Because the human visual system has its limitation Thus, it is preferable to transfer the tampering decision to an objective algorithm.

Hence in this work, we make an important step in reducing the user interaction for an illuminant-based tampering decision- making. So proposed a new semiautomatic method that is also significantly more reliable than earlier approaches. Quantitative evaluation study shows that this particular proposed method achieves a detection rate of 86%, where as existing illumination-based work is slightly better than guessing. We exploit the fact that local illuminant estimates are most discriminative when comparing objects of the same (or similar) material. Thus, we focus on the automated comparison of human skin, and more specifically faces, to classify the illumination on a pair of faces as either consistent or inconsistent. In the proposed method User interaction is limited to marking bounding boxes around the faces in an image under investigation. In the simplest case, this reduces to specifying two corners (upper left and lower right) of a bounding box.

In summary, the main contributions of this work are:

- Interpretation of the illumination distribution as object texture for feature computation.
- A novel edge-based characterization method for illuminant maps which explores edge attributes related to the illumination process.
- The creation of a benchmark dataset comprised of 100 skillfully created forgeries and 100 original photographs³

RELATED WORK

Illumination-based methods for forgery detection are either geometry-based or color-based. Geometry-based methods focus at detecting inconsistencies in light source positions between specific objects in the scene [5]–[11]. Color-based methods search for inconsistencies in the interactions between object color and light color. Johnson and Farid proposed a method which computes a low-dimensional descriptor of the lighting environment in the image plane (i.e., in 2-D). It estimates the illumination direction from the intensity distribution along manually annotated object boundaries of homogeneous color. Farid along with Kee extended this approach to exploiting known 3-D surface geometry. In the case of faces, a dense grid of 3-D normal improves the estimate of the illumination direction. Fan *et al.* Propose a method for estimating 3-D illumination using shape-from-shading in which no 3-D model of the object is required. The applicability of both approaches, however, is somewhat limited by the fact that people's eyes must be visible and available in high resolution.

Gholap and Bora introduced physics-based illumination cues to image forensics. The authors examined inconsistencies in specularities based on the dichromatic reflectance model. the authors require manual annotation of specular highlights. Additionally, specularities have to be present on all regions of interest, which limits the method's applicability in real-world scenarios. To avoid this problem, Wu and Fang assume purely diffuse (i.e., specular-free) reflectance, and train a mixture of Gaussians to select a proper illuminant color estimator. The angular distance between illuminant estimates from selected regions can then be used as an indicator for tampering. Unfortunately, the method requires the manual selection of a "reference block", where the color of the illuminant can be reliably estimated. This is a significant limitation of the method.

Riess and Angelopoulou followed a different approach by using a physics-based color constancy algorithm that operates on partially specular pixels. In this approach, the automatic detection of highly specular regions is avoided, which used *illuminant map*. Implausible illuminant color estimates point towards a manipulated region.

In the field of color constancy, descriptors for the illuminant color have been extensively studied. Most research in color constancy focuses on uniformly illuminated scenes containing a single dominant illuminant. For an overview, see e.g., However, in order to use the color of the incident illumination as a sign of image tampering, we require multiple, spatially-bound illuminant estimates.

Ebner presented an early approach to multi-illuminant estimation. Assuming smoothly blending illuminants, the author proposes a diffusion process to recover the illumination distribution. Unfortunately, in practice, these approach over smoothes the illuminant boundaries. Gijzenij *et al.* proposed a pixelwise illuminant estimator. It allows segmenting an image into regions illuminated by distinct illuminants. Differently illuminated regions can have crisp transitions, for instance between sunlit and shadow areas. While this is an interesting approach, a single illuminant estimator can always fail. Thus, for forensic purposes, we prefer a scheme that combines the results of multiple illuminant estimators. In this paper, we build upon the ideas in which, We use the relatively rich illumination information provided by both physics-based and statistics-based color constancy methods. Decisions with respect to the illuminant color estimators are completely taken away from the user, which differentiates this paper from prior work.

EXISTING SYSTEM

In existing, many methods has been proposed for detecting the forged images .Tiago jose de carvalho proposed that illumination-based methods for forgery detection are either geometry-based or color-based has been used . Geometry-based methods focus at detecting inconsistencies in light source positions between specific objects in the scene has been use. Color-based methods search for inconsistencies in the interaction between object color and light color has been used .

An early approach of multi-illuminant estimation has been done.In this smoothly blending illuminants used a diffusion process to recover the illumination distribution.By exploring with this pixelwise illuminant estimator is used . It allows to segment an image into regions illuminated by distinct illuminants. Differently illuminated regions can have crisp transitions, for instance between sunlit and shadow areas. The issues of the existing system are it oversmooths the illuminant boundaries.And it donot scale well on smaller image regions.A single illuminant estimator always fails.

PROPOSED SYSTEM

We make an important step towards minimizing user interaction for an illuminant-based tampering decision-making. We propose a forgery detection method that exploits subtle inconsistencies in the color of the illumination of images. Interpretation of the illumination distribution as object texture for feature computation. Our approach is machine-learning-based and requires minimal user interaction.

We classify the illumination for each pair of faces in the image as either consistent or inconsistent. The proposed method consists of five main components:

- 1) *Dense Local Illuminant Estimation (IE)*: The input image is segmented into homogeneous regions. Per illuminant estimator, a new image is created where each region is colored with the extracted illuminant color. This resulting intermediate representation is called illuminant map (IM).
- 2) *Face Extraction*: This is the only step that may require human interaction. An operator sets a bounding box around each face (e.g., by clicking on two corners of the bounding box) in the image that should be investigated. Alternatively, an automated face detector can be employed. We then crop every bounding box out of each illuminant map, so that only the illuminant estimates of the face regions remain.
- 3) *Computation of Illuminant Features*: for all face regions, texture-based and gradient-based features are computed on the IM values. Each one of them encodes complementary information for classification.
- 4) *Paired Face Features*: Our goal is to assess whether a pair of faces in an image is consistently illuminated. For an image with faces, we construct joint feature vectors, consisting of all possible pairs of faces.
- 5) *Classification*: We use a machine learning approach to automatically classify the feature vectors. We consider an image as a forgery if at least one pair of faces in the image is classified as inconsistently illuminated.

In the proposed system, an important step towards minimizing user interaction for an illuminant-based tampering decision-making was made. A new semiautomatic method that is also significantly more reliable than earlier approaches has been proposed.

The technique is applicable to images containing two or more people and requires no expert interaction for the tampering decision. To achieve this, we incorporate information from physics- and statistical-based illuminant estimators on image regions of similar material. From these illuminant estimates, we extract texture and edge-based features which are then provided to a machine-learning approach for automatic decision-making.

We use the relatively rich illumination information provided by both physics-based and statistics-based color constancy methods. Decisions with respect to the illuminant color estimators are completely taken away from the user. In order to describe the edge information, we propose a new algorithm based on edge-points and the HOG descriptor, called HOGedge.

The Fig.4 shows the overview of the proposed method. It gives the complete knowledge of the work done in the project. Initially the images are taken and it is splitted into original and edited image. The images are splitted for the purpose of comparison of detection of forged and original image. Here it describes two types of process. One is test stage while the other one is training process. First the dense illuminant estimation is extracted from the images of the training examples. The illuminant is found for all images in the database. Then the face extraction is done where here the faces is cropped by using a rectangle boxes. And the images are splitted to extract the illuminant features. These features are extracted using SASI and HOGedge algorithm. The features are then paired to give a combination of features which is used to detect the forgery image for future use. These processes are done in the training database. The test stage also follows the same steps done in the training set, but the only change is that an individual image is taken for the process. At the last the SVM (Support Vector Machine) is used to classify the images which are from training feature vector and test stage. In the classification step, the forged image is detected if any of the features mismatch each other, so that image is called as forged image.

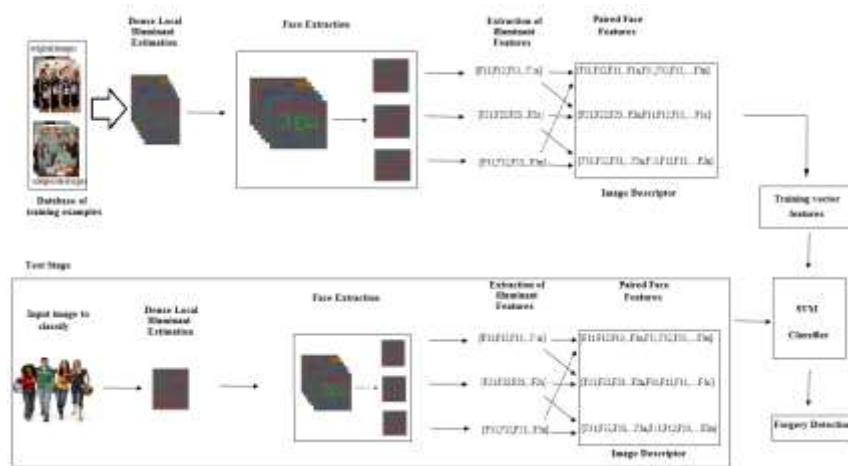


Fig.4. Overview of the proposed method

Algorithm:

Texture Description: SASI Algorithm: We use the Statistical Analysis of Structural Information (SASI) descriptor to extract texture information from illuminant maps. In our work, the most important advantage of SASI is its capability of capturing small granularities and discontinuities in texture patterns. Distinct illuminant colors interact differently with the underlying surfaces, thus generating distinct illumination “texture”. This can be a very fine texture, whose subtleties are best captured by SASI. SASI is a generic descriptor that measures the structural properties of textures. It is based on the autocorrelation of horizontal, vertical and diagonal pixel lines over an image at different scales. Instead of computing the autocorrelation for every possible shift, only a small number of shifts is considered.

One autocorrelation is computed using a specific fixed orientation, scale, and shift. Computing the mean and standard deviation of all such pixel values yields two feature dimensions. Repeating this computation for varying orientations, scales and shifts yields a 128-dimensional feature vector. As a final step, this vector is normalized by subtracting its mean value, and dividing it by its standard deviation.

2. Interpretation of Illuminant Edges: HOGedge Algorithm

Differing illuminant estimates in neighboring segments can lead to discontinuities in the illuminant map. Dissimilar illuminant estimates can occur for a number of reasons: changing geometry, changing material, noise, retouching or changes in the incident light. Thus, one can interpret an illuminant estimate as a low-level descriptor of the underlying image statistics. When an image is spliced, the statistics of these edges is likely to differ from original images. To characterize such edge discontinuities, we propose a new feature descriptor called *HOGedge*. It is based on the well-known HOG-descriptor, and computes visual dictionaries of gradient intensities in edge points. We first extract approximately equally distributed candidate points on the edges of illuminant maps. At these points, HOG descriptors are computed. These descriptors are summarized in a visual words dictionary.

The SASI and HOGedge descriptors capture two different properties of the face regions. From a signal processing point of view, both descriptors are *signatures* with different behavior. We then computed the mean value and standard deviation per feature dimension. SASI and HOGedge, in combination with the IIC-based and gray world illuminant maps create features that discriminate well between original and tampered images, in at least some dimensions. Secondly, the dimensions, where these features have distinct value, vary between the four combinations of the feature vectors. We exploit this property during classification by fusing the output of the classification on both feature sets.

CONCLUSIONS AND FUTURE WORK

In proposed work, new method for detecting forged images of people using the illuminant color has been described. The illuminant color using a statistical gray edge method and a physics-based method which exploits the inverse intensity chromaticity color space has been estimated. These illuminant maps are treated as texture maps. Information on the distribution of edges on these maps is extracted. In order to describe the edge information, a new algorithm based on edge-points and the HOG descriptor, called HOGedge is proposed. We combine these complementary cues (texture and edge-based) using machine learning late fusion. The results are

encouraging, yielding an AUC of over 86% correct classification. Good results are also achieved over internet images and under cross-database training/testing.

The proposed method is custom-tailored to detect splicing on images containing faces. The proposed method requires only a minimum amount of human interaction and provides a crisp statement on the authenticity of the image. Another advantage is, the exploitation of illuminant color in forensic area.

Methods that operate on illuminant color are inherently prone to estimation errors. Thus, future enhancements can be achieved when more advanced illuminant color estimators become available. An incorporation of a machine-learning based illuminant estimator particularly for faces is subject of future work. Incorporating effective skin detection methods & techniques can further expand the applicability of our method. Such an improvement could be employed, for example, in detecting pornography compositions.

REFERENCES:

- [1] A. Rocha, W. Scheirer, T. E. Boult, and S. Goldenstein, "Vision of the unseen: Current trends and challenges in digital image and video forensics," *ACM Comput. Surveys*, vol. 43, pp. 1–42, 2011
- [2] C. Riess and E. Angelopoulou, "Scene illumination as an indicator of image manipulation," *Inf. Hiding*, vol. 6387, pp. 66–80, 2010
- [3] Y. Ostrovsky, P. Cavanagh, and P. Sinha, "Perceiving illumination inconsistencies in scenes," *Perception*, vol. 34, no. 11, pp. 1301–1314, 2005
- [4] M. Johnson and H. Farid, "Exposing digital forgeries by detecting inconsistencies in lighting," in *Proc. ACM Workshop on Multimedia and Security*, New York, NY, USA, 2005, pp. 1–10
- [5] M. Johnson and H. Farid, "Exposing digital forgeries in complex lighting environments," *IEEE Trans. Inf. Forensics Security*, vol. 3, no. 2, pp. 450–461, Jun. 2007
- [6] M. Johnson and H. Farid, "Exposing digital forgeries through specular highlights on the eye," in *Proc. Int. Workshop on Inform. Hiding*, 2007, pp. 311–325
- [7] E. Kee and H. Farid, "Exposing digital forgeries from 3-D lighting environments," in *Proc. IEEE Int. Workshop on Inform. Forensics and Security (WIFS)*, Dec. 2010, pp. 1–6.
- [8] W. Fan, K. Wang, F. Cayre, and Z. Xiong, "3D lighting-based image forgery detection using shape-from-shading," in *Proc. Eur. Signal Processing Conf. (EUSIPCO)*, Aug. 2012, pp. 1777–1781.
- [9] J. F. O'Brien and H. Farid, "Exposing photo manipulation with inconsistent reflections," *ACM Trans. Graphics*, vol. 31, no. 1, pp. 1–11, Jan. 2012
- [10] S. Gholap and P. K. Bora, "Illuminant colour based image forensics," in *Proc. IEEE Region 10 Conf.*, 2008, pp. 1–5.
- [11] X. Wu and Z. Fang, "Image splicing detection using illuminant color inconsistency," in *Proc. IEEE Int. Conf. Multimedia Inform. Networking and Security*, Nov. 2011, pp. 600–603.
- [12] P. Saboia, T. Carvalho, and A. Rocha, "Eye specular highlights telltales for digital forensics: A machine learning approach," in *Proc. IEEE Int. Conf. Image Processing (ICIP)*, 2011, pp. 1937–1940.
- [13] C. Riess and E. Angelopoulou, "Physics-based illuminant color estimation as an image semantics clue," in *Proc. IEEE Int. Conf. Image Processing*, Nov. 2009, pp. 689–692.
- [14] M. Bleier, C. Riess, S. Beigpour, E. Eibenberger, E. Angelopoulou, T. Tröger, and A. Kaup, "Color constancy and non-uniform illumination: Can existing algorithms work?," in *Proc. IEEE Color and Photometry in Computer. Vision Workshop*, 2011, pp. 774–781.
- [15] M. Ebner, "Color constancy using local color shifts," in *Proc. Eur. Conf. Comput. Vision*, 2004, pp. 276–287.
- [16] J. van de Weijer, T. Gevers, and A. Gijssenij, "Edge-based color constancy," *IEEE Trans. Image Process.*, vol. 16, no. 9, pp. 2207–2214, Sep. 2007.
- [17] R. Tan, K. Nishino, and K. Ikeuchi, "Color constancy through inverse- intensity chromaticity space," *J. Opt. Soc. Amer. A*, vol. 21, pp. 321–334, 2004
- [18] C. Riess, E. Eibenberger, and E. Angelopoulou, "Illuminant color estimation for real-world mixed-illuminant scenes," in *Proc. IEEE Color and Photometry in Computer Vision Workshop*, Barcelona, Spain, Nov. 2011

Performance Enhancement of Charge Pump using Modified Wilson Current Mirror

Sandhya Save, B.K.Mishra and Jalpaben Pandya

Thakur College of Engineering and Technology, pandyajalpa7@gmail.com, 9561769957

Abstract—Phase locked loops (PLLs) are integral parts of communication devices used in various applications such as frequency synthesizer, clock recovery circuits, synchronization for digital communications, carrier phase, frequency tracking, etc. Charge Pump PLL (CP-PLL) is a type of PLL widely used for today's SoC environment. The non-ideal effects such as jitter, phase noise, reference spur, phase error, etc. influence the CP-PLL performance which significantly affects the performance of the overall system.

Charge Pump is a small but one of the important components of CP-PLL that significantly affects its performance. The Charge Pump circuit generates non-ideal effects such as leakage current, timing mismatch and current mismatch which causes phase error, reference spurs, jitter, etc. at the CP-PLL output.

In this work, the Charge Pump circuit is designed in Matlab Simulink environment to reduce the current mismatch. Simulated results show that current mismatch for the Charge Pump circuit using Modified Wilson current mirror and transmission gate is 1.94% and phase error is also reduced. This set up can be easily utilized to design various Charge Pump to achieve minimum current mismatch for SoC applications.

Keywords—Charge Pump, CAD Tools, Current Mismatch, Current Mirror, Phase Error, Reference Spur, Matlab Simulink

INTRODUCTION

Charge Pump PLL (CP-PLL) is a type of hybrid PLL. CP-PLLs form an integral part of communication systems such as frequency synthesizer, clock recovery circuits, synchronization for digital communications, carrier phase and frequency tracking, etc. CP-PLLs are used for synchronizing the output signal with the input signal in both frequency and phase. The block diagram of CP-PLL is as shown in figure 1. The major building blocks of a CP-PLL are Phase/Frequency Detector (PFD), Charge Pump (CP), Loop Filter (LF) and Voltage-Controlled Oscillator (VCO) [1].

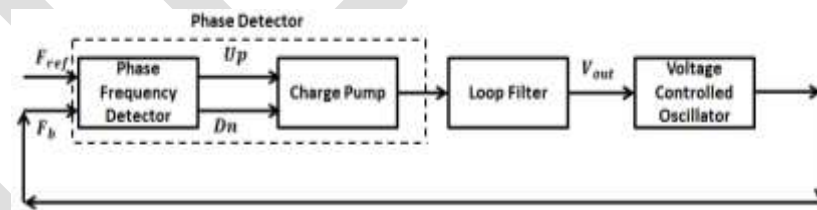


Figure 1: Block diagram of CP-PLL

The Charge Pump (CP) circuit is a small part of CP-PLL which converts the digital error pulses into analog current pulses. The CP circuit plays an important role in determining the CP-PLL performance. The CP circuit consists of two switched current sources I_{UP} (charging current source) and I_{DN} (discharging current source), that pump charge into or out of the LF as shown in figure 2. The capacitor C_p acts as a LF. The inputs to the CP circuit are the Up or Dn signals obtained from the PFD and the output current is coupled to the capacitor C_p . The current sources and switches in CP are usually implemented using MOS transistors. Ideally, the charge pump currents I_{UP} and I_{DN} need to be equal in magnitude but the inherent mismatches between the MOS transistors result in mismatching between the current sources. The mismatch between charging and discharging current is known as current mismatch and it degrades the performance of CP [2].

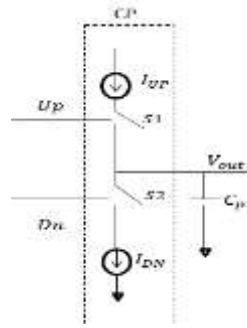


Figure 2: Basic Charge Pump

This mismatch gives rise to phase error and reference spurs in CP-PLL.

The paper is organized as follows. In section 2, phase detector non-idealities are discussed. In section 3, mixed signal CAD tools used for design of phase detector circuit are discussed. In section 4, design of phase detector circuit in Matlab /Simulink /Simscape /Simelectronics environment is presented. In section 5, simulation results are reported and the phase error and reference spurs for the different CP circuits are investigated.

PHASE DETECTOR NON-IDEALITIES

Phase detector circuit exhibits non-ideal behaviour which contributes to phase error and reference spur in CP-PLL [3], [4].

The different non-idealities that occur in phase detector circuit are as given below:

1. Leakage Current

One of the issues in the CP is the leakage current which might be caused by the CP itself, by the on-chip varactor, or by any leakage in the board. This gives rise to change in the output voltage and causes phase error which is given by [3]:

$$\Delta\phi_{leakage} = 2\pi \frac{I_{leakage}}{I_{cp}} (rad) \dots\dots\dots (1)$$

Where,

Ileakage - Leakage current occurring in MOS transistors

Icp – CP current

The leakage current is in the order of μA ; therefore, the phase error due to leakage current can be ignored.

2. Charge Sharing

The capacitors at nodes ‘a’ and ‘b’ consist of the parasitic source/drain capacitances of MOS transistor. As shown in figure 3, when the switching transistors are open, the charges on the nodes ‘a’ and ‘b’ move towards VDD and GND respectively. When the switches close instantaneously, some of the charge stored on these parasitic capacitors will be transferred to the LF, and cause voltage spikes on the VCO control line. The charge sharing cannot be completely eliminated but it can be reduced by proper design of switches.

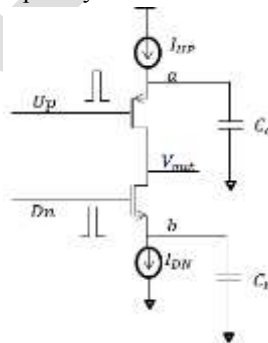


Figure 3: Charge Sharing in CP

3. Clock Feedthrough

When the Up and Dn signals of the MOS switch change their logic levels, due to the overlap of the MOS transistors, some charges are coupled to the LF which causes spikes on the control voltage which leads to reference spurs at the output.

4. Charge Injection

Charge injection is a phenomenon that arises due to leakage of charge into a capacitive node during the turn on and turn off of a switch that is connected to that node. Charge injection and clock feedthrough is directly proportional to gate capacitance.

5. Dead Zone

Dead zone problem occurs when the rising edges of the two clocks to be compared are very close. To mitigate the dead zone issue, the reset signal inside the tri-state PFD as shown in figure 4 needs to be designed carefully as given in equation (2).

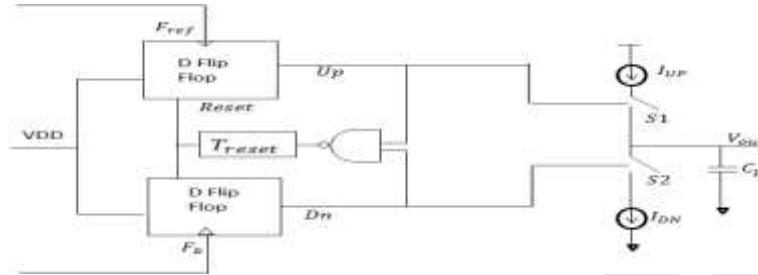


Figure 4: D Flip-Flop based PFD

The reset delay represents the minimum pulse width of the PFD output that is needed to turn on the CP completely.

$$T_{reset} = \frac{1}{(2 \times F_{max})} \dots \dots \dots (2)$$

Where,

T_{reset} – Reset Delay in PFD

F_{max} – Maximum operating frequency of PFD

Dead zone contributes to timing mismatch which in turn contributes to phase error and CP non-idealities. Thus, designing a PFD with no dead zone is important for accurate frequency generation, low phase noise in frequency synthesizer PLLs, and low timing jitter in clock generator PLLs.

6. Missing Edge Phenomenon

The PFD suffers from another problem known as missing edge phenomenon. The PFD should provide the clock pulses correctly in the arriving order of the two signals, but it may sometimes miss edges which is known as missing edge phenomenon [5, 6]. This missing edge problem occurs when a rising edge of F_{ref} or F_b signal arrives during the reset delay (T_{reset}) as shown in figure 5.

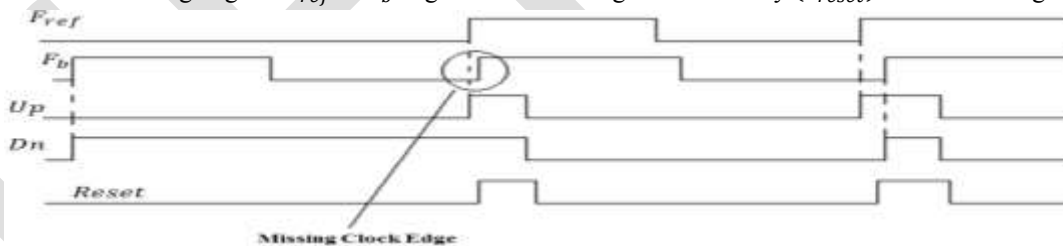


Figure 5: Missing Edge Phenomenon

Some of the rising edges can be missed in the detection when the edges are overlapped with the reset signal internally generated in the PFD, which is called the missing edge problem. Missing edges induce wrong polarity in the PFD output, leading to incorrect behaviour and making the CP-PLL spend more time to acquire phase or frequency. As circuit speed increases, the possibility of missing edges increases.

7. Timing Mismatch

Timing mismatch is inherent with the CP circuit. As the input to the CP is the PFD outputs (Up and Dn) signals; there exists a delay in the PFD outputs reaching the CP. This delay introduces a certain amount of phase error given by [3]:

$$\Delta\phi_{timing} = 2\pi \frac{\Delta T_{delay} \cdot T_{on}}{T_{ref}^2} \dots \dots \dots (3)$$

Where

ΔT_{delay} - Timing Mismatch in PFD,

T_{ref} - Reference cycle time,

T_{on} - Turn-on time of the PFD.

In all the previous works, ΔT_{delay} does not consider the switch non-idealities. Therefore, in this work to estimate the non-idealities, the timing mismatch is segregated as given below.

Timing mismatch consists of a) propagation delay between the logical output of PFD and the CP switches, b) Propagation delay for the CP switches to change the state, c) Dead Zone of PFD.

Therefore,

$$\Delta T_{delay} = T1 + T2 + T3 \dots \dots \dots (4)$$

Where,

$T1$ - Propagation delay due to connection between PFD and CP switch

$T2$ - Propagation delay for the switch to change state

$T3$ - Dead Zone of the PFD

Substituting the values of ΔT_{delay} in equation (3), we get,

$$\Delta \phi_{timing} = 2\pi \frac{(T1 + T2 + T3) \cdot T_{on}}{T_{ref}^2} \text{ (rad)} \dots \dots \dots (5)$$

7. Current Mismatch

Current mismatch consists of Mismatch between the drain currents of the current sources. The current sources present in CP are designed using MOS transistors. Due to the inherent mismatches present in transistors such as 2nd order effects and random device mismatches, CP suffers from current mismatches [7]. Current mismatching refers to the magnitude difference of charging and discharging currents. Phase error due to charge pump current mismatch is given by [3]:

$$\Delta \phi_{mismatch} = 2\pi \frac{\Delta i}{I_{cp}} \cdot \frac{T_{on}}{T_{ref}} \text{ (rad)} \dots \dots \dots (6)$$

Where,

I_{cp} - Rating current of CPs,

T_{ref} - Reference cycle time,

T_{on} - Turn-on time of the PFD

Δi - Mismatching of charging and discharging currents

The total phase error $\Delta \phi_{tot}$ caused by these non-idealities can be approximated as:

$$\Delta \phi_{tot} = 2\pi (\Delta \phi_{leakage} + \Delta \phi_{mismatch} + \Delta \phi_{timing}) \dots \dots \dots (7)$$

Also, the reference spurs can be given by [4],

$$P_r = 20 \log \frac{N F_{bw} \Delta \phi_{tot}}{\sqrt{2} F_{ref}} - 20 \log \left(\frac{F_{ref}}{F_{pl}} \right) \dots \dots \dots (8)$$

Where,

P_r - Reference Spur

N - Division ratio of the divider

F_{bw} - Loop Bandwidth

$\Delta \phi_{tot}$ - Total Phase Error

F_{ref} - Reference Frequency

F_{pl} - Frequency of the pole in the LF

MIXED SIGNAL CAD TOOL

CP-PLL is a mixed signal block involving the co-design of analog and digital circuits. There are different tools available to design the CP-PLL as shown in table 1 with its advantages and limitations. Referring to table 1, Matlab is a tool which can provide analog and digital design on a common platform [10].

As compared to other tools, Matlab is better for computation than LabVIEW. Simulations execute faster in Matlab (nearly 3 times) as compared to LabVIEW. The maximum error in the delay, computed using Matlab, is less than 8% compared to HSPICE simulation results [8].

Table 1: Mixed Signal Design Tools

S. No	Description	Matlab [8], [9], [10]	Mentor Graphics [10], [11], [12]	Synopsys [10], [13]	Cadence [10], [14],[15]	National Instruments – LabVIEW [10], [16], [17]	Scilab [9],[10],[18], [19]	Oscad [20]
1.	Year of Introduction	1970	1981	1986	1988	1990	2009	2013
2.	Function	Multi-paradigm numerical computing environment	Complete CAD Flow	Complete CAD Flow	Complete CAD Flow	Graphical Programming Environment	Numerical computational package and a high-level, numerically oriented programming language	CAD tool for circuit design, simulation, analysis and PCB design.
3.	Availability	Licensed	Licensed	Licensed	Licensed	Licensed	Open Source	Open Source
4.	AMS Design supported	Yes (Simulink)	Yes (Eldo)	Yes (HSpice)	Yes (Pspice)	Co-Simulation with Matlab	Yes (Scicos)	Yes
5.	MOS Models Supported	Spice model level 1 and 3. Other models can be imported from Pspice.	Supports Eldo level 1-47, 53-70,101 Mosfet models.	Levels 1 to 71	Spice Levels 1 to 7	Spice models can be imported from Pspice, Matlab	In-Built PMOS and NMOS transistors with default parameters is present.	Models can be imported from Ngspice
6.	Programming	Easy	Complex as compared to Matlab	Easy	-	Complex as compared to Matlab	Easy	-
7.	Industry Acceptance	Widely used by scientists and researchers and has good industry acceptance	Moderate	Moderate	Moderate	Moderate	Limited to the developer community	Still in development stage
8.	Co-Simulation	Scilab, Cadence-Pspice, NI-Multisim, Mentor Graphics-ModelSim, NI-LabVIEW	Matlab	Matlab	Matlab	Matlab, Pspice	Matlab	Ngspice, Scilab

Also, Matlab includes a rich set of plotting capabilities, Matlab help is user friendly and highly descriptive; Matlab GUI is better than other tools. Matlab has a large collection of toolboxes in a variety of domains such as signal processing, communications, image and video processing, control systems, test and measurement, computational finance, etc. One of the key features of this tool is the integration ability with other languages and third-party applications. Therefore, Matlab has become the preferred language of computing for the researchers [10].

Considering the advantages of Matlab environment, the CP and PFD circuit is designed in Matlab Simulink Simelectronics environment.

PHASE DETECTOR DESIGN

The set up for phase detector circuit used in CP-PLL circuit is designed in Matlab Simulink Simelectronics, Spice compatible environment by using $0.18 \mu\text{m}$ level 3 CMOS model with 3.3V supply as shown in figure 6. The output of the CP is captured on scope as shown in figure 7. The designed CP system is combination of two main sub system PFD and a single ended CP. The subsystem gives the flexibility to reduce the complexity and size of the circuit [21]. The design of sub system PFD is shown in figure 8. The PFD subsystem consists of two edge-triggered, resettable D Flip-Flops (DFF) with their D inputs connected to logic "1". When one of the PFD inputs rises, the corresponding output becomes high. The phase or frequency difference information is stored in the capacitor which is used to tune the VCO.

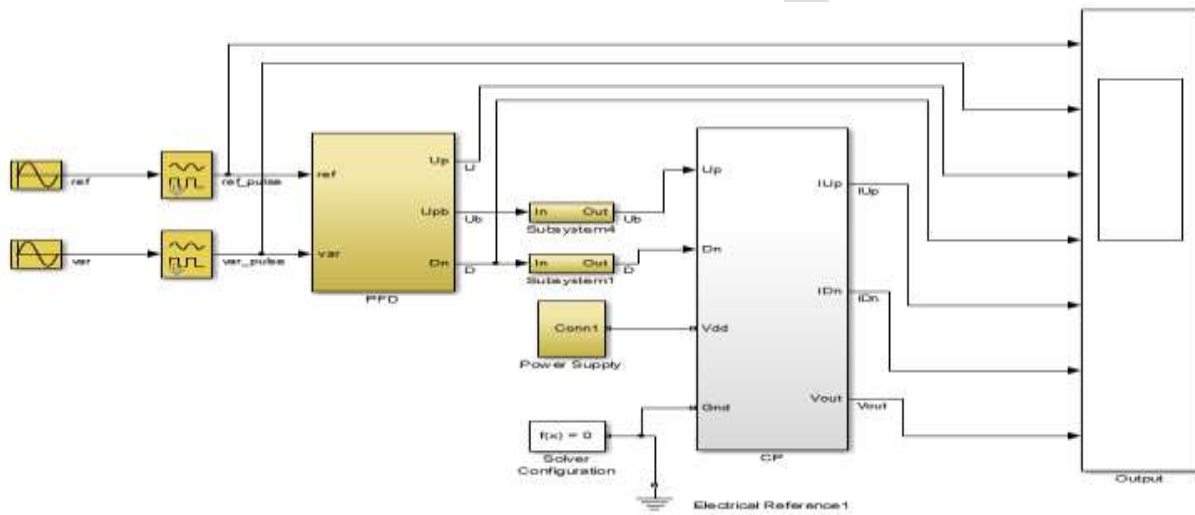


Figure 6: Phase Detector setup used in CP-PLL

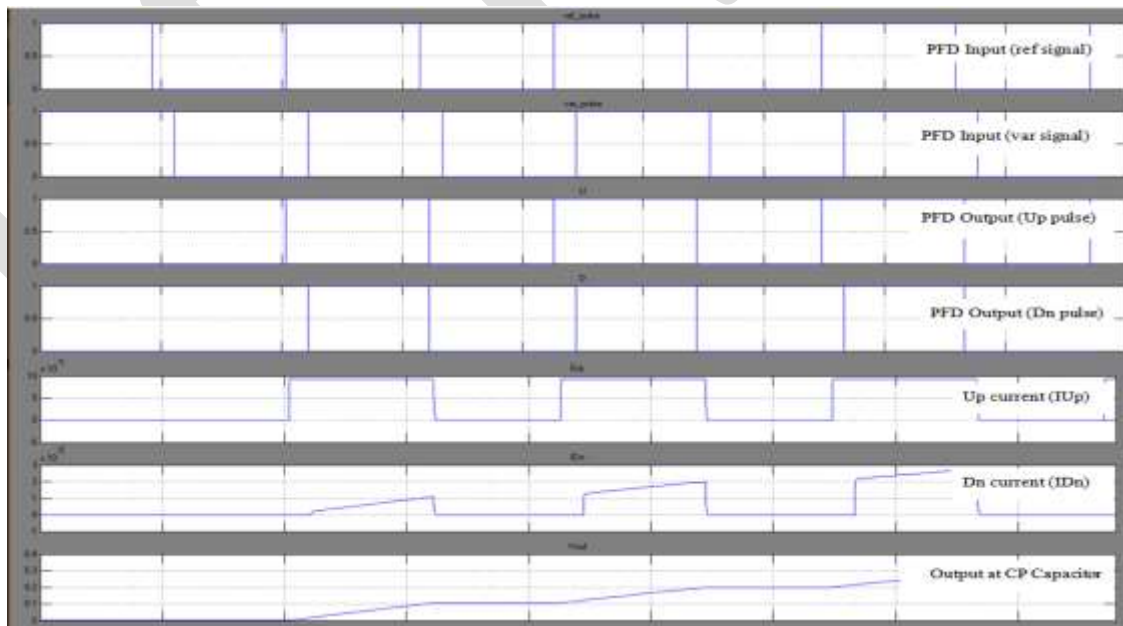


Figure 7: CP response for Reference signal leading Variable signal

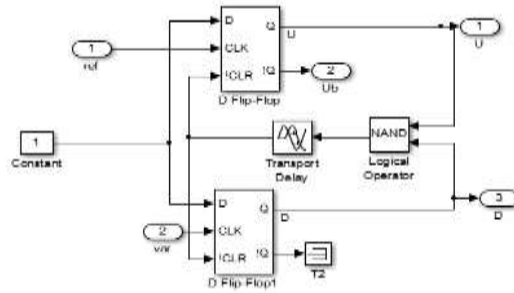


Figure 8: PFD subsystem

The design of single ended CP subsystem is shown in figure 9. CP subsystem consists of PMOS and NMOS current mirror subsystem with Up switch and Dn switch. The current sources in the CP are designed using current mirror circuits [22]. The current mirror circuit uses the principle that if the gate-source potentials of two identical MOS transistors are equal, then the current flowing through their drain terminals should be the same. The charge pump circuits are designed using different combinations of current sources and switches.

1. Basic Current Mirror circuit with PMOS/NMOS switch

In this the CP uses the basic current mirror circuits using PMOS and NMOS transistors (figure 10 and figure 11) whereas the switches used are PMOS and NMOS transistors (figure 12 and figure 13) acting as a switch. The current mismatch caused is estimated as 12.19%.

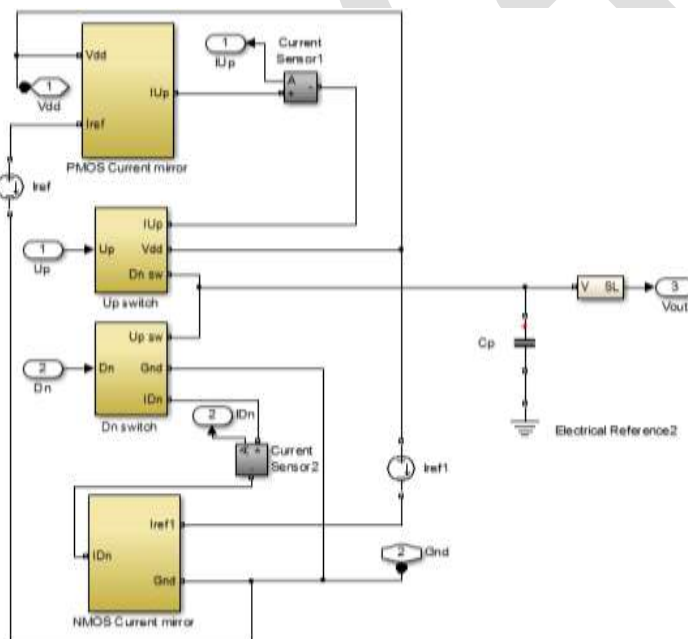


Figure 9: CP subsystem

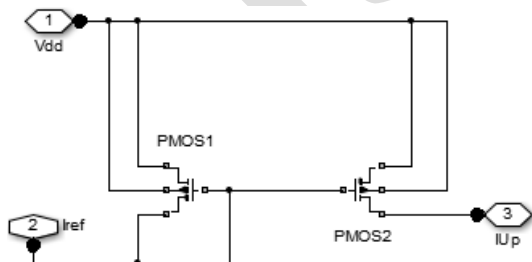


Figure 10: PMOS current mirror subsystem

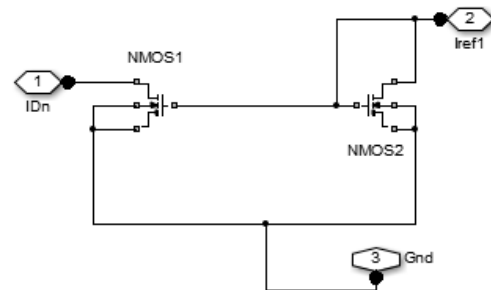


Figure 11: NMOS current mirror subsystem

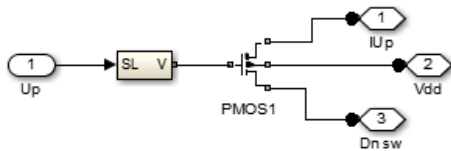


Figure 12: Up switch subsystem

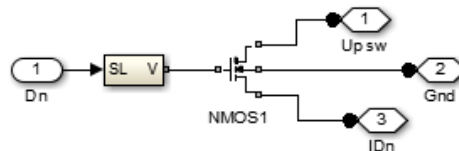


Figure 13: Dn switch subsystem

2. Cascode Current Mirror circuit with PMOS/NMOS switch

As discussed above, the current mismatch can be reduced by increasing the output resistance of the current sources, therefore a Cascode current mirror (figure 14 and 15) is implemented using PMOS/NMOS switch (figure 12 and 13). The current mismatch caused is 10.70%.

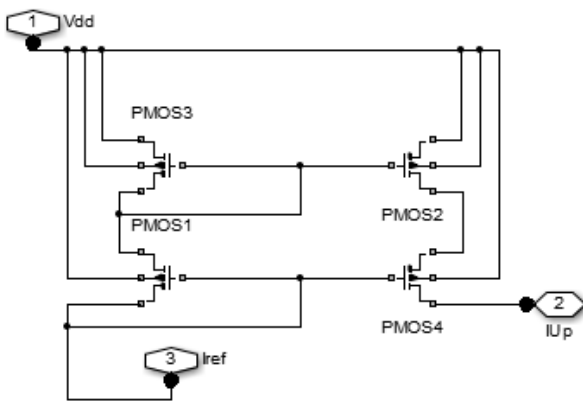


Figure 14: PMOS Cascode Current Mirror

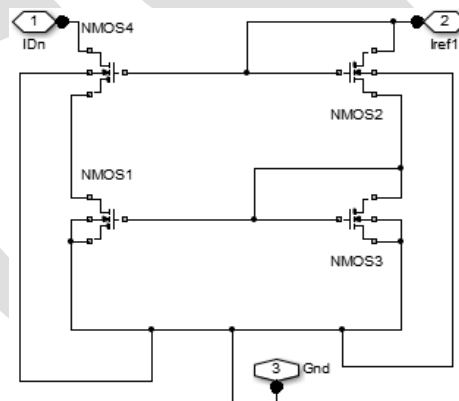


Figure 15: NMOS Cascode Current Mirror

3. Cascode Current Mirror circuit with Transmission gate switch

It is observed that the current mismatch reduces as the output resistance of the current sources increases. To further reduce the charge injection and charge sharing caused due to the PMOS/NMOS switch, a transmission gate (figure 16) is used. The current mismatch caused is 10.06%.

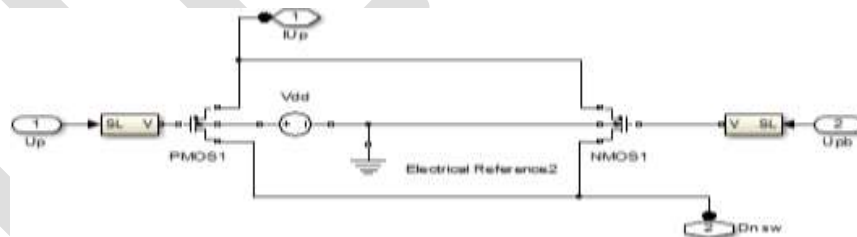


Figure 16: Transmission gate used as a switch in CP circuit

4. Modified Wilson Current Mirror circuit with Transmission gate switch

To further reduce the current mismatch and obtain an improved CP circuit Modified current mirror circuit (figure 17 and 18) is used with transmission gate (figure 16). The current mismatch of the CP is reduced to 6.56%.

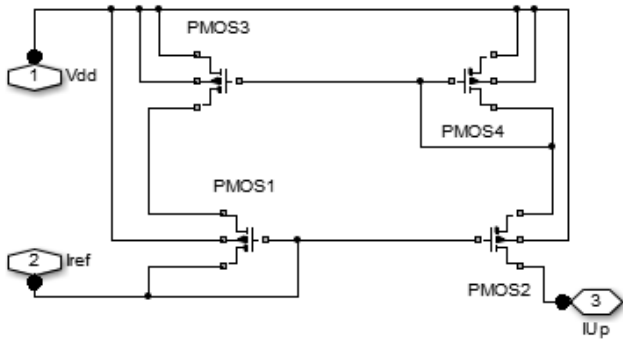


Figure 17: Modified Wilson PMOS Current Mirror

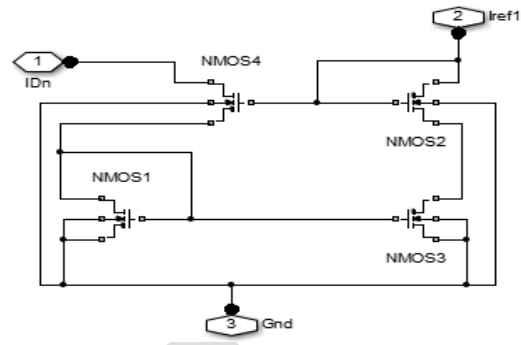


Figure 18: Modified Wilson NMOS Current Mirror

RESULTS AND DISCUSSIONS

When the ref signal leads the var signal, the PFD detects a rising edge on the reference frequency and produces an Up signal. This Up signal from the PFD will turn the Up switch on. This Up pulse will turn on the charging current source and it will cause the CP to inject current into the LF, thus increasing Vout. The obtained simulated result is shown in figure 7.

The designed set up for phase detector of CP-PLL is simulated at 450 MHz with two different current sources and MOS designed switches. The current matching graphs for the different circuits designed are shown in figure 19, 20, 21 and 22 respectively.

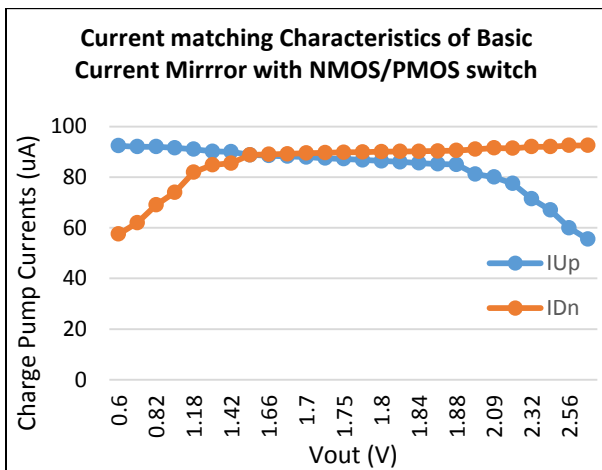


Figure 19: Current matching characteristics of Basic current mirror with PMOS/NMOS switch

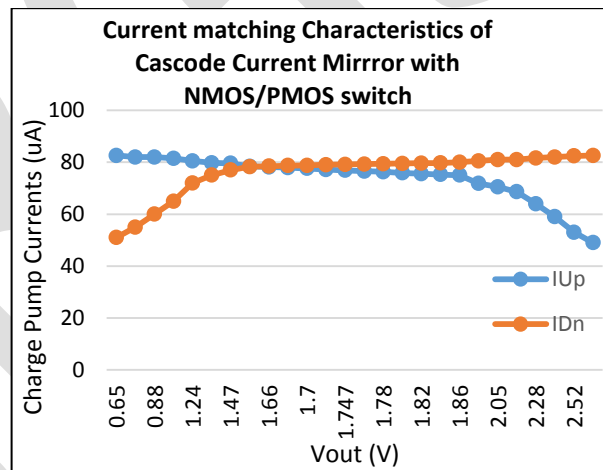


Figure 20: Current matching characteristics of Cascode current mirror with PMOS/NMOS switch

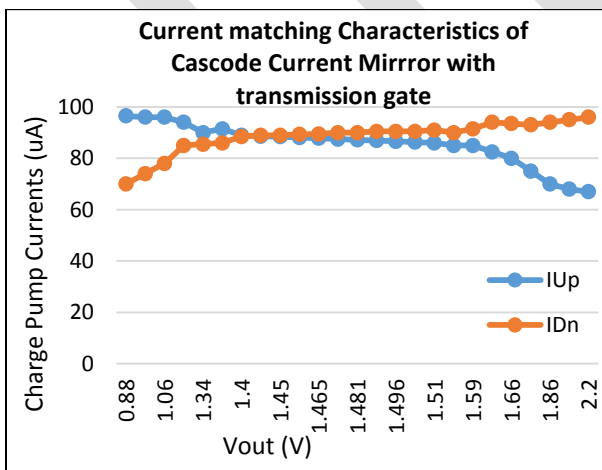


Figure 21: Current matching characteristics of Cascode current mirror with transmission gate

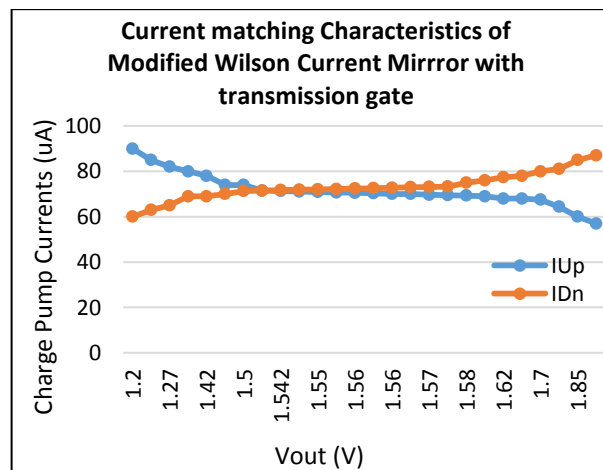


Figure 22: Current matching characteristics of Modified Wilson current mirror with transmission gate

From the graphs it is concluded that current mismatch is reduced for the CP which uses Modified Wilson current mirror with transmission switch. As the PFD circuit suffers from missing edge phenomenon, the PFD circuit is analyzed at different frequencies to estimate the missing edge as shown in table 2.

Table 2. Missing edge Phenomenon at different frequencies and phases

Freq\Phase Diff.	0	10	50	100	150	200	250	300	350
1 MHz	□	□	□	□	□	□	□	□	□
8 MHz	□	□	□	□	□	□	□	□	□
20 MHz	□	□	□	□	□	□	□	□	X
30 MHz	□	□	□	□	□	□	□	□	X
50 MHz	□	□	□	□	□	□	□	□	X
70 MHz	□	□	□	□	□	□	□	□	X
100 MHz	□	□	□	□	□	□	□	X	X
150 MHz	□	□	□	□	□	□	□	X	X
200 MHz	□	□	□	□	□	□	X	X	X
250 MHz	□	□	□	□	□	X	X	X	X
300 MHz	□	□	□	□	X	X	X	X	X
350 MHz	□	□	□	□	X	X	X	X	X
400 MHz	□	□	□	X	X	X	X	X	X
450 MHz	□	□	X	X	X	X	X	X	X

The current mismatch evaluated for the CP using Modified Wilson current mirror circuits and transmission gates is reduced which reduces the phase error and reference spurs. For, this configuration of CP it is found out that the current mismatch is $1.94 \mu A$ in the range where no missing edge phenomenon occurs as compared to $14.36 \mu A$ in the missing edge phenomenon range at 450 MHz reference frequency. At 230 MHz reference frequency, the current mismatch is $11.78 \mu A$ in the range where no missing edge phenomenon occurs as compared to $44.26 \mu A$ in the missing edge phenomenon range.

Missing edge phenomenon is not taken into consideration into the previous works. The previous works only focus on reducing the current mismatch by using the op-amp circuits, but at the same time it also increases the area which is a concern for SoC applications. The different designed CP circuits are compared on grounds of Area and Current Mismatch achieved as shown in table 3.

Table 3: Current mismatch in different CP configurations

S. No	CP Circuit	Current Mismatch (%)	Area (μm^2)
1.	Basic Current Mirror with NMOS/PMOS switch	12.19	8.5
2.	Cascode Current Mirror with NMOS/PMOS switch	10.70	23.1
3.	Cascode Current Mirror with Transmission gate	10.06	23.2
4.	Modified Wilson Current Mirror with Transmission gate	6.56*	23.2
		1.94	

*- Count for Missing Edge Phenomenon over all the frequency range

The current mismatch is calculated in table 3 and the timing mismatch is calculated in table 4. Referring to equations 4 and 5, $T1$ is found out to be $100 ps$. $T2$ is calculated from different CP circuits and PFD is designed such that no dead zone ($T3$) occurs. But for the worst condition ($T3$) is taken as $100 e - 15 sec$.

Table 4: Timing Mismatch for the different CP configurations

S. No.	Circuit	T1 (Propagation delay due to connection between PFD and CP)	T2 (Propagation delay for the switch to change)	T3 (Dead Zone)	$\Delta T_{delay} = T1 + T2 + T3$
--------	---------	---	---	----------------	-----------------------------------

		switch)	state)		
1.	Basic Current Mirror with NMOS/PMOS switch	100e-12	2.8e-11	100e-15	1.28e-10
2.	Cascode Current Mirror with NMOS/PMOS switch	100e-12	6.79e-11	100e-15	1.68e-10
3.	Cascode Current Mirror with Transmission gate	100e-12	6.7e-11	100e-15	1.67e-10
4.	Modified Wilson Current Mirror with Transmission gate	100e-12	6.5e-11	100e-15	1.65e-10

Referring table 3 and 4 and referring equations 7 and 8, the phase error and reference spurs are estimated as shown in table 6. From the table it is concluded that the CP using Modified Wilson current mirror and transmission gate achieves reduced current mismatch and occupies less area on chip making it suitable for SoC applications. Therefore, a CP with reduced current mirror is designed and compared with the previous works as shown in table 7 below.

Table 6: Phase error and Reference spur of different CP circuits

S. N.	Circuit	Phase error due to leakage current (rad)	Phase error due to current Mismatch (rad)	Phase error due to timing mismatch (rad)	Reference Spur due to leakage current (dBc/Hz)	Reference Spur due to current mismatch (dBc/Hz)	Reference Spur due to timing mismatch (dBc/Hz)	Total phase error (rad)	Total reference spur (dBc/Hz)
1.	Basic Current Mirror with NMOS/PMOS switch	6.28e-6	0.3480	0.1661	-143.0753	-38.6688	-38.6688	0.5141	-44.8142
2.	Cascode Current Mirror with NMOS/PMOS switch	6.28e-6	0.3054	0.2180	-143.0753	-40.2253	-36.3068	0.5234	-44.6574
3.	Cascode Current Mirror with Transmission gate	6.28e-6	0.2872	0.2167	-143.0753	-40.7611	-36.3587	0.5039	-44.9883
4.	Modified Wilson Current Mirror	6.28e-6	0.0554	0.2141	-143.0753	-55.0570	-36.4633	0.2695	-50.4241
	Current Mirror with Transmission gate	6.28e-6	0.1873	0.2141	-143.0753	-44.4749	-36.4633	0.4014	-46.9639*

*- Count for Missing Edge Phenomenon over all the frequency range

Table 7: Comparison with previous works

S. No	Parameters	[23]	[24]	[25]	[26]	This work
1	Process (μm)	0.18	0.18	0.09	0.09	0.18
2	CP Architecture	-	-	Single Ended	Single Ended	Single Ended
3	Supply Voltage (V)	1.8	1	1	1.8	3.3

4	Current Mismatch (%)	- < 1	- < 1	< 6.8	7	1.94*
5	CP current (μA)	100	-	20	-	100
6	Reference Freq. (MHz)	-	-	-	2500	450
7	Area (μm^2)	-	-	-	85.5	23.2
8	Circuit Simulated in	Spectre	Tanner Tool	Spectre	Cadence design environment	Matlab - Simulink environment

*- Count for Missing Edge Phenomenon over all the frequency range

CONCLUSION

A CP circuit design for current mirror and switch reducing current mismatch and phase error is proposed. The complete circuit is designed and simulated in Matlab Simulink Simelectronics in 0.18 μm CMOS technology. The current mismatch can be further reduced by employing a feedback which uses operational amplifiers but at the cost of more area and design complexity. Improved current matching reduces the static phase offset and reference spurs of a charge pump PLL. CP circuit using Modified Wilson current mirror improves the performance of charge pump with reduced area. This CP circuit can be used to achieve minimum current mismatch for SoC applications.

REFERENCES:

- [1] R. Best, Phase-Locked Loops Design, Simulation, and Applications, Fifth Edition. New York: McGraw-Hill, 2003.
- [2] B. Razavi, Design of Analog CMOS Integrated Circuits, McGraw-Hill, New York, NY, USA, 2000, ISBN 0-07-238032-2.
- [3] Woogeun Rhee, "Multi-Bit, Delta Sigma Modulation Technique for fractional $-N$ Frequency Synthesizers, University of Illinois, PhD Thesis, 2001.
- [4] Li Zhiquan, Zheng Shuangshuang and Hou Ningbing "Design of a high performance CMOS charge pump for phase-locked loop synthesizers," Journal of Semiconductors, vol. 32, no. 7, 2011.
- [5] Kangwoo Park and In-Cheol Park, "Fast Frequency Acquisition Phase Frequency Detectors with Prediction-Based Edge Blocking," IEEE Symposium on Circuits and Systems, pp. 1891-1894, 2009.
- [6] Mozghan Mansuri, Dean Liu and Chih - Kong Ken Yang, "Fast frequency acquisition phase-frequency detectors for Gsamples/s phase locked loops," IEEE Journal of Solid-State Circuits, vol. 37, no. 10, pp. 1331-1334, 2002.
- [7] Marcel J. M. Pelgrom et.al, "Matching Properties of MOS Transistors", IEEE Journal of Solid-State Circuits, vol. 24, No. 5, pp. 1433-1440, 1989.
- [8] www.mathworks.com
- [9] Comparative Study of Matlab and its Open Source Alternative Scilab: OSSRC Technical Report OSS 0601.
- [10] CMC Product Catalogue: <http://www.cmc.ca/~media/NewsAndEvents/BizDev/Product%20Catalogue%20V30%20V30.pdf>
- [11] Eldo User's Manual- Software Version 6.8_1 Release AMS 2006.2
- [12] www.mentor.com
- [13] www.synopsys.com
- [14] www.cadence.com
- [15] www.orcad.com
- [16] <http://www.ni.com/labview/>
- [17] Tadej Tasner, Darko Lovrec, Francisek Tasner and Jorg Edler, "Comparison Of Labview and Matlab For Scientific Research," Annals of the Faculty of Engineering Hunedoara - International Journal of Engineering, vol. 10, no. 3, pp. 389-394, 2012.
- [18] <http://www-rocq.inria.fr/scilab/>
- [19] <http://pdfoiogr.org/k-440974.html>
- [20] <http://www.oscad.in/resource/book/oscad.pdf>
- [21] B. K. Mishra, Sandhya Save and Rupali Mane, "A Novel Method to Design Analog Circuits Using Simulink," Proceedings published by International Journal of Computer Applications, pp. 6-13, 2011.
- [22] D.R. Holberg P.E.Allen. CMOS Analog Circuit Design. New York: Oxford University Press, 2002.\
- [23] Jae Hyung Noh and Hang Geun Jeong, "Charge pump with a regulated cascode circuit for reducing current mismatch in PLLs," Proceedings of World Academy of Science, Engineering and Technology, vol. 25, pp. 185-187, 2008.
- [24] J.S. Lee, M.S. Keel, "Charge pump with perfect current matching characteristics in phase-locked loops," Electronics Letters, no. 36, pp.1907-1908, 2000.

- [25] L.F. Tanguay, M. Sawan, Y. Savaria, "A very-high output impedance charge pump for low-voltage low-power PLLs," *Microelectronics Journal*, vol. 40, no. 6, pp. 1026-1031, 2009.
- [26] Umakanta Nanda, Debiprasad Priyabrata Acharya and Sarat Kumar Patra, "A New Transmission Gate Cascode Current Mirror Charge Pump for Fast Locking Low Noise PLL," *Circuits, Systems, and Signal Processing*, vol.33, no. 9, pp. 2709–2718, 2014

IJERGS

INTERLEAVEDBUCK BOOST INVERTER FOR DISTRIBUTED GENERATION SYSTEM

Akhiljith P J, Reenu George, Salice Peter
P G Student, akhiljith90@gmail.com, +91 9400506759

Abstract—This paper presents a non-inverting interleaved buck boost inverter for DC-AC energy conversions. The energy derived from the renewable energy sources cannot be directly connected to the load. For applications that require a stable DC bus voltage, an efficient converter is needed. Two non inverting buck boost converters are integrated with an interleaved operation for DC-DC conversion. Thus, a switch and a diode can be omitted, reducing cost. A modified z source inverter is integrated with the buck boost converter for DC-AC energy conversion. The operating principle and steady-state analysis are discussed in detail. The interleaved operation reduces current ripple at the output. The converter is simulated using MATLAB 2010 and waveforms are analyzed. Higher voltage conversion ratio can be obtained without using transformer topologies.

Keywords— Buck boost converter, Distributed Generation (DG) system, Continuous conduction mode (CCM), z-source inverter, Interleaving technique.

INTRODUCTION

Conventional fossil-fuel-based energy sources such as crude oil, coal and natural gas are rapidly being exhausted, and energy derived from these sources causes serious environmental pollutions. Renewable energy technologies have become a prominent and rapidly growing portion of the world's energy portfolio. Renewable energy comes from many commonly known sources such as solar power, wind, running water and geothermal energy. Renewable energy sources are wonderful options because they are limitless. Also another great benefit from using renewable energy is that many of them do not pollute our air and water, the way burning fossil fuels does. Among these two major forms are fuel cell based and photovoltaic cell based energy sources. Any such renewable energy system requires a suitable converter to make it efficient. Several converter types are capable of providing both step-up and step-down voltage conversion for renewable energy systems, including the inverting buck boost converter, the flyback converter, the Cuk converter and the single-ended primary-inductance converter (SEPIC)[4][6]. However, these converters greatly stress the switches. The Cuk and SEPIC converters utilize two pairs of inductors and capacitors to transform energy into the output, and are thus large and inefficient. Another disadvantage is that the output polarity is reversed in the inverting buck boost and Cuk converters[3]. The flyback converter has a high-leakage inductance and its efficiency is low. The main application of a step-down/step-up or buck-boost converter is in regulated DC power supplies, where a negative-polarity output may be desired with respect to the common terminal of the input voltage, and the output voltage can be either higher or lower than the input voltage. But single-switch buck-boost topology have the problem of an increase in the component stresses and component sizes[1]. In order to solve the common-ground issue for the input and output, a two-switch non-inverting buck boost converter can be used. High efficiency can be achieved by using the interleaving technique. Interleaved converters are used for sharing the load current in high power applications[2][5]. It has the advantage of high equivalent switching frequency and reduced output current ripples. Two non-inverting buck boost converters are integrated with an interleaved operation[7]. Thus, a switch and a diode can be omitted, reducing cost. The interleaved operation reduces both the current ripple at the output and the current stress of the diodes. Traditional full bridge inverters do not have the flexibility of handling a wide range of dc input voltages. Especially when the dc voltage is lower than the ac voltage, heavy line frequency step up transformers are required. Although these inverters demonstrate robust performance and high reliability, they demand higher volume, weight and cost for DG system applications. By using Z source network[10] as an intermediate circuit it can control the dc link voltage[11][12]. So the interleaved buck boost converter is integrated with a modified z-source inverter. DC voltage obtained from the renewable energy sources is efficiently converted.

PRINCIPLE AND WORKING

Figure 1 shows the general block diagram of renewable energy conversion system. From the block diagram it can be seen that voltage supplied from energy sources goes through two stages of conversion before it is supplied to grid.

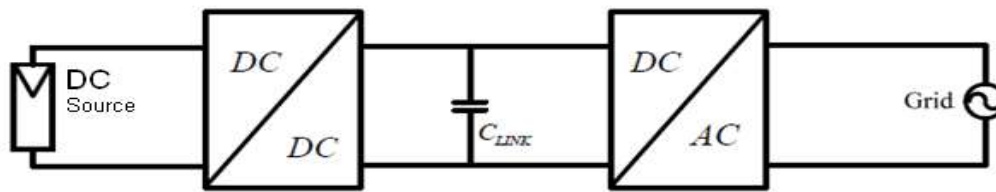


Figure 1. General block diagram of renewable energy conversion system

The voltage from the energy source is first converted to into variable dc using a non-inverting interleaved buck boost converter. This variable dc voltage is then converted to ac voltage by using a modified z-source inverter and is given to grid. The capacitor link acts as a voltage source to the inverter.

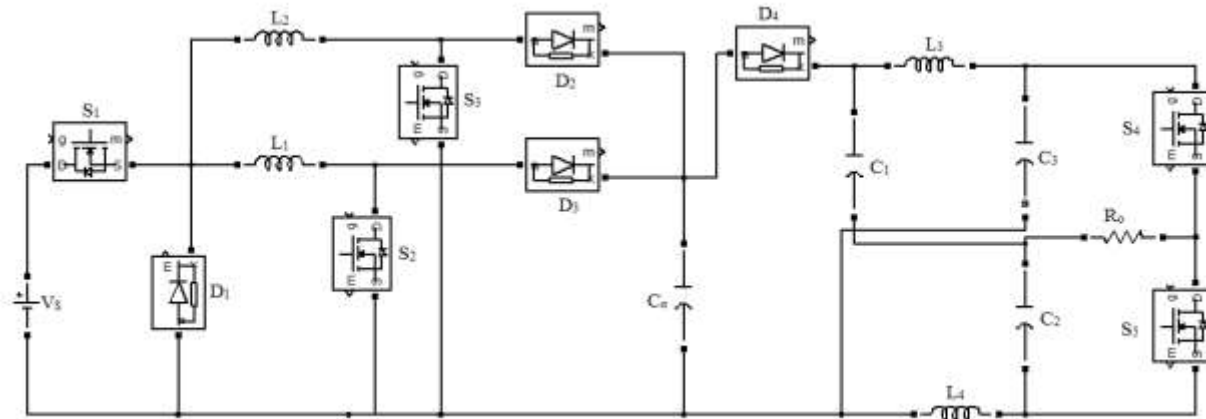


Figure 2. Interleaved buck boost inverter

The circuit can be divided into two sections, first is a DC-DC converter where a buck boost converter effectively converts the DC input voltage and the second is a DC-AC converter where a modified z-source inverter is used for the conversion. A DC link connects both the sections. Figure 2 shows the circuit configuration of the interleaved buck boost inverter. The first section consists of three power switches, two inductors, three diodes and one capacitor. Two non-inverting buck boost converters are integrated with an interleaved operation. To simplify the circuit analysis, the following conditions are assumed. The power metal oxide field-effect transistors(MOSFET) and the diodes are ideal. The output capacitor C_0 is large enough so that the output voltage ripple can be ignored. Thus, V_{c0} is considered to be constant in one-switching period. Inductors L_1 and L_2 are equal. Inductor currents i_{L1} and i_{L2} are operated in continuous conduction mode (CCM). Second section consists of two power switches, two inductors, one diode and three capacitors. The load is connected between the common node of the two series capacitors and the common node of the two switches. Working of first section consists of 4 modes and that of second stage consists of 3 modes.

A. DC-DC Converter

Mode I: In mode I, S_1 , S_2 and D_3 are turned on and S_3 , D_1 and D_2 are turned off. Figure.3(a). shows the current flow path of the converter in this mode. In, inductors L_1 and L_2 store their energies from input voltage V_s . Inductor current i_{L1} increases linearly and i_{L2} increases or decreases linearly this interval depending on whether the converter is operating in buck or boost mode. In this mode, inductor current i_{L2} decreases linearly. The load is supplied by capacitor C_0 and inductor L_2 .

Mode II: In this mode, S_1 , S_2 and S_3 are turned off and D_1 , D_2 and D_3 are turned on. Figure.3(b). shows the current flow path for this mode. In this interval, the energy stored in inductors L_1 and L_2 is released to capacitor C_0 and load R_0 . Inductor currents i_{L1} and i_{L2} decrease linearly.

Mode III: In mode III S_1 , S_3 and D_2 are turned on and S_2 , D_1 and D_3 are turned off. Figure.3(c) shows the current flow path of the converter in this mode. In this interval, inductors L_1 and L_2 store their energies from input voltage V_s . Inductor current i_{L2} increases linearly, and i_{L1} increases or decreases depending on whether the converter is operating in buck or boost mode. In this mode, inductor current i_{L1} decreases linearly. The load is supplied by capacitor C_0 and inductor L_1 .

Mode IV: In this mode, S_1 , S_2 and S_3 are turned off and D_1 , D_2 and D_3 are turned on. The current owing path in this mode is the same as mode II. Figure. 3(d.) shows the current flow path of the converter in this mode. In this interval, the energy stored in inductors L_1 and L_2 is released to capacitor C_0 and load R_0 . Inductor currents i_{L1} and i_{L2} decrease linearly.

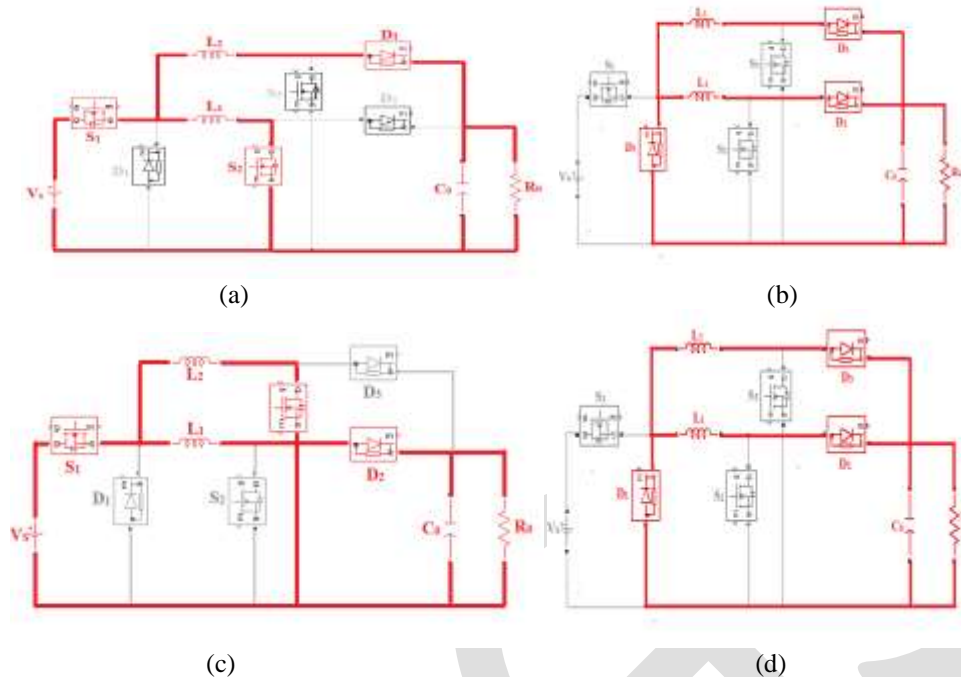


Figure 3.(a).Mode I operation. (b).Mode II operation. (c).Mode III operation.(4).Mode IV operation

B. Modified z-source inverter

Figure 4 shows the diagram of modified z source inverter. It consists of three operating modes.

- 1) *Model I*: Figure 5(a) shows the circuit diagram of mode I operation. The inverter is in active state. Upper transistor is conducting and lower transistor is substituted by its freewheeling diode.
- 2) *Model II*: Figure 5(b) shows the circuit diagram of mode II operation. The inverter is in active state. Lower transistor is conducting and upper transistor is actively like a diode.
- 3) *Model III*: Figure 5(c) shows the circuit diagram of mode III operation. In this mode upper and lower switches are conducting. The inverter is in shoot through state.

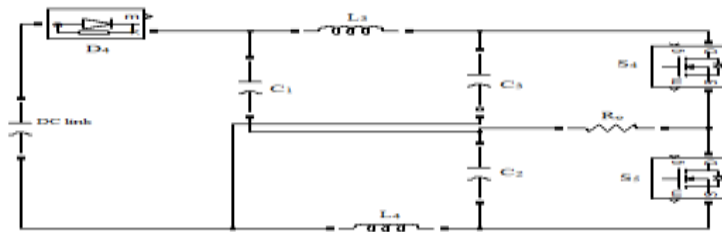


Figure 4. Modified z source inverter

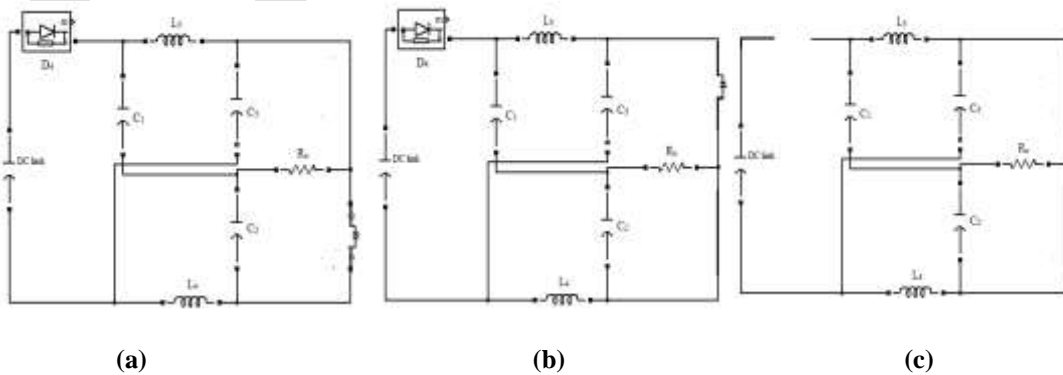


Figure 5.(a).Mode I operation. (b).Mode II operation. (c).Mode III operation.

DESIGN OF COMPONENTS

Input voltage $V_s = 36V$
 Output voltage $V_o = 28V$
 Switching frequency $f_s = 50kHz$

Voltage gain $\frac{V_o}{V_s} = \frac{2D}{1-D}$ (1)

Duty cycle $D = 28\%$

Inductor $L_1 = L_2 = \frac{R_o(1-2D)}{f_s} = 10\mu H$ (2)

Capacitor $C_o = \frac{V_o D}{V_{co} R_o f_s} = 874\mu F$ (3)

Inductor $L_3 = L_4 = 10\mu H$

Capacitor $C_1 = C_2 = 47\mu F$
 $C_3 = 100\mu F$

SIMULINK MODEL AND RESULTS

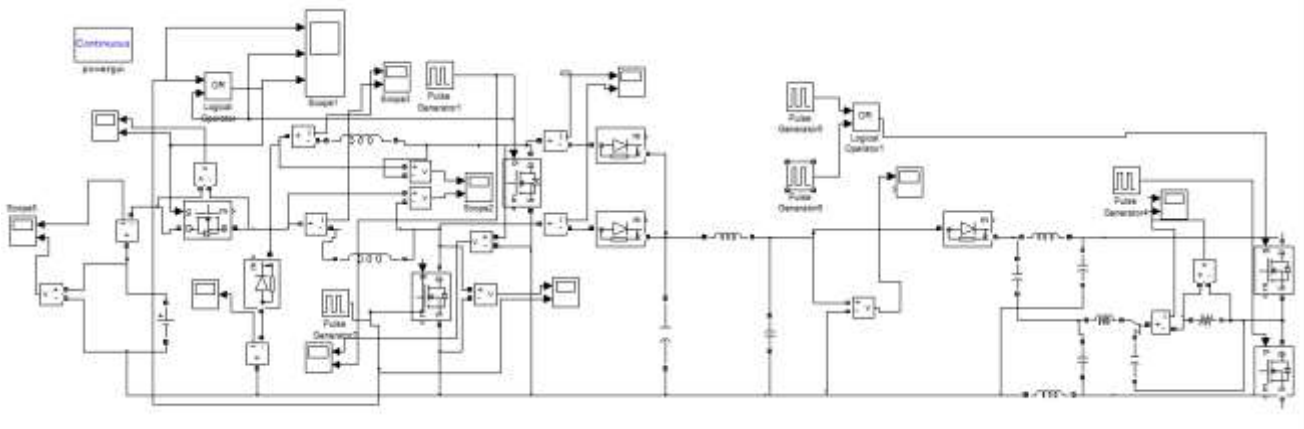


Figure 6. Simulink model of buck boost inverter

Simulink model of interleaved buck boost inverter with Π filter is shown in figure 6. Output voltage and current ripples are significantly reduced with the addition of Π filter. For simulation of the DC-DC converter, parameters of the different circuit components are taken as: For an input voltage of $V_s = 36V$, f_s (switching frequency) = 50kHz, simulation is performed in MATLAB 2010 for non-inverting interleaved buck boost converter for an output voltage of $V_o = 28V$. The parameters used includes $L_1=L_2 = 10\mu H$ and C_o (Output capacitor) = 874 μF , duty cycle $D = 28\%$.

SIMULATION RESULTS

Simulated waveforms obtained are shown below:

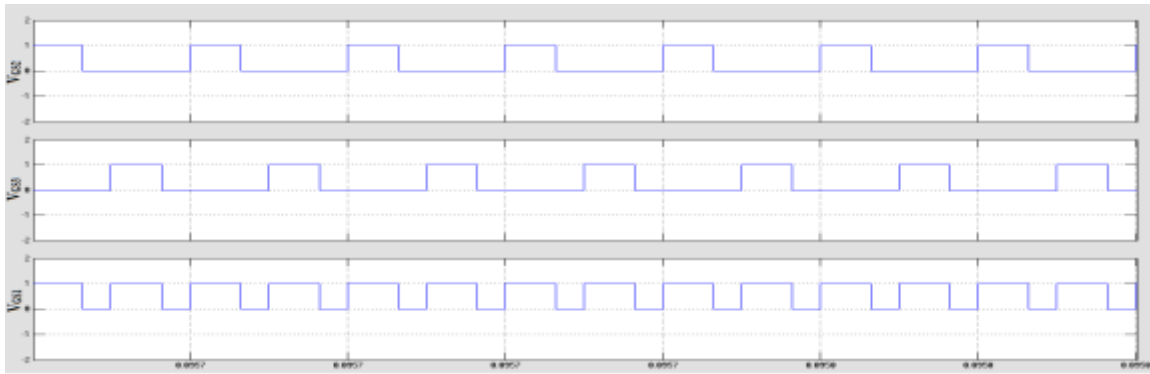


Figure 7. Switching pulses $V_{GS1}, V_{GS2}, V_{GS3}$

Figure 7 shows the waveform of switching pulses provided to the three switches, where V_{gs1} - the gate signal of the switch S_1 , V_{gs2} - the gate signal of the switch S_2 and V_{gs3} - the gate signal of the switch S_3 . The frequencies of switches S_2 and S_3 are twice those of the main switches, which mean that the circuit can behave as an interleaved circuit during two phases, which increases power density and reduces the output voltage ripple.

Figure 8 shows the current waveform of inductor L_1 and L_2 . During one switching period 4 modes of operations have occurred. In mode I, i_{L1} increased and i_{L2} decreased. In mode II energy stored in both inductors are released so both inductor currents are decrease linearly. In mode III i_{L1} decrease linearly and i_{L2} increases linearly. Mode IV same as that of mode II.

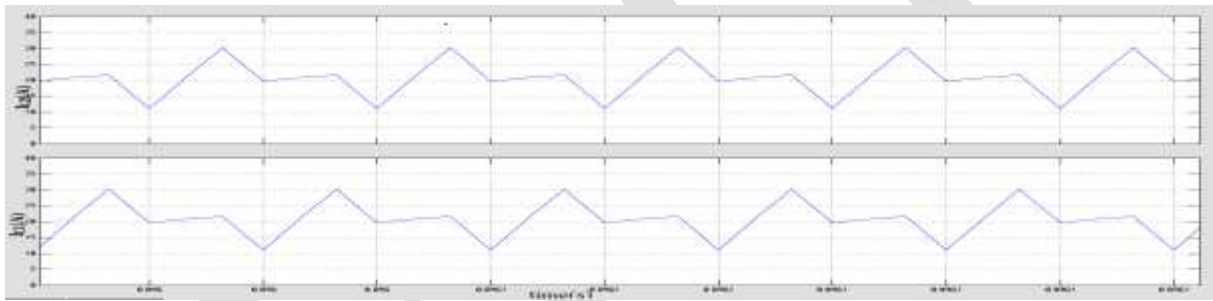


Figure 8. Inductor currents I_{L2} & I_{L1}

Figure 9 shows voltage waveforms of inductor L_1 and L_2 . During one switching period 4 modes of operations have occurred. In mode I voltage across L_1 is V_s and across L_2 is $V_s - V_o$. In mode II voltage across L_1 is $-V_o$ and across L_2 is $-V_o$. In mode III voltage across L_1 is $V_s - V_o$ and across L_2 is V_s . Mode IV same as that of mode II.

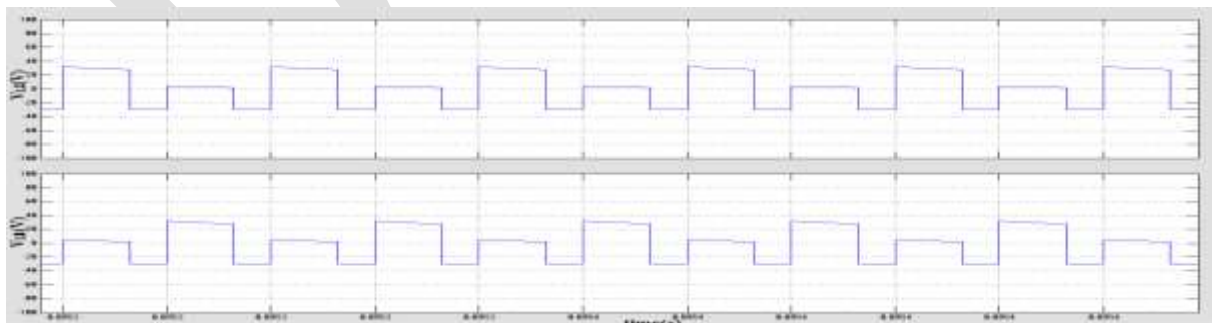


Figure 9. Inductor voltages V_{L2} & V_{L1}

Figure 10 shows the output voltage and current waveform of the inverter. Z source network acts as a dc link energy storage sub circuit. It reduce the inrush current and harmonics due to the two inductors and act as a second order filter and handle undesirable voltage sags.

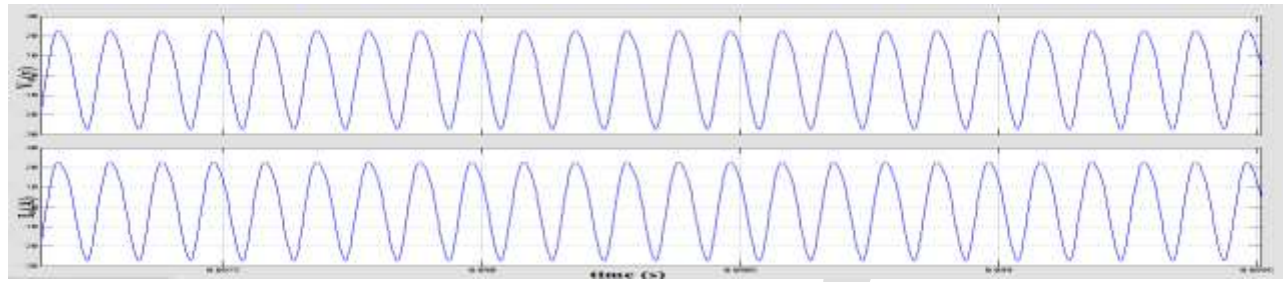


Figure 10. a).Output voltage b). Output current

ACKNOWLEDGMENT

It is a great pleasure to acknowledge all those who have assisted and supported me for successfully completing my work. First of all, I thank God Almighty for his blessings as it is only through his grace that I was able to complete my work successfully. I am deeply indebted to Prof. Geetha B, Principal, Mar Athanasius College of Engineering. Her encouragement and patience will be a guiding spirit in all endeavors of my future. I express my deep sense of gratitude to Prof. Salice Peter, Head of Electrical & Electronics Engineering Department for the valuable guidance as well as timely advice which helped me a lot in doing my work successfully. I also extend my deep sense of gratitude to PG Coordinator, Sri. George John P, Professor, EEE Dept. and our Faculty Advisor Smt. Beena M Varghese, Associate Professor, EEE Dept. for their creative suggestions during the preparation of the mini project. I take this opportunity to extend my sincere thanks to my project guide Smt. Reenu George, Assistant Professor, EEE Dept. and all the faculty members of the Department of Electrical & Electronics Engineering for sharing their valuable critical comments during the preparation of the paper. I wholeheartedly thank all my classmates, for their valuable suggestions and for the spirit of healthy competition that existed between us.

CONCLUSION

Non-inverted interleaved buck boost inverter was analysed and simulated using MATLAB 2010. A non-inverting interleaved buck boost converter is integrated with a modified z source inverter to form an efficient DC-AC conversion system for distributed generation system. The interleaved buck boost converter can achieve higher voltage conversion ratio without using transformer. From input voltage of 36V the DC-DC converter can achieve the targeted output voltage 28V with reduced current ripples. Since the output polarity is non-inverting, the common ground issue is resolved. One power switch and one diode are omitted and thereby saving cost and increasing power density. The interleaved technique is used to produce a low-output current ripples. This converter is well suited for fuel cell powered applications. Instead of high voltage rated electrolytic capacitors, series smaller rated capacitors are used in modified z source inverter. The integrated operation of interleaved buck boost converter and modified z source inverter provide efficient DC-AC energy conversion system.

REFERENCES:

- [1] H.K Liao, T.J Liang, L.S Yang, J.F Chen "Non-inverting interleaved buck-boost converter with interleaved technique for fuel cell system", *IET Power electronics*, vol.5, pp.1379-1388, 2012.
- [2] Ahmad, A.A., Abrishamifar, A, "A simple current mode controller for two switches buck-boost converter for fuel cells", *Electrical Power Conf., EPC 2007*, October 2007, pp. 363-366.
G. Xiao, S. Xie, "Interleaving double-switch buckboost converter", *IET Power Electron.*, Vol. 5, Iss. 6, pp. 899-908, 2012.
- [3] Ned Mohan, Tore M Undeland, William P Robbins, "Power Electronics Converters, Applications and Design".
- [4] Vahid Samavatian, Ahmed Radan "A novel low-ripple interleaved buck-boost converter with high efficiency and low oscillation for fuel-cell applications.", *Electrical Power and Energy Systems*, 2014
- [5] Ren X, Tang Z, Xuan R, Wei J, Hua G, "Four switch buck-boost converter for telecom DC-DC power supply applications", *IEEE APEC*, 2008, pp. 1527-1530..
- [6] Gert K. Andersen, Frede Blaabjerg, "Current Programmed Control of a Single-Phase Two-Switch BuckBoost Power Factor Correction Circuit", *IEEE Transactions On Industrial Electronics*, Vol. 53, no. 1, February 2006
- [7] Tao H, Duarte J L, Hendrix M.A, "Line-interactive UPS using a fuel cell as the primary source", *IEEE Trans. Ind. Electron.*, 2008, 55, (8), pp. 3012-3021.

- [8] Chen J, Maksimovic D, Erickson R, "Buck–boost PWM converters having two independently controlled switches". *Proc. IEEE 32nd Annual Power Electronics Specialists Conf.*, June 2001, pp. 736–741
- [9] F. Z. Peng, "Z-Source Inverter," *IEE Transactions on Industry Applications*, vol. 39, pp. 504-510, March April 2003.
- [10] B. M. Ge, Q. Lei, W. Qian, and F. Z. Peang, "A family of Z- Source matrix converters," *IEEE Trans. Ind. Electron.*, vol. 59, no. 1, pp. 35–46, Jan. 2012.
- [11] Eduardo I. Ortiz Rivera, Member Luis A. Rodríguez , "The Z- Source Converter as an Introduction to Power Electronics and Undergraduate Research", *37th ASEE/IEEE Frontiers in Education Conference*

IJERGS

A Lossless Image Compression Based On Hierarchical Prediction and Context Adaptive Coding

Ann Christa Antony, Cinly Thomas

P G Scholar, Dept of Computer Science, BMCE, Kollam, Kerala, India

annchristaantony2@gmail.com, 9037621808

Abstract: This paper introduces a new lossless compression. This is based on the hierarchical prediction and context adaptive coding. Here first we convert the RGB image into YCuV transform. The Y component is converted by using any of the lossless gray scale image compression method. The hierarchical schema is used for the compression of the chrominance channel. Here we are using four predictors. For the prediction we are using the upper, right, left diagonal and right diagonal for the image compression. The arithmetic coding is used for the error signal calculation. This provides better compression of the images on the boundary as compared to the existing system based on the hierarchical prediction. It also reduces the bit rate when compared with other lossless compression methods.

Keywords: YCuV, lossless compression, hierarchical prediction, Huffman coding, context adaptive coding, RGB, RCT,

I INTRODUCTION

Digital images are acquiring a wide audience nowadays. Most of the cameras used today are digital cameras. The main problem comes when there is a need for transferring the image and also storing the image. The digital images are of huge size, and hence they need to be stored in a low memory, for this the only solution is to compress it. When we want to transfer an image of huge size, the only possible way is to compress it and then transfer.

Compression is mainly of two types. While compressing, if some part of the image is lost, then it is called lossy compression. But in the lossless compression the entire image is preserved even after the decompression. Due to the wide application of the image in the medical fields and other important areas, we can't afford image loss. So the lossless compression acquires wide spread acceptance. In a lossless compression technique two steps are there. The first one is that we may create a statistical model for the input data. And in the second step this model is used for the mapping of the input data. Many lossless compression techniques are there and the most commonly used ones include Lossless JPEG [1], JPEG LS [2], LOCO-1[3], CALIC [4], JPEG 2000[5], and JPEG XR [6]. Among this CALIC and JPEG are based on the JPEG standardization. CALIC provides better compression performance but more computation.

Mainly for the compression of the colour images, a colour transform is used for splitting the colour component. After that, each of the colour component is compressed independently by any of the above mentioned colour transform method. In the case of lossy image compression the RGB component is converted into YCbCr transform [7], but in colour lossless compression, as a result of the uninvertability with integer arithmetic most of the colour transform cannot be used. So, it is better to use a reversible colour transform. Hence an RCT was defined and used in JPEG 2000[5].

In this paper, we are proposing a hierarchical prediction schema. Based on this prediction schema, the predictors are being calculated. Here four predictors are calculated and from it the most significant and apt value is chosen as the actual predictor and that particular pixel is encoded on the basis of that predictor.

A lot of existing prediction methods are there for the lossless compression. The main problem is that they all are based on the raster scan prediction method which is inefficient for some cases, mainly high frequency regions [9]. The method of hierarchical prediction was also proposed in many other papers [10], where only two predictors are used. Here in this method an edge directed predictor and context adaptive modelling is used. Here the lower rows as well as left and upper row alone are used for the prediction.

The main problem is that while predicting edge pixel, we can't accurately predict the edges. So there is a chance of improper decompression of the image.

The rest of the paper is organised as follows. The section II includes proposed method and the section III includes the conclusion and the last section covers the references.

II PROPOSED METHOD

A. Compression of RGB to YCuCv

Normally the images are in the RGB form. The RGB colour space is widely used in computer graphics. The RGB image is converted into YCuCv form by using the RCT form mentioned in [8]. The YCuCv components are split into different components like Y, Cu and Cv.

B. Y channel encoding

The extracted Y channel needs to be encoded. That encoding is done on the basis of the gray scale image compression algorithm. The gray scale image compression is necessary due to some reasons like simplicity, that is gray scale images only contain one image plane with gray scale intensity values and data reduction.

C. Cu and Cv encoding

The Cu and Cv components are encoded on the basis of hierarchical prediction. At first the Cu and Cv are subdivided into odd $X_o^{(1)}$ and even $X_e^{(1)}$ subimages. The even subimage is used for encoding the odd subimage. The first subdivision is based on the rows. For more accuracy, the even row is again subdivided into odd $X_o^{(2)}$ and even $X_e^{(2)}$ on the basis of the column. This result in a more specific encoding as the subdivision is more specific. Here also the even sub image is used for the encoding of the odd one.

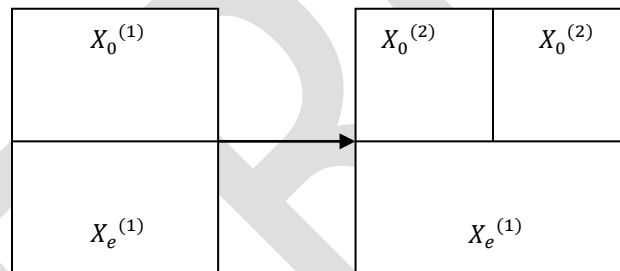


Fig 1 Images Subdivision

D. Predictors

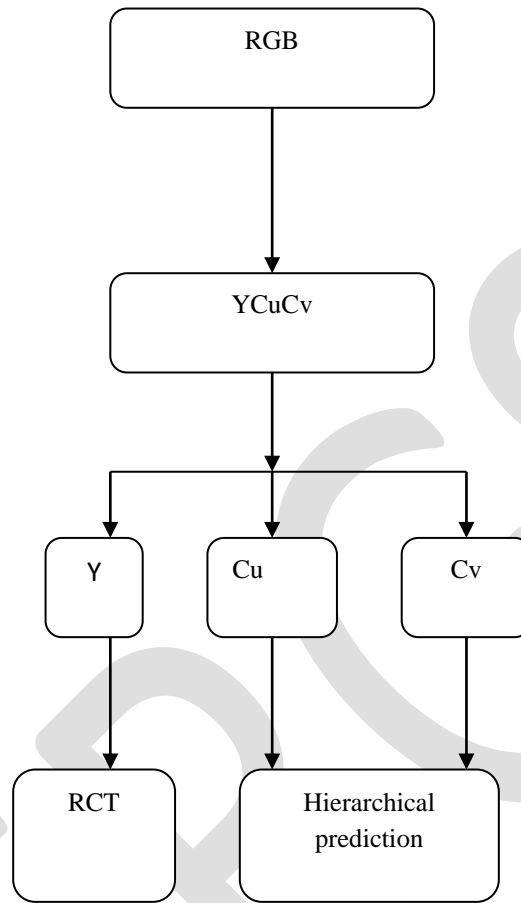


Fig 2 System Architecture of the Proposed System

For encoding the pixel in the image, we are using four predictors. The four predictors are calculated based on the following equation.

$$Xp_0(i, j) = X_0^{(2)}(i, j) \quad (1)$$

$$Xp_1(i, j) = \text{round}((X_0^{(2)}(i + 1, j - 1) + X_0^{(2)}(i - 1, j + 1))/2) \quad (2)$$

$$Xp_2(i, j) = X_0^{(2)}(i - 1, j) \quad (3)$$

$$Xp_3(i, j) = \text{round}((X_0^{(2)}(i - 1, j - 1) + X_0^{(2)}(i + 1, j + 1))/2) \quad (4)$$

After calculating the predictors, the next step is to find the predictor with the maximum value. This can be obtained by comparing the four values. After obtaining the actual predictor, we have to compare this with a particular threshold value. This value is chosen based on the object. Based on the threshold value the value of the predicted value change. Then only the exact prediction process will happen. This can be calculated based on the following algorithms.

Algorithm 1

Calculate the prediction vector

$$\text{Prediction vector} = (X_{p_0}, X_{p_1}, X_{p_2}, X_{p_3})$$

Algorithm II

Prediction algorithm

if (prediction vector < threshold)

$$\text{prediction}(i, j) = \left((X_0^{(2)}(i, j + 1) + X_0^{(2)}(i - 1, j + 1) + X_0^{(2)}(i - 1, j) + X_0^{(2)}(i - 1, j - 1) + X_0^{(2)}(i, j - 1) + X_0^{(2)}(i + 1, j - 1) + X_0^{(2)}(i + 1, j) + X_0^{(2)}(i + 1, j + 1)) / 8 \right)$$

else

$$\text{prediction}(i, j) = 0.85 \left((X_0^{(2)}(i - 1, j + 1) + X_0^{(2)}(i + 1, j - 1)) / 2 \right) + 0.15 \left((X_0^{(2)}(i, j + 1) + X_0^{(2)}(i - 1, j) + X_0^{(2)}(i - 1, j - 1) + X_0^{(2)}(i, j - 1) + X_0^{(2)}(i + 1, j) + X_0^{(2)}(i + 1, j + 1)) / 6 \right)$$

The above algorithm calculates the exact prediction of each pixel is calculated. Based on this prediction the entire image is being encoded. For the proper working of the algorithm the threshold value need to be perfectly chosen based on the property of the images.

E. Error Calculation

After the prediction process, the error of each sub image is calculated; we need to calculate the error value. The context adaptive coding can be used for the actual modelling of the image. For the purpose of context adaptive coding, the error value which is found by using the equation given below is fed into any of the variable length coding.

Error = original image – predicted image

$$\text{ie, error}(i, j) = X(i, j) - \text{prediction}(i, j) \quad (5)$$

The error of each sub image is calculated by subtracting the prediction image from the actual image. Either Huffman or arithmetic coding can be used for the context adaptive coding. The best one is the Huffman coding. The obtained error image is fed on to the Huffman coding for the purpose of context adaptive coding[11]. Many coding techniques are there [12]. The Huffman coding is an algorithm which is used mainly for the lossless compression. The reason for which the Huffman coding is used is that the output of the algorithm can be viewed as variable length code. The Huffman code is mainly used for creating the prefix codes. The output obtained by using the Huffman coding is much more accurate.

III CONCLUSION

Here we have proposed a method for lossless compression based on the hierarchical prediction schema and context adaptive coding is used for the error calculation. At first the RGB is converted into YCuCv colour space using any reversible colour transform. Then Y channel is encode by using any of the gray scale conversion. The chrominance channel is encoded by using hierarchical prediction. Four predictors are being calculated and one among them (here it is minimum valued predictor) is chosen as the prediction vector. And based on this prediction of individual pixels are done. Finally the arithmetic or Huffman coding is used for the error calculation and thereby for the context adaptive coding.

REFERENCES:

- [1] W B. Pennebaker and J. L. Mitchell, Jpeg Still Image Data Compression Standard. New York, NY, USA: Van Nostrand Reinhold, 1993.
- [2] Information Technology—Lossless and Near-Lossless Compression Of Continuous-Tone Still Images (JPEG-LS), ISO/IEC Standard 14495-1, 1999.
- [3] M. Weinberger, G. Seroussi, And G. Sapiro, “The Loco-I Lossless Image Compression Algorithm: Principles And Standardization Into Jpeg-Ls,” IEEE Trans. Image Process, Vol. 9, No. 8, Pp. 1309–1324, Aug. 2000.
- [4] W. Wu And N. Memon, “Context-Based, Adaptive, Lossless Image Coding,” IEEE Trans. Commun., Vol. 45, No. 4, Pp. 437–444, Apr. 1997.
- [5] Information Technology—Jpeg 2000 Image Coding System—Part 1: Core Coding System, INCITS/ISO/IEC Standard 15444-1, 2000.
- [6] ITU-T And ISO/IEC, JPEG XR Image Coding System—Part 2: Image Coding Specification, ISO/IEC Standard 29199-2, 2011.
- [7] S. Pei And J. Ding, “Improved Reversible Integer-To-Integer Color Trans- Forms,” In Proc. 16th IEEE ICIP, Nov. 2009, Pp. 473–476.
- [8] G. Sullivan, “Approximate Theoretical Analysis Of RGB To YCbCr To RGB Conversion Error,” Iso/Iec Jtc1/Sc29/Wg11 And ITU-T Sg16 Q.6 Document Jvt-I017, 2003
- [9] P. Roos, M. A. Viergever, M. C. A. Van Dijke, and J. H. Peters, “Reversible Intraframe Compression of Medical Images,” IEEE Trans. Med. Image, Vol. 7, No. 4, Pp. 328–336, Dec. 1988.
- [10] Seyun Kim, Student Member, IEEE, And Nam Ik Cho, Senior Member, IEEE “Hierarchical Prediction And Context Adaptive Coding For Lossless Color Image Compression” IEEE Transactions On Image Processing, Vol. 23, No. 1, January 2014
- [11] Shrusti Porwal , Yashi Chaudhry, Jitendra Joshi Manish Jain , “ Data Compression Methodologies For Lossless Data And Compression Between Algorithms”, in ISSN 2319-5967 Volume 2, Issue 2, March 2013
- [12] A. Said, “Arithmetic Coding,” In Lossless Compression Handbook, K. Sayood, Ed. San Diego, Ca, USA: Academic, 2003

A Voltage Quadruple DC-DC Converter with PFC

Cicy Mary Mathew, Kiran Boby, Bindu Elias

P.G. Scholar, cicymary@gmail.com , +91-8289817553

Abstract— A two inductor, interleaved power factor corrected converter exhibiting voltage quadruple characteristic is introduced. The proposed converter operates at a duty cycle more than 50%. The input P.F is improved along with reduced voltage stress Across the semiconductor devices. Also a high voltage gain is obtained almost 4 times that of a conventional boost converter. The simulation are carried out for 25 V AC input in MATLAB/SIMULINK 2010a, to justify the properties of the proposed converter

Keywords— Volt-sec balance, High voltage gain, Voltage quadruple, power factor, active PFC, Ripple cancellation, interleaved converter

INTRODUCTION

To meet the challenges of ever-increasing power densities of today's AC/DC power supplies, designers are continuously looking for opportunities to maximize the power-supply efficiency, minimize its component count, and reduce the size of components. Full-bridge diode rectifier has long been used in AC/DC conversion due to its simple and robust circuit. A single DC/DC converter, which is connected after the rectifier, is then able to perform power factor correction (PFC) and output voltage regulation .When an electric load has a PF lower than 1, the apparent power delivered to the load is greater than the real power that the load consumes. Only the real power is capable of doing work, but the apparent power determines the amount of current that flows into the load, for a given load voltage. Power factor correction (PFC) is a technique of counter acting the undesirable effects of electric loads that create a power factor PF that is less than 1. Most of the research on PFC for nonlinear loads is actually related to the reduction of the harmonic content of the line current. There are several solutions to achieve PFC. There are two types of PFC 1) Passive PFC 2) Active PFC. The Active PFC is further classified into low-frequency and high-frequency Active PFC depending on the switching frequency.

The block diagram of power supply with Active PFC network is shown in figure. 1. Here we see it has an active PFC and a DC DC converter which works as a power conditioner and the load is connected. The load may be a DC load or an AC load connected through an inverter.

The operating principle of the proposed circuit is explained in detail in the following sections The circuit is divided into two sections : the PFC stage and the converter stage. Design of the components is also explained briefly in the third section. Section 4 shows the simulation results.

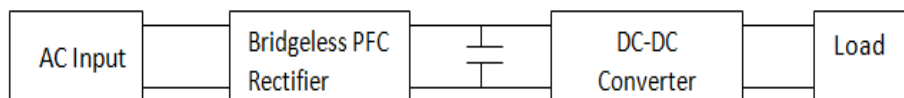


Figure.1 : Block diagram of power supply with an Active PFC

OPERATING PRINCIPLES

An Active power factor correction makes the load behave like a resistor leading to near unity load power factor and the load generating negligible harmonics. The input current is similar to the input voltage waveform's wave shape. The proposed circuit consists of an input PFC stage connected to a boost DC DC converter via a DC link. The figure 1 shows the block diagram of power supply with an Active PFC.

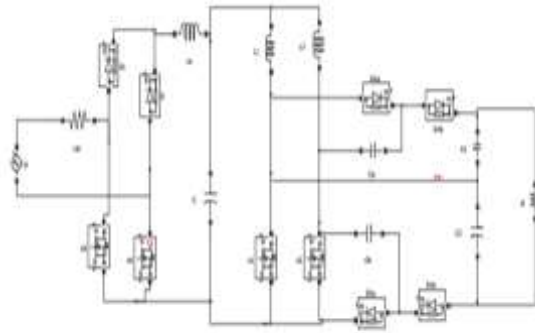


Figure. 2: Circuit diagram of the proposed DC DC converter with PFC

A bridgeless PFC circuit is used in the proposed circuit. In a conventional PFC rectifier, the output ground is always connected to the AC source through the full-bridge rectifier whereas, in the bridgeless PFC rectifier in Figure3, the output ground is connected to the AC source only during a positive half-line cycle, through the body diode of switch S_2 , while during a negative half-line cycle the output ground is pulsating relative to the AC source with a high frequency (HF) and with an amplitude equal to the output voltage. This High Frequency pulsating voltage source charges and discharges the equivalent parasitic capacitance between the output ground and the AC line ground, resulting in a significantly increased common-mode noise. An inductor is connected at the DC side, the current through which is continuous for a large value of L_a .

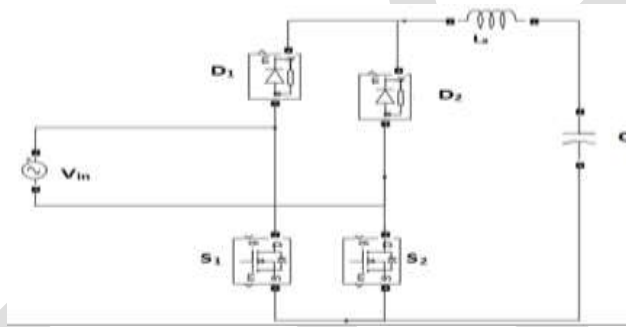


Figure3. Active PFC Stage

The rectified output from the AC-DC PFC stage is stored in a DC-Link capacitor. This capacitor Acts like an input to the DC-DC boost converter stage. A voltage quadrupler DC-DC converter is used in this stage. This converter is so named as the gain is almost four times the gain of a conventional boost converter. The circuit is as shown in figure.4.

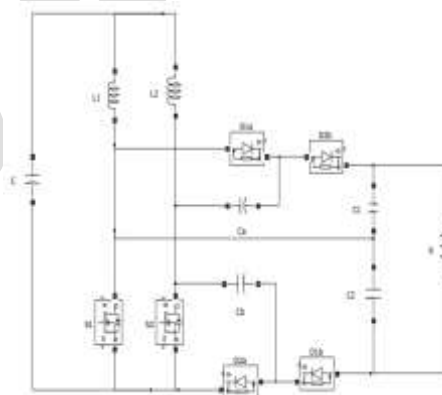


Figure. 4: DC-DC boost converter stage

The operation of this converter can be explained through its four operating modes. It has two switches S_1 and S_2 , the switching signals of whose are 180° out of phase with each other. The modes of operation of this converter is explained below.

1) *Mode I* ($t_0 < t < t_1$): The switches S_1 and S_2 are ON, $D_{1a}, D_{1b}, D_{2a}, D_{2b}$ are all OFF. The corresponding equivalent circuit is shown in Figure.5. From figure.5, it is seen that both i_{L1} and i_{L2} are increasing to store energy in L_1 and L_2 , respectively. The voltages Across diodes D_{1a} and D_{2a} are clamped to capacitor voltage V_{CA} and V_{CB} , respectively, and the voltages Across the diodes D_{1b} and D_{2b} are clamped to V_{C2} minus V_{CB} and V_{C1} minus V_{CA} , respectively. Also, the load power is supplied from capacitors C_1 and C_2 .

2) *Mode II* ($t_1 < t < t_2$): For this operation mode, switch S_1 remains conducting and S_2 is turned OFF. Diodes D_{2a} and D_{2b} become conducting. The corresponding equivalent circuit is shown in Figure.6. It is seen from Figure.6 that part of stored energy in inductor L_2 as well as the stored energy of C_A is now released to output capacitor C_1 and load. Meanwhile part of stored energy in inductor L_2 is stored in C_B . In this mode, capacitor voltage V_{C1} is equal to V_{CB} plus V_{CA} . Thus, i_{L1} still increases continuously and i_{L2} decreases linearly.

3) *Mode III* ($t_3 < t < t_4$): For this operation mode, both S_1 and S_2 are turned ON. The corresponding equivalent circuit turns out to be the same as Figure.7

4) *Mode IV* ($t_4 < t < t_5$): For this operation mode, switch S_2 remains conducting and S_1 is turned OFF. Diodes D_{1a} and D_{1b} become conducting. The corresponding equivalent circuit is shown in Figure.8 It is seen from Figure. 8 that the part of stored energy in inductor L_1 as well as the stored energy of C_B is now released to output capacitor C_2 and load. Meanwhile, part of stored energy in inductor L_1 is stored in C_A . In this mode, the output capacitor voltage V_{C2} is equal to V_{CB} plus V_{CA} . Thus, i_{L2} still increases continuously and i_{L1} decreases linearly.

The equivalent theoretical waveforms of currents and voltages for the afore said modes is shown in figure9. Note that the voltage Across switches is low and also the circuit exhibits automatic current sharing without any need of extra circuitry.

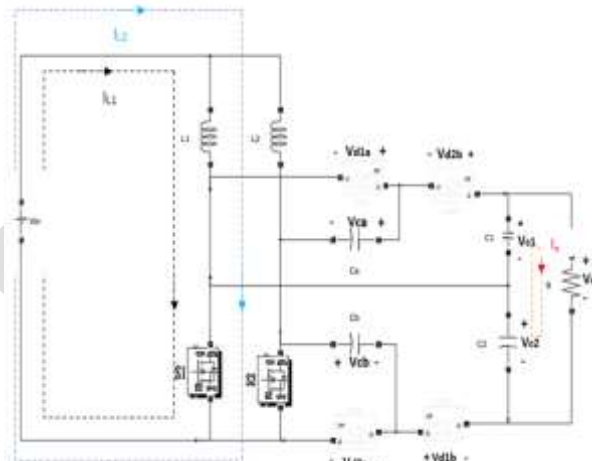


Figure.5: Equivalent circuit of Mode 1 and 3 operation

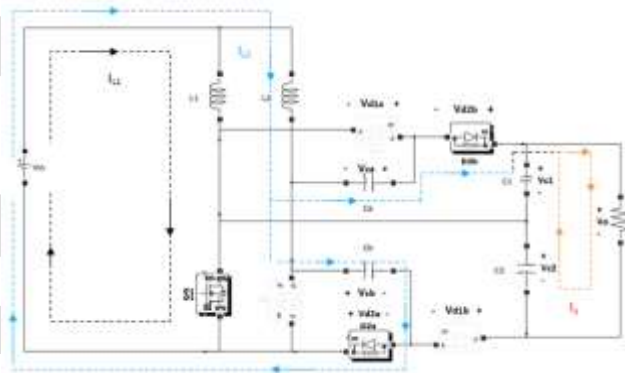


Figure.6: Equivalent circuit of Mode 2 operation

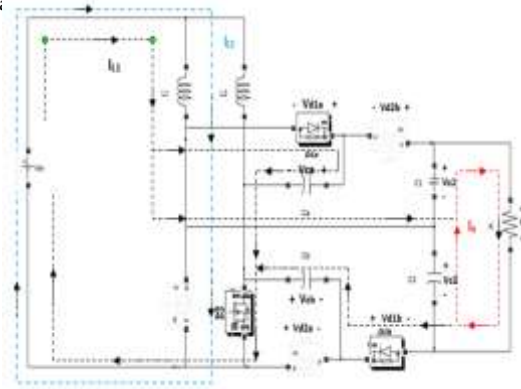


Figure7 :Equivalent circuit of Mode 4 operation

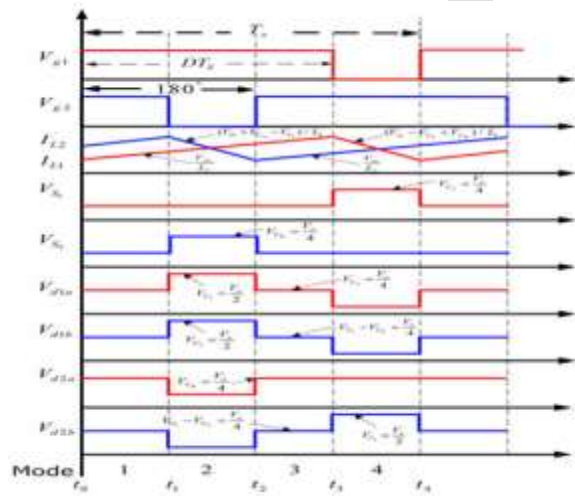


Figure 8: Theoretical Waveforms

DESIGN OF COMPONENTS

The value of the Input filter inductor , DC link capacitor , input inductors, blocking capacitors and output capacitors can be found by the equations discussed in subsection below.

The value of the inductor appropriate for proper working of the converter can be decided by the voltage sec balance of the inductor current. From voltage-sec balance principle

$$\Delta i_{L1} = \frac{V_{in}DT_s}{L_1} \quad (1)$$

Since $L_1 \approx L_2$, therefore

$$\Delta i_{L2} = \frac{V_{in}DT_s}{L_2} \quad (2)$$

Thus, for:

$$V_{in} = 25V \quad D = 0.75 \quad T_s$$

Let us assume a standard acceptable value of ΔI_L as 2.4A. we get $L_1 \approx L_2 \approx 197.5H$

The value of the capacitor appropriate for proper working of the converter can be decided by the charge balance of capacitor. The voltage Across the capacitor is approximately constant. Hence, the voltage ripple ΔV_c is taken to be a very small value approximately 0.1V. The equations for the capacitor value are:

$$C_a = I_c + I_L \left(\frac{1-D}{\Delta V_c} T_s \right) \quad (3)$$

Since $C_a \approx C_b$ therefore

$$C_b = I_c + I_L \left(\frac{1-D}{\Delta V_c} T_s \right) \quad (4)$$

Thus we get the values as $C_a \approx C_b \approx 30\mu F$

The value of the capacitor appropriate for proper working of the converter can be decided by the charge balance of capacitor. The voltage across the capacitor is approximately constant. Hence, the voltage ripple, ΔV_c is taken to be a very small value approximately 0.1V The equations for the capacitor value are:

$$C_2 = I_c + I_L \left(\frac{1-D}{\Delta V_C} T_s \right) \quad (5)$$

Since $C_1 \approx C_2$ therefore

$$C_2 = I_c + I_L \left(\frac{1-D}{\Delta V_C} T_s \right) \quad (6)$$

Thus we get the values as $C_1 \approx C_2 \approx 250 \mu\text{F}$

From the equivalent circuits of mode 1 and mode 2, we can get the relationship between the output voltage and voltage Across output capacitors as

$$V_o = V_{c1} + V_{c2} = \frac{4V_{in}}{1-D} \quad (7)$$

Thus the voltage gain of the converter, M is

$$M = \frac{V_o}{V_{in}} = \frac{4}{1-D} \quad (8)$$

To simplify the voltage stress analyses of the components of the proposed converter, the voltage ripples on the capacitors are ignored. The voltage stresses on Active powers switches S_3 and S_4 can be obtained directly as shown in the following equation:

$$V_{s3max} = V_{s2max} = \frac{V_o}{4}$$

Hence the voltage stress of Active switches of the converter is equal to one fourth of the output voltage, which enables one to adopt lower voltage rating devices to further reduce both switching and conduction losses. Also, from the equivalent circuits of mode 1 and 2 operation, the circuit voltage stress of diodes D_{1a} , D_{1b} , D_{2a} and D_{2b} can be obtained directly be written as:

$$V_{D1amax} = V_{D1bmax} = V_{D2bmax} = \frac{V_o}{2}$$

$$V_{D2amax} = \frac{V_o}{4}$$

SIMULATION RESULTS

The proposed circuit was simulated in MATLAB/SIMULINK. The AC input given was 25V, peak to peak. It is fed through a bridgeless PFC rectifier. Figure 10 shows input current. Figure 11 shows the voltage Across DC link. The value of inductor chosen is $300 \mu\text{H}$ and capacitor value is $30 \mu\text{F}$. The inductors L_1 and L_2 are chosen as $190 \mu\text{H}$. The blocking capacitors, C_a and C_b are chosen as $30 \mu\text{F}$ and output capacitors, C_1 and C_2 are chosen as $250 \mu\text{F}$. MOSFET is chosen as switch. Switches S_1 and S_2 work at 40kHz switching frequency at 75% duty cycle. For the positive cycle only switch S_1 works while S_2 works for negative half cycle. Similarly the Switches S_3 and s_4 work at 40 kHz switching frequency and with 75% duty cycle. The signal to switches S_3 and S_4 are 180° out of phase with each other. Figure 10 shows the Simulink model. Figure 14 to figure 19 show the low voltage stresses on the semiconductor devices.

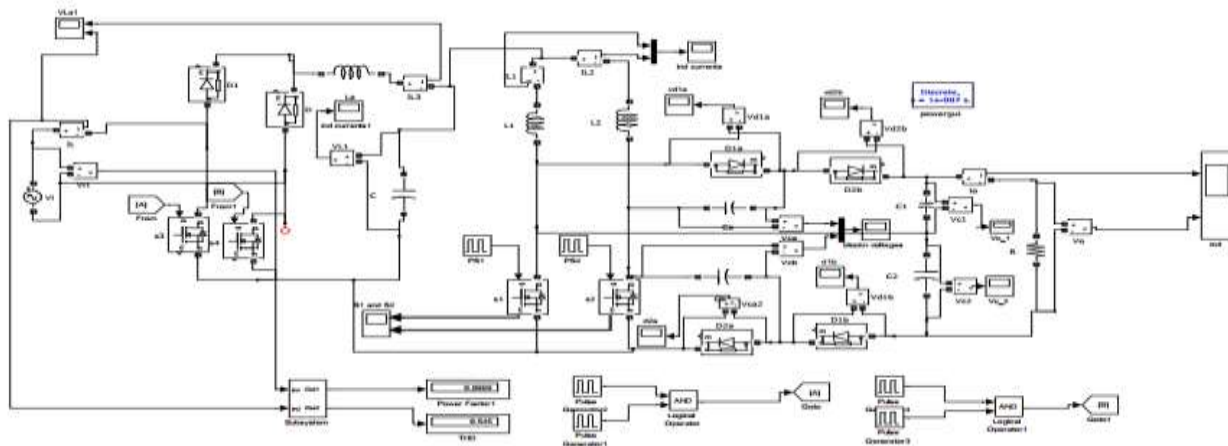


Fig.9 Simulation diagram

Fig 10 shows the input current waveform. From this we see that the input current is almost in phase with the input voltage. Therefore the power factor is nearer to unity. The simulation value of pf 0.98. also the input harmonic distortion is less than 40 percent.

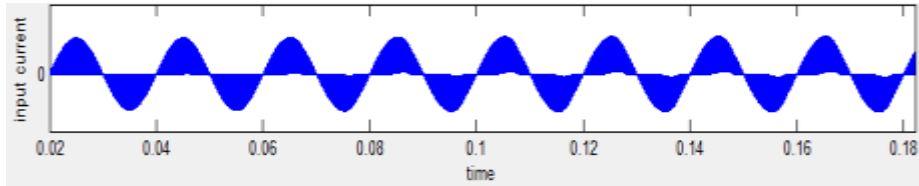


Figure.10: Input A.C. Current

Figure 11 shows the DC link voltage. This voltage is the input to the boost converter section. For an input of 25 V A.C about 21.33V dc link voltage is obtained.

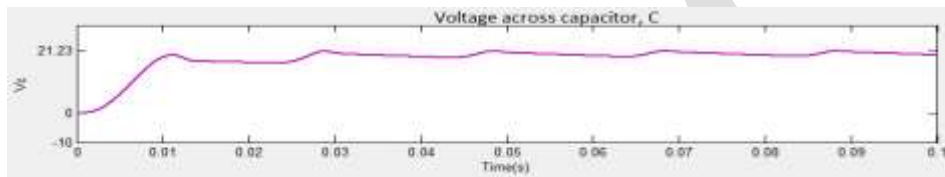


Figure.11: Voltage Across DC-Link Capacitor.

Figure 12 shows the inductor currents. From the result it is clear that input current ripple cancellation is taking place in effect as both the currents are seen to be in 180° phase shift.

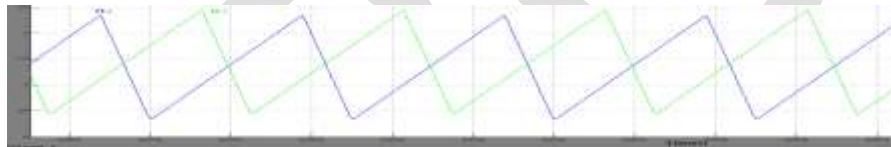


Figure 12: Inductor currents I_{11} and I_{12}

Figure 13 shows the output voltage. For a 25V A.C input a 325.33 output DC voltage is obtained.

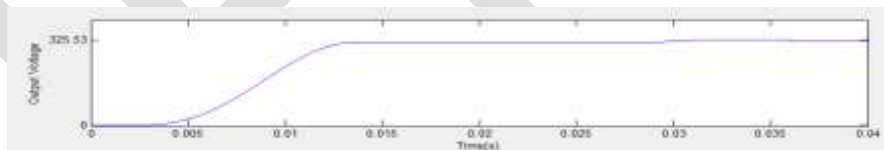


Figure. 13 Output Voltage

Figure 14 to 17 show the voltage across diodes D_{1a} , D_{1b} , D_{2a} and D_{2b} respectively. From the results it is clear that the maximum voltage across D_{1a} , D_{1b} , D_{2b} is $V_o/2$, whereas the maximum voltage across D_{2a} is $V_o/4$. This justifies the low voltage stress across diodes.

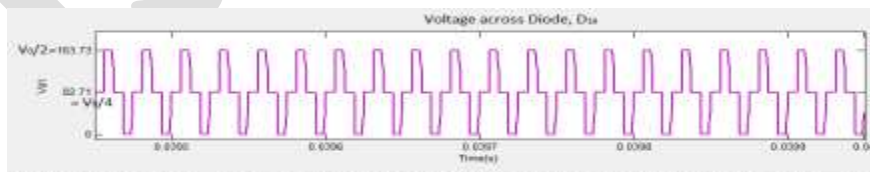


Figure. 14 Voltage Across Diode D_{1a}

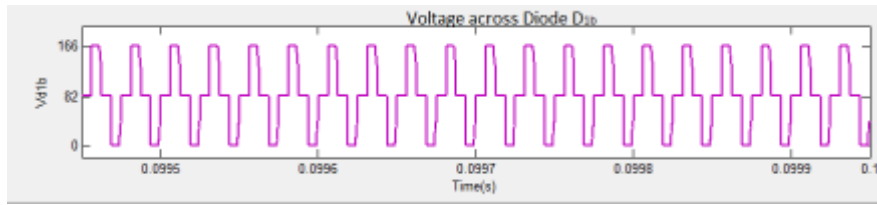


Figure. 15 Voltage Across Diode D_{1b}

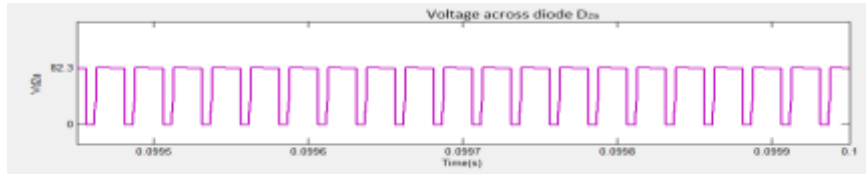


Figure. 16 Voltage Across Diode D_{2a}

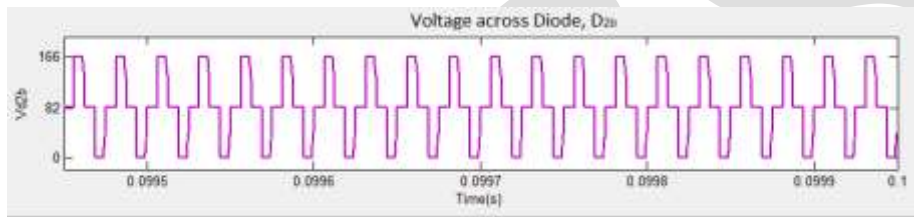


Figure. 17 Voltage Across Diode D_{2b}

Figure 18 and 20 show the voltage across switches S_1 and S_2 respectively. From the results it is clear that the maximum voltage across S_1 , S_2 is $V_o/4$. This justifies the low voltage stress across switches.

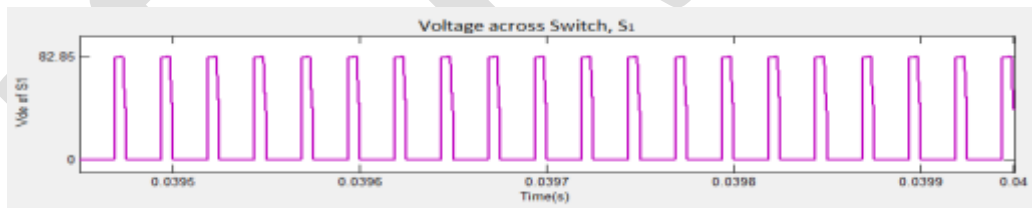


Figure. 18 Voltage Across Switch S_1

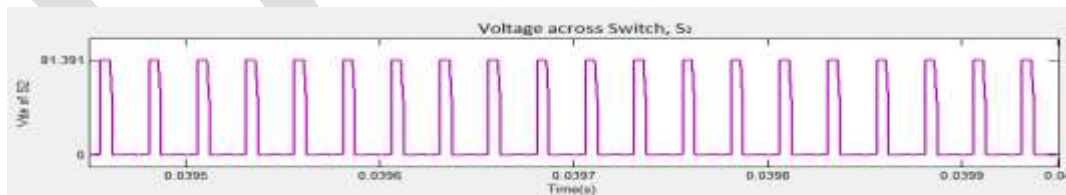


Figure. 19 Voltage Across Switch S_2

CONCLUSION

The proposed circuit was simulated in MTALAB/SIMULINK210a and the results were verified. For an input of 25V AC, a 325.33 V output was obtained. The input power factor obtained was approximately nearer to unity about 0.98 and THD found was 54%. The steady state analysis was done. The voltage Across semiconductor devices is low. The voltage stress Across switches is $\frac{1}{4}$ th the output voltage and that of the diodes D_{1a} D_{1b} , D_{2b} is $V_o/2$ while that for diode D_{2a} is $V_o/4$. Also a high gain output is obtained. Therefore the proposed circuit can be used at applications where a PFC and high gain are required.

REFERENCES:

- 1) R.Lakshmi Narayan, Sriramalakshmi, V.T. Sreelakshmi Comparison Of High Gain DC-DC Boost Converters, Proceedings of 21st IRF International Conference, 15th March 2015, Chennai, India.
- 2) Yungtaek Jang, Milan M. Jovanovic 'Interleaved Boost Converter With Intrinsic Voltage-Doubler Characteristic for Universal-Line PFC Front End', IEEE Transactions On Power Electronics, Vol. 22, No. 4, July 2007
- 3) Ching-Tsai Pan, Chen-Feng Chuang Chia-Chi Chu, "A Novel Transformer-less Adaptable Voltage Quadrupler DC Converter with Low Switch Voltage Stress," IEEE Transactions On Power Electronics, Vol. 29, No. 9, September 2014
- 4) Ahmed M. Al Gabri, Esam H. Ismail, "Bridgeless PFC Modified SEPIC Rectifier with Extended Gain for Universal Input Voltage Applications," IEEE Transactions On Power Electronics
- 5) Dragon Maksimovic, Robert Erickson "Universal input, high power factor, boost doubler rectifiers" Applied Power Electronics Conference and Exposition, 1995. APEC '95. Conference Proceedings, 1995
- 6) Rectifiers for Power Factor Correction, Application Note, Vishay General Semiconductor
- 7) Fariborz Musavi, Wilson Eberle William G. Dunford "A High-Performance Single-Phase Bridgeless Interleaved PFC Converter for Plug-in Hybrid Electric Vehicle Battery Chargers" IEEE Transactions On Industry Applications, Vol. 47, No. 4, July/August 2011
- 8) Dylan Dah-Chuan Lu, Wenfei Wang "Bridgeless Power Factor Correction Circuits with Voltage-Doubler Configuration" IEEE PEDS 2011, Singapore, 5 - 8 December 2011
- 9) Bing Lu Ron Brown, Marco Soldano "Bridgeless PFC Implementation Using One Cycle Control Technique," APEC '05
- 10) Michel Ioughlin, "An interleaving PFC pre-regulator for high power converters", Application Note Texas Instruments
- 11) A.Ramesh Babu, Dr.T.A.Raghavendiran "Analysis of non-isolated two phase interleaved high voltage gain boost converter for PV application" 2014 International Conference on Control, Instrumentation, Communication and Computational Technologies (ICCICCT)
- 12) [12] H. M. Mallikarjuna Swamy, K.P.Guruswamy, Dr.S.P.Singh, "Design And Implementation Of Two Phase Interleaved Dc-Dc Boost Converter With digital Pid Controller", International Journal of Electrical and Electronics Engineering (IJEET) ISSN (PRINT):2231 -5284 Volume-3, Issue-1, 2013.

An Efficient Approach for Contrast Enhancement of Medical Image Using Dual Tree Complex Wavelet with High Pass Filter

Swati Gupta
M.Tech. Scholar
Department of CSE
LNCT, Bhopal
swatigupta13dec@gmail.com

Shweta Shrivastava
Assistant Professor
Department of CSE
LNCT, Bhopal
shwetashri.26@gmail.com

Dr. Vineet Richariya
Professor & Head,
Department of CSE
LNCT, Bhopal
vineet_rich@yahoo.com

ABSTRACT- Image processing is extensively used area for the research and this is used for various applications such as remote sensing image data, medical image and weather forecasting etc. In this we are mainly focusing on medical image data and to get enhance quality of medical image becomes very challenging task nowadays. The low contrast medical image is very critical to analyze and obtain false results from such image. A lot of techniques have been developed to improve the quality of image. In this paper, we propose Dual Tree Complex Wavelet Transform (DTCWT) with High Boost Filtering to improve the quality of medical image. Here first method is used for enhancing the contrast of image and subsequent filtering technique is used for sharpening or eliminating the noise and blur from the image. The simulation of our proposed method is done using the MATLAB2012a simulator which comprises several functions for image simulation and the comparative analysis of our methodology uses performance measuring metrics such as PSNR and MSE. The experimental results of our methodology give improved quality of image than the existing approach.

Keywords- Image processing; Medical image; DTCWT; MATLAB; PSNR; MSE; MAE

INTRODUCTION

In digital image processing, it deals with increasing a digital system that acts upon operations on a digital image. The image is not anything further than a two dimensional signal. It has been defined by the geometric function $f(x, y)$ in which x and y are horizontally and vertically co-ordinates of the image and the amplitude of f at any couple of coordinate (x, y) is labeled the intensity or gray level of the image at that position. This is used for many applications such as Gamma ray imaging, X-ray, microwave band and ultraviolet band etc. In medical application, low contrast image analysis is a challenging predicament [1]. The low contrast digital image decreases the aptitude of spectator in analyzing the image. Histogram based methods are used to augment contrast of every type of medical images. They are chiefly used for all categories of medical images such as for Miasmammogram images, these methods are used to discover precise localities of cancerous regions and for low-dose CT images, these methods are used to overstate inconsequential anatomies analogous to containers, lungs nodules, airways and pulmonary fissures. The most effective method used for contrast augmentation is Histogram Equalization (HE). Image enrichment is principally humanizing the interpretability or sensitivity of information in images for human spectators and provided that `healthier contribution for other automated image processing techniques. The foremost intention of image enhancement is to transform aspects of an image to formulate it more appropriate for a specified task and a precise spectator. During this progression, one or more aspects of the image are personalized. The selection of aspects and the way they are personalized are detailed to a given task. Furthermore, spectator-specific factors, for instance the human visual system and the spectator's understanding, will commence an enormous covenant of subjectivity into the alternative of image enhancement methods. There subsist a lot of techniques that can augment a digital image lacking of blemishing it. The enhancement techniques can largely be divided in to the following two classes:

1. Spatial Domain Methods
2. Frequency Domain Methods

Basically in spatial domain the value of pixel strength are operated directly as equation given below:

$$G(x, y) = T [f(x, y)] \dots \dots \dots (1)$$

In frequency domain technique, the image is former transmitted in to frequency domain [2]. This means that, the Fourier transform of the image is calculated formerly. The overall enhancement operations are performed on the Fourier transform of the image and after that the Inverse Fourier transform is act upon to obtain the resultant image. These improvement functions are performed in order to

transform the image brightness, contrast or the allocation of the grey levels. As a consequence, the pixel value (intensity) of the resultant image will be customized according to the transformation function operated on the input values. In the frequency domain the image development can be done according to this equation:

$$G(u, v) = H(u, v) * F(u, v) \dots \dots \dots (2)$$

Where $F(u, v)$ is input image, $G(u, v)$ is improved image, and $H(u, v)$ is the transfer function. Image enhancement basically represents that transforming an image f into image g using T . (Where T is the transformation. The values of pixels in images f and g are nominated by r and s , correspondingly. Seeing that said, the pixel values r and s are associated by the expression

$$s = T(r) \dots \dots \dots (3)$$

Where T is a conversion that maps a pixel value R into a pixel value S . The outcomes of this transformation are mapped into the grey scale range while we are relating here simply with grey scale digital images. I will consider simply gray level images. A digital gray image should have pixel values in the range of 0 to 255. In this, we uses wavelet transform based approach to develop the excellence of medical image also diminish the noise and blur of the image using filtering technique (high boost filtering). This paper is arranged in such way: In section II presents the review of literature of earlier work done in medical image enhancement. In section III discuss our proposed methodology with its flowchart and section IV shows experimental results and analysis of our methodology. Last but not least, this section presents overall conclusion of this paper with its future work scope.

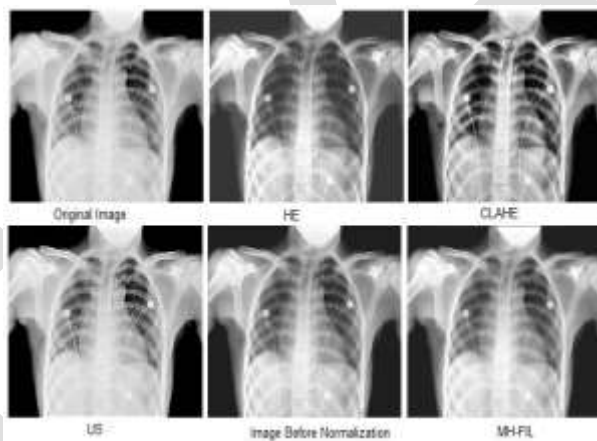


Figure1: Image enhancement process using Histogram Equalization

RELATED WORK

The area of medical image enhancement is the significant characteristic of medical image processing, as of their mammoth applications in several areas of our live particularly in the medical diseases diagnosis. Lots of articles and literature evaluation are published in this area and we will enlighten some of these works.

In 2014, **Subir Singh Lamba et al. [9]** proposed a novel MH-FIL for medical images. This method used two step of processing, in primary step global contrast of image is improved using histogram amendment followed by histogram equalization and then in subsequently step homomorphic filtering is used for image sharpening, this filtering if followed by image normalization. To estimate the effectiveness of their method they preferred two extensively used metrics absolute mean brightness error (AMBE) and entropy. Based on consequences of these two metrics this algorithm is confirmed as a bendable in use and effectual way for medical image enhancement and can be used as a pre-processing step for medical image understanding and investigation.

In 2013, **Qasima Abbas Kazmi et al. [8]** presented the specified process to oversimplify the diffusion procedure further into forward-and-backward progression. Additionally, the Forward - and Backward diffusion process could once more be used in perfection of the resolution of the given image. A particular image is being used for improvement of resolution of that image by means of interpolation and a forward-and-backward non-linear diffusion post-processing presents suppression of ringing. Process was initiated to be

extremely productive in distinctive those medical images which gives analogous images for two or more hazardous diseases. The process compliments the boundaries among the edges.

In 2013, **Rajesh Nema et al. [10]** proposed a system to get better the eminence of image using Kernel Padding and DWT with Image Fusion that augmented the contrast of Images that has varying intensity allocation predominantly satellite images, sustains the brightness of images, sharpens the edges and eradicates the blurriness of images. Primarily this is a pixel based edge guided image fusion procedure. In this system LL sub band of Image DWT is routed by contrast enhancement section where based on image brilliance level image is decomposed in dissimilar layers and then each & every layer intensity is stressed or compressed by engendering intensity transformation function. The partitioned intensity layers are too processed by canny edge recognition method as all the satellite images incorporates the noise due to atmospheric turbulence and this is Gaussian by character. The Canny edge detector is the preeminent method for detecting edges of image in the subsistence of Gaussian noise. Finally the contrast enhanced images are amalgamated according to the weight map concluded by edge map of image.

In 2012, **Uma Maheswari et al. [4]** presented a hybrid method to recover the image Excellency of Digital Imaging and communications in medicine (DICOM) images. The proposal of image enhancement technique is to advance the eminence of an image for early diagnosis. Subsequently, followed by a noise diminution using speckle diminution anisotropic filter. They suggested that the use of contrast enhancement method as an attempted to transform the intensity allocation of the image and to lessen the multiplicative noise. The performance of the proposed method is compared with the existing conventional algorithm and real time medical diagnosis image.

In 2012, **Yuanfeng Jin et al. [5]** this paper concerned regarding the applications of the partial differential equation (PDE) in image refurbishment and image enhancement. They primarily analyzed conventional methods of image investigation, study applications of the diverse method and diffusion equations in image refurbishment, as well as their enhanced algorithm for image enhancement.

In 2012, **S.M. Chao et al. [6]** Presented the customized method that considers also the incongruity of the brightness levels in a local neighborhood around each pixel was offered. On the other hand, the predicament of the automatic assessment of the decisive parameters was not addressed. A modified diffusion method, appropriate for images with low-contrast and jagged illumination, was portrayed in [7].

In 2010, **Ovidiu Ghita et al. [3]** concerned with the introduction of a novel gradient vector flow (GVF) field formulation that illustrates increased robustness in the presence of assorted noise and with its estimation when incorporated in the improvement of image enhancement algorithms. In this observation, the foremost contribution associated with this work exists in the enlargement of an adaptive image enhancement structure that couples the anisotropic dispersion models through the adaptive median filtering that is premeditated for the reinstatement of digital images corrupted with miscellaneous noise. To further exemplify the advantages allied with the anticipated GVF field formulation, additional experiments are conducted when the proposed approach is functioned in the creation of anisotropic models for texture enhancement

PROPOSED WORK

In this section, we briefly discuss about our proposed methodology to enhance the brightness, contrast and sharpening the images

Discrete Wavelet Transform

The CWT performs a multi-resolution analysis by retrenchment and dilatation of the wavelet functions. The discrete wavelet transform employs filter banks for the construction of the multi-resolution time frequency plane. The DWT [11] employs multi-resolution filter banks and individual wavelet filters for the analysis and reconstruction of signals. In many image processing applications wavelets plays an important role. In 2-D wavelet decomposition of an image, the 1-D discrete wavelet transform (DWT) is applying along the rows of image and after that results are decomposed along the columns. The results of this operation gives four decomposed sub band images that are low-high (LH), low-low (LL), high-high (HH) and high-low (HL). The absolute frequency spectrum of the input image is covered by frequency components of all these sub-

bands cover the complete frequency spectrum of the original image.

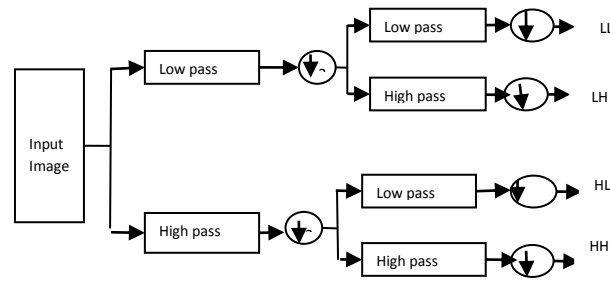


Figure 2: Decomposition of image using DWT

Dual Tree Complex Wavelet Transform (DT-CWT)

The DTCWT [12] is a comparatively modern enhancement to the discrete wavelet transform (DWT), with significant supplementary properties like; it is just about shift invariant and directionally discriminating in two and higher dimensions. It accomplishes this with a redundancy factor of only for 2-dimensional signals, which is considerably lower than the undecimated DWT. The multi-dimensional (M-D) dual-tree CWT is non-separable. It is based on a computationally proficient, distinguishable filter bank (FB). DT-CWT determines the complex transform of a signal using two split DWT decompositions (tree a and tree b). It is shown in Fig. 3. If the filters used in one are particularly designed dissimilar from those in the other it is promising for one DWT to fabricate the real coefficients and the other the imaginary. This redundancy of the two offers superfluous information for analysis but at the disbursement of extra computational power. It also supplies estimated shift-invariance (unlike the DWT). It agrees to perfect reconstruction of the signal. The Dual Tree Complex Wavelet Transform (DTCWT) has been anticipated to de-noise the ultrasound images.

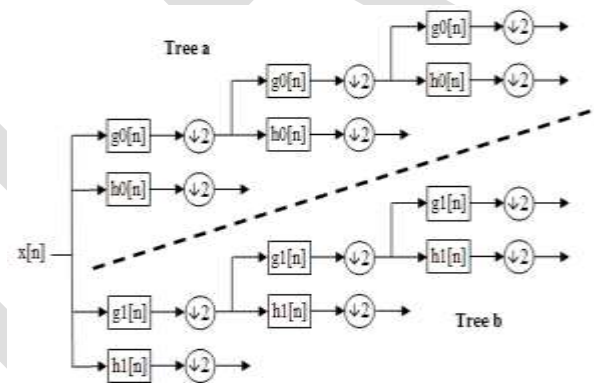


Figure 3: Tree structure diagram of DTCWT

Kernel Filtering

It initial defines a universal linear translation-variant filtering procedure, which engrosses a guidance image I, an input image p, and output image q. Both I and p are given beforehand according to the application, and they can be indistinguishable [14]. The filtering output at a pixel I is expressed as a weighted average:-

$$q_i = \sum_j w_{ij}(p)p_j \dots \dots \dots (4)$$

In this eqn. “i” and “j” are pixel index. The filter kernel W_{ij} is a function of the guidance image I and independent of p. This filter is linear with respect to p.

The guided filtering kernel W_{ij} is given by:-

$$w_{ij} = \frac{1}{|w|^2} \sum_{k:(ij) \in w_k} \left(1 + \frac{(I_i - \mu_k)(I_j - \mu_k)}{\sigma_k^2 + \epsilon} \right) \dots \dots \dots (5)$$

In this eqn. I is the guidance image, p is the input image, w_{ij} is the filter kernel is the variance, K_i is the normalizing parameter, w_k is the window centered pixel at pixel k and μ_k is mean of I.

Zero Padding:

It is preferable to periodic replication in various applications because it circumvents wrap-around problems with little increase in computational cost. In this way wavelet analysis is different from Fourier analysis, in which periodic replication is necessary due to the periodic nature of the basis function. In Fourier analysis the term “zero padding” refers to extending the signal with a finite number of zeros. Periodic replication does retain certain attractiveness in wavelet analysis, however, due to its computational simplicity and its convenient analytical properties [13].

For signals that do not begin or end on the baseline, the appropriate methods of extension are mirroring or extrapolation, in order to prevent discontinuities at the boundaries. The relative pros and cons of extrapolation versus mirroring are less clear than those zero padding versus periodizing. Generally filters are used to filter discarded belongings or thing in a spatial domain or its surface area. In the area of image processing maximum time the images are pretentious by several of noises. The major objectives of filters are to improve the quality of an image by improving interoperability of the present information into images.

Frequency Domain

The frequency domain method is based on the convolution theorem. It splits an image from its spatial domain form of intensity into frequency domain [2] components and it is symbolized as the above equation 1 & equation 2.

Spatial Filters

When filtering functions are unswervingly performed on the pixels of an image are referred as Spatial Filtering. Spatial filtering consists basically affecting the filter mask from point to point in an image. At every point(x, y), the reaction of the filter at that point is designed using a predefined relationship.

3.4 Proposed Method

High pass filters: A high pass filter is mostly used for sharpening purpose. When an image is sharpened and contrast is superior between bordering areas with little variation in brightness or low eminence information.

High pass = $f(x, y) - low\ pass$

High-boost Filtering: A high-boost filter is also acknowledged as a high-frequency prominence filter. A high-boost filter is used to conserve numerous of the low-frequency apparatus to abet in the elucidation of an image. In high-boost filtering input image h (m, n) is multiplied by an amplification factor A prior to subtracting the low-pass image. Accordingly, the high-boost filter expression is:

$$High\ Boost = A * f - low\ pass \dots \dots \dots (7)$$

Adding and subtracting 1 with gain factor, then

$$High\ Boost = (A - 1) * f(x, y) + f - low\ pass$$

So

$$High\ Boost(A - 1) * f + High\ pass \dots \dots \dots (8)$$

Steps Followed by enhancement are:

1. Input an image (x-ray, MRI).
2. Apply DWT (dual tree).

3. Decompose image into (LL, LH, HL, HH) sub bands.
4. Apply Kernel with zero padding in LL band using the given equation

$$w_{ij} = \frac{1}{|w|^2} \sum_{k:(ij) \in w_k} \left(+ \frac{(I_i - \mu_k)(I_j - \mu_k)}{\sigma_k^2 + \epsilon} \right)$$

5. Apply high pass filter into LL, LH, HH bands using the given formula.

$$\text{High pass} = f(x, y) - \text{low pass}$$

6. Then apply Gaussian filter to remove noise

$$h(m, n) = \left[\frac{1}{\sqrt{2\pi}\sigma} e^{-\frac{m^2}{2\sigma^2}} \right] \times \left[\frac{1}{2\pi\sigma} e^{-\frac{n^2}{2\sigma^2}} \right]$$

7. In parallel apply HE into padded LL band.
8. Apply high boost filter after removed noise from LH, HL, HH sub bands.

$$\text{High Boost} = (A - 1) * f(x, y) + \text{High pass}$$

9. Compose all layers.
10. Apply inverse function of DWT (IDWT).
11. Measure MSE (original image ,

Enhanced image)

$$MSE = \frac{1}{mn} \sum_{i=0}^{m-1} \sum_{j=0}^{n-1} [I(i, j) - K(i, j)]^2$$

12. Measure PSNR (peak signal-to-noise ratio).

$$PSNR = 10 \log_{10} \frac{MAX_I^2}{MSE}$$

13. Measure MAE (mean absolute error)

$$MAE = \frac{1}{n} \sum_{t=1}^n |x_t - \hat{x}_t|$$

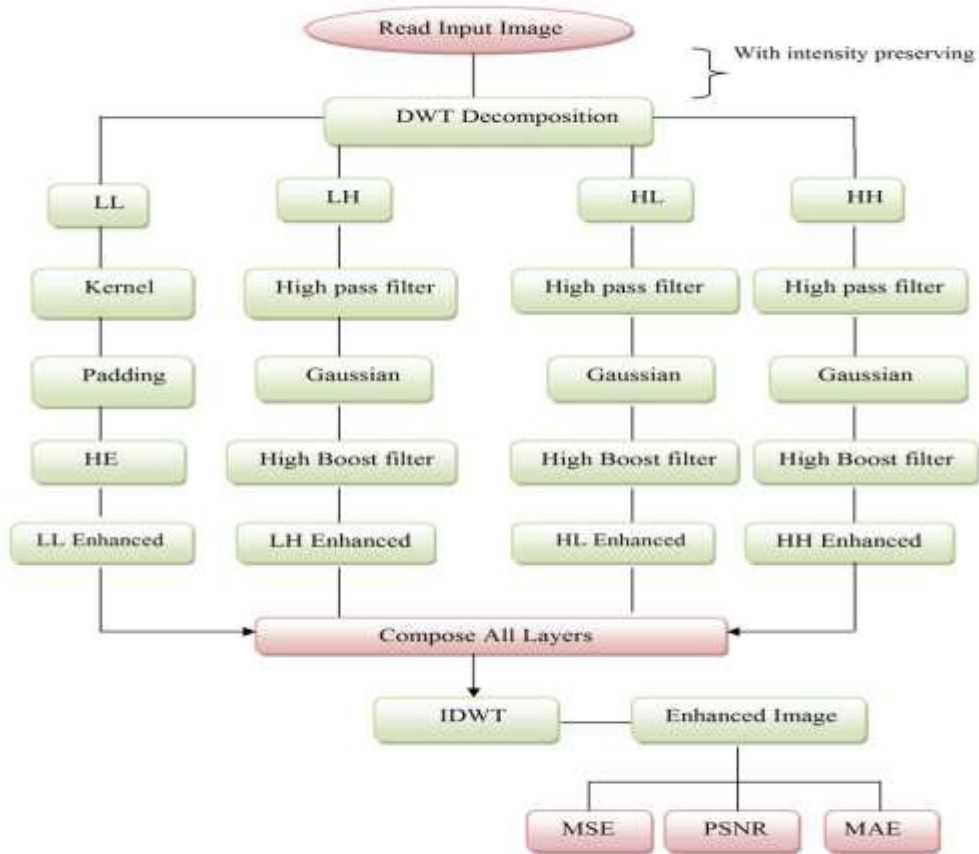


Figure 4: Block Diagram of proposed enhancement method

Figure 4 shows that the working diagrams of proposed system where low quality images are enhanced with it. Additionally Gaussian filter is embedded into this system, who removes the noise from the images. Basically Gaussian filter is linear smoothing filter with the weights selected according to the Gaussian functions. Primarily these kind filters are used to level

4. EXPERIMENTAL RESULTS & ANALYSIS

In this section we demonstrate the effectiveness of our proposed methodology DTCWT with HBF in comparison with some existing approach HE, DWT and High Boost Filter for contrast enhancement. The simulation is done on MATLAB2012a [15] & analysis of our method is performs using performance metrics such as MSE and PSNR.

For the experimental process they have tested 5 X-ray-MRI images, and in figure 5 show the comparison of different methods for chest x-ray image, similarly they have tested contrast enhancement foot-x-ray, hands-bone, head-x-ray and mummy-x-ray images.

MSE: Mean Square Error

The MSE is the cumulative squared error between the compressed and the original image

$$MSE = \frac{1}{mn} \sum_{i=0}^{m-1} \sum_{j=0}^{n-1} [I(i,j) - K(i,j)]^2$$

PSNR: Peak Signal-To-Noise Ratio

It is the ratio between the maximum probable power of a signal and the power of corrupting noise that influences the fidelity of its representation. For the reason that many signals have a extremely extensive dynamic range, PSNR is typically expressed in terms of the logarithmic decibel scale.

The PSNR (in dB) is defined as

$$PSNR = 10 \log_{10} \frac{MAX_I^2}{MSE}$$

MAE: Mean Absolute Error

MAE measures the average magnitude of the errors and is defined as follows:

$$MAE = \frac{1}{n} \sum_{t=1}^n |x_t - \hat{x}_t|$$

Where x_t and \hat{x}_t denote the samples of original image and enhanced image, respectively. M and N are number of pixels in row and column directions, respectively.

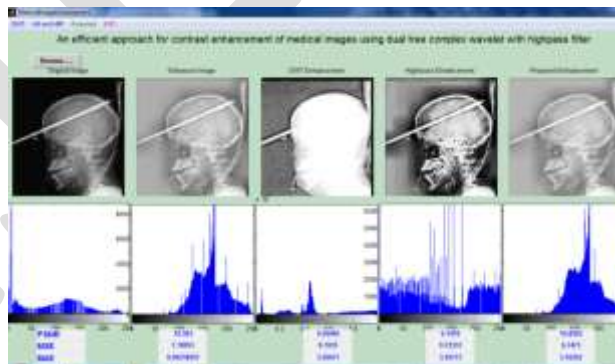


Figure 5: Shows the result produced by method HE, DWT, HBF and Proposed on mummy- x-ray

From the above figure we observe that the existing HE, DWT and HBF method does not execute well that part of the image which is much darker region but after analyzing our method with these method, we found that our method DTCWT with HBF produce much better results and enhance the contrast of the images.

Here, we are showing the performance of five medical images and analyze it on the basis of MSE (mean square error) and PSNR (peak signal noise ratio), MAE (mean absolute error)

After observing the table 1 found that the MSE value of our proposed method is much better than the HE, DWT and High Boost.

Table 1: Comparison of 5 medical images using various methods on MSE

MSE comparison				
Method/ Image	HE	DWT	High Boost	Proposed
chest-x-ray	6.6923	12.1548	6.13787	5.52765
mummy-x-ray	10.1678	7.02954	11.3795	12.1732
hands-bone	7.25542	11.4552	7.17098	5.90256
foot-x-ray	12.7051	7.71594	10.3744	10.4141
head-x-ray	10.8502	9.69466	9.19786	8.64066

In table 2 we also analyze that the result of PSNR value of five medical images comparing it with methods and obtain more PSNR than the HE, DWT and High boost which efficiently reduce and enhance the contrast or brightness of the image.

Table 2: Comparison of 5 medical images using various method on PSNR

PSNR comparison				
Method/ Image	HE	DWT	High boost	Proposed
chest-x-ray	15.1418	4.77495	16.6441	18.4632
mummy-x-ray	7.8757	7.02954	11.3795	12.1732
hands-bone	13.7383	5.80466	13.9416	17.3232
foot-x-ray	4.00569	12.6692	7.5262	7.45994
head-x-ray	6.7473	8.7035	9.61732	10.7029

In table 3 we also analyze that the result of MAE value of five medical images comparing it with methods and obtain less MAE than the HE, DWT and High boost which efficiently reduce and enhance the contrast or brightness of the image.

Table 3: Comparison of 5 medical images using various methods on MAE

MAE comparison				
Method/ Image	HE	DWT	High Boost	Proposed
chest-x-ray	6.6923	12.1548	6.13787	5.52765
mummy-x-ray	3.1678	7.02954	6.3795	2.1732
hands-bone	7.25542	6.4552	6.17098	5.90256
foot-x-ray	3.7051	4.71594	6.3744	2.4141
head-x-ray	7.8502	9.6946	4.1978	1.6406

5. CONCLUSION & FUTURE SCOPE

In medical application, to acquire improved quality of medical data various techniques has been implemented which enhance the contrast and preserve the brightness of image but they are not much efficient. Our proposed method DTCWT with high boost filter enhances the contrast of medical image it also reduces the noise and blur of the image than the existing methods. The MSE and PSNR results show that our method is more suitable for contrast enhancement.

REFERENCES:

- [1]. Bhabatosh Chanda and Dwijest Dutta Majumder, "Digital Image Processing and Analysis", 2002.
- [2]. Raman Maini and Himanshu Aggarwal "A Comprehensive Review of Image Enhancement Techniques", Journal of Computing, Volume 2, Issue 3, March 2010.
- [3]. Ovidiu Ghita Paul F. Whelan, "A new GVF-based image enhancement formulation for use in the presence of mixed noise", Journal Pattern Recognition, Volume 43, Issue 8, pp-2646-2658, Aug 2010.
- [4]. Umamaheswari, J. and G. Radhamani, "An Enhanced Approach for Medical Brain Image Enhancement", Journal of Computer Science, Volume 8, Issue 8, pp. 1329-1337, ISSN 1549-3636, 2012.
- [5]. Yuanfeng Jin, Tinghuai Ma, Donghai Guan, Weiwei Yuan and Chengmin Hou, "Review of applications of partial differential equations for image enhancement", Scientific Research and Essays, Volume. 7, Issue 44, pp. 3766 - 3783, November, 2012.
- [6]. S.M. Chao, D.M. Tsai, "An improved anisotropic diffusion model for detail and edge-preserving smoothing", Journal Pattern Recognition, Volume 31, Issue 13, PP 2012-2023, October 2012.
- [7]. S.M. Chao, D. Tsai, "Anisotropic diffusion with generalized diffusion coefficient function for defect detection in low-contrast surface images, Pattern Recognition 43 1917–1931, (5) 2010.
- [8]. Qasima Abbas Kazmi, Krishna Kant Agrawal and Vimal Upadhyay, "Image Enhancement Processing Using Anisotropic Diffusion", International Journal of Computer Science Engineering and Information Technology Research (IJCEITR), ISSN 2249-6831, Volume 3, Issue 1, pp. 293-300, Mar 2013.

- [9]. Tarun Kumar Agarwal, Mayank Tiwari, Subir Singh Lamba, “*Modified Histogram Based Contrast Enhancement using Homomorphic Filtering for Medical Images*”, ”, IEEE International Advance computing conference (IACC), DOI: 10.119/AdCC.2014.6779453, pp. 964-968, Feb 2014.
- [10]. Deepak Kumar Pandey, Rajesh Nema, “*Efficient Contrast Enhancement using Kernel Padding and DWT with Image Fusion*”, International Journal of Computer Applications (0975 – 8887) Volume 77, No.15, September 2013.
- [11]. P.Bala Srinivas, B.Venkatesh, “*Comparative Analysis of DWT, SWT, DWT&SWT and DTCWT-Based Satellite Image Resolution Enhancement*”, International Journal of Electronics & Communication Technology (IJECT) Vol. 5, Issue 4, Oct - Dec 2014, ISSN : 2230-7109 (Online).
- [12]. Anil Dudy, Kanwaljit Singh, “*A New Approach For Denoising Ultrasonographic Images Using DTCWT*”, International Journal of Latest Research in Science and Technology Vol.1, Issue 2: Page No.106-108, July-August (2012), ISSN (Online):2278-5299.
- [13]. Kevin C McGill and Carl Taswell “*Length- Preserving Wavelet Transform Algorithm for Zero-padded and Linearly-Extended Signals*”, Scientific Computing Computational Mathematics Jacks Hall-314, Stanford University, Stanford, CA 94305-2140.
- [14]. DEVI. S, JINI CHERIYAN, “*Image Enhancement Using Guided Image Filter and Wavelet Based Edge Detection*”, International Journal of Modern Engineering Research (IJMER) Vol. 3, Issue.3, pp-1702-1706, ISSN: 2249-6645, May.-June. 2012.
- [15]. <http://in.mathworks.com/matlabcentral/answers/40897-links-to-matlab-documentation-in-published-html-pages>

Improved biomedical sensing technologies and applications by using TEDS

Priyanka verma and Shilpa Sharma
M.Tech(VLSI)
CGC Landran, Mohali
priverma77@gmail.com
shilpa1992sharma@gmail.com

ABSTRACT- A In biomedical sensors having advancement in micro fabrication and in signal processing techniques, the use of transducer electronic data sheet (TEDs) is to suggest new features to improve performance of biomedical sensors and its applications. The development of smart transducers and sensors uses a family of standards.ISO/IEC/IEEE21451-X also known as IEEE1451.X is a family of standards that allows designer to project smart transducers and sensors having reference to protocols, TEDS, networks, web services, radio frequency identification and so on. TEDS are mainly used to store information related to patient clinical history and diagnostic criteria.

Keywords: TEDS, Biomedical sensors, reliability, patient adapting system, Diagnostic algorithm.

1. INTRODUCTION

A modern biomedical sensor consists of a biologically or biophysically-derived sensing element integrated with a physical transducer that performs a measurand into an output signal. In biomedical sensor it having ability to pick out one parameter without any interference to the other parameters. It having ability to measure small changes in a given measurand such as accuracy, time response, bio compatibility, aging characteristics, size, ruggedness, robustness, low cost.

Transducers, sensors and actuators, are defined by ISO/IEC /IEEE21451-X standards, are mostly used in different fields : industrial, biomedical, environmental, energy,etc. The ISO/IEC/IEEE21451-X is a growing family of standards responsible for the development of smart sensors. TEDS can be used to improve performances of biomedical sensors and instrumentation. The data processing algorithms can accommodate itself to the patient by learning his/her health history.

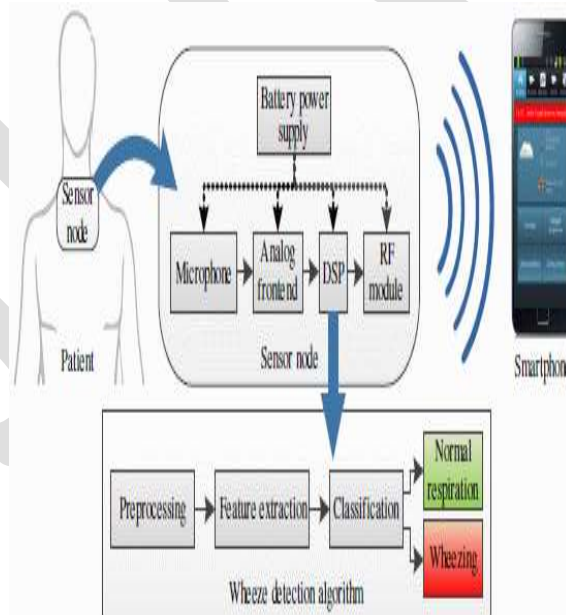


Figure. 1.1 Biomedical sensor.

The microscopic physical, chemical changes are produced when measurand interacts with sensing element.

Sensing technologies are: electrochemical bio-sensing technologies, optical bio-sensing technologies, Acoustic biomedical sensor. These are sensing technologies used in modern biomedical sensors.

1.1 TRANSDUCER ELECTRONIC DATA SHEET(TEDS).

TEDS is a standardized method of storing transducer identification, checking, correction data and manufacturer related information. The formats are defined in the IEEE1451 set of smart transducer interface which in turn contains an EEPROM memory called TEDS. It is a standard developed by the IEEE Instrumentation and Measurement society's sensor technology technical committee.

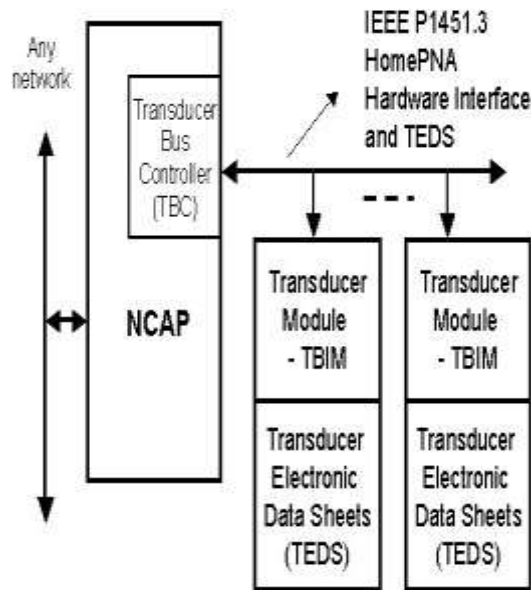


Figure. 1.2 TEDS.

A TEDS can store information related to sensor characteristics and parameters like type of device, designer, model number, serial number, accuracy, resolution, electrical output, frequency response etc. TEDS can include algorithms and additional information for data processing. TEDS having a family of standards and are open to allow user to define additional information concerning the data processing.

2. BIOMEDICAL SENSOR AND APPLICATION:

In biomedical sensor it having three application cases:

A SMART ECG SENSOR : A Smart ECG sensor is used for diagnosing cardiac arrhythmias. There are some portable devices available for monitoring the health care of patient at their homes. It provides both advantages for health care service and for the emotional status of same patient.

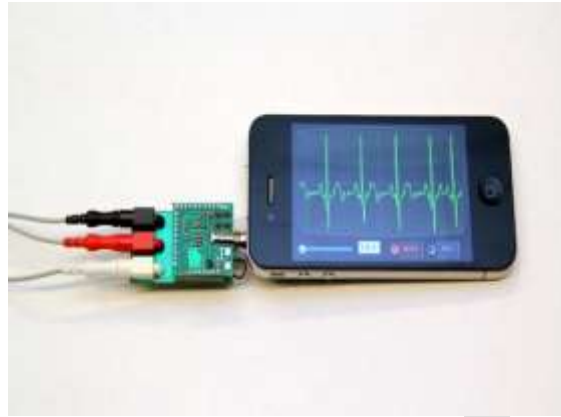


Figure 2.1 The smart ECG Sensor.

The ECG Sensor checks the microelectric signals of heart at fixed sampling frequency. The system is based on a smart phone or a personal digital assistant(PDA) and ECG Sensor.

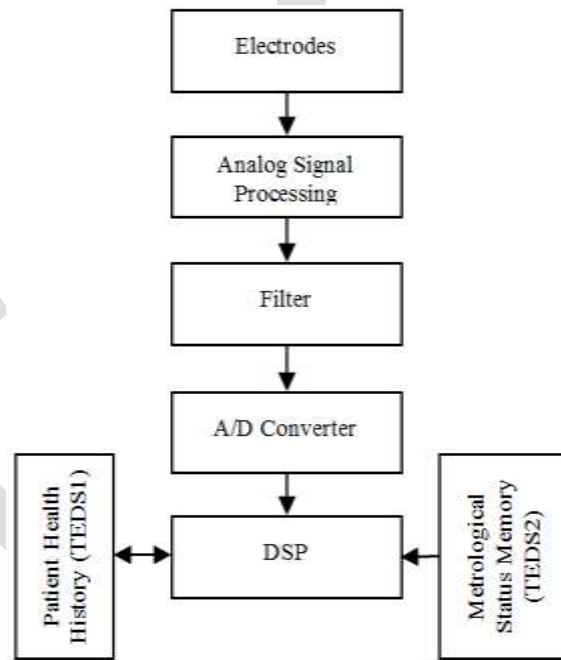


Figure 2.2. block diagram of ECG Sensor.



Figure 2.3: Final results of ECG sensor.

2.1 SMART VIBRATION SENSOR:

Smart vibration sensor is used for monitoring hand-arm vibration exposure. During their activity workers are continuously exposed to risks. So in work places requirements of accident prevention and security are required.



Figure 2.4: A Smart Vibration Sensor.

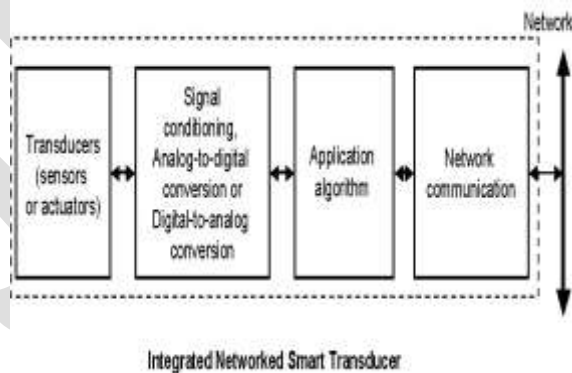


Figure 2.5: architecture of Smart vibration sensor.

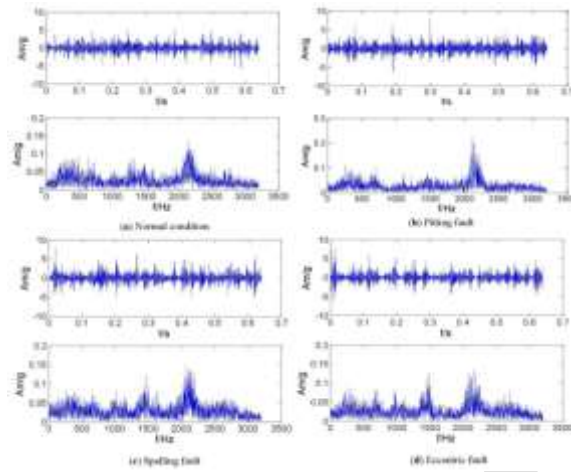


Figure 2.6: Final results of A Smart Vibration Sensor.

2.2 SMART EGG SENSORS:

Smart EGG Sensors are used for diagnosing gastric disorders. Population of any age mostly suffering from gastric disorders.(EEG) Electrogastrographic technique records myoelectric signals of the stomach activity.

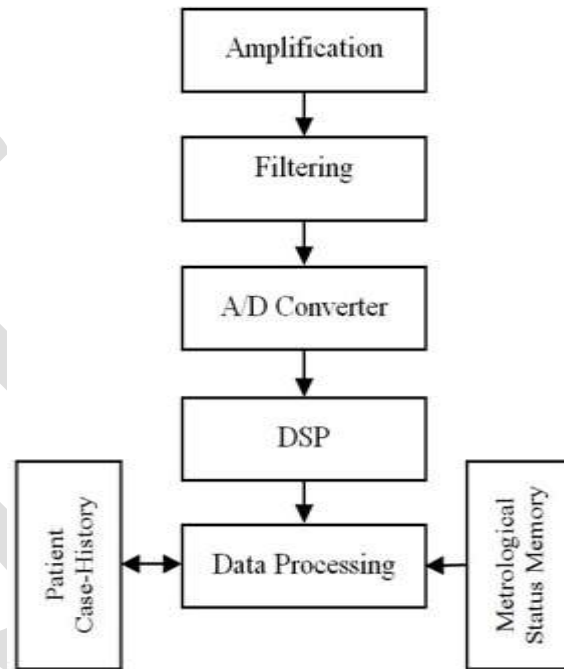


Figure 2.7: architecture of smart EGG sensor

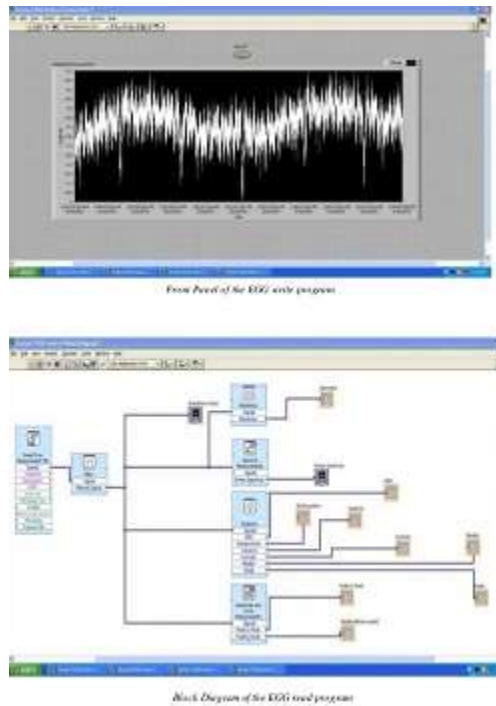


Figure 2.8: Diagnosing with EEG Sensor.

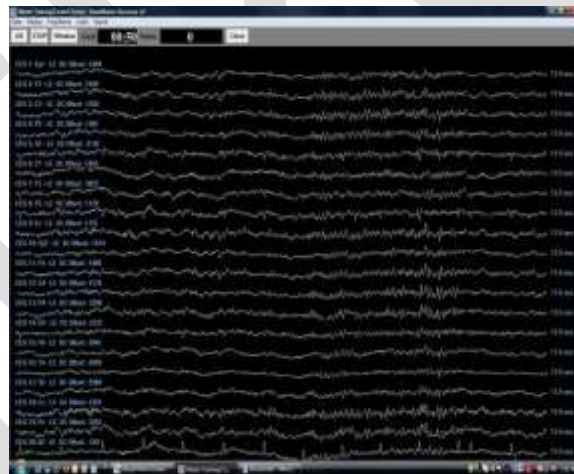


Figure 2.9: Final results of EGG Sensor.

These are the applications cases of biomedical sensors.

3..CONCLUSION

Testing causes significant time delays in reporting results because of specialized laboratories located away from a patient, doctor or hospital. Modern sensors having techniques becoming inexpensive, accurate, reliable and reduce delay time. The use of TEDS is to provide the identification, clinical history and diagnostic criteria of patient. It improves the performance of biomedical sensors and instrumentation. Biomedical sensors can make medical care more personal by using personal monitoring devices.

REFERENCES:

- [1]. Kumar, I. P. Singh and S. K. Sud "Energy efficient and low-cost indoor environment monitoring system based on the IEEE 1451 standard", IEEE Sensors J., vol. 11, no. 10, pp.2598 -2610 2011.
- [2]. G. de Haan and V. Jeanne "Robust pulse rate from chrominance-based RPPG", IEEE Trans. Biomed. Eng., vol. 60, no. 10, pp.2878 -2886 2013.
- [3]. A. H. Al-Timemy, G. Bugmann, J. Escudero and N. Outram "Classification of finger movements for the dexterous hand prosthesis control with surface electromyography", IEEE J. Biomed. Health Inform., vol. 17, no. 3, pp.608 -618 2013.
- [4]. G. R. Naik, D. K. Kumar and M. Palaniswami "Signal processing evaluation of myoelectric sensor placement in low-level gestures: sensitivity analysis using independent component analysis", Expert Syst., vol. 31, pp.91 -99 2014.
- [5]. P. Geethanjali and K. Ray "Statistical pattern recognition technique for improved real-time myoelectric signal classification", Biomed. Eng.: Appl. Basis Comm., vol. 25, pp.1 -9 2013.
- [6]. C. Oliveira, N. Almeida and J. Machado da Silva "A stent-graft endoleakage monitor: Telemetry system based on inductive-coupling transmission for implantable pressure sensors", Proc. IEEE 3rd Portuguese Meeting Bioeng., pp.1 -4 2013

**D & R
I & A**



Publication

International Journal of Engineering Research and general science is an open access peer review publication which is established for publishing the latest trends in engineering and give priority to quality papers which emphasis on basic and important concept through which there would be remarkable contribution to the research arena and also publish the genuine research work in the field of science, engineering and technologies

**International Journal Of Engineering Research and
General Science**

ISSN 2091 - 2730